National Library
of Canada

Bibliothèque nationale
du Canada

Canadian Theses Service

Services des thèses canadiennes

Ottawa, Canada
K1A 0N4

CANADIAN THESES

THÈSES CANADIENNES

NOTICE

The quality of this microfiche is heavily dependent upon the quality of the original thesis submitted for microfilming. Every effort has been made to ensure the highest quality of reproduction possible.

If pages are missing, contact the university which granted the degree.

Some pages may have indistinct print especially if the original pages were typed with a poor typewriter ribbon or if the university sent us an inferior photocopy.

Previously copyrighted materials (journal articles, published tests, etc.) are not filmed.

Reproduction in full or in part of this film is governed by the Canadian Copyright Act, R.S.C. 1970, c. C-30.

AVIS

La qualité de cette microfiche dépend grandement de la qualité de la thèse soumise au microfilmage. Nous avons tout fait pour assurer une qualité supérieure de reproduction.

S'il manque des pages, veuillez communiquer avec l'université qui a conféré le grade.

La qualité d'impression de certaines pages peut laisser à désirer, surtout si les pages originales ont été dactylographiées à l'aide d'un ruban usé ou si l'université nous a fait parvenir une photocopie de qualité inférieure.

Les documents qui font déjà l'objet d'un droit d'auteur (articles de revue, examens publiés, etc.) ne sont pas microfilmés.

La reproduction, même partielle, de ce microfilm est soumise à la Loi canadienne sur le droit d'auteur, SRC 1970, c. C-30.

THIS DISSERTATION
HAS BEEN MICROFILMED
EXACTLY AS RECEIVED

LA THÈSE A ÉTÉ
MICROFILMÉE TELLE QUE
NOUS L'AVONS REÇUE

NL-339 (r.86/06)

Canada

THE UNIVERSITY OF ALBERTA

# UNDRAINED STRENGTH OF ATHABASCA OIL SAND

by

HOWARD DOUGLAS PLEWES

A THESIS

SUBMITTED TO THE FACULTY OF GRADUATE STUDIES AND RESEARCH
IN PARTIAL FULFILMENT OF THE REQUIREMENTS FOR THE DEGREE
OF MASTER OF SCIENCE

DEPARTMENT OF CIVIL ENGINEERING

EDMONTON, ALBERTA

SPRING 1987

Permission has been granted to the National Library of Canada to microfilm this thesis and to lend or sell copies of the film.

The author (copyright owner) has reserved other publication rights, and neither the thesis nor extensive extracts from it may be printed or otherwise reproduced without his/her written permission.

L'autorisation a été accordée à la Bibliothèque nationale du Canada de microfilmer cette thèse et de prêter ou de vendre des exemplaires du film.

L'auteur (titulaire du droit d'auteur) se réserve les autres droits de publication; ni la thèse ni de longs extraits de celle-ci ne doivent être imprimés ou autrement reproduits sans son autorisation écrite.

ISBN 0-315-37795-X

## THE UNIVERSITY OF ALBERTA

## RELEASE FORM

NAME OF AUTHOR HOWARD DOUGLAS PLEWES

TITLE OF THESIS UNDRAINED STRENGTH OF ATHABASCA OIL SAND

DEGREE FOR WHICH THESIS WAS PRESENTED MASTER OF SCIENCE

YEAR THIS DEGREE GRANTED SPRING 1987

Permission is hereby granted to THE UNIVERSITY OF ALBERTA LIBRARY to reproduce single copies of this thesis and to lend or sell such copies for private, scholarly or scientific research purposes only.

The author reserves other publication rights, and neither the thesis nor extensive extracts from it may be printed or otherwise reproduced without the author's written permission.

(SIGNED) ....................

PERMANENT ADDRESS:

781 Village Drive
Sherwood Park, Alta
T8A 4H9

DATED March 9 19 87

THE UNIVERSITY OF ALBERTA

FACULTY OF GRADUATE STUDIES AND RESEARCH

The undersigned certify that they have read, and recommend to the Faculty of Graduate Studies and Research, for acceptance, a thesis entitled UNDRAINED STRENGTH OF ATHABASCA OIL SAND submitted by HOWARD DOUGLAS PLEWES in partial fulfilment of the requirements for the degree of MASTER OF SCIENCE.

J. D. Scott

Supervisor

D. C. Sego

Date October 14, 1986

# ABSTRACT

The mobility of the pore fluid in saturated Athabasca oil sand ranges between two and three orders of magnitude less than water saturated dense sand due to the viscosity of the interstitial bitumen. This introduces a spectrum of geotechnical problems in oil sand technology governed by the strength and deformation properties of oil sand under undrained or partially drained conditions. The research documented in this thesis investigates the undrained behaviour of Athabasca oil sand under axial compression and extension in laboratory triaxial tests at 20 °C. Stress levels up to 8 MPa are covered in the test program. Strain rates are varied up to 3.5 $s^{-1}$ to investigate the influence of transient loading. The influence of initial pore pressure, effective confining stress, stress path and strain rate on undrained strength and deformation behaviour are examined. A predictive procedure for undrained strength and strain to failure in axial compression under generalized stress conditions is presented.

# ACKNOWLEDGEMENTS

The research documented in this thesis was conducted under a scholarship provided by the Alberta Oil Sands Technology and Research Authority (AOSTRA). The laboratory research facilities were supported in part by the National Sciences and Engineering Research Council (NSERC) and the University of Alberta.

The research was performed under the guidance of Dr. J.D. Scott of the Department of Civil Engineering. The advice and ready assistance provided by Dr. Scott is greatly appreciated by the author.

Tanya Shulz and Peter Doell provided capable assistance during the experimental research. Technical assistance was also provided by Hal Soderberg, Denis Gagnon, Steve Gamble, Sean Maloney, Gerry Cyre and other staff members.

Hardy Associates (1978) Ltd. was generously supportive during the time period of this research.

I wish to especially acknowledge my wife, Sheri, who has been patient and provided encouragement throughout the course of study.

# Table of Contents

Chapter Page

1. INTRODUCTION ........................................1

1.1 Statement of Problem ..........................1

1.2 Objective of Thesis ...........................3

1.3 Organization of Thesis ........................3

1.4 Sign Conventions for Stresses and Deformations ..4

2. UNDRAINED SHEAR STRENGTH OF SANDS ...................6

2.1 Introduction ..................................6

2.2 Components of Shear Resistance of Sand ..........6

2.3 Stress-Dilatancy Theory .........................8

2.4 Critical Void Ratio .............................11

2.5 Conditions at Failure in Undrained Tests .......13

2.6 Undrained Stress-Strain Behavior ...............18

2.7 Pore Pressure Parameters A and B ...............19

2.8 Influence of Strain Rate .......................21

2.9 Summary ........................................25

3. STRENGTH OF OIL SANDS ..............................34

3.1 The Athabasca Oil Sands ........................34

3.2 Problem of Sampling and Sample Disturbance .....35

3.3 Past Studies of Shear Strength of Oil Sands ....38

3.4 Drained Strength of Oil Sands ..................39

3.5 Undrained Strength of Oil Sands ................41

3.6 Tensile Strength of Oil Sand ...................42

3.7 Summary ........................................45

4. UNDRAINED TRIAXIAL TESTING OF SALINE CREEK OIL SAND .59

4.1 Introduction ...................................59

4.2 High Pressure Triaxial Testing Facility ........61

4.2.1 Description ..............................61

4.2.2 Calibration of Electronic Monitoring Devices ..............................64

4.2.3 Design of Frictionless Loading Platens ...64

4.2.4 Compliance of Testing Apparatus ..........65

4.2.4.1 Axial Deformation of Frictionless Platens .............65

4.2.4.2 Piston Friction in Triaxial Cell .66

4.2.4.3 Response Time of Pore Pressure Transducer ......................67

4.2.4.4 Stress Wave Propagation and Inertia Forces under Transient Loading .........................68

4.2.4.5 Stiffness of Test Apparatus ......70

4.3 Proof Testing of Frictionless Loading Platens ..75

4.3.1 Introduction ..............................75

4.3.2 Sample Preparation of Ottawa Sand ........75

4.3.3 Saturation of the Test Specimens .........77

4.3.4 Triaxial Testing Procedures .............79

4.3.5 Influence of Specimen Size on Undrained Behavior ................................81

4.3.5.1 Pore Pressure Parameter B ........81

4.3.5.2 Undrained Strength and Pore Pressure Response ................82

4.3.5.3 Strain and Mode of Failure .......85

4.3.6 Pore Pressure Measurements under Transient Loading Conditions .............88

4.3.7 Influence of Strain Rate on Undrained Strength ................................88

4.3.8 Summary ..................................90

4.4 Triaxial Testing of Saline Creek Oil Sand ......91

4.4.1 Introduction ..............................91

4.4.2 Sampling and Sample Preparation ..........91
4.4.3 Index Testing ............................93
4.4.4 Saturation of the Test Specimens .........96
4.4.5 Isotropic Compressibility ................99
4.4.6 Undrained Triaxial Compression Tests ....101
4.4.7 Pore Pressure Measurements under Transient Loading ........................103
4.4.8 Assessment of Grain Crushing during Testing ................................104
4.5 Summary ......................................107
5. TRIAXIAL TESTING OF SYNCRUDE OIL SAND ..............132
5.1 Introduction .................................132
5.2 Low Pressure Triaxial Testing Facility ........133
5.2.1 Description ..............................133
5.2.2 Calibration of Electronic Measuring Devices ................................135
5.3 Sampling and Sample Preparation ...............136
5.3.1 Preparation of Triaxial Test Specimens ..136
5.3.2 Preparation of Unconfined Tension Test Specimens ...............................137
5.4 Index Testing .................................139
5.5 Saturation of the Test Specimens ..............140
5.6 Isotropic Compressibility .....................141
5.7 Drained Axial Compression Test ................145
5.8 Axial Extension Tests .........................146
5.8.1 Test Procedures and Analyses ............146
5.8.2 Mode of Failure of Test Specimens .......148
5.8.3 Straining During Triaxial Tension Tests .149
5.8.4 Membrane Corrections to Triaxial Test Results ..................................152

5.8.4.1 Extension Modulus of the Rubber Membranes ........................152

5.8.4.2 Membrane Extension Tests in the Triaxial Cell ....................154

5.8.4.3 Correction for Membrane Area ....157

5.9 Unconfined Extension Tests ...................158

5.9.1 Failure of Test Specimens ...............158

5.10 Summary .......................................161

6. DISCUSSION OF EXPERIMENTAL RESULTS ................186

6.1 Drained and Undrained Compressibility .........186

6.2 Undrained Strength ............................187

6.2.1 Assessment of Sample Disturbance ........187

6.2.2 Maximum Stress Ratio ....................188

6.2.3 Ultimate Strength .......................190

6.2.4 Undrained Stress Path ...................191

6.3 Critical Void Ratio ...........................192

6.4 Prediction of Undrained Strength ..............193

6.4.1 Shear Strength in Non-Cavitating Tests ..193

6.4.2 Shear Strength in Cavitating Tests ......195

6.5 Undrained Stress-Strain Behavior ..............198

6.5.1 Undrained Modulus of Deformation ........198

6.5.2 Strain at Failure .......................201

6.6 Influence of Strain Rate ......................203

6.7 Behavior of Oil Sand under Axial Extension ....205

6.7.1 Effective Shearing Resistance ...........205

6.7.2 Stress Path .............................206

6.7.3 Comparison with other Dense Sands .......207

6.7.4 Comparison with Stress-Dilatancy Theory .209

6.7.5 Stress-Strain Behavior ..................210

6.7.6 Implications of Unconfined Extension Tests ..................................211

7. CONCLUSIONS AND RECOMMENDATIONS ..................253

7.1 General ..................................253

7.2 Conclusions ..............................254

7.3 Practical Implications of the Research ........259

REFERENCES ......................................262

APPENDIX A - Compliance and Calibrations of Triaxial Test Apparatus ..................................268

APPENDIX B - Ottawa Sand Triaxial Test Results ..........274

APPENDIX C - Saline Creek Oil Sand Triaxial Test Results 303

APPENDIX D - Comparitive Grain Size Distribution of Saline Creek Oil Sand Before And After Testing ......388

APPENDIX E - Syncrude Oil Sand Triaxial Test Results ....393

## List of Tables

Table Page

1.1 Geotechnical Design Problems Controlled by Undrained or Partially Drained Behavior of Oil Sand ....5

3.1 Classification of Sample Quality with the Disturbance Index (After Dusseault and Van Domselaar, 1982) ....47

4.1 Ottawa Sand: Summary of Specimen Data ....108

4.2 Ottawa Sand: Summary of Triaxial Test Results ....109

4.3 Saline Creek Oil Sand: Summary of Specimen Data ....110

4.4 Saline Creek Oil Sand: Grain Size Data ....111

4.5 Saline Creek Oil Sand: Summary of Pore Fluid Saturation Pressure and Pore Pressure Parameter B ....112

4.6 Saline Creek Oil Sand: Summary of Isotropic Compression Tests ....113

4.7 Saline Creek Oil Sand: Summary of Triaxial Test Results ....114

4.8 Saline Creek Oil Sand: Comparative Grain Size Analyses Before and After Testing ....115

5.1 Syncrude and Saline Creek Oil Sand: Summary of Test Specimen Data ....162

5.2 Syncrude Oil Sand: Grain Size Data ....163

5.3 Syncrude Oil Sand: Summary of Pore Fluid Saturation Pressure and Pore Pressure Parameter B ....164

5.4 Syncrude Oil Sand: Summary of Isotropic Compressibility Tests ....165

5.5 Syncrude Oil Sand: Summary of Triaxial Test Results ....166

5.6 Coefficient of Consolidation and Requisite Time to Failure for SYN-C-1 ....167

5.7 Time to Failure and Average Degree of Consolidation for Triaxial Tests ....168

Table Page

5.8 Tensile Stresses Developed in Unconfined Extension Tests ....169

6.1 Comparison of Predicted and Measured Undrained Strength of Undisturbed Oil Sand ....213

6.2 Comparison of Predicted and Measured Undrained Strength of Disturbed and Remolded Oil Sand ....214

6.3 Comparison of Axial Compression and Extension Tests on Dense Sands ....215

6.4 Calculation of $\phi_\mu$ and $\phi_{cv}$ from Stress Dilatancy Theory for Syncrude Oil Sand ....216

A.1 Calibration of Electronic Measuring Devices in High Pressure Triaxial Testing Facility ....269

A.2 Measurement Of Piston Friction in High Pressure Triaxial Cell ....270

A.3 Response of Pore Pressure Transducer Under Maximum Rate of Deformation ....271

A.4 Calibration of Electronic Measuring Devices in Low Pressure Triaxial Testing Facility ....272

## List of Figures

Figure Page

2.1 Schematic Illustration of Contribution of Components of Shearing Resistance for Drained Tests on Dense Sands (After Lee and Seed, 1967a) ....26

2.2 Experimental Relationship Between $\phi_{cv}$ and $\phi_{\mu}$ (After Rowe, 1969) ....27

2.3 Relationship Between Volume Change at Failure, Void Ratio and Confining Pressure in Drained Triaxial Compression Tests ....28

2.4 Relationship Between Pore Pressure Change at Failure, Void Ratio and Consolidation Pressure in Undrained Triaxial Compression Tests ....29

2.5 Undrained Behavior of Dense Sands in Triaxial Compression Tests ....30

2.6 Ultimate Undrained Strength of Dense Sands in Terms of Total Stress ....31

2.7 Stress Path to Failure in Undrained Triaxial Compression Tests ....32

2.8 Typical Undrained Stress-Strain Response for Dense Sands ....33

3.1 Oil Sands Deposits of Alberta ....48

3.2 Composition of In Situ Oil Sand (After Dusseault, 1977) ....49

3.3 Grain Size Distribution for Athabasca Oil Sand (After Dusseault, 1977) ....50

3.4 Drained Triaxial Compression Test Data for Oil Sand, Bulk Densities Greater Than 2.00 $Mg/m^3$ ....51

3.5 Typical Stress-Strain Curves for Drained Triaxial Compression Tests at Low and High Confining Pressures (After Dusseault, 1983) ....52

3.6 Axial Strain at Failure in Drained Triaxial Compression Tests ....53

Figure Page

3.7 Modulus of Deformation for Drained Triaxial Compression Tests at $\epsilon_a$ = 0.25 Percent ....54

3.8 Shear Strength at the Maximum Principal Stress Ratio in Undrained Triaxial Compression Tests ....55

3.9 Ultimate Shear Strength in Undrained Triaxial Compression Tests ....56

3.10 Axial Strain at Ultimate Strength in Undrained Triaxial Compression Tests ....57

3.11 Theoretical Prediction of Undrained Shear Strength by Rowe's Stress-Dilatancy Theory ....58

4.1 High Pressure Air Activated Diaphragm Pump System ....116

4.2 Nitrogen Charged Low Pressure System ....116

4.3 Assembly of Frictionless Loading Platens ....117

4.4 Spring Analogy Representing the Interaction of the Triaxial Test Apparatus and the Test Specimens ....118

4.5 Mold Assembly for Ottawa Sand Samples ....119

4.6 Ottawa Sand: Pore Pressure Parameter B Versus Length/Diameter Ratio of the Test Specimens ....120

4.7 Test Series A and B: Conditions at the Ultimate Strength and Maximum Stress Ratio Versus l/d Ratio of the Test Specimens ....121

4.8 Test Series A and B: Shape of the Test Specimens after Testing ....122

4.9 Nonuniformity of Straining and Developed Shear Plane using Conventional Steel Loading Platens (After Rowe and Barden, 1964) ....123

4.10 Variation in Pore Pressure Measurements with Strain Rate for Ottawa Sand ....124

Figure Page

4.11 Test Series C: Conditions at the Ultimate Strength and Maximum Stress Ratio Versus Strain Rate ....................125

4.12 Measurement of Pore Fluid Saturation Pressure and Pore Pressure Parameter B ....................126

4.13 Pore Pressure Parameter B Versus Effective Confining Pressure ....................127

4.14 Coefficient of Volume Compressibility Versus Effective Confining Pressure ....................128

4.15 Variation in Pore Pressure Measurements with Strain Rate for Saline Creek Oil Sand ....................129

4.16 Fines Generation in Undrained Triaxial Compression Tests Versus Effective Confining Stress at Failure, Strain Rates less than $10^{-3}$ $s^{-1}$ ....................130

5.1 Schematic Layout of Low Pressure Testing Facility ....................170

5.2 Air Activated Low Pressure System ....................170

5.3 Notching of Tension Test Specimens ....................171

5.4 Convolution of Rubber Membrane for Tension Test Specimens SYN-T-2 Through SYN-T-5 ....................171

5.5 Suspension of Unconfined Tension Test Specimens in the Triaxial Cell ....................172

5.6 Coefficient of Volume Compressibility Versus Effective Confining Pressure ....................173

5.7 Calculation of $t_{100}$ From Isotropic Compression Tests ....................174

5.8 Stresses Acting on Tension Test Specimens ....................175

5.9 Measurement of Axial Deformation Along SYN-T-5 During Axial Extension Test ....................176

5.10 Volume Change During Axial Extension of SYN-T-1 ....................177

5.11 Volume Change During Axial Extension of SYN-T-2 ....................178

Figure Page

5.12 Volume Change During Axial Extension of SYN-T-3 ....179

5.13 Measurement of Extension Modulus of Rubber Membranes ....180

5.14 Results of Rubber Membrane Extension Test ....181

5.15 Replicate Steel Sample for Membrane Extension Tests in the Triaxial Cell ....182

5.16 Calculation of Membrane Resistance for Extension Tests in the Triaxial Cell ....183

5.17 Test Results for Membrane Extension Tests in the Triaxial Cell ....184

6.1 Relation Between Pore Pressure Parameter B and Compressibility of Oil Sand ....217

6.2 Predicted Variation of Pore Pressure Parameter B with Confining Stress, $C_b$ = $2.0 \times 10^{-6} s^{-1}$ ....218

6.3 Maximum Principal Stress Ratio Versus Index of Disturbance for Initial Effective Confining Pressures of 2 MPa ....219

6.4 Shear Strength at Maximum Principal Stress Ratio in Undrained Triaxial Compression Tests ....220

6.5 Comparison of Drained Triaxial Compression Tests with Undrained Failure Line at the Maximum Principal Stress Ratio ....221

6.6 Comparison of Drained Triaxial Compression Tests Corrected for Dilatancy with Undrained Failure Line at the Maximum Principal Stress Ratio ....222

6.7 Shear Strength of Disturbed Oil Sand at the Maximum Stress Ratio in Undrained Triaxial Compression Tests ....223

6.8 Ultimate Shear Strength in Undrained Triaxial Compression Tests ....224

6.9 Stress Path for Undrained Triaxial Compression Tests on Conventional Specimens (l/d = 2) of Undisturbed Oil Sand ....225

Figure Page

6.10 Stress Path for Undrained Triaxial Compression Tests on Short Specimens (l/d = 0.5) of Undisturbed Oil Sand using Frictionless Platens ....226

6.11 Pore Pressure Parameter A at Ultimate Strength for Non-Cavitating Undrained Triaxial Compression Tests ....227

6.12 Effective Minor Principal Stress at Ultimate Strength in Undrained Triaxial Compression Tests ....228

6.13 Critical Confining Pressure From Drained Triaxial Compression Tests on Saline Creek Oil Sand (After Au, 1984 and Agar, 1984) ....229

6.14 Critical Confining Pressure from Drained Triaxial Compression Tests on Lean Oil Sand (After Dusseault, 1983) ....230

6.15 Critical State Line for Oil Sand ....231

6.16 Ultimate Shear Strength in Non-Cavitating Undrained Triaxial Compression Tests on Undisturbed Saline Creek Oil Sand ....232

6.17 Ultimate Shear Strength in Non-Cavitating Undrained Triaxial Compression Tests on Disturbed Saline Creek Oil Sand ....233

6.18 Predicted Ultimate Shear Strength for Undrained Triaxial Compression Tests on Undisturbed Oil Sand ....234

6.19 Predicted Ultimate Shear Strength for Undrained Triaxial Compression Tests on Disturbed Oil Sand ....235

6.20 Stress-Strain Curves for Conventional Specimens (l/d = 2) of Undisturbed Saline Creek Oil Sand ....236

6.21 Tangent Modulus at 0.25 Percent Strain for Undrained Triaxial Compression Tests on Oil Sand ....237

6.22 Stress-Strain Curves for Short Specimens (l/d = 0.5) of Undisturbed Saline Creek Oil Sand using Frictionless Platens ....238

Figure Page

6.23 Comparison of Undrained Triaxial Compression Test Results for Conventional Specimens (l/d = 2) and Short Specimens (l/d = 0.5) using Frictionless Platens ............239

6.24 Comparison of Modulus of Deformation for Undrained Triaxial Compression Tests at $\Delta u/\Delta\epsilon = 0$ and Drained Tests at $\Delta v/\Delta\epsilon = 0$ ..........240

6.25 Axial Strain at Maximum Stress Ratio Versus Index of Disturbance ........................241

6.26 Axial Strain at Ultimate Strength Versus Stress Difference $\sigma'_{3_f} - \sigma'_{3_i}$ .........................242

6.27 Ultimate Undrained Strength Versus Strain Rate of Testing ...................................243

6.28 Relative Increase in Ultimate Undrained Strength with Strain Rate .........................244

6.29 Axial Strain at Ultimate Strength Versus Strain Rate ..........................................245

6.30 Initial Tangent Modulus of Deformation Versus Strain Rate ...................................246

6.31 Triaxial Test Results for Syncrude Oil Sand ..................................................247

6.32 Comparison of Triaxial Compression Test SYN-C-1 with Test Series 84S .......................248

6.33 Stress Path To Failure for Triaxial Tests on Syncrude Oil Sand ...............................249

6.34 Comparison of $\phi_\mu$ and $\phi_{cv}$ for Syncrude Oil Sand with other Dense Sands at Low Stresses (After Rowe, 1969) .......................250

6.35 Tangent Modulus of Deformation Versus Initial Effective Confining Pressure for Extension Tests .........................................251

6.36 Effective Stress Modulus of Deformation, E' at 1.0 Percent Strain for Extension Tests ..............................................252

A.1 Axial Compliance of Frictionless Platens (Steel Insert Sample Not Cyclically Compressed) ...........................................273

B.1 Grain Size Distribution of Ottawa Sand ............275

Figure Page
B.2 OS-S1: Triaxial Test Results ........................276
B.3 OS-S2: Triaxial Test Results ........................277
B.4 OS-S3: Triaxial Test Results ........................278
B.5 OS-S4: Triaxial Test Results ........................279
B.6 OS-1A: Triaxial Test Results ........................280
B.7 OS-1B: Triaxial Test Results ........................281
B.8 OS-2A: Triaxial Test Results ........................282
B.9 OS-3B: Triaxial Test Results ........................283
B.10 OS-4: Triaxial Test Results .........................284
B.11 OS-5: Triaxial Test Results .........................285
B.12 OS-6A: Triaxial Test Results ........................286
B.13 OS-6B: Triaxial Test Results ........................287
B.14 OS-7A: Triaxial Test Results ........................288
B.15 OS-7B: Triaxial Test Results ........................289
B.16 OS-8A: Triaxial Test Results ........................290
B.17 OS-8B: Triaxial Test Results ........................291
B.18 OS-11: Triaxial Test Results ........................292
B.19 OS-12: Triaxial Test Results ........................293
B.20 OS-13: Triaxial Test Results ........................294
B.21 OS-14: Triaxial Test Results ........................295
B.22 OS-15A: Triaxial Test Results .......................296
B.23 OS-16A: Triaxial Test Results .......................297
B.24 OS-18A: Triaxial Test Results .......................298
B.25 OS-19A: Triaxial Test Results .......................299
B.26 OS-19B: Triaxial Test Results .......................300
B.27 OS-21: Triaxial Test Results ........................301
B.28 OS-22: Triaxial Test Results ........................302

Figure Page
C.1 SC-83-22D: Triaxial Test Results ..................305
C.2 SC-83-22U: Triaxial Test Results ..................307
C.3 SC-84-1: Triaxial Test Results ....................309
C.4 SC-84-3A: Triaxial Test Results ...................311
C.5 SC-84-3B: Triaxial Test Results ...................313
C.6 SC-84-4A: Triaxial Test Results ...................315
C.7 SC-84-4B: Triaxial Test Results ...................317
C.8 SC-84-5A: Triaxial Test Results ...................319
C.9 SC-84-5B: Triaxial Test Results ...................321
C.10 SC-84-8A: Triaxial Test Results ..................323
C.11 SC-84-8B: Triaxial Test Results ..................325
C.12 SC-84-10: Triaxial Test Results ..................327
C.13 SC-84-13: Triaxial Test Results ..................329
C.14 SC-84-14A: Triaxial Test Results .................331
C.15 SC-84-14B: Triaxial Test Results .................333
C.16 SC-84-15A: Triaxial Test Results .................335
C.17 SC-84-15B: Triaxial Test Results .................337
C.18 SC-84-17: Triaxial Test Results ..................339
C.19 SC-84-22: Triaxial Test Results ..................341
C.20 SC-84-23: Triaxial Test Results ..................343
C.21 SC-84-24: Triaxial Test Results ..................345
C.22 SC-84-25A: Triaxial Test Results .................347
C.23 SC-84-25B: Triaxial Test Results .................349
C.24 SC-84-29: Triaxial Test Results ..................351
C.25 SC-84-30: Triaxial Test Results ..................353
C.26 SC-84-31: Triaxial Test Results ..................355
C.27 SC-84-33: Triaxial Test Results ..................357

Figure Page

C.28 SC-84-34: Triaxial Test Results ....................359

C.29 SC-84-39: Triaxial Test Results ....................361

C.30 SC-84-40A: Triaxial Test Results ....................363

C.31 SC-84-40B: Triaxial Test Results ....................365

C.32 SC-84-43: Triaxial Test Results ....................367

C.33 SC-84-49: Triaxial Test Results ....................369

C.34 SC-84-51: Triaxial Test Results ....................371

C.35 SC-84-52: Triaxial Test Results ....................373

C.36 SC-84-53: Triaxial Test Results ....................375

C.37 SC-84-55A: Triaxial Test Results ....................377

C.38 SC-84-55B: Triaxial Test Results ....................379

C.39 SC-84-60: Triaxial Test Results ....................381

C.40 SC-84-115A: Triaxial Test Results ....................383

C.41 SC-84-115B: Triaxial Test Results ....................385

C.42 SC-84-117: Triaxial Test Results ....................387

D.1 SC-84-10: Grain Size Distribution Before And After Testing ....................389

D.2 SC-84-30: Grain Size Distribution Before And After Testing ....................389

D.3 SC-84-110: Grain Size Distribution Before And After Testing ....................390

D.4 SC-84-3B And SC-84-4A: Composite Grain Size Distribution Before And After Testing ....................390

D.5 SC-84-5B And SC-84-15A: Composite Grain Size Distribution Before And After Testing ....................391

D.6 SC-84-31 And SC-84-43: Composite Grain Size Distribution Before And After Testing ....................391

Figure Page

D.7 SC-84-49 And SC-84-52: Composite Grain Size Distribution Before And After Testing ....................392

D.8 SC-84-23, SC-84-55A And SC-84-55B: Composite Grain Size Distribution Before And After Testing ....................392

E.1 SYN-T-1,T-2,T-3: Grain Size Distribution ..........394

E.2 SYN-T-4,T-5,C-1: Grain Size Distribution ..........394

E.3 SYN-C-1: Pore Pressure Parameter B ..............396

E.4 SYN-C-1: Cyclic Compressibility Test ..............396

E.5 SYN-C-1: Drained Axial Compression Test Results ....................397

E.6 SYN-C-1: Condition of Sample After Testing ....................398

E.7 SYN-C-1: Consolidation Under Loading Increment of Isotropic Stress From 81 To 198 kPa ....................399

E.8 SYN-C-1: Consolidation Under Loading Increment of Isotropic Stress From 198 To 389 kPa ....................399

E.9 SYN-C-1: Consolidation Under Loading Increment of Isotropic Stress From 389 To 589 kPa ....................400

E.10 SYN-C-1: Consolidation Under Loading Increment of Isotropic Stress From 589 To 791 kPa ....................400

E.11 SYN-T-1: Pore Pressure Parameter B ................402

E.12 SYN-T-1: Cyclic Compressibility Test ..............402

E.13 SYN-T-1: Drained Axial Extension Test Results ....................403

E.14 SYN-T-1: Condition of Sample After Testing ....................404

E.15 SYN-T-2: Pore Pressure Parameter B ................406

E.16 SYN-T-2: Cyclic Compressibility Test ..............406

Figure Page

E.17 SYN-T-2: Drained Axial Extension Test Results ....................................407

E.18 SYN-T-2: Condition of Sample After Testing ....................................408

E.19 SYN-T-3: Pore Pressure Parameter B ...............410

E.20 SYN-T-3: Cyclic Compressibility Test ..............410

E.21 SYN-T-3: Drained Axial Extension Test Results ....................................411

E.22 SYN-T-3: Condition of Sample After Testing ....................................412

E.23 SYN-T-4: Pore Pressure Parameter B ...............414

E.24 SYN-T-4: Cyclic Compressibility Test ..............414

E.25 SYN-T-4: Undrained Axial Extension Test Results ....................................415

E.26 SYN-T-4: Condition of Sample After Testing ....................................416

E.27 SYN-T-5: Pore Pressure Parameter B ...............418

E.28 SYN-T-5: Cyclic Compressibility Test ..............418

E.29 SYN-T-5: Undrained Axial Extension Test Results ....................................419

E.30 SYN-T-5: Condition of Sample After Testing ....................................420

E.31 SYN-T-6: Initial Sample Dimensions ...............422

E.32 SC-84-T-1: Initial Sample Dimensions .............424

E.33 SC-84-T-1: Condition of Sample After 5 Days ....................................425

E.34 SC-84-T-2: Initial Sample Dimensions .............427

E.35 SC-84-T-2: Condition of Sample After Failure ....................................428

## List of Plates

Plate Page

4.1 Indentation of Ottawa Sand Grains into Surface of Conventional Steel Loading Platens ....................................131

5.1 Assembly of Test Specimen SYN-T-5 in Triaxial Cell (After Testing) ....................185

## LIST OF SYMBOLS

The following list of symbols is included to assist the interpretation of the equations within the text:

| SYMBOL | MEANING |
|---|---|
| $A, B$ | Parameters relating pore pressure response with undrained total stress change |
| $A_f$ | Pore pressure parameter A at ultimate strength |
| $A_e, A_n$ | Sectional area through ends and notch of tension test specimens |
| $A_m$ | Sectional area through membrane enclosing triaxial test specimens |
| $A_o$ | Initial sectional area through triaxial specimens |
| $C$ | Drained isotropic compressibility |
| $C_b$ | Compressibility of bitumen |
| $C_s$ | Compressibility of soil grains |
| $C_w$ | Compressibility of water |
| $C_v$ | Coefficient of consolidation |
| $C_u$ | Uniformity coefficient ($C_u = D_{10}/D_{60}$) |
| $c$ | Longitudinal wave velocity through soil |
| $D$ | Dilatancy correction ($D = 1 - d\epsilon_v/d\epsilon_a$) |

| | |
|---|---|
| $D_n$ | Mean particle diameter greater than n percent by mass of the soil particles in a sample |
| $D_r$ | Relative density |
| $d$ | Mean diameter of triaxial test specimens |
| $d_m$ | Mean diameter of triaxial membranes |
| $d_n$ | Notch diameter of extension test specimens |
| $E$ | Drained modulus of deformation |
| $E_u$ | Undrained modulus of deformation |
| $H$ | Henry's coefficient |
| $h$ | One-half height of triaxial test specimens |
| $I_D$ | Index of disturbance for oil sand |
| $K$ | Experimental coefficient |
| $k$ | Absolute permeability |
| $k_m$ | Axial stiffness of triaxial test apparatus |
| $k_s$ | Axial stiffness of triaxial test specimens |
| $k_1, k_2$ | Constants for drainage condition of triaxial test specimens |
| $l$ | Length of triaxial test specimens |
| $M$ | Compression modulus of triaxial membranes |

| | |
|---|---|
| $m_v$ | Coefficient of volume compressibility |
| $n$ | Soil porosity |
| $n_b$ | Bitumen porosity |
| $n_i$ | In situ porosity from geophysical logs |
| $n_w$ | Water porosity |
| $p$ | $(\sigma_1 + \sigma_3)/2$ |
| $p'$ | $(\sigma'_1 + \sigma'_3)/2$ |
| $q$ | $(\sigma_1 - \sigma_3)/2$ |
| $R$ | Effective principal stress ratio, $\sigma'_1/\sigma'_3$ |
| $R_u$ | Ratio of pore fluid pressure to the pore fluid saturation pressure, $u/u_s$ |
| $S$ | Saturation |
| $T$ | Tensile resistance |
| $T_m$ | Tensile resistance of triaxial membranes |
| $t_d$ | Time to develop 100 percent saturation of pore fluid |
| $t_f$ | Time to failure in axial compression tests |
| $t_{100}$ | Empirical time for 100 percent consolidation of triaxial test specimens |
| $U_f$ | Average degree of consolidation at ultimate strength |

| | |
|---|---|
| $u$ | Pore pressure |
| $u_a$ | Absolute atmospheric pore fluid pressure |
| $u_f$ | Pore fluid pressure at ultimate strength in triaxial tests |
| $u_i$ | Initial pore fluid pressure in triaxial tests |
| $u_s$ | Pore fluid gas saturation pressure |
| $\Delta u$ | Change in pore fluid pressure |
| $V$ | Volume of test specimens |
| $\Delta V$ | Change in volume of test specimens |
| $v_o$ | Axial rate of deformation |
| $X$ | Experimental coefficient |
| $\epsilon$ | Strain |
| $\epsilon_1, \epsilon_2, \epsilon_3$ | Major principal strains |
| $\epsilon_a$ | Axial strain in triaxial tests |
| $\epsilon_f$ | Axial strain at ultimate strength in triaxial tests |
| $\epsilon_v$ | Volumetric strain |
| $\dot{\epsilon}$ | Strain rate |
| $\sigma$ | Total stress |

| | |
|---|---|
| $\sigma'$ | Effective stress |
| $\sigma_1, \sigma_2, \sigma_3$ | Major principal total stresses |
| $\sigma'_1, \sigma'_2, \sigma'_3$ | Major principal effective stresses |
| $\sigma'_{1f}, \sigma'_{2f}, \sigma'_{3f}$ | Major principal effective stresses at ultimate strength |
| $\sigma_c$ | Confining cell pressure |
| $\sigma'_c$ | Effective confining cell pressure |
| $\sigma_{crit}$ | Critical confining stress or pressure |
| $\sigma_e$ | Total stress acting in the plane through the ends of the triaxial extension test specimens |
| $\sigma_n$ | Total stress acting in the plane through the notch of the triaxial extension test specimens |
| $\sigma_r$ | Membrane correction for compressive strength in triaxial compression test |
| $\tau$ | Shear stress or shearing resistance |
| $\tau_u$ | Undrained shearing resistance |
| $\tau_p, \tau_{de}, \tau_{df}, \tau_r$ | Components of internal shearing resistance |
| $\phi'$ | Angle of internal shearing resistance |
| $\phi_f$ | Empirical angle of shearing resistance |
| $\phi_{cv}$ | Angle of shearing resistance under conditions of constant volume |

| | |
|---|---|
| $\phi_\mu$ | Intergranular angle of friction |
| $\mu$ | Dynamic viscosity |
| $\Delta_m$ | Axial deformation of test specimens contributed by stress relaxation in triaxial test apparatus |
| $\Delta_s$ | Total axial deformation of test specimens |

# 1. INTRODUCTION

## 1.1 Statement of Problem

The mobility of the pore fluid in saturated rich Athabasca oil sand at in situ temperatures (generally less than 20°C) ranges between two and three orders of magnitude less than water saturated dense sand due to the viscosity of the interstitial bitumen. The impeded mobility of the pore fluid introduces a spectrum of geotechnical problems in which stresses and deformations are governed by the strength and stress-strain behaviour of oil sand under undrained or partially drained conditions. A range of potential problems likely to be encountered in surface mining, in situ process recovery and mine assisted in situ process (MAISP) recovery schemes are listed in Table 1.1.

The types of problems listed in Table 1.1 are broadly classified into three categories:

1. Undrained behaviour under transient changes of stress,
2. Undrained behaviour during "rapid" changes of stress, and
3. Partially drained behaviour during "slow" changes of stress or following rapid stress changes.

Under transient and "rapid" stress changes, there is insufficient time for significant drainage of the pore fluid to occur during the time interval of the applied stress change and the behaviour is completely undrained. Partially drained conditions occur when the rate of stress change is slow enough to allow simultaneous drainage of the pore fluid and dissipation of pore pressures. Conditions of partially drained behaviour may also occur with pore fluid drainage following "rapid" increments of stress change. The behaviour is a time dependent function of the rate of pore fluid drainage and pore pressure dissipation.

In situ process heating of oil sand by injection of condensed steam or in situ combustion is intended to decrease the viscosity of the bitumen allowing recovery by pumping or gravity drainage. A broad range of undrained and partially drained behaviour is encompassed by the spacial variation of temperature and fluid mobility. At elevated temperatures approaching 300°C, the mobility of the pore fluid increases approximately 10 times while the physical properties of the quartzose grains and structure of the Athabasca oil sand are largely unaltered (Agar, 1984). Hence, the effects of elevated temperatures over this range on the undrained strength and deformation behaviour of Athabasca oil sand are projected to exert a minor secondary influence only. The time dependent behaviour under partially drained conditions will, however, be influenced by faster rates of fluid drainage with increased fluid mobility.

## 1.2 Objective of Thesis

The objective of the research documented in this thesis is to investigated the undrained behaviour of Athabasca oil sand in triaxial laboratory tests at room temperature (20°C). The triaxial test program is divided into two major parts:

1. Undrained triaxial compression tests are conducted covering the range of effective confining stress levels up to 8 MPa. The strain rate of testing is also varied between $10^{-5}$ and 3.5 $s^{-1}$ to investigate the influence of transient loading.
2. The undrained behaviour of oil sand during unloading in axial extension is examined. Undrained and drained extension tests are conducted for comparison of behaviour.

The influence of initial pore pressure, effective confining stress, stress path and strain rate on the undrained strength and deformation behaviour are examined. A predictive procedure for the undrained strength and strain to failure in axial compression under generalized stress conditions is presented.

## 1.3 Organization of Thesis

Research on the behaviour of sands has proliferated in the past 50 years and matured to high levels of understanding on many aspects. The volume of the literature is immense and out of the scope of this thesis to review its entirety. Chapter 2 introduces selected behavioural aspects and concepts pertinent to this thesis.

Chapter 3 discusses the unique interpenetrative or "locked" structure of oil sands and the problems of sample disturbance. Available published laboratory test data on the drained and undrained behaviour of oil sand is presented.

The laboratory test facilities and test procedures developed for the undrained triaxial compression tests are described in Chapter 4. The test facilities and testing procedures adopted for the axial extension tests are described in Chapter 5.

Discussion of the experimental results and comparison with other published data is contained in Chapter 6. Chapter 7 concludes with a summary of the findings of the research and discussion of practical implications.

### 1.4 Sign Conventions for Stresses and Deformations

The sign convention adhered to in this thesis defines compressive stress as positive in magnitude and tensile stress as negative. Compressive and expansive volumetric strains are defined as negative and positive quantities, respectively.

Table 1.1 Geotechnical Design Problems Controlled by Undrained or Partially Drained Behavior of Oil Sand

| CATEGORY | SURFACE MINING | INSITU PROCESS RECOVERY | MINE ASSISTED IN SITU PROCESS RECOVERY |
|---|---|---|---|
| Undrained behavior under transient loading | - Design of blasting patterns for rubbilization of oil sand<br>- Design of dynamically loaded foundations<br>- Stability of oil sand during movements of bucketwheel excavators or draglines<br>- Stability of stacker dumps | - Deformations and fracture propagation using explosives<br>- Stability of wellbores under explosive fracturing<br>- Rubbilization of oil sand around wellbores using explosives to increase mass permeablility | - Same as in situ process recovery |
| Undrained behavior under rapid stress changes | - Deformations and stability of excavations | - Deformations and propagation of hydraulic fractures under very high rates of fluid injection<br>- Stability of wellbores under high rates of fluid injection | - Same as in situ process recovery<br>- Stability and standup time of tunnels and cavities |
| Partially drained behavior | - Deformations and stability of excavations and mine high walls<br>- Pore pressure generation and stability of embankments | - Deformations and hydraulic fracture propagation<br>- Stability of wellbores during hydraulic fracturing<br>- Deformations and stresses during heating of oil sand | - Same as in situ process recovery<br>- Deformations and convergence of tunnel and cavity faces<br>- Design of tunnel liners |

# 2. UNDRAINED SHEAR STRENGTH OF SANDS

## 2.1 Introduction

This chapter introduces selected aspects and concepts of the undrained behaviour of sands pertinent to discussions in subsequent chapters.

## 2.2 Components of Shear Resistance of Sand

Work by Rowe(1962), Rowe, Barden and Lee(1964), Lee and Seed(1967), and Ladanyi and Archambault(1969) suggest that the shearing resistance, $\tau$ of a cohesionless particulate mass is the sum of four components:

$$\tau = \tau_f + \tau_{de} + \tau_{df} + \tau_r \qquad 2.1$$

where $\tau_f$ is derived from shear across grain asperities,

$\tau_{de}$ is derived from dilation of the soil structure against external forces,

$\tau_{df}$ is derived from internal friction due to dilatancy, and

$\tau_r$ is derived from internal friction under conditions of constant volume.

Figure 2.1 shows a schematic illustration of the contributing components of shearing resistance for drained tests on sand. The shearing resistance $\tau_r$, denoted by the friction angle $\phi_{cv}$, represents the sliding resistance of one mineral grain against another without contributing effects of volume change or grain shearing. Horn and Deere(1962) report values of $\phi_{cv}$ ranging from 22 degrees for quartz to about 37 degrees for feldspar. Layered lattice minerals such as mica exhibit $\phi_{cv}$ as low as 13 degrees and explain the lower strength of micaceous sands. Rowe(1962) shows that the coefficient of friction decreases only slightly with increasing pressures for materials that remain essentially elastic at contact points as for example sound quartz. Lee and Seed(1967a) suggest that the crushing of particles under very high confining pressures increases the number of particle contacts so that the load per particle and the value of $\phi_{cv}$ is not likely to change appreciably.

For dense sands at low confining pressures, the sand dilates against the external confining pressure as it is sheared. This dilation requires energy and contributes significantly to the observed shearing resistance. Measurements by Lee and Seed(1967a) on dense Ottawa sand indicate that the components of dilatancy, $\tau_{de} + \tau_{df}$, contribute up to 14 degrees to the total angle of internal friction at low stresses. Bishop and Eldin(1953) found the dilational component of shear strength increases with lower porosity reflecting higher potential for dilation in a dense, more tightly packed sand. Sowers and Sowers(1951) show that the angularity and gradation of the sand also contribute to the interlocking of the sand and increase the angle of friction.

As the confining pressure is increased, dilation is suppressed in favour of shearing of the sand grains under the high contact stresses. As indicated in Figure 2.1, higher confining pressures yield increased shearing resistance due to grain shearing, but a net decrease in the total angle of shearing resistance due to the decreased dilational component. The progressive decrease in total angle of shearing resistance results in the curvi-linear failure envelope at high stresses observed by Vesic and Barksdale(1963), Bishop, Webb and Skinner(1965) and Vesic and Clough(1968). Lee and Seed(1967a) show that grain shearing is initiated at lower stresses in sands with higher porosity. This results from fewer particle contacts yielding higher contact stresses. Similar effects are found in poorly graded sands for the same reason.

### 2.3 Stress-Dilatancy Theory

Taylor(1948), Bishop(1954) and Rowe(1962) have independently proposed "energy" relationships to correlate the strength and deformation behaviour of cohesionless soils. Taylor and Bishop deduct the component of shear resistance derived from dilation of the soil structure, $\tau_{de}$ from the total shear strength. Rowe separates the combined components of dilational shearing resistance, $\tau_{de} + \tau_{df}$ on the basis of energy balance. Thus, since the Taylor-Bishop analysis for evaluating dilatancy accounts for $\tau_{de}$ only, the derivation by Rowe for dilatancy is generally considered theoretically more satisfactory.

Rowe, Barden and Lee(1964) present the stress dilatancy equations for axial compression and extension in the triaxial cell on the basis of Rowe's theory. The equation for axial compression is:

$$R = D\ K \tag{2.2}$$

and for axial extension:

$$R = \frac{K}{D} \tag{2.3}$$

where

$$R = \sigma'_1/\sigma'_3 \tag{2.4}$$

$$D = \text{Dilatancy Correction} = \left(1 - \frac{d\epsilon_v}{d\epsilon_a}\right) \tag{2.5}$$

$$K = \tan^2(45 + \phi_f/2) \tag{2.6}$$

and $\epsilon_v$ is the volumetric strain, $\epsilon_a$ is the major principal strain, $\epsilon_1$, in a compression test and the minor principal strain, $\epsilon_3$, in an extension test. The angle $\phi_f$ is an empirical angle of shearing resistance corrected for dilation during testing. The component $d\epsilon_v/d\epsilon_a$ is the volumetric rate of dilatancy during testing.

Rowe(1969) concludes from examination of test results at low stresses for normal dense sands in triaxial compression and extension that the approximate value of $\phi_f$ varies as:

$$\phi_\mu \leq \phi_f \leq \phi_{cv} \tag{2.7}$$

where $\phi_\mu$ is the intergranular angle of friction and $\phi_{cv}$ is the friction angle at constant volume or critical void ratio state. The minimum value of $\phi_f = \phi_\mu$ occurs when only a few particle contacts are sliding. The maximum value of $\phi_f = \phi_{cv}$ occurs at the critical state (shearing under constant volume) when all possible contacts are sliding. Hence, for sand in the densest state, $\phi_f = \phi_\mu$ up to the the peak stress ratio and decreases from peak to the critical state at which $\phi_f = \phi_{cv}$. The experimental relation between $\phi_\mu$ and $\phi_{cv}$ for various cohesionless materials at low confining stresses is shown in Figure 2.2.

Lee and Seed(1967a) show the relationship in Equation 2.7 is only valid at very low stresses where shearing and crushing of particles is minimal, or $\tau_f = 0$. At higher stresses, particle crushing contributes substantially to the measured angle of shearing resistance. Hence, measurements of $\phi_f$ appear to overestimate the value of $\phi_\mu$.

The major factors governing the value of the dilatancy correction D are the relative density of the assemblage of particles and the degree of grain crushing. The most important material properties influencing crushing are the grain strength with particle shape, rugosity and grading also having an effect. Assuming no particle crushing, Horne(1965) has deduced a theoretical upper limit of $D_{max}$ = 2 at failure for a dense assembly of rotund particles in triaxial compression. The lower limit for a very loose assembly at the critical state establishes $D_{min}$ = 1. Hence:

$$1 \leq D \leq 2 \qquad 2.8$$

Rowe(1969) shows this relation has good agreement with experimental results for remolded sands at low pressures. Values of D greater than 2 have been observed in highly dilatant angular grained sands, sands with high surface rugosity and "locked" sands (Morgenstern and Dusseault, 1978 and Frossard, 1979).

## 2.4 Critical Void Ratio

The compression of loose sands and the dilation of dense sands during shear led Casagrande(1936) to postulate the concept of a critical void ratio, $e_{crit}$, for which no volume change would occur at failure. The relationship between volume change, void ratio and confining pressure in drained triaxial compression tests on a cohesionless soil is illustrated in Figure 2.3. If a series of drained tests is conducted, using the same confining pressure, on samples having different void ratios, e, the relationship between volume change at failure and the initial void ratio is shown in Figure 2.3(a). From the plot, the critical void ratio, $e_{crit}$ for which there is no volume change at failure can be determined. Repeated series of tests at different confining pressures leads to a series of values of $e_{crit}$ as shown in Figure 2.3(b). The variation of the critical void ratio with the magnitude of the confining pressure takes the form in Figure 2.3(c). Tests conducted at confining pressures to the left of the critical void ratio line in Figure 2.3(c) dilate during drained shearing. Conversely, tests conducted at pressures to the right of the line contract during shear. This predicts that sand with a given density or void ratio increasingly behaves as loose sand as the effective confining pressure is increased.

In an analagous manner, the values of the critical void ratio and critical confining pressure may be obtained from observations of the pore water changes during completely undrained triaxial compression tests. As shown in Figure 2.4(a), the void ratio and confining pressure for which there is no change in pore pressure at failure may be interpreted as the critical void ratio and critical confining pressure. From Figure 2.4(a), it is possible to determine the combinations of critical confining pressure and critical void ratio which take the form in Figure 2.4(b).

A third method of determining the critical confining pressure from undrained tests is simply to note the effective minor principal stress at failure in completely undrained tests. This stress is equivalent to the critical confining pressure for the corresponding void ratio of the soil sample.

Lee and Seed(1967b) conducted drained and undrained triaxial compression tests on Sacremento River sand and found the difference in measurement of the critical confining pressure to be 30 percent between the three methods for loose sample (e = 0.90) and decreasing to less than 6 percent for dense samples (e < 0.60). Lee and Seed(1967b) also compile values of the critical confining pressure for various granular materials from the literature. For fine to medium grained sands in a dense state (e < 0.60) comparable to Athabasca oil sand, the critical confining pressures range between 1.7 and 7.5 MPa.

## 2.5 Conditions at Failure in Undrained Tests

Seed and Lee(1967b) explain the undrained behaviour of sands during shear using the concept of the critical void ratio and critical confining pressure. The concept is illustrated in Figure 2.5. If the initial confining pressure is less than the critical confining pressure, the tendency to dilate during loading leads to a decrease in the pore water pressure and a corresponding increase in the effective confining pressure. The pore water pressure continues to decrease until one of two limiting conditions are reached (Figure 2.5(b)):

1) The effective confining pressure builds up to a value equal to the critical confining pressure, at which stage there is no further tendency for volume change. Thus, the pore water would have no tendency to change further and the sample would ultimately fail with the effective confining pressure equal to the critical confining pressure.
2) The pore water pressure drops to a value below the pore fluid gas saturation pressure at which stage cavitation occurs and bubbles of water vapour or air form in the voids of the sand. Once cavitation occurs, volume change of the sample is permitted and there is no further decrease in the pore water pressure. The sample is brought to failure with the pore water pressure equal to the gas saturation pressure.

Conversely, if the initial effective confining pressure is greater than the critical confining pressure, the sample tends to compress during loading causing an increase in the pore water pressure (Figure 2.5(c)). The effective confining pressure decreases until it reaches a value equal to the critical confining pressure at which point there is no longer any tendency for volume change. Correspondingly, there are no further changes in pore water pressure and the sample ultimately fails with the effective confining pressure equal to the critical confining pressure.

On this basis, if a series of samples of saturated sand are compacted initially to a void ratio, $e_i$, and then consolidated under different total confining pressures, $\sigma_3$, and back pressure, $u_i$, the effective consolidation pressure will be:

$$\sigma_3' = (\sigma_3 - u_i) \qquad 2.9$$

The samples will attain equilibrium void ratios $e_c$ where $e_c$ is a function of the initial void ratio, $e_i$, and the effective consolidation pressure, $\sigma_3'$:

$$e_c = f(e_i, \sigma_3') \qquad 2.10$$

Corresponding to the void ratios after consolidation, there will be a particular value of the critical confining pressure, $\sigma_{crit}$ where:

$$\sigma_{crit} = F(e_c) = F(e_i, \sigma_3') \qquad 2.11$$

During undrained loading of the samples to failure, one of the two following conditions will occur:

1) In a cavitating test, the pore water pressure in the

sample will decrease until it reaches the pore fluid gas saturation pressure, $u_s$. At failure, the confining pressure will then be:

$$\sigma'_{3f} = \sigma_3 - u_s \qquad 2.12$$

The strength of the sample will be governed by the drained angle of frictional resistance, $\phi'$ at the effective confining stress level, $\sigma'_{3f}$:

$$\sigma'_{1f} = (\sigma'_3 + u_i - u_s) \tan^2(45 + \phi'/2) \qquad 2.13$$

2) In a non-cavitating test, the pore water pressure in the sample will change until the effective confining pressure becomes equal to $\sigma_{crit}$. Under this condition, the strength will be governed by the frictional resistance at the critical confining pressure:

$$\sigma'_{3f} = \sigma_{crit} = F(e_i, \sigma'_3) \qquad 2.14$$

$$\sigma'_{1f} = \sigma_{crit} \tan^2(45 + \phi'/2) \qquad 2.15$$

The significance of these two conditions is shown in the corresponding envelope of strength in terms of total stresses in Figure 2.6. For non-cavitating tests ($u_i - u_s \geq \sigma_{crit}$), the envelope of strength may exhibit a shallow slope reflecting the slight decrease in porosity at higher consolidation pressures. The corresponding increase in $\sigma_{crit}$ leads to higher strength as per Equations 2.14 and 2.15.

For cavitating tests with $u_i - u_s = 0$, cavitation occurs immediately on commencing loading and the strength is determined by the drained failure envelope with $\sigma'_{3f} = \sigma'_3$. For cavitating tests with $0 < u_i - u_s < \sigma_{crit}$, the effective confining pressure at failure is increased to $\sigma'_3 + u_i - u_s$. The corresponding strength governed by Equation 2.13 is represented by shifting of the drained failure envelope towards the origin by the magnitude $(u_i - u_s)$. This points out the importance not only of the initial effective stress condition on undrained strength, but also the initial pore water pressure.

Bishop and Eldin(1950) demonstrate that the maximum principal stress ratio, $\sigma'_1/\sigma'_3$ and the ultimate strength, $(\sigma_1 - \sigma_3)_f$ occur at different stages of an undrained test. Thus, the angle of shearing resistance in terms of effective stresses will vary with the criterion of failure adopted. The stress path to failure for an undrained test on dense sand is shown in Figure 2.7. The maximum stress ratio occurs early in the test at lower strains and lower stresses than the ultimate strength. The effective stresses within the specimens progressively increase with strain as the critical confining pressure is approached. Lower angles of shearing resistance are mobilized due to the decrease in shearing resistance with increasing confining pressure noted in Section 2.1. Ultimately, the angle of shearing resistance under conditions of constant volume is mobilized at the critical confining pressure.

The angle of shearing resistance at the maximum stress ratio is less than measured in drained triaxial compression tests due to external work performed in dilatancy. The angles of shearing resistance are generally in good agreement after external work due to dilatancy in the drained tests has been deducted in accordance with Equation 2.2 (Lee and Seed, 1967b).

## 2.6 Undrained Stress-Strain Behavior

A typical stress-strain response for an undrained triaxial compression test of dense sand is shown in Figure 2.8. The fact that dense sands have a tendency to elastically compress to some extent before they dilate leads to the increase in pore pressure at low strains. At higher strains, the tendency to dilate begins to predominate and the pore pressures decrease. The decrease in the pore pressure with strain often leads to a strain-hardening stress-strain response. The drop in pore pressure with strain increases the magnitude of the intergranular stresses resulting in higher shear resistance and a progressive increase in stiffness of the sample. This behaviour is observed in data by Bishop and Eldin(1950), Bjerrum, Kringstad and Kummeneje(1961) and Nash and Dixon(1961). Failure occurs when the critical confining pressure is reached or cavitation occurs and the pore pressures cease to drop.

## 2.7 Pore Pressure Parameters A and B

Skempton(1954) expresses the change in pore pressure, $\Delta u$ in the triaxial test under changes of axial deviatoric stress, $(\Delta\sigma_1 - \Delta\sigma_3)$ and all round confining stress, $\Delta\sigma_3$ by the following equation:

$$\Delta u = B(\Delta\sigma_3 + A(\Delta\sigma_1 - \Delta\sigma_3)) \qquad 2.16$$

where A and B are the pore pressure parameters.

Bishop(1966,1973) developed the following expression for the pore pressure parameter B expressed as the pore pressure response, $\Delta u$ of a saturated porous material to an undrained isotropic stress increment, $\Delta\sigma_3$:

$$B = \frac{\Delta u}{\Delta\sigma_3} = \frac{1}{1 + n\ (C_w - C_s)/(C - C_s)} \qquad 2.17$$

where n is the soil porosity, C is the compressibility of the soil structure, $C_w$ denotes the compressiblity of the pore water, and $C_s$ denotes the compressiblity of the soil grains. For most sands, $C_s$ is several magnitudes less than C and $C_w$, so Equation 2.17 may be re-written as:

$$B = \Delta u/\Delta\sigma_3 = 1/(1 + nC_w/C) \qquad 2.18$$

In dry sands, $C_w/C$ approaches infinity since the compressiblity of air far exceeds that of the soil structure and therefore, B equals zero. In saturated sands, the compressibility of the water is generally less than the soil structure, so $C_w/C$ is approaches zero and the value of B approaches unity. Hence,

$$0 < B < 1 \qquad 2.19$$

The changes in the pore pressure during the application of a deviatoric stress, $(\Delta\sigma_1 - \Delta\sigma_3)$ is given by the following expression:

$$A = \frac{\Delta u}{B\ (\Delta\sigma_1 - \Delta\sigma_3)} \qquad 2.20$$

Skempton(1954) theoretically found the value of A under conditions of purely elastic behaviour to be 1/3. However, the behaviour of soils is rarely in accordance with elastic theory and the value of A must be found experimentally. Bjerrum, Kringstad and Kummeneje(1961) calculated the value of A at failure in a series of undrained triaxial compression tests on fine sand at different porosities. In loose sands, the value of A is positive because the pore pressures increase due to the tendency to contract under loading. In dense sand, the pore pressures decrease due to dilation and the value of A becomes negative at failure.

## 2.8 Influence of Strain Rate

The behaviour of sands under transient loads has been studied by a number of researchers. As the behaviour of sands under transient loading is still not well defined, the findings are synthesized below in some detail for purposes of dicussion in a later section.

Casagrande and Shannon(1948, 1949) appear to be the first to study the effect of strain rate on the strength of soil. They performed transient loading tests on dry Manchester sand over the range of strain rates between 1.6 x $10^{-4}$ and 1.3 $s^{-1}$. The tests were conducted using a vacuum pressure of 30 kPa. The strength of the sand was observed to increase about 10 to 15 percent over the range of strain rate. The modulus of deformation was found to be independent of the strain rate.

Seed and Lungren(1954) performed transient loading tests on samples of dense saturated fine-grained Sacremento River sand at strain rates up to 1.2 $s^{-1}$. They observed that at high strain rates, the drained and undrained strengths became equal. This was attributed to the insufficient time to allow water to drain from the sample. The transient undrained strength of the dense saturated samples were found to be 15 to 20 percent greater than undrained static tests on saturated samples. The modulus of deformation was found to be 30 percent greater than in the static undrained tests. Analogous results were obtained for the well graded, coarse grained Monterey Sand No. 5.

Whitman(1957) performed a series of transient loading tests on dry, moist and saturated dense samples of Ottawa sand. Strain rates up to 16 $s^{-1}$ were achieved. An increase in the compressive strength of 10 to 15 percent was observed for the dry and moist samples tested under a confining pressure of 101 kPa. The tests on the saturated samples were conducted at cell and pore pressures of 414 and 212 kPa. The strength of the sand was observed to increase 25 percent. The increase in the strength was attributed to the migration of pore water in the samples. As the speed of deformation increases, more energy must be expended to overcome the resistance of the flow of pore water.

Nash and Dixon(1961) report pore pressure measurements in slow and transient undrained compression tests on samples of medium grained Leighton Buzzard sand. The tests were conducted at cell and pore pressures of 100 and 95 kPa. The stress-strain curves for the static tests were marked by short "jerky" collapses in strength with corresponding increases in the pore pressure. It was suggested that the collapse of strength corresponded to fracturing of sand particles during progressive failure of the sand. In the rapid tests, this behaviour did not appear. It was reasoned that the sand particles did not have sufficient time to adjust their positions to offer a minimum resistance to the strain and complete collapse takes place when the peak strength is reached, rather than occuring progressively.

Healy(1963) and Whitman and Healy(1963) report undrained triaxial tests with pore pressure measurements on dense and loose saturated coarse (20-30 mesh) Ottawa sand. Initial cell and pore pressures of 276 and 241 kPa were used. Measurements of pore pressure were made at the middle and bottom of the test specimens. The pore pressure measurements at the bottom were observed to lag the decrease in pore pressure at midheight for loose specimens at the strain rate of 6.7 $s^{-1}$. In dense specimens ($D_r$ = 100%), the time lag in pore pressure response was observed at the lower strain rate of 0.27 $s^{-1}$. This was attributed to the higher rate of pore pressure decrease due to dilation in the dense samples which was over 10 times faster than in the loose samples. The time allowed for pore pressure redistribution within the specimens was therefore more than one-tenth less. No significant increase in the compressive strength was observed over the range of strain rate between 2 and 450 percent per second. The maximum strengths were coincident with pore water cavitation and the failure was under drained conditions. The pore water is reported to have cavitated at the same pressure regardless of the strain rate.

Lee, Seed and Dunlop(1969) investigated the effects of transient loading under high confining stresses. A series of transient loading tests were conducted on dense dry Antioch sand ($D_r$ = 100%) at confining pressures of 100, 600 and 1500 kPa. At the confining stresses of 100 and 600 kPa, the ultimate strength of the sand increased only by 10 percent over the range of strain rate of $1.7 \times 10^{-6}$ to $1.6\ s^{-1}$. At 1500 kPa confining pressure, the increase was 30 percent. At all pressures, the initial tangent modulus was found to increase by up to 100 percent. The greater increase in strength at the highest confining pressure was thought to be indicative of the effect of strain rate on the energy required for grain crushing. The authors explored this concept with a series of undrained load-creep tests on saturated samples. Initial stress levels were maintained below failure. The pore pressures were observed to increase over a period of time leading to eventual sample failure. It was concluded that particle crushing was the primary mechanism to compress the soil and increase the water pressure. The time to failure decreased with higher stresses. The crushing of the sand grains was therefore suggested to be a time-dependent process accelerated by higher stresses.

## 2.9 Summary

This chapter gives a broad overview of the undrained behaviour of cohesionless sands. The theory of shearing resistance of cohesionless particulate masses, and the relationship of shearing resistance with soil dilatancy and interparticle friction are introduced. The theoretical concepts of the critical void ratio, mechanisms of undrained strength and deformation behaviour, and drained and undrained compressibility are discussed.

The behaviour of dense sands under transient loading reported in the literature is synthesized. In summary, increases in the undrained strength of 25 percent and deformation modulus up to 100 percent have been measured for water saturated dense sands over the range of strains rates up to 16 $s^{-1}$.

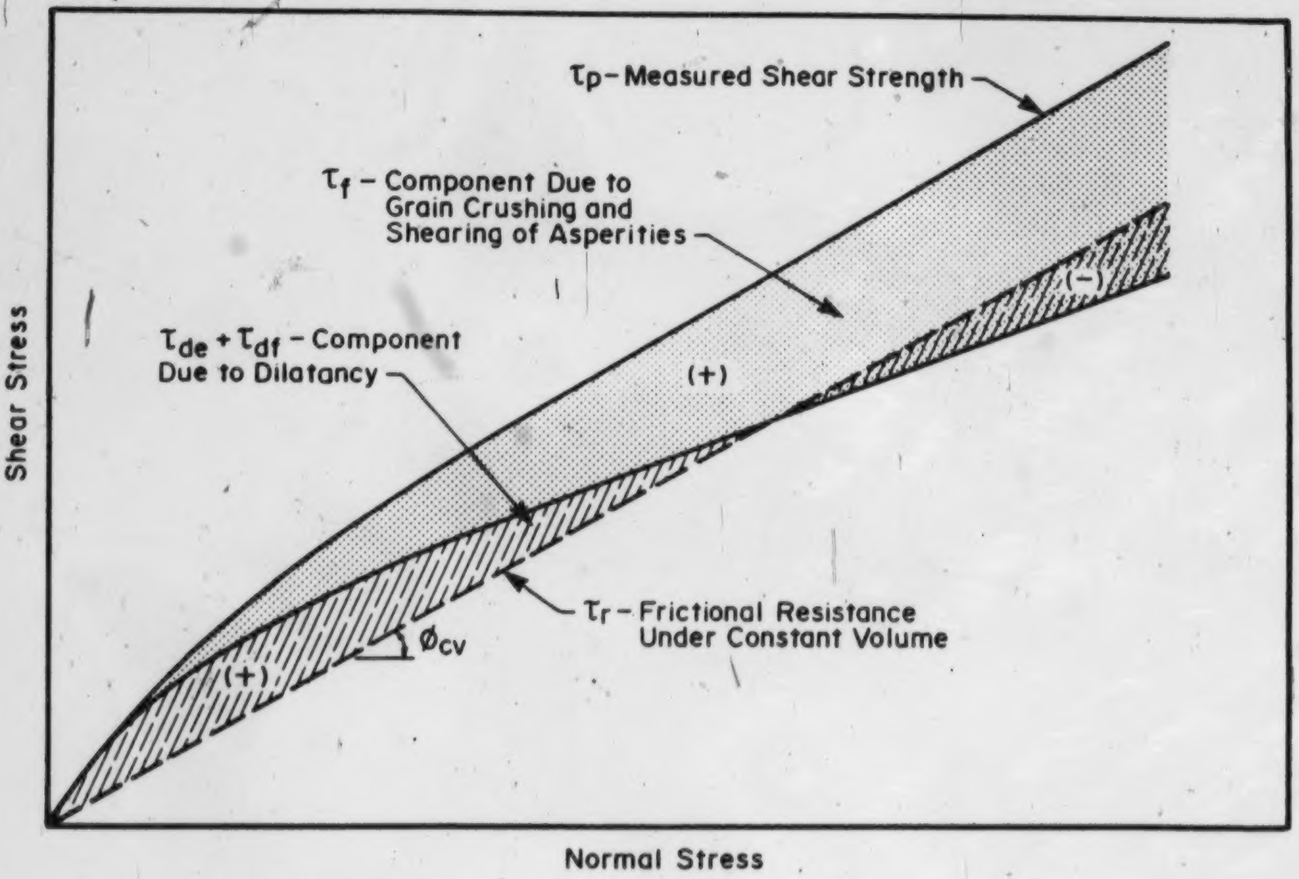

Figure 2.1 Schematic Illustration of Contribution of Components of Shearing Resistance for Drained Tests on Dense Sands (After Lee and Seed, 1967a)

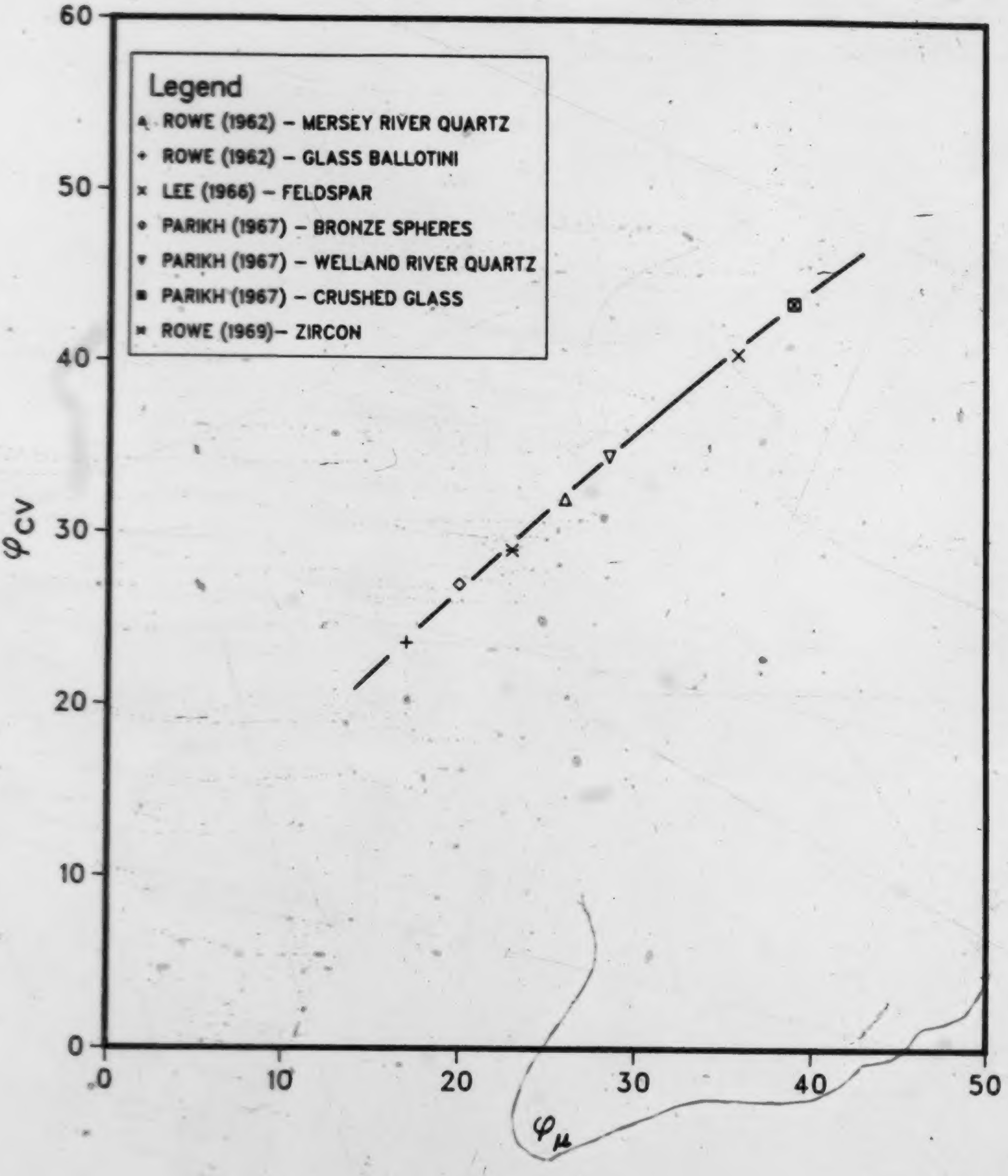

Figure 2.2 Experimental Relationship Between $\phi_{cv}$ and $\phi_\mu$
(After Rowe, 1969)

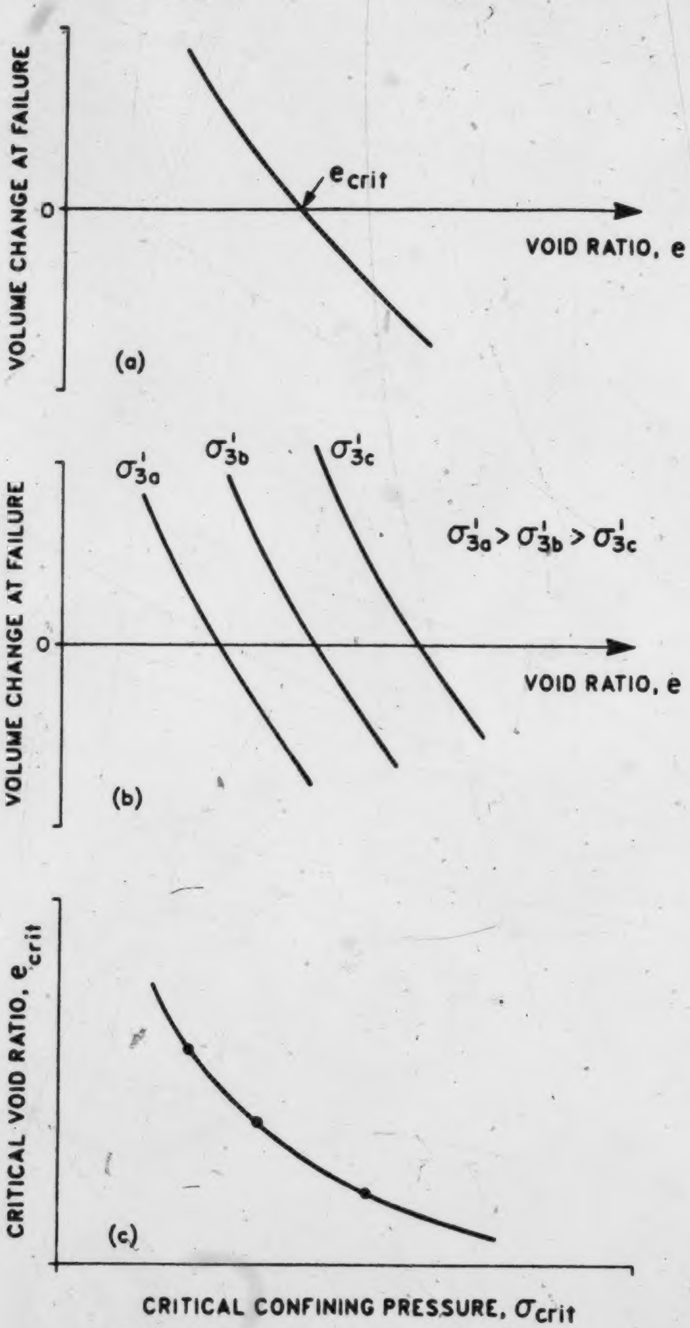

Figure 2.3 Relationship Between Volume Change at Failure, Void Ratio and Confining Pressure in Drained Triaxial Compression Tests

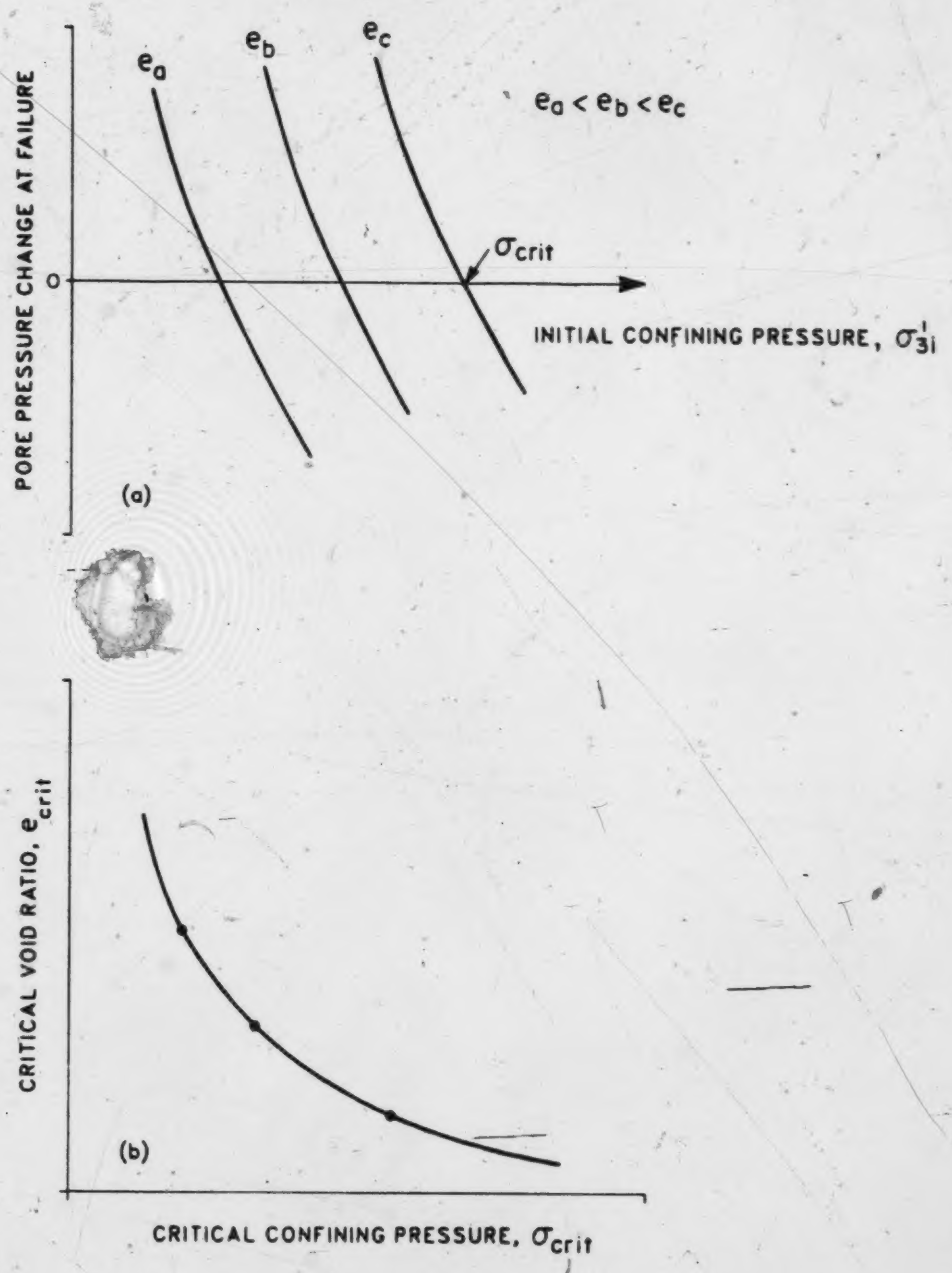

Figure 2.4 Relationship Between Pore Pressure Change at Failure, Void Ratio and Consolidation Pressure in Undrained Triaxial Compression Tests

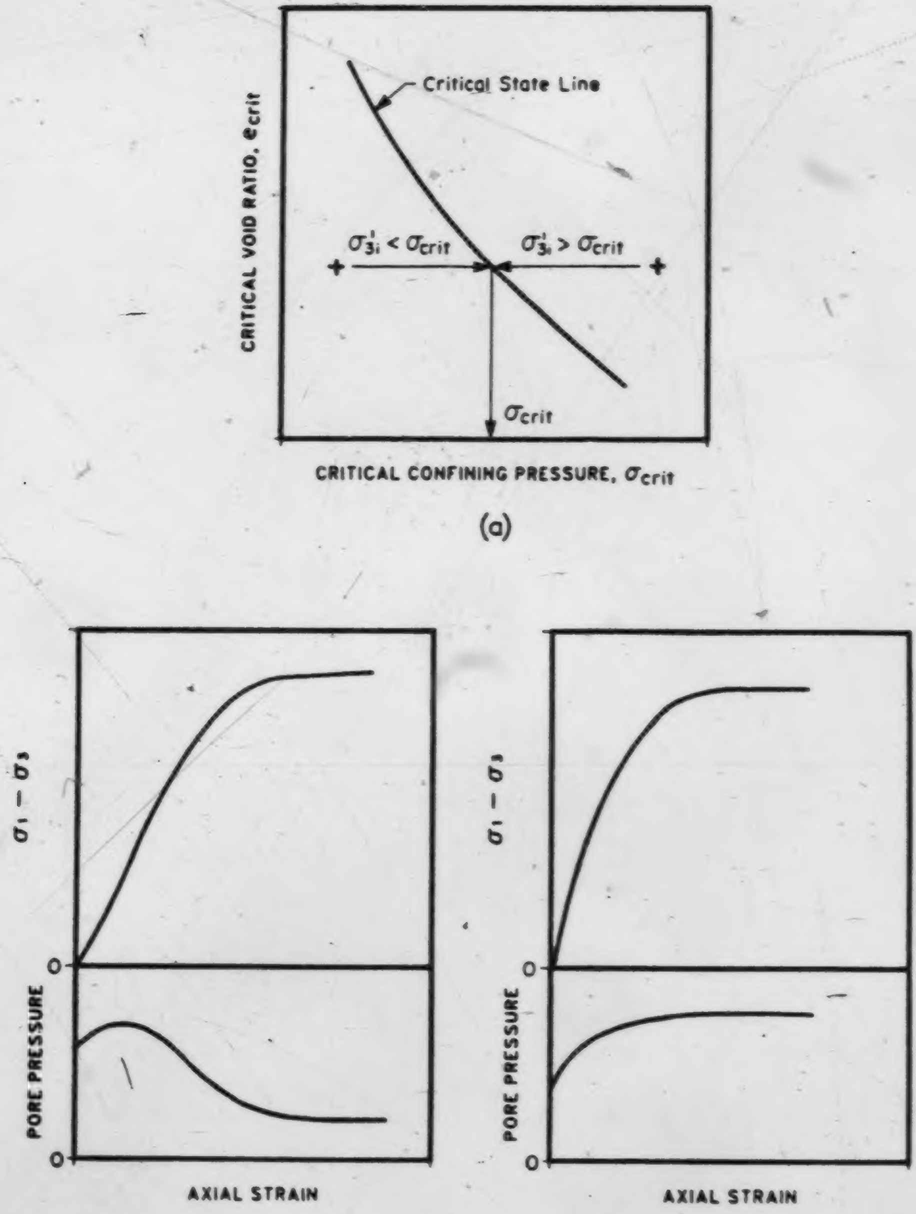

(b) $\sigma_{crit} > \sigma_{3i}'$

(c) $\sigma_{3i}' > \sigma_{crit}$

Figure 2.5 Undrained Behavior of Dense Sands in Triaxial Compression Tests

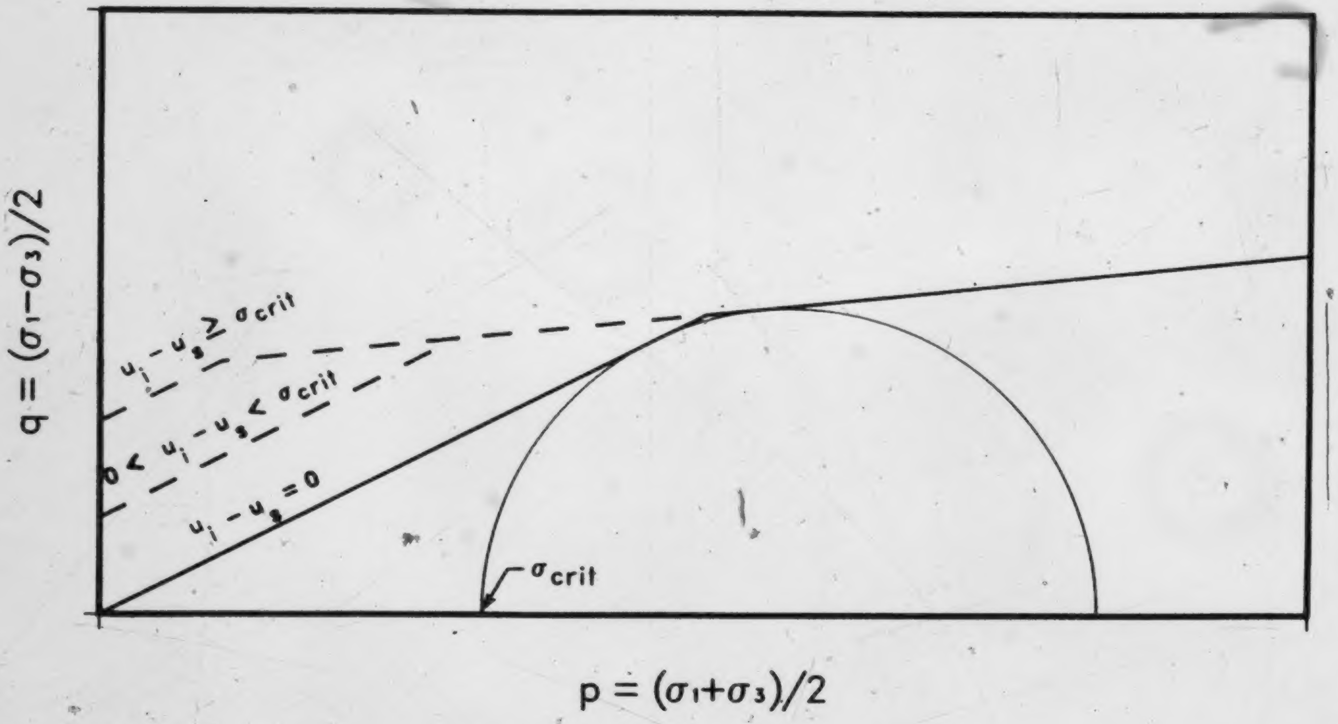
$q = (\sigma_1 - \sigma_3)/2$
$p = (\sigma_1 + \sigma_3)/2$
$u_i - u_s \geq \sigma_{crit}$
$0 < u_i - u_s < \sigma_{crit}$
$u_i - u_s = 0$
$\sigma_{crit}$

Figure 2.6 Ultimate Undrained Strength of Dense Sands in Terms of Total Stress

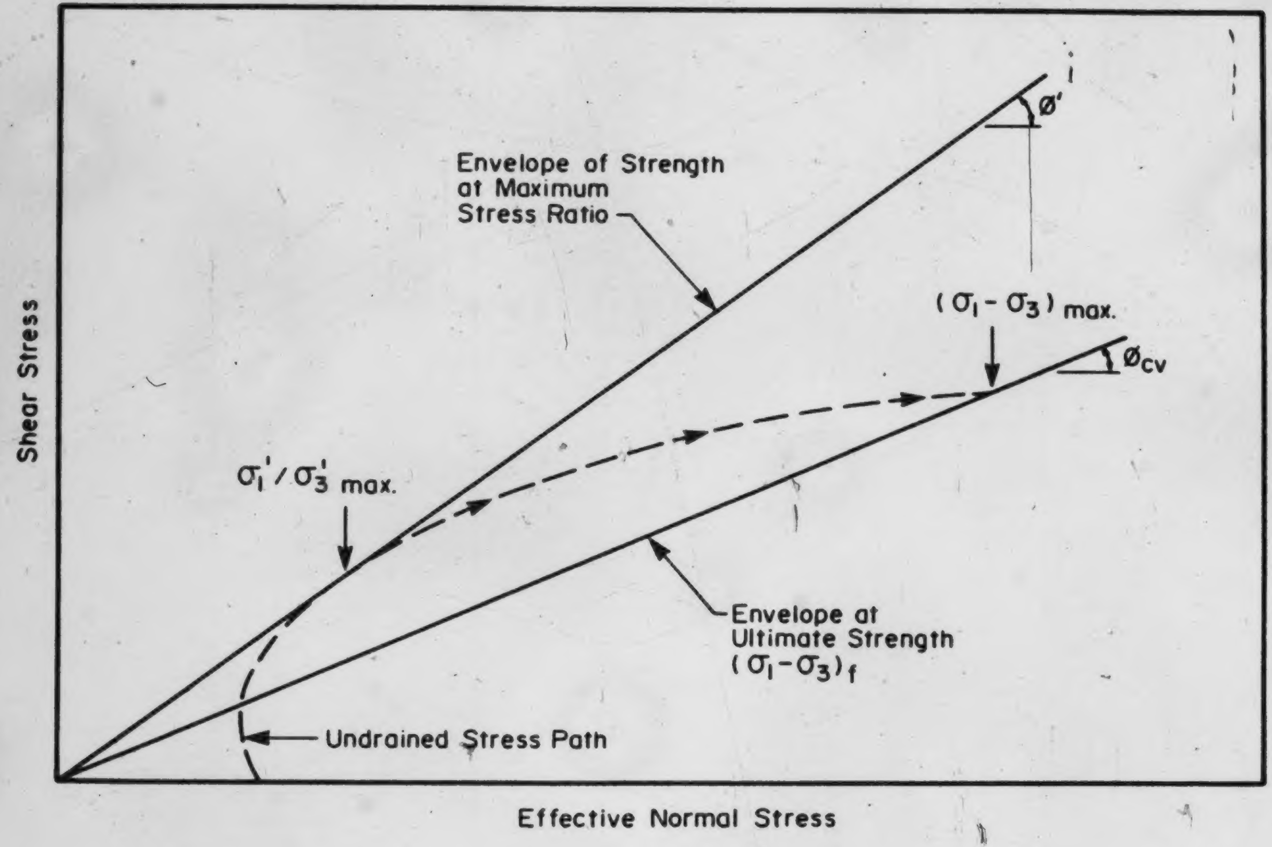
Envelope of Strength
at Maximum
Stress Ratio
$\phi'$
$(\sigma_1 - \sigma_3)_{max.}$
$\phi_{cv}$
$\sigma_1'/\sigma_3'{}_{max.}$
Envelope at
Ultimate Strength
$(\sigma_1-\sigma_3)_f$
Undrained Stress Path
Shear Stress
Effective Normal Stress

Figure 2.7 Stress Path to Failure in Undrained Triaxial Compression Tests

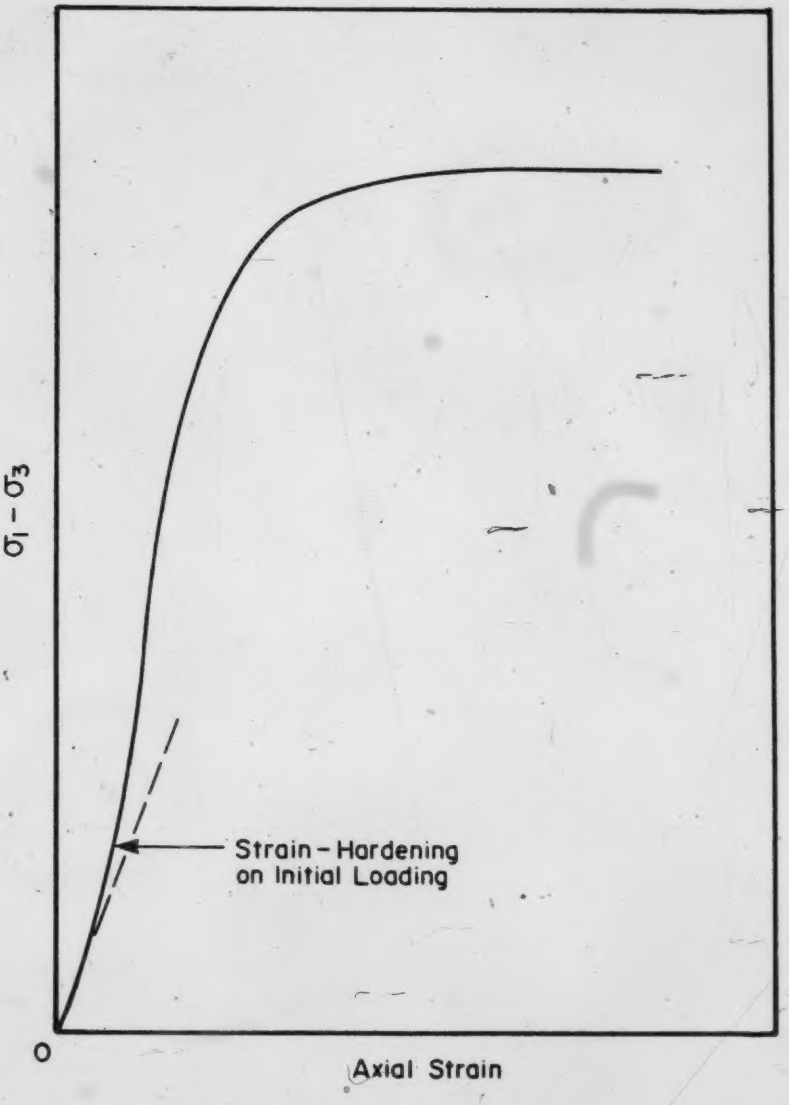

Figure 2.8 Typical Undrained Stress-Strain Response for Dense Sands

# 3. STRENGTH OF OIL SANDS

## 3.1 The Athabasca Oil Sands

The oil sands considered in this thesis are from the Athabasca Oil Sands Deposit, the largest of the four major oil sands deposits in Alberta. The Athabasca deposit is located in northern Alberta (Figure 3.1) and underlies an area of approximately 32,000 square kilometers with estimated in-place reserves of about 146 billion cubic metres (Outrim and Evans, 1978 and Mossop, 1980). The vast majority of the reserves of the Athabasca deposit are found in the Lower Cretaceous sands of the Lower Manville McMurray Formation. The McMurray Formation typically varies in thickness between 40 and 60 m (Mossop, 1978). The Athabasca deposit is unique in that about 10 percent of the reserves have less than 50 m of overburden and can be recovered by surface mining methods.

The composition of the Athabasca oil sands typically consists of approximately 95 percent silica quartz, 2 to 3 percent feldspar, 2 to 3 percent mica and clay minerals, and traces of other minerals (Mossop, 1980). The sand structure is dense and interpenetrative owing to diagenetic processes of dissolution and re-crystallization of quartz at grain boundaries during the time of burial (Milligan, 1976 and Dusseault, 1977). The grains are water wet with the remaining pore space occupied by bitumen which forms a continuous phase throughout the oil sand structure (Figure 3.2). Gases are dissolved within the liquid phases and depending on in situ temperatures and pore fluid pressures are occasionally present as free gas.

Dusseault(1977, 1980) reports saturated bulk densities for uniformly graded, rich Athabasca oil sand of 2.05 to 2.18 $Mg/m^3$ and porosities of 28 to 36 percent. Mossop(1980) reports bitumen and water contents in rich oil sands of 18 and 2 percent, respectively, by weight. Grain size distributions for Athabasca oil sands are given in Figure 3.3.

### 3.2 Problem of Sampling and Sample Disturbance

Uncemented oil sand is highly susceptible to expansion and microstructure disturbance when in situ stresses are released rapidly during sampling. Dissolved gases in the bitumen and pore water phases exsolve under the release of stress and are unable to drain from the sample due to the low effective permeability of the bitumen in the oil sand. Undrained expansion of the oil sand thus occurs as the dissolved gases expand but are prevented from draining. Core recoveries in excess of 100 percent is common when standard sampling techniques are employed. Hardy and Hemstock(1963) identified the mechanics of sample disturbance and showed that the disruption of the interpenetrative grain structure dramatically decreases the strength and increases the compressibility of oil sands.

Several methods to sample undisturbed oil sand have been tried. Hardy and Hemstock(1963) used a pressure core barrel to obtain high quality core from depths up to 50 m. The pressure core barrel allowed the oil sand core to be sealed in the core barrel at the bottom-hole fluid pressure, thereby keeping the pore fluid pressure above the fluid saturation pressure when remove from the hole. The core barrels were frozen in dry ice prior to removing the sample to inhibit expansion of the core. The performance of the samples in triaxial tests, however, gave mixed results. It was concluded that the in situ stress conditions had not been maintained somewhere in the sampling, handling or test set-up procedures.

Dusseault and Morgenstern(1977) attempted to freeze the oil sand downhole by circulating chilled diesel fuel in the hole prior to coring. The method worked well for bitumen poor and fine grained oil sands. Oil rich samples were found to still expand excessively for purposes of geotechnical testing.

High quality oil sand samples are reported to have been attained at the exposure of the McMurray Formation in the Saline Creek valley by: (1) conventional vertical wet rotary diamond coring (Smith et al, 1978), and (2) diamond coring directly into oil sand exposures on the slopes of the creek valley (Dusseault and Sterne, 1980 and Agar, 1984). The formation of the Saline Creek valley took place over a period of approximately 10,000 years. The gradual removal of confining stress and reduction of pore pressures due to erosion of the valley face has allowed the gases to exsolve slowly from the pore liquids without disturbance of the sand micro-structure. Smith reports bulk densities ranging between 2.06 and 2.11 $Mg/m^3$. Dusseault and Sterne experienced problems with tensile and torsional shear failure of samples during diamond coring into the oil sand exposures. Agar reports that these problems were largely overcome by coring during the late winter when the oil sand exposures were frozen. Agar concluded that the freezing of the oil sand prevents disturbance during sampling by:

1) freezing the pore water to provide a tensile resistance to expansion,
2) increasing the bitumen viscosity to very high values,
3) depressing the pore liquid pressures and the bubble point pressure by shrinkage,and
4) increasing the solubility of gas in the bitumen and pore water thereby limiting the rate and amount of gas exsolution upon stress release.

Dusseault and Van Domselaar(1982) studied the effects of sample disturbance on the laboratory measurement of geotechnical properties and recommended that the disturbance index, $I_D$, be used to evaluate the quality of oil sand samples for testing purposes. The disturbance index is defined as:

$$I_D = \frac{n - n_i}{n_i} \times 100 \qquad 3.1$$

where n is the laboratory measurement of the porosity of the sample and $n_i$ is the in situ porosity from downhole geophysical density logs. Dusseault and Van Domselaar recommend the classification in Table 3.1 to relate the disturbance index to the degree of disturbance and the suitability for testing purposes.

### 3.3 Past Studies of Shear Strength of Oil Sands

A comprehensive compilation of published strength and stress-strain properties of Alberta oil sands has already been presented by Au(1984) and will not be repeated in this thesis. Attention is directed to Appendix C "Summarizing Notes on Selected References" in Au where a brief descriptive review of the available source literature is contained. All of the information presented is for Athabasca oil sands. Au reports that the oil sands in the Cold Lake deposit may be weaker than the Athabasca oil sands, probably due to weaker feldspar grains. Subsequent to Au, Agar(1984) has completed a detailed study of the mechanical behaviour of Athabasca oil sand recovered from Saline Creek at elevated temperatures up to 300°C.

### 3.4 Drained Strength of Oil Sands

The peak strength from available drained triaxial compression tests are plotted in Figure 3.4 where:

$$p' = \frac{\sigma_1' + \sigma_3'}{2} \qquad 3.2$$

$$q = \frac{\sigma_1' - \sigma_3'}{2} \qquad 3.3$$

Samples with initial bulk densities greater than 2.0 Mg/m$^3$ are plotted only to represent in situ densities. The test data shows an unusually high angle of friction of about 60 degrees at low stresses. The failure envelope also exhibits a distinct curvature with increasing stress. Dusseault and Morgenstern(1977, 1978) show that this behaviour is characteristic of the interpenetrative or "locked" structure of the oil sand. The interpenetrative fabric results in abnormally high rates of dilation and strength at low stresses. The curvature of the failure envelope at higher stresses is caused by the suppression of the dilatancy in favour of the shear of grains and grain asperities. Dusseault and Morgenstern(1979) observed this phenomena in several other "locked" sands.

Two typical stress-strain curves for drained triaxial compression tests on oil sand at low and high confining pressures are shown in Figure 3.5. Strains to failure for high density test specimens are generally less than 3 percent with the majority of the samples failing betweeen 1 and 2 percent as shown in Figure 3.6. Substantial increases in failure strain are observed in the samples with lower densities and are typical of other fine grained sands of similar density (Bjerrum, Kringstad, Kummeneje, 1961).

At low stresses, the mode of failure is brittle with substantial strain-softening past failure. Dusseault(1977) found from direct shear tests that the drop in the post peak strength is coincident with the sudden decrease in the rate of dilation as the peak strength is passed. Dusseault and Morgenstern(1978) conclude that while the fabric of the oil sands is responsible for the high strengths, this fabric is destroyed by shear straining and the specimens ultimately behave as ordinary dense sands. Direct shear tests taken to large strains by Dusseault(1977) and Barnes(1980) indicate the ultimate or residual angle of shearing resistance for oil sand under conditions of constant volume ranges between 30° and 33° for normal stresses up to 5 MPa.

The difference between the peak and ultimate strength decreases with higher confining stresses. This is caused by the suppression of the high dilational component of shear strength in favour of grain shearing. The fabric of the oil sand exerts less influence on the behaviour at higher stresses and the oil sand behaves more like an ordinary dense sand.

The relationship between the modulus of deformation and confining pressure for the drained triaxial compression tests with bulk densitites greater than 2.0 Mg/m$^3$ is shown in Figure 3.7. Initially, the modulus of deformation increases markedly with the confining pressure. At high confining pressures, the rate of increase decreases and reflects the lower contribution of frictional resistance as grain shearing becomes the predominant mechanism of failure.

### 3.5 Undrained Strength of Oil Sands

The strength at the maximum principal stress ratio for undrained triaxial compression tests on Athabasca oil sand are plotted in Figure 3.8. The test data to date extends only to the mean stress of 2.5 MPa. The effective angle of shearing resistance, $\phi'$, for the upper bound of the test data over this range is 59°, slightly less than observed for the drained compression tests at low stresses in Figure 3.4.

The ultimate strength for the undrained tests are plotted in Figure 3.9. The corresponding angle of shearing resistance is about 53°. The decrease in shearing resistance is contributed by the loss of strength associated with higher strains to reach failure in undrained tests as shown in Figure 3.10. The ultimate strength in all tests shown in

Figure 3.9 was accompanied by pre-mature cavitation of the pore fluid. The undrained decrease in pore pressure prior to cavitation among the tests ranges up to 0.7 MPa. Based on the critical confining pressures reported in Section 2.4 for other dense sands, the potential decrease in pore pressure may range as high as 7.5 MPa. Hence, substantially higher strains and lower angles of shearing resistance at the ultimate strength will be observed in completely undrained tests.

A theoretical prediction of the undrained strength of oil sands can be made by subtracting the contribution of dilatancy from drained triaxial compression tests using Rowe's(1962) stress-dilatancy theory presented in Section 2.3. Figure 3.11 presents the corresponding undrained strength envelope derived from the drained triaxial compression test data in Figure 3.4 with corrections for dilatancy.

### 3.6 Tensile Strength of Oil Sand

In current engineering practice, oil sand is not considered to have any tensile strength due to the lack of cementation between the sand grains. Milligan(1976), Dusseault(1977) and Barnes(1980) conclude from inspection of triaxial compression and direct shear test data that any tensile strength derived from the interpenetrative grain structure may also be discounted. Dusseault(1977) justifies the extension of the Mohr-Coulomb failure envelopes to the origin primarily for the following two laboratory observations:

1) Specimens of oil free sandy silt from a borehole depth of 42 m segregated almost totally when immersed in water for 24 hours, indicating the absence of tensile strength; and
2) Outcrop samples from oil-free portions of the McMurray Formation display no apparent cohesion in a saturated state.

Notwithstanding the convincing evidence presented by Milligan(1976), Dusseault(1977) and Barnes(1980), it is noted that any tensile strength derived from the interpenetrative grain structure of the oil sand would be quite small, and a highly structure sensitive property that may be obscured by very small changes in density from stress relief during sampling. There is ample observational data from natural slopes, mine pit walls and tunnels to show that oil sand mobilizes an apparent effective cohesion during unloading at in situ densities. The mobilization of an effective tensile strength may be stress path dependent as well.

At the present time, it is believed the only attempt to measure the tensile strength of oil sand is that reported by McRoberts(1986). Ten Brazlian tests were conducted on cylindrical specimens, 38 mm diameter and 76 mm long, cut from block samples of rich oil sand. The tests were conducted at room temperature of 18.5°C and a deformation rate of 0.38 mm per minute. The measured tensile strength ranged between 8.1 and 17.1 kPa. The density and bitumen content of the samples varied between 1.84 and 1.89 Mg/m$^3$ and 15.3 and 17.1 percent, respectively.

Five unconfined direct tensile tests are also reported by McRoberts(1986). Cylindrical specimens were bonded to end bearing plates and a tensile force applied with the long axis of the cylindrical specimens lying horizontally. The measured tensile strength varied between 2.1 and 6.2 kPa. The temperature and axial strain rate at which the tests were conducted are not reported. The bulk density and bitumen contents ranged between 1.84 and 1.91 Mg/m$^3$ and 15.3 and 16.7 percent.

Given the low density of the test specimens reported by McRoberts(1986), it must be concluded that the tensile strength observed is mobilized by the viscosity of the bitumen and/or negative pore pressures developed during testing rather than from the grain structure. However, it is interesting to note that rich oil sand can mobilize some short term tensile strength due to these factors.

### 3.7 Summary

The grain structure of Athabasca oil sand is very dense and interpenetrative owing to diagenetic processes of pressure solution and re-crystallization of quartz at the the grain boundaries. At low stresses, high rates of dilation of the interpenetrative grain structure result in effective angles of shearing resistance of 60 degrees. The failure envelope of shear strength is highly curvi-linear caused by the suppression of dilatancy in favour of shear of grains and grain asperities at higher stresses.

The pore phase of oil sand is comprised of water, bitumen and gases. The gases are dissolved within the liquid phases depending on the in situ temperature and pore fluid pressure. The structure of oil sand is highly susceptible to disturbance during sampling caused by undrained expansion with exsolution of gases under rapid release of stresses. High quality samples have been obtained from surface exposures of oil sand along natural creek valleys where gradual removal of stress and reduction of pore fluid pressures has allowed the gases to exsolve slowly. Dusseault and Van Domselaar(1982) propose a disturbance index to quantify the effects of sample disturbance.

Experimental measurements of ultimate undrained compressive strength of Athabasca oil sand reported in the literature were limited by pre-mature cavitation of the pore fluid in all tests. A theoretical prediction of the undrained shear strength at the maximum stress ratio for Athabasca oil sand using the stress-dilatancy theory proposed by Rowe(1962) is presented.

Observational data from natural slopes, mine pit walls and tunnels show that in situ oil sand mobilizes an apparent cohesion during unloading. Available experimental data suggests that a finite short term tensile strength may be mobilized by the viscosity of the interstitial bitumen and/or negative pore pressures developed during unloading.

Table 3.1 Classification of Sample Quality with the Disturbance Index (After Dusseault and Van Domselaar, 1982)

| DISTURBANCE INDEX (%) | SAMPLE QUALITY | SUITABILITY FOR TESTING PURPOSES |
|---|---|---|
| 0 - 10 | Intact or slightly disturbed | High quality geomechanical tests and petrophysical tests |
| 10 - 20 | Intermediate disturbance | Petrophysical research |
| 20 - 40 | Highly disturbed | Qualitative and descriptive tests |
| > 40 | Generally disrupted | Behavior as loose sand |

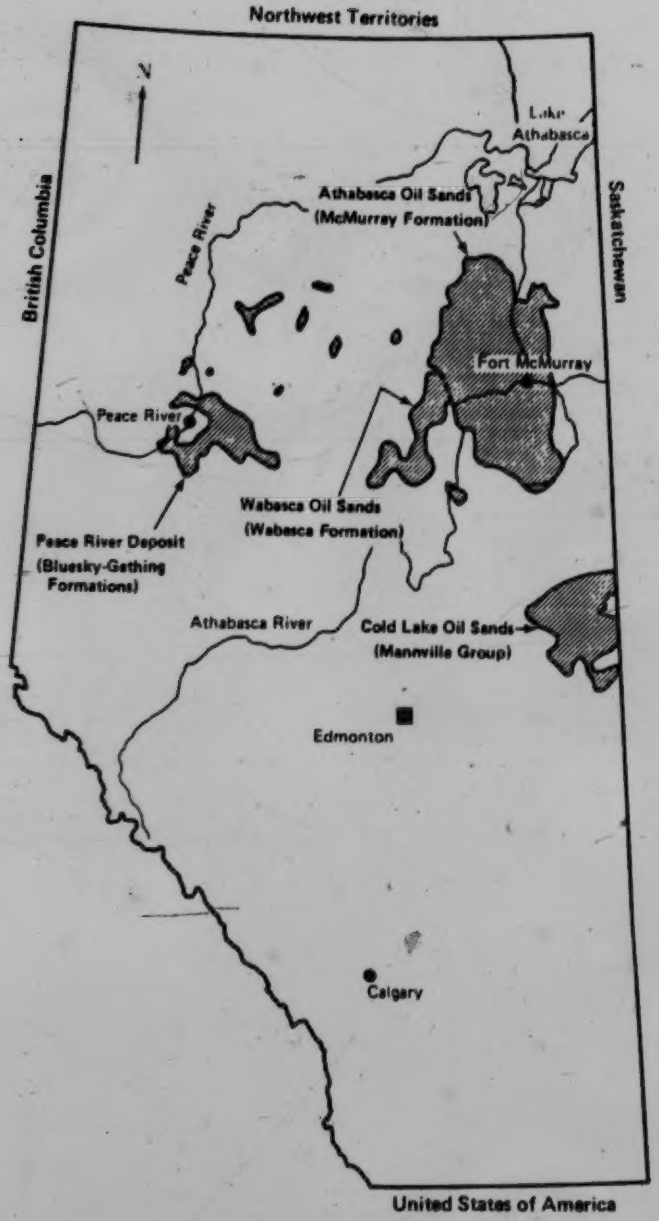
Northwest Territories
N
Lake Athabasca
British Columbia
Saskatchewan
Peace River
Athabasca Oil Sands (McMurray Formation)
Fort McMurray
Peace River
Peace River Deposit (Bluesky-Gething Formations)
Wabasca Oil Sands (Wabasca Formation)
Athabasca River
Cold Lake Oil Sands (Mannville Group)
Edmonton
Calgary
United States of America

Figure 3.1 Oil Sands Deposits Of Alberta

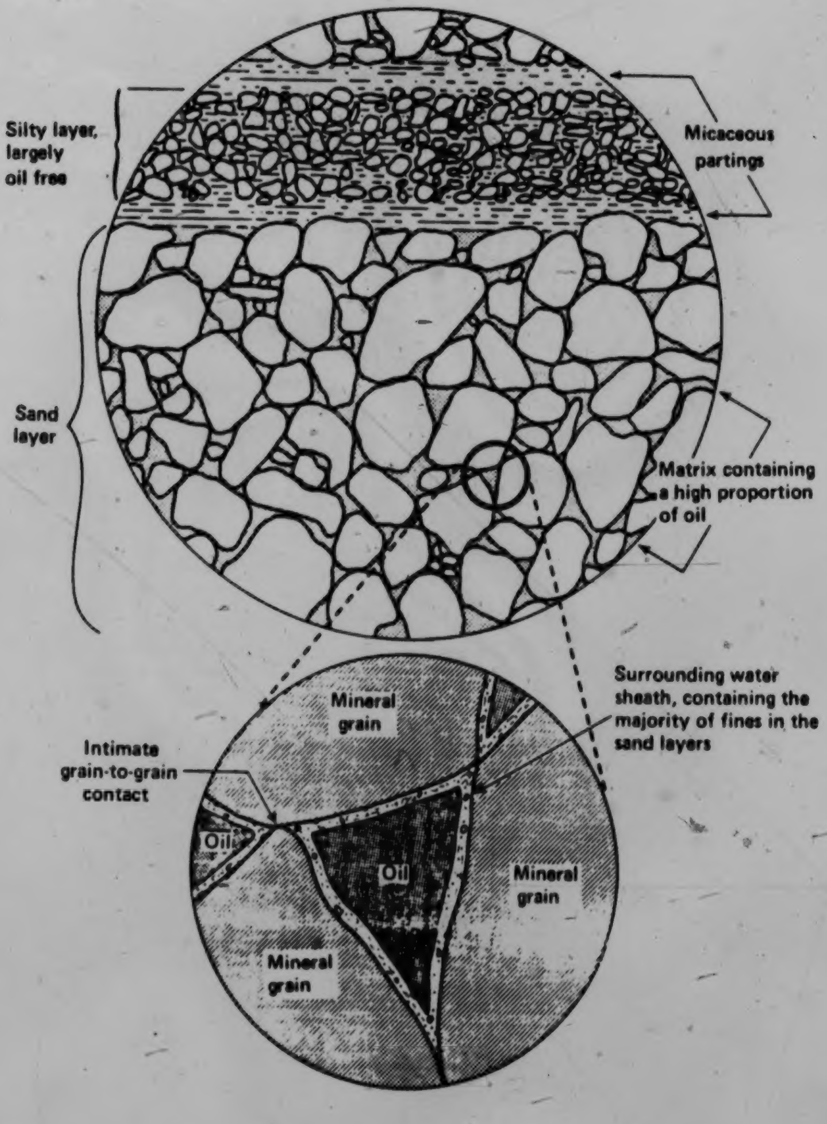
Silty layer, largely oil free
Micaceous partings
Sand layer
Matrix containing a high proportion of oil
Surrounding water sheath, containing the majority of fines in the sand layers
Mineral grain
Intimate grain-to-grain contact
Oil
Oil
Mineral grain
Mineral grain

Figure 3.2 Composition of In Situ Oil Sand (After Dusseault, 1977)

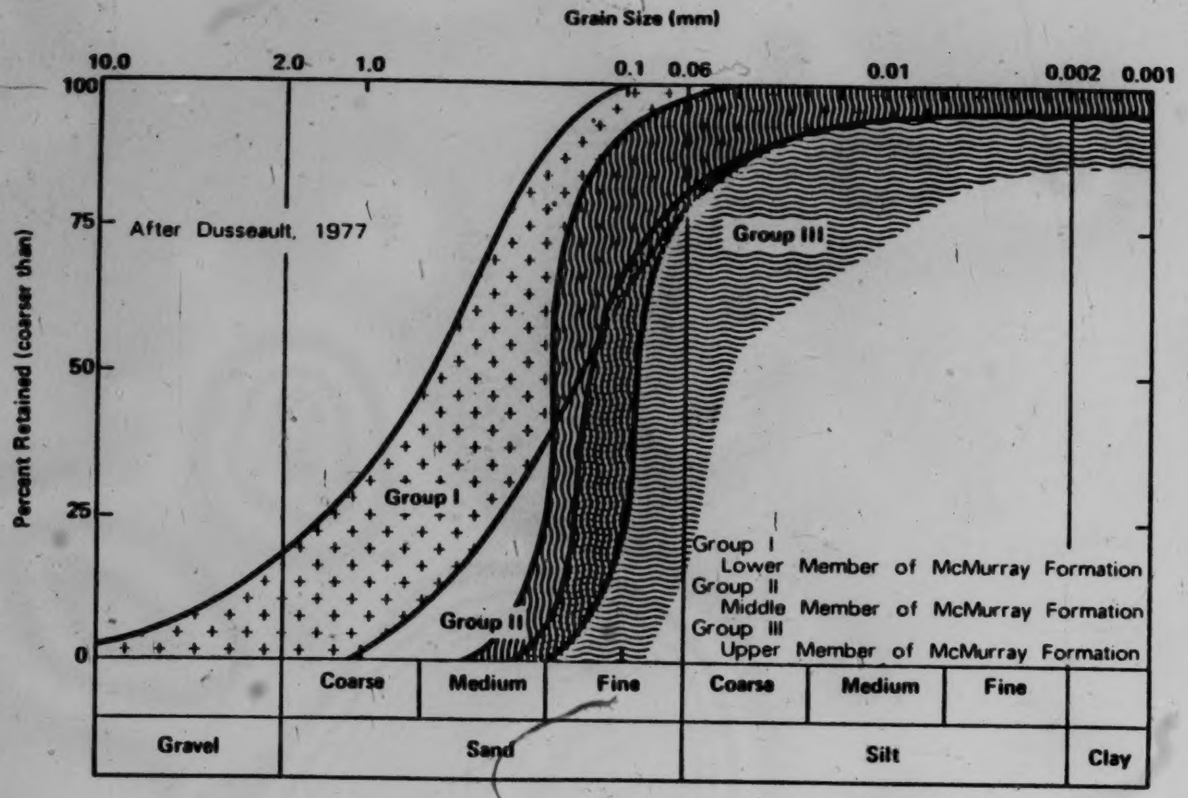

Figure 3.3 Grain Size Distribution For Athabasca Oil Sand
(After Dusseault, 1977)

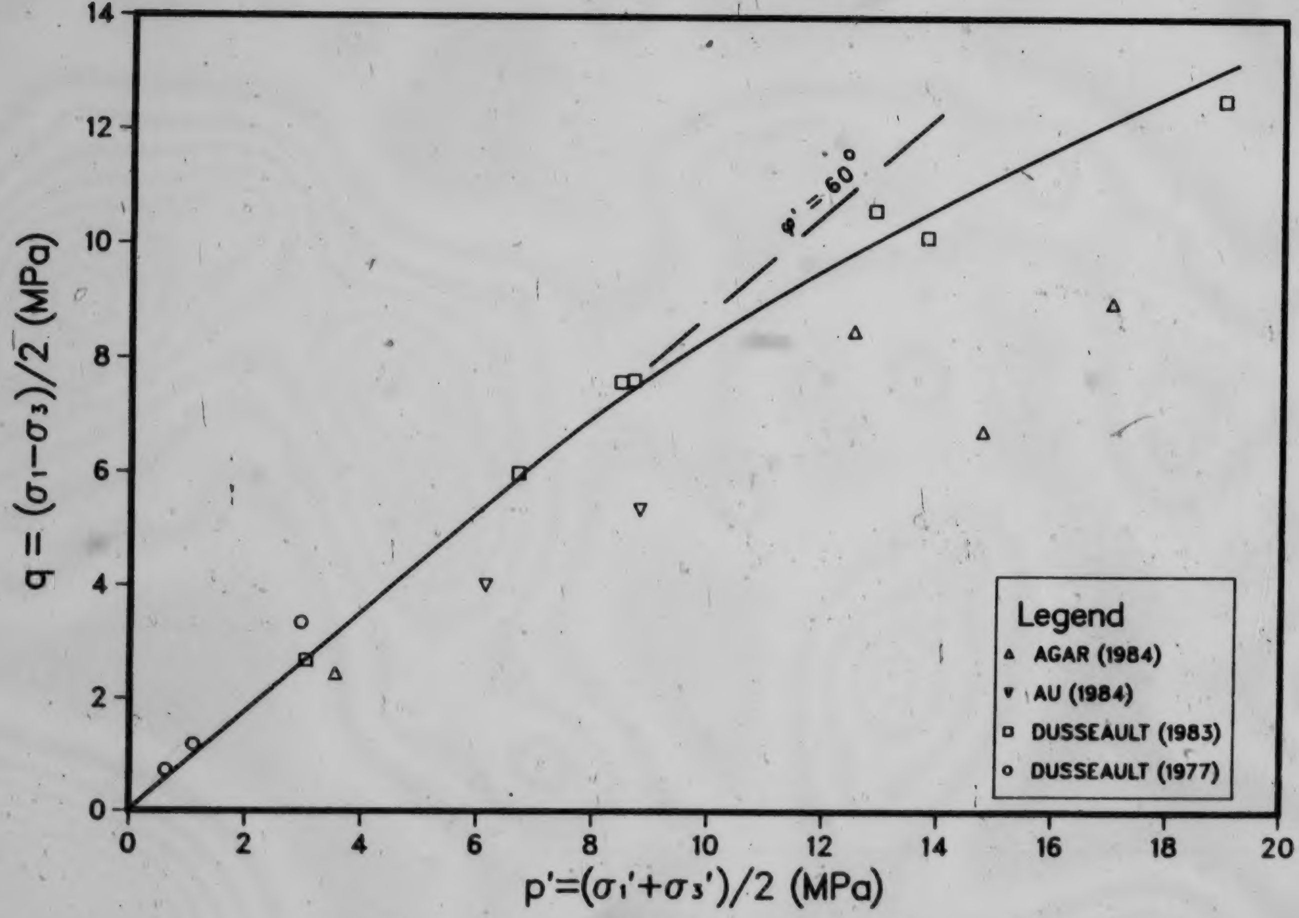

Figure 3.4 Drained Triaxial Compression Test Data for Oil Sand, Bulk Densities Greater Than 2.00 Mg/m³

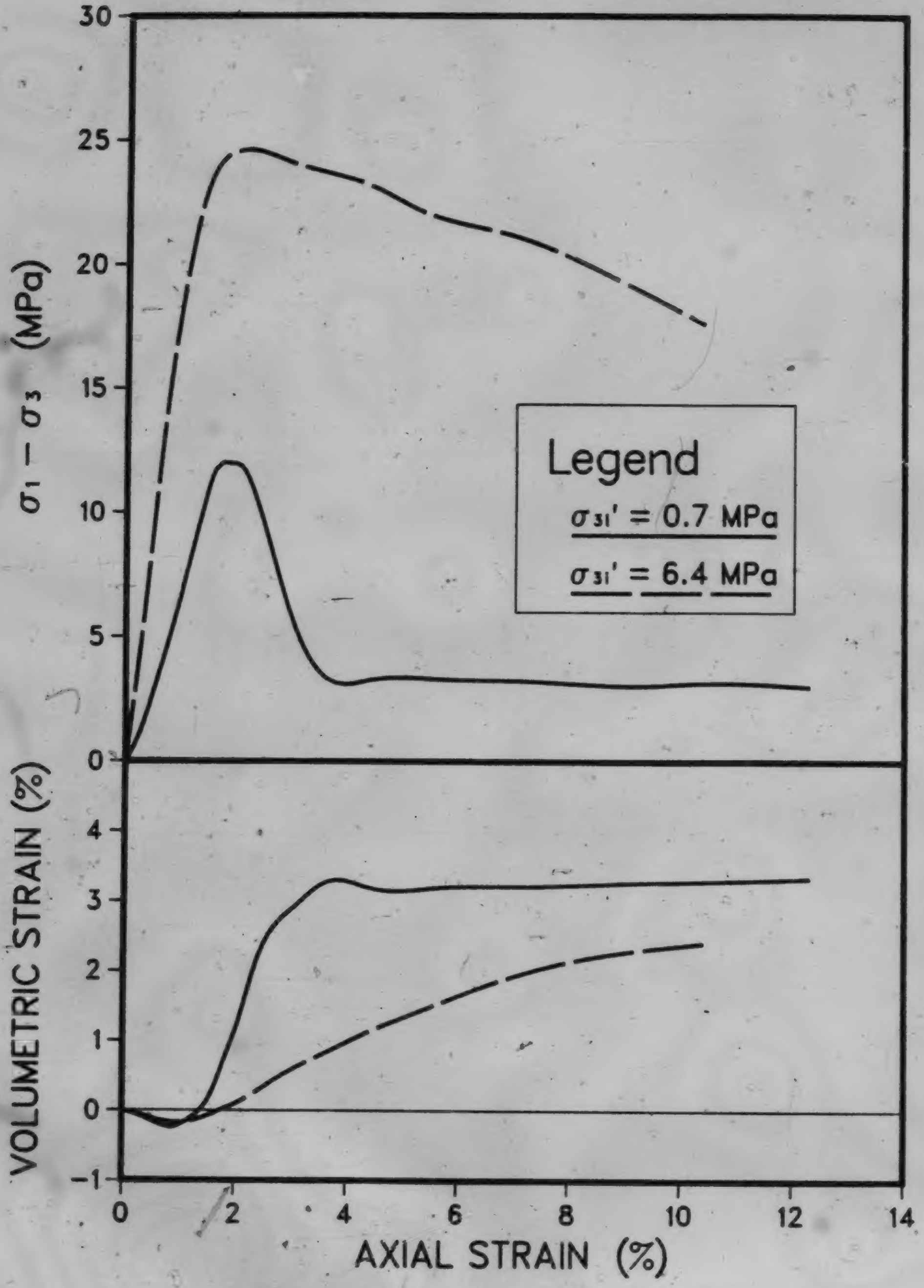

Figure 3.5 Typical Stress-Strain Curves for Drained Triaxial Compression Tests at Low and High Confining Pressures (After Dusseault, 1983)

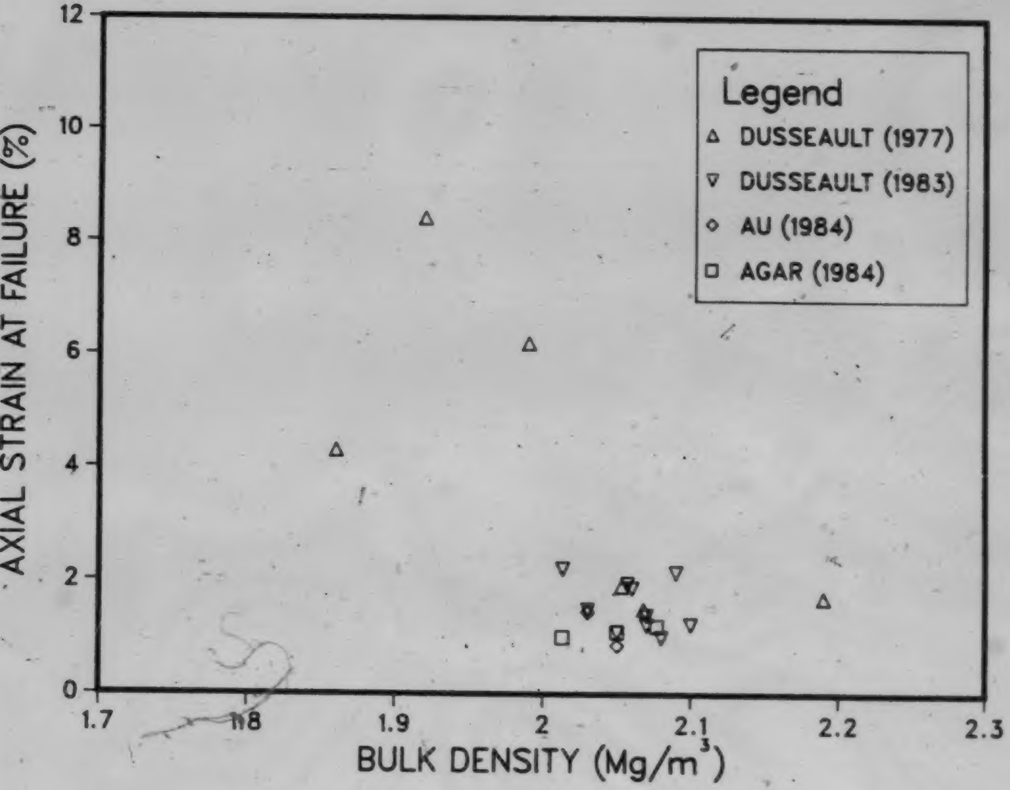

Figure 3.6 Axial Strain at Failure in Drained Triaxial Compression Tests

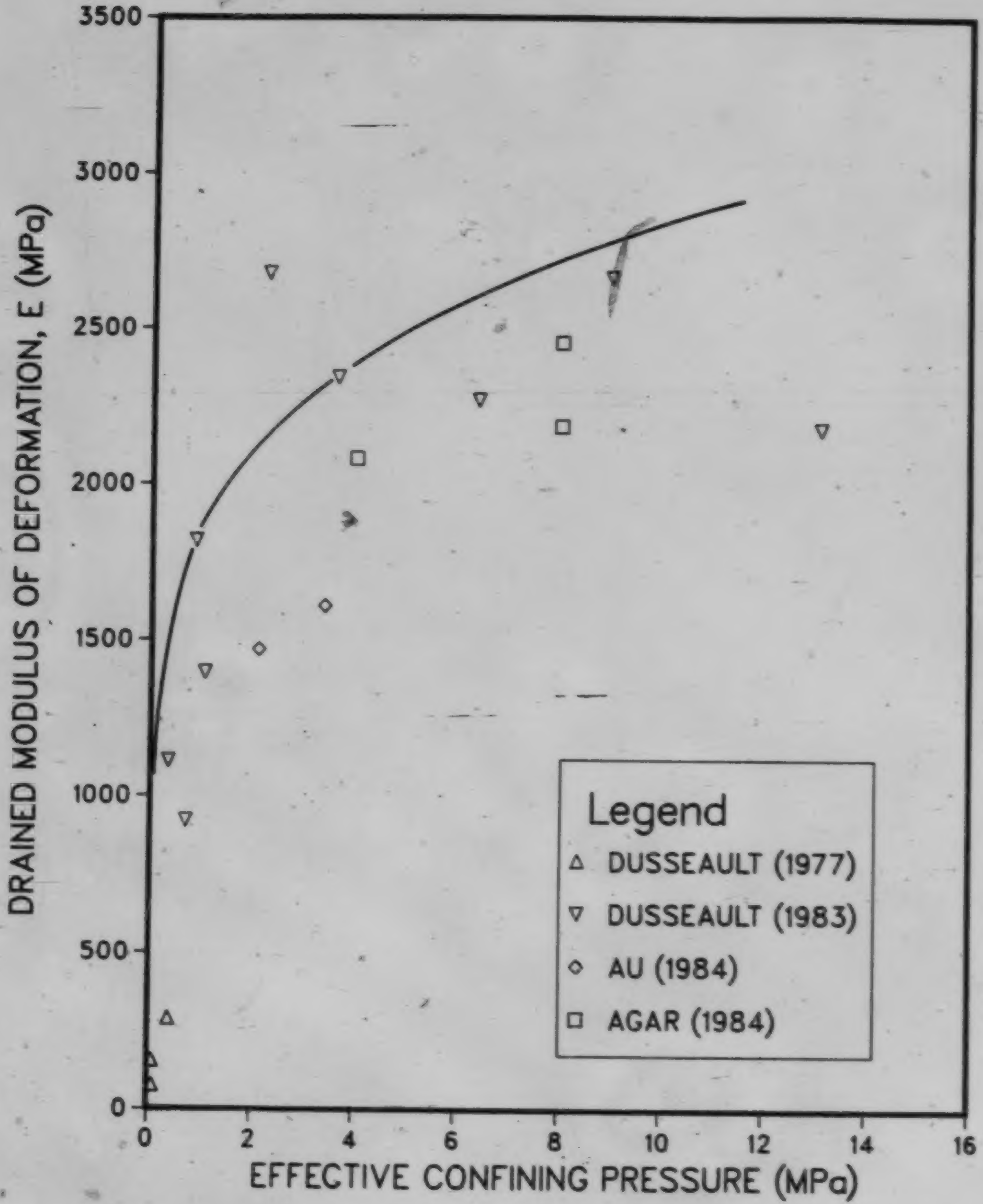

Figure 3.7 Modulus of Deformation for Drained Triaxial Compression Tests at $\epsilon_a$ = 0.25 Percent

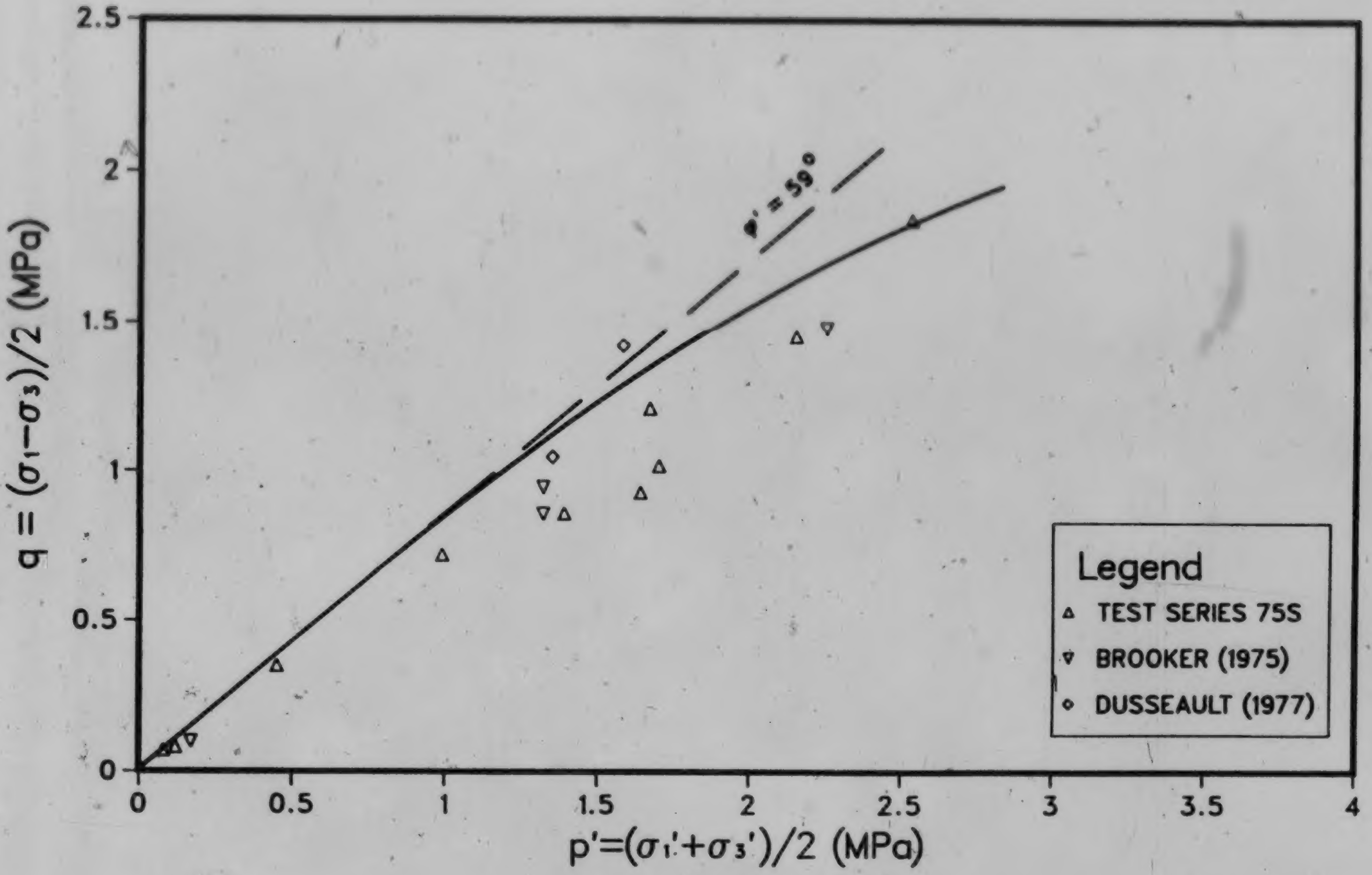

Figure 3.8 Shear Strength at the Maximum Principal Stress Ratio in Undrained Triaxial Compression Tests

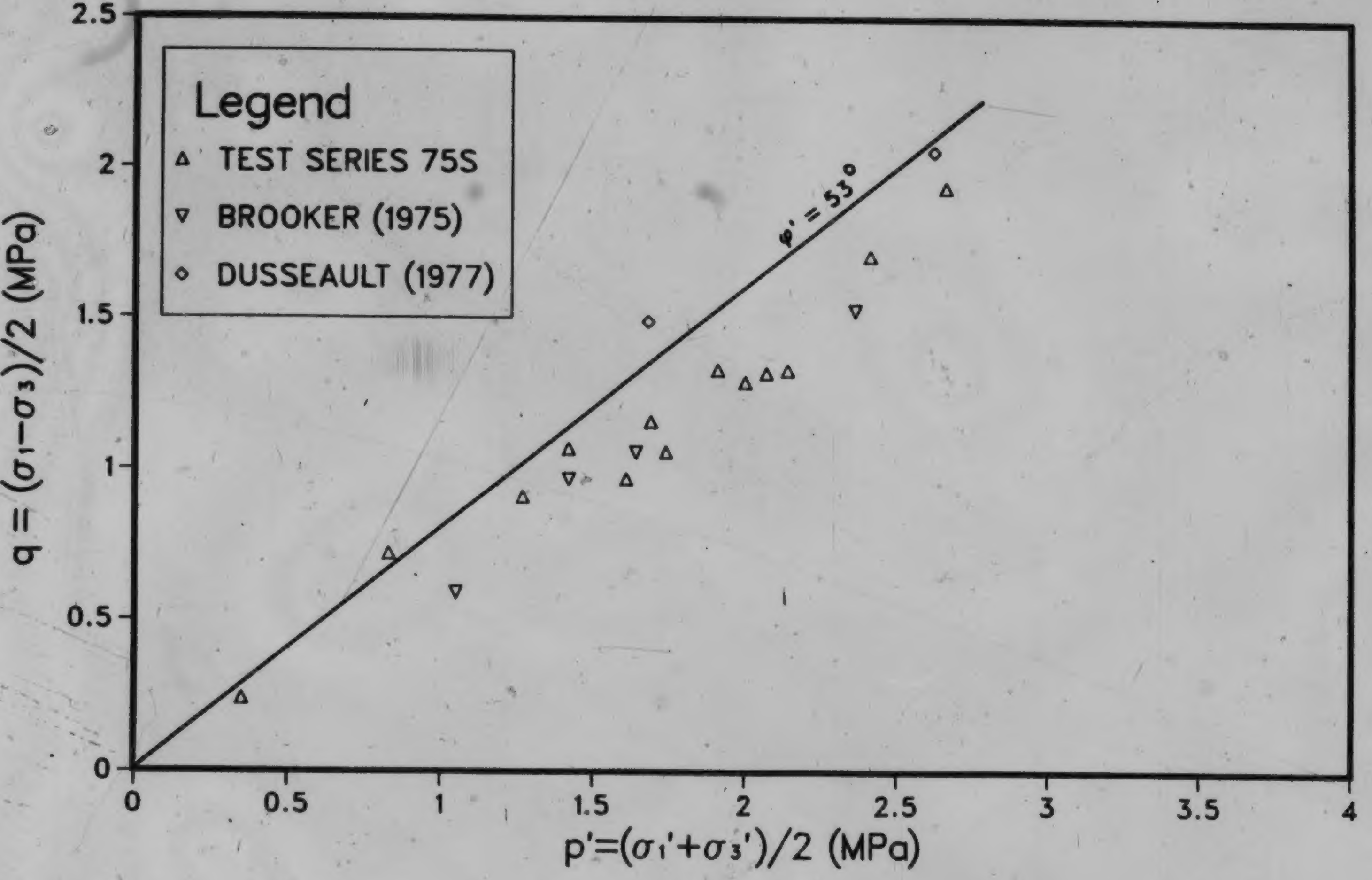

Figure 3.9 Ultimate Shear Strength in Undrained Triaxial Compression Tests

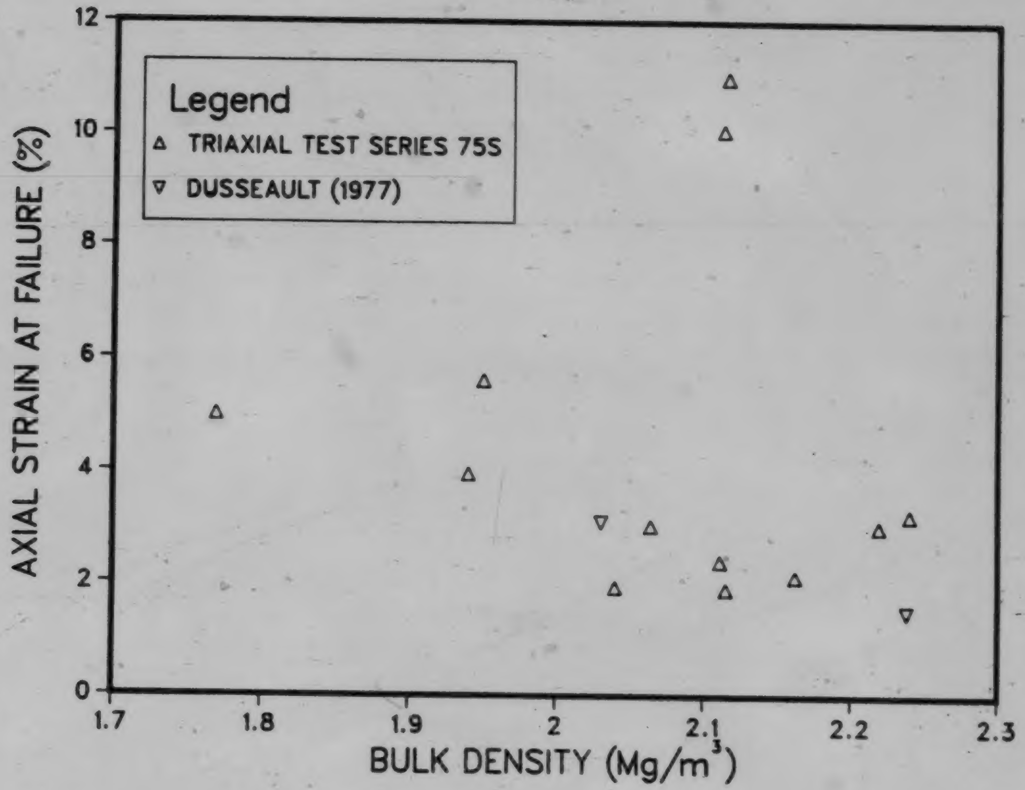

Figure 3.10 Axial Strain at Ultimate Strength in Undrained Triaxial Compression Tests

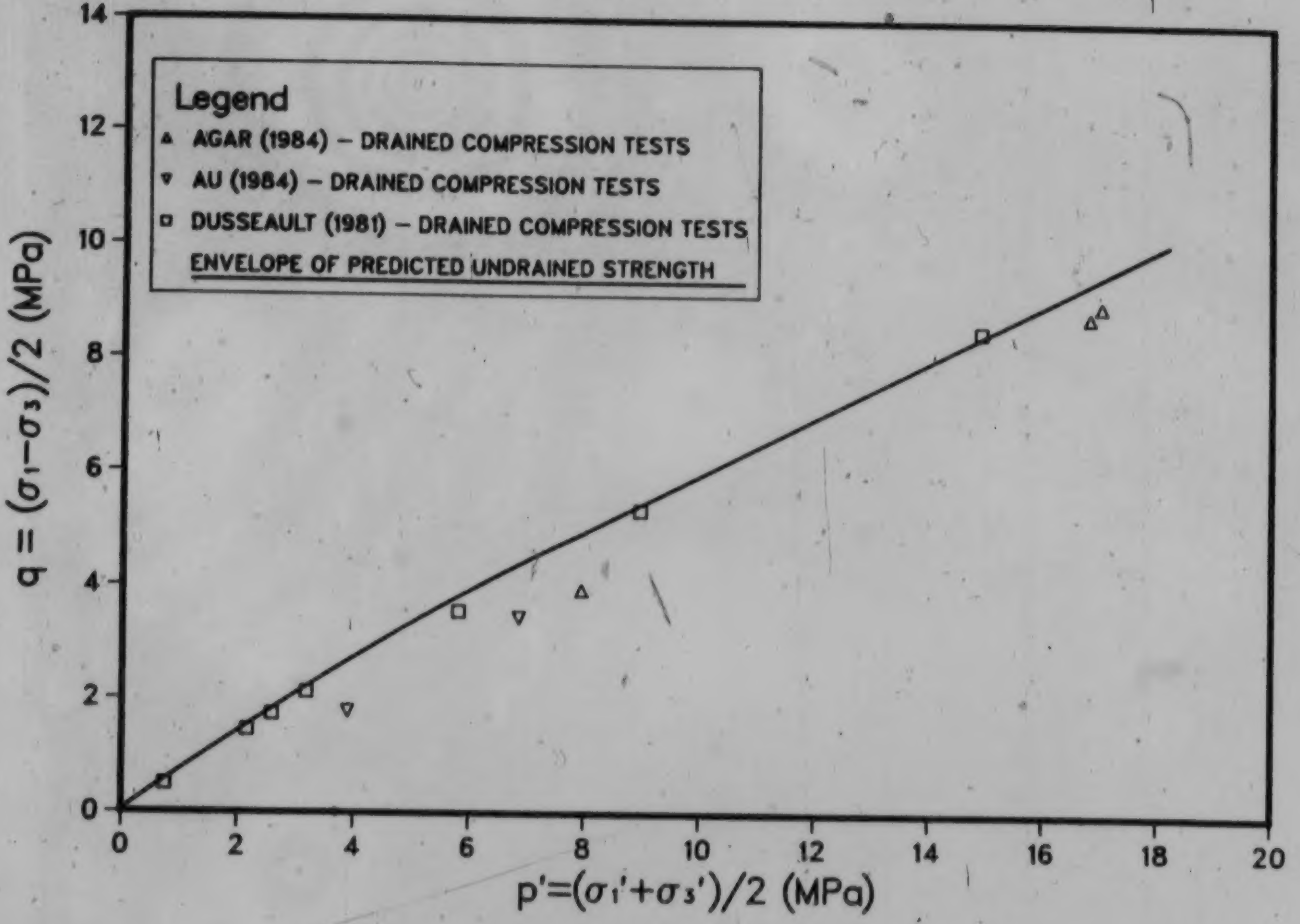

Figure 3.11 Theoretical Prediction of Undrained Shear Strength by Rowe's Stress-Dilatancy Theory

# 4. UNDRAINED TRIAXIAL TESTING OF SALINE CREEK OIL SAND

## 4.1 Introduction

A series of undrained triaxial compression tests were conducted to investigate the undrained stress-strain behaviour and strength properties of Saline Creek oil sand. The tests were performed at initial effective confining pressures between 1 and 8 MPa to evaluate the behaviour over a range of in situ stress levels. The strain rate of testing was also varied nominally between $10^{-5}$ and 3.5 $s^{-1}$ to study the influence of transient loading.

The absence of previous completely undrained triaxial test data for oil sand has been largely predicated by the requirement of unusually high pressure triaxial test equipment. As reviewed in Chapter 2, pore pressures may decrease up to 7.5 MPa during undrained compression loading of dense sands. The triaxial test equipment must therefore be capable of applying both pore and cell pressures in excess of 7.5 MPa which are well beyond the capacity of conventional testing apparatus. For this test program, a high pressure triaxial testing facility was assembled capable of pore and cell pressures up to 14 MPa. This allowed a minimum initial pore pressure of 6 MPa at the highest initial effective confining test pressure of 8 MPa.

It was recognized that the higher viscosity of the interstitial bitumen in the Saline Creek oil sand could impede the dissipation of pore pressures generated during undrained loading at high strain rates as noted by Healy(1963). It was reasoned that reduction of pore pressure gradients and more accurate measurements of pore pressure could be achieved using specimens of smaller height. A brief study of the influence of sample size and frictional end restraint on the undrained behaviour of dense Ottawa sand was conducted. The tests showed that the use of short specimens (length/diameter = 0.5) and "frictionless" loading platens negates the development of pore pressure gradients in the specimens for strain rates up to $10^{-1}$ $s^{-1}$. This method of testing was adopted for the testing of Saline Creek oil sand at strain rates greater than $10^{-4}$ $s^{-1}$.

## 4.2 High Pressure Triaxial Testing Facility

### 4.2.1 Description

The high pressure triaxial testing facility includes the following major components:

1) high pressure triaxial cell;
2) high load capacity testing machines;
3) confining pressure system;
4) low and high pore pressure systems;
5) pore fluid volume change measuring device; and
6) high speed data acquistion systems.

The Wykeham-Farrance WF40020 high pressure triaxial cell was selected for the test program. The cell is capable of withstanding cell and back pressures up to 14 MPa and applying axial ram loads up to 35 kN.

The confining cell pressures were applied by an air activated diaphragm pump. The pump is driven by a 600 kPa compressed air supply. The capacity of the pump is 30 times the inlet air pressure or 18 MPa. The pump diaphragm maintains constant pressure by activating at slight reductions in the water pressure. Each time the pump is activated, an instantaneous pressure decline of approximately 5 percent occurs in the line before the set point pressure is restored. A nitrogen charged accumulator was placed in the high pressure water line to help maintain constant line pressure in the event of sudden changes in pump pressure. A schematic of the high pressure air activated diaphragm pump system is given in Figure 4.1.

Pore pressures in the low pressure range (0 to 4 MPa) were provided by a nitrogen charged pressure board shown in Figure 4.2. Compressed nitrogen at 17 MPa pressure is regulated through relief valves to charge a series of nitrogen-oil and oil-water fluid interface reservoirs. Pore pressures above 4 MPa were applied by a second air activated diaphragm pump.

Three high load capacity testing machines were used during the test program. The first was the Material Test System Model 207.70 which has a capacity of 2650 kN and can achieve ram speeds up to 8 mm/s. The second machine was the Gilmore Model 426-50 fatique testing frame which has a 245 kN loading capacity and achieves speeds up to 64 mm/s. The third machine was the Wykeham-Farrance Model 1008 which has a load capacity of 175 kN. This machine was used only for very slow tests at strain rates less than $10^{-4}$ $s^{-1}$. Each system controls the displacement of the loading ram for constant rate of strain testing.

Changes in volume of the samples during testing were measured by a fluid volume change indicator placed in the pore pressure line between the pressure board or pump and the cell. The volume change indicator was a standard volumetric displacement type similar to the "paraffin volume gauge" described by Bishop and Henkel(1962). The central glass tube was graduated in 0.01 cm$^3$ divisions.

Axial deformations of the sample were measured by means of a LVDT fastened to the loading piston ram of the cell. The confining and pore pressures were measured by strain gauge pressure transducers attached to ports at the base of the cell. The axial load applied to the samples was measured with a 90 kN capacity strain gauge load cell placed between the piston ram and the loading frame.

The excitation voltages for the LVDT, pressure transducers and load cell were supplied by a constant voltage power supply. At strain rates less than $10^{-1}$ s$^{-1}$, the output voltage signals were recorded by the Servigor 460 six channel chart recorder which has chart speeds up to 1 cm/s. At the faster strain rates, the signals from the load cell and pore pressure transducer were amplified and electronically filtered to minimize the interference of transient "noise" in the signals. The signals were recorded by the SE Labs SE6150 oscillograph. Chart speeds up to 1 m/s are achieved by this recorder.

### 4.2.2 Calibration of Electronic Monitoring Devices

The electronic monitoring devices were calibrated prior to undertaking the test program. Calibration checks were repeated periodically during the testing program and a second full suite of calibrations was carried out half way through the testing program.

The strain gauge pressure transducers were calibrated using a dead weight table hydraulic pressure calibrator. The load cell was calibrated against the internal load cell of the Materials Testing Systems loading frame which had been calibrated by the manufacturer on the same day to an accuracy of less than 1 percent over the range of load 0 to 267 kN. The load cell was re-calibrated half way through the testing program against a proving ring of compatible load capacity. The LVDT was calibrated against a micrometer scale. The calibrations are summarized in Table A.1.

### 4.2.3 Design of Frictionless Loading Platens

A set of frictionless loading platens were designed in the manner used by Bishop and Green(1965). The conventional 38.1 mm diameter base pedestal and top loading cap that accompanied the triaxial cell were replaced with pedestals and cap enlarged to 43.2 mm diameter as shown in Figure 4.3. The purpose of the enlargement is to accomodate the radial expansion of the test specimens during undrained compression. The enlarged platens accomodate up to 22.2

percent axial straining of the specimens assuming the specimens deform as perfect right cylinders. Pore pressure measurements are made through a 12.7 mm diameter coarse porous stone inset flush into the centre of the base pedestal.

The surface of the top loading platen was lubricated with a thin smear of silicone grease and a sandwich of two 0.39 mm thick latex rubber membranes placed over it. The upper facing sides of the membranes were also lubricated. The same procedure was carried out on the base pedestal. A 12.7 mm diameter hole was cut in the centre of each membrane to provide contact of the porous stone with the test specimen. The porous stone was covered with filter paper and care was taken not to contaminate the stone with the silicone grease.

### 4.2.4 Compliance of Testing Apparatus

#### 4.2.4.1 Axial Deformation of Frictionless Platens

Axial deformations measured in the triaxial cell using the frictionless loading platens include the deformation of the lubricated membranes above and below the specimen as well as the specimen itself. Compliance tests to correct for the membranes were carried out in the following manner:

1) A steel disk, 38.1 mm diameter and 23.5 mm in length, was installed in the triaxial cell using the

frictionless loading platens described in Section 4.3.3.

2) The pore pressure system was allowed to saturate under an effective confining pressure of 2.0 MPa and a pore pressure of 10.5 MPa.

3) The pore pressure port was closed and axial load was incrementally applied to the specimen under undrained conditions and the deformation response recorded by the LVDT.

The results of the compliance test are shown in Figure A.1. The correction for the membranes was simplified into a bilinear relationship as shown in the figure. This correction was applied to the triaxial test results.

#### 4.2.4.2 Piston Friction in Triaxial Cell

Piston friction increases the magnitude of the axial load measured by the load cell. To quantify the piston friction, the triaxial cell was assembled without a test specimen and a series of piston loading tests were conducted against a cell pressure of 12.5 MPa. Piston speeds of 0.10, 0.51 and 5.08 mm per second were tried to assess the effects of loading rate. The test results are summarized in Table A.2. The piston friction increased slightly with velocity due to inertia forces required to drive the piston into the cell at higher speeds. Failure loads for the test specimens in this test program were generally 10 kN or more. Hence, the maximum piston friction of 300 N amounts to less than 3 percent of the total load. Typically, the loading piston travelled about 0.5 mm before reaching the top of the test specimen in the triaxial tests. Load measurements during this travel were used as the reference for zero load, thereby automatically compensating for most of the piston friction. Given this practice and the small relative magnitude of the piston friction, no corrections to the triaxial test data were deemed necessary.

#### 4.2.4.3 Response Time of Pore Pressure Transducer

At the highest strain rates, it was recognized that a time lag could occur between the base of the test specimens and the pore pressure transducer. To investigate this possibility, the cell was assembled without a test specimen and pressurized at 4.9, 6.7, 10.1 and 12.1 MPa. The cell pressures were "locked" in by closing the cell pressure port valve. At each pressure, the piston was driven into the cell at a constant speed of 50 mm per second. The increase in cell pressure as the piston was driven into the cell was measured both by the pore pressure transducer and by the increase in piston load recorded by the load cell. The calculated changes in cell pressure are compared in Table A.3.

The increases in cell pressure recorded by the pore pressure transducer range up to 10 percent less than calculated from the load cell readings. The difference in pore pressure measurements consistently vary between 0.09 and 0.13 MPa despite the difference in initial cell pressures. The differences are therefore attributed to the inertia force required to drive the piston ram into the cell rather than a time lag in pore pressure measurement by the pore pressure transducer. The calculated inertial forces are given in Table A.3 and range between 49 and 69 N. These forces are negligible compared to the total loads applied to the test specimens and have been neglected in the analyses of the test results.

#### 4.2.4.4 Stress Wave Propagation and Inertia Forces under Transient Loading

Longitudinal stress waves are induced in the test specimens as the top of the specimen is loaded by the piston ram. Unless the stress waves can pass back and forth through the specimen many times before the peak stress is reached, there will be a complex stress pattern at the time of failure. Whitman and Healy(1962) proposed an approximate rule by stipulating that the initial stress wave pass back and forth at least ten times before the failure strain is reached. The permissible time to failure and permissible piston velocity are given by:

$$t_f > \frac{20\ l}{c} \qquad 4.1$$

and

$$v_o < \frac{c\epsilon_f}{20} \qquad 4.2$$

where $t_f$ is the time to failure, l is the length of the specimen, c is the longitudinal wave velocity, $v_o$ is the applied loading velocity, and $\epsilon_f$ is the average axial strain at failure.

Typical values of the longitudinal wave velocities for dense sands are 350 to 600 metres per second. The fastest strain rate achieved during this test program was 3.1 $s^{-1}$. Given the sample height of 14.28 mm and the strain at the maximum stress ratio to be 10.4 percent, the minimum time to failure, $t_f$ is 0.001 seconds and the maximum piston velocity, $v_o$ is 1820 mm per second. The time of loading at the maximum stress ratio and the loading velocity were 0.033 seconds and 44 mm per second, respectively. These values are well within the recommended magnitudes. Hence, nonuniform stress conditions resulting from longitudinal stress waves were not expected to be a factor in the test results.

Radial strains of the outer portions of the test specimen can be resisted by the radial inertia of the soil particles at very high strain rates. The radial inertia force increases the effective horizontal confining stress and, for short periods of time, the specimen may sustain axial loads in excess of the axial failure stress. For typical dense sands and 38 mm diameter test specimens, Whitman and Healy(1962) report that radial inertia forces only become significant at times to failure less than 0.001 second. This is more than an order of magnitude faster than the times to failure achieved in this test program.

### 4.2.4.5 Stiffness of Test Apparatus

The post-failure behaviour of a brittle material like a hard rock can be very strongly influenced by the release of energy stored within the components of the tests apparatus. Coates(1981) considered the post-failure equilibrium between a test specimen (rock or soil) under axial compression and the test apparatus. By the spring analogy illustrated in Figure 4.4, the maximum deformation of the test specimen, $\Delta_m$ contributed by the relaxation of stress in the test apparatus with the decreased load reaction of the test specimen in post-failure (or post-ultimate strength) is derived as:

$$\Delta_m = \Delta_s \, k_s/k_m \qquad 4.3$$

where $\Delta_s$ is the total axial deformation of the test specimen,

$k_s$ is the apparent axial stiffness of the test specimens at the ultimate strength, and $k_m$ is the apparent axial stiffness of the test apparatus.

From Equation 4.3, the magnitude of $\Delta_m$ approaches zero as $k_m$ becomes large for a very stiff testing apparatus. In the case of a testing apparatus of soft stiffness, the post-failure deformation $\Delta_m$ applied to the test specimen can lead to a substantial further reduction in the strength. Where a stable equilibrium between the strength of the test specimens and the strain released by the test apparatus cannot be reached, a chain reaction leading to uncontrolled rapid failure occurs.

The stiffness of the testing apparatus, $k_m$ is comprised of (1) the stiffness of the testing machine, and (2) the stiffness of the triaxial cell apparatus. Among the three testing machines used in the test program, the Wykeham-Farrance Model 1008 is the least stiff. In test configuration, the reaction of the testing machine to the load applied to the test specimens is carried by two circular steel bars, 64 mm diameter and 430 mm in length. If the deflection of the cross members supporting the top and bottom of the steel bars is neglected, the calculated stiffness of the testing apparatus is $3.1 \times 10^6$ kN/m.

Two drained loading tests were conducted on the triaxial cell to estimate the stiffness of the triaxial cell apparatus itself. A 38.1 mm diameter and 20.6 mm long steel disk was inserted into the cell in replacement of the oil sand test specimens. The stiffness of the triaxial cell apparatus was measured to be 214,000 and 230,000 during successive loading cycles up to 30 kN. By comparison, the theoretical total stiffness of the combined components of the triaxial cell is estimated to be 239,000 kN/m.

The total combined stiffness of the testing apparatus including the testing machine and assuming an average stiffness of 222,000 kN/m for the triaxial cell is calculated to be 207,000 kN/m. It is evident that the overall stiffness of the test apparatus is controlled by the stiffness of the triaxial cell. Any additional reduction in stiffness due to neglect of the influence of the cross members in the testing machine would therefore contribute very little to the overall stiffness of the testing apparatus.

In review of the test results for the undrained triaxial compression tests conducted on the Saline Creek oil sand, the bulk stiffness, $k_s$ at the ultimate strength for the samples tested ranges up to 9000 kN/m. According to Equation 4.3, the maximum potential magnitude of $\Delta_m$ therefore does not exceed 4.3 percent of the total axial deformation, $\Delta_s$ applied to the test specimens. This magnitude of $\Delta_m$ is considered to be sufficiently low enough as to be considered inconsequential to the results of the test program. This conclusion is based on the following:

1) The magnitude of $\Delta_m$ from Equation 4.3 is very conservatively estimated assuming perfectly brittle post-failure behaviour with complete loss of strength. In reality, soil and rock maintain some strength during post-failure deformation and the magnitude of $\Delta_m$ is less. Ultimately, $\Delta_m$ is zero for materials which behave perfectly plastic during post-failure deformation.

2) In all undrained triaxial compression tests conducted on the Saline Creek oil sand, the axial loads applied to the test specimens increased constantly with the applied deformation up to the 20 percent strain reached in the tests. Hence, whereas a drop in strength in terms of stress is observed in the undrained stress-strain response of the oil sand, the axial load continued to increase with strain. The potential magnitude of $\Delta_m$ estimated from Equation 4.3 is therefore overestimated in view of the characteristic non-brittle load

behaviour of the oil sand under undrained axial compression.

## 4.3 Proof Testing of Frictionless Loading Platens

### 4.3.1 Introduction

A preliminary series of undrained triaxial compression tests on Ottawa sand were performed in the high pressure triaxial test apparatus to investigate the effects of sample size and strain rate on the undrained behaviour of a dense sand. The tests were conducted using the conventional and modified "frictionless" loading platens to study the influence of frictional end restraint. Strain rates were varied between $10^{-5}$ and 2.5 $s^{-1}$.

### 4.3.2 Sample Preparation of Ottawa Sand

The sand is a 20-30 mesh Ottawa sand supplied from Ottawa, Illinois. The gradation of the sand is given in Figure B.1. The specimens were formed in a three piece steel split mold, 38.1 mm in diameter and 127 mm in length. The mold was assembled and lined with a 38.1 mm diameter latex rubber membrane passed through the centre of the mold and stretched over the ends. The mold was then fitted over a steel base pedestal to seal off the bottom. The assembly of the mold is illustrated in Figure 4.5.

The mold was held on a vibrating table and layers of saturated sand were placed in the mold in 25 mm lifts. Each lift was tamped gently with a 12.7 mm diameter steel rod for 30 seconds. Filling of the mold was stopped when the sand reached within 15 mm of the top of the mold. A 25 mm high by 37 mm diameter aluminum "plug" with 2 mm diameter holes drilled through it was then placed on top of the sample.

The sample was placed in a refrigerated room with temperatures maintained between 0 and -5°C. The base pedestal was connected to a refrigeration unit and antifreeze cooled to -15 to -20°C circulated through it. The freezing of the specimens from the base tends to force water expelled by freezing upwards through the sample and out the holes of the plug. A 5 Kg weight was placed on the top of the "plug" to help minimize heaving of the specimens during freezing. The samples were frozen after about 4 hours. The frozen samples were stored in a cold room at a temperature of -15°C.

The final test specimen preparations were carried out in the cold room. The samples were cut to the appropriate test length with a diamond saw and the ends were squared in a lathe. The height, diamater and weight of the samples were then measured. On selected specimens, the water content of the end trimmings was measured to allow calculation of the porosity. The bulk density and porosity of the specimens vary between 1.960 and 2.061 Mg/m$^3$ and 33.6 and 37.7 percent, respectively. The majority of the densities exceed 2.00 Mg/m$^3$. Table 4.1 is a summary of the specimen data.

The test specimens were transported to the test facility in a styrofoam container filled with dry ice (-80°C) and allowed to chill in the container for a minimum of 15 minutes. The specimens were mounted in the cell in a frozen state. In view of the high confining stresses applied to the specimens, three 0.39 mm thick latex membranes were used to enclose the specimens. The time from the start of specimen mounting to the application of the confining pressure was no more than 10 minutes and improved to less than 5 minutes with practice. Observations of specimens allowed to thaw at room temperatures showed that significant thawing of the specimens only occurred after 20 minutes for samples chilled in the dry ice.

### 4.3.3 Saturation of the Test Specimens

Lowe and Johnson(1960) show the theoretical back pressure, $u_s$ required to reach complete saturation of the pore fluid in a soil sample is:

$$u_s = u_a(1 - S_i)\frac{(1 - H)}{H} \qquad 4.4$$

where $u_a$ is the initial absolute pressure corresponding to the initial saturation, $S_i$ and H is Henry's constant. Henry's constant at room temperature for water is approximately equal to 0.02 $cms^3$ of air to 1 $cms^3$ of water. This simplifies the equation to:

$$u_s = 49\ u_s(1 - S_i) \tag{4.5}$$

Black and Lee(1973) experimentally investigated the use of elevated back pressures to produce complete saturation of Ottawa sand samples. They found the time to reach saturation to be an exponential function of the initial saturation, $S_i$ and the ratio of the applied back pressure, u to the fluid saturation pressure, $u_s$. The following relationship was developed to estimate the time for complete saturation:

$$t_d = \{\frac{1}{Y}\ [\frac{1 - S_i}{1 + 49R_u(1 - S_i)}]\}^{1/X} \tag{4.6}$$

where $t_d$ is the time required for complete saturation and $R_u$ is the ratio of the applied back pressure to the fluid saturation pressure, $u/u_s$. The parameters X and Y are experimental coefficients determined by curve fitting to be:

$$Y = 0.0014 \text{ for } S_i > 0.8 \tag{4.7}$$

$$X = 0.085 + 0.133\ S_i \tag{4.8}$$

The test specimens were thawed under a nominal effective confining pressure of 2.0 MPa and minimum back pressure of 4.6 MPa. The purpose of the high back pressure was twofold: (1) to allow for pore pressure decreases during undrained shear and (2) to accelerate the time required to saturate the pore pressure system. The pore pressure lines in the cell were flushed with water to ensure as high an initial saturation as possible. If it is assumed that the saturation was as low as 95 percent at atmospheric pressure, then the time required to completely saturate the sample can be calculated:

$S_i = 0.95$

$u = 4600$ kPa

$u_a = 1$ atmosphere $= 101.3$ kPa

$u_s = 49 \times 101.3 \times (1 - 0.95) = 248$ kPa

$R_u = 4600/248 = 18.54$

$Y = 0.0014$

$X = 0.085 + 0.133 \times 0.95 = 0.211$

$$t_d = \{\frac{1}{0.0014}[\frac{1 - 0.95}{1 + 49 \times 18.54 \times (1 - 0.95)}]\}^{1/0.211}$$

$$= 0.3 \text{ minutes}$$

The calculations suggest that complete saturation is reached almost immediately and is reasonable considering the very high back pressure used. Black and Lee(1973) caution the use of the equation as only an estimate of the order of magnitude of time required to bring a soil to complete saturation. The test specimens were therefore allowed to consolidate for at least 1 hour to ensure saturation.

### 4.3.4 Triaxial Testing Procedures

The pore pressure parameter B was measured on most of the specimens prior to the triaxial compression tests. The pore pressure valve was closed and the cell pressure raised. The value of B is defined as:

$$B = \frac{\Delta u}{\Delta \sigma_3} \tag{4.9}$$

where $\Delta u$ is the change in the pore pressure resulting from the change in the cell pressure, $\Delta \sigma_3$. The measurements of the pore pressure parameter B are summarized in Table 4.2.

Undrained triaxial compression tests were conducted on the specimens under an initial effective confining pressure of 2.0 MPa and initial pore pressures between 4.6 and 10.2 MPa. Three series of tests were carried out:

Series A - Seven tests were conducted using the conventional 38.1 mm diameter base pedestal and top loading platens on specimens with length/diameter (l/d) ratios of 0.5, 1.0, 1.5 and 2.0. Another 2 specimens were tested using the enlarged 43.2 mm platens. A nominal strain rate of $10^{-2}$ $s^{-1}$ was used for all tests.

Series B - Six specimens with l/d ratios between 0.5 and 2.0 were tested at a nominal strain rate of $10^{-2}$ $s^{-1}$ using the frictionless end platens described in Section 4.2.3. The purpose of these tests were to comparatively evaluate the effect of radial friction developed between the loading platens and the ends of the specimens.

**Series C** - Eight specimens with l/d = 0.5 were tested using the frictionless platens at nominal strain rates of $10^{-5}$, $10^{-4}$, $10^{-1}$ and 2.5 $s^{-1}$. Three specimens with l/d = 2.0 were tested at strain rates of $10^{-5}$, $10^{-4}$ and $10^{-1}$ $s^{-1}$ using the conventional platens for purposes of comparison.

Continuous measurements of axial deformation, axial load, cell pressure and pore pressure were taken during testing. Measurements and observations of the condition of the specimens after failure were noted. The procedural details and test results for each of the triaxial tests are presented in Appendix B. The triaxial test results are summarized in Table 4.2.

### 4.3.5 Influence of Specimen Size on Undrained Behavior

#### 4.3.5.1 Pore Pressure Parameter B

The value of pore pressure parameter B generally ranged between 0.8 and 0.9 with a mean of 0.85. The magnitude of B is plotted against the length/diameter ratio of the test specimens in Figure 4.6. The value of B decreases for shorter specimens using the conventional loading platens. This is caused by the frictional end restraint between the shorter specimens and the loading platens which increases the rigidity and decreases the compressibility of the grain structure. Hence, the magnitude of B decreases in accordance with Equation 2.17.

Within the limits of the test data, it is concluded that the frictionless platens increase the apparent compressibility of the specimens as reflected by the slightly higher magnitude of B at l/d = 0.5. The higher compressibility is derived from the reduction in frictional restraint at the ends of the specimens and by the compressibility of the rubber membranes used in the frictionless platens themselves. At l/d = 0.5, the range of B using the frictionless platens remains within the range of B measured using the conventional platens and l/d = 2. This shows that undrained pore pressure responses caused by changes in total confining stress are not adversely altered by the frictionless platens.

#### 4.3.5.2 Undrained Strength and Pore Pressure Response

The conditions at the ultimate strength or maximum deviator stress, $(\sigma_1 - \sigma_3)_f$ and maximum principal stress ratio, $\sigma'_1/\sigma'_3$ for Test Series A and B are plotted against the length/diameter ratio of the test specimens in Figures 4.7. The pore pressure parameter A is used to define the pore pressure conditions. The average value of B of 0.85 was assumed for specimens OS-S1 through OS-3B where initial measurements of B were not made.

Using the conventional platens, the ultimate strength and maximum stress ratio increase for l/d ratios less than 1.5 with up to a twofold increase for l/d = 0.5. Using the frictionless platens, equivalent measurements of the ultimate strength and maximum stress ratio were made for l/d ratios between 2 and as low as 0.5. It is obvious that the frictional end restraint between the test specimens and the loading platens is substantially reduced using the frictionless platens.

The average ultimate strength and maximum stress ratio measured using the conventional platens and l/d = 2 are 16.5 MPa and 3.7, respectively. The maximum stress ratio corresponds to an effective friction angle of shearing resistance of 35°. The tests using frictionless platens indicate an average maximum strength of 15.0 MPa and a maximum stress ratio of 3.4 corresponding to an effective friction angle of 33°. Lee(1978) also observed an approximate 1° decrease in the friction angle using frictionless platens for undrained triaxial compression tests on dense, fine grained Sacremento River sand over a range of consolidation pressures up to 2.5 MPa. It is evident that slightly lower angles of shearing resistance are measured using the frictionless platens and suggests that frictional end restraint using conventional platens exerts a minor influence even at comparatively slender l/d ratios of 2.

At the initial effective confining pressure of 2 MPa, the Ottawa sand is a highly dilatant material as indicated by the negative value of the pore pressure parameter A at failure. Using conventional platens, the dilatancy of the sand structure is suppressed by frictional end restraint for lower l/d as indicated by the more positive magnitude of $A_f$. The value of $A_f$ measured using both the conventional and frictionless platens at l/d = 2 was -0.32. The value of $A_f$ using the frictionless platens and l/d = 0.5 ranged between -0.31 and -0.42 with a mean of -0.35. The lower value of $A_f$ at l/d = 0.5 using the frictionless platens suggests that strain and shear dilation occurs more uniformly throughout the test specimens as the height is decreased. Straining of the test specimens is discussed further in the next section.

All tests were conducted with initial pore pressures between 4.63 and 4.93 MPa. The pore pressures at the ultimate strength using the frictionless loading platens vary between 0.0 and 0.68 MPa with a mean of 0.28 MPa. The pore fluid saturation pressure for the specimens was conservatively estimated to be as high as 0.25 MPa in Section 4.3.3. It appears that the maximum strength of the test specimens was concurrent with the cavitation of the pore fluid. This was confirmed in Test Series C by conducting the Tests OS-11, OS-18A and OS-19A at initial pore pressures of 9.92, 10.17 and 5.41 MPa. The pore pressures at failure decreased 6.63, 5.46 and 5.09 MPa giving final pore pressures of 3.29, 4.71 and 0.32 MPa, respectively. Cavitation of the pore fluid occurred for OS-19A, but not for OS-11 and OS-18A. A minimum initial pore pressure greater than 7 MPa was therefore required to prevent cavitation.

#### 4.3.5.3 Strain and Mode of Failure

The strains at the maximum strength and maximum stress ratio approximately doubled as the l/d ratio decreased from 2 to 0.5 for both the conventional and frictionless platens. Four shapes of the test specimens after testing were typically observed and are sketched in Figure 4.8:

a) All specimens with l/d greater than 1.5 failed by the development of a single shear plane when using the conventional loading platens. The bottom of the shear plane passed through the bottom edge of the test specimens as shown by Figure 4.8(a).

b) Specimens tested with l/d less than 1.0 using the conventional platens failed by radially bulging at the mid-height of the specimen. Radial expansion at the contact between the specimen and the platens was minimal due to frictional restraint.

c) Specimens tested using the frictionless platens and l/d = 2 failed by bulging at mid-height. Radial expansion decreased towards the ends of the specimen.

d) Specimens tested using the frictionless loading platens and l/d less than 1 expanded uniformly throughout the height of the specimen.

Rowe and Barden(1964) observed similar trends in the shape of test specimens in drained tests on dense Mersey River sand using conventional and frictionless platens. They concluded that the friction developed between the specimens and the conventional steel loading platens inhibits radial straining causing large "dead zones" at the ends of the specimens as shown in Figure 4.9. The concentration of shear straining and dilation in narrow zones in the centre of the specimen causes these zones to pre-maturely fail ahead of the rest of the specimen. The failure plane that develops is drawn to the corners of the platen by the "singularity" in the strain field formed by the dead zones.

Rowe and Barden(1964) also found that frictionless platens permit unrestrained radial expansion at the ends of the test specimens and shear straining develops unsuppressed in all parts of the specimens. Numerous failure planes form simultaneously in the specimens under the condition of general shear. The multiple formation of failure planes causes the observed bulging of the specimens. Higher strains to failure are required to mobilize many shear planes evenly distributed throughout the specimens rather than in a localized zone.

For the test specimens using the frictionless platens and l/d = 2, the observed reduction in radial expansion towards the end of the specimens suggests that the frictional end restraint is not completely eliminated by the frictionless platens. Hence, the observed "uniform" radial expansion of the shorter specimens with l/d less than 1 may not entirely imply complete elimination of end restraint. The uniform expansion is probably the combination of reduced frictional end restraint and the kinematics of particle motion enforced between two rigid boundaries.

Evidence of the frictional restraint at the ends of the Ottawa sand specimens using the conventional loading platens was visually observed by examining the faces of the steel platens after the first series of tests. The indentations of the sand grains into the steel surface were evident as shown in Plate 4.1. Radial grooves up to 2 mm long were also noted where the sand grains moved radially during the tests. Conversely, no indentations or scratches in the surface of the platens were observed when the frictionless platens were used.

### 4.3.6 Pore Pressure Measurements under Transient Loading Conditions

The pore pressure measurements during the undrained compression tests using the conventional and frictionless loading platens are compared in Figure 4.10 for the range of strain rates tested. Using the conventional platens, there is no evidence of pore pressure gradients or time lag of pore pressure measurements up to the maximum strain rate of 7.4 x $10^{-2}$ $s^{-1}$. A slight time lag of pore pressure measurement within the specimens at the strain rate of 2.4 $s^{-1}$ is noted using the shorter specimens and the frictionless platens. The time lag is indicative of pore pressure gradients within the specimens. It is therefore concluded that the use of the shorter specimens and the frictionless platens does not negate pore pressure gradients in Ottawa sand significantly beyond the strain rate of 0.27 $s^{-1}$ reported by Healy(1963).

### 4.3.7 Influence of Strain Rate on Undrained Strength

The conditions at the ultimate strength and maximum stress ratio for Test Series C are plotted against the strain rate of testing in Figures 4.11. The maximum stress ratio appears to be largely unaffected by strain rate. Between the strain rates of $10^{-5}$ and $10^{-1}$ $s^{-1}$, a modest increase of about 10 percent in the ultimate strength is gained irrespective of the loading platens used. Work by other researchers presented in Section 2.8 show similar gains in strength of sands over the same range of strain rate. Noticeably higher ultimate strengths were found for test specimens OS-11 and OS-18A at the strain rate of 2.5 $s^{-1}$. The reason for the higher strength is primarily the prevention of pre-mature cavitation of the pore pressure by use of higher initial back pressures as already discussed. A portion of the additional strength may presumably also be derived from the resistance of the flow of the pore water, as indicated by the pore pressure gradients within the specimens at these strain rates.

The strain and pore pressure response at the ultimate strength using the conventional platens was largely unchanged by the strain rate which is consistent with the small increase in strength. A much wider variation in the A parameter and strains was found using the frictionless platens. The scatter in the test data even at the same strain rate suggests that the variation is due to statistical variation in the density and manufacture of the test specimens rather than a physical phenomena. The larger strains observed at the strain rate of 2.5 $s^{-1}$ are caused by the higher initial pore pressures used to prevent cavitation of the pore fluid in these specimens. Failure is prolonged by further decreases in the pore pressure with dilation until the critical confining pressure is reached.

### 4.3.8 Summary

In summary, this series of tests has shown the following:

1) Representative measurements of strength and pore pressure response in undrained triaxial compression tests on dense sand can be made on specimens with l/d as low as 0.5 if properly designed frictionless loading platens are employed. Axial strains are found to increase with lower l/d ratios due to the change from a local mobilization of shear strain to a condition of general shear.
2) The test facility can perform undrained triaxial tests at elevated pressures with accurate measurements of strength and strain for strain rates up to 2.5 $s^{-1}$. Measurements of the pore pressures in dense sand specimens cannot be made at strain rates much greater than $10^{-1}$ $s^{-1}$ due to the pore pressure gradients established within the specimens.
4) Test results at the static and transient strain rates are in agreement with work of other researchers.

## 4.4 Triaxial Testing of Saline Creek Oil Sand

### 4.4.1 Introduction

Undrained triaxial compression tests on Saline Creek oil sand were conducted in the high pressure triaxial test apparatus at initial effective confining pressures of 1, 2, 5 and 8 MPa. An almost six order of magnitude range of strain rate between $10^{-5}$ and 3.5 $s^{-1}$ was covered in the test program to investigate the behaviour under transient loading. Tests at strain rates greater than $10^{-4}$ $s^{-1}$ were conducted on specimens with l/d ratios of 0.5. The frictionless loading platens described in Section 4.2.3 were used to negate the effects of frictional end restraint. Tests using conventional loading platens and specimens with l/d of 2 were also conducted at each confining pressure at the slowest strain rate of $10^{-5}$ $s^{-1}$ to verify the effectiveness of the frictionless loading platens.

### 4.4.2 Sampling and Sample Preparation

The majority of the samples used in the testing program were cored during February 1984 from the oil sand outcrop in the Saline Creek valley wall, approximately 1 km south of Fort McMurray, Alberta. Two test specimens (SC-83-22D and SC-83-22U) were taken from the same location during February 1983 in a previous coring program. The coring equipment and technique is described in detail in Agar(1984). The retrieved frozen cores were double wrapped in plastic and shipped to Edmonton in a portable electric freezer. Power for the freezer was supplied by a portable electric generator. The samples were stored in a climate controlled cold room at -20°C until testing.

The oil sand cores were pre-chilled in a styrofoam cooler packed with dry ice for at least 12 hours prior to trimming. The samples were sealed in a paint can to prevent permeation of carbon dioxide into the samples while chilling in the dry ice. The specimens were trimmed in the cold room to the final 38.1 mm diameter on a lathe using a diamond tipped trimming bit. The samples were cut to the desired length in a diamond saw. The specimens were then re-mounted in the lathe to finish the ends at right angles to the cylindrical axis. Initial trimming of the samples was performed in 0.250 to 0.375 mm cuts. Final trimming and finishing cuts were performed in 0.050 to 0.100 mm cuts to ensure a smooth surface and prevent chipping of the edges.

The initial diameter of the cores were 50 and 64 mm. The 64 mm diameter cores were trimmed in two stages to the final test diameter. The specimens were re-cooled in dry ice for at least 15 minutes between stages. Otherwise, the specimens were found to expand from the heat generated by the bit during trimming.

The specimens were chilled in the dry ice until mounting in the triaxial cell. The base and top loading platen of the cell were also chilled in dry ice for a minimum of 15 minutes before the specimens were installed. Three 0.39 mm thick latex membranes were used to confine the specimens. A confining pressure of 500 kPa was applied to the specimens immediately upon completion of the cell assemblage.

The mounting procedures were carried out at room temperature. The time from start of specimen mounting to the application of the confining pressure was generally kept to about 5 minutes and not more than 10 minutes. No thaw of the samples was visibly noticeable in this time period.

### 4.4.3 Index Testing

A 100-200 gram intact chunk of the oil sand was retained from each core during the lathing of the test specimens. The quantities of bitumen and water occupying the pore spaces in the sample were determined by soxhlet refluxing. The technique used is described by Agar(1984) and will not be repeated here.

The weight of each test specimen was measured immediately after completion of lathing. At the same time, the diameter and height of the specimen was determined by making precise caliper measurements. The initial bulk density of the specimens were calculated from these measurements.

Knowing the bulk density, water content, bitumen content, and density of the mineral grains; the dry density, porosity and saturation were also calculated. A density of 2.65 $Mg/m^3$ was assumed for the sand grains which are primarily quartzose. The bitumen was assumed to have a density of 1.03 $Mg/m^3$ at room temperature and atmospheric pressure. Table 4.3 is a summary of the specimen data.

The disturbance index, $I_D$ calculated from Equation 3.1 is listed in Table 4.3 for all samples tested. Since borehole geophysical data is not available, an average in situ porosity value of 0.33 was used. This is consistent with the in situ densities reported for the Saline Creek Tunnel project (Smith et al, 1978).

Mechanical grain size analysis of each soxhlet extraction sample was conducted according to the procedure outlined in American Society for Testing and Materials ASTM D422-72 "Particle Size Analysis of Soils". It should be noted that a small portion of fine silt and clay size particles are absorbed by the filter bag during the soxhlet process. The grain size curves for each core are contained in Appendix C. The grain size data are summarized in Table 4.4.

The Saline Creek oil sand consists of a fine to medium grained uniform sand. The fines content is quite small, ranging between 1.3 and 5.1 percent by weight. X-ray diffraction analyses by Agar(1984) indicate the sand grains are predominantly silica (quartz). Scanning electron microscope studies also conducted by Agar show the sand grains in the undisturbed state to be interlocked with concavo-convex grain contacts due to pressure solution and authigenic overgrowth as described by Dusseault(1977) and Barnes(1980).

The bitumen and water contents range between 9.4-17.8 and 1.2-7.6 percent, respectively, with average contents of 14.9 and 2.8 percent. Agar(1984) reports bitumen and water contents for 27 samples of Saline Creek oil sand which similarily average 17.3 and 2.8 percent. The bedding of the deposit is highlighted by the occasional seams of very rich oil sand. The bedding is inclined approximately 30° to the axis of the core. This is caused by coring at an angle into the valley wall of Saline Creek which is inclined about 60° to horizontal. Occassional thin (less than 1 mm thick) partings of silt are present. The triaxial test specimens were trimmed between these partings to prevent the partings from acting as potentially weak failure planes.

### 4.4.4 Saturation of the Test Specimens

Entrapped gas bubbles in the pore system can significantly influence the pore pressure response in undrained tests because of the relatively high compressibility of the gases. Consequently, it was deemed necessary that two criteria be established for the undrained triaxial compression tests:

1) The test specimens must be saturated; and
2) The pore pressures during testing should not fall below the pore saturation pressure or bubble point to prevent cavitation of the pore fluid.

The method described by Wissa(1969) was adopted to evaluate the degree of saturation of the specimens. The method is base on the observation that the pore pressure parameter B increases with pore pressure until the pore fluid saturation pressure is reached. All gas is dissolved into solution and the magnitude of B remains constant with further increases in the pore pressure. The test procedure adopted from these observations is as follows:

1) With the pore pressure port to the cell closed, an increment of isotropic confining stress (usually 500 - 1000 kPa) is applied to the specimen and the pore pressure response measured and the value of B calculated;
2) The pore pressure port is then opened and the pore pressure increased to restore the initial confining

pressure;

3) Steps (1) and (2) are then repeated at the new pore pressure. Incremental B-tests are conducted until the value of B becomes constant.

The pore fluid saturation pressure and the value of the pore pressure parameter B at saturation can be found graphically as shown in Figure 4.12. For the specimens subjected to isotropic compressibility tests as described in the next section, a series of B-tests were carried out at several pore pressures after to re-assess the conditions of saturation. The results of the B-tests are given in Appendix C. The pore fluid saturation pressures and pore pressure parameter B are summarized in Table 4.5.

The pore fluid saturation pressure estimated from the initial B-tests varies over a broad range between 1.0 and 7.5 MPa. In theory, the gas saturation pressure of saturated Saline Creek oil sand cored immediately at the ground surface should be equivalent to the atmospheric or zero gauge pressure. Since the test specimens were not initially saturated ($S_i$ = 76.9 - 99.3 percent), either in situ or by sample disturbance, a pore pressure is necessary to dissolve the gases into the pore fluid. Based on measurements by Peacock(1986) for rich oil sand cored from depth, the pore fluid saturation pressure should nominally be less than 650 kPa.

The discrepancy between the measurements is attributed to the relatively rapid rate at which the initial B-tests are conducted. As presented in Section 4.3.4, Black and Lee(1973) show the time for complete saturation is exponentially proportional to the inverse of the applied pore pressure. The rapid application of increments of pore pressure during the initial B-tests therefore underpredicts the value of B at lower pore pressures due to the time required for the interstitial gases to dissolve into the pore fluid. Hence, higher apparent saturation pressures are observed as higher pore pressures drive the gases into solution faster.

This behaviour was verified by re-checking the conditions of saturation following the cyclic compression of the test specimens. From the data presented in Appendix C, the apparent saturation pressure fell between 1.0 and 2.0 MPa for all test specimens. Lower pressures may have been observed if B-tests were conducted at pore pressures below 1.0 MPa.

The variation of the pore pressure parameter B with the effective confining pressure at test is shown in Figure 4.13. There is an obvious trend for the magnitude of B to decrease with higher confining pressures which is shown in the next section to mirror the decrease in compressibility of the sand grain structure at higher stresses. Overall, there is virtually no difference between the measurements using the conventional platens and the frictionless platens with shorter specimens as noted for the Ottawa sand. This indicates the compressibility of the rubber membranes in the frictionless platens adds very little to the compressibility of the combined oil sand-membrane system as a whole. Also, there is minor difference in B between specimens for $I_D$ less than and greater than 10 percent. In this respect, the isotropic compression of the specimens to 5.0 MPa, as described in the next section, appears to overcome small disturbances in the compressibility of the oil sand.

### 4.4.5 Isotropic Compressibility

Isotropic compressibility tests were conducted on the first nineteen specimens tested. The purpose of the cyclic compression of the specimens was to re-compact the samples to the undisturbed density and measure the coefficient of volume compressibility as an index of sample quality. The effective confining stress applied to the specimens was raised by increasing the cell pressure and keeping the pore pressure constant. Changes in the pore fluid volume were recorded by the volume change indicator attached to the pore fluid pressure line. The effective confining pressure was cycled three times between approximately 700 and 5000 kPa. Increments of pressure were generally 500 to 1000 kPa. The coefficient of volume compressibility measured on each loading cycle of the tests are summarized in Table 4.6.

It was evident from the isotropic compression test results in Table 4.6 that changes in compressibility in the second and third loading cycles is minor suggesting the majority of re-compaction of the specimens is largely completed in the first loading cycle to 5 MPa. Subsequently, the remaining test specimens were thawed and consolidated at an effective confining pressure of 5 MPa prior to triaxial testing in lieu of cyclic compression of the test specimens.

The isotropic compressibility over the range of confining stress of 2 to 4 MPa varies between 0.88 x $10^{-6}$ and 2.36 x $10^{-6}$ $kPa^{-1}$ on the last loading cycle. Measurements of isotropic compressibility of Athabasca oil sand by other researchers vary between 0.25 x $10^{-6}$ and 4.4 x $10^{-6}$ $kPa^{-1}$ (Au, 1984). Dusseault(1981) and Agar(1984) conducted cyclic compressibility tests and report volume compressibilities between 0.25 x $10^{-6}$ and 0.79 x $10^{-6}$ $kPa^{-1}$ on the last loading cycle. These latter values are lower than measured in this report. However, the stress levels covered by Dusseault (2.76 - 13.3 MPa) and Agar(4 - 25 MPa) are far higher.

The variation of the compressibility of the Saline Creek oil sand on the final loading cycle is plotted against the effective confining pressure in Figure 4.14. The coefficient of volume compressibility is a stress dependent function, decreasing up to 10 times in magnitude between 0.5

and 5.0 MPa. The compressibility at stresses between 4 and 5 MPa ranges between $0.37 \times 10^{-6}$ and $2.47 \times 10^{-6}$ $kPa^{-1}$ with a mean of $0.96 \times 10^{-6}$ $kPa^{-1}$. The measurements by Agar(1984) for Saline Creek oil sand are in agreement at the same stress levels. The compressibility of oil sand should then be expressed according to the confining stress rather than a broad range of stress, especially at stress levels less than 5 MPa where the relation is distinctly non-linear.

### 4.4.6 Undrained Triaxial Compression Tests

Undrained triaxial compression tests were performed on each specimen. The tests were conducted at nominal initial effective confining pressures of 1, 2, 5 and 8 MPa to evaluate the behaviour over a range of stress levels. Strain rates over the range between $10^{-5}$ and 3.5 $s^{-1}$ were also covered.

Initially, three tests (SC-83-22U, SC-84-22 and SC-84-39)were conducted to measure the magnitude of the pore pressure decrease to be expected during undrained loading. These specimens were 50 mm diameter with l/d = 2 and conventional steel loading platens were used. The tests were conducted at initial confining pressures of 2.03, 1.81 and 0.08 MPa, respectively, and a static strain rate of $10^{-5}$ $s^{-1}$. Initial pore pressures of 1.52, 11.46 and 4.46 MPa were used. The pore pressures at failure dropped to 0.22, 7.67, and 0.59 MPa. Cavitation of the pore fluid likely occurred for SC-83-22U and SC-84-39. A minimum initial pore pressure of 4 MPa above the pore fluid saturation pressure appeared to be required to prevent cavitation. A minimum initial pore pressure of 6 MPa was subsequently used for all remaining tests to keep well above the pore fluid saturation pressure. The pore fluid saturation pressures reported in Table 4.5 were not reached during any subsequent undrained compression tests.

Measurements of the axial deformation, axial load, confining pressure and pore pressure were recorded continuously throughout the tests. Measurements and observations of the specimens on completion of testing were noted. The test results are presented in Appendix C and summarized in Table 4.7.

A compliance test to evaluate the effect of the rubber membranes in the frictionless platens on the measurement of axial deformations during the axial compression tests was repeated in the manner outlined in Section 4.2.4.1. In this case, the steel disk was isotropically consolidated to 5 MPa prior to conducting the test. The results of the test are shown in Figure A.5. The calculated vertical compressibility of the membranes is 9.93 x $10^{-3}$ mm/kN. This correction factor was been applied to the test results. The magnitude of the correction factor is slightly less than that measured in Section 4.2.4.1 and reflects the somewhat improved seating of the samples against the frictionless platens with the isotropic compression to 5 MPa.

### 4.4.7 Pore Pressure Measurements under Transient Loading

The pore pressure measurements during the undrained triaxial compression tests at initial confining pressures of 2 and 5 MPa are compared at strain rates between $10^{-5}$ and $10^{0}$ $s^{-1}$ in Figure 4.15. At both confining pressures, an apparent time lag in pore pressure measurement begins at the strain rate of $10^{-2}$ $s^{-1}$. At strain rates greater than $10^{0}$ $s^{-1}$, pore pressure measurements are virtually redundant under the high pore pressure gradients established within the specimens. Pore pressure measurements at strain rates greater than $10^{-2}$ $s^{-1}$ cannot be considered representative of the pore pressure conditions in the test specimens and are excluded from Table 4.7.

In comparison to the tests on Ottawa sand, the initiation of the pore pressure gradients in the oil sand occurs at strain rates approximately two orders of magnitude lower. Bishop and Henkel(1963) show the time required for adequate dissipation of pore pressure gradients during undrained compression tests is proportional to the inverse of the coefficient of consolidation, $C_v$. Inversely, the allowable strain rate is then directly proportional to $C_v$:

$$\dot{\epsilon}_{allowable} \propto C_v \qquad 4.10$$

The coefficient of consolidation, $C_v$ is defined as the ratio of the fluid mobility, $k/\mu$ to the compressibility of the soil skeleton, $m_v$:

$$C_v = \frac{k/\mu}{m_v} \qquad 4.11$$

Hence,

$$\dot{\varepsilon}_{allowable} \propto \frac{k/\mu}{m_v} \qquad 4.12$$

Agar(1984) shows the coefficient of consolidation of undisturbed bitumen-rich Saline Creek oil sand ranges between 100 to 200 times less than water saturated bitumen-extracted Saline Creek oil sand. The allowable strain rate for bitumen-rich oil sand is therefore approximately two orders of magnitude less than water saturated oil sand. This also agrees with the difference in allowable strain rates observed between the Ottawa sand and Saline Creek oil sand. It is then apparent that the onset of time lag in dissipation of excess pore pressures at slower strain rates in the Saline Creek oil sand is caused by the viscosity of the interstitial bitumen.

### 4.4.8 Assessment of Grain Crushing during Testing

Grain shearing and crushing will occur under the high effective stresses achieved during fully undrained compression tests. It was also recognized that greater grain crushing could occur under the conditions of general shear using the frictionless platens. The crushing of the sand grains may also be a time dependent process as thought by Lee, Seed and Dunlop(1969) and grain crushing could be suppressed at higher strain rates.

To assess the influence of initial confining stress, loading platens and strain rate, a careful series of grain size analyses before and after testing was conducted on selected specimens. The results of the grain size analyses are presented in Appendix D and summarized in Table 4.8. It is noted that the short specimens (l/d = 0.5) using the frictionless platens were combined at the same initial confining stress and strain rate to enable a more accurate grain size analyses on a larger mass. The initial grain size distributions were accordingly taken as the average between the samples in Table 4.4.

Sample SC-84-110 was isotropically consolidated to a confining pressure of 5 MPa only. Virtually no grain crushing occurred from the application of isotropic stress as indicated by the negligible generation of additional fines or alteration of the grain size distribution in Figure D.1. Agar(1984) also reports only very minor fines generation in test specimens of Saline Creek oil sand isotropically consolidated up to 25 MPa. Isotropic stress alone therefore does not contribute significantly to grain crushing of Saline Creek oil sand.

Among the test specimens subjected to undrained compression tests at "static" strain rates less than $10^{-2}$ $s^{-1}$, grain crushing has generated between 4.4 and 7.0 percent additional fines in the samples. Overall, there does not appear to be any relationship between the amount of grain crushing and the initial confining pressure. In Figure 4.16, there is a trend for the amount of fines generation to increase with the effective confining stress at failure. The degree of grain crushing is then not so much a function of the initial confining stress as the effective confining stress reached at failure. The amount of fines generation for the short specimens using the frictionless platens is greater than conventional specimens over the range of stresses shown. It appears that the degree of grain crushing is increased by more uniform shear straining that occurs using the shorter specimens and the frictionless platens.

The grain size distribution of three sets of specimens (SC-84-31/43, SC-84-49/53 and SC-84-23/55A/55B) at the highest strain rate of $10^{0}$ $s^{-1}$ were measured at initial confining pressures of 1,2 and 5 MPa. Due to the pore pressure gradients established in the specimens at strain rates greater than $10^{-2}$ $s^{-1}$, it is not possible to correlate the amount of fines generation with the effective confining stress at failure. The amount of fines generation, ranging between 4.9 and 7.2 percent, is consistent with the tests at slower strain rates.

## 4.5 Summary

This chapter describes the test equipment and experimental procedures followed for the undrained triaxial compression tests conducted on Saline Creek oil sand. The undrained behaviour under axial compression loading was determined for confining stresses up to 8 MPa and strain rates between $10^{-5}$ and 3.5 $s^{-1}$. Supplementary test procedures were performed to measure drained and undrained compressibility and evaluate grain alteration during testing.

A preliminary series of undrained triaxial compression tests were conducted on dense Ottawa sand to evaluate the performance of a set of frictionless loading platens using varied specimen aspect ratios and strain rates up to 2.5 $s^{-1}$. This series of tests showed that representative measurements of strength and pore pressure response in undrained triaxial compression tests can be made on specimens with l/d as low as 0.5 utilizing the frictionless loading platens described in this chapter. The frictionless loading platens were adopted in conjunction with short specimens (l/d = 0.5) of Saline Creek oil sand to attempt to eliminate pore pressure gradients developed within the oil sand during undrained triaxial compression tests at strain rates greater than $10^{-4}$ $s^{-1}$.

Table 4.1 Ottawa Sand: Summary of Specimen Data

| SAMPLE | DIAMETER D (mm) | LENGTH L (mm) | INITIAL DENSITY $\gamma$ (Mg/m$^3$) | POROSITY n |
|---|---|---|---|---|
| OS-S1 | 37.97 | 19.58 | 2.061 | - |
| OS-S2 | 38.13 | 56.93 | 2.056 | - |
| OS-S3 | 38.07 | 77.23 | 2.059 | - |
| OS-S4 | 38.10 | 38.57 | 2.047 | - |
| OS-1A | 38.12 | 20.75 | 2.000 | 0.377 |
| OS-1B | 38.15 | 38.60 | 2.056 | 0.336 |
| OS-2A | 38.10 | 19.37 | 2.000 | 0.352 |
| OS-3B | 38.13 | 19.08 | 2.006 | 0.363 |
| OS-4 | 38.17 | 38.37 | 2.036 | 0.348 |
| OS-5 | 38.20 | 38.25 | 2.039 | 0.364 |
| OS-6A | 38.18 | 20.27 | 2.039 | 0.347 |
| OS-6B | 38.10 | 19.68 | 1.994 | 0.361 |
| OS-7A | 38.06 | 19.32 | 1.998 | 0.374 |
| OS-7B | 38.05 | 17.28 | 2.014 | 0.366 |
| OS-8A | 38.04 | 19.28 | 2.004 | 0.360 |
| OS-8B | 38.10 | 19.30 | 2.014 | 0.356 |
| OS-11 | 37.76 | 19.08 | 1.959 | - |
| OS-12 | 38.07 | 72.13 | 2.058 | - |
| OS-13 | 38.18 | 73.98 | 2.045 | - |
| OS-14 | 38.07 | 76.32 | 2.061 | - |
| OS-15A | 38.14 | 19.72 | 2.022 | - |
| OS-16A | 38.19 | 19.30 | 2.014 | - |
| OS-18A | 38.73 | 19.93 | 1.936 | - |
| OS-19A | 38.07 | 76.42 | 2.049 | - |
| OS-19B | 37.98 | 19.30 | 2.021 | - |
| OS-21 | 38.05 | 71.57 | 2.055 | - |
| OS-22 | 37.93 | 19.30 | 2.018 | - |

Table 4.2 Ottawa Sand: Summary of Triaxial Test Results

| SAMPLE | L/D | LOADING PLATENS | STRAIN RATE $\dot{\varepsilon}$ ($s^{-1}$) | INITIAL TEST CONDITIONS | | | CONDITIONS AT MAXIMUM STRESS RATIO | | | | | | CONDITIONS AT MAXIMUM STRENGTH | | | | |
|---|---|---|---|---|---|---|---|---|---|---|---|---|---|---|---|---|---|
| | | | | B | $\sigma_{3i}'$ (MPa) | $u_i$ (MPa) | $\sigma_1'/\sigma_3'$ | $(\sigma_1-\sigma_3)$ (MPa) | $\sigma_3$ (MPa) | u (MPa) | $\varepsilon$ (%) | A | $(\sigma_1-\sigma_3)_f$ (MPa) | $\sigma_{3f}$ (MPa) | $u_f$ (MPa) | $\varepsilon_f$ (%) | $A_f$ |
| OS-S1 | 0.52 | 1* | $6.4\times10^{-3}$ | (0.85)** | 2.03 | 4.64 | 8.7 | 9.33 | 6.67 | 5.45 | 4.4 | 0.10 | 23.41 | 6.62 | 1.93 | 13.1 | -0.14 |
| OS-S2 | 1.49 | 1 | $7.7\times10^{-3}$ | (0.85) | 2.14 | 4.71 | 4.0 | 10.16 | 6.88 | 3.49 | 3.0 | -0.14 | 18.03 | 6.88 | -0.01 | 6.3 | -0.31 |
| OS-S3 | 2.03 | 1 | $8.5\times10^{-3}$ | (0.85) | 2.29 | 4.63 | 3.8 | 7.33 | 6.95 | 4.32 | 2.8 | -0.05 | 16.54 | 6.95 | -0.04 | 7.0 | -0.33 |
| OS-S4 | 1.01 | 1 | $8.1\times10^{-3}$ | (0.85) | 2.26 | 4.66 | 4.1 | 6.89 | 6.92 | 4.69 | 3.6 | 0.01 | 16.29 | 6.92 | 0.43 | 9.9 | -0.31 |
| OS-1A | 0.54 | 1 | $9.0\times10^{-3}$ | (0.85) | 1.98 | 4.76 | 6.5 | 12.66 | 6.74 | 4.42 | 4.9 | -0.04 | 19.17 | 6.74 | 2.41 | 13.4 | -0.14 |
| OS-1B | 1.01 | 1 | $8.9\times10^{-3}$ | (0.85) | 2.13 | 4.72 | 4.2 | 11.80 | 6.85 | 3.44 | 4.3 | -0.14 | 16.26 | 6.85 | 0.98 | 7.8 | -0.27 |
| OS-2A | 0.51 | 1 | $8.3\times10^{-3}$ | (0.85) | 2.04 | 4.72 | 6.8 | 12.92 | 6.74 | 4.50 | 6.6 | -0.02 | 18.97 | 6.74 | 2.98 | 14.9 | -0.11 |
| OS-3B | 0.50 | 3 | $8.8\times10^{-3}$ | (0.85) | 2.06 | 4.77 | 3.1 | 8.24 | 6.83 | 2.88 | 7.9 | -0.27 | 12.86 | 6.83 | 0.22 | 16.2 | -0.42 |
| OS-4 | 1.00 | 3 | $8.9\times10^{-3}$ | 0.91 | 2.01 | 4.89 | 3.5 | 9.47 | 6.90 | 3.10 | 5.5 | -0.21 | 15.50 | 6.88 | 0.19 | 10.4 | -0.33 |
| OS-5 | 1.00 | 3 | $8.8\times10^{-3}$ | 0.88 | 1.90 | 4.65 | 3.6 | 9.74 | 6.55 | 2.76 | 5.0 | -0.22 | 15.60 | 6.55 | 0.06 | 9.0 | -0.33 |
| OS-6A | 0.53 | 3 | $8.7\times10^{-3}$ | 0.84 | 2.14 | 4.76 | 3.3 | 9.94 | 6.90 | 2.48 | 6.1 | -0.27 | 15.40 | 6.90 | 0.23 | 10.5 | -0.35 |
| OS-6B | 0.52 | 3 | $1.1\times10^{-4}$ | 0.82 | 1.84 | 4.83 | 3.1 | 8.06 | 6.62 | 2.69 | 5.5 | -0.32 | 12.96 | 6.58 | 0.23 | 12.8 | -0.43 |
| OS-7A | 0.51 | 3 | $1.1\times10^{-1}$ | 0.79 | 2.06 | 4.72 | 3.1 | 12.25 | 6.78 | 1.03 | 7.8 | -0.38 | 13.90 | 6.78 | 0.28 | 13.3 | -0.40 |
| OS-7B | 0.45 | 3 | $1.6\times10^{-5}$ | 0.84 | 1.84 | 4.83 | 3.4 | 5.93 | 6.67 | 4.20 | 4.7 | -0.13 | 14.37 | 6.67 | 0.46 | 12.3 | -0.36 |
| OS-8A | 0.51 | 3 | $8.6\times10^{-3}$ | 0.86 | 1.78 | 4.80 | 3.3 | 13.83 | 6.60 | 0.51 | 8.8 | -0.36 | 14.58 | 6.60 | 0.28 | 10.4 | -0.36 |
| OS-8B | 0.51 | 2 | $8.5\times10^{-3}$ | 0.74 | 2.11 | 4.86 | 9.8 | 14.27 | 6.97 | 5.35 | 2.2 | 0.05 | 25.69 | 6.97 | 2.51 | 8.2 | -0.12 |
| OS-11 | 0.51 | 3 | $2.4\times10^{0}$ | 0.83 | 2.26 | 9.92 | 3.6 | 8.53 | 12.20 | 8.90 | 6.4 | -0.14 | 21.02 | 12.20 | 3.29 | 18.8 | -0.38 |
| OS-12 | 1.89 | 2 | $8.8\times10^{-3}$ | 0.83 | 2.06 | 4.72 | 3.7 | 11.31 | 6.81 | 2.62 | 3.6 | -0.22 | 16.35 | 6.85 | 0.33 | 6.3 | -0.32 |
| OS-13 | 1.94 | 3 | $8.7\times10^{-3}$ | 0.90 | 2.20 | 4.72 | 3.6 | 7.92 | 6.95 | 3.85 | 2.9 | -0.12 | 13.99 | 6.99 | 0.68 | 6.2 | -0.32 |
| OS-14 | 2.01 | 2 | $1.1\times10^{-4}$ | 0.90 | 2.06 | 4.93 | 3.8 | 8.87 | 6.90 | 3.68 | 2.9 | -0.16 | 16.17 | 6.76 | 0.28 | 7.0 | -0.32 |
| OS-15A | 0.52 | 3 | $1.1\times10^{-1}$ | 0.90 | 2.15 | 4.75 | 3.5 | 16.01 | 6.90 | 0.55 | 7.3 | -0.29 | 16.01 | 6.90 | 0.55 | 7.3 | -0.29 |
| OS-16A | 0.51 | 3 | $1.1\times10^{-4}$ | 0.84 | 2.07 | 4.83 | 3.2 | 13.32 | 6.85 | 0.62 | 7.6 | -0.38 | 14.05 | 6.81 | 0.14 | 10.2 | -0.40 |
| OS-18A | 0.53 | 3 | $3.1\times10^{0}$ | 0.83 | 2.14 | 10.17 | 3.5 | 10.92 | 12.31 | 7.90 | 7.7 | -0.25 | 16.83 | 12.31 | 4.71 | 15.9 | -0.39 |
| OS-19A | 2.01 | 2 | $7.4\times10^{-2}$ | 0.89 | 2.13 | 5.40 | 4.2 | 5.38 | 7.48 | 5.80 | 1.5 | 0.08 | 17.85 | 7.48 | 0.48 | 6.6 | -0.31 |
| OS-19B | 0.51 | 3 | $1.5\times10^{-5}$ | 0.79 | 1.95 | 4.79 | 3.4 | 7.47 | 6.74 | 3.57 | 4.9 | -0.21 | 13.91 | 6.74 | 0.41 | 10.4 | -0.40 |
| OS-21 | 1.88 | 2 | $1.6\times10^{-5}$ | 0.90 | 1.93 | 4.79 | 4.0 | 7.52 | 6.72 | 4.21 | 2.4 | -0.09 | 15.84 | 6.72 | 0.44 | 7.6 | -0.31 |
| OS-22 | 0.51 | 3 | $9.2\times10^{-3}$ | 0.82 | 2.11 | 4.71 | 3.4 | 16.14 | 6.90 | 0.00 | 7.5 | -0.36 | 16.14 | 6.90 | 0.00 | 7.5 | -0.36 |

* (1) Conventional 38.1 mm diameter loading platens
(2) Enlarged 43.2 mm diameter loading platens
(3) Enlarged 43.2 mm diameter loading platens with frictionless end preparations

** The average value of B of 0.85 assumed for these samples

# Table 4.3 Saline Creek Oil Sand: Summary of Specimen Data

| SAMPLE | DIAMETER $D$ (mm) | LENGTH $L$ (mm) | INITIAL DENSITY $\gamma$ (Mg/m$^3$) | INITIAL POROSITY $n_i$ | INITIAL SATURATION $S_i$ (%) | WATER CONTENT $w_w$ (%)* | BITUMEN CONTENT $w_b$ (%)* | DISTURBANCE INDEX $I_D$ (%)** |
|---|---|---|---|---|---|---|---|---|
| SC-83-22D | 50.86 | 101.70 | 1.989 | 0.360 | 79.1 | 1.3 | 13.4 | 9.1 |
| SC-83-22U | 50.80 | 102.24 | 2.012 | 0.352 | 81.8 | 1.6 | 13.1 | 6.7 |
| SC-84-1 | 38.69 | 19.49 | 2.018 | 0.364 | 89.0 | 1.7 | 14.8 | 10.3 |
| SC-84-3A | 38.45 | 19.33 | 2.002 | 0.383 | 93.5 | 2.6 | 15.8 | 16.1 |
| SC-84-3B | 38.44 | 19.35 | 1.994 | 0.386 | 92.5 | 2.6 | 15.8 | 17.0 |
| SC-84-4A | 38.27 | 20.03 | 1.970 | 0.399 | 92.2 | 3.2 | 15.9 | 20.9 |
| SC-84-4B | 38.27 | 18.20 | 1.969 | 0.399 | 92.1 | 3.2 | 15.9 | 20.9 |
| SC-84-5A | 38.31 | 19.43 | 2.002 | 0.375 | 90.1 | 3.3 | 14.0 | 13.6 |
| SC-84-5B | 38.35 | 19.63 | 1.952 | 0.391 | 84.4 | 3.3 | 14.0 | 18.5 |
| SC-84-8A | 38.33 | 20.07 | 1.985 | 0.360 | 78.1 | 2.0 | 12.6 | 9.1 |
| SC-84-8B | 38.28 | 19.35 | 1.974 | 0.363 | 76.9 | 2.0 | 12.6 | 10.0 |
| SC-84-10 | 38.75 | 75.25 | 2.006 | 0.361 | 85.4 | 3.6 | 12.2 | 9.4 |
| SC-84-13 | 38.50 | 18.68 | 2.015 | 0.371 | 91.6 | 2.1 | 15.2 | 12.4 |
| SC-84-14A | 38.00 | 18.81 | 1.966 | 0.396 | 91.9 | 5.1 | 13.4 | 20.0 |
| SC-84-14B | 38.10 | 18.51 | 1.941 | 0.403 | 89.2 | 5.1 | 13.4 | 22.1 |
| SC-84-15A | 37.95 | 17.36 | 2.021 | 0.373 | 93.4 | 1.2 | 16.5 | 13.0 |
| SC-84-15B | 37.95 | 18.78 | 1.985 | 0.384 | 89.1 | 1.2 | 16.5 | 16.4 |
| SC-84-17 | 38.22 | 77.40 | 1.966 | 0.393 | 88.6 | 2.1 | 16.1 | 19.1 |
| SC-84-22 | 50.95 | 102.50 | 2.035 | 0.362 | 92.7 | 2.8 | 14.1 | 9.7 |
| SC-84-23 | 38.50 | 21.70 | 1.986 | 0.395 | 93.7 | 3.3 | 15.8 | 19.7 |
| SC-84-24 | 38.20 | 20.72 | 1.956 | 0.408 | 91.5 | 3.5 | 16.2 | 23.6 |
| SC-84-25A | 38.00 | 21.72 | 2.005 | 0.370 | 88.3 | 3.8 | 12.9 | 12.1 |
| SC-84-25B | 38.00 | 19.85 | 2.000 | 0.371 | 87.8 | 3.8 | 12.9 | 12.4 |
| SC-84-29 | 38.40 | 20.73 | 1.929 | 0.394 | 80.1 | 2.0 | 14.8 | 19.4 |
| SC-84-30 | 38.23 | 76.93 | 1.934 | 0.401 | 84.4 | 4.0 | 13.9 | 21.5 |
| SC-84-31 | 38.65 | 17.40 | 1.930 | 0.408 | 86.3 | 2.3 | 16.4 | 23.6 |
| SC-84-33 | 38.70 | 19.94 | 2.005 | 0.377 | 91.6 | 3.9 | 13.7 | 14.2 |
| SC-84-34 | 38.50 | 67.51 | 2.061 | 0.352 | 95.4 | 1.9 | 14.8 | 6.7 |
| SC-84-39 | 50.98 | 102.10 | 2.034 | 0.364 | 94.0 | 1.4 | 15.8 | 10.3 |
| SC-84-40A | 39.00 | 18.83 | 1.964 | 0.395 | 89.1 | 2.6 | 15.8 | 19.7 |
| SC-84-40B | 38.95 | 20.53 | 1.987 | 0.388 | 91.7 | 2.6 | 15.8 | 17.6 |
| SC-84-43 | 38.45 | 19.78 | 1.953 | 0.411 | 94.0 | 2.7 | 17.4 | 24.1 |
| SC-84-49 | 38.50 | 19.30 | 1.890 | 0.411 | 78.6 | 3.1 | 14.4 | 24.5 |
| SC-84-51 | 38.47 | 20.16 | 1.947 | 0.401 | 87.3 | 1.6 | 16.9 | 21.5 |
| SC-84-52 | 38.55 | 19.68 | 2.027 | 0.339 | 79.7 | 4.2 | 9.4 | 2.7 |
| SC-84-53 | 38.52 | 19.75 | 1.947 | 0.416 | 93.5 | 2.7 | 17.8 | 26.1 |
| SC-84-55A | 38.65 | 18.19 | 1.964 | 0.398 | 90.1 | 2.4 | 16.3 | 20.6 |
| SC-84-55B | 38.63 | 20.98 | 1.999 | 0.387 | 94.3 | 2.4 | 16.3 | 17.3 |
| SC-84-60 | 38.80 | 19.11 | 1.974 | 0.384 | 86.6 | 2.0 | 15.3 | 16.4 |
| SC-84-110 | 38.20 | 52.73 | 1.976 | 0.385 | 88.4 | 3.2 | 14.3 | 16.7 |
| SC-84-115A | 38.58 | 19.91 | 1.959 | 0.392 | 86.0 | 2.2 | 15.5 | 18.8 |
| SC-84-115B | 38.50 | 14.28 | 1.948 | 0.395 | 85.1 | 2.2 | 15.5 | 19.7 |
| SC-84-117 | 38.51 | 19.45 | 1.997 | 0.384 | 93.7 | 2.9 | 15.7 | 16.4 |

* By total mass of sample

** $I_D = (n_i - 0.33)/(0.33) \times 100$

## Table 4.4 Saline Creek Oil Sand: Grain Size Data

| SAMPLE | GRAIN SIZE DATA<br>$D_{10}$ (mm) | $D_{50}$ (mm) | $D_{60}$ (mm) | UNIFORMITY COEFFICIENT $C_u = D_{60}/D_{10}$ | FINES CONTENT (%<0.074 mm) |
|---|---|---|---|---|---|
| SC-83-22U | 0.15 | 0.19 | 0.21 | 1.4 | 5.10 |
| SC-84-1 | 0.12 | 0.19 | 0.21 | 1.8 | 1.60 |
| SC-84-3A | 0.10 | 0.19 | 0.20 | 2.0 | 3.11 |
| SC-84-3B | 0.10 | 0.19 | 0.20 | 2.0 | 3.11 |
| SC-84-4A | 0.10 | 0.19 | 0.20 | 2.0 | 2.96 |
| SC-84-4B | 0.10 | 0.19 | 0.20 | 2.0 | 2.96 |
| SC-84-5A | 0.13 | 0.19 | 0.21 | 1.6 | 1.36 |
| SC-84-5B | 0.13 | 0.19 | 0.21 | 1.6 | 1.36 |
| SC-84-8A | 0.13 | 0.20 | 0.21 | 1.6 | 2.30 |
| SC-84-8B | 0.13 | 0.20 | 0.21 | 1.6 | 2.30 |
| SC[illegible]-10 | 0.13 | 0.20 | 0.21 | 1.6 | 2.07 |
| SC-84-13 | 0.13 | 0.20 | 0.21 | 1.6 | 2.56 |
| SC-84-14A | 0.13 | 0.19 | 0.21 | 1.6 | 1.80 |
| SC-84-14B | 0.13 | 0.19 | 0.21 | 1.6 | 1.80 |
| SC-84-15A | 0.11 | 0.19 | 0.20 | 1.8 | 2.13 |
| SC-84-15B | 0.11 | 0.19 | 0.20 | 1.8 | 2.13 |
| SC-84-17 | 0.11 | 0.19 | 0.21 | 1.9 | 3.75 |
| SC-84-22 | 0.12 | 0.19 | 0.20 | 1.7 | 1.71 |
| SC-84-23 | 0.14 | 0.23 | 0.25 | 1.8 | 1.81 |
| SC-84-24 | 0.15 | 0.23 | 0.26 | 1.7 | 1.27 |
| SC-84-25A | 0.12 | 0.19 | 0.21 | 1.8 | 3.11 |
| SC-84-25B | 0.12 | 0.19 | 0.21 | 1.8 | 3.11 |
| SC-84-29 | 0.11 | 0.19 | 0.20 | 1.8 | 2.02 |
| SC-84-30 | 0.12 | 0.20 | 0.21 | 1.8 | 2.28 |
| SC-84-31 | 0.13 | 0.19 | 0.20 | 1.5 | 2.40 |
| SC-84-33 | 0.12 | 0.19 | 0.21 | 1.8 | 1.81 |
| SC-84-34 | 0.14 | 0.20 | 0.21 | 1.5 | 1.45 |
| SC-84-40A | 0.10 | 0.18 | 0.20 | 2.0 | 3.54 |
| SC-84-40B | 0.10 | 0.18 | 0.20 | 2.0 | 3.54 |
| SC-84-43 | 0.10 | 0.19 | 0.20 | 2.0 | 3.02 |
| SC-84-49 | 0.11 | 0.19 | 0.20 | 1.8 | 1.77 |
| SC-84-51 | 0.11 | 0.20 | 0.22 | 2.0 | 3.25 |
| SC-84-52 | 0.12 | 0.19 | 0.21 | 1.6 | 1.71 |
| SC-84-53 | 0.11 | 0.19 | 0.20 | 1.9 | 3.36 |
| SC-84-55A | 0.10 | 0.18 | 0.20 | 2.0 | 3.77 |
| SC-84-55B | 0.10 | 0.18 | 0.20 | 2.0 | 3.77 |
| SC-84-60 | 0.13 | 0.19 | 0.21 | 1.6 | 2.33 |
| SC-84-110 | 0.15 | 0.24 | 0.28 | 1.9 | 1.87 |
| SC-84-115A | 0.12 | 0.19 | 0.21 | 1.8 | 3.23 |
| SC-84-115B | 0.12 | 0.19 | 0.21 | 1.8 | 3.23 |
| SC-84-117 | 0.13 | 0.20 | 0.21 | 1.6 | 2.93 |

# Table 4.5 Saline Creek Oil Sand: Summary of Pore Fluid Saturation Pressure and Pore Pressure Parameter B

| SAMPLE | NOMINAL DIAMETER | L/D | PORE FLUID SATURATION PRESSURE | PORE PRESSURE PARAMETER B | | | |
|---|---|---|---|---|---|---|---|
| | | | | AFTER INITIAL SATURATION | | AFTER CYCLIC COMPRESSION | |
| | D (mm) | | $P_s$ (MPa) | $\sigma_3'$ AT TEST (MPa) | B | $\sigma_3'$ AT TEST (MPa) | B |
| SC-83-22D | 50 | 2.00 | 1.2 | 0.14 | 0.91 | 2.2 | 0.60 |
| SC-83-22U | 50 | 2.01 | 1.2 | 0.05 | 0.94 | 2.1 | 0.64 |
| SC-84-1 | 38 | 0.50 | 4.4 | 5.0 | 0.50 | - | - |
| SC-84-3A | 38 | 0.50 | 3.5 | 0.5 | 0.87 | 2.2 | 0.69 |
| SC-84-3B | 38 | 0.50 | 3.2 | 0.5 | 0.86 | 2.3 | 0.65 |
| SC-84-4A | 38 | 0.52 | 3.0 | 0.4 | 0.86 | 2.2 | 0.68 |
| SC-84-4B | 38 | 0.48 | 2.0 | 0.4 | 0.88 | 2.2 | 0.70 |
| SC-84-5A | 38 | 0.51 | 3.3 | 0.6 | 0.85 | 2.2 | 0.66 |
| SC-84-5B | 38 | 0.51 | 3.0 | 0.5 | 0.79 | 2.2 | 0.66 |
| SC-84-8A | 38 | 0.52 | 3.5 | 0.5 | 0.87 | 2.0 | 0.68 |
| SC-84-8B | 38 | 0.51 | 3.4 | 0.5 | 0.77 | 2.3 | 0.64 |
| SC-84-10 | 38 | 1.94 | 3.5 | 1.0 | 0.87 | - | - |
| SC-84-13 | 38 | 0.49 | 4.7 | 1.0 | 0.79 | - | - |
| SC-84-14A | 38 | 0.50 | 6.2 | 5.0 | 0.68 | - | - |
| SC-84-14B | 38 | 0.49 | 3.1 | 1.0 | 0.84 | - | - |
| SC-84-15A | 38 | 0.46 | 3.2 | 0.7 | 0.85 | 2.2 | 0.68 |
| SC-84-15B | 38 | 0.49 | 3.0 | 0.8 | 0.87 | 3.4 | 0.72 |
| SC-84-17 | 38 | 2.03 | 2.5 | 0.4 | 0.90 | 1.8 | 0.82 |
| SC-84-22 | 50 | 2.00 | 1.1 | 0.07 | 1.00 | 2.9 | 0.75 |
| SC-84-23 | 38 | 0.56 | 2.4 | 0.5 | 0.87 | slow pore pressure response | |
| SC-84-24 | 38 | 0.54 | 2.2 | 0.3 | 0.90 | 2.2 | 0.82 |
| SC-84-25A | 38 | 0.57 | 2.5 | 0.4 | 0.84 | 2.0 | 0.61 |
| SC-84-25B | 38 | 0.52 | 3.3 | 0.3 | 0.88 | 2.4 | 0.62 |
| SC-84-29 | 38 | 0.54 | - | 8.0 | 0.49 | - | - |
| SC-84-30 | 38 | 2.01 | - | 8.0 | 0.49 | - | - |
| SC-84-31 | 38 | 0.45 | 4.5 | 1.0 | 0.85 | - | - |
| SC-84-33 | 38 | 0.51 | 4.2 | 5.0 | 0.54 | - | - |
| SC-84-34 | 38 | 1.75 | 4.1 | 5.0 | 0.65 | - | - |
| SC-84-39 | 50 | 2.00 | 1.1 | 0.15 | 0.90 | 2.1 | 0.76 |
| SC-84-40A | 38 | 0.48 | 4.4 | 5.0 | 0.62 | - | - |
| SC-84-40B | 38 | 0.53 | slow pore pressure response | | | | |
| SC-84-43 | 38 | 0.51 | slow pore pressure response | | | | |
| SC-84-49 | 38 | 0.50 | 4.2 | 5.0 | 0.70 | - | - |
| SC-84-51 | 38 | 0.52 | 4.8 | 1.0 | 0.88 | - | - |
| SC-84-52 | 38 | 0.51 | 4.8 | 5.0 | 0.52 | - | - |
| SC-84-53 | 38 | 0.51 | slow pore pressure response | | | | |
| SC-84-55A | 38 | 0.52 | 7.5 | 2.0 | 0.71 | - | - |
| SC-84-55B | 38 | 0.37 | 6.8 | 2.0 | 0.76 | - | - |
| SC-84-60 | 38 | 0.49 | 6.4 | 1.0 | 0.82 | - | - |
| SC-84-115A | 38 | 0.47 | 6.2 | 2.0 | 0.75 | - | - |
| SC-84-115B | 38 | 0.54 | 5.6 | 2.1 | 0.79 | - | - |
| SC-84-117 | 38 | 0.52 | 5.0 | 5.0 | 0.62 | - | - |

Table 4.6 Saline Creek Oil Sand: Summary of Isotropic Compression Tests

| SAMPLE | NOMINAL DIAMETER D (mm) | L/D | INITIAL DENSITY $\gamma$ (Mg/m$^3$) | COEFFICIENT OF VOLUME COMPRESSIBILITY, $m_v$ ($10^{-6}$ kPa$^{-1}$) | | | |
|---|---|---|---|---|---|---|---|
| | | | | RANGE OF STRESS (MPa) | FIRST LOADING CYCLE | SECOND LOADING CYCLE | THIRD LOADING CYCLE |
| SC-83-22D | 50 | 2.00 | 1.989 | 2-4 | 1.67 | 1.26 | - |
| SC-83-22U | 50 | 2.01 | 2.012 | 2-4 | 8.12 | 1.62 | 1.42 |
| SC-84-3A | 38 | 0.50 | 2.002 | 2-4 | 1.52 | 0.95 | 1.07 |
| SC-84-3B | 38 | 0.50 | 1.994 | 2-4 | 1.03 | 1.26 | 1.02 |
| SC-84-4A | 38 | 0.52 | 1.970 | 2-4 | 1.73 | 1.06 | 1.07 |
| SC-84-4B | 38 | 0.48 | 1.969 | 2-4 | 0.96 | 1.13 | 0.94 |
| SC-84-5A | 38 | 0.51 | 2.002 | 2-4 | - | 0.84 | 1.00 |
| SC-84-5B | 38 | 0.51 | 1.952 | 2-4 | 1.82 | 1.07 | 1.38 |
| SC-84-8A | 38 | 0.52 | 1.985 | 2-4 | 1.73 | 1.14 | 0.99 |
| SC-84-8B | 38 | 0.51 | 1.974 | 2-4 | 1.02 | 1.50 | 1.04 |
| SC-84-15A | 38 | 0.46 | 2.021 | 2-4 | 1.34 | 1.94 | 1.12 |
| SC-84-15B | 38 | 0.49 | 1.985 | 2-4 | 2.82 | 1.95 | 2.12 |
| SC-84-17 | 38 | 2.03 | 1.966 | 2-4 | 1.64 | 1.02 | 0.88 |
| SC-84-22 | 50 | 2.00 | 2.035 | 2-4 | 2.27 | 1.53 | 1.41 |
| SC-84-23 | 38 | 0.56 | 1.986 | 2-4 | Bitumen in porous stone inhibiting volume change | | |
| SC-84-24 | 38 | 0.54 | 1.956 | 2-4 | 1.57 | 2.06 | 1.98 |
| SC-84-25A | 38 | 0.57 | 2.005 | 2-4 | 1.47 | 0.99 | 0.98 |
| SC-84-25B | 38 | 0.52 | 2.000 | 2-4 | 1.69 | 0.81 | 0.94 |
| SC-84-39 | 50 | 2.00 | 2.034 | 2-4 | 3.18 | 2.79 | 2.36 |

## Table 4.7 Saline Creek Oil Sand: Summary of Triaxial Test Results

| SAMPLE | NOMINAL DIAMETER D (mm) | L/D | INITIAL DENSITY $\gamma$ (Mg/m$^3$) | LOADING PLATENS | STRAIN RATE $\dot{\varepsilon}$ (s$^{-1}$) | INITIAL TEST CONDITIONS $\sigma'_{3i}$ (MPa) | $u_i$ (MPa) | $B$ | CONDITIONS AT MAXIMUM STRENGTH $(\sigma_1-\sigma_3)_f$ (MPa) | $\sigma'_{3f}$ (MPa) | $u_f$ (MPa) | $\varepsilon_f$ (%) | $A_f$ | CONDITIONS AT MAXIMUM STRESS RATIO $\sigma'_1/\sigma'_3$ | $(\sigma_1-\sigma_3)$ (MPa) | $\sigma'_3$ (MPa) | $u$ (MPa) | $\varepsilon$ (%) | $A$ |
|---|---|---|---|---|---|---|---|---|---|---|---|---|---|---|---|---|---|---|---|
| SC-83-22U | 50 | 2.01 | 2.012 | 1* | $1.4\times10^{-5}$ | 2.03 | 1.52 | 0.64 | 8.95 | 3.60 | 0.22 | 3.8 | -0.23 | 3.8 | 7.66 | 3.80 | 1.06 | 2.1 | -0.13 |
| SC-84-1 | 38 | 0.50 | 2.018 | 3 | $1.4\times10^{-2}$ | 3.55 | 8.48 | 0.50 | 14.75 | 12.10 | - | 10.6 | - | - | - | - | - | - | - |
| SC-84-3A | 38 | 0.50 | 2.002 | 3 | $8.4\times10^{-4}$ | 2.25 | 10.63 | 0.69 | 10.53 | 12.88 | 6.93 | 11.9 | -0.51 | 3.5 | 4.86 | 12.88 | 10.92 | 2.3 | 0.09 |
| SC-84-3B | 38 | 0.50 | 1.994 | 3 | $1.2\times10^{-5}$ | 2.17 | 10.71 | 0.65 | 10.39 | 12.88 | 7.66 | 12.8 | -0.45 | 3.4 | 4.80 | 12.88 | 10.92 | 2.2 | 0.07 |
| SC-84-4A | 38 | 0.52 | 1.970 | 3 | $1.4\times10^{-5}$ | 2.01 | 10.69 | 0.68 | 9.20 | 12.70 | 7.82 | 7.4 | -0.46 | 3.5 | 3.43 | 12.70 | 11.32 | 1.9 | 0.27 |
| SC-84-4B | 38 | 0.48 | 1.969 | 3 | $8.4\times10^{-4}$ | 2.15 | 10.61 | 0.70 | 9.65 | 12.76 | 7.30 | 10.4 | -0.49 | 3.0 | 2.94 | 12.76 | 11.30 | 2.4 | 0.34 |
| SC-84-5B | 38 | 0.51 | 1.952 | 3 | $7.5\times10^{-2}$ | 1.97 | 10.23 | 0.66 | 13.97 | 12.30 | 4.11 | 10.2 | -0.67 | - | - | - | - | - | - |
| SC-84-8A | 38 | 0.52 | 1.985 | 3 | $2.1\times10^{-1}$ | 2.07 | 10.46 | 0.68 | 14.79 | 12.53 | - | 9.4 | - | - | - | - | - | - | - |
| SC-84-8B | 38 | 0.51 | 1.974 | 3 | $2.2\times10^{-1}$ | 2.07 | 10.28 | 0.64 | 16.09 | 12.35 | - | 7.4 | - | - | - | - | - | - | - |
| SC-84-10 | 38 | 1.94 | 2.006 | 2 | $2.6\times10^{-5}$ | 0.93 | 10.98 | 0.87 | 8.56 | 12.33 | 7.80 | 6.8 | -0.48 | 4.3 | 3.94 | 11.96 | 10.77 | 1.2 | -0.06 |
| SC-84-13 | 38 | 0.49 | 2.015 | 3 | $1.3\times10^{-5}$ | 1.05 | 10.89 | 0.79 | 12.05 | 12.24 | 6.34 | 11.6 | -0.51 | 6.3 | 1.58 | 12.01 | 11.71 | 2.8 | 0.66 |
| SC-84-14A | 38 | 0.50 | 1.966 | 3 | $1.5\times10^{-5}$ | 4.92 | 7.80 | 0.68 | 9.03 | 12.88 | 7.66 | 15.0 | -0.04 | 2.7 | 7.10 | 12.83 | 8.55 | 8.2 | 0.14 |
| SC-84-14B | 38 | 0.49 | 1.941 | 3 | $1.5\times10^{-2}$ | 0.97 | 9.33 | 0.84 | 10.62 | 10.33 | - | 11.7 | - | - | - | - | - | - | - |
| SC-84-15A | 38 | 0.46 | 2.021 | 3 | $1.1\times10^{-2}$ | 2.06 | 10.18 | 0.68 | 10.71 | 12.24 | - | 13.1 | - | - | - | - | - | - | - |
| SC-84-15B | 38 | 0.49 | 1.985 | 3 | $8.4\times10^{-3}$ | 2.20 | 10.24 | 0.72 | 12.49 | 12.44 | 5.86 | 12.4 | -0.49 | 3.7 | 8.80 | 12.44 | 9.14 | 5.3 | -0.17 |
| SC-84-17 | 38 | 2.03 | 1.966 | 3 | $3.1\times10^{-2}$ | 2.30 | 10.07 | 0.82 | 6.57*** | 12.42 | - | 1.7 | - | - | - | - | - | - | - |
| SC-84-22 | 50 | 2.00 | 2.035 | 3 | $1.9\times10^{-5}$ | 1.81 | 11.46 | 0.75 | 10.68 | 13.20 | 7.67 | 8.7 | -0.47 | 4.6 | 4.10 | 13.35 | 12.22 | 1.6 | 0.23 |
| SC-84-23 | 38 | 0.56 | 1.986 | 3 | $2.4\times10^{0}$ | 1.96 | 10.02 | 0.87 | 12.44 | 12.82 | - | 16.0 | - | - | - | - | - | - | - |
| SC-84-24 | 38 | 0.54 | 1.956 | 3 | $8.7\times10^{-5}$ | 2.12 | 10.69 | 0.82 | 6.96 | 12.81 | 9.22 | 19.1 | -0.26 | 2.9 | 5.94 | 12.81 | 9.59 | 11.2 | -0.23 |
| SC-84-25A | 38 | 0.57 | 2.005 | 3 | $8.4\times10^{-5}$ | 2.10 | 10.32 | 0.61 | 14.53 | 12.42 | 5.13 | 10.1 | -0.59 | 4.2 | 5.26 | 12.42 | 10.76 | 2.2 | 0.14 |
| SC-84-25B | 38 | 0.52 | 2.000 | 3 | $8.4\times10^{-5}$ | 2.01 | 10.52 | 0.62 | 13.25 | 12.53 | 5.27 | 8.9 | -0.64 | 3.9 | 3.71 | 12.53 | 11.25 | 2.4 | 0.32 |
| SC-84-29 | 38 | 0.54 | 1.929 | 3 | $1.1\times10^{-5}$ | 7.89 | 3.23 | 0.49 | 10.40 | 11.12 | 5.85 | 11.3 | 0.51 | 3.4 | 6.09 | 11.11 | 8.57 | 4.5 | 1.79 |
| SC-84-30 | 38 | 2.01 | 1.934 | 2 | $1.3\times10^{-5}$ | 7.96 | 3.18 | 0.49 | 10.69 | 11.21 | 6.40 | 9.6 | 0.61 | 3.4 | 8.03 | 11.17 | 7.82 | 4.6 | 1.18 |
| SC-84-31 | 38 | 0.45 | 1.930 | 3 | $1.3\times10^{0}$ | 1.04 | 9.72 | 0.85 | 9.97 | 11.73 | - | 17.1 | - | - | - | - | - | - | - |
| SC-84-33 | 38 | 0.52 | 2.005 | 3 | $1.1\times10^{-1}$ | 5.00 | 6.31 | 0.54 | 14.08 | 11.58 | - | 7.9 | - | - | - | - | - | - | - |
| SC-84-34 | 38 | 1.75 | 2.062 | 2 | $9.6\times10^{-6}$ | 5.01 | 6.49 | 0.65 | 14.44 | 11.78 | 5.67 | 4.5 | -0.09 | 4.0 | 11.89 | 11.64 | 7.62 | 1.6 | 0.15 |
| SC-84-39 | 50 | 2.00 | 2.034 | 1 | $1.8\times10^{-5}$ | 0.08 | 4.46 | 0.76 | 9.12 | 4.73 | 0.74 | 12.4 | -0.54 | 12.2 | 0.88 | 4.55 | 4.47 | 0.4 | 0.00 |
| SC-84-40A | 38 | 0.48 | 1.964 | 3 | $1.5\times10^{-2}$ | 4.83 | 7.20 | 0.62 | 8.87 | 12.33 | - | 12.1 | - | - | - | - | - | - | - |
| SC-84-40B | 38 | 0.53 | 1.987 | 3 | $1.3\times10^{-2}$ | 5.04 | 4.83 | 0.62** | 9.50 | 9.89 | - | 15.1 | - | - | - | - | - | - | - |
| SC-84-43 | 38 | 0.51 | 1.953 | 3 | $1.3\times10^{0}$ | 0.92 | 9.48 | 0.85** | 10.62 | 11.38 | - | 19.3 | - | - | - | - | - | - | - |
| SC-84-49 | 38 | 0.51 | 1.899 | 3 | $1.6\times10^{0}$ | 4.85 | 5.59 | 0.70 | 12.43 | 11.68 | - | 24.1 | - | - | - | - | - | - | - |
| SC-84-52 | 38 | 0.51 | 2.027 | 3 | $1.5\times10^{0}$ | 5.00 | 5.58 | 0.52 | 19.13 | 11.64 | - | 16.4 | - | - | - | - | - | - | - |
| SC-84-53 | 38 | 0.51 | 1.947 | 3 | $1.1\times10^{-5}$ | 8.01 | 3.07 | 0.49** | 7.55 | 11.18 | 5.09 | 18.0 | 0.53 | 2.1 | 7.55 | 11.18 | 5.09 | 18.0 | 0.53 |
| SC-84-55A | 38 | 0.52 | 1.964 | 3 | $2.9\times10^{0}$ | 2.07 | 10.38 | 0.71 | 14.23 | 12.87 | - | 14.9 | - | - | - | - | - | - | - |
| SC-84-55B | 38 | 0.37 | 1.999 | 2 | $2.3\times10^{0}$ | 2.02 | 10.29 | 0.76 | 18.76 | 12.58 | - | 17.8 | - | - | - | - | - | - | - |
| SC-84-60 | 38 | 0.49 | 1.974 | 3 | $1.4\times10^{-1}$ | 1.02 | 10.94 | 0.82 | 11.22 | 12.27 | - | 9.5 | - | - | - | - | - | - | - |
| SC-84-115A | 38 | 0.47 | 1.959 | 3 | $2.3\times10^{0}$ | 2.35 | 9.71 | 0.75 | 13.81 | 12.24 | - | 14.6 | - | - | - | - | - | - | - |
| SC-84-115B | 38 | 0.54 | 1.948 | 3 | $3.1\times10^{0}$ | 2.13 | 10.20 | 0.79 | 10.38 | 12.57 | - | 23.5 | - | - | - | - | - | - | - |
| SC-84-117 | 38 | 0.51 | 1.997 | 3 | $1.1\times10^{-1}$ | 4.96 | 6.43 | 0.62 | 12.47 | 11.56 | - | 16.3 | - | - | - | - | - | - | - |

* (1) Conventional 38.1 mm diameter loading platens
(2) Enlarged 43.2 mm diameter loading platens
(3) Enlarged 43.2 mm diameter loading platens with frictionless end preparations

** The average value of B at the appropriate stress level assumed for these samples.

*** Failure along bedding plane.

# Table 4.8 Saline Creek Oil Sand: Comparative Grain Size Analyses Before and After Testing

| SAMPLE | STRAIN RATE ($s^{-1}$) | INITIAL CONSOLIDATION PRESSURE (MPa) | GRAIN SIZE DATA | | | | |
|---|---|---|---|---|---|---|---|
| | | | $D_{10}$ (mm) | $D_{50}$ (mm) | $D_{60}$ (mm) | UNIFORMITY COEFFICIENT $C_u = D_{60}/D_{10}$ | FINES CONTENT (%<0.074 mm) |
| SC-84-10 | $2.6 \times 10^{-5}$ | 0.9 | | | | | |
| -before testing | | | 0.13 | 0.20 | 0.21 | 1.6 | 2.07 |
| -after testing | | | 0.09 | 0.18 | 0.20 | 2.2 | 6.45 |
| SC-84-30 | $1.3 \times 10^{-5}$ | 8.0 | | | | | |
| -before testing | | | 0.12 | 0.20 | 0.21 | 1.8 | 2.28 |
| -after testing | | | 0.08 | 0.18 | 0.20 | 2.5 | 7.35 |
| SC-84-34 | $9.6 \times 10^{-6}$ | 5.0 | | | | | |
| -before testing | | | 0.14 | 0.20 | 0.21 | 1.5 | 1.45 |
| -after testing | | | 0.08 | 0.18 | 0.20 | 2.5 | 7.83 |
| SC-84-110 | - | 5.0 | | | | | |
| -before testing | | | 0.15 | 0.24 | 0.28 | 1.9 | 1.87 |
| -after testing | | | 0.15 | 0.23 | 0.26 | 1.7 | 1.84 |
| SC-84-3B/4A* | $1.0 \times 10^{-5}$ | 2.0 | | | | | |
| -before testing | | | 0.10 | 0.19 | 0.20 | 2.0 | 3.02 |
| -after testing | | | 0.08 | 0.18 | 0.19 | 2.4 | 8.96 |
| SC-84-5B/15A* | $1.0 \times 10^{-2}$ | 2.0 | | | | | |
| -before testing | | | 0.12 | 0.19 | 0.20 | 1.7 | 1.75 |
| -after testing | | | 0.08 | 0.18 | 0.20 | 2.5 | 8.74 |
| SC-84-31/43* | $1.3 \times 10^{0}$ | 1.0 | | | | | |
| -before testing | | | 0.12 | 0.19 | 0.20 | 1.7 | 2.71 |
| -after testing | | | 0.08 | 0.19 | 0.20 | 2.5 | 7.68 |
| SC-84-49/52* | $1.6 \times 10^{0}$ | 5.0 | | | | | |
| -before testing | | | 0.12 | 0.19 | 0.21 | 1.8 | 1.74 |
| -after testing | | | 0.08 | 0.17 | 0.19 | 2.4 | 8.95 |
| SC-84-23/55A/55B* | $2.5 \times 10^{0}$ | 2.0 | | | | | |
| -before testing | | | 0.12 | 0.20 | 0.22 | 1.8 | 2.79 |
| -after testing | | | 0.08 | 0.18 | 0.20 | 2.5 | 8.75 |

* Combined samples after testing.

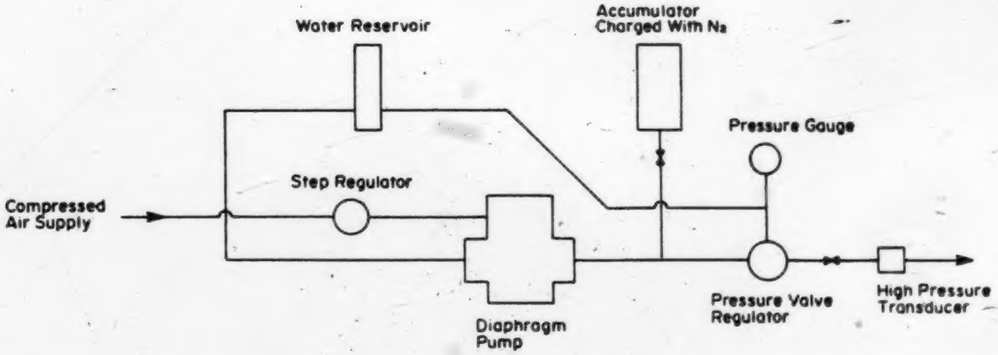
Water Reservoir
Accumulator Charged With $N_2$
Pressure Gauge
Step Regulator
Compressed Air Supply
Diaphragm Pump
Pressure Valve Regulator
High Pressure Transducer

Figure 4.1 High Pressure Air Activated Diaphragm Pump System

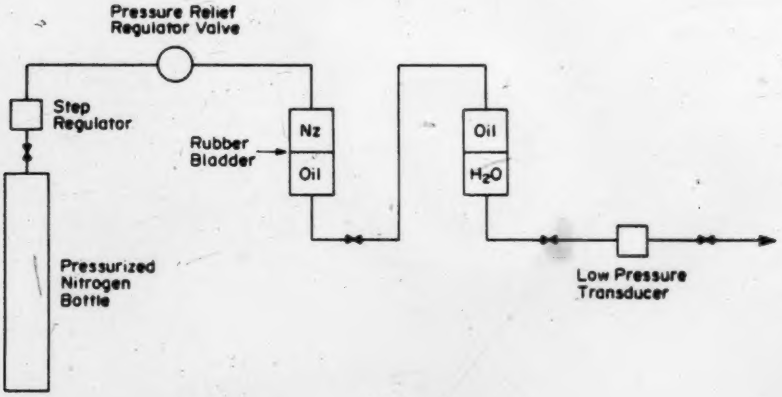
Pressure Relief Regulator Valve
Step Regulator
Rubber Bladder
Nz
Oil
Oil
$H_2O$
Pressurized Nitrogen Bottle
Low Pressure Transducer

Figure 4.2 Nitrogen Charged Low Pressure System

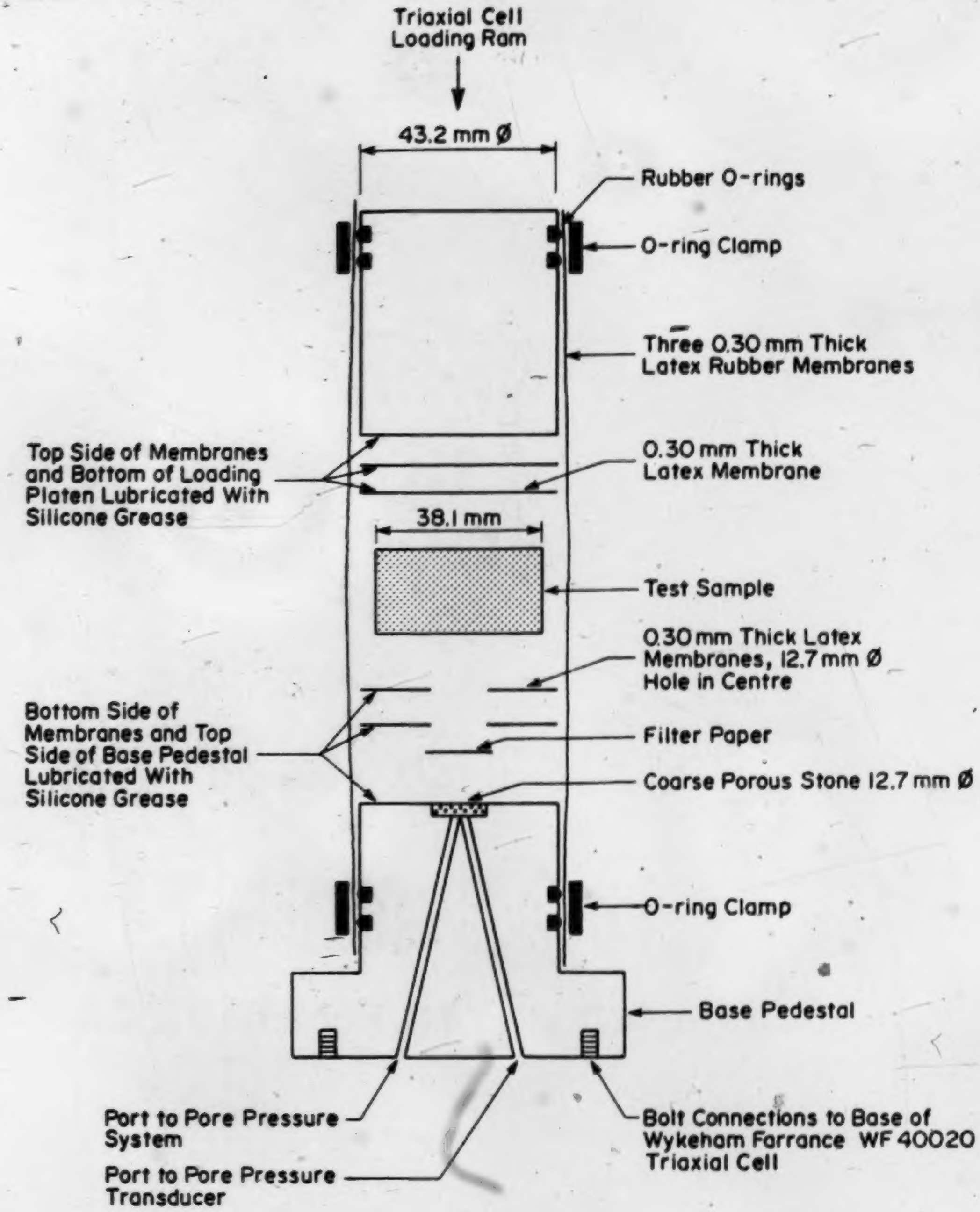
Triaxial Cell Loading Ram
43.2 mm Ø
Rubber O-rings
O-ring Clamp
Three 0.30 mm Thick Latex Rubber Membranes
Top Side of Membranes and Bottom of Loading Platen Lubricated With Silicone Grease
0.30 mm Thick Latex Membrane
38.1 mm
Test Sample
0.30 mm Thick Latex Membranes, 12.7 mm Ø Hole in Centre
Bottom Side of Membranes and Top Side of Base Pedestal Lubricated With Silicone Grease
Filter Paper
Coarse Porous Stone 12.7 mm Ø
O-ring Clamp
Base Pedestal
Port to Pore Pressure System
Port to Pore Pressure Transducer
Bolt Connections to Base of Wykeham Farrance WF 40020 Triaxial Cell

Figure ~~4.3~~ Assembly of Frictionless Loading Platens

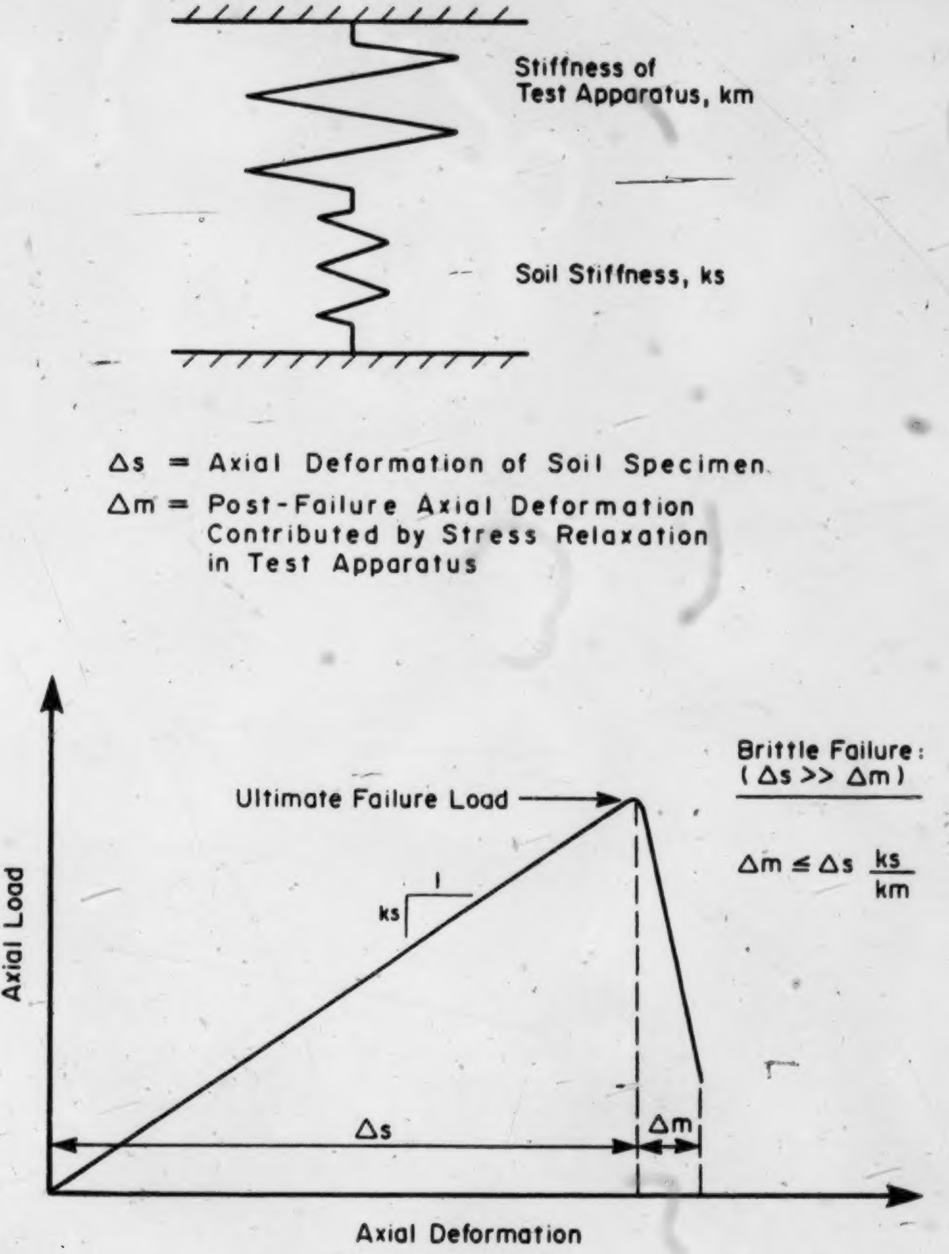
Stiffness of
Test Apparatus, km
Soil Stiffness, ks
Brittle Failure:
( Δs >> Δm )
Δm ≤ Δs ks/km
Ultimate Failure Load
ks
1
Axial Load
Δs
Δm
Axial Deformation

$\Delta s$ = Axial Deformation of Soil Specimen

$\Delta m$ = Post-Failure Axial Deformation Contributed by Stress Relaxation in Test Apparatus

Figure 4.4 Spring Analogy Representing the Interaction of the Triaxial Test Apparatus and the Test Specimens

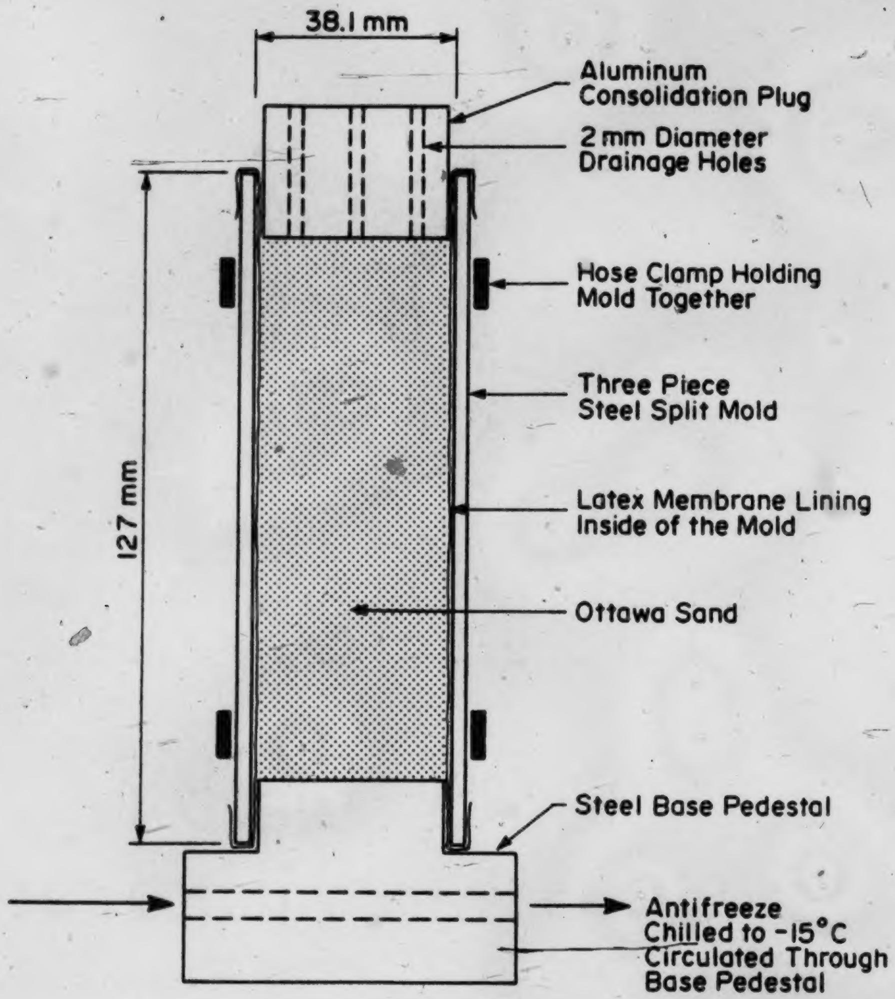
38.1 mm
Aluminum Consolidation Plug
2 mm Diameter Drainage Holes
Hose Clamp Holding Mold Together
Three Piece Steel Split Mold
127 mm
Latex Membrane Lining Inside of the Mold
Ottawa Sand
Steel Base Pedestal
Antifreeze Chilled to -15°C Circulated Through Base Pedestal

Figure 4.5 Mold Assembly for Ottawa Sand Samples

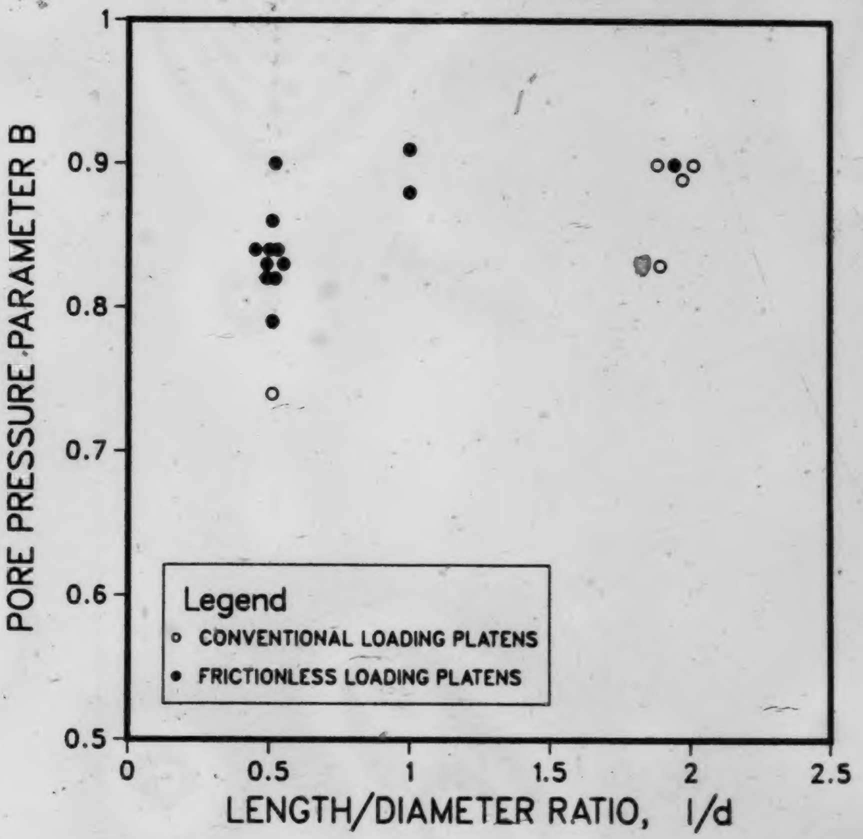

Figure 4.6 Ottawa Sand: Pore Pressure Parameter B Versus Length/Diameter Ratio of the Test Specimens

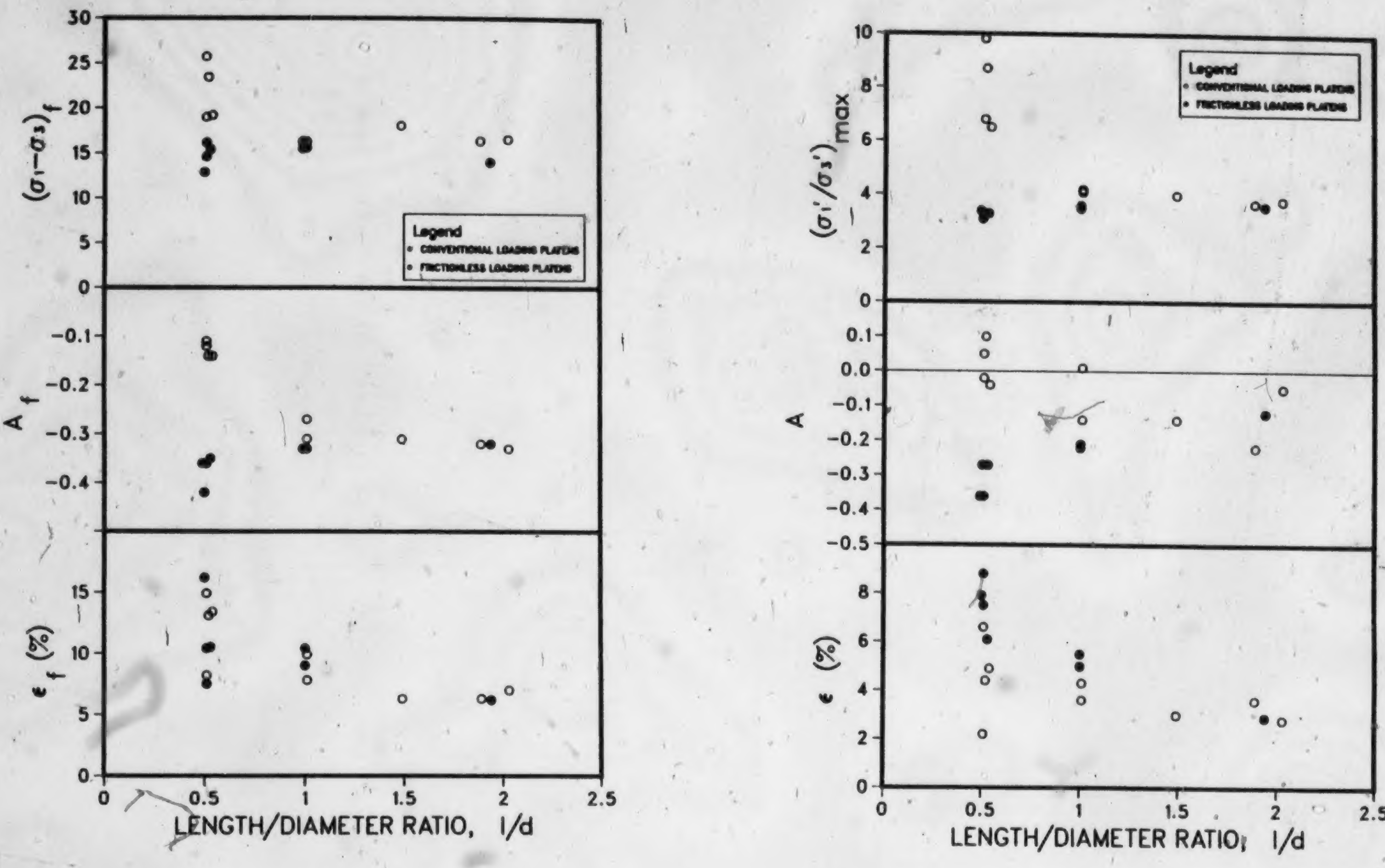

Figure 4.7 Test Series A and B: Conditions at the Ultimate Strength and Maximum Stress Ratio Versus l/d Ratio of the Test Specimens

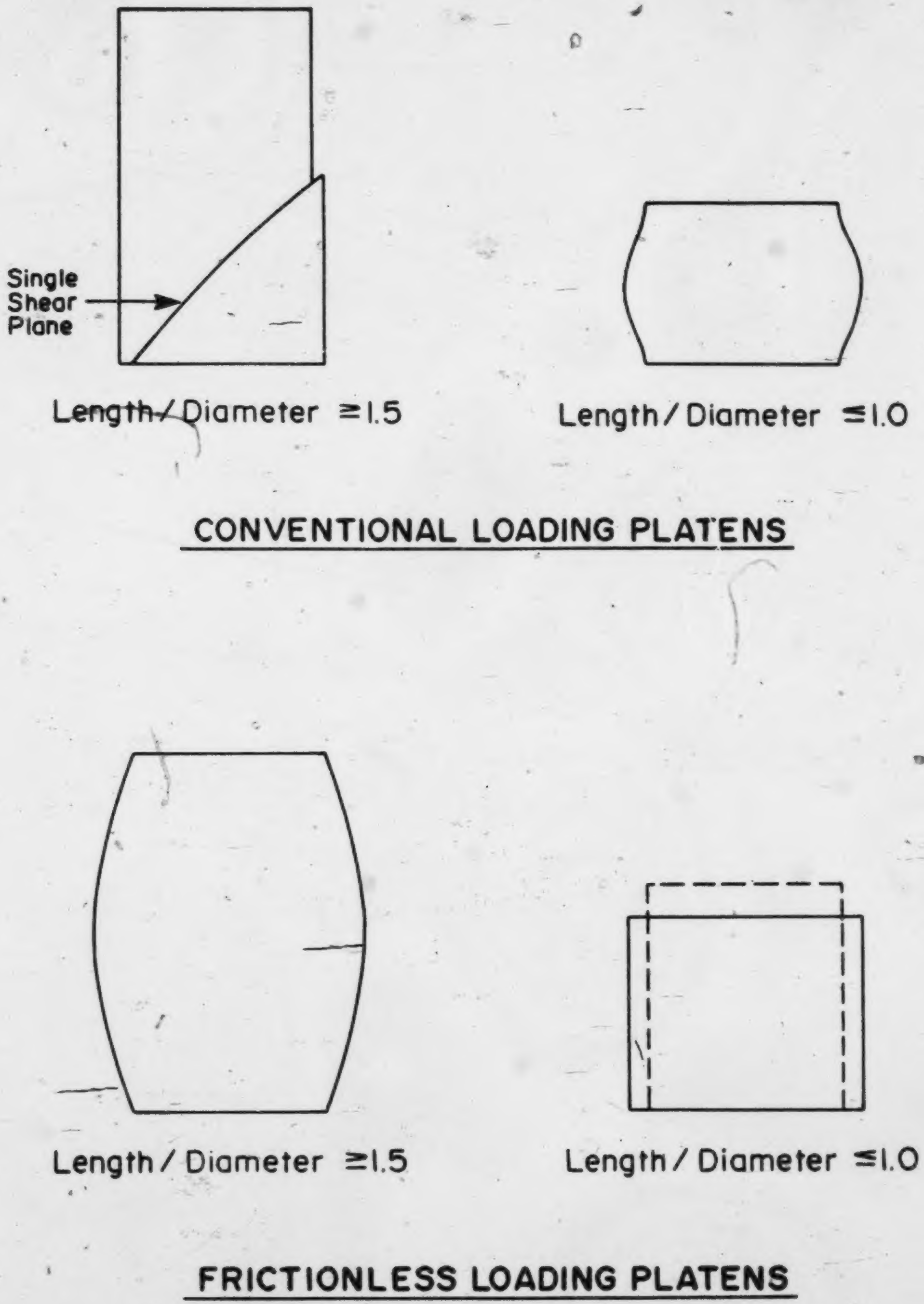
Single Shear Plane
Length/Diameter ≥1.5
Length/Diameter ≤1.0
CONVENTIONAL LOADING PLATENS
Length/Diameter ≥1.5
Length/Diameter ≤1.0
FRICTIONLESS LOADING PLATENS

Figure 4.8 Test Series A and B: Shape of the Test Specimens after Testing

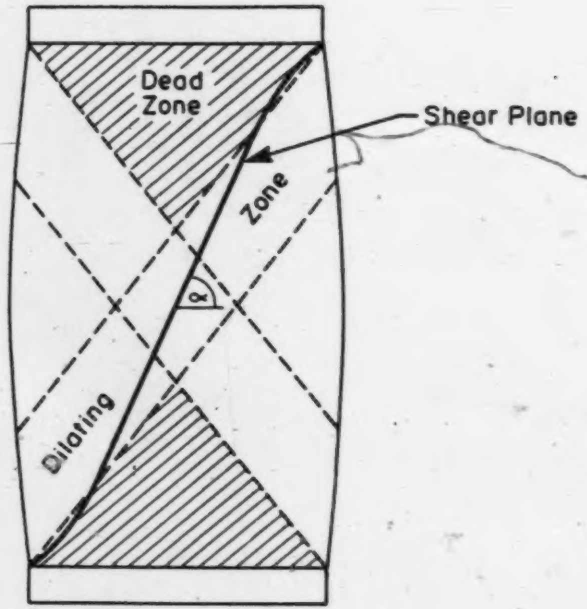
Dead
Zone
Shear Plane
Zone
α
Dilating

Figure 4.9 Nonuniformity of Straining and Developed Shear Plane using Conventional Steel Loading Platens (After Rowe and Barden, 1964)

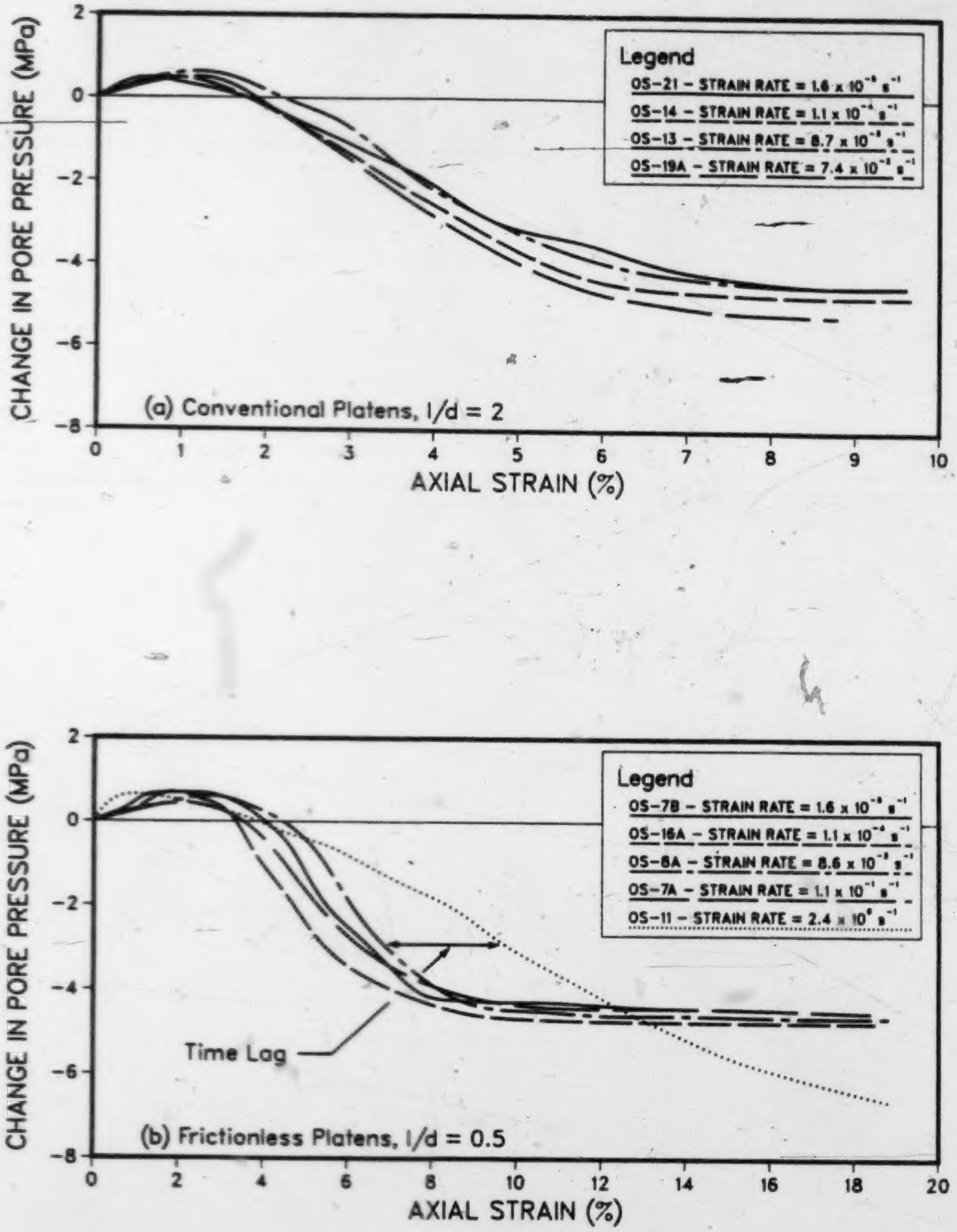

Figure 4.10 Variation in Pore Pressure Measurements with Strain Rate for Ottawa Sand

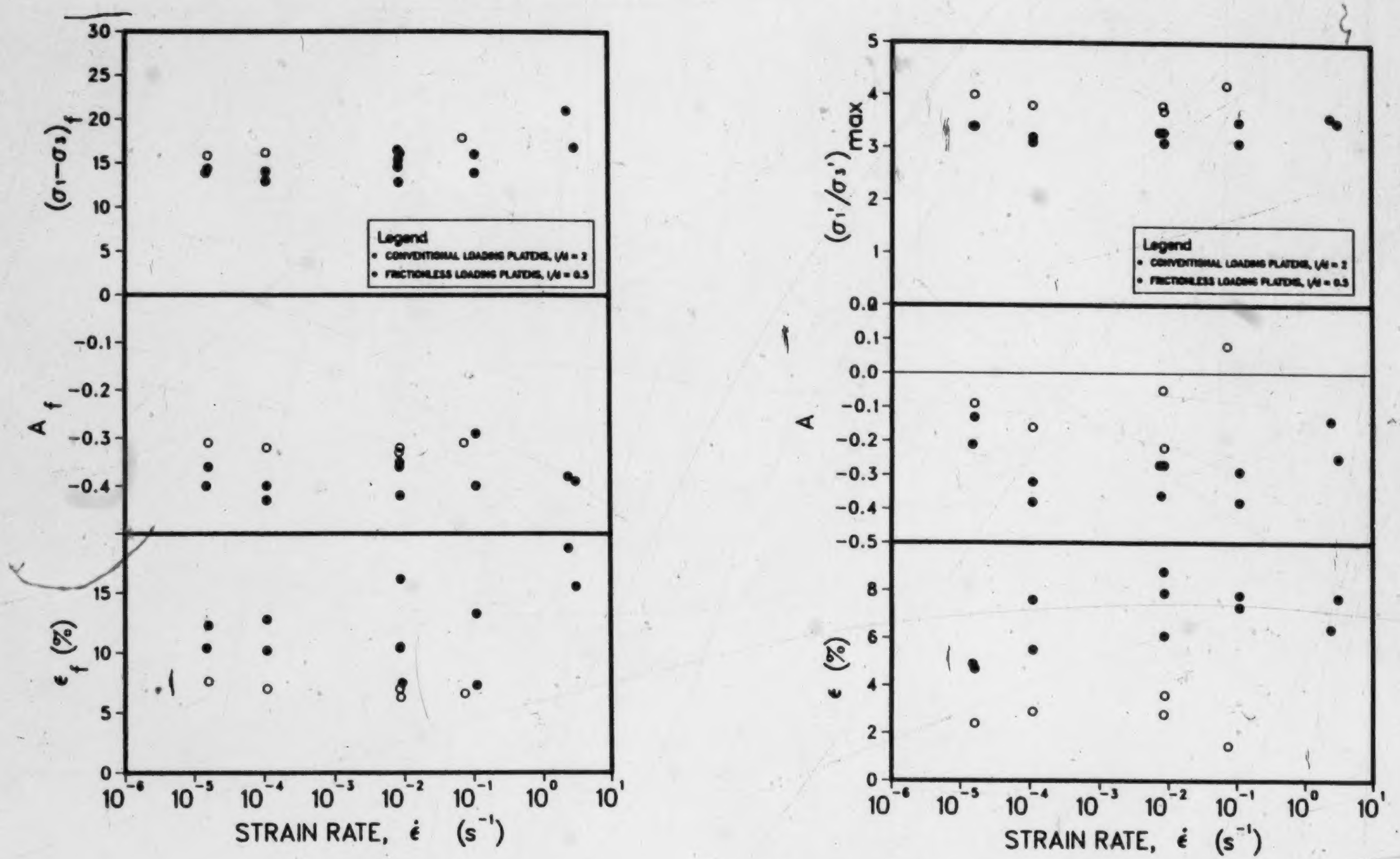

Figure 4.11 Test Series C: Conditions at the Ultimate Strength and Maximum Stress Ratio Versus Strain Rate

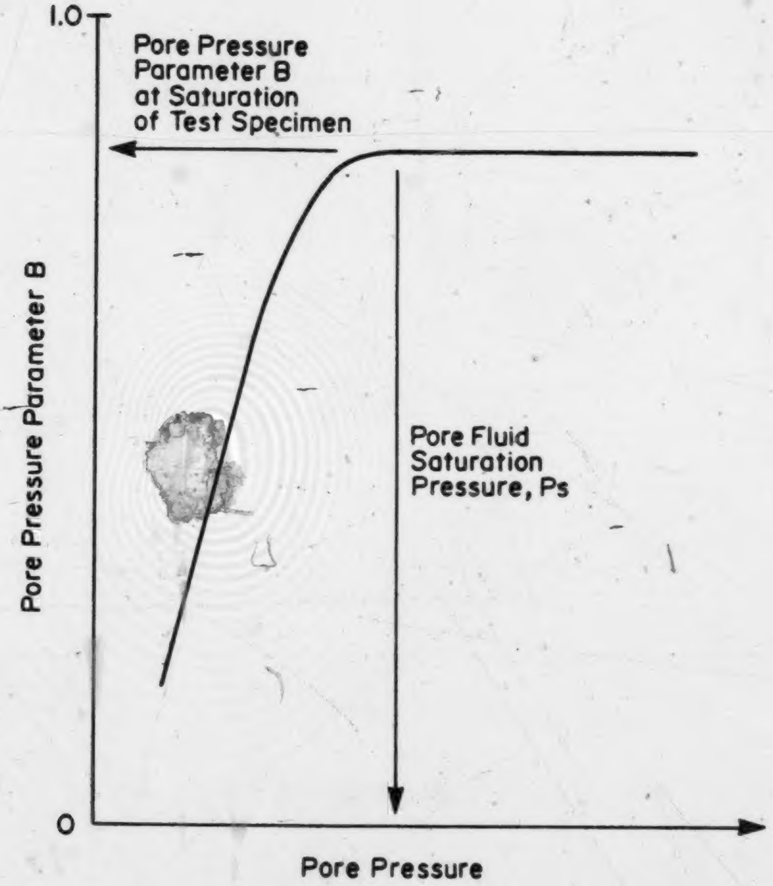

Figure 4.12 Measurement of Pore Fluid Saturation Pressure and Pore Pressure Parameter B

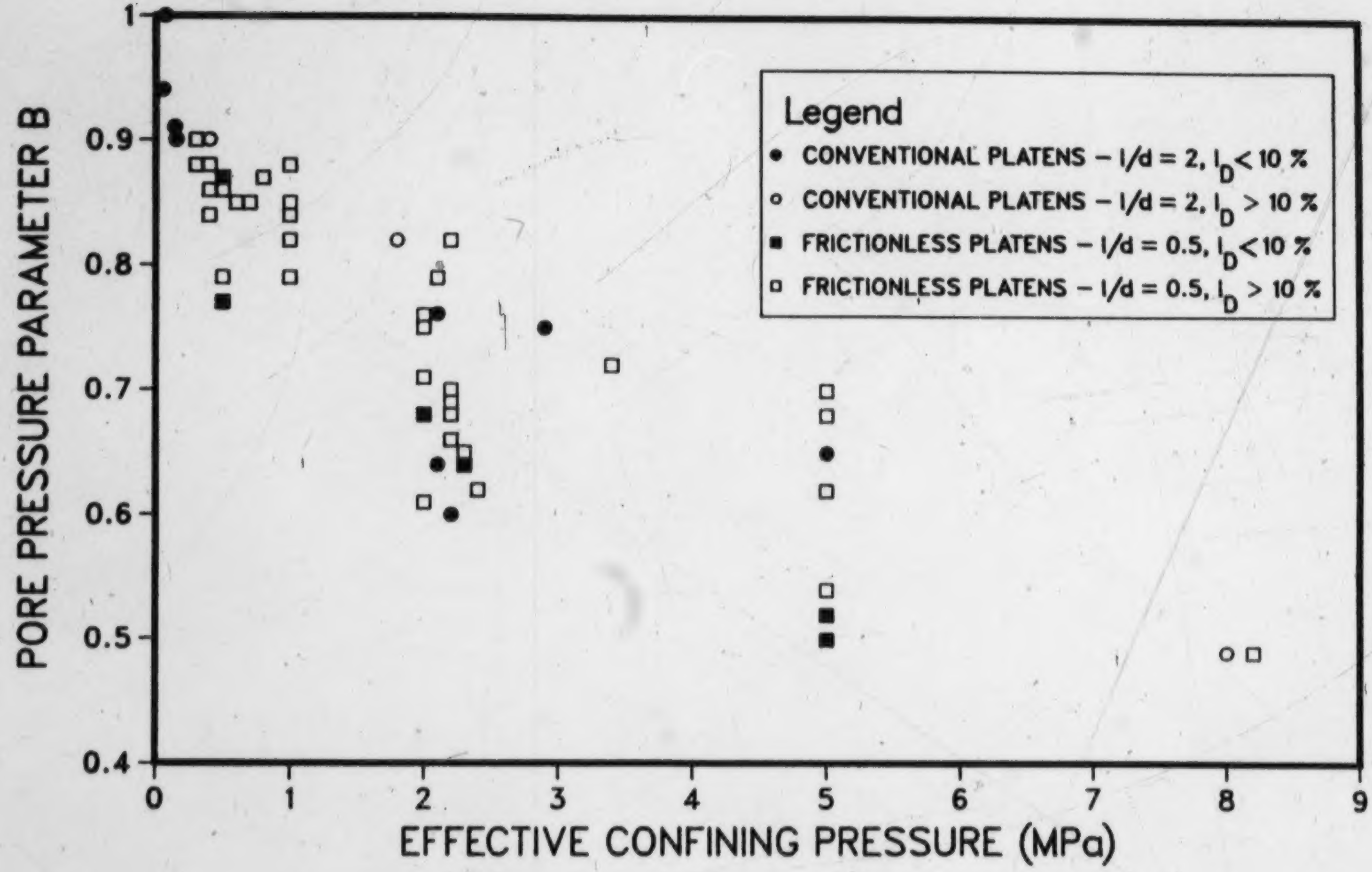

Figure 4.13 Pore Pressure Parameter B Versus Effective Confining Pressure

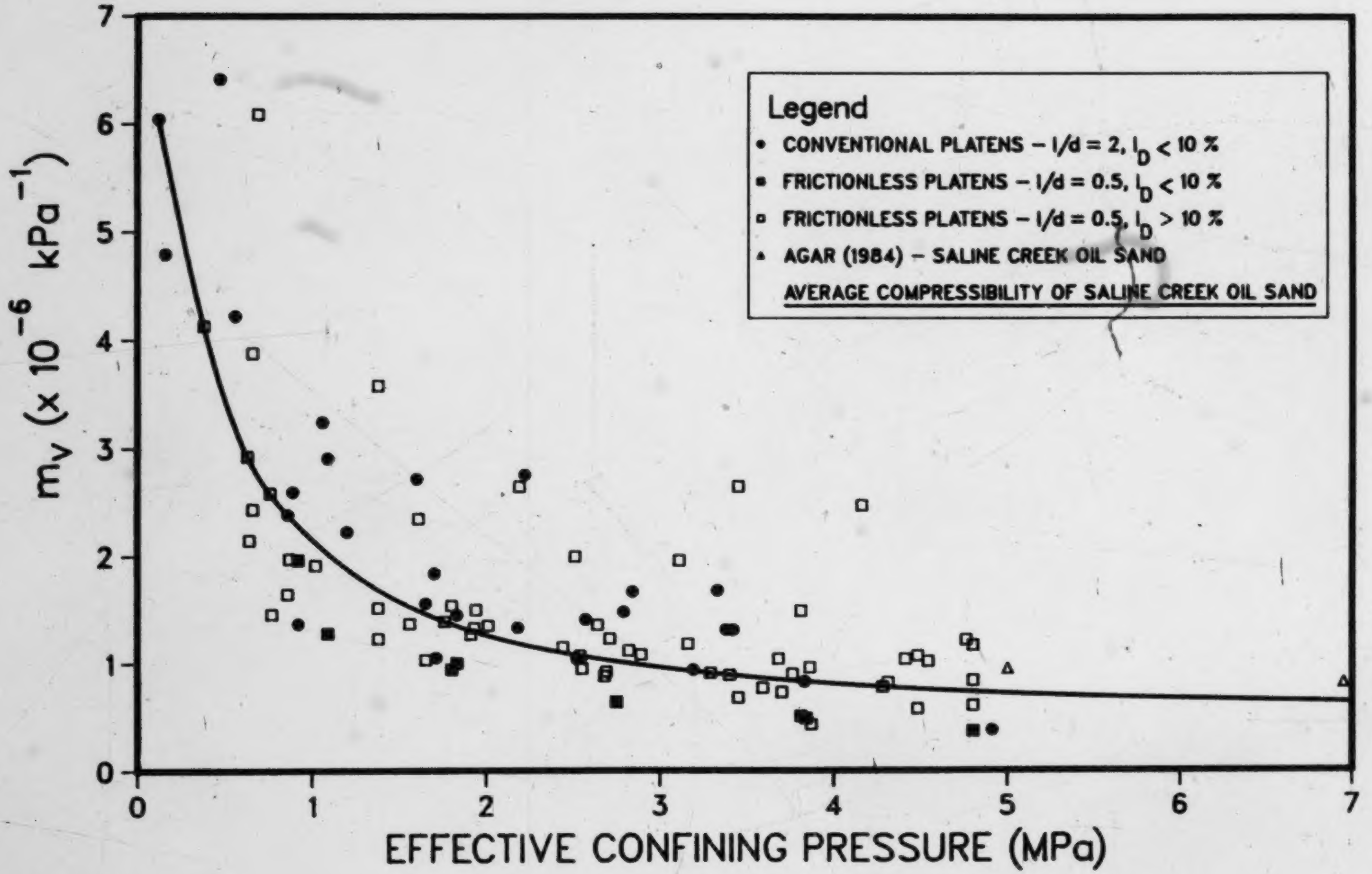

Figure 4.14 Coefficient of Volume Compressibility Versus Effective Confining Pressure

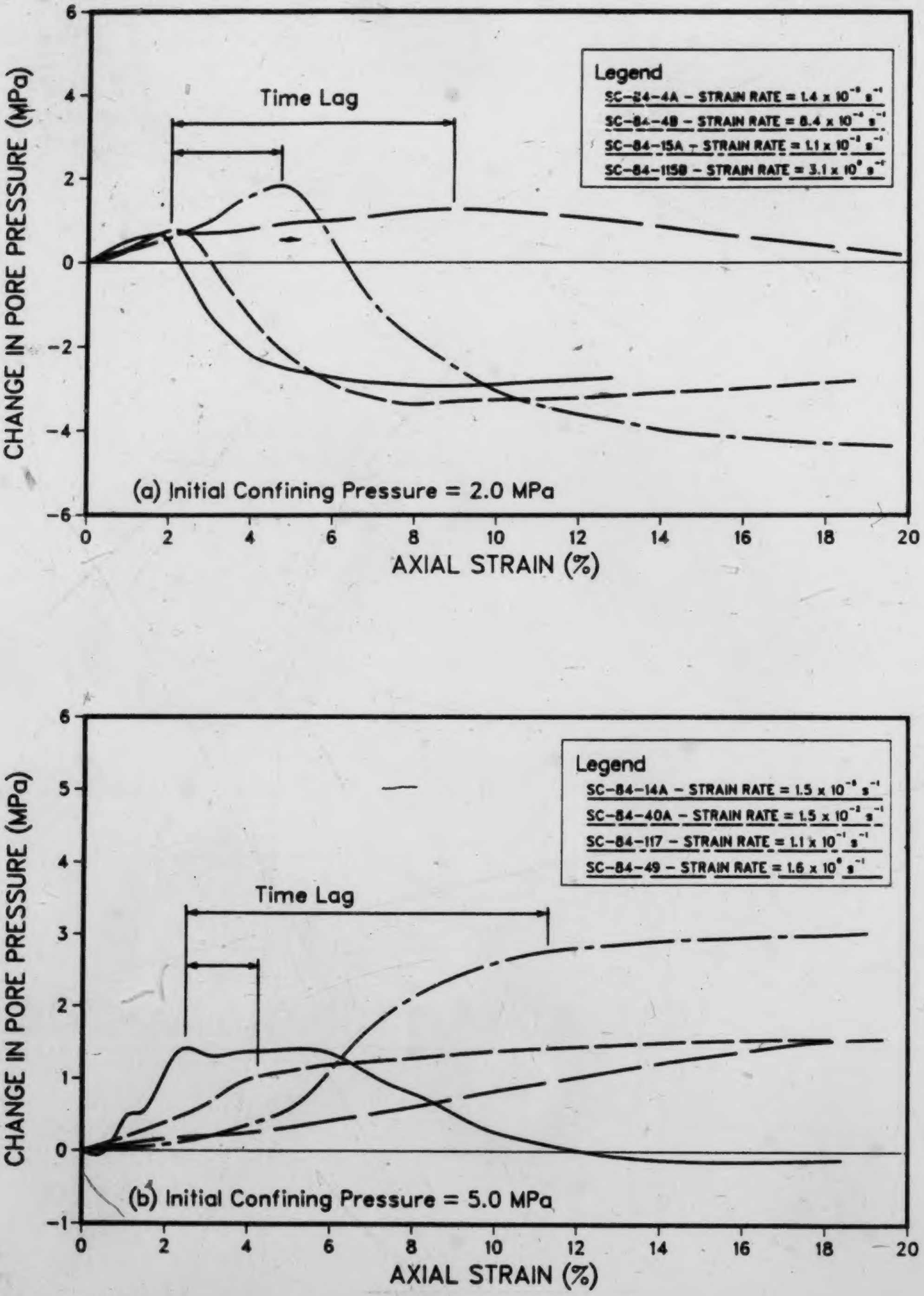

Figure 4.15 Variation in Pore Pressure Measurements with Strain Rate for Saline Creek Oil Sand

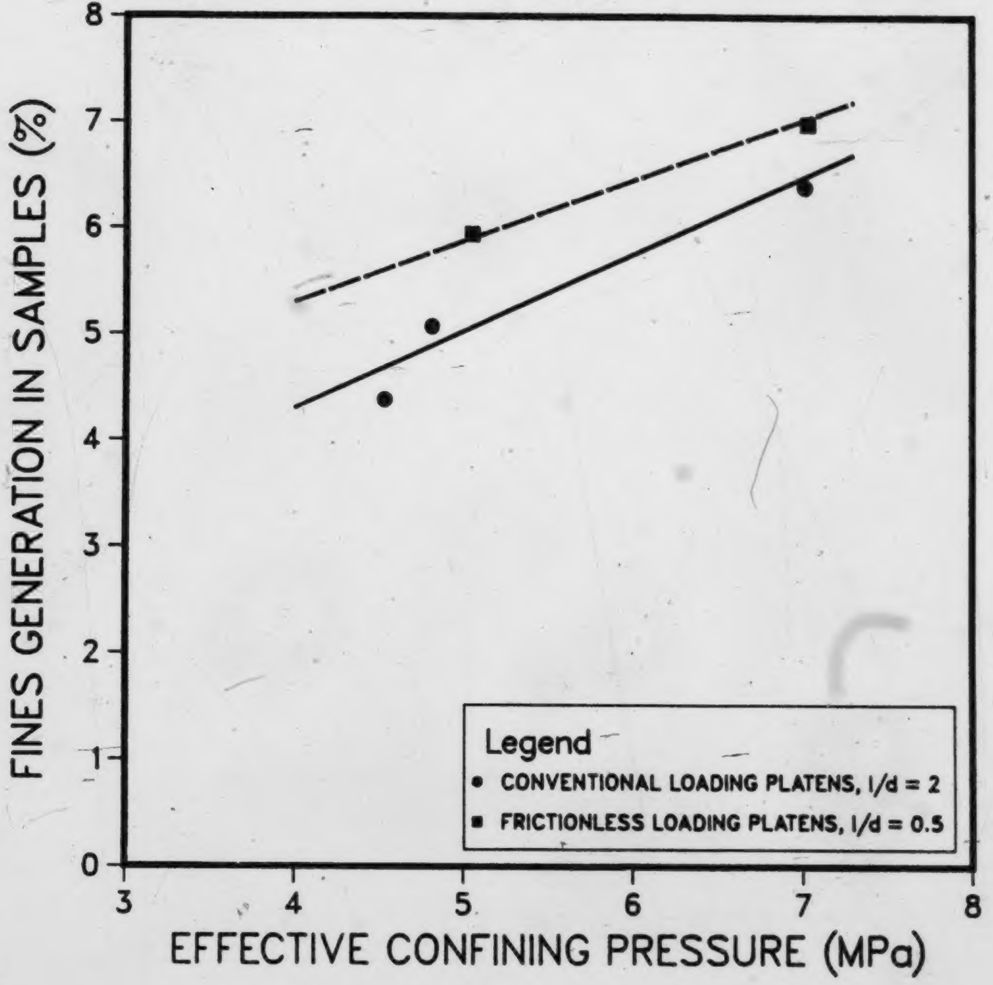

Figure 4.16 Fines Generation in Undrained Triaxial Compression Tests Versus Effective Confining Stress at Failure, Strain Rates less than $10^{-3}$ $s^{-1}$

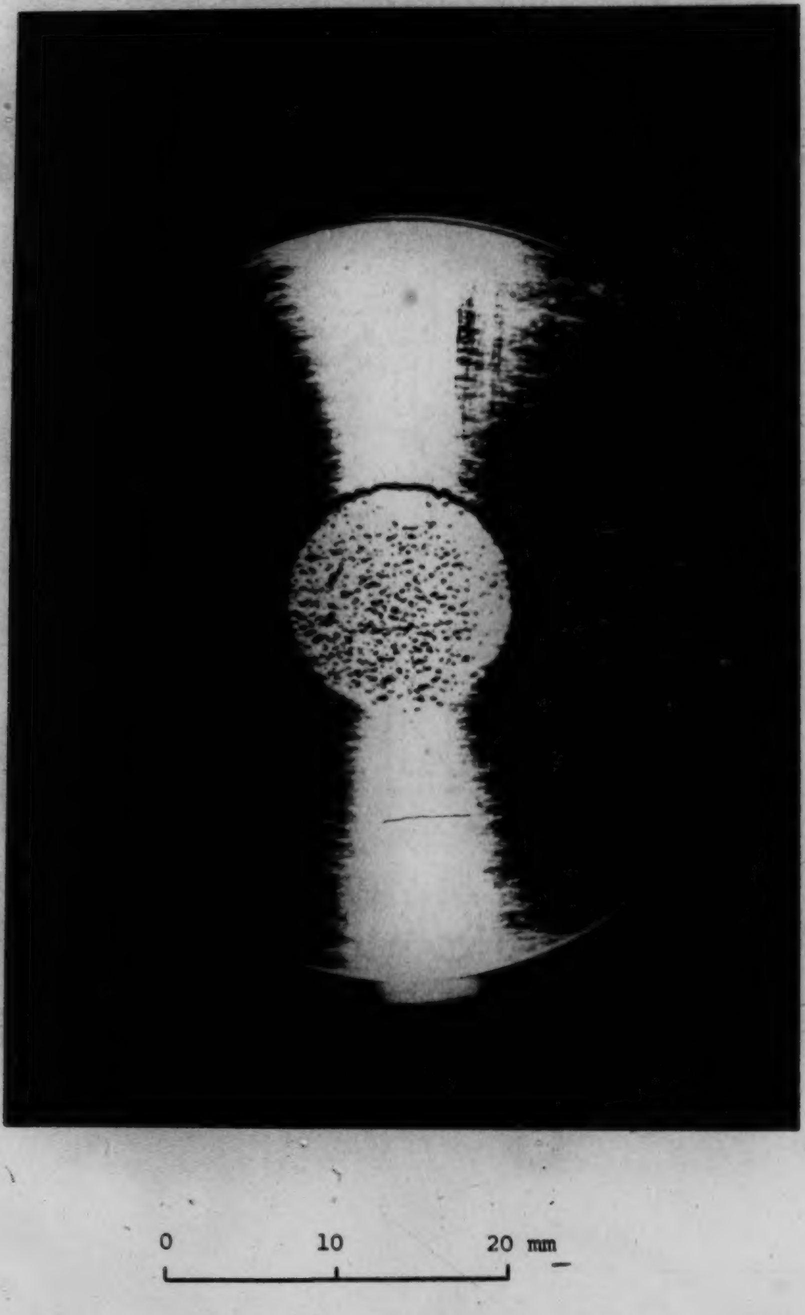

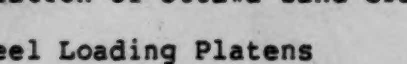

Plate 4.1 Indentation of Ottawa Sand Grains into Surface of Conventional Steel Loading Platens

# 5. TRIAXIAL TESTING OF SYNCRUDE OIL SAND

## 5.1 Introduction

A number of high quality, low bitumen content oil sand cores were recovered from shallow depths within the Syncrude Canada Limited oil sands lease near Fort McMurray, Alberta. These cores were considered suitable to investigate the behaviour of oil sand in axial extension because the influence of bitumen viscosity on strength measurement at very low stresses would be minimized by the low bitumen contents. The methodology of the investigation was conducted as follows:

1) A series of drained triaxial compression tests on the Syncrude oil sand, Test Series 84S, were previously conducted at the University of Alberta at effective confining stresses of 138, 276 and 414 kPa. An additional drained triaxial compression test designated SYN-C-1 was conducted at an effective confining stress of 15 kPa to extend the Mohr-Coulomb envelope to lower stresses.
2) Three drained and two undrained triaxial extension tests, SYN-T-1 through SYN-T-5, were conducted by the procedure described by Bishop and Garga(1969).
3) An unconfined static "self-weight" tension test, SYN-T-6, was conducted in a triaxial cell. Cell pressures were maintained above the pore fluid gas saturation pressure to prevent gas exsolution and

sample expansion. Two samples of disturbed bitumen-rich Saline Creek oil sand, SC-84-T-1 and SC-84-T-2, were also tested by the same method to evaluate the tensile resistance mobilized by the interstitial bitumen.

## 5.2 Low Pressure Triaxial Testing Facility

### 5.2.1 Description

A low pressure triaxial testing system was assembled for the test program. The layout of the system is shown schematically in Figure 5.1.

The Wykeham Farrance WF12400 stress path cell was used for the triaxial compression and extension tests. The Wykeham Farrance WF11004 triaxial cell was substituted for the unconfined tension tests to accomodate taller specimens.

The Wykeham Farrance WF12400 stress path cell is illustrated and described in detail by Bishop and Wesley(1975). Briefly, the cell is operated by a hydraulic ram mounted internally in the base of the cell. The ram applies axial load to the test specimen by raising and lowering the base pedestal supporting the specimen. The ram is activated by a digitally controlled stepping motor which turns a screw cylinder to increase or decrease the pressure in the ram. The ram can be controlled to run tests in axial compression and axial extension and at controlled rate of loading or controlled rate of strain.

The axial load cell is a strain gauge type and is mounted inside the cell above the top loading cap on the specimen. Vertical load in a compression test is applied by moving the specimen upward thereby pushing the top cap against the load cell. Extension tests are conducted by attaching the top cap to the load cell by a bayonet catch. The specimen is lowered and the decrease in the axial load is recorded by the pull on the load cell. Measurements of changes in axial load are made directly by the load cell, independent of the cell pressure or mechanical friction.

The ports for the confining and pore pressures are located at the base of the cell. The pore pressure is led up through the loading ram to the base of the sample. The cell and pore pressures were both applied by compressed air (1200 kPa) regulated through relief valves into air-water interface reservoirs. A schematic diagram of the pressure systems is shown in Figure 5.2.

Volume changes during testing were measured by the volume change indicator described in Section 4.2.1. Axial deformations were measured by 2 LVDT fastened to opposite sides of the cell. The LVDT record the movement of the hydraulic ram relative to the top of the cell. The cell and pore pressures were measured by strain gauge transducers attached off the ports at the base of the cell. To provide precise measurements of the effective confining pressure applied to the samples, a differential pressure mercury manometer was attached between the cell and the pore pressure lines.

The excitation voltages for the LVDT's, pressure transducers and load cell were suppplied by a constant voltage signal conditioning system. A Fluke 2240B Datalogger was used to electronically record the output signals onto paper tape.

### 5.2.2 Calibration of Electronic Measuring Devices

The electronic monitoring devices were calibrated prior to and upon completion of the testing program. The LVDT's were calibrated against a micrometer scale. The cell and pore pressure transducers had been previously calibrated using a dead weight table hydraulic pressure calibrator. The calibrations were checked against another pressure transducer which had been calibrated independently. The load cell was calibrated in tension by hanging dead weights from the load cell. The load cell was calibrated in compression against a calibrated proving ring. The calibrations are summarized in Table A.4.

## 5.3 Sampling and Sample Preparation

The Syncrude oil sand samples were cored within the Syncrude Canada Limited oil sands lease during September 1984. The cores were recovered with a pitcher sampler at depths between 11 and 14 m, just below the upper surface of the Upper McMurray Formation. The cores were immediately re-pressurized in nitrogen gas to the insitu hydrostatic pressure and frozen. The samples were transported to Edmonton and stored in a cold room at -15 to -20°C until testing.

### 5.3.1 Preparation of Triaxial Test Specimens

The preparation of the triaxial test specimens was carried out in the cold room at -15°C. The cores were lathed from the initial diameter of 73 mm to approximately 38.1 mm in the manner described in Section 4.4.2. The triaxial extension test specimens SYN-T-1 through SYN-T-5 were additionally inscribed with a approximately 6 mm deep by 25 mm long notch through the midsection of the specimens as shown in Figure 5.3. The ends of the notch were cut to approximately 1.5:1 to 2:1 slopes to minimize stress concentrations. The ends of the samples were finished in the conventional manner.

The test specimens were chilled in dry ice (-80°C) until mounting in the triaxial cell. The mounting procedures were carried out at room temperature. Porous stones placed above and below the specimen were also frozen in dry ice to prevent thawing of the ends of the samples during the mounting procedures. A single 0.39 mm thick latex membrane with a nominal diameter of 38.1 mm was used to confine the specimens. For test specimens SYN-T-2 through SYN-T-5, a single horizontal convolution or fold in the membrane was formed at mid-height as shown in Figure 5.4. The object of the fold was to minimize the tensile resistance of the membrane during the test. Radial drainage filter papers were also wrapped around the specimens. For the tension test specimens, the filters were cut at mid-height to eliminate tensile resistance that may be developed by the filter paper. The assembly of SYN-T-5 in the triaxial cell (after testing) is shown in the photograph in Plate 5.1.

A 100 kPa confining pressure was applied to the specimens immediately upon completion of the cell assembly. The time to install the specimens was less than 10 minutes and no thaw of any of the specimens during this time period was visibly apparent. The specimens were consolidated under back pressures between 146 and 550 kPa for periods ranging from 12 to 46 hours.

### 5.3.2 Preparation of Unconfined Tension Test Specimens

The unconfined test specimens were fabricated from a 200 mm length of full diameter core (nominally 70 mm diameter). The cores were inscribed with a 10 to 14 mm deep by 25 mm long notch through the upper third of the core length as shown in Figure 5.5. The ends of the notch were cut to approximately 2:1 slopes to minimize stress concentrations.

The test specimens were seated in the hanger shown in Figure 5.5. The hanger is manufactured of four aluminum "pie" plates with the centres cut out to form a seat to support the upper annulus of the notch zone. An undersized 64 mm diameter latex rubber membrane was used to confine the aluminum plates against the specimen and to attach the specimen to the top cap.

The taller Wykeham Farrance WF11004 triaxial cell was substituted for this test series. The cores were installed in the triaxial cell in the frozen state. The top cap was fastened to the loading ram of the cell by two universal joints in series. The universal joints allowed the test specimens to suspend themselves vertically under their own weight. The triaxial cell was then filled with water and the cell pressure increased to the estimated pore fluid saturation pressure of the oil sand. This step was taken to prevent gas exsolution and undrained expansion of the test specimens. Based on the measurements of pore fluid saturation pressure in Sections 4.4.4 and 5.5, cell pressures of 200 and 700 kPa were applied to the Syncrude and Saline Creek oil sand, respectively.

## 5.4 Index Testing

Index testing and grain size analysis of the test specimens were conducted as described in Section 4.4.3. Table 5.1 is a summmary of the specimen data. The grain size data is summarized in Table 5.2.

The Syncrude oil sand is comprised of lean, silty, fine grained oil sand of the Upper McMurray Formation. Bitumen contents measured in this study were 2.4 and 5.3 percent by total weight. Seto(1985) and other research conducted at the University of Alberta report bitumen contents between 2.2 and 6.0 percent for this oil sand.

The index of disturbance tabulated in Table 5.1 range between 5.8 and 10.0 percent and indicate the test specimens to be of sufficient quality for measurement of geotechnical strength properties. The in situ porosity was estimated to be 0.310 assuming an average total in situ pore fluid content of 14.5 percent and 100 percent saturation. The in situ porosity is a conservative lower bound since full pore fluid saturation was assumed.

Occassional clay clasts are present within the Syncrude oil sand. The clay clasts are generally less than 1 mm in thickness and are oriented horizontal or very slightly inclined. Examination of sections through the core indicate the clasts are discontinuous rather than continuous seams.

The high fines content shown in the grain size curves in Appendix E are probably caused by the clay clasts and does not entirely reflect the amount of fine material in the sand grain matrix.

### 5.5 Saturation of the Test Specimens

The fluid saturation pressure and the B parameter at saturation were measured on all triaxial test specimens by the method outlined in Section 4.4.4. Saturation was generally established over a period of 6 hours. A second series of B tests were conducted after the isotropic compressibility tests to check the conditions of saturation. The pore fluid saturation pressures and pore pressure parameter B are summarized in Table 5.3.

The magnitude of the pore pressure paramater B at initial saturation ranged from 0.81 to 0.93. In comparison, the measurement of B at initial saturation for high quality Saline Creek oil sand ($I_D$<12 %) in Chapter 4 range from 0.90 to 1.0 at effective confining pressures between 50 and 150 kPa. A slight increase in B was noted following cyclic compression of SYN-T-3, SYN-T-5 and SYN-C-1. This is due to the decrease in effective confining pressures for the latter B tests. The largest increase in B from 0.81 to 0.90 was observed for SYN-T-5 as $\sigma_3'$ at test was halved from 160 to 70 kPa. The change in B points out the sensitivity of the compressibility to confining stress, particularily at the lower stress levels.

The pore fluid saturation pressure of the Syncrude oil sand estimated from the initial B-tests varies between 400 and 680 kPa. Peacock(1986) conducted long term saturation tests on the Syncrude oil sand and measured the pore fluid saturation pressure to be 170 kPa at room temperature (20°C). The discrepancy between the measurements is attributed to the relatively rapid rate at which the initial B-tests were conducted as discussed in Section 4.4.4. This behaviour was again verified by re-checking the conditions of saturation following the cyclic compression of the test specimens. From the data presented in Appendix E, the apparent saturation pressure dropped to less than 300 kPa among the test specimens and is more consistent with the measurements reported by Peacock(1986).

## 5.6 Isotropic Compressibility

Isotropic compressibility tests were conducted on all triaxial test specimens. The test procedure described in Section 4.4.5 was followed. For test specimens SYN-T-1 through SYN-T-5, the effective confining pressure was cycled twice between 80 and 780 kPa in increments of 100 and 200 kPa. A single cycle was carried out on the compression test specimen SYN-C-1. The coefficient of volume compressibility measured for each loading cycle is summarized in Table 5.4.

The coefficient of volume compressibility, $m_v$ varies between $0.97 \times 10^{-5}$ and $1.61 \times 10^{-5}$ $kPa^{-1}$ on the second loading cycle over the range of isotropic stress between 400 and 700 kPa. In comparison, measurements of $m_v$ in Chapter 4 on samples of high quality Saline Creek oil sand range between $1.5 \times 10^{-6}$ and $6.0 \times 10^{-6}$ $kPa^{-1}$, up to one order of magnitude lower. The apparent conundrum between the higher compressibility and the otherwise high quality of the Syncrude oil sand is attributed to the clay clasts interspersed within the oil sand. The fines content (< 0.074 mm) of the grain size distributions ranges between 13.5 and 15.0 percent by weight. If it is assumed that the fines originate solely from the clay clasts, then the clasts contribute up to 15 percent of the total solids volume. Given the volume compressibility of a heavily overconsolidated clay to be approximately $1 \times 10^{-4}$ $kPa^{-1}$ (Carrier,1985), the bulk volume compressibility of a specimen comprised of 15 percent clay clasts by volume would be $1.59 \times 10^{-5}$ $kPa^{-1}$. The volume compressibility of the oil sand in the remaining 85 percent of the solids volume is assumed to be $1 \times 10^{-6}$ $kPa^{-1}$ for high quality oil sand. It is concluded that the use of volume compressibility as an index of oil sand quality can underestimate the quality of oil sand when inclusions of more compressible argillaceous material are present. In this case, the index of disturbance is a more reliable indicator of sample quality with respect to the in situ state.

Overall, the volume of the test specimens decreased less than 0.4 percent upon completion of the cyclic compression tests. The slight compaction of the specimens reflects the very high initial density. The coefficient of compressibility, $m_v$ measured on each loading cycle is plotted against the effective confining stress in Figure 5.6. The compressibility of the oil sand at stresses less than 100 kPa is up to 5 times greater than at stresses above 500 kPa. This shows the sensitivity of compressibility to confining stress as inferred from the B-tests in the previous section.

The volume change in SYN-C-1 for the loading increments of isotropic stress of 81-198, 198-389, 389-589 and 589-791 kPa are plotted against the square root of time in Figures E.7 through E.10. The coefficient of consolidation, $C_v$ can be estimated from the plots by the method proposed by Bishop and Henkel(1962). The coefficient of consolidation is given by:

$$C_v = \frac{k_1 h^2}{t_{100}} \qquad 5.1$$

where h is one-half the height of the specimen, $k_1$ is a constant for the sample drainage conditions, and $t_{100}$ is measured from the plot of volume change versus the square root of time by the construction shown in Figure 5.7. For the specimen height/diameter ratio of 2 and conditions of drainage from the radial boundary and one end of the specimen as for SYN-C-1, the value value of $k_1$ is $\pi/81$. The coefficient of consolidation calculated from Equation 5.1 for each loading increment is tabulated in Table 5.6.

Gibson and Henkel(1954) and Bishop and Gibson(1963) found the average degree of consolidation at failure, $\overline{U}_f$, in an undrained compression test may be expressed in the form:

$$\overline{U}_f = 1 - \frac{h^2}{k_2 C_v t_f} \qquad 5.2$$

where $t_f$ is the time to failure, and $k_2$ is a factor depending upon drainage conditions at the sample boundary. Bishop and Henkel(1962) show that a theoretical degree of consolidation of 95 percent is sufficient to ensure a negligible error in the measurement of drained strength. The requisite time to failure for a drained triaxial test may then be written as:

$$t_f = \frac{20h^2}{k_2 C_v} \qquad 5.3$$

For the conditions of drainage for Test SYN-C-1, the value of $k_2$ is 35.8. Hence:

$$t_f = \frac{0.559\ h^2}{C_v} \qquad 5.4$$

The requisite time for failure at each confining stress is also tabulated in Table 5.6. The time to failure ranges between 35 and 91 minutes and increases with the confining stress, reflecting the decrease in sample permeability with higher confining stress.

## 5.7 Drained Axial Compression Test

The drained compression test SYN-C-1 was conducted at an effective confining pressure of 15 kPa. Due to the very low confining pressure, the difference between the confining cell and pore pressures were set by the mercury manometer. The slowest strain rate attainable by the test apparatus of $8.7 \times 10^{-7}$ $s^{-1}$ was used, giving a conservative time to failure of 7.1 hours. Assuming the magnitude of $C_v$ from Table 5.6 to be $3.86 \times 10^{-2}$ $cm^2/s$ or greater, the predicted degree of consolidation at failure was at least 99.5 percent.

The load cell, LVDT's, cell pressure and pore pressure transducers were monitored continuously throughout the test by the electronic data acquistion system. The effective confining pressure was checked periodically by the mercury manometer. Volume changes were regularly recorded from the volume change indicator. Measurements and observations of the condition of the specimens were noted on the completion of testing. The final bulk water content was measured by air drying the specimen after testing. The test results are presented in Appendix E and summarized in Table 5.5.

## 5.8 Axial Extension Tests

### 5.8.1 Test Procedures and Analyses

The axial extension tests were conducted by the method described by Bishop and Garga(1969). Three drained tests (Tests SYN-T-1, SYN-T-2 and SYN-T-3) were conducted at effective confining pressures of 58, 71 and 63 kPa respectively. Two undrained tests (Tests SYN-T-4 and SYN-T-5) were conducted at initial effective confining pressures of 32 and 80 kPa.

The rate of axial deformation for Test SYN-T-1 was 1.12 mm per hour. The remaining tests were conducted at 0.233 mm per hour, the slowest rate attainable by the test apparatus. The time to failure and the degree of consolidation estimated by Equation 5.2 for each drained test are tabulated in Table 5.7. The minimum degree of consolidation is predicted to be 98 precent for SYN-T-1. Pore pressures throughout the undrained tests were maintained above the pore fluid saturation pressure measured in Section 5.5 to prevent cavitation of the pore fluid during testing.

The configuration of stresses and forces acting on the extension test specimens are shown in Figure 5.8. The magnitude of the total vertical stress acting through plane

A-A' within the notched section of the specimen is given by:

$$\sigma_n = \sigma_c - \frac{T}{A_n} \qquad 5.5$$

and the effective stress is:

$$\sigma'_n = \sigma_c - \frac{T}{A_n} - u = \sigma'_c - \frac{T}{A_n} \qquad 5.6$$

The maximum magnitude of the tension force T is limited by the condition at which the end caps will become detached from the ends of the specimen so the effective vertical stress along plane B-B' at the end of the sample drops to zero. Hence:

$$\sigma'_e = \sigma'_c - \frac{T_{max}}{A_e} = 0 \qquad 5.7$$

or

$$T_{max} = \sigma'_c \, A_e \qquad 5.8$$

Thus, the limiting value of the tensile stress developed along plane A-A' is:

$$\sigma'_{n_{min}} = -\sigma'_c \left(\frac{A_e}{A_n} - 1\right) \qquad 5.9$$

Failure of specimens will not occur if the magnitude of the tensile strength exceeds $\sigma'_{n_{min}}$. For initial effective confining pressures between 50 and 100 kPa, the required minimum area ratio to attain a maximum anticipated tensile strength of 20 kPa for oil sand ranges between 1.2 and 1.4. Area ratios ranging between 1.72 and 2.27 were therefore selected for the test program.

Measurements of the load cell, LVDT's, cell and pore pressure transducers, and volume change were made in the same manner as for the compression test. Measurements and observations of the specimens after failure were noted. Samples for water content determination were taken at the zone of parting and at the ends of the specimen. The samples were air dried to estimate the final water content. The triaxial test results are presented in Appendix E and summarized in Table 5.5.

### 5.8.2 Mode of Failure of Test Specimens

Measurements of the specimens upon the completion of testing are presented in Appendix E. SYN-T-1, SYN-T-2 and SYN-T-4 failed by a brittle fracture parting within the notch zone perpendicular to the vertical axis of the specimens. Slight inclinations between 4 and 7 degrees to horizontal were observed in the initial parting surfaces for SYN-T-3 and SYN-T-5. It was not possible to determine if the partings exhibited the conical "cup and cone" tensile fracture due to the necking of the specimens around the parting with further axial extension. The majority of the axial elongation of the specimens occurred in the zone of parting. In retrospect, it is intuitively obvious that once a parting occurs all further axial extension of the specimen occurs as widening of the parting only. The observed necking of the specimens at the parting is caused by shear failure of material around the outer edges of the parting surface.

The changes in water content within the specimens during testing concur with the mode of failure. As tabulated in Table 5.5, the final water content within the notch zone exceeds the water content at the ends of the specimens in all tests. This reflects the concentration of straining and increase in porosity with dilation in the notch zone. Much higher differences in water content are noted in the undrained tests caused by suction of water from the ends of the specimens into the notch zone. The tests are consequently only partially undrained as the consolidation of the specimen ends allows an increase in volume or dilation in the notch zone.

### 5.8.3 Straining During Triaxial Tension Tests

Measurements of axial deformation along the length of SYN-T-5 were attempted during the undrained extension test. Thin strips of filter paper were dyed red and placed at approximately 5 mm intervals along the length of the specimens. The displacement of the strips were measured by a vertical vernier telescope. The bottom of the top loading ram immediately above the sample was used as the reference point for the measurements. The displacement of only two points along the top half of the notch as shown in Figure 5.9 could be recorded as the reinforcing bands around the exterior of the plexiglass cell blocked the view of the vernier telescope. The displacement and strain between the two points are plotted against the total axial extension of the sample in Figure 5.9. The following observations are clearly evident from the figure:

1) The displacement of both measurement points prior to the formation of a parting indicates that vertical axial straining with the reduction of vertical stress occurs throughout the notch height of the specimen. The strain between the two points correlates well with the strain predicted assuming that axial elongation of the notch height only occurs during the test.
2) The effective ceasation of the displacements after the parting of the specimen confirms that almost all further axial extension occurs as widening of the parting. Recompression of the notch zone outside the parting, as suggested by the negative straining, occurs as the resistance of the specimen is overcome.
3) Theoretically, the formation of the parting occurs as the minimum minor principal stress is reached. Visible indications of the parting are not apparent until the parting is opened by further axial

extension, approximately 0.40 mm for SYN-T-5.

The volume change during the drained axial extension of SYN-T-1, SYN-T-2 and SYN-T-3 are plotted in Figures 5.10 through 5.12 respectively. For comparison, the volume change predicted as:

$$\Delta V = (\text{Axial Extension}) \times (\text{Initial Area of Notch}) \qquad 5.10$$

is also shown in the figures. The match between the predicted and measured volume changes are markedly close for SYN-T-1 and SYN-T-2. For SYN-T-3, the predicted volume change overestimates the measured volume change roughly by 25 percent throughout the the test. Interestingly, the formation of a parting in the specimens does not affect the rate of volume change in the specimens. This is not unexpected considering that deformation of the notch zone is merely changed to widening of the parting or high straining of a localized portion of the notch rather than uniform straining throughout.

Based on the foregoing observations, the axial straining of the tension test specimens were accordingly calculated as uniform axial elongation of the notch height only. Corrections to the cross-sectional area of the notch were calculated assuming the notch zone deforms as a right cylinder. Compensation for dilation of the specimens were made for the drained tension tests. Calculation of strain in this manner is accurate up to parting of the specimens as the minor principal stress is reached. After parting, very high local straining takes place as widening of the parting over a localized length of the notch occurs. The area corrections are also underestimated as the specimens begin to "neck" in at the parting.

### 5.8.4 Membrane Corrections to Triaxial Test Results

It is common practice in conventional geotechnical testing to neglect the strength corrections for membrane effects since they are small and become negligible at confining pressures greater than 100 kPa. In this series of tests, it was recognized that membrane effects may contribute significantly to the measurement of strength at the very low stress levels. A series of tests to evaluate the effects of the membranes were conducted and are described in the following sections.

#### 5.8.4.1 Extension Modulus of the Rubber Membranes

The extension modulus, M of the rubber membranes was measured by the method described by Henkel and Gilbert(1962). A 47.3 mm wide circumferential strip of the latex rubber membrane was suspended between two glass rods as shown in Figure 5.13. Load was applied to the strip by dead weights and the extension of the membrane measured by a vertical vernier telescope. The results of the test are shown in Figure 5.14. The load-strain behaviour is slightly non-linear on loading. The extension modulus for the 0.39 mm thick membrane is 75.5 g/mm for extension strains less than 7.0 percent.

Henkel and Gilbert(1952) present a method for calculating the correction for the membrane effects in triaxial compression tests. The method is based on the following assumptions:

1) the membrane is held against the sample by the cell pressure and is capable of taking compression;
2) the deformation modulus of the membrane is the same in compression as in extension; and
3) the sample deforms as a right cylinder.

The correction to be applied to the measured compressive strength is:

$$\sigma_r = \frac{-\pi d M \epsilon (1 - \epsilon)}{A_o} \qquad 5.11$$

where D is the initial diameter of the specimen, $A_o$ is the initial sample area, $\epsilon$ is the sample strain, and M is the compression modulus of the membrane.

The compression test SYN-C-1 was observed to fail generally by bulging without the development of a single distinct shear plane. The application of this method of correction for membrane effects was therefore felt justified and was applied to the test data. The maximum strain reached in SYN-C-1 was 6.90 percent and the compression modulus of 75.5 g/mm was used.

#### 5.8.4.2 Membrane Extension Tests in the Triaxial Cell

A series of membrane extension tests were conducted in the triaxial cell by substituting a replicate steel sample for the tension test specimens. The replicate steel sample is shown in Figure 5.15. The centre notch section consists of a sleeve assembly to model the straining of the test specimens in the notched zone. The inside of the assembly was lubricated with light oil to provide free movement. The steel replicate was installed in the cell in the same manner as for the oil sand samples. The sample was saturated under an effective confining pressure of 75-100 kPa and pore pressure of 400 kPa.

Two extension tests were conducted. In the first test, a membrane was form fitted over the sample to model the conditions of SYN-T-1. For the second test, a convolution or fold in the membrane was formed at the mid-height of the notch to evaluate the reduction in membrane resistance for SYN-T-2 through SYN-T-5. Increments of axial extension were applied to the sample and maintained until the load equilibrated, generally 10 minutes or less. The configuration of the net forces and stresses acting during the extension tests is illustrated in Figure 5.16. The steel sample exhibits no tensile strength due to the sleeve in the notched section, hence $\sigma'_3 = 0$. The resistance of the membrane, $T_m$ is then calculated as:

$$T_m = T - \sigma'_c A_n - \sigma'_c A_m \qquad 5.12$$

where T is the measured axial load, $\sigma'_c$ is the effective confining cell pressure, $A_n$ is the cross-sectional area of the specimen within notch, and $A_m$ is the sectional area of the membrane. The results of the tests are shown in Figure 5.17.

For comparison purposes, the calculated equivalent resistance of a 38.1 mm diameter membrane is shown in Figure 5.17 assuming an extension modulus of 75.5 g/mm as found in Section 5.8.1. Two cases of axial extension are shown: (1) extension of the membrane over the 25.3 mm length of the notched section of the sample only, and (2) extension over the full 76.6 mm height of the sample. Several observations can be drawn from the figure:

1) For axial extensions less than 1.0 mm, the very close correlation between the resistance of the unconvoluted membrane and the predicted resistance assuming extension of the membrane over the notch

height indicates the membrane strain is confined to the notched zone only. As axial extension increases, slippage occurs between the membrane and the sample and the membrane resistance decreases. The parallel slope between the membrane resistance and the predicted resistance assuming uniform extension of the membrane over the full sample height suggests that the slippage is almost complete at axial extensions greater than 2 mm.

SYN-T-1 reached failure at an axial extension of 1.47 mm. The measured axial load for SYN-T-1 was corrected for membrane resistance assuming the axial extension of the membrane occurred over the notch height of the specimen only. This correction is conservative and will cause a slight underestimation of the strength of SYN-T-1.

2) The resistance of the convoluted membrane is roughly equal to the unconvoluted membrane up to 2.5 mm of axial extension. The drop in load with further axial extension is probably caused by the stick-slip sliding between the faces of the convolution as it tries to open. The eventual opening of the fold releases the tension in the membrane and the resistance is observed to fall substantially.

Given the uncertainity of the stick-slip phenomena, it was chosen to assume the convoluted membrane was ineffective in reducing the membrane resistance. The membrane correction for SYN-T-1 was applied to the axial load for SYN-T-2 through SYN-T-5. In retrospect, this assumption was found not unreasonable as the axial extension at failure among the specimens was less than 1.70 mm.

### 5.8.4.3 Correction for Membrane Area

As shown in Figure 5.16, enclosing the tension specimens with the latex rubber membrane increases the cross-sectional area through the notch zone by the area:

$$A_m = \pi d_m t_m \qquad 5.13$$

where $D_m$ and $t_m$ are the diameter and thickness of the membrane. The axial load in the drained tests must therefore be corrected by the force, ($\sigma_c'$ x $A_m$), to compensate for membrane area. In the undrained tests, the correction increases throughout the tests with the drop in pore pressure and increase in effective confining cell pressure, $\sigma_c'$.

## 5.9 Unconfined Extension Tests

An unconfined axial extension test (SYN-T-6) was conducted on the Syncrude oil sand to evaluate the effect of confining stress on the measurement of strength in axial extension and attempt to correlate the membrane corrections applied in the confined tension tests. Two samples of disturbed (estimated $I_D$ = 15.5 and 24.2) bitumen-rich Saline Creek oil sand, SC-84-T-1 and SC-84-T-2, were also tested to measure the tensile resistance mobilized by the interstitial bitumen. The detailed test procedures followed and test results are presented in Appendix [illegible].

### 5.9.1 Failure of Test Specimens

A field of tensile stresses are developed in the suspended test specimens under the bouyant "self-weight", with the maximum tensile stresses occuring in the notch zone. The average tensile stress developed within the notch zone of each specimen is tabulated in Table 5.8. Very low tensile stresses ranging between 2 and 3 kPa are achieved.

Specimens SYN-T-6 and SC-84-T-1 were suspended in the triaxial cell and thawed under the applied cell pressures. SYN-T-6 failed by parting horizontally within the notch zone. SC-84-T-1 failed by a combination of horizontal parting and shear along the inclined bedding planes in the core. The specimens failed at 5 and 1 minutes, respectively, after application of the cell pressure. It is judged that both failures were concurrent with thaw of the specimens through the notch zone.

SC-84-T-2 was thawed for 3 hours while resting on the bottom of the triaxial cell. The specimen was then raised off the bottom of the cell at the rate of 0.5 mm per minute. Initiation of parting was observed to occur at the bottom edge of the notch zone and propagate through the specimen. The parting of the specimen in this manner appeared to be caused by the slight eccentricity of loading while raising the specimen off the bottom of the cell.

SYN-T-6 and SC-84-T-1 were left in the triaxial cell to observe the slaking of the specimens over a period of 4 and 5 days, respectively. SYN-T-6 totally segregated over the four day period. The primary mechanism was the dispersion of the clay clasts. SC-84-T-1 displayed virtually no tendency to slake over the period of 5 days due to the viscosity of the bitumen. Less than a 0.3 percent increase in the sample dimensions was measured after testing.

The dimensions of SC-84-T-2 were also re-measured immediately after failure. Virtually no swell of the sample was measured. The absence of expansion in SC-84-T-1 and SC-84-T-2 suggests that gas exsolution and undrained expansion of the oil sand was effectively suppressed by maintaining pore pressures above the pore fluid gas saturation pressure.

## 5.10 Summary

This chapter describes the testing equipment and experimental procedures followed for the triaxial tests on bitumen-poor Syncrude oil sand. A total of eight drained and undrained extension tests were performed under confined and unconfined stress conditions. The method of shaped test specimens described by Bishop and Garga(1969) was used to evaluate the presence of any tensile resistance in the interpenetrative "locked" structure of the oil sand tested. An additional single drained axial compression test was conducted under very low effective confining stress.

Table 5.1 Syncrude and Saline Creek Oil Sand: Summary of Test Specimen Data

| SAMPLE | DIAMETER | | LENGTH | | INITIAL DENSITY $\gamma$ ($Mg/m^3$) | INITIAL POROSITY $n_i$ | INITIAL SATURATION $S_i$ (%) | WATER CONTENT $w_w$ (%)[1] | BITUMEN CONTENT $w_b$ (%)[1] | INDEX OF DISTURBANCE $I_D$ (%)[2] |
|---|---|---|---|---|---|---|---|---|---|---|
| | ENDS (mm) | NOTCHED SECTION (mm) | TOTAL (mm) | NOTCHED SECTION (mm) | | | | | | |
| SYN-C-1 | 37.95 | - | 75.77 | - | 2.089 | 0.331 | 94.3 | 9.8 | 5.3 | 6.8 |
| SYN-T-1 | 37.90 | 28.95 | 70.22 | 15.60 | 2.066 | 0.328 | 86.5 | 11.4 | 2.4 | 5.8 |
| SYN-T-2 | 37.90 | 28.70 | 89.05 | 16.40 | 2.059 | 0.330 | 85.6 | 11.4 | 2.4 | 6.5 |
| SYN-T-3 | 37.68 | 25.50 | 81.73 | 28.35 | 2.060 | 0.330 | 85.7 | 11.4 | 2.4 | 6.5 |
| SYN-T-4 | 38.35 | 25.60 | 89.60 | 30.00 | 2.092 | 0.330 | 94.8 | 9.8 | 5.3 | 6.5 |
| SYN-T-5 | 38.62 | 26.08 | 75.32 | 22.30 | 2.058 | 0.341 | 90.2 | 9.8 | 5.3 | 10.0 |
| SYN-T-6 | 73.20 | 45.60 | 200.8 | 27.40 | 2.162 | | | | | |
| SC-84-T-1 | 60.00 | 40.40 | 201.1 | 18.00 | 1.902 | 0.410[3] | 80.1 | 2.8 | 14.9 | 24.2 |
| SC-84-T-2 | 68.40 | 45.20 | 194.1 | 24.00 | 1.992 | 0.381[3] | 90.2 | 2.8 | 14.9 | 15.5 |

1. By total mass of sample

2. Using $n_i$ = 0.310 assuming in situ pore fluid content equals 14.5 percent of the total mass and 100 percent saturation.

3. Using average values of $w_w$ = 2.8 % and $w_b$ = 14.9 % for Saline Creek oil sand.

Table 5.2 Syncrude Oil Sand: Grain Size Data

| SAMPLE | GRAIN SIZE DATA | | | | |
|---|---|---|---|---|---|
| | $D_{10}$ (mm) | $D_{50}$ (mm) | $D_{60}$ (mm) | UNIFORMITY COEFFICIENT $C_u = D_{60}/D_{10}$ | FINES CONTENT (%<0.074 mm) |
| SYN-T-1 | 0.04 | 0.11 | 0.13 | 3.3 | 13.5 |
| SYN-T-2 | 0.04 | 0.11 | 0.13 | 3.3 | 13.5 |
| SYN-T-3 | 0.04 | 0.11 | 0.13 | 3.3 | 13.5 |
| SYN-T-4 | 0.03 | 0.16 | 0.18 | 6.0 | 15.0 |
| SYN-T-5 | 0.03 | 0.16 | 0.18 | 6.0 | 15.0 |
| SYN-C-1 | 0.03 | 0.16 | 0.18 | 6.0 | 15.0 |

Table 5.3 Syncrude Oil Sand: Summary of Pore Fluid Saturation Pressure and Pore Pressure Parameter B

| SAMPLE | PORE FLUID SATURATION PRESSURE | PORE PRESSURE PARAMETER B | | | |
|---|---|---|---|---|---|
| | | AFTER INITIAL SATURATION | | AFTER CYCLIC COMPRESSION | |
| | $P_s$ (kPa) | $\sigma_3'$ AT TEST (kPa) | B | $\sigma_3'$ AT TEST (kPa) | B |
| SYN-T-1 | 600 | 90 | 0.90 | 75 | 0.90 |
| SYN-T-2 | 560 | 100 | 0.88 | 90 | 0.85 |
| SYN-T-3 | 525 | 125 | 0.88 | 70 | 0.92 |
| SYN-T-4 | 400 | 105 | 0.93 | 85 | 0.94 |
| SYN-T-5 | 660 | 160 | 0.81 | 70 | 0.90 |
| SYN-C-1 | 680 | 150 | 0.87 | 85 | 0.91 |

Table 5.4 Syncrude Oil Sand: Summary of Isotropic Compressibility Tests

| SAMPLE | INITIAL DENSITY $\gamma$ (Mg/m$^3$) | COEFFICIENT OF VOLUME COMPRESSIBILITY, $m_v$ ($10^{-5}$ kPa$^{-1}$) | | |
|---|---|---|---|---|
| | | RANGE OF STRESS (kPa) | FIRST LOADING CYCLE | SECOND LOADING CYCLE |
| SYN-T-1 | 2.066 | 400-750 | 1.33 | 0.97 |
| SYN-T-2 | 2.059 | 400-750 | 1.73 | 1.31 |
| SYN-T-3 | 2.060 | 400-750 | 1.82 | 1.56 |
| SYN-T-4 | 2.092 | 400-750 | 2.56 | 1.61 |
| SYN-T-5 | 2.058 | 400-750 | 1.98 | 1.11 |
| SYN-C-1 | 2.089 | 400-750 | 1.84 | - |

# Table 5.5 Syncrude Oil Sand: Summary of Triaxial Test Results

| SAMPLE | INITIAL DENSITY $\gamma$ (Mg/m$^3$) | INITIAL TEST CONDITIONS | | CONDITIONS AT FAILURE IN NOTCH ZONE | | | | | | FINAL WATER CONTENT[2] | | |
|---|---|---|---|---|---|---|---|---|---|---|---|---|
| | | $\sigma'_{3i}$ (kPa) | $u_i$ (kPa) | $(\sigma_1-\sigma_1)_f$ (kPa) | $\sigma'_{1f}$ (kPa) | $\sigma'_{3f}$ (kPa) | $\Delta u$ (kPa) | AXIAL EXTENSION (mm) | $\epsilon_f$ (%) | NOTCHED ZONE (%) | ENDS OF SAMPLE (%) | TOTAL SAMPLE (%) |
| SYN-C-1 | 2.089 | 14.8 | 178 | 200.9 | 216.0 | 15.1 | 0. | - | 2.2 | 11.6 | 11.1 | - |
| SYN-T-1 | 2.066 | 57.5 | 849 | 56.1 | 57.5 | 1.4 | 0. | 1.47 | 9.4[3] | 11.5 | 10.3 | - |
| SYN-T-2 | 2.059 | 70.9 | 592 | 57.0 | 70.9 | 13.9 | 0. | 1.70 | 10.4[3] | 12.0 | 11.5 | - |
| SYN-T-3 | 2.060 | 63.1 | 546 | 63.4 | 65.0 | 1.5 | 0. | 1.15 | 4.1[3] | 13.0 | 10.6 | - |
| SYN-T-4 | 2.092 | 32.1 | 620 | 40.5[1] | 43.9 | 3.4 | -11.8 | 1.39 | 4.6[3] | 12.0 | 9.9 | - |
| SYN-T-5 | 2.058 | 86.9 | 598 | 156.1[1] | 162.8 | 6.7 | -82.6 | 0.81 | 3.6[3] | - | - | 12.5 |

1. Conditions at minimum minor principal stress, $\sigma'_{3f}$.

2. By total mass of sample.

3. Strain calculated over notch height of specimen.

Table 5.6 Coefficient of Consolidation and Requisite Time to Failure for SYN-C-1

| STRESS INCREMENT (kPa) | $t_{100}$ (minutes) | COEFFICIENT OF CONSOLIDATION $C_v = k_2h^2/t_{100}$ ($10^{-3}$ $cm^2/s$) | TIME TO FAILURE[1] $t_f = 0.559\ h^2/C_v$ (min) |
|---|---|---|---|
| 89-198 | 2.40 | 3.86 | 35 |
| 198-389 | 3.24 | 2.86 | 47 |
| 389-589 | 4.62 | 2.01 | 67 |
| 589-791 | 6.25 | 1.48 | 90 |

1. For average degree of consolidation of 95 percent in drained triaxial test.

Table 5.7 Time to Failure and Average Degree of Consolidation for Triaxial Tests

| SAMPLE | TIME TO FAILURE $t_f$ (hours) | AVERAGE DEGREE OF CONSOLIDATION $\overline{U}_f$ (%) |
|---|---|---|
| SYN-T-1 | 1.3 | 98.1 |
| SYN-T-2 | 9.9 | 99.7 |
| SYN-T-3 | 5.8 | 99.4 |
| SYN-T-4 | 6.0 | 99.3 |
| SYN-T-5 | 3.5 | 99.2 |
| SYN-C-1 | 7.1 | 99.5 |

Table 5.8 Tensile Stresses Developed in Unconfined Extension Tests

| SAMPLE | AVERAGE TENSILE STRESS IN NOTCH ZONE UNDER BUOYANT SELF-WEIGHT OF SAMPLE (kPa) |
|---|---|
| SYN-T-6 | 3.0 |
| SC-84-T-1 | 2.6 |
| SC-84-T-2 | 2.5 |

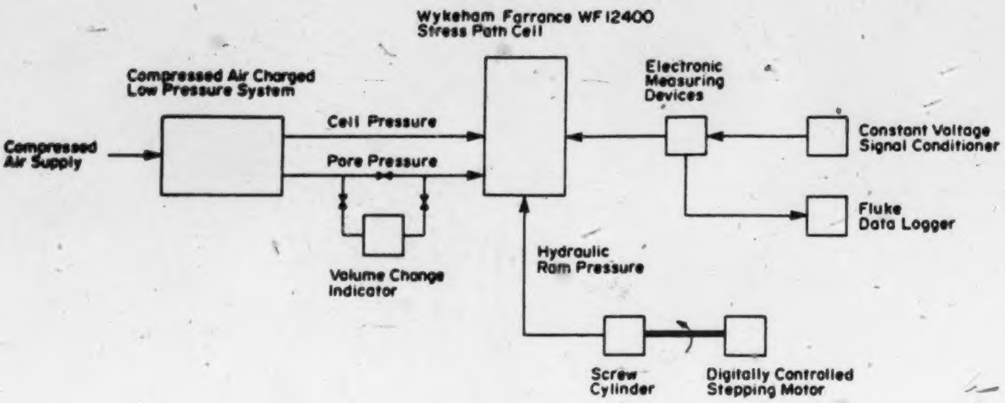
Wykeham Farrance WF 12400
Stress Path Cell
Compressed Air Charged
Low Pressure System
Compressed
Air Supply
Cell Pressure
Pore Pressure
Volume Change
Indicator
Electronic
Measuring
Devices
Constant Voltage
Signal Conditioner
Fluke
Data Logger
Hydraulic
Ram Pressure
Screw
Cylinder
Digitally Controlled
Stepping Motor

Figure 5.1 Schematic Layout of Low Pressure Testing Facility

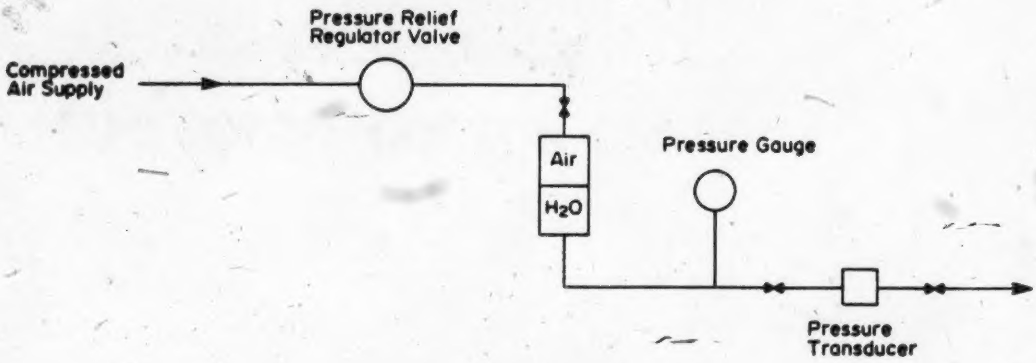
Pressure Relief
Regulator Valve
Compressed
Air Supply
Air
$H_2O$
Pressure Gauge
Pressure
Transducer

Figure 5.2 Air Activated Low Pressure System

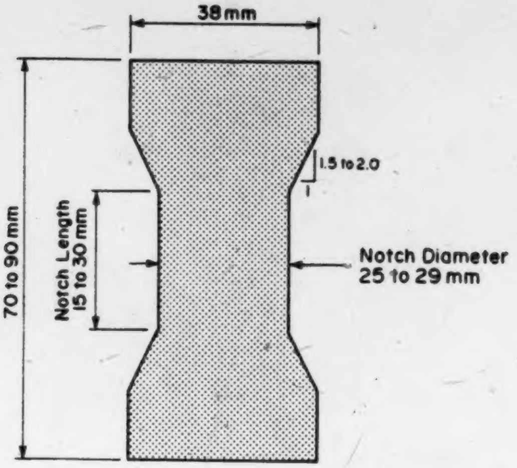
38mm
1.5 to 2.0
1
70 to 90 mm
Notch Length
15 to 30 mm
Notch Diameter
25 to 29 mm

Figure 5.3 Notching of Tension Test Specimens

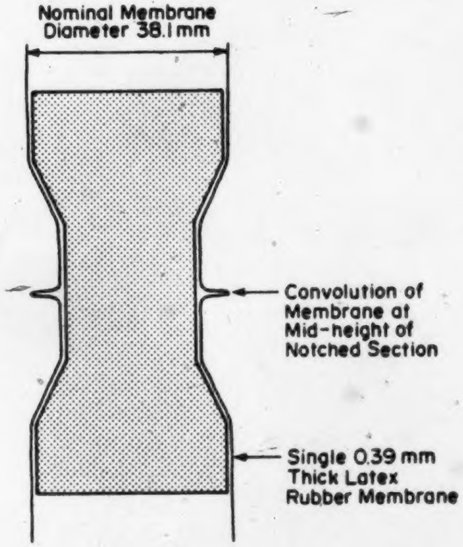
Nominal Membrane
Diameter 38.1 mm
Convolution of
Membrane at
Mid-height of
Notched Section
Single 0.39 mm
Thick Latex
Rubber Membrane

Figure 5.4 Convolution of Rubber Membrane for Tension Test Specimens SYN-T-2 Through SYN-T-5

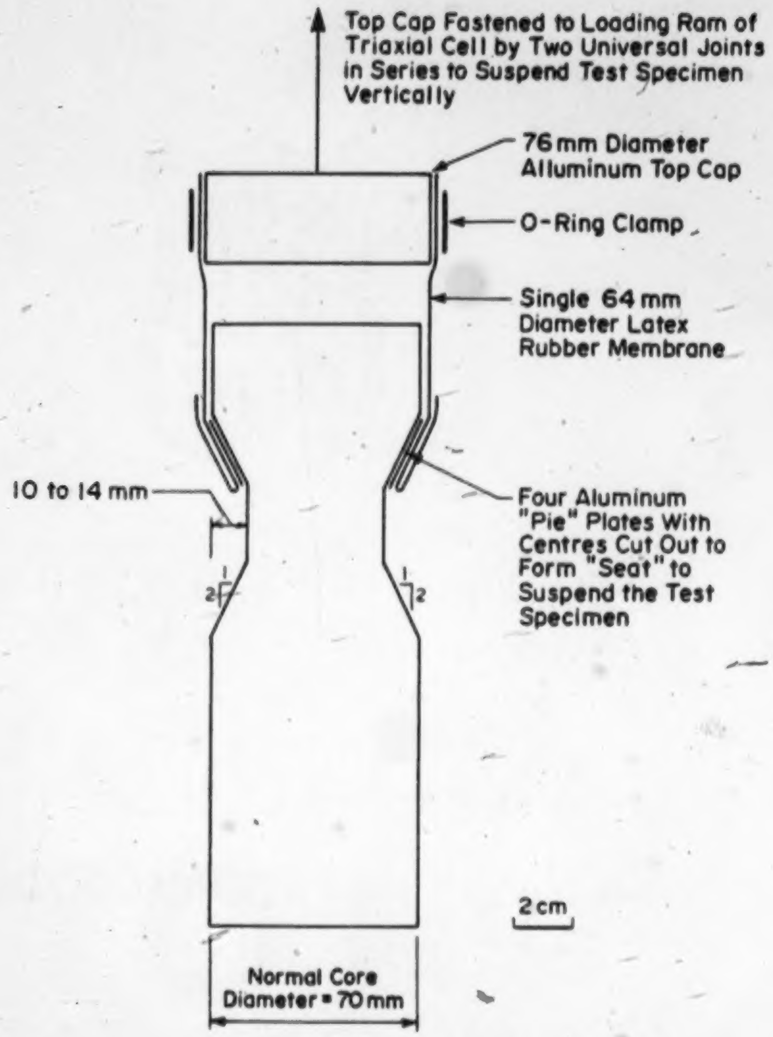
Top Cap Fastened to Loading Ram of Triaxial Cell by Two Universal Joints in Series to Suspend Test Specimen Vertically
76 mm Diameter Alluminum Top Cap
O-Ring Clamp
Single 64 mm Diameter Latex Rubber Membrane
Four Aluminum "Pie" Plates With Centres Cut Out to Form "Seat" to Suspend the Test Specimen
10 to 14 mm
1
2
1
2
2 cm
Normal Core Diameter = 70 mm

Figure 5.5 Suspension of Unconfined Tension Test Specimens in the Triaxial Cell

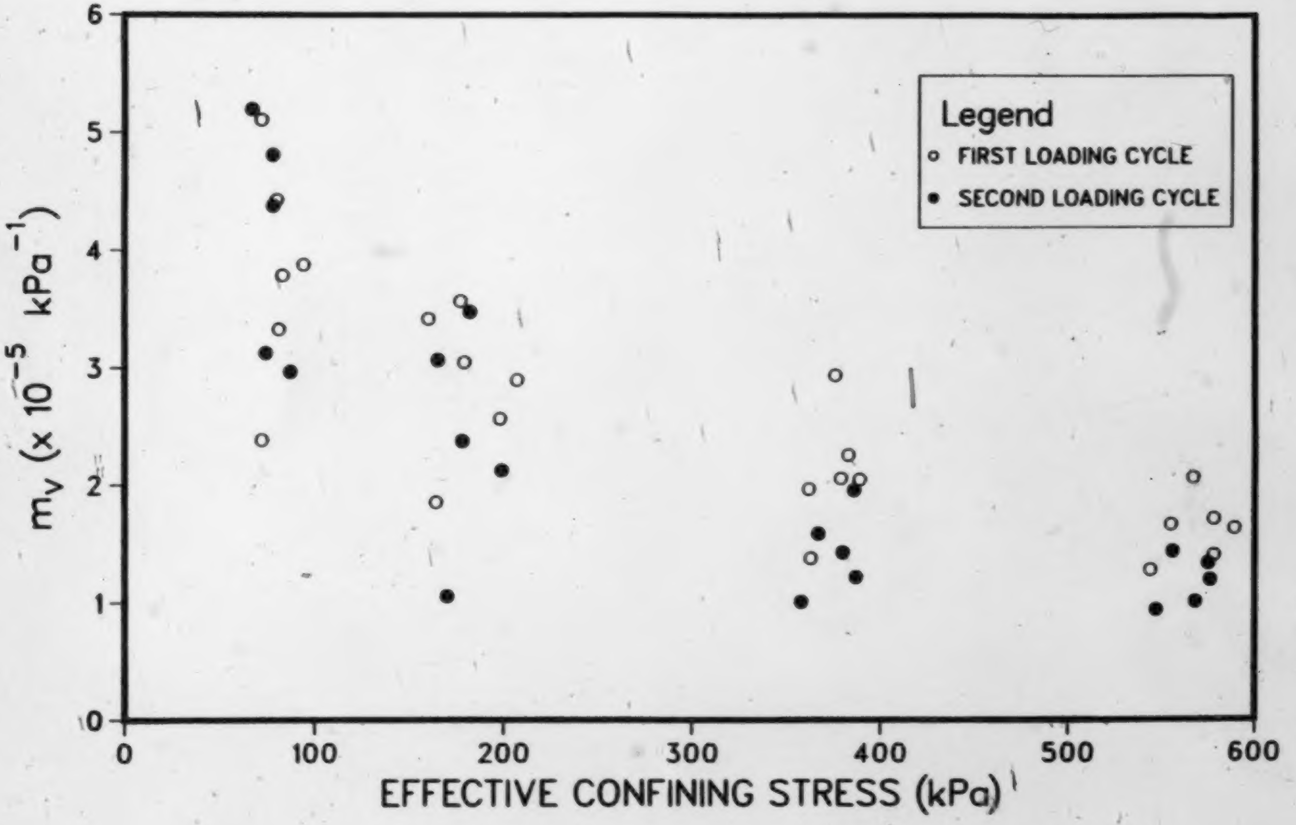

Figure 5.6 Coefficient of Volume Compressibility Versus Effective Confining Pressure

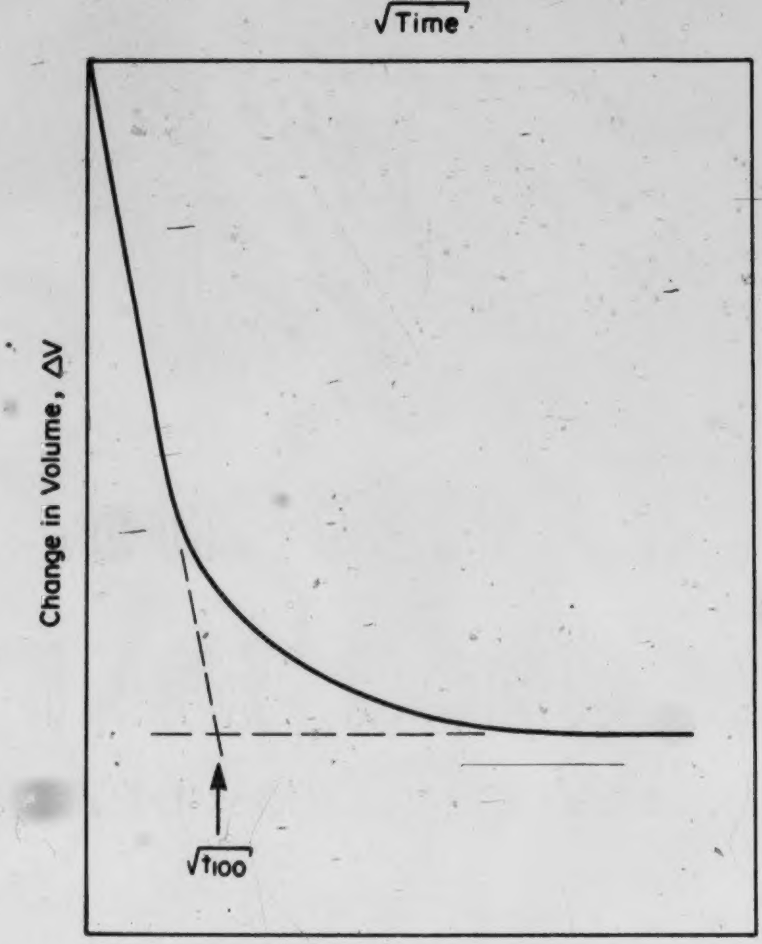

Figure 5.7 Calculation of $t_{100}$ From Isotropic Compression Tests

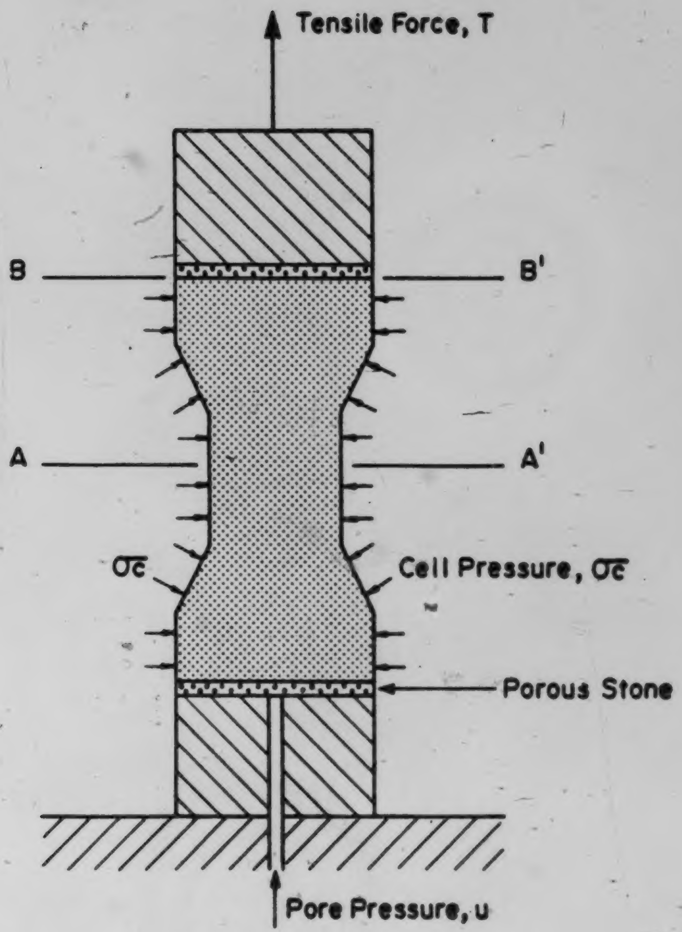
Tensile Force, T
B
B'
A
A'
σc
Cell Pressure, σc
Porous Stone
Pore Pressure, u

$A_n$ = Area Through Plane A—A'
$A_e$ = Area Through Plane B—B'

Figure 5.8 Stresses Acting on Tension Test Specimens

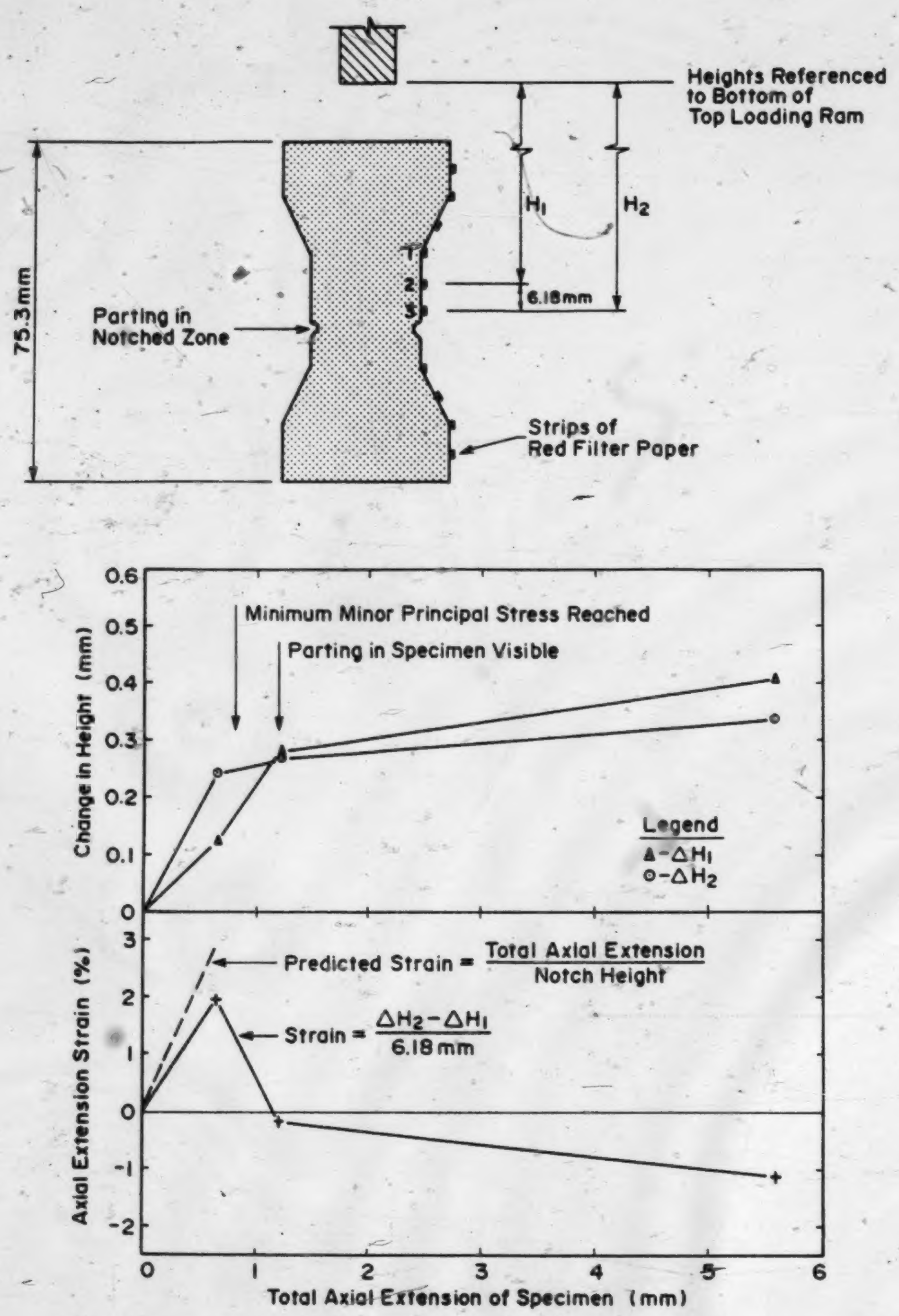

Figure 5.9 Measurement of Axial Deformation Along SYN-T-5 During Axial Extension Test

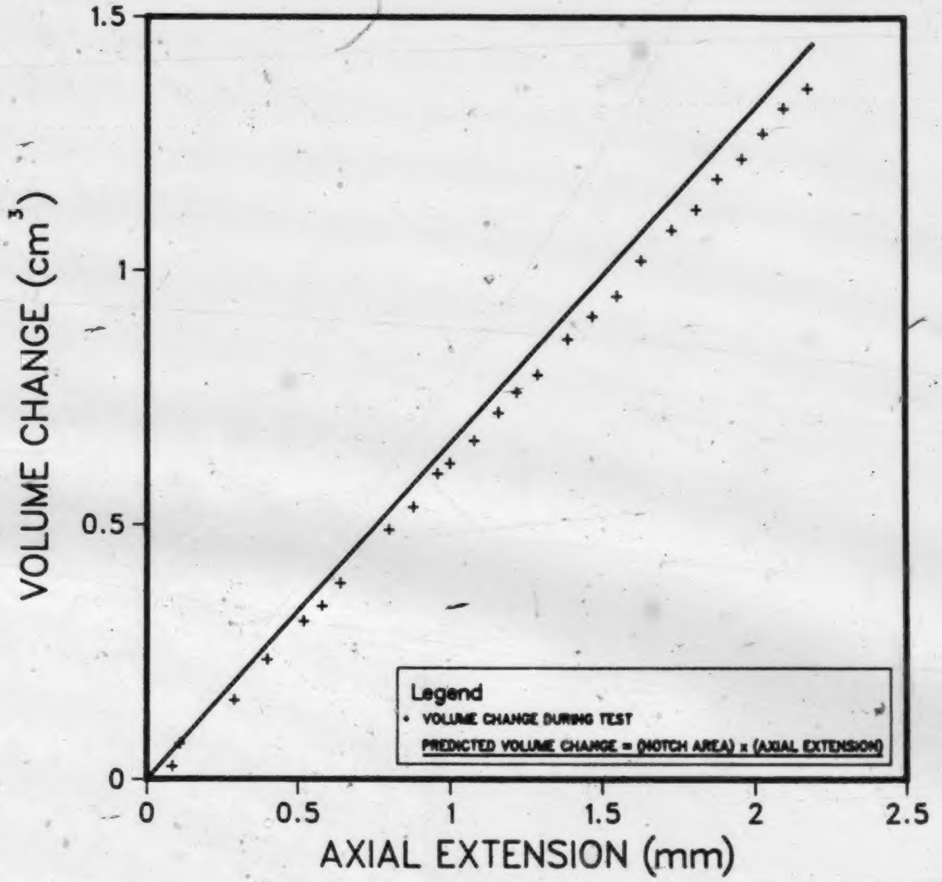

Figure 5.10 Volume Change During Axial Extension of SYN-T-1

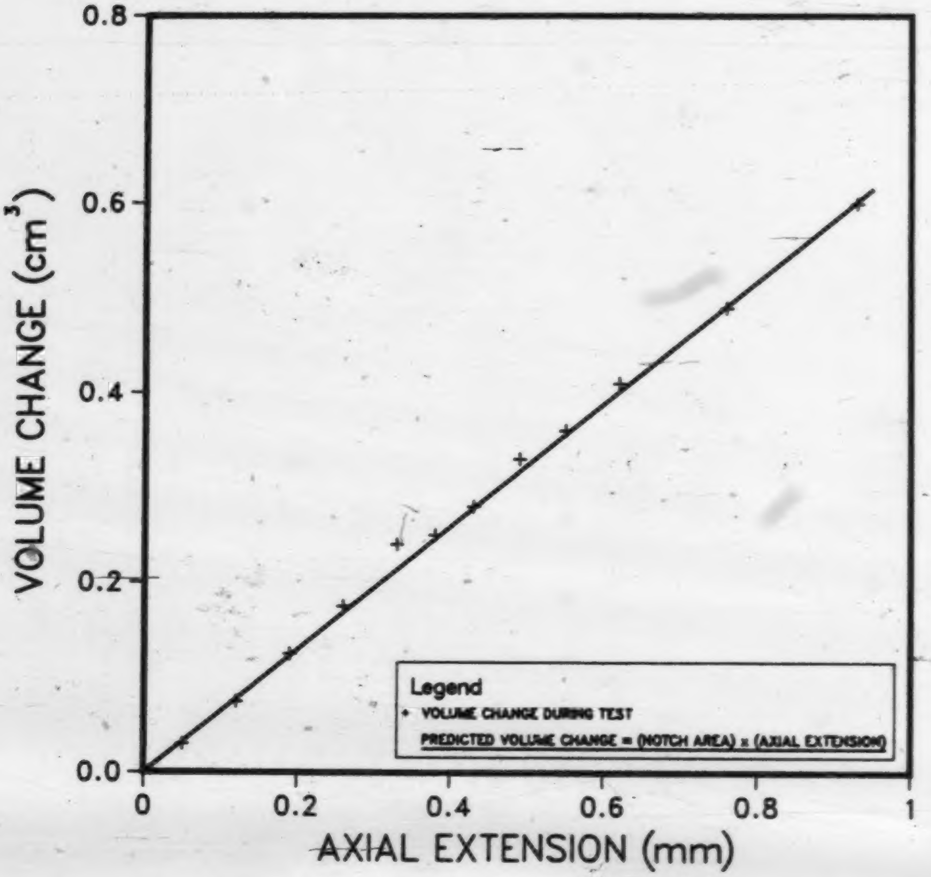

Figure 5.11 Volume Change During Axial Extension of SYN-T-2

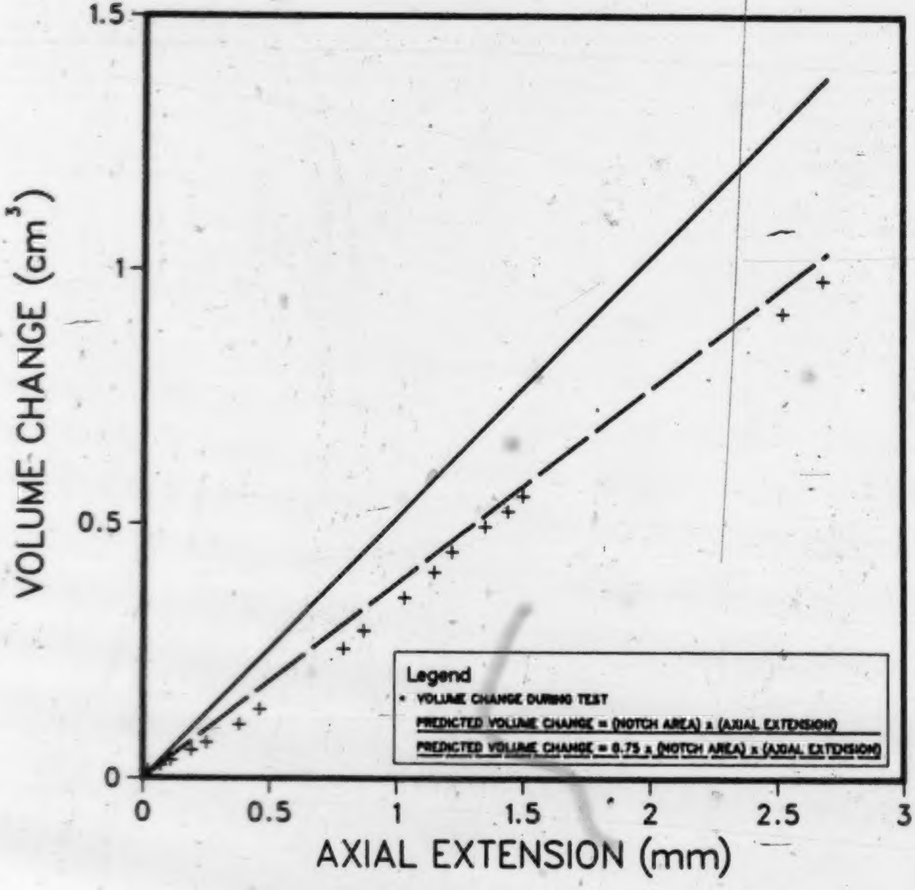

Figure 5.12 Volume Change During Axial Extension of SYN-T-3

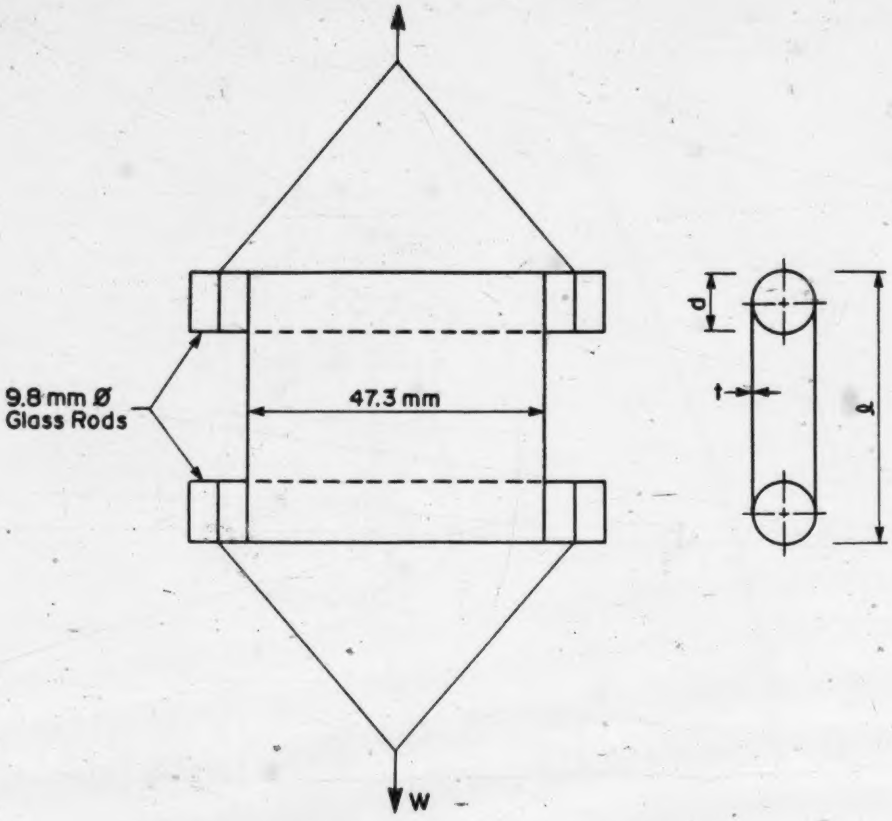
9.8 mm Ø
Glass Rods
47.3 mm
d
t
ℓ
W
Load Applied By
Dead Weights On Hanger

Mean Length of Membrane $= 2(\ell - d - 2t) + \pi(d - t)$

Strain $= \Delta\ell$ / Mean Length of Membrane

$$\text{Load Per mm} = \frac{W\ (g)}{2 \times 47.3\ (mm)}$$

$$\text{Extension Modulus } M = \frac{\text{Load Per mm}}{\text{Strain}}$$

Figure 5.13 Measurement of Extension Modulus of Rubber Membranes

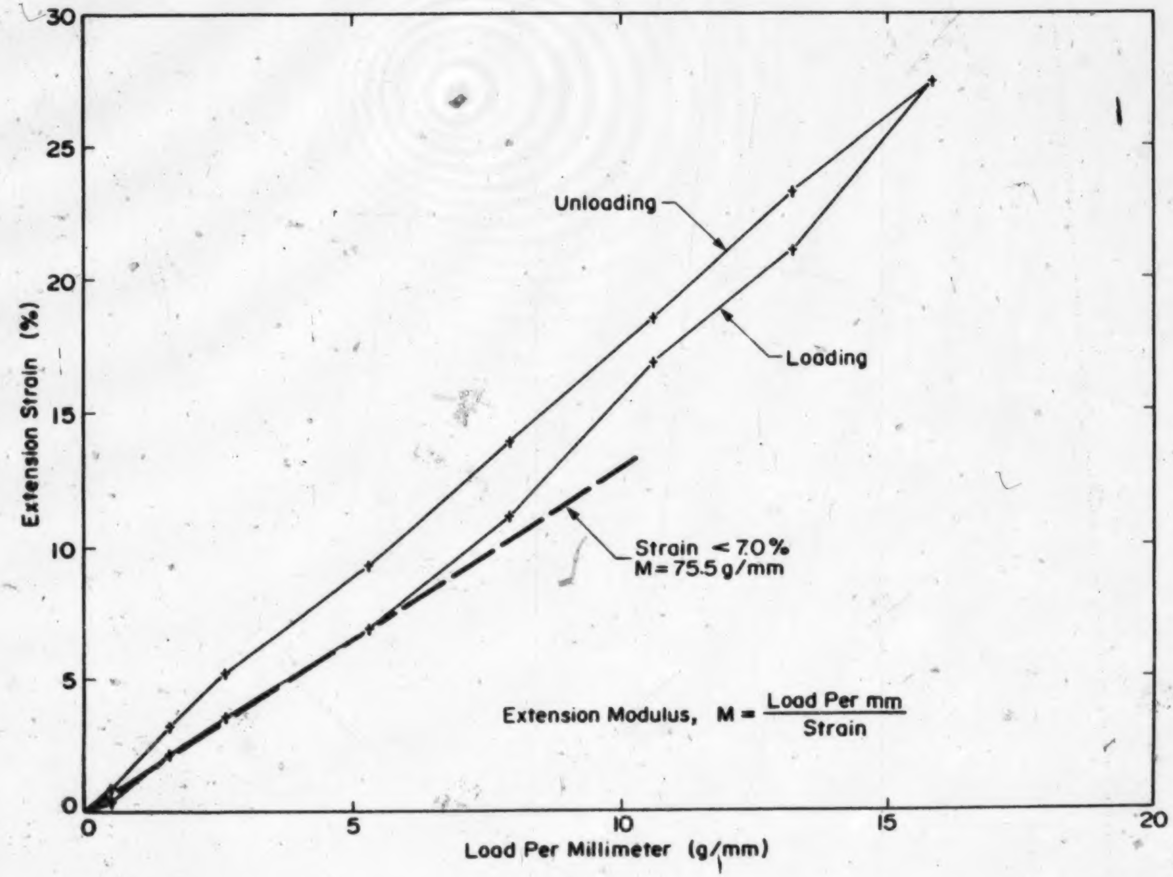

Figure 5.14 Results of Rubber Membrane Extension Test

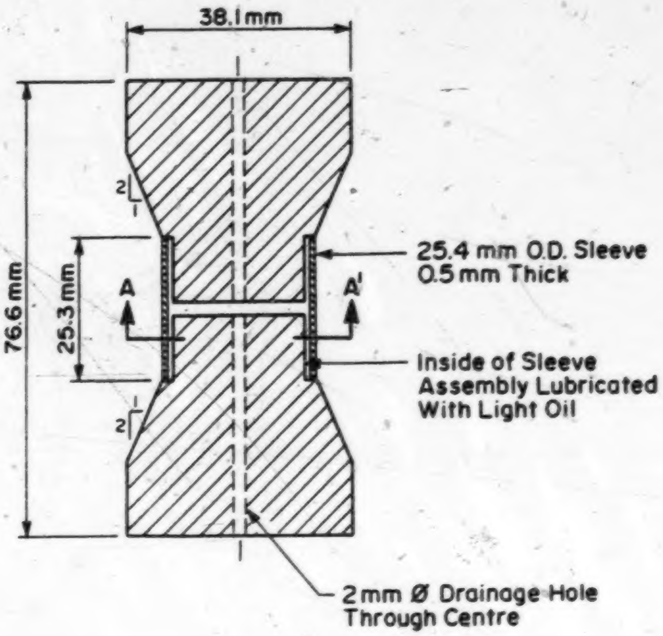
38.1mm
76.6mm
25.3mm
2
1
A
A'
25.4 mm O.D. Sleeve
0.5 mm Thick
Inside of Sleeve
Assembly Lubricated
With Light Oil
2mm Ø Drainage Hole
Through Centre

VERTICAL SECTION THROUGH SAMPLE

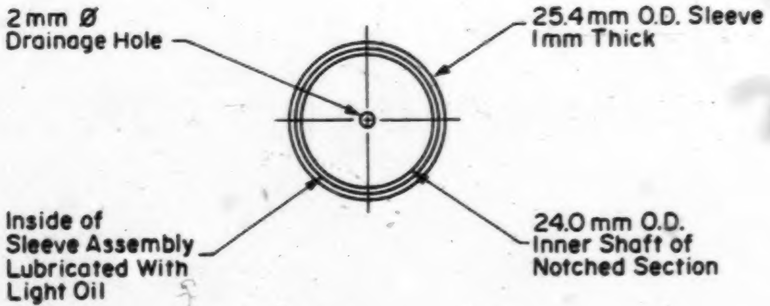
2mm Ø
Drainage Hole
25.4mm O.D. Sleeve
1mm Thick
Inside of
Sleeve Assembly
Lubricated With
Light Oil
24.0 mm O.D.
Inner Shaft of
Notched Section

SECTION A-A'

Figure 5.15 Replicate Steel Sample for Membrane Extension Tests in the Triaxial Cell

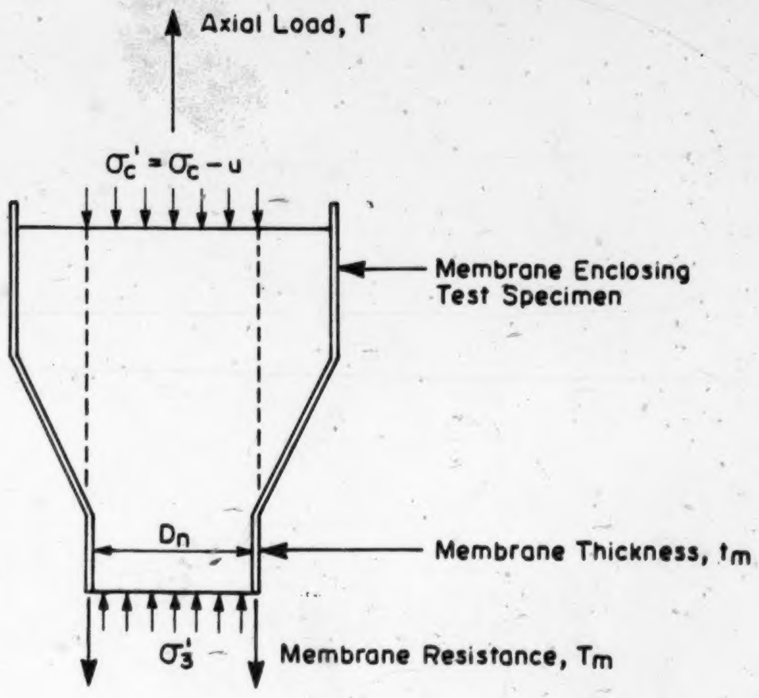
Axial Load, T
$\sigma_c' = \sigma_c - u$
Membrane Enclosing Test Specimen
$D_n$
Membrane Thickness, $t_m$
$\sigma_3'$
Membrane Resistance, $T_m$

Sectional Area of Notch, $A_n = \frac{\pi}{4} D_n^2$

Sectional Area of Membrane, $A_m = \pi D_m t_m$

$$T = (\sigma_c - u) A_n + (\sigma_c - u) A_m + T_m - \sigma_3' A_n$$

$$\sigma_3' = \sigma_c' - \frac{(T - \sigma_c' A_m - T_m)}{A_n}$$

Figure 5.16 Calculation of Membrane Resistance for Extension Tests in the Triaxial Cell

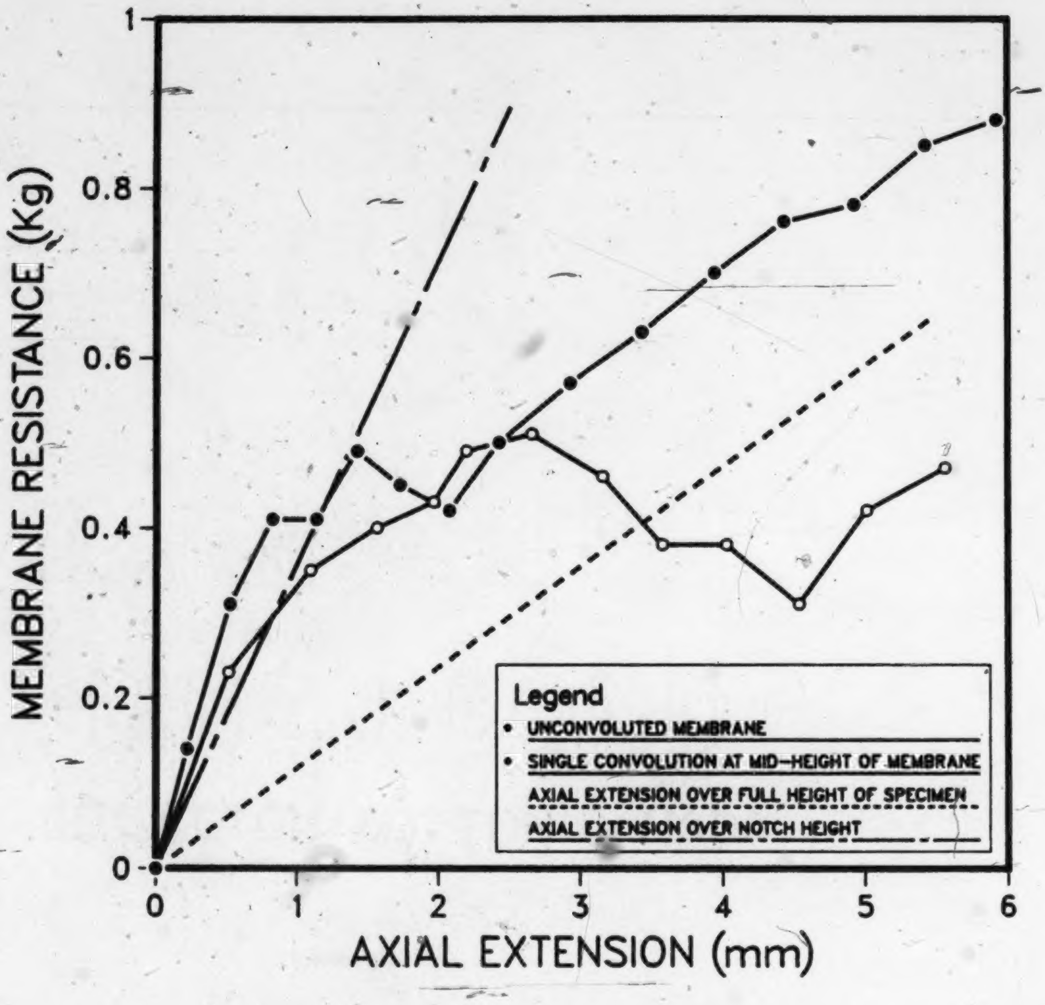

Figure 5.17 Test Results for Membrane Extension Tests in the Triaxial Cell

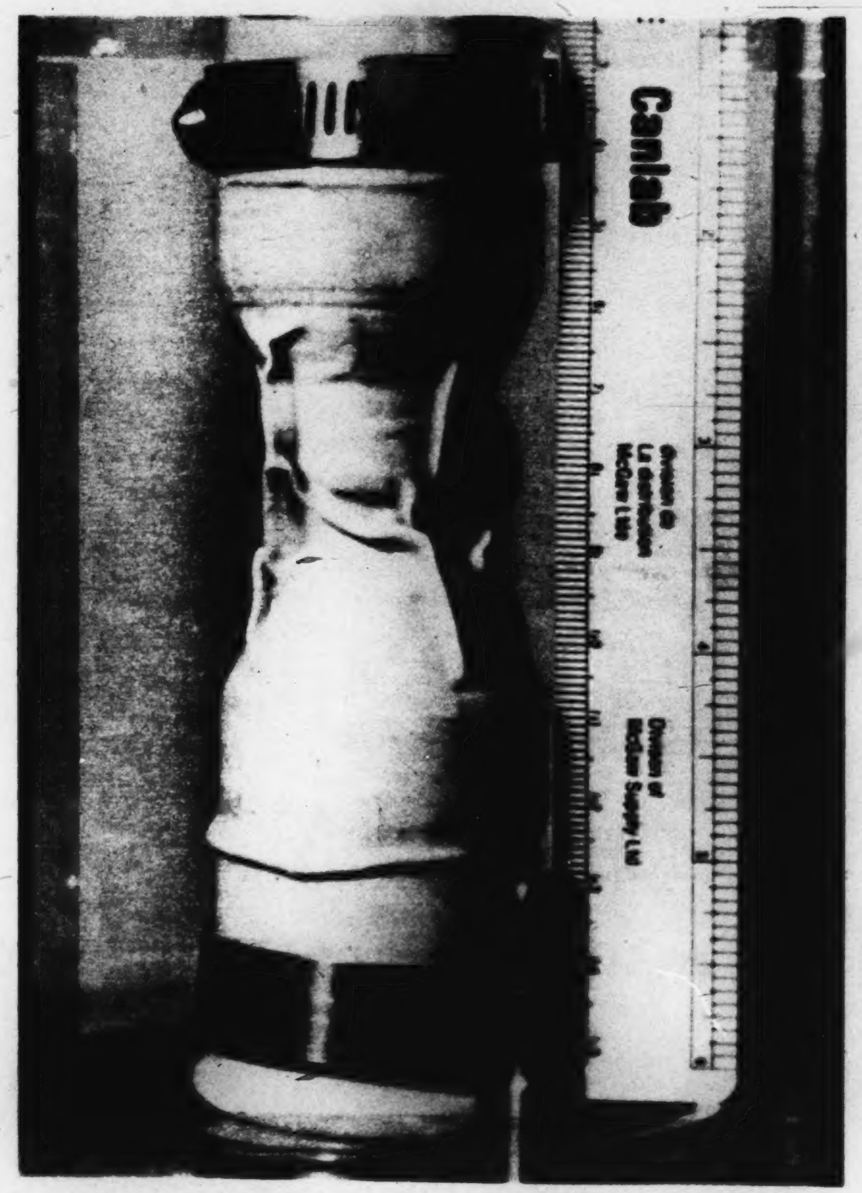

Plate 5.1 Assembly of Test Specimen SYN-T-5 in Triaxial Cell (After Testing)

# 6. DISCUSSION OF EXPERIMENTAL RESULTS

## 6.1 Drained and Undrained Compressibility

The expression presented in Equation 2.18 relating the pore pressure response, $\Delta u$ of a saturated porous material to an undrained isotropic stress increment, $\Delta\sigma_3$ may be re-written for the two phase pore fluid of saturated oil sand as:

$$B = \frac{\Delta u}{\Delta\sigma_3} = \frac{1}{1 + (n_w\, C_w + n_b\, C_b)/C} \qquad 6.1$$

where $C_b$ denotes the compressibity of the bitumen, and $n_w$ and $n_b$ represent the water and bitumen porosities. The compressibilities of liquid water and bitumen at room temperature are approximately $4.5 \times 10^{-7}$ kPa$^{-1}$ and $2.0 \times 10^{-6}$ kPa$^{-1}$, respectively, and are relatively independent of the fluid pressure (Kosar, 1983). Figure 6.1 shows the theoretical variation of B with the compressiblity of oil sand from Equation 6.1. For comparison, the relation assuming $Cb = Cw = 4.5 \times 10^{-7}$ kPa$^{-1}$ and $Cb = 5.0 \times 10^{-6}$ kPa$^{-1}$ are also shown. The average porosity of 0.358 and average water and bitumen contents of 2.8 and 14.9 percent for Saline Creek oil sand were assumed.

The corresponding measurements of B and compressiblity of the Saline Creek oil sand after initial saturation and following cyclic compression of the test specimens are also plotted in Figure 6.1. The measurements are in agreement with the compressibility of the bitumen, Cb = 2.0 x $10^{-6}$ $kPa^{-1}$, as reported by Kosar(1983).

Figure 6.2 shows the predicted variation of B with confining stress from Equation 6.1 using Cb = 2.0 x $10^{-6}$ $kPa^{-1}$. The relation between the average compressiblity and confining stress for Saline Creek oil sand in Figure 4.14 was assumed. The predicted values of B correlate quite well with the laboratory measurements. The theoretical relation between drained and undrained compressibility for saturated oil sand is considered to be validated.

## 6.2 Undrained Strength

### 6.2.1 Assessment of Sample Disturbance

Figure 6.3 shows the relationship between the maximum principal stress ratio and index of disturbance for the undrained compression tests on Saline Creek oil sand conducted at the initial confining pressure of 2.0 MPa. Tests at strain rates less than $10^{-2}$ $s^{-1}$ only are shown to eliminate transient loading effects. There is an obvious trend for the maximum stress ratio to decrease with higher disturbance indices. With consideration of the compositional variation of the test specimens, it is reasonable to extend the range of the index of disturbance for geomechanical measurements from 10 percent as proposed by Dusseault and

Van Domselaar(1981) to 14 percent. Samples with disturbance indices less than 14 percent are then considered representative for comparison of in situ strength and stress-strain behaviour in this thesis. Specimens with disturbance index values greater than 14 percent are considered separately. These specimens are still of considerable engineering significance for modelling the behaviour of "softened" oil sand disturbed by stress relief, as in mine excavations or underground cavities.

### 6.2.2 Maximum Stress Ratio

The triaxial test results at the maximum principal stress ratio are plotted in terms of p' and q in Figure 6.4. The strength of the high quality test specimens ($I_D < 14$ percent) correlate well with other undrained tests reported in Test Series 75S, Brooker(1975) and Dusseault(1977). There is no apparent difference in measured strength between the conventional test specimens and the shorter specimens ($l/d = 0.5$) using the frictionless platens. The loss of strength with disturbance is evident by the lower strength for specimens with $I_D$ greater than 14 percent. Accepting that some disturbance and weakening has occurred to all specimens, the failure line (Kf-line) representative of in situ strength may be taken as the upper bound envelope. At mean stresses less than 1.5 MPa, the failure line is defined by the Mohr-Coulomb parameters $c' = 0$ and $\phi' = 59°$. The failure line is characterized by a distinct curvature between 1.5 and 4.0 MPa. At mean stresses greater than 4.0 MPa, the failure line is defined by c' = 500 kPa and $\phi'$ = 30°.

The failure envelope for the undrained tests is compared in Figure 6.5 to the drained compression tests on oil sand presented in Section 3.4. The shear strength measured at the maximum principal stress ratio in the undrained tests is less over the range of stresses tested, particularily at mean stresses greater than 4.0 MPa. Figure 6.6 compares the undrained failure envelope with the drained tests corrected for volume change during testing by Rowe's stress-dilatancy theory presented in Section 3.5. The correlation between the undrained failure envelope and the upper bound of the corrected drained strength is remarkably close. On this basis, it is reasonable to extend the undrained failure envelope to the mean stress of 17 MPa as suggested by the dashed line in the figure.

The undrained shear strength at the maximum principal stress ratio for the disturbed test specimens ($14 < I_D < 24$ percent) is compared in Figure 6.7 with undrained triaxial tests on recompacted oil sand and densified tailings sand reported by Dusseault(1977). The undrained tests conducted by Dusseault cavitated prior to the maximum stress ratio, hence slightly higher strengths are observed due to dilatancy of the samples. With this in consideration, the strength of the disturbed oil sand clearly reverts to a normal dense sand with $\phi' = 33^\circ$.

### 6.2.3 Ultimate Strength

The triaxial test results at the ultimate strength or maximum deviator stress, $(\sigma_1 - \sigma_3)_f$ are shown in Figure 6.8. The test results do not agree with the ultimate strength of undrained tests by other researchers. It was noted in Section 3.5 that the ultimate strength of previous undrained tests was concurrent with cavitation of the pore fluid. The strengths observed will then be more consistent if corrections for volume change subsequent to cavitation are made. The same considerations apply to specimens SC-83-22U and SC-84-39 indicated in the figure which also cavitated in this series of tests. Volume change measurements to make these corrections, however, are not available.

The ultimate strength of the completely undrained tests is predicted by the residual strength for oil sand defined by $\phi'_r = 30^\circ$. The higher strains associated with the undrained tests to reach the critical confining pressure are sufficient to reduce the angle of shearing resistance of the oil sand to the residual angle. The similarity in ultimate strength between the undisturbed ($I_D < 14$ percent) and disturbed ($14 < I_D < 14$ percent) test specimens is then explained as large strains are apt to eradicate any differences in the initial structure of the sand grains.

### 6.2.4 Undrained Stress Path

The undrained stress paths for two conventional test specimens (SC-84-22 and SC-84-34) are shown in Figure 6.9. Both specimens are undisturbed with $I_D$ less than 14 percent. The initial curvature of the stress paths towards the origin is caused by the tendency of the oil sand to elastically contract upon loading thereby increasing the pore pressure and decreasing the minor principal stress, $\sigma'_3$. The maximum principal stress ratio occurs as the tendency to dilate begins to dominate the behaviour of the oil sand. Subsequent to the maximum stress ratio, the stress paths converge towards the residual strength envelope defined by $\phi'_r = 30°$. The progression to residual strength is emphasized by the passing of the stress paths down the residual strength envelope after the ultimate strength is reached.

The undrained stress paths for SC-84-13 and SC-84-25A using short specimens (1/d = 0.5) and frictionless platens are shown in Figure 6.10. The curvature of the stress paths for the short specimens is slightly more distinct, particularily at the lower stresses, suggesting the initial contraction of the specimens is enhanced. This is due in part to the reduction of frictional restraint at the ends of the specimens and the compressiblity of the membranes used in the frictionless platens. Otherwise, the stress paths between the conventional specimens and the short specimens using frictionless platens are virtually identical.

## 6.3 Critical Void Ratio

The pore pressure parameter, $A_f$ at the ultimate strength for the non-cavitating undrained compression tests on Saline Creek oil sand is plotted against the initial confining pressure in Figure 6.11. The initial confining pressure for which there is no change in pore pressure at failure due to shearing ($A_f = 0$) may be interpreted as the critical confining pressure, $\sigma_{crit}$. From Figure 6.11, the critical confining pressure ranges between 5.0 and 6.0 MPa for the Saline Creek oil sand. The corresponding critical porosity (analogous to critical void ratio) for this range of critical confining pressures may be taken as 0.365 representing the average porosity of the specimens shown in Figure 6.11.

As proposed by Lee and Seed(1967b), the critical confining pressure can also be determined as the effective minor principal stress, $\sigma'_{3f}$ at the ultimate strength in non-cavitating undrained tests. The effective minor principal stress at the ultimate strength for each test shown in Figure 6.11 is plotted against the initial confining pressure in Figure 6.12 according to $I_D$ greater and less than 14 percent. By this method, the critical confining pressure for the Saline Creek oil sand ranges between 5.5 and 7.3 MPa for $I_D$ less than 14 percent, and 4.7 and 6.0 MPa for $I_D$ greater than 14 percent.

For comparison, the critical confining pressure determined in Figure 6.13 for drained compression tests on Saline Creek oil sand conducted by Au(1984) and Agar(1984) ranges between 3.5 and 6.0 MPa for an average porosity of 0.355. The critical confining pressure for drained compression tests conducted by Dusseault(1983) on lean Athabasca oil sand is determined in Figure 6.14 to range between 6.0 and 10.5 MPa for a lower average porosity of 0.350.

The ranges of the critical confining pressure for all the above tests are plotted against the average porosities in Figure 6.15. The corresponding critical porosities and critical confining pressures for Athabasca oil sand tailings from Test Series 78S are also shown. These measurements were made from non-cavitating triaxial compression tests. The band of test data in Figure 6.15 defines the critical state line for Athabasca oil sand.

## 6.4 Prediction of Undrained Strength

### 6.4.1 Shear Strength in Non-Cavitating Tests

In non-cavitating or fully undrained compression tests, the pore fluid pressure in the sample will change until the effective minor principal stress becomes equal to the critical confining pressure, $\sigma_{crit}$. For samples initially consolidated to a pressure greater than $\sigma_{crit}$ (to the right of the critical state line in Figure 6.15), the pore pressures will increase during loading and the behaviour is intrinsically undrained. Conversely, the pore pressures will decrease during loading for consolidation pressures less than $\sigma'_{crit}$.

The shear strength under these conditions is governed by the frictional resistance at the critical confining pressure, regardless of the initial confining pressure, according to Equation 2.15 repeated below:

$$\sigma'_{1f} = \sigma_{crit} \tan^2(45 + \phi'/2) \qquad 6.2$$

As determined in Section 6.2.3, the angle of shearing resistance, $\phi'$ at the ultimate undrained strength for Saline Creek oil sand is equivalent to the residual angle of shearing resistance for oil sand, $\phi'_r = 30°$. Hence:

$$\sigma'_{1f} = 3\ \sigma_{crit} \qquad 6.3$$

or

$$\tau_u = \frac{(\sigma_1 - \sigma_3)_f}{2} = \sigma_{crit} \qquad 6.4$$

The undrained shear strength for Saline Creek oil sand is then identically equal to $\sigma_{crit}$. The magnitude of $\sigma_{crit}$ for undisturbed oil sand may be taken as the upper bound of

7.3 MPa from Figure 6.12(a), representing the lowest porosity or densest state among the test specimens. Hence, the undrained shear strength mobolized under completely undrained conditions is:

$$\tau_u = \frac{(\sigma_1 - \sigma_3)_f}{2} = 7.3 \text{ MPa} \qquad 6.5$$

The ultimate shear strength of the undisturbed test specimens ($I_D$ < 14 percent) in the non-cavitating tests are plotted in terms of total stress in Figure 6.16. The upper bound of the undrained shear strength mobolized is 7.3 MPa as predicted by Equation 6.5. The lower strengths observed among the test data reflect the sensitivity of strength to the degree of sample disturbance among the test specimens.

By the same procedure, the predicted ultimate undrained shear strength for disturbed oil sand (14 < $I_D$ < 24 percent) may be estimated by the mean value of $\sigma_{crit}$ of 5.2 MPa from Figure 6.12(b). The predicted undrained shear strength of 5.2 MPa also correlates very well with the test measurements in Figure 6.17.

### 6.4.2 Shear Strength in Cavitating Tests

In a cavitating test, the pore water pressure in the sample decreases until the pore fluid saturation pressure, $u_s$ is reached. The strength of the sample is governed by the drained angle of shearing resistance, $\phi'$ at the effective confining stress level, $\sigma'_{3f}$ where:

$$\sigma'_{3f} = \sigma'_{3i} + u_i - u_s \qquad 6.6$$

$$\sigma'_{1f} = \sigma'_{3f} \tan^2(45 + \phi'/2) \qquad 6.7$$

For cavitating tests with initial pore pressures equal to the saturation pressure ($u_i - u_s = 0$), cavitation occurs shortly after commencing loading and the shear strength is determined by the failure envelope for drained tests with $\sigma'_{3f} = \sigma'_{3i}$. The drained envelope for undisturbed Saline Creek oil sand determined by Au(1984) and Agar(1984) is shown in Figure 6.18. As $\sigma'_{3i}$ increases, the magnitude of shearing resistance contributed by dilation decreases, and at $\sigma'_{3i} = \sigma_{crit}$ the value of $\phi'$ is 30° corresponding to constant volume conditions.

For cavitating tests with initial pore pressures greater than the saturation pressure ($0 < u_i - u_s < \sigma_{crit}$), the effective confining pressure at failure is increased by the magnitude ($u_i - u_s$). The corresponding strength governed by Equation 6.7 is represented in terms of total stresses by the shifting of the drained envelope towards the origin by the magnitude ($u_i - u_s$). A unique failure envelope is then generated for each condition over the range ($0 < u_i - u_s <$ 7.3 MPa) as shown in Figure 6.18 for Saline Creek oil sand.

The general relationship between the undrained shear strength and the difference in initial pore pressure ($u_i$ - $u_s$) in Figure 6.18 can be used to predict the undrained shear strength of undisturbed oil sand for which cavitation or partial drainage occurs. The measured undrained shear strengths in cavitating undrained compression tests on undisturbed oil sand are compared in Talbe 6.1 to the predicted shear strengths from Figure 6.18. The difference between the measured and predicted strengths ranges between ± 20 percent. This is within acceptable limits for predictive purposes. It is also reflected that the predicted undrained shear strength represents the upper bound of laboratory measurements. Hence, the majority of the measured strengths are less than the predicted strength due to sample disturbance.

The foregoing analysis is repeated for disturbed oil sand ($14 < I_D < 24$ percent) in Figure 6.19. The drained failure envelope for ($u_i - u_s = 0$) is defined by drained triaxial compression tests on dense re-compacted oil sand by Dusseault(1977). The upper limit of undrained shear strength is 5.2 MPa as discussed in Section 6.4.1. The undrained shear strength predicted from Figure 6.19 is compared with laboratory meaurements for disturbed and remolded oil sand in Table 6.2. The difference between the predicted and measured undrained strengths ranges between ± 25 percent. The range of difference in strength is not unexpected given the variations in density between the natural and remolded test specimens.

## 6.5 Undrained Stress-Strain Behavior

### 6.5.1 Undrained Modulus of Deformation

The deviatoric stress versus axial strain for five conventional test specimens of Saline Creek oil sand covering the range of initial effective confining pressures between 0.08 and 5.0 MPa are shown in Figure 6.20. Specimens SC-84-22U and SC-84-39 cavitated during testing and the portion of the stress-strain curves up to the point of cavitation are shown only. Each stress-strain curve shows a distinct strain-hardening at low strains. This behaviour was noted for other dense sands in Section 2.6. The tendency for the oil sand to elastically compress to some extent upon initial loading causes an increase in pore pressure and decrease in the effective confining pressure. As dilation begins to dominate the behaviour of the oil sand, a progressive increase in stiffness in the stress-strain response occurs as the pore pressures decrease and the effective confining or isotropic stresses increase with straining.

The relation between the initial tangent modulus to the stress-strain curves and the initial effective confining pressure is shown in Figure 6.21. The tangent modulus was measured at the axial strain of 0.25 percent to account for seating of the loading platens on initial loading. The tangent modulus measured in this manner for other undrained tests are also shown in Figure 6.21. In comparison to Figure 3.7, the modulus of deformation under undrained conditions is approximately one-third that mobilized in drained compression tests.

The stress-strain curves for SC-84-13 and SC-84-25A (l/d = 0.5 using the frictionless platens) at initial effective confining pressures of 1 and 2 MPa are shown in Figure 6.22. Both specimens show a markedly greater non-linear stress-strain response than the conventional specimens in Figure 6.20. The complete triaxial test results for SC-84-13 and SC-84-25A are compared in Figure 6.23 with SC-84-10 and SC-84-22 (l/d = 2 using conventional platens) at the same initial confining pressures of 1 and 2 MPa. By comparison, the increase in pore pressure upon initial loading using the frictionless platens is larger and sustained until greater strain. As was noted in the undrained stress paths, the apparent compressibility of the oil sand is enhanced by the reduction of frictional end restraint and the compressibility of the membranes in the frictionless platens themselves. Consequently, a lower initial tangent modulus and a delayed strain-hardening response is observed.

The deformation modulus for the undrained compression tests may be separated into two components as follows:

$$E_u = \frac{\Delta(\sigma_1 - \sigma_3)}{\Delta\epsilon} = \frac{\Delta\sigma_1'}{\Delta\epsilon} + \frac{\Delta u}{\Delta\epsilon} \qquad 6.8$$

where the term $\Delta\sigma_1'$ represents the change in deviator stress due to the increase in effective axial stress and $\Delta u$ is the increase in deviator stress due to the decrease in pore water pressure. At the strain at which the pore pressure reaches a peak during initial loading, $\Delta u/\Delta\epsilon = 0$ and the modulus of deformation is represented by the change in effective axial stress alone:

$$E = \frac{\Delta\sigma_1'}{\Delta\epsilon} \qquad 6.9$$

Given the same effective confining stress and level of strain, the undrained stiffness under the conditions described above should be equivalent to the stiffness in a drained compression test at the strain where $\Delta v/\Delta\epsilon = 0$. A comparison of the modulus of deformation and effective confining stress for the undrained tests at the strain where $\Delta u/\Delta\epsilon = 0$ and drained tests where $\Delta v/\Delta\epsilon = 0$ is shown in Figure 6.24. The modulus of deformation for the drained and undrained tests correlate very well over the same range of stresses. There also does not appear to be any difference in the modulus of deformation between the conventional and shorter specimens using frictionless platens. The modulus of deformation appears to be a function of the stress path rather than a difference in material behaviour between the types of tests or the types of platens used.

### 6.5.2 Strain at Failure

The strains at the maximum stress ratio for the "static" undrained tests (strain rates less than $10^{-2}$ $s^{-1}$) are compared with drained tests on Saline Creek oil sand according to the index of disturbance in Figure 6.25. Using conventional test specimens ($l/d = 2$), the strain at the maximum stress ratio generally ranges between 1 and 2 percent for undisturbed oil sand ($I_D < 14$ percent) and is independent of stress path in the drained and undrained tests. Slightly higher strains are observed using the frictionless platens. The difference is attributed to the higher strains mobolized under the more uniform shear straining within the specimens using the frictionless platens as noted for the preliminary tests on Ottawa sand discussed in Section 4.3.5.3.

In comparison of the triaxial test results between the test specimens in Figure 6.23, it is evident that the strain to ultimate strength increases with the magnitude of the pore pressure decrease, $\Delta u_f$, during testing. The change in pore pressure at ultimate strength is equivalent to the difference between the final and initial effective confining pressures, $(\sigma'_{3f} - \sigma'_{3i})$. The strain at ultimate strength for the undisturbed specimens is plotted against the stress difference $(\sigma'_{3f} - \sigma'_{3i})$ in Figure 6.26. A direct relationship between the strain and stress difference is apparent for both non-cavitating and cavitating tests. Interestingly, as the difference $(\sigma'_{3f} - \sigma'_{3i})$ approaches zero, the strains converge to 2 percent corresponding to the strain at ultimate strength for drained tests in Figure 6.25. This is consistent with satisfying the following two conditions:

1) The initial pore pressure is equivalent to the gas saturation pressure and the oil sand behaves in a drained manner, or
2) The initial confining pressure $\sigma'_{3i}$ equals $\sigma_{crit}$ and the change in pore pressure at failure $\Delta u_f = 0$. The failure occurs under conditions of constant volume and is equivalent to loading under drained conditions.

The average strain in percent at ultimate strength may be estimated from Figure 6.26 for predictive purposes as:

$$\epsilon_f = 2.0 + 1.6\,(\sigma'_{3f} - \sigma'_{3i}) \quad \text{(MPa)} \qquad 6.10$$

For non-cavitating conditions, $\sigma'_{3f}$ is taken equal to $\sigma_{crit}$. For cavitating conditions, $(\sigma'_{3f} - \sigma'_{3i})$ is equivalent to the difference between the initial pore pressure and gas saturation pressure, $(u_i - u_s)$.

## 6.6 Influence of Strain Rate

The ultimate strength for the non-cavitating undrained compression tests on Saline Creek oil sand are plotted against strain rate in Figure 6.27. As predicted in Section 6.4.1, the upper bounds of undrained strength for the undisturbed ($I_D < 14$ percent) and disturbed ($14 < I_D < 24$ percent) specimens are consistently defined by 14.6 MPa and 10.4 MPa, respectively, for the "static" strain rates less than $10^{-2}$ $s^{-1}$. An increase in measured undrained strength is apparent at strain rates greater than $10^{-2}$ $s^{-1}$. To illustrate the effect of strain rate more clearly, the data in Figure 6.27 is re-plotted in Figure 6.28 to show the increase in strength relative to the predicted "upper" bound of "static" undrained strength. The increase in undrained strength ranges between 30 and 35 percent at the highest strain rate of 3.5 $s^{-1}$ reached in the test program.

The absence of any significant additional fines generation from grain shearing at the higher strain rates discussed in Section 4.4.8 suggests that the behaviour of the sand grain structure is not a major factor for the increase in strength. It is interesting to note that the increase in strength with strain rate in Figure 6.28 coincedes exactly with the time lag of pore pressure response beginning at $10^{-2}$ $s^{-1}$ observed in Section 4.4.7. Hence, the increase in strength appears to be largely related to the migration of the pore fluid in the specimens during testing as suggested by Whitman(1957). As the speed of deformation is increased, more energy must be expended to overcome the resistance of the flow of the pore fluid. Seed and Lungren(1954), Whitman(1957), and Whitman and Healy(1963) report increases in undrained strength up to 25 percent for dense water saturated sands at strain rates up to 16 $s^{-1}$. By comparison, the viscosity of the bitumen in the oil sand appears to contribute at least 10 to 15 percent additional strength over the same range of strain rates.

The variation of strain at the ultimate strength with strain rate is plotted in Figure 6.29. In general, slight increases in the strain were observed at strain rates higher than 1.0 $s^{-1}$. The relationship between the initial tangent modulus to the stress-strain curves and strain rate is given in Figure 6.30. A relative increase of up to 600 percent in the tangent modulus is observed among the test specimens. Over the same range of strain rates, the increase in deformation modulus reported by other researchers for water saturated dense sands in Section 2.8 is less than 100 percent. It appears that the stiffness of the oil sand is attenuated more significantly with strain rate due to the viscosity of the interstitial bitumen.

## 6.7 Behavior of Oil Sand under Axial Extension

### 6.7.1 Effective Shearing Resistance

The triaxial extension test results are plotted in terms of p' and q in Figure 6.31. The region of tensile stresses lies to the left of the 45° line as shaded in the figure. It is apparent that no tensile strength was exhibited in the drained or undrained extension tests. The triaxial compression test SYN-C-1 agrees with the upper bound envelope for axial compression tests defined by $\phi' = 60°$ in Figure 3.4. The angle of shearing resistance at failure for the extension tests ranges between 42° and 73°. The parameters for the average failure line ($K_f$ - line) shown in Figure 6.31 are $c' = 0$ and $\phi' = 68°$. There is no obvious distinction between the strength for the drained and undrained extension tests. The strength for SYN-T-2 is noticeably lower than the other tests. This is suspected to be caused by overestimation of the correction for membrane resistance due to the shorter notch height for this specimen in comparison to the other test specimens. The strength of SYN-T-2 calculated using 25 percent of the membrane correction is shown in the figure and correlates well with the remaining tests.

The triaxial compression test SYN-C-1 is re-plotted with Triaxial Test Series 84S in Figure 6.32. Comparatively, the strength measured in Test Series 84S is lower than measured in this report. The parameters for the failure line of shear strength are given by $c' = 0$ and $\phi' = 51^\circ$. Given the consistency of the test results and the low index of disturbance of the Syncrude test specimens, sample disturbance is not considered a factor in the lower strengths. It is noted that the core samples tested in Test Series 84S were from a different borehole and have a higher fines content (22-26 percent compared to 13-15 percent). The lower shearing resistance is then probably caused by the difference in composition, likely by collective weakening of the oil sand from the inclusion of the clay clasts.

### 6.7.2 Stress Path

The stress paths to failure for the triaxial compression and extension tests on the Syncrude oil sand are presented in the generalized three dimensional stress space in Figure 6.33. The stress path for SYN-C-1 compares very well with the upperbound failure envelope for triaxial compression tests defined by $\phi' = 60^\circ$. The effective stress paths for the drained and undrained extension tests are consistently bounded by the failure line defined by $\phi' = 68^\circ$.

The undrained stress paths to failure in terms of total stress are also plotted for SYN-T-4 and SYN-T-5 in Figure 6.33. Much larger deviator stresses, $(\sigma_1-\sigma_3)_f$, are required to reach failure in these tests due to the undrained drop in pore pressure and increase in confining stress. The undrained deviator stress mobilized ranges up to almost twice that mobilized in the drained tests at roughly the same initial effective confining stress. In terms of total stress, it appears that a significant apparent tensile strength can be mobilized during in situ undrained unloading of oil sand.

### 6.7.3 Comparison with other Dense Sands

The influence of stress path on the strength of dense sands in axial compression and extension has been investigated by numerous researchers. Cornforth(1964), Barden and Proctor(1969), Reades and Green(1976) and Arthur et al(1977) compare the results of axial compression and extension in the triaxial cell. Sutherland and Medsary(1969), Barden and Proctor(1971), Lade and Duncan(1973), Reades and Green(1976) and Arthur et al(1977) report comparative test for cubical specimens in independent stress control (ISC) cells. Table 6.3 summarizes the test results.

Overall, a maximum increase of 5° or 13 percent in the angle of shearing resistance in extension as compared to compression has been measured in the triaxial cell. Slightly larger increases for extension has been reported for cubical specimens (Reades and Green, 1976 and Arthur et al, 1977) but not for others (Sutherland and Medsary, 1969). Barden and Proctor(1971) and Reades and Green(1976) conducted exhaustive studies to evaluate corner effects in the ISC extension tests and found the influence to be minor. Barden and Proctor(1976) conclude the angle of shearing resistance in extension is bounded by the condition of plane strain. Bishop(1966) and Lee(1970) review the literature for plane strain tests on sand and conclude an increase of 3° to 6° or about 10 percent in the angle of shearing resistance for normal dense sands under conditions of plane strain.

The average increase of 8° or 13 percent in the angle of shearing resistance in axial extension for the Syncrude oil sand agrees with other dense sands in the literature cited in terms of relative magnitude. The absolute magnitude of the increase is, however, greater and may partly be contributed by the curvi-linearity of the Mohr-Coulomb envelope for oil sand at low stresses (Dusseault, 1977 and Barnes, 1980). It is also reflected that the interpenetrative grain structure of oil sand is a unique material which results in almost twice the angle of shearing resistance in compression as compared to "normal" dense sands. The greater increase in angle of shearing resistance in axial extension may therefore also reflect the nature of the sand fabric.

### 6.7.4 Comparison with Stress-Dilatancy Theory

As presented in Section 2.3, Rowe(1969) concludes from examination of test results at low stresses for normal dense sands in triaxial compression and extension that the approximate value of $\phi_f$ varies as:

$$\phi_\mu \le \phi_f \le \phi_{cv} \tag{6.11}$$

where $\phi_\mu$ is the intergranular angle of friction and $\phi_{cv}$ is the friction angle at constant volume or critical void ratio state. For sand in the densest state, $\phi_f = \phi_\mu$ up to the maximum stress ratio and decreases to the critical state at which $\phi_f = \phi_{cv}$. On this basis, the values of $\phi_\mu$ and $\phi_{cv}$ were calculated from the compression test SYN-C-1 and for Test Series 84S. The value of $\phi_\mu$ was also calculated for the drained axial extension tests SYN-T-1 and SYN-T-3 for which there are complete volume change measurements at failure. The results are summarized in Table 6.4.

The measurement of $\phi_\mu$ among the compression and extension test specimens are in close agreement despite the differences in stress path in axial compression and extension. This suggests the observed higher angle of shearing resistance for oil sand in axial extension is derived solely from the dilatancy of the interpenetrative grain structure. The measurements of $\phi_\mu$ and $\phi_{cv}$ for SYN-C-1 and Test Series 84S are compared with other granular materials at low stresses in Figure 6.34. The relation between $\phi_{\mu}$ and $\phi_{cv}$ for SYN-C-1 correlates favourably. The magnitude of $\phi_{cv}$ for Triaxial Test Series 84S is lower. The reduction in $\phi_{cv}$ for Triaxial Test Series 84S is attributed to the influence of the higher fines content on the frictional resistance as the samples are remolded with straining.

### 6.7.5 Stress-Strain Behavior

Appreciable strains ranging 3.6 and 10.4 percent were observed in the notch zone before failure. These strains reflect high dilatancy of the sand grain matrix as supported by the significant water content changes in the notch zone. The variation of the initial tangent deformation modulus with confining pressure for axial extension is shown on Figure 6.35. In terms of total stress, the tangent modulus for undrained extension ranges up to 75 percent greater than for drained extension.

The deformation modulus for the undrained extension tests may be separated into two components as follows:

$$E_u = \frac{\Delta(\sigma_1 - \sigma_3)}{\Delta\epsilon} = \frac{\Delta\sigma_3'}{\Delta\epsilon} + \frac{\Delta u}{\Delta\epsilon} \qquad 6.12$$

where the term $\Delta\sigma_3'$ represents the change in deviator stress due to the decrease in effective axial stress and $\Delta u$ is the increase in deviator stress due to the decrease in pore water pressure. The effective stress modulus of deformation, E' may then be defined to represent the change in effective axial stress with axial strain:

$$E' = \frac{\Delta\sigma'_3}{\Delta\epsilon} \qquad 6.13$$

The effective stress modulus, E' at 1.0 percent strain for the drained and undrained extension tests are plotted against the corresponding effective confining pressure in Figure 6.36. The figure suggests that the modulus of deformation in terms of effective stresses alone is linear with effective confining pressure and independent of the stress path.

### 6.7.6 Implications of Unconfined Extension Tests

The failure of the unconfined extension tests on disturbed Saline Creek oil sand, SC-84-T-1 and SC-84-T-2, shows that the tensile resistance mobilized by the bitumen in very rich oil sand is nominally less than 2 kPa at 20°C. Dusseault(1977) reports that significant cohesion may be developed by the bitumen due to dessication and evaporation of volatile hydrocarbons in the upper few metres of exposed oil sand slopes. This effect is not apparent in the Saline Creek oil sand.

The failure of SYN-T-6 indicates the strength mobolized by the bitumen in the Syncrude oil sand is also very small.

The complete segregation of SYN-T-6 precludes the presence of any cementation or bonding in the clay clasts.

Table 6.1 Comparison of Predicted and Measured Undrained Strength of Undisturbed Oil Sand

| REFERENCE | LABORATORY MEASUREMENTS | | | PREDICTED UNDRAINED SHEAR STRENGTH $C_{up}$ | PERCENTAGE DIFFERENCE |
|---|---|---|---|---|---|
| | $\sigma'_{3i}$ (MPa) | $\Delta u_f$ (MPa) | $C_u$ (MPa) | (MPa) | $\frac{C_{up} - C_u}{C_u} \times 100$ (%) |
| **PLEWES(1986)** - SC-83-22U | 2.03 | -1.30 | 4.5 | 5.2 | 15.5 |
| - SC-83-39 | 0.08 | -3.87 | 4.6 | 5.5 | 19.5 |
| **TEST SERIES 75S** | 0.01 | -0.35 | 1.06 | 1.10 | 3.8 |
| | 0.69 | -0.03 | 1.94 | 1.90 | -2.1 |
| | 0.41 | -0.16 | 1.33 | 1.35 | 1.5 |
| | 0.21 | -0.32 | 1.16 | 1.20 | 3.4 |
| **DUSSEAULT(1977)** | 0.36 | -0.29 | 2.06 | 1.65 | -20.0 |

Table 6.2 Comparison of Predicted and Measured Undrained Strength of Disturbed and Remolded Oil Sand

| REFERENCE | LABORATORY MEASUREMENTS |  |  | PREDICTED UNDRAINED SHEAR STRENGTH $C_{up}$ | PERCENTAGE DIFFERENCE |
|---|---|---|---|---|---|
|  | $\sigma'_{3i}$ (MPa) | $\Delta u_f$ (MPa) | $C_u$ (MPa) | (MPa) | $\frac{C_{up} - C_u}{C_u} \times 100$ (%) |
| TEST SERIES 75S | 0.21 | -0.55 | 1.32 | 1.35 | 2.2 |
|  | 0.69 | -0.12 | 1.33 | 1.40 | 5.2 |
| DUSSEAULT(1977) |  |  |  |  |  |
| - Remolded Oil Sand | 0.69 | -0.65 | 1.88 | 1.90 | 1.1 |
|  | 0.51 | -0.47 | 1.37 | 1.50 | 9.4 |
|  | 0.35 | -0.31 | 0.95 | 1.20 | 26.3 |
|  | 0.17 | -0.17 | 0.63 | 0.65 | 4.8 |
|  | 0.35 | -0.34 | 1.19 | 1.25 | 5.0 |
| - Tailings Sand | 0.83 | -0.51 | 1.61 | 1.70 | 5.6 |
|  | 0.75 | -0.79 | 2.55 | 2.10 | -17.7 |
|  | 0.35 | -0.60 | 1.50 | 1.55 | 3.3 |
|  | 0.34 | -0.39 | 1.16 | 1.35 | 16.4 |
|  | 0.69 | -1.29 | 2.20 | 2.40 | 9.1 |

Table 6.3 Comparison of Axial Compression and Extension Tests on Dense Sands

| REFERENCE | MATERIAL | INITIAL POROSITY (%) | ANGLE OF SHEARING RESISTANCE, $\phi'$ (DEGREES) | | | |
|---|---|---|---|---|---|---|
| | | | TRIAXIAL COMPRESSION | TRIAXIAL EXTENSION | ISC COMPRESSION[1] | ISC EXTENSION[1] |
| Cornforth(1964) | Brasted Sand | 36 | 39 | 40 | | |
| Green(1965) | Ham River Sand | 39 | 39 | 40 | | |
| Sutherland and Mesdary(1969) | Loch Aline Sand | 37 | 40 | | 40.5 | 40.5 |
| Barden and Proctor(1971) | River Welland Sand | 39 | 44.5 | 44.5 | 44.5 | 49.8 |
| Lade and Duncan(1973) | Monterey No. 0 Sand | 37<br>44 | | | 48.5<br>39.6 | 57.0<br>41.0 |
| Reades and Green(1976) | Ham River Sand | 39 | 40 | 42-44, 45[2] | | 45-46 |
| Arthur et al(1977) | Leighton Buzzard Sand | 34 | 38 | 43 | 39 | 47 |

1. Independant stress control test on cubical specimens.

2. Cylindrical specimen with "flared"ends.

Table 6.4 Calculation of $\phi_\mu$ and $\phi_{cv}$ from Stress Dilatancy Theory for Syncrude Oil Sand

| SAMPLE | $(d\epsilon_v/d\epsilon_a)_{peak}$ | $(\sigma_1'/\sigma_3')_{peak}$ | $(\sigma_1'/\sigma_3')_{residual}$ | $\phi_\mu$ | $\phi_{cv}$ |
|---|---|---|---|---|---|
| SYN-C-1 | -1.81 | 14.3 | 7.0 | 42.2 | 48.6 |
| SYN-T-1 | 0.86 | 41.1 |  | 44.7 |  |
| SYN-T-3 | 0.89 | 43.3 |  | 40.8 |  |
| Test Series 84S |  |  |  |  |  |
| $\sigma_3' = 138$ kPa | -0.30 | 6.35 | 3.53 | 41.3 | 34.0 |
| $\sigma_3' = 276$ kPa | -0.29 | 7.56 | 3.53 | 45.1 | 34.0 |
| $\sigma_3' = 414$ kPa | -0.42 | 8.20 | 3.79 | 44.8 | 35.6 |

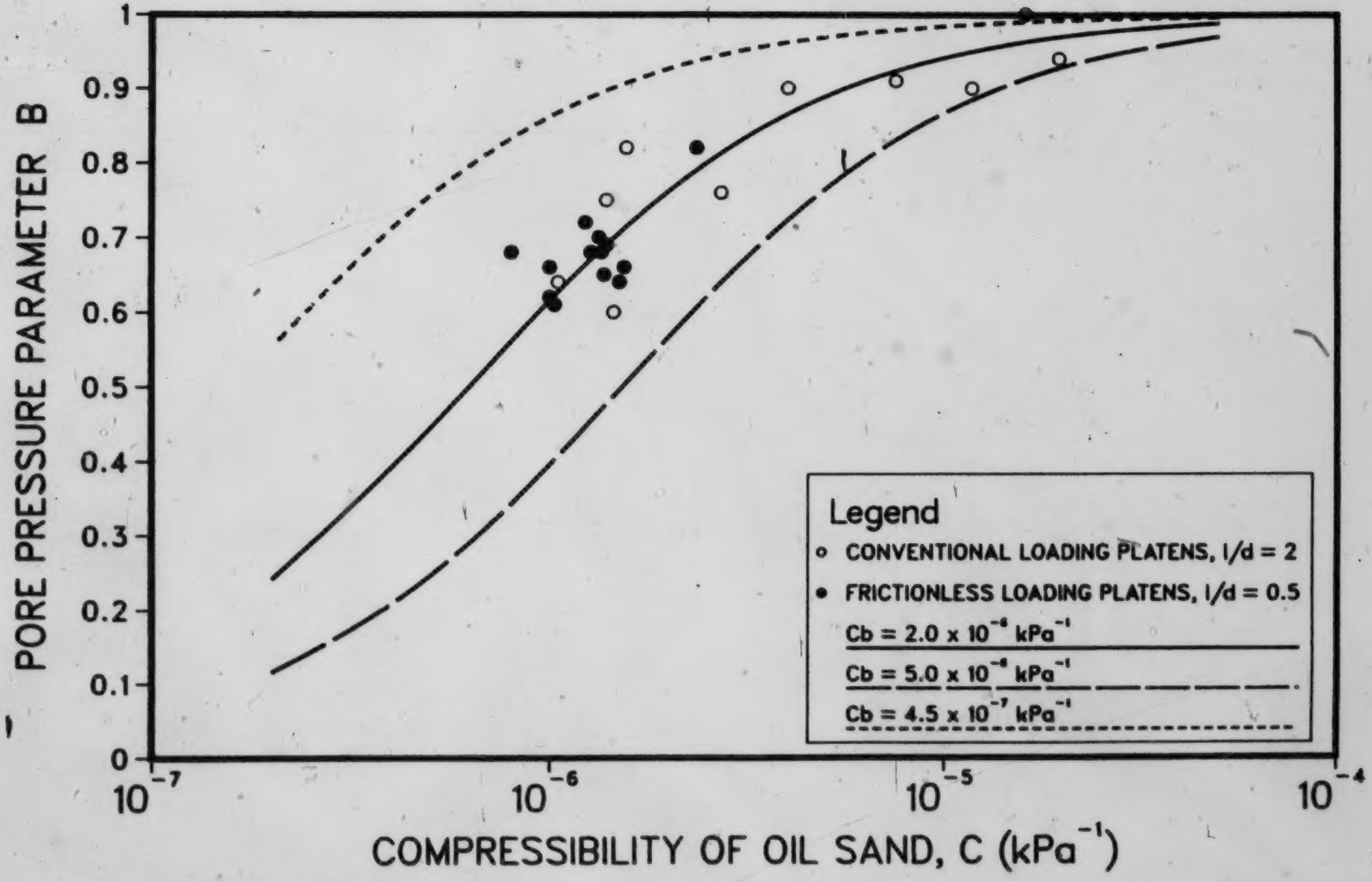

Figure 6.1 Relation Between Pore Pressure Parameter B and Compressibility of Oil Sand

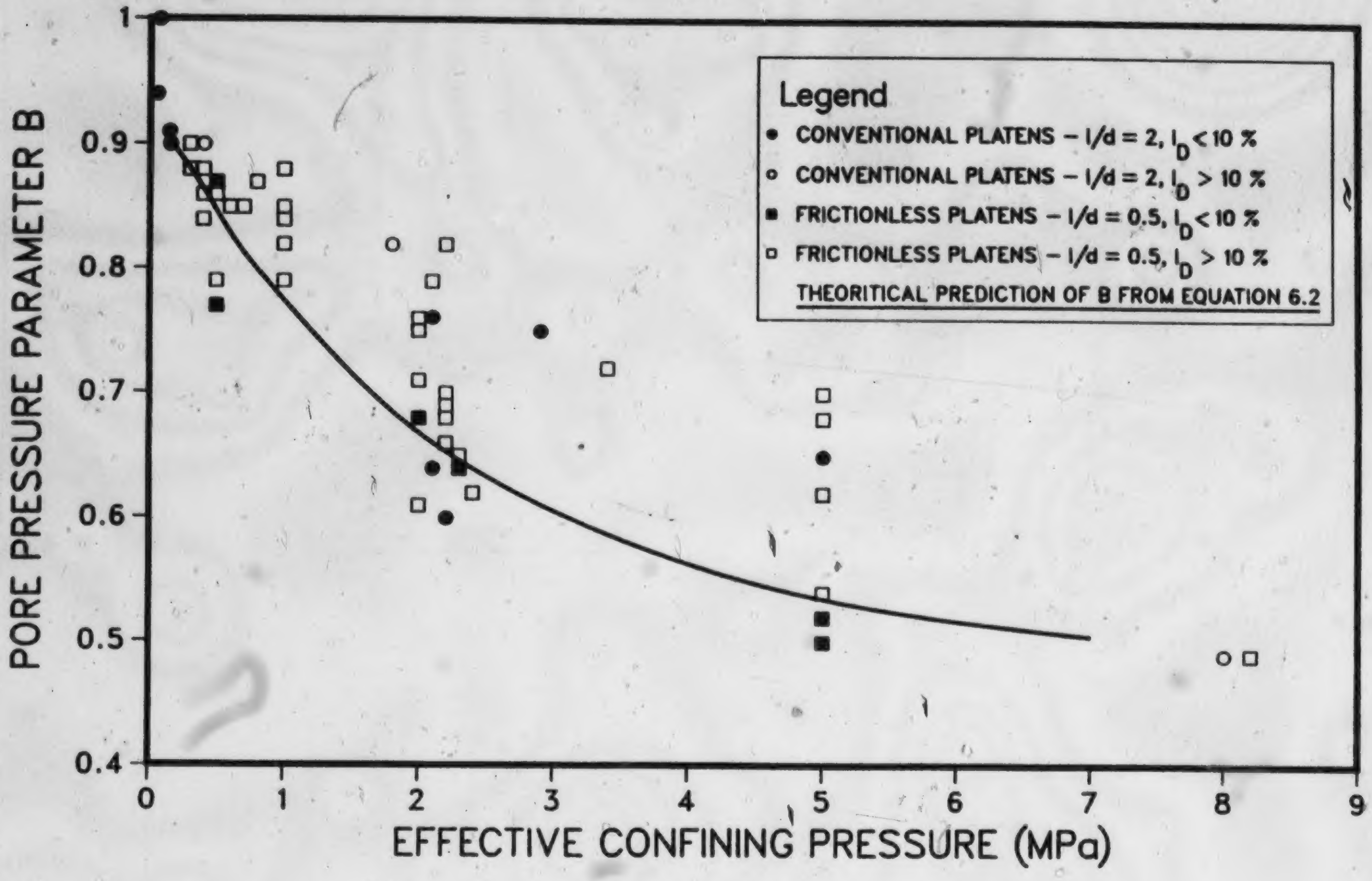

Figure 6.2 Predicted Variation of Pore Pressure Parameter B with Confining Stress, $C_b = 2.0 \times 10^{-4}\ s^{-1}$

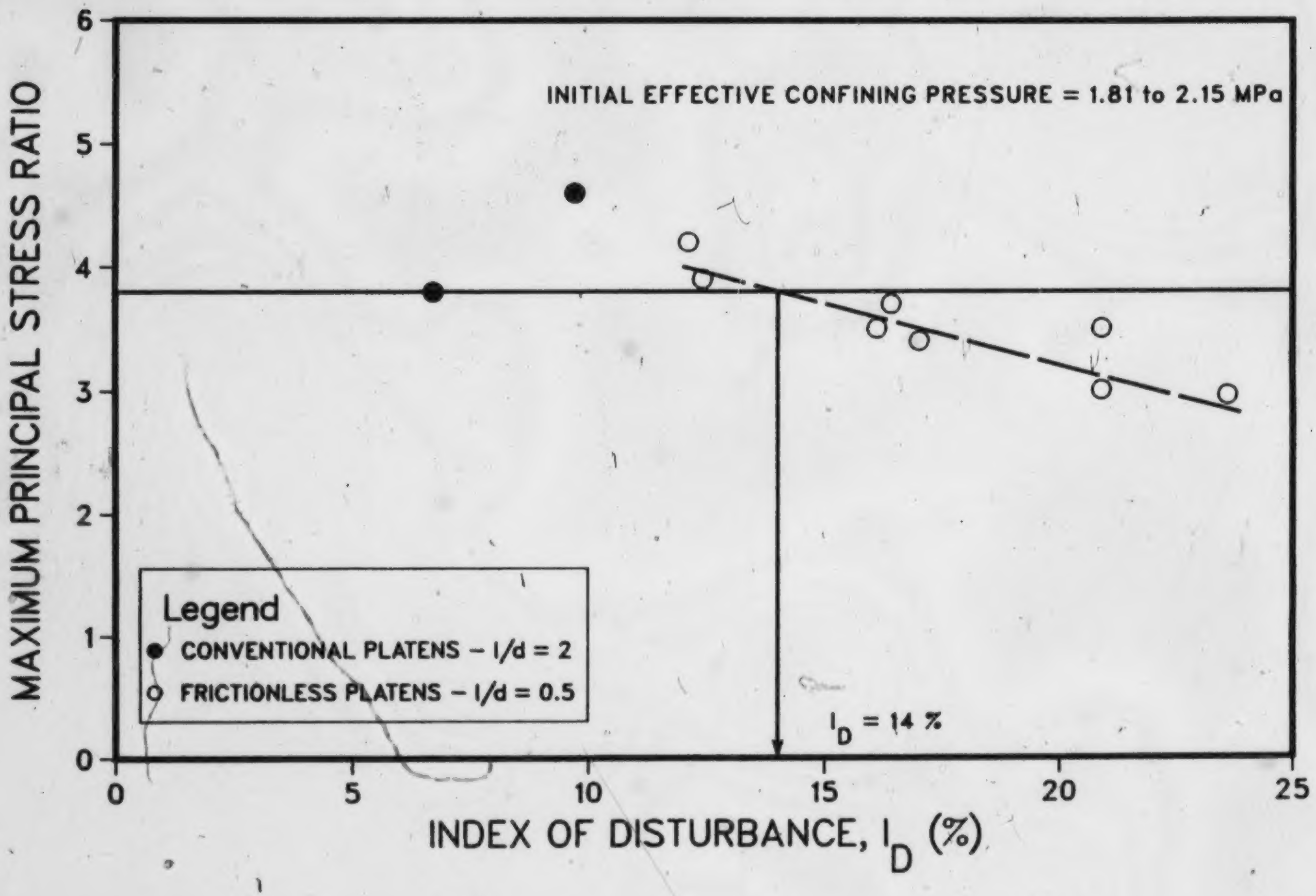

Figure 6.3 Maximum Principal Stress Ratio Versus Index of Disturbance for Initial Effective Confining Pressures of 2 MPa

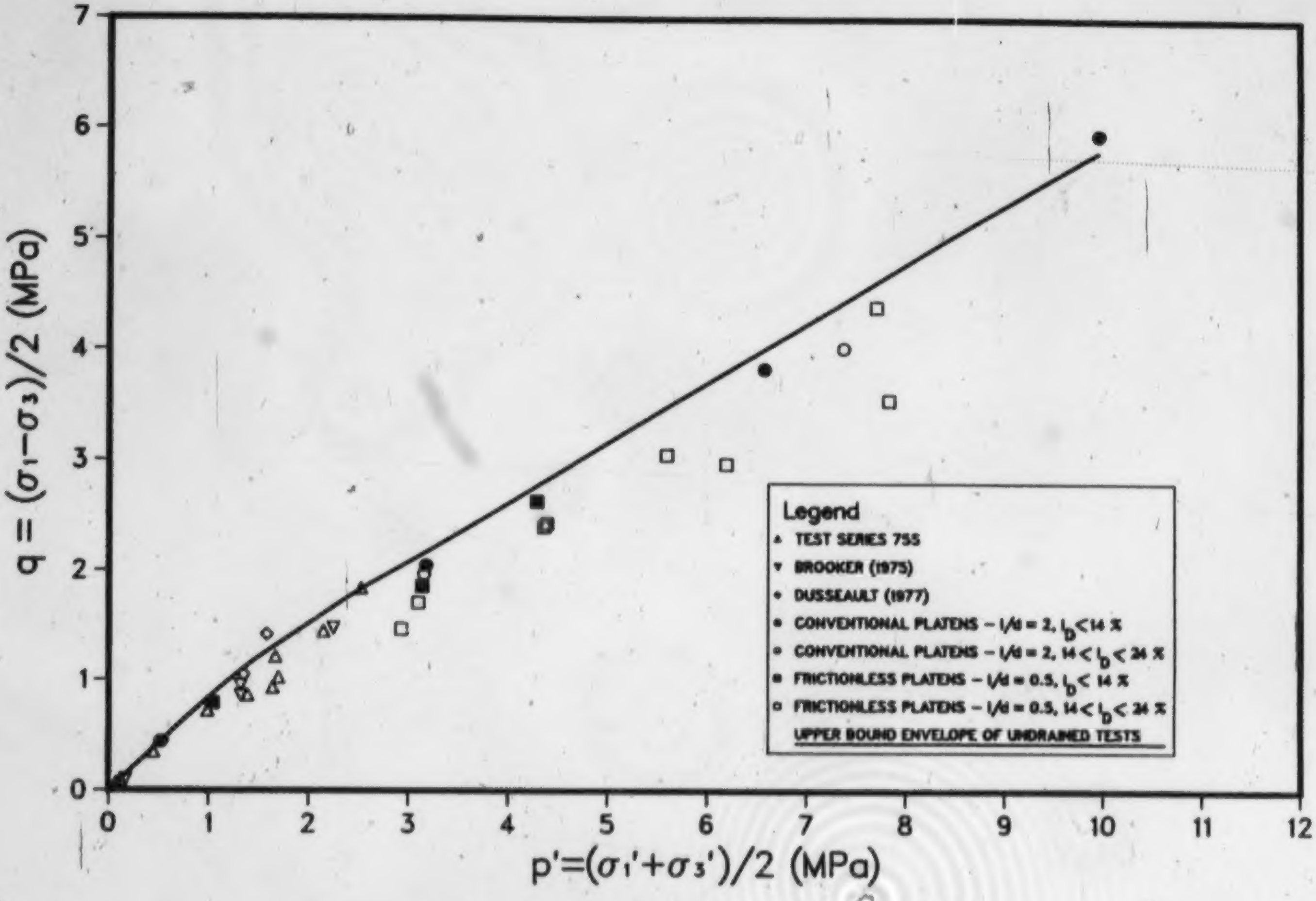

Figure 6.4 Shear Strength at Maximum Principal Stress Ratio in Undrained Triaxial Compression Tests

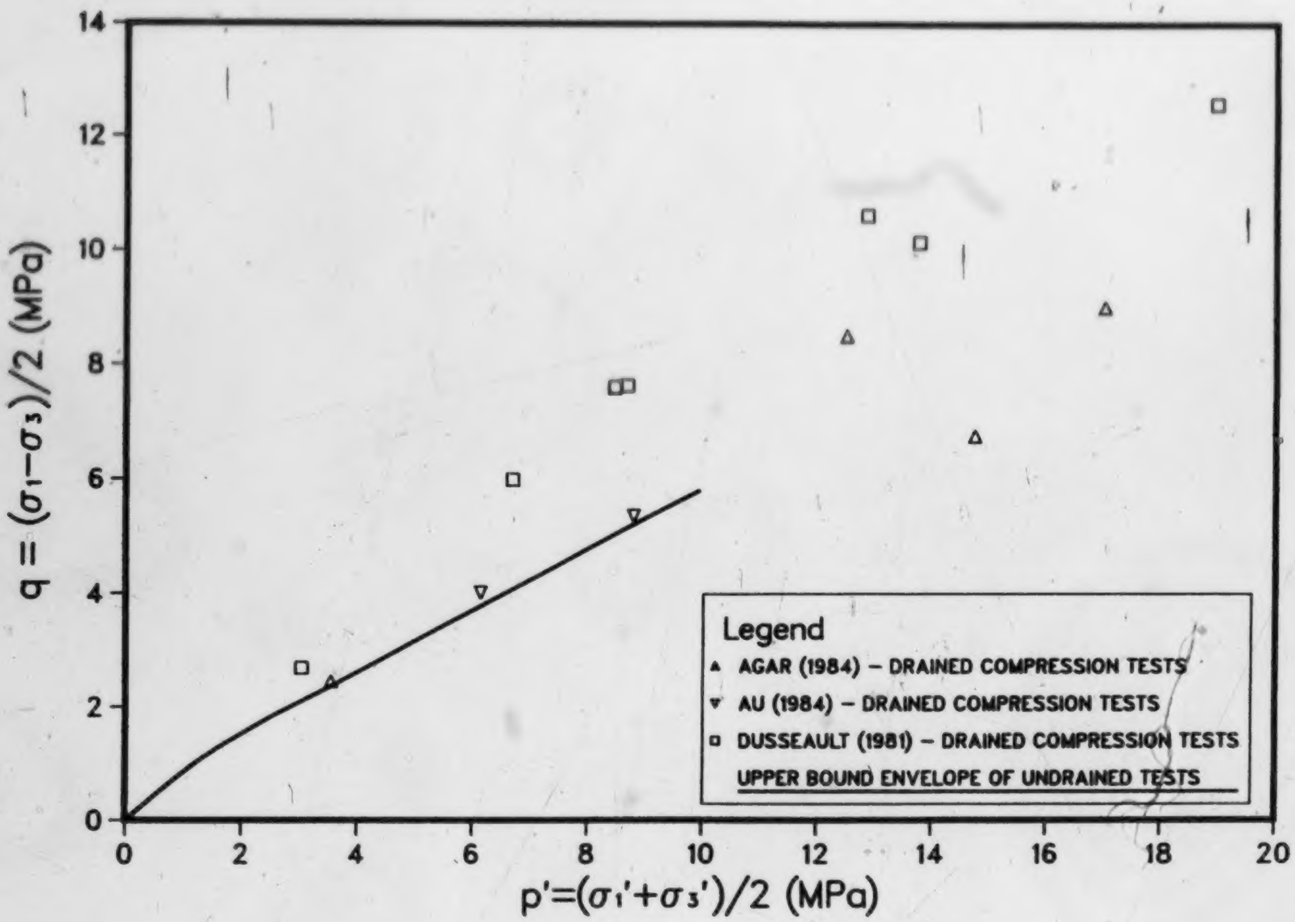

Figure 6.5 Comparison of Drained Triaxial Compression Tests with Undrained Failure Line at the Maximum Principal Stress Ratio

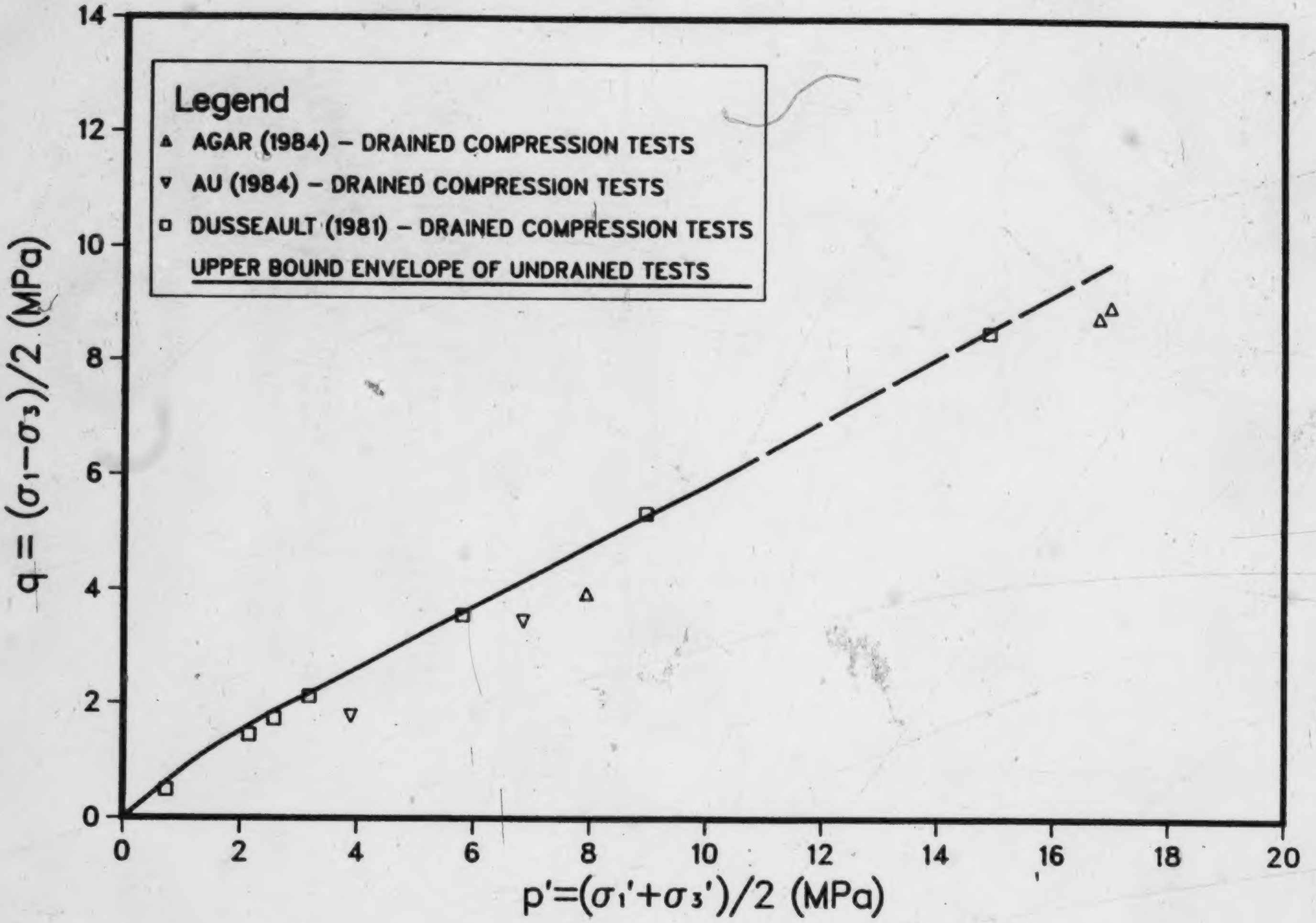

Figure 6.6 Comparison of Drained Triaxial Compression Tests Corrected for Dilatancy with Undrained Failure Line at the Maximum Principal Stress Ratio

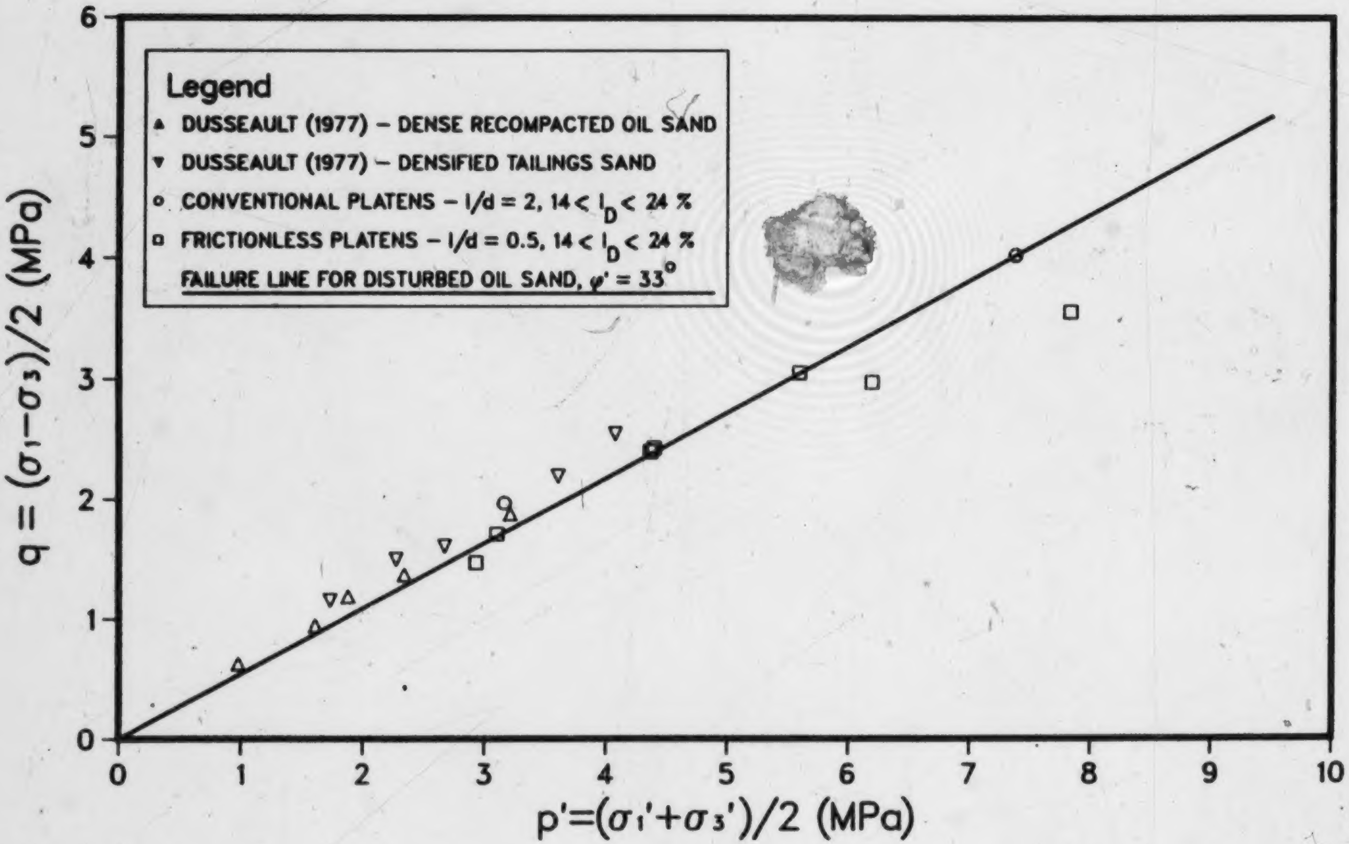

Figure 6.7 Shear Strength of Disturbed Oil Sand at the Maximum Stress Ratio in Undrained Triaxial Compression Tests

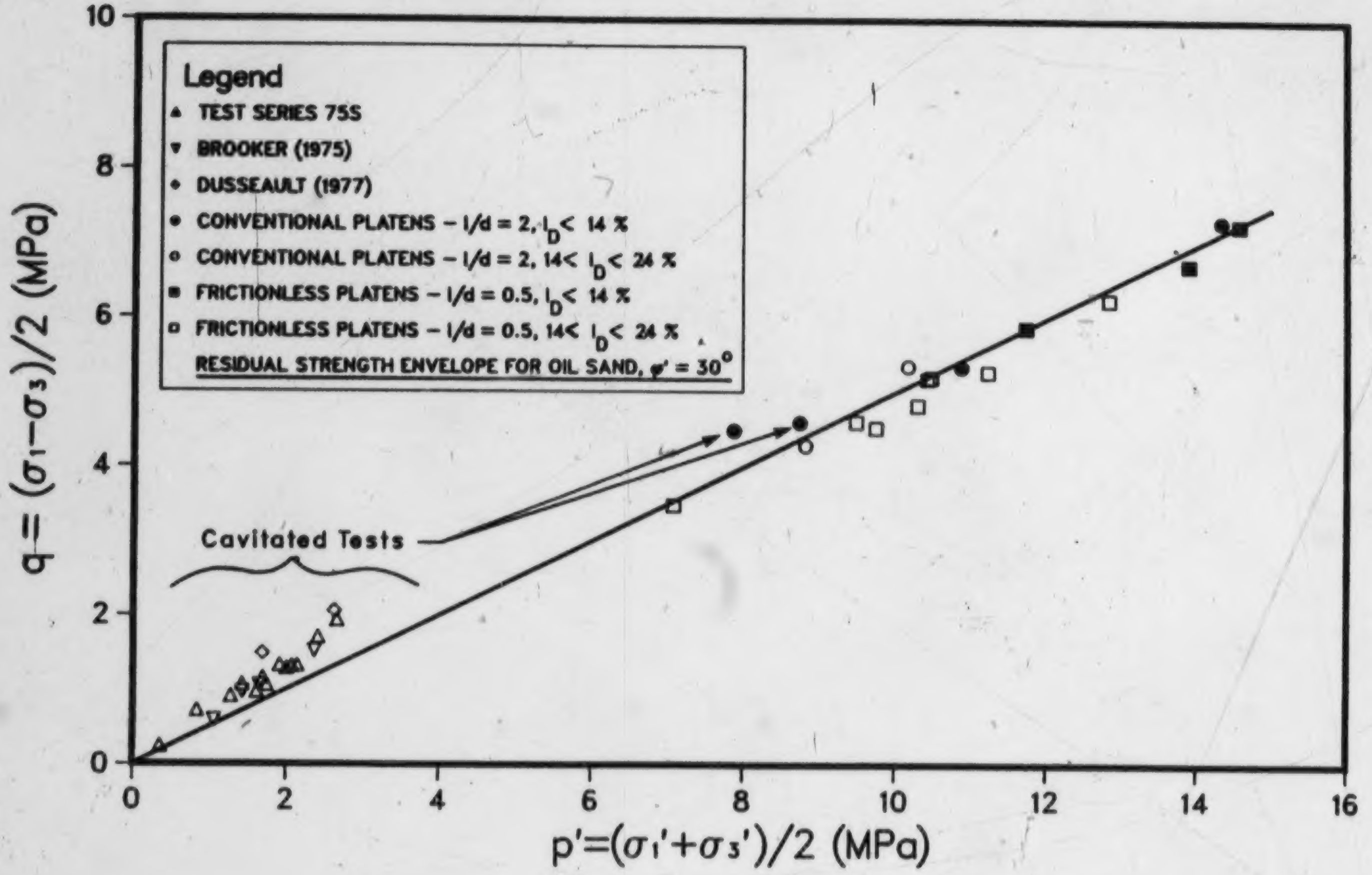

Figure 6.8 Ultimate Shear Strength in Undrained Triaxial Compression Tests

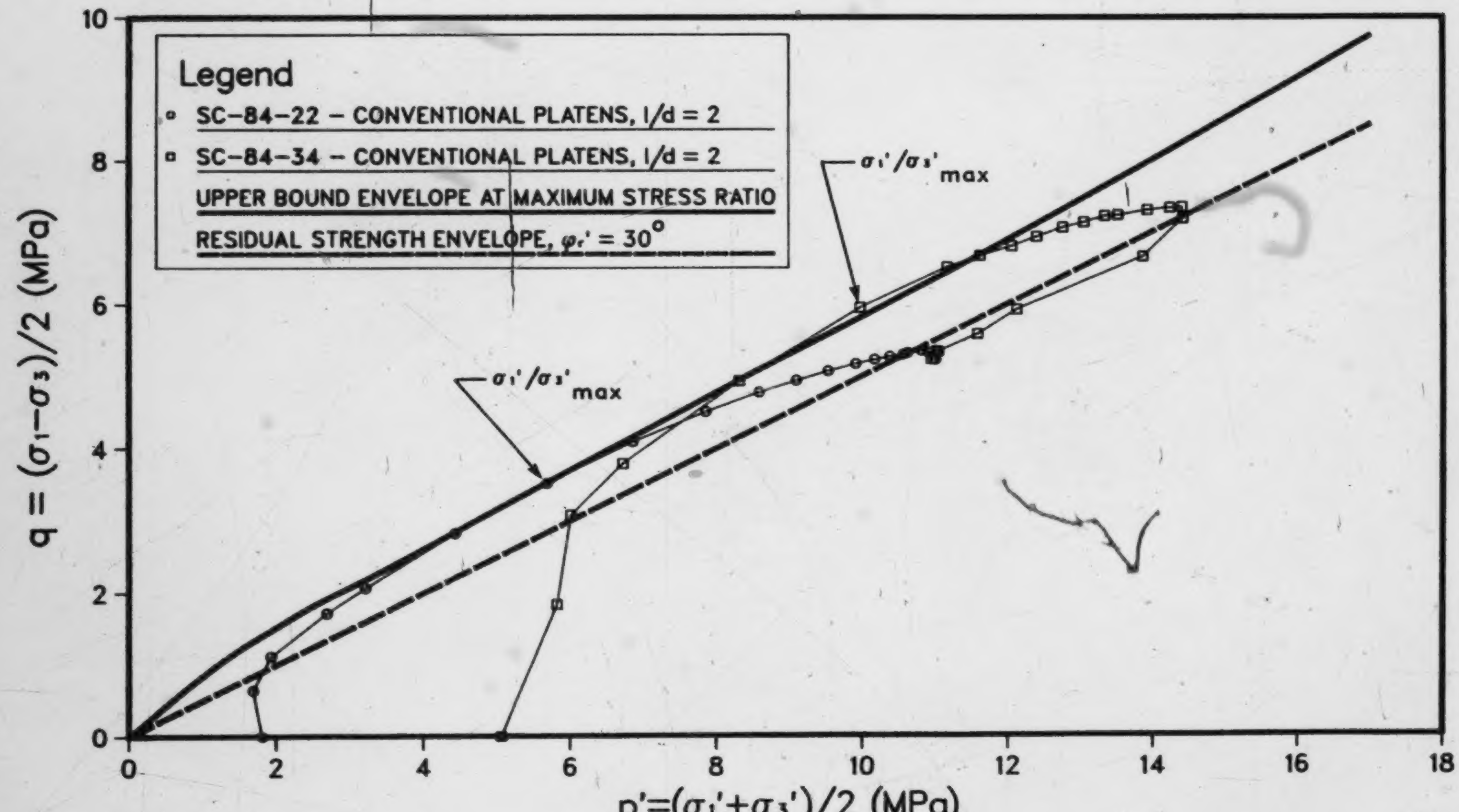

Figure 6.9 Stress Path for Undrained Triaxial Compression Tests on Conventional Specimens (l/d = 2) of Undisturbed Oil Sand

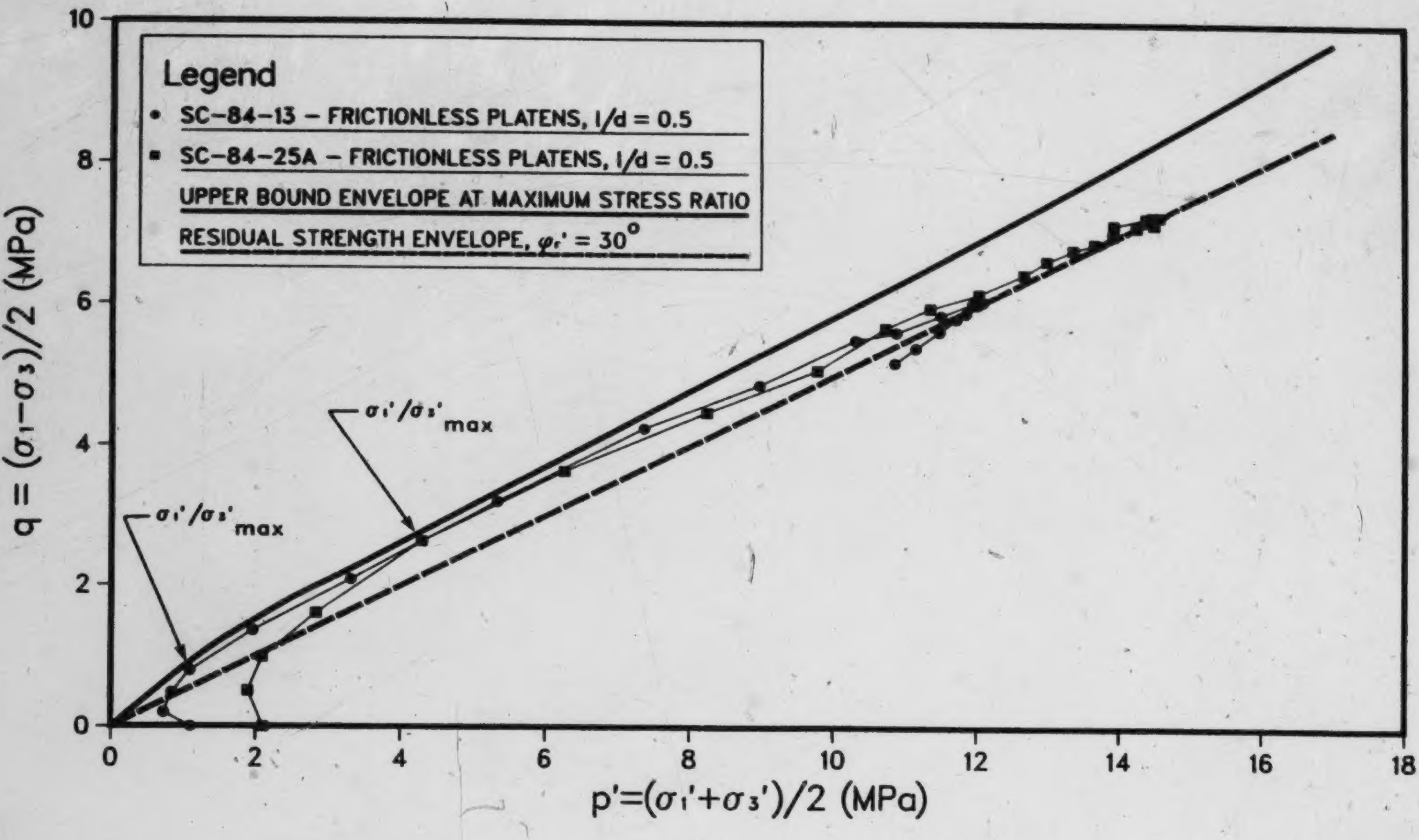

Figure 6.10 Stress Path for Undrained Triaxial Compression Tests on Short Specimens (l/d = 0.5) of Undisturbed Oil Sand using Frictionless Platens

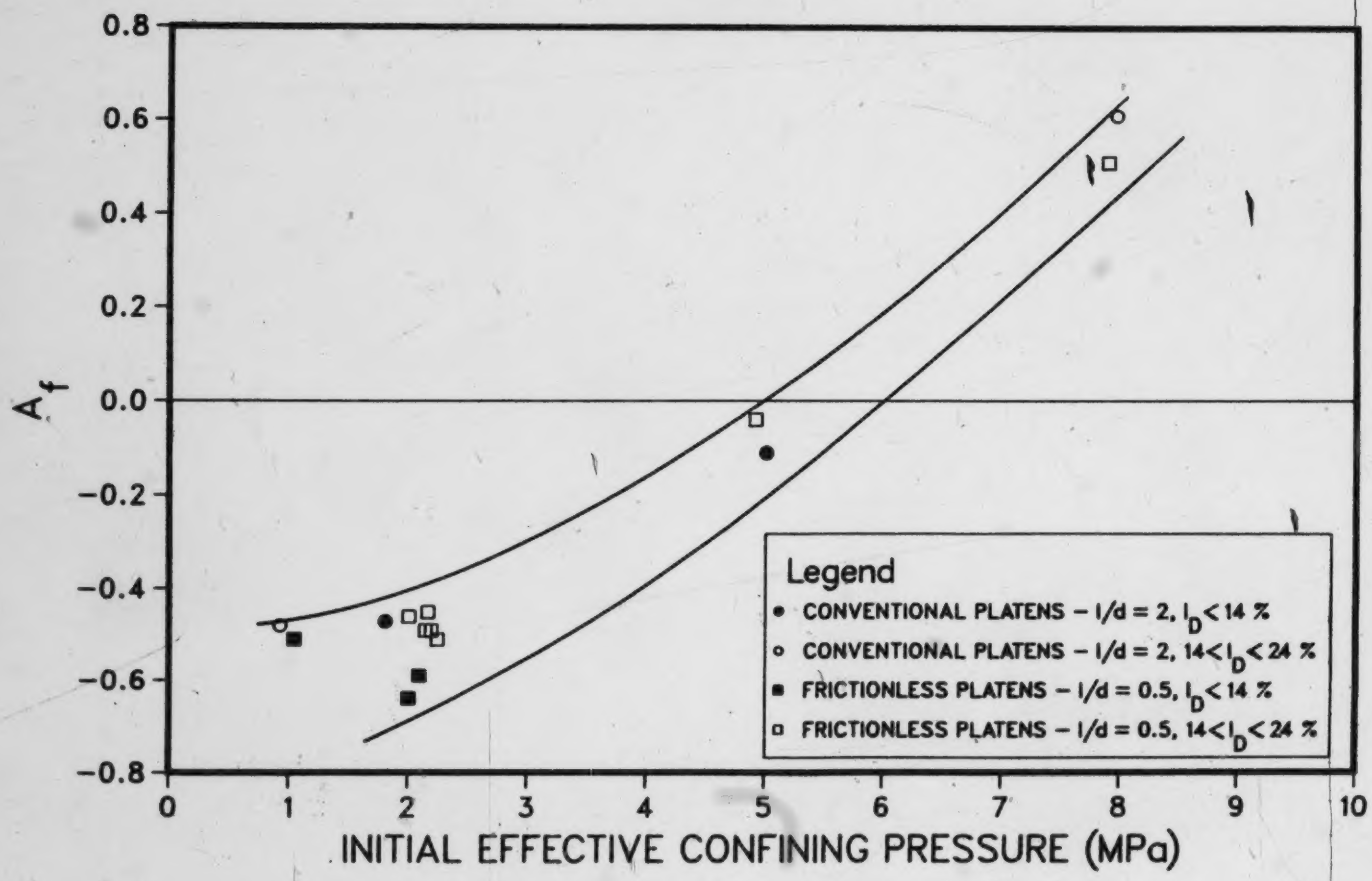

Figure 6.11 Pore Pressure Parameter A at Ultimate Strength for Non-Cavitating Undrained Triaxial Compression Tests

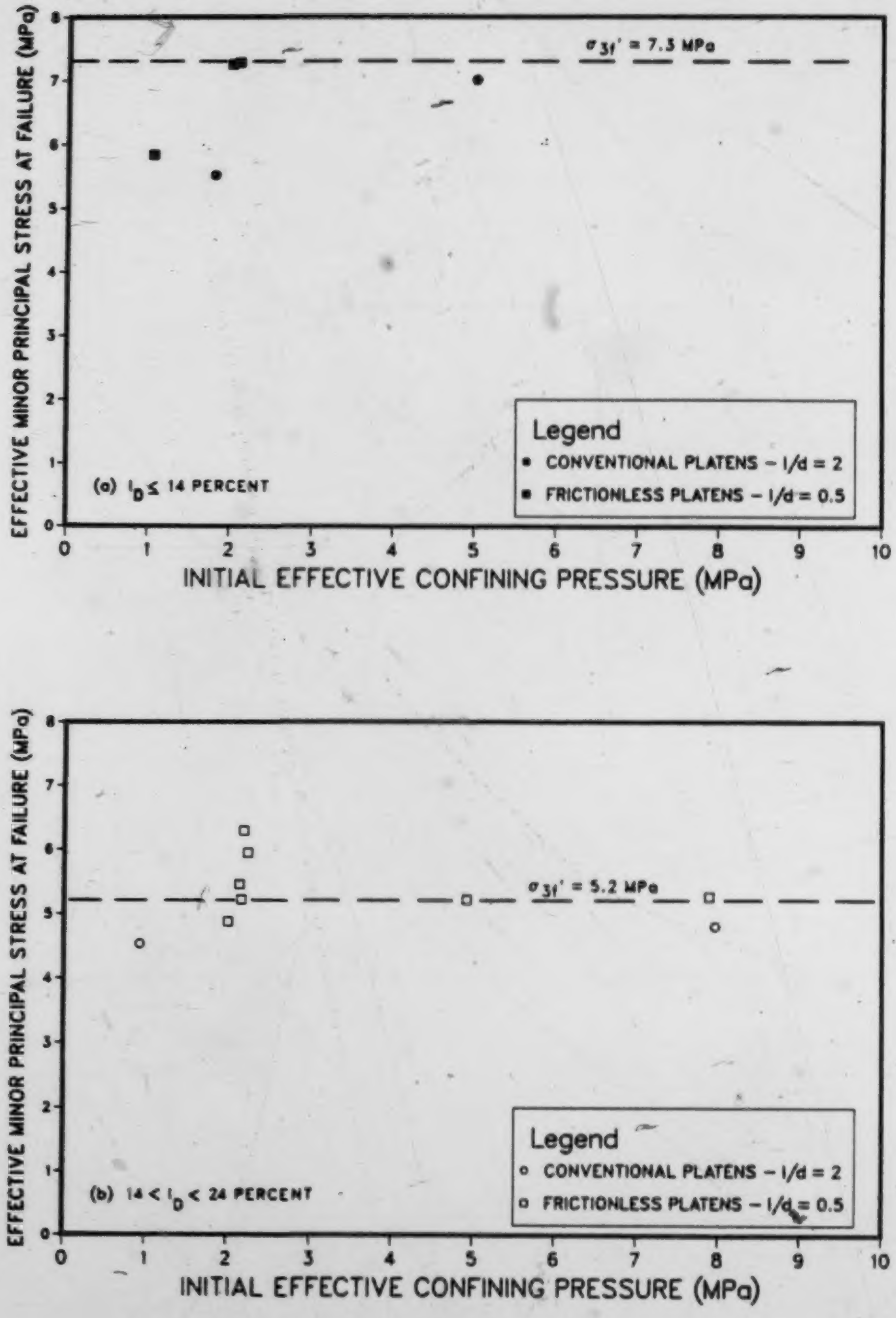

Figure 6.12 Effective Minor Principal Stress at Ultimate Strength in Undrained Triaxial Compression Tests

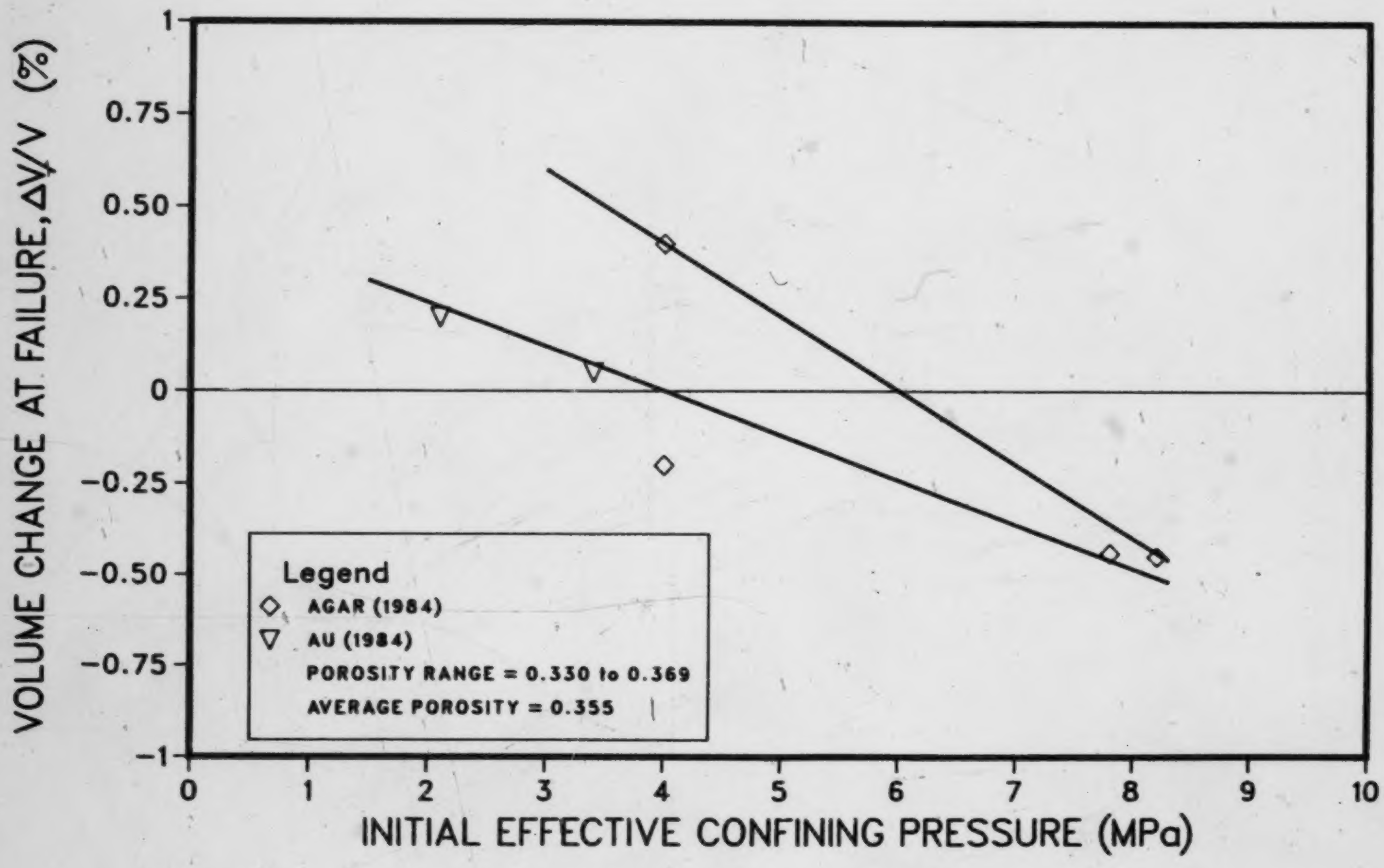

Figure 6.13 Critical Confining Pressure From Drained Triaxial Compression Tests on Saline Creek Oil Sand (After Au, 1984 and Agar, 1984)

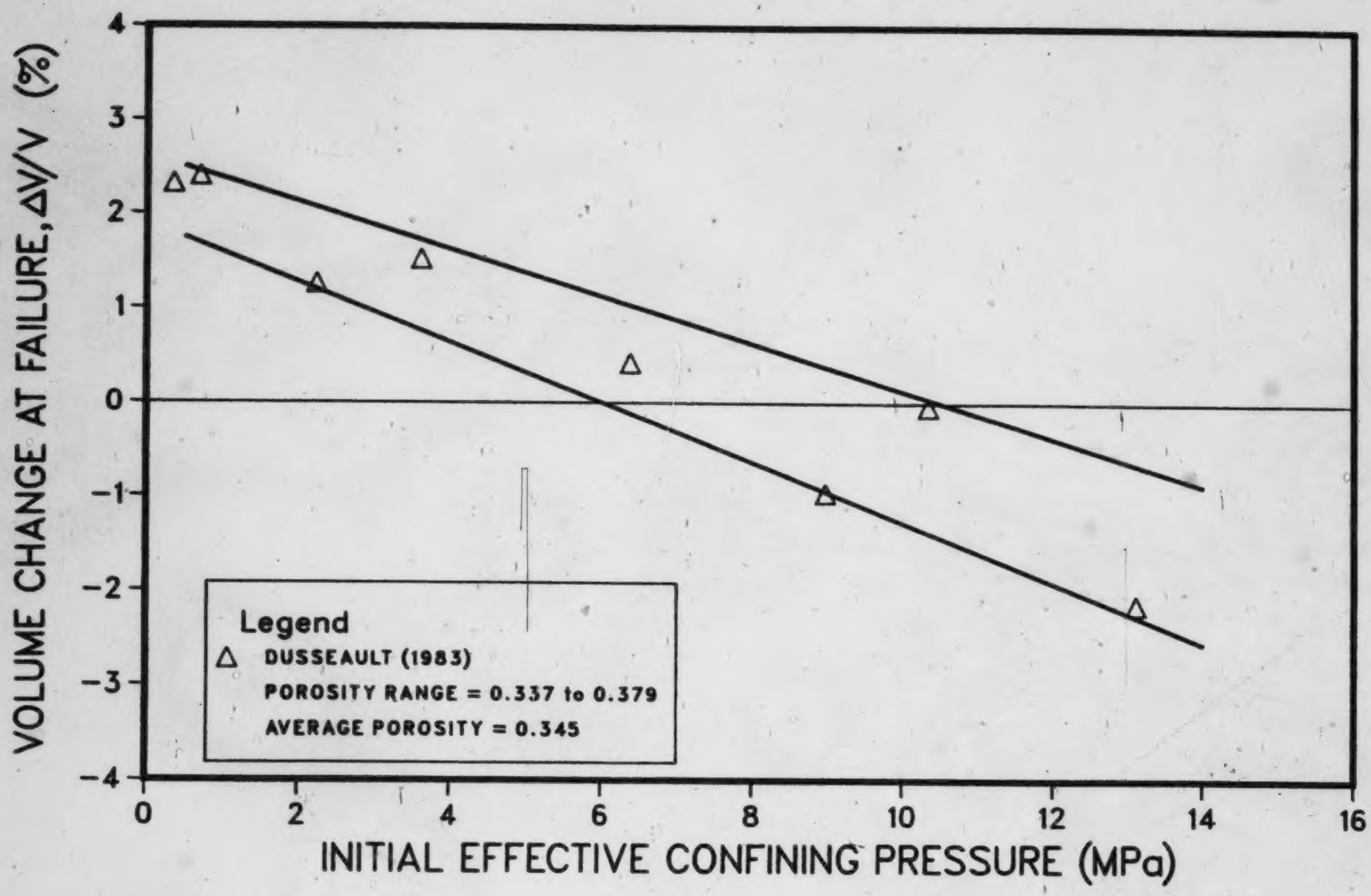

Figure 6.14 Critical Confining Pressure from Drained Triaxial Compression Tests on Lean Oil Sand (After Dusseault, 1983)

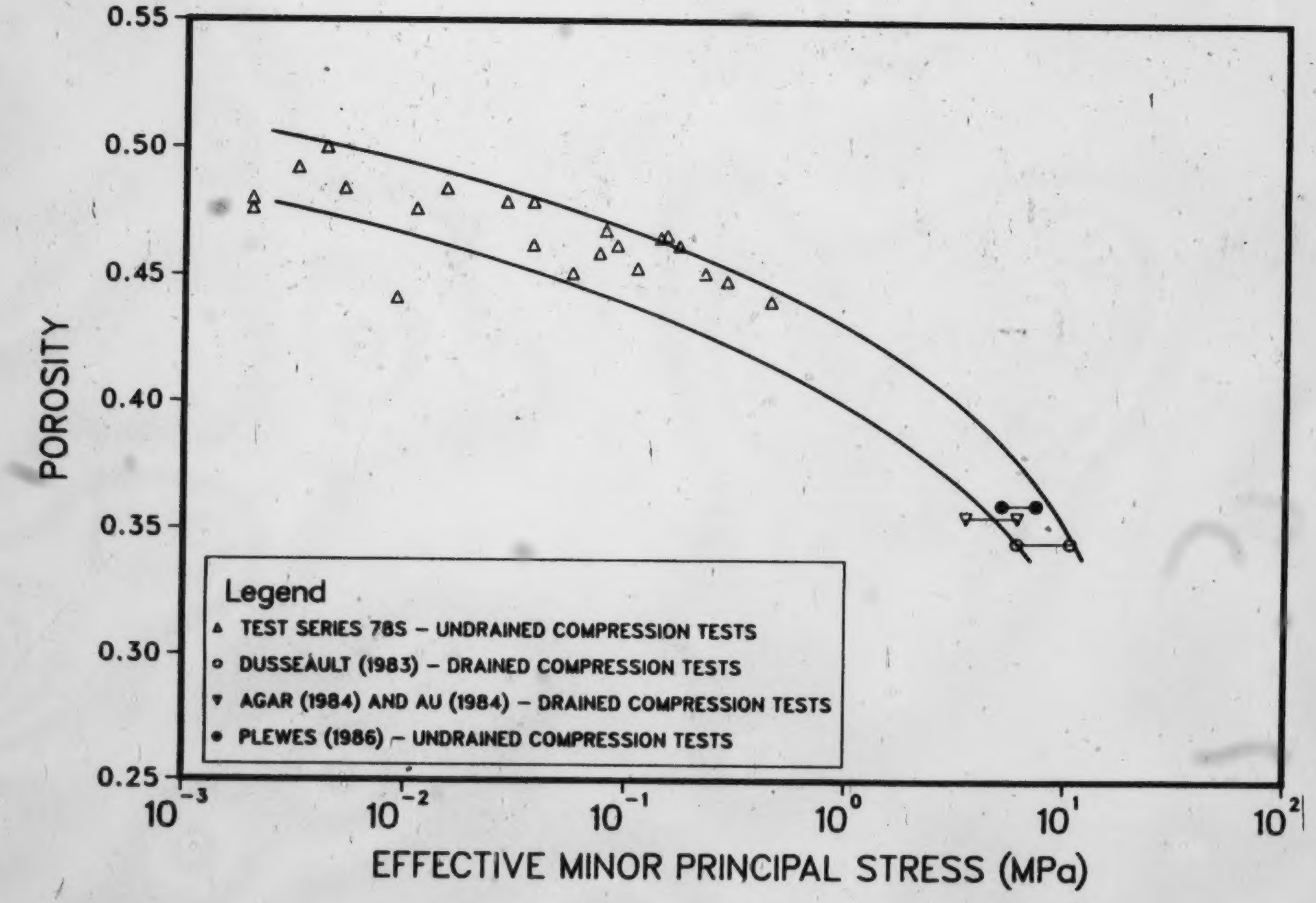

Figure 6.15 Critical State Line for Oil Sand

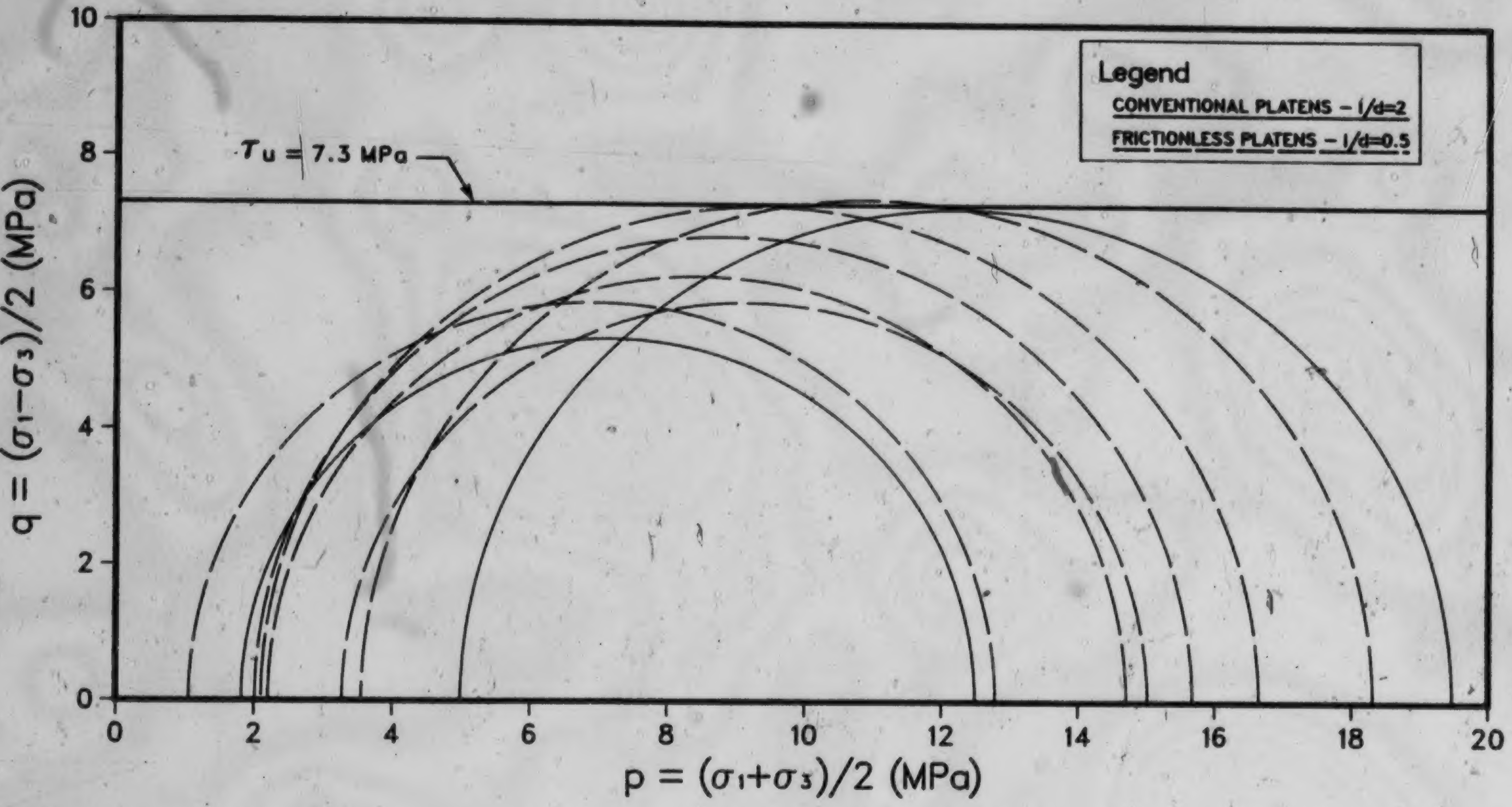

Figure 6.16 Ultimate Shear Strength in Non-Cavitating Undrained Triaxial Compression Tests on Undisturbed Saline Creek Oil Sand

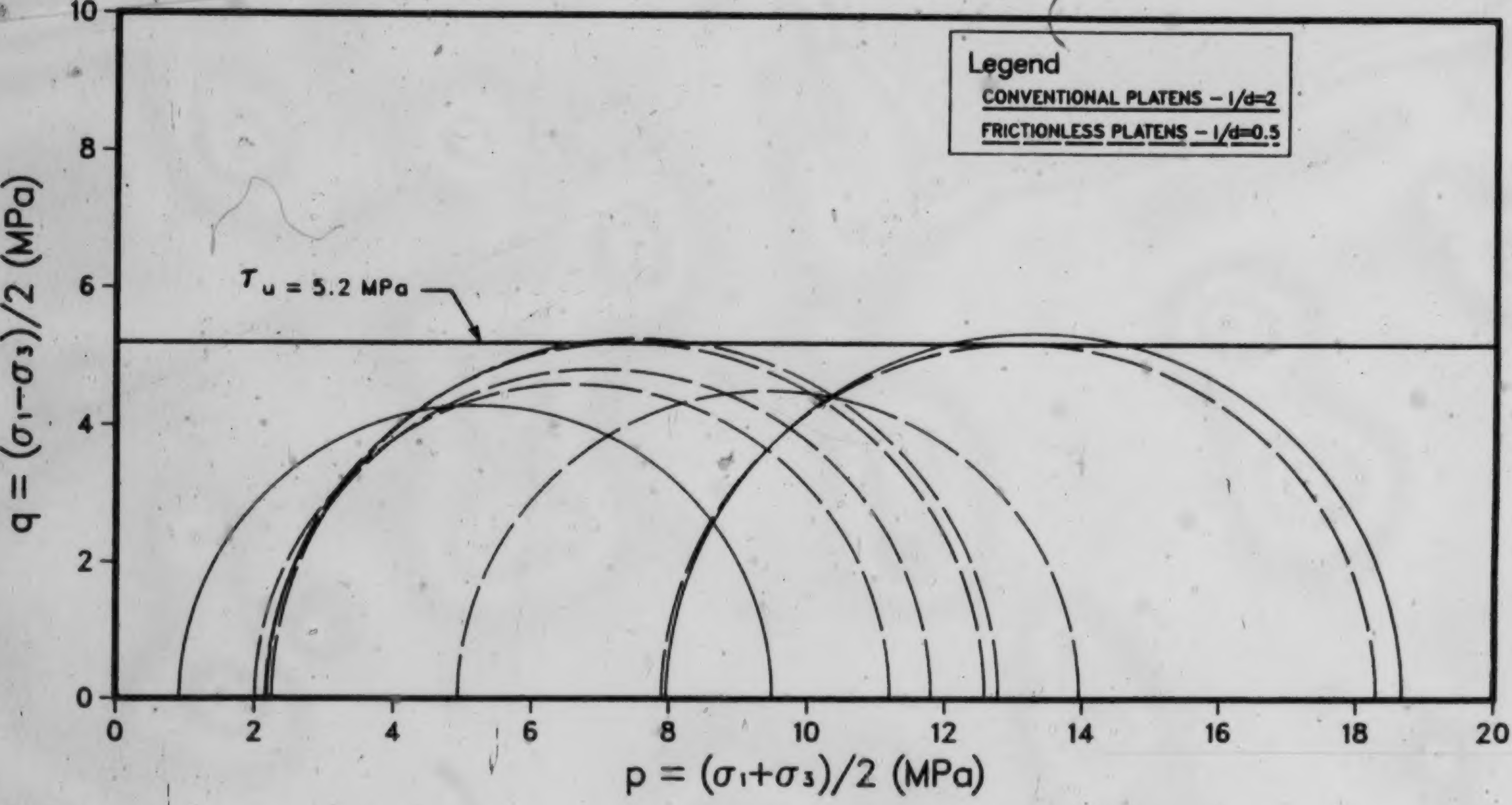

Figure 6.17 Ultimate Shear Strength in Non-Cavitating Undrained Triaxial Compression Tests on Disturbed Saline Creek Oil Sand

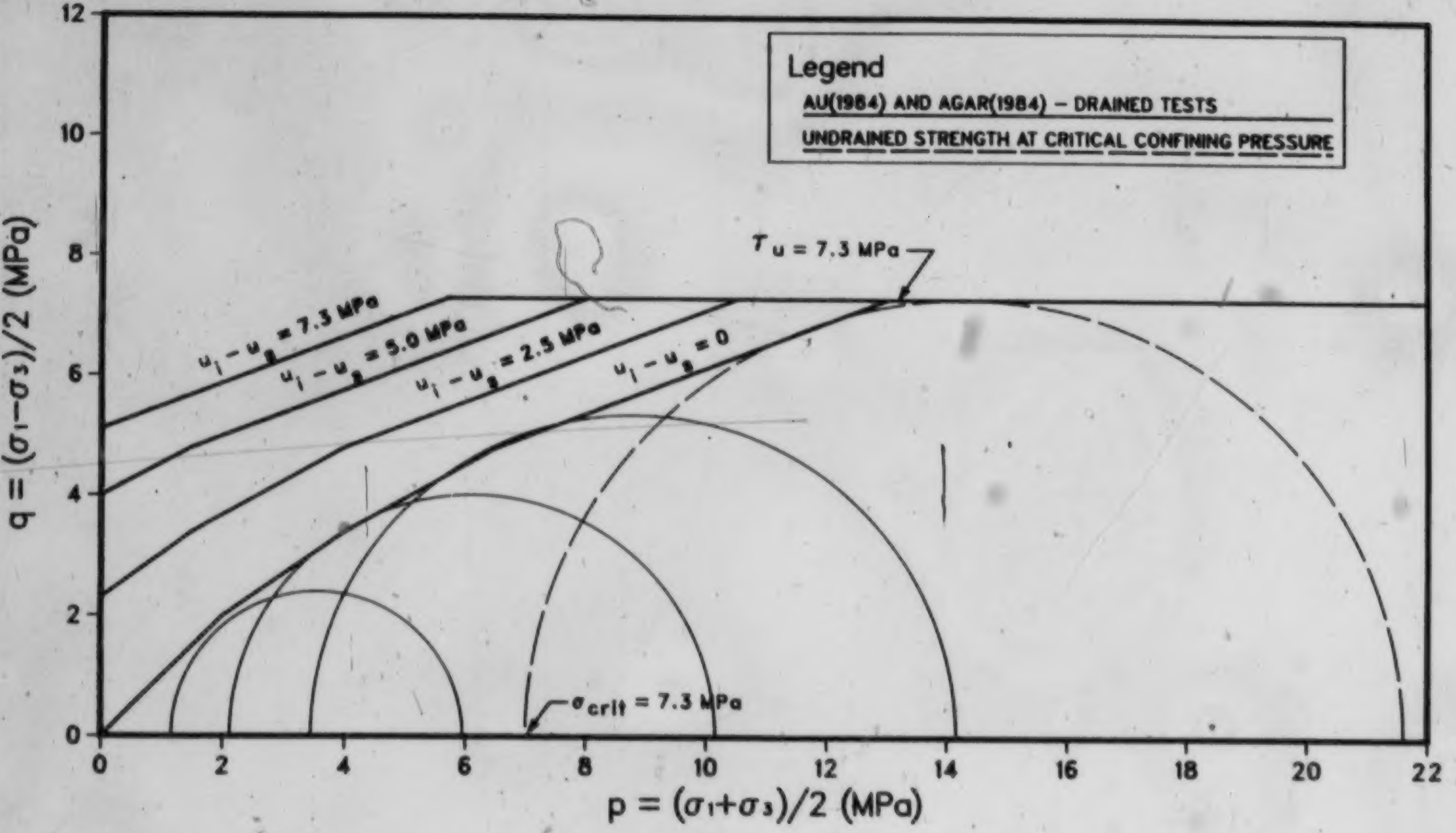

Figure 6.18 Predicted Ultimate Shear Strength for Undrained Triaxial Compression Tests on Undisturbed Oil Sand

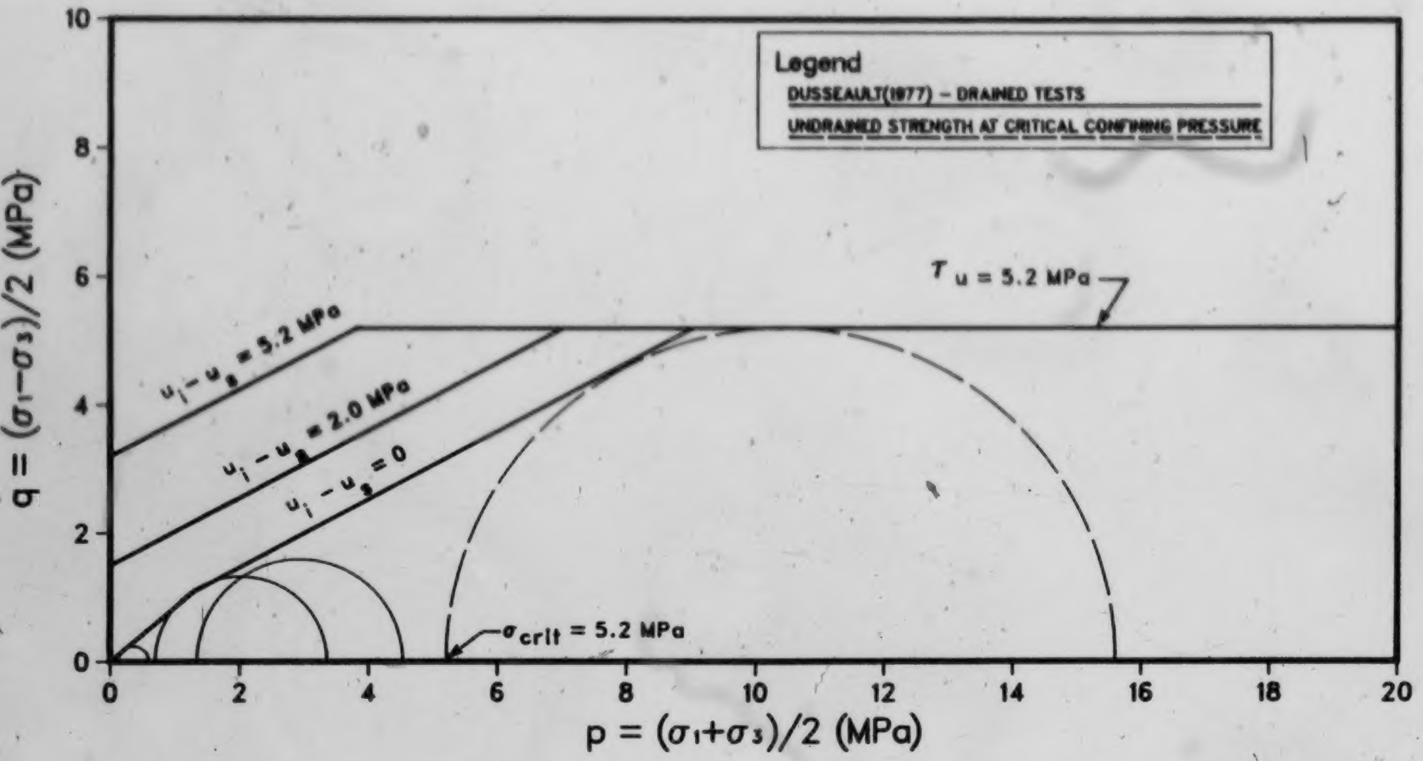

Figure 6.19 Predicted Ultimate Shear Strength for Undrained Triaxial Compression Tests on Disturbed Oil Sand

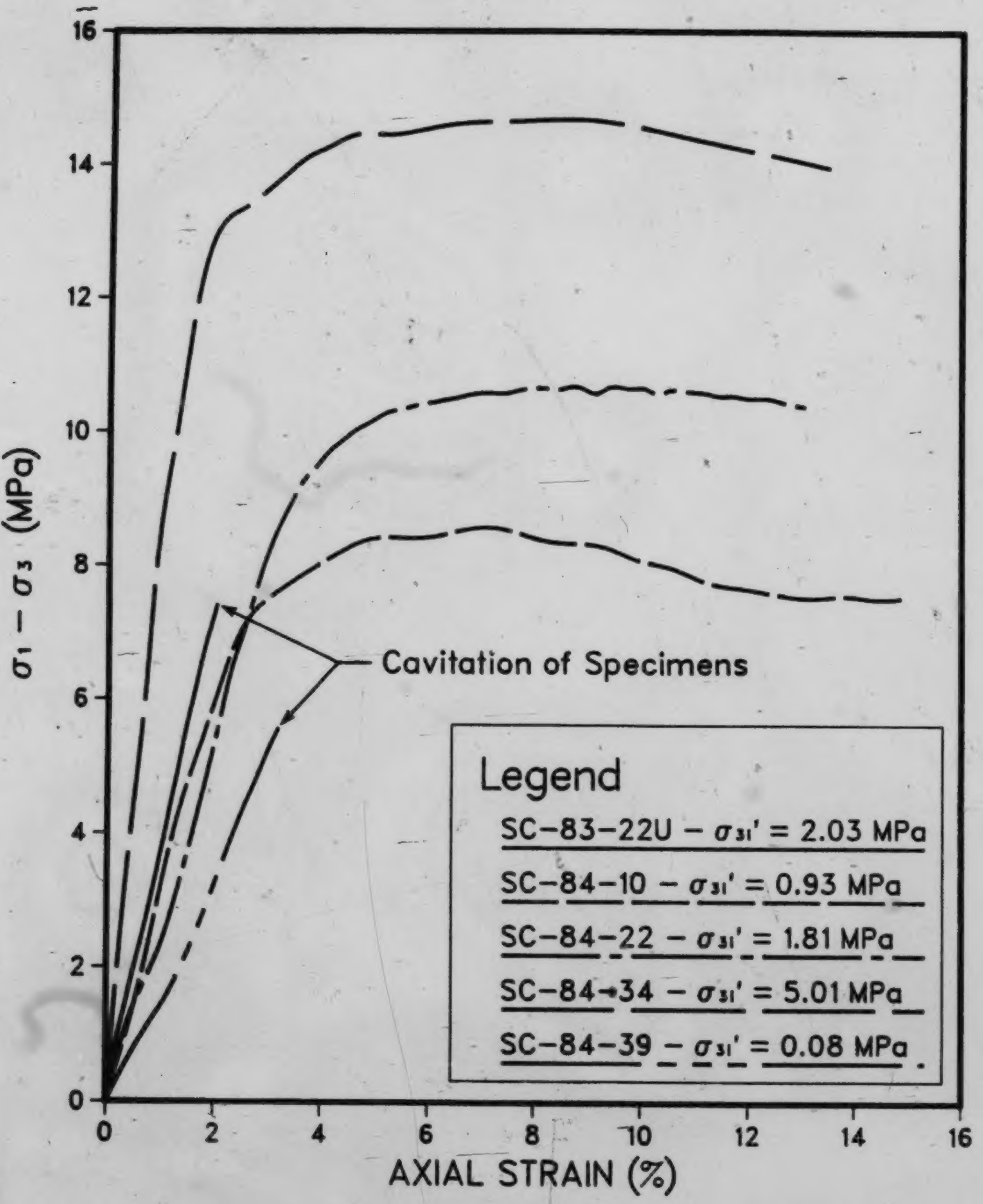

Figure 6.20 Stress-Strain Curves for Conventional Specimens (l/d = 2) of Undisturbed Saline Creek Oil Sand

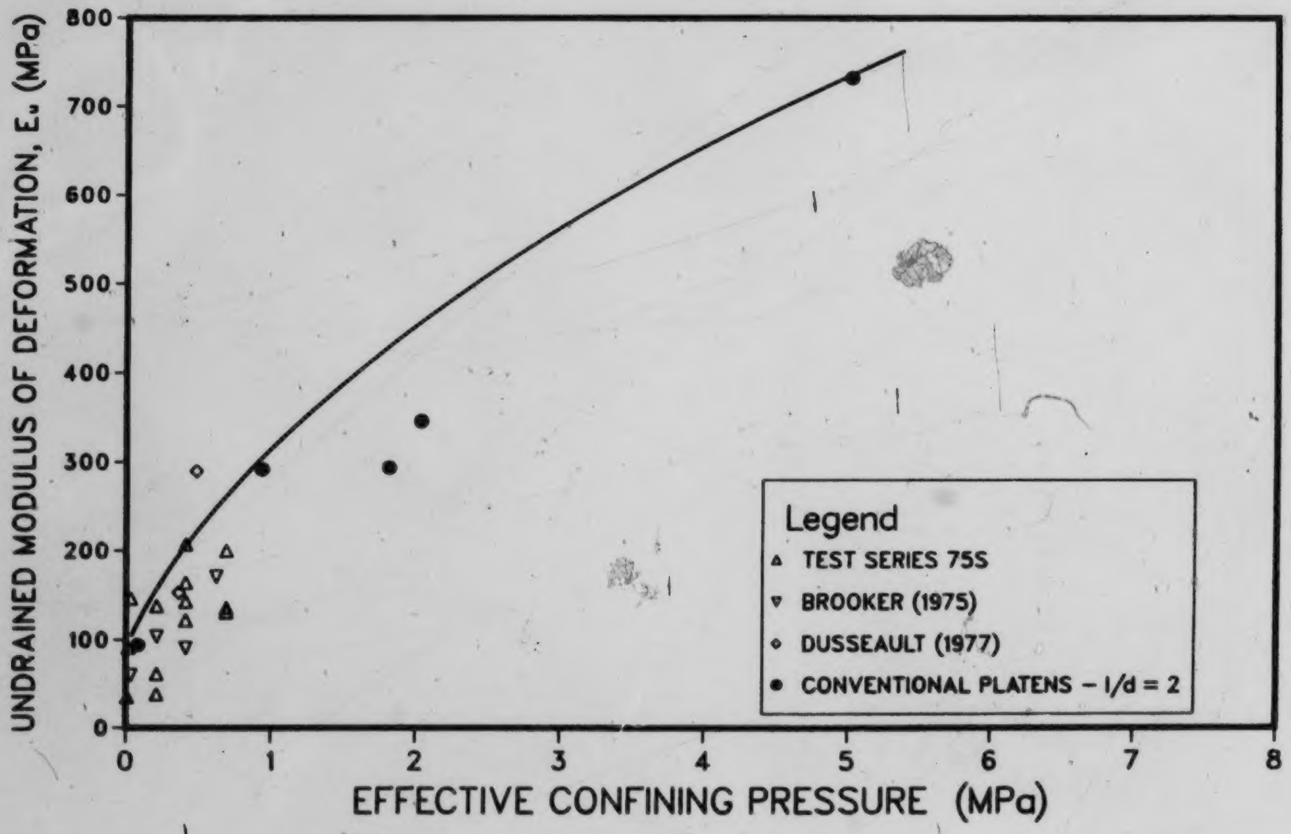

Figure 6.21 Tangent Modulus at 0.25 Percent Strain for Undrained Triaxial Compression Tests on Oil Sand

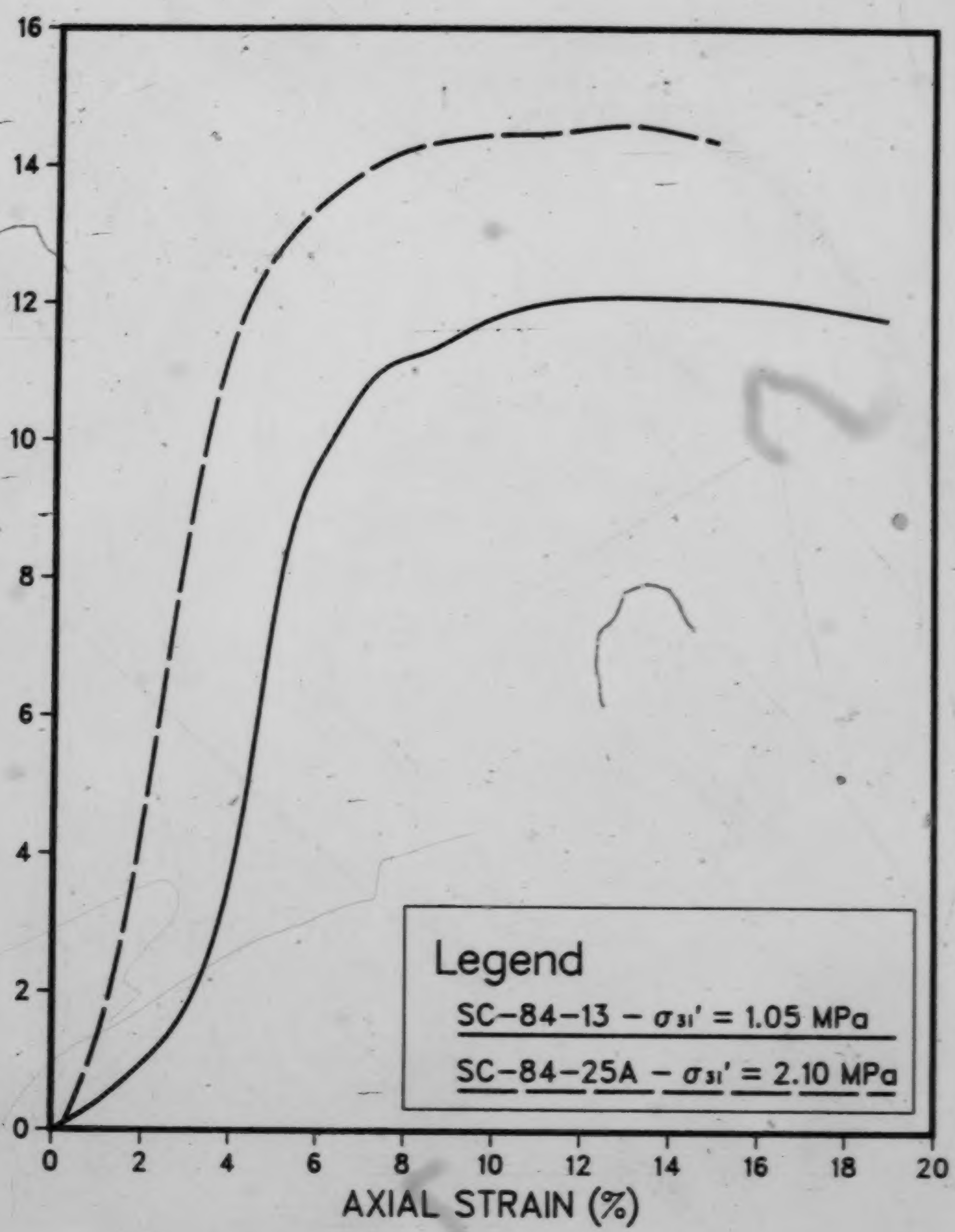

Figure 6.22 Stress-Strain Curves for Short Specimens (l/d = 0.5) of Undisturbed Saline Creek Oil Sand using Frictionless Platens

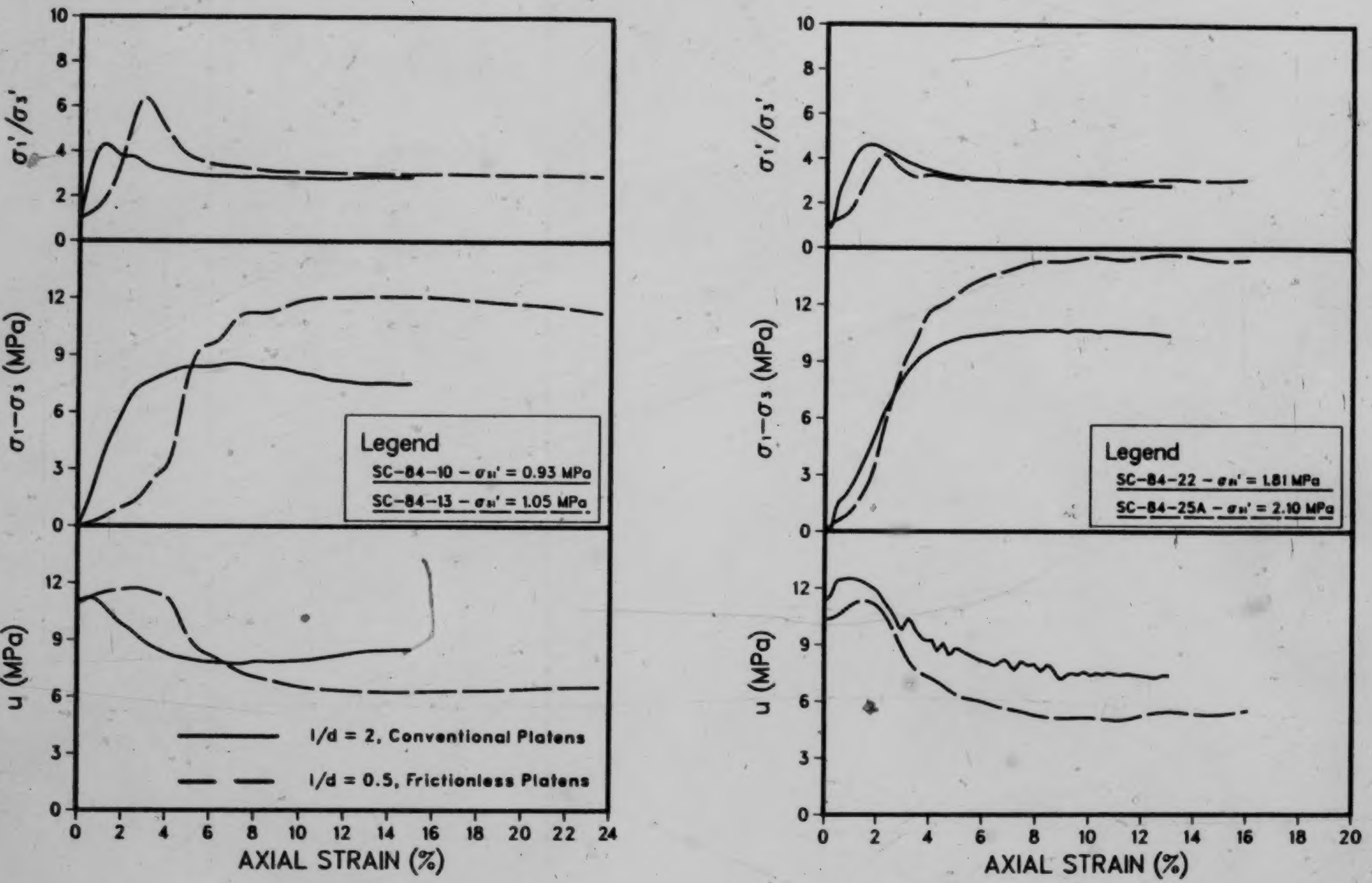

Figure 6.23 Comparison of Undrained Triaxial Compression Test Results for Conventional Specimens (l/d = 2) and Short Specimens (l/d = 0.5) using Frictionless Platens

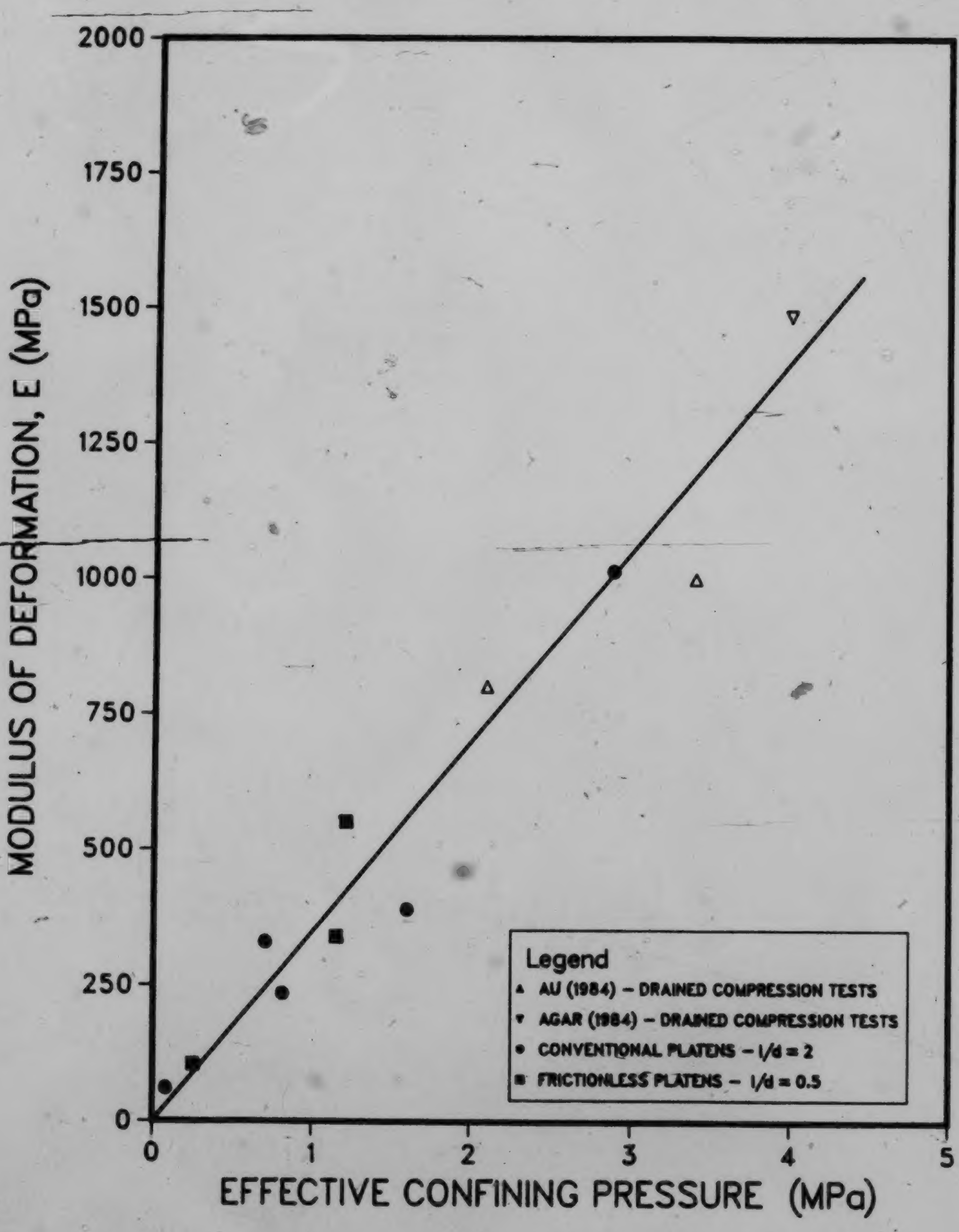

Figure 6.24 Comparison of Modulus of Deformation for Undrained Triaxial Compression Tests at $\Delta u/\Delta \epsilon = 0$ and Drained Tests at $\Delta v/\Delta \epsilon = 0$

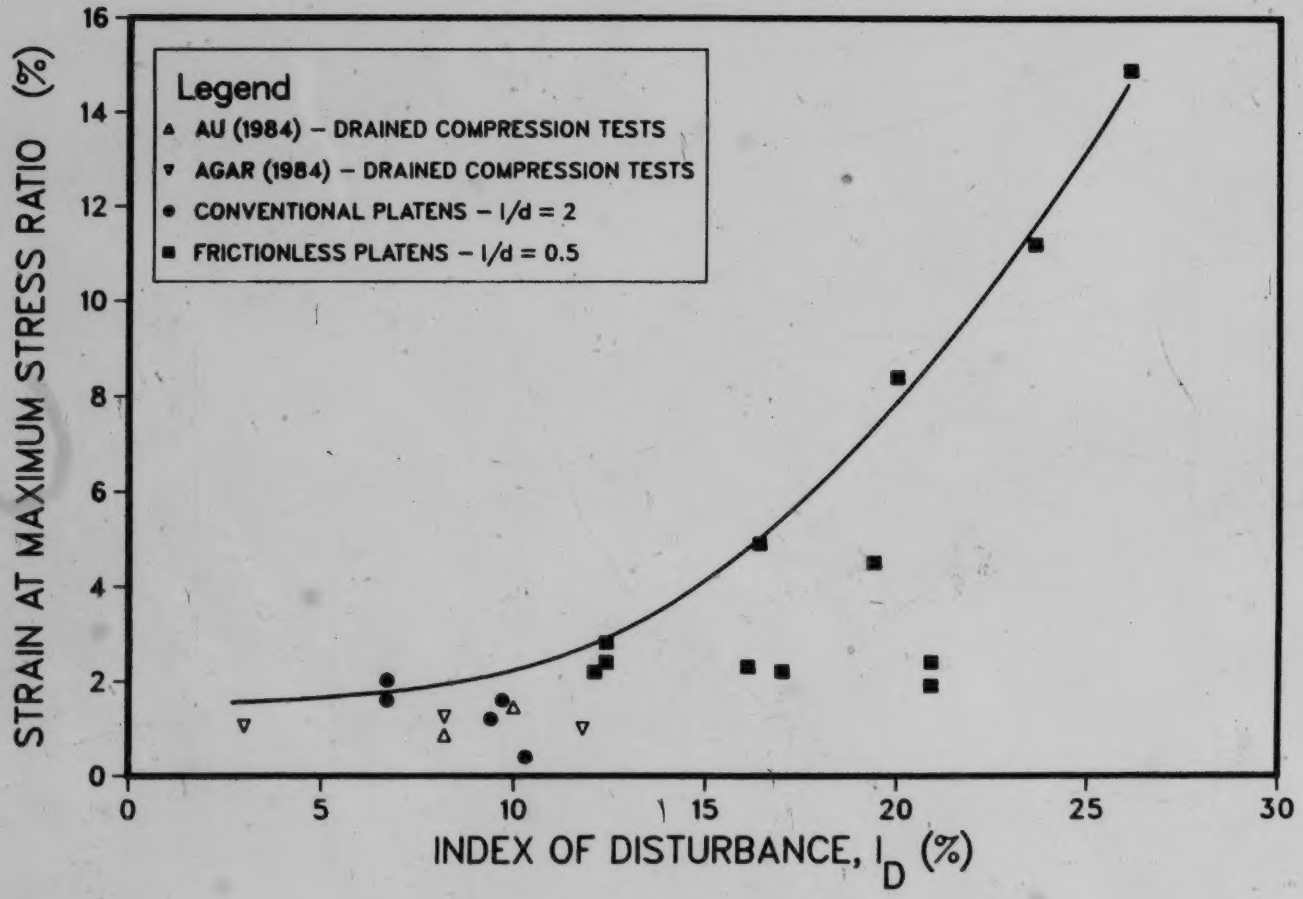

Figure 6.25 Axial Strain at Maximum Stress Ratio Versus Index of Disturbance

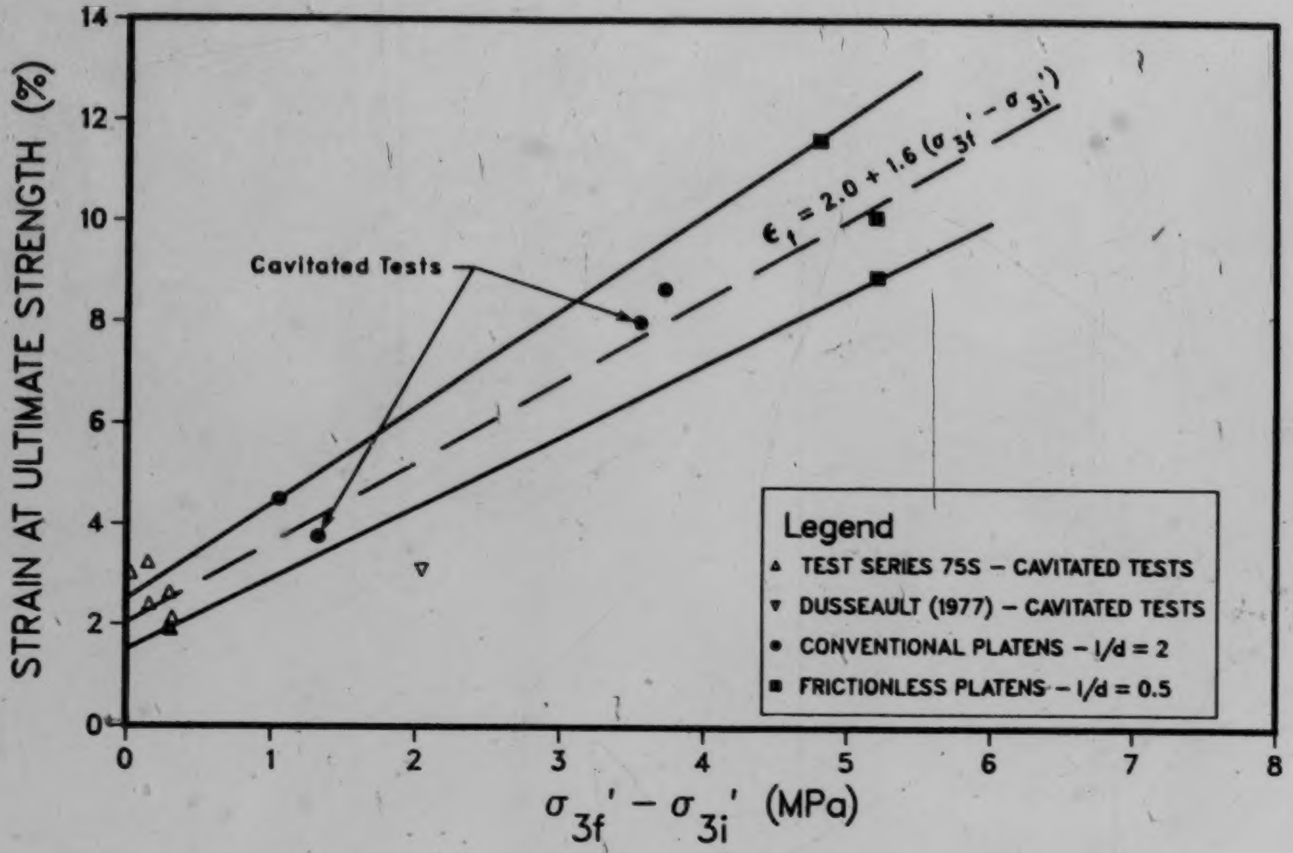

Figure 6.26 Axial Strain at Ultimate Strength Versus Stress Difference $\sigma_{3f}' - \sigma_{3i}'$

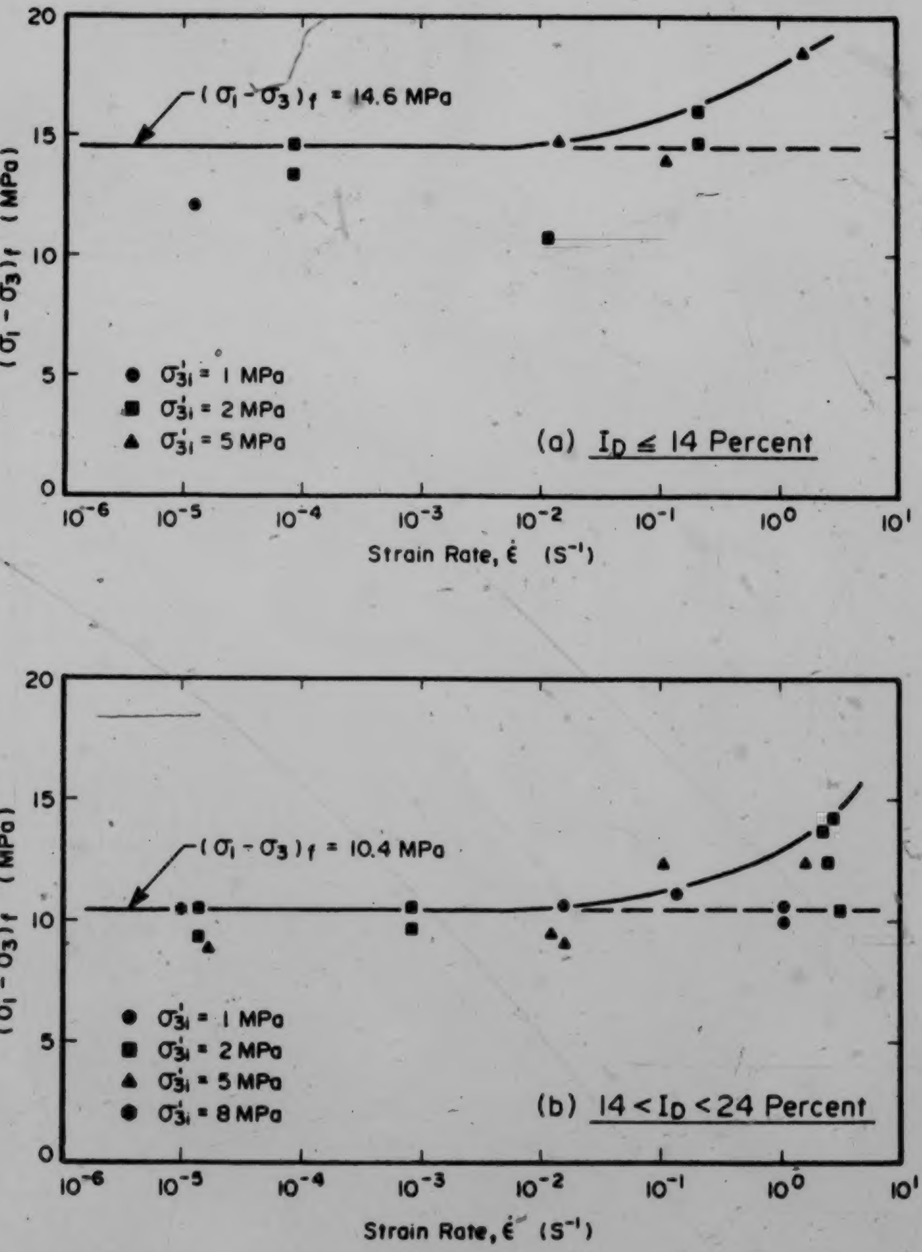

Figure 6.27 Ultimate Undrained Strength Versus Strain Rate of Testing

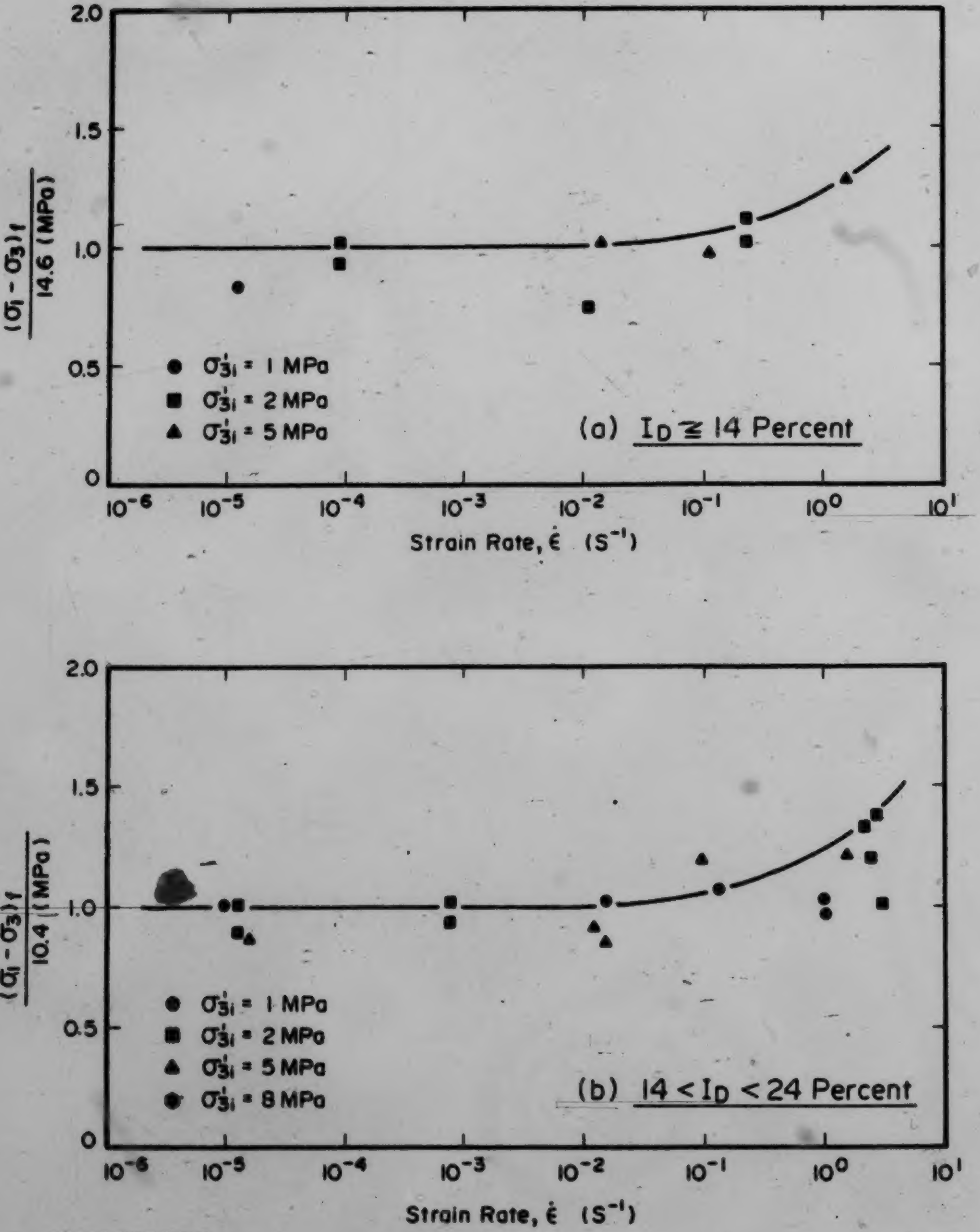

Figure 6.28 Relative Increase in Ultimate Undrained Strength with Strain Rate

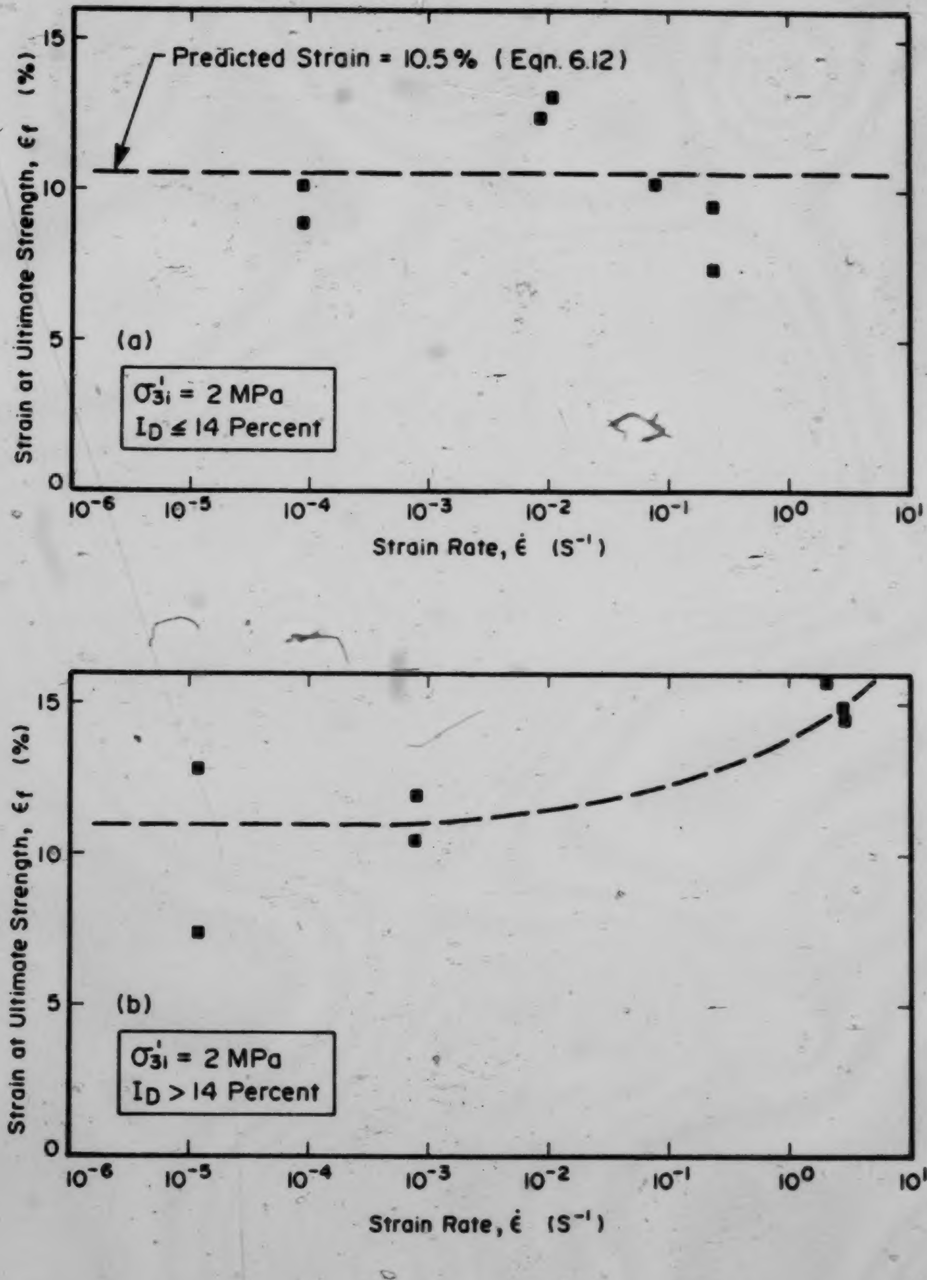

Figure 6.29 Axial Strain at Ultimate Strength Versus Strain Rate

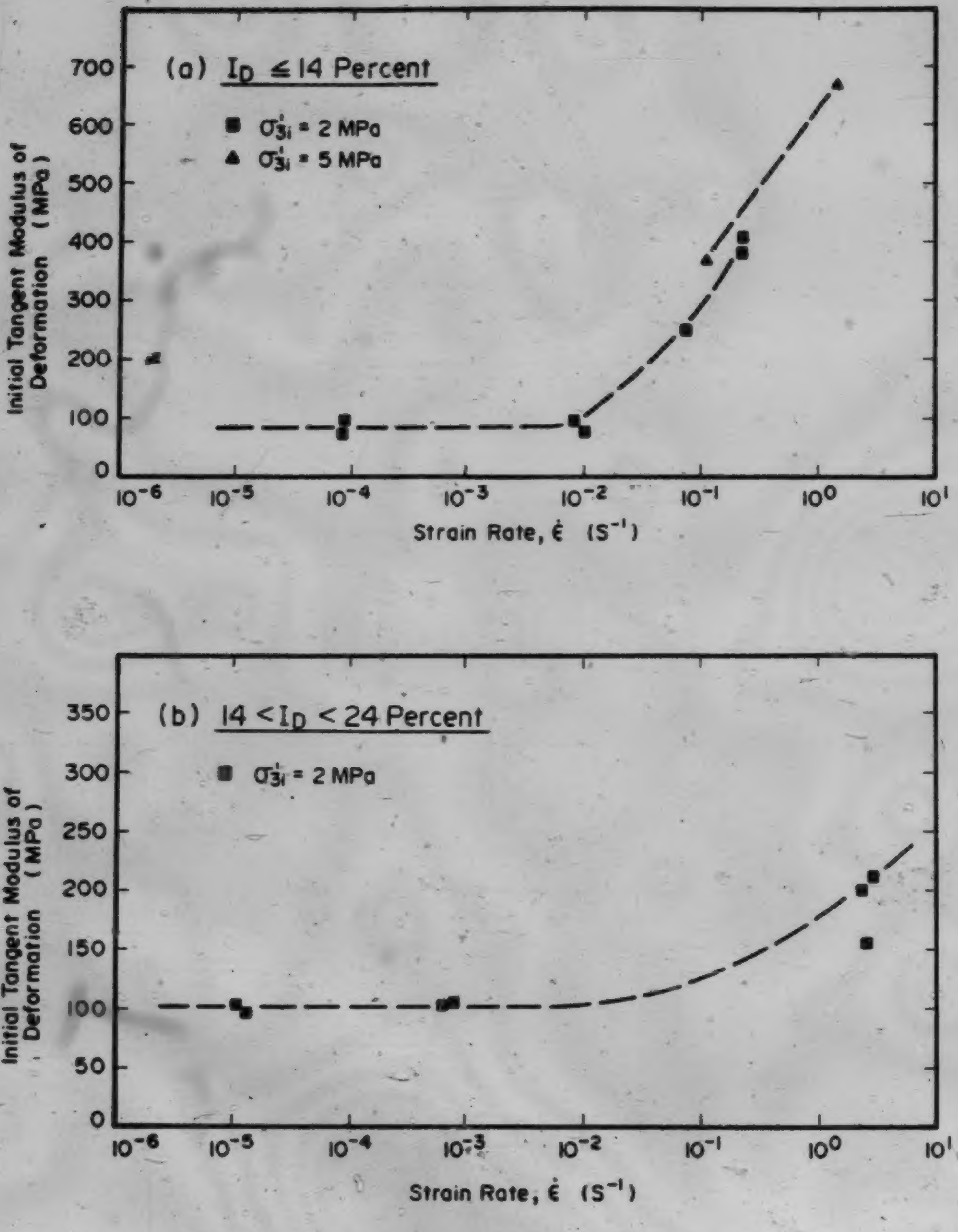

Figure 6.30 Initial Tangent Modulus of Deformation Versus Strain Rate

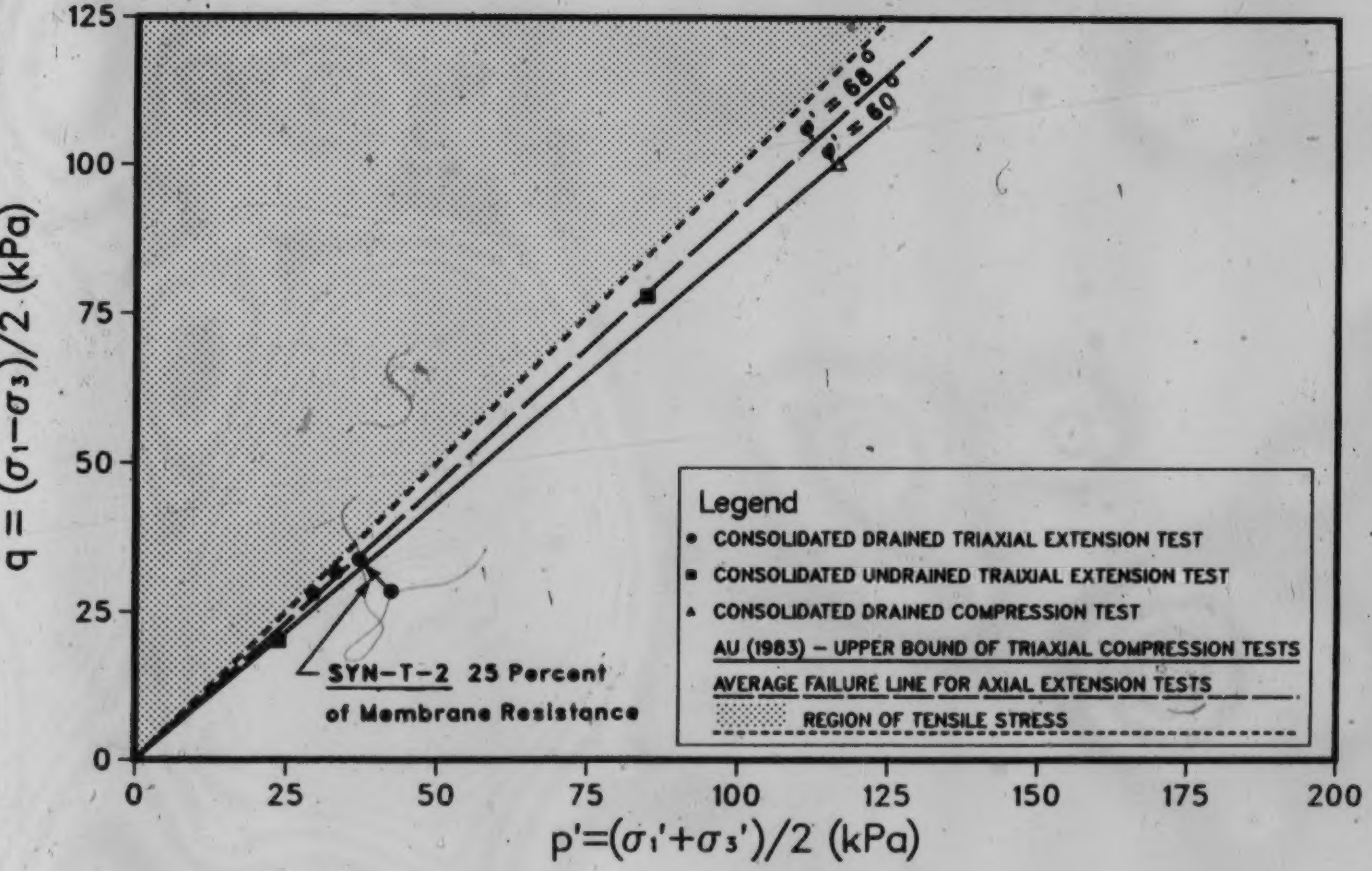

Figure 6.31 Triaxial Test Results for Syncrude Oil Sand

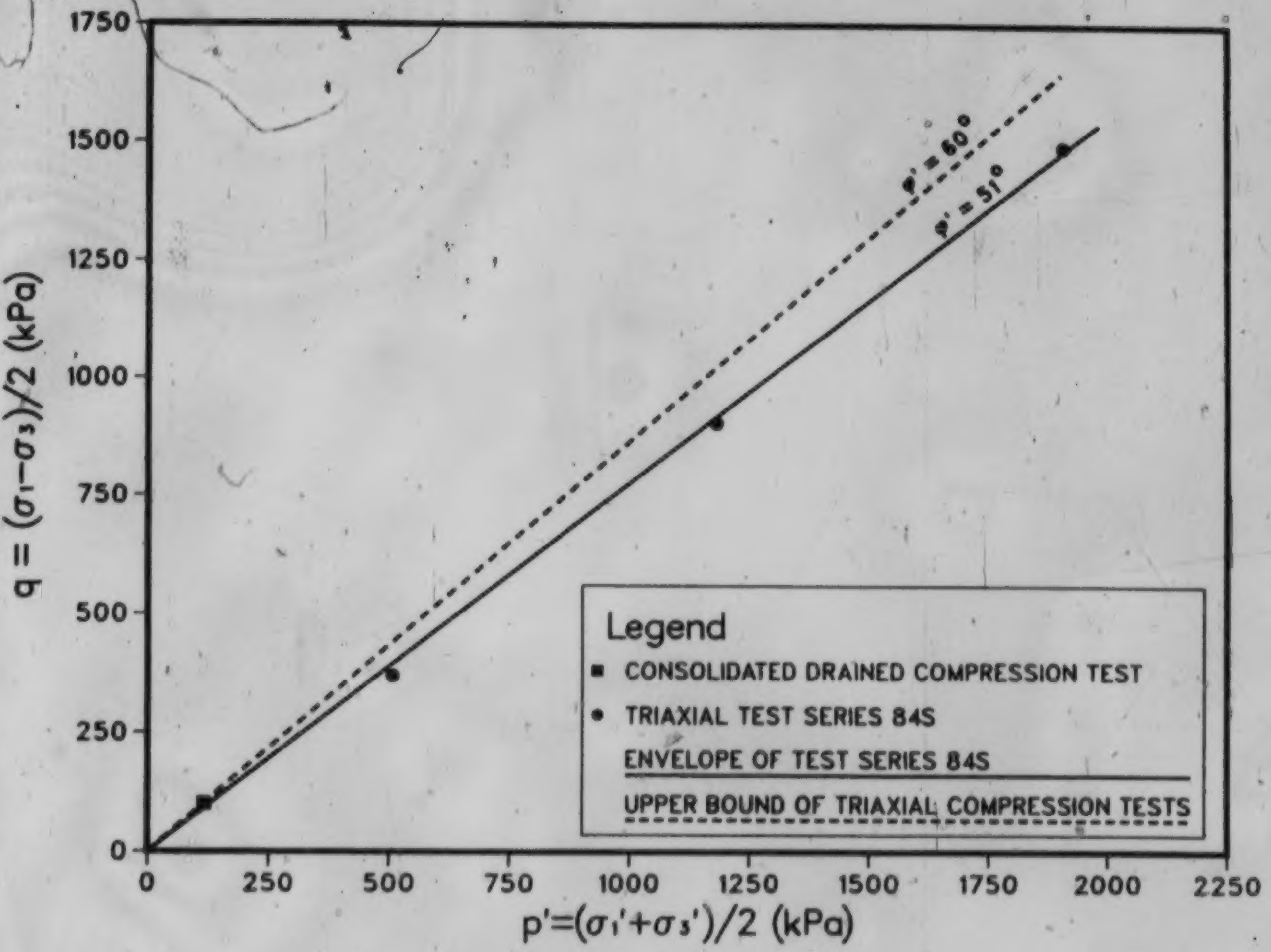

Figure 6.32 Comparison of Triaxial Compression Test SYN-C-1 with Test Series 84S

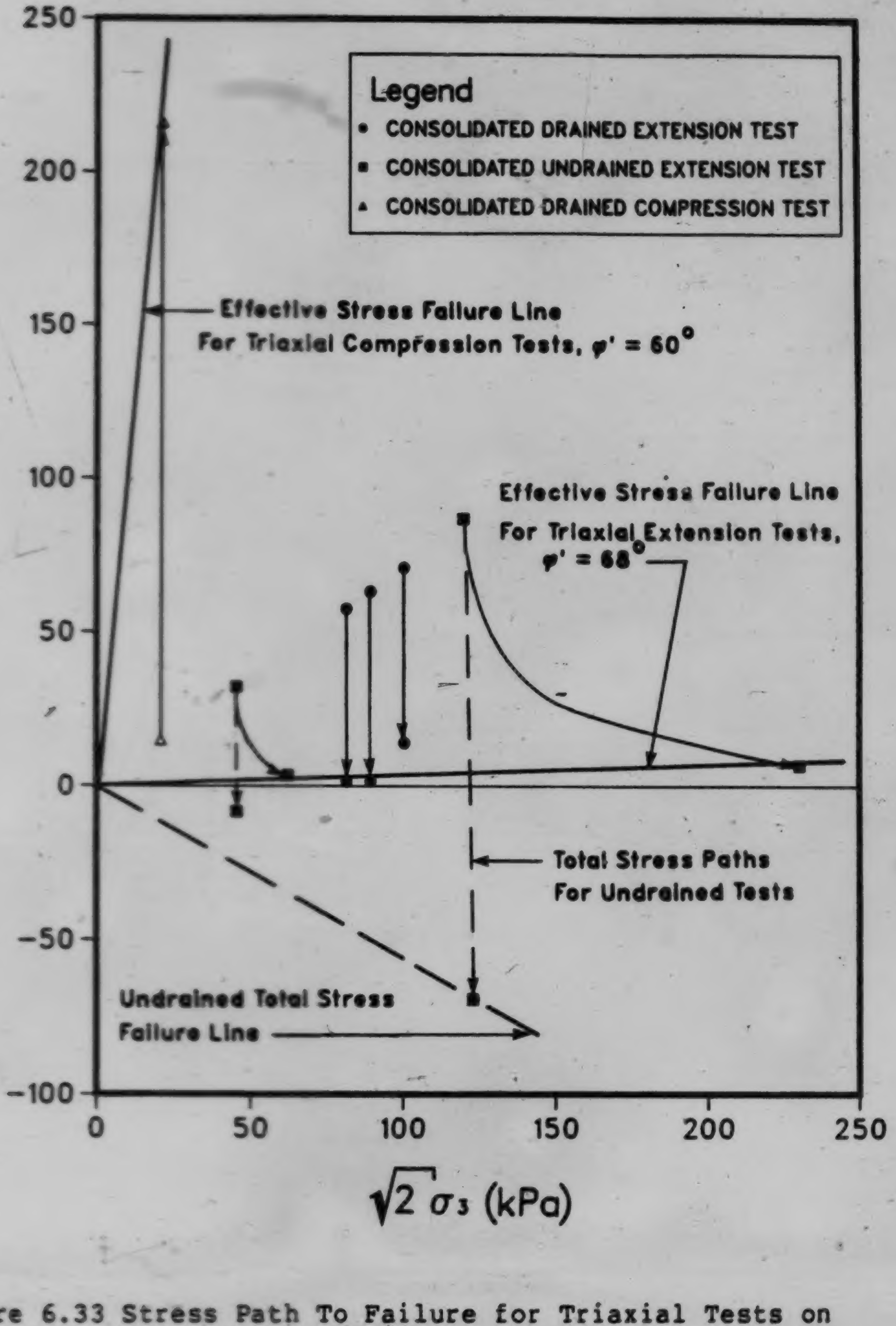

Figure 6.33 Stress Path To Failure for Triaxial Tests on Syncrude Oil Sand

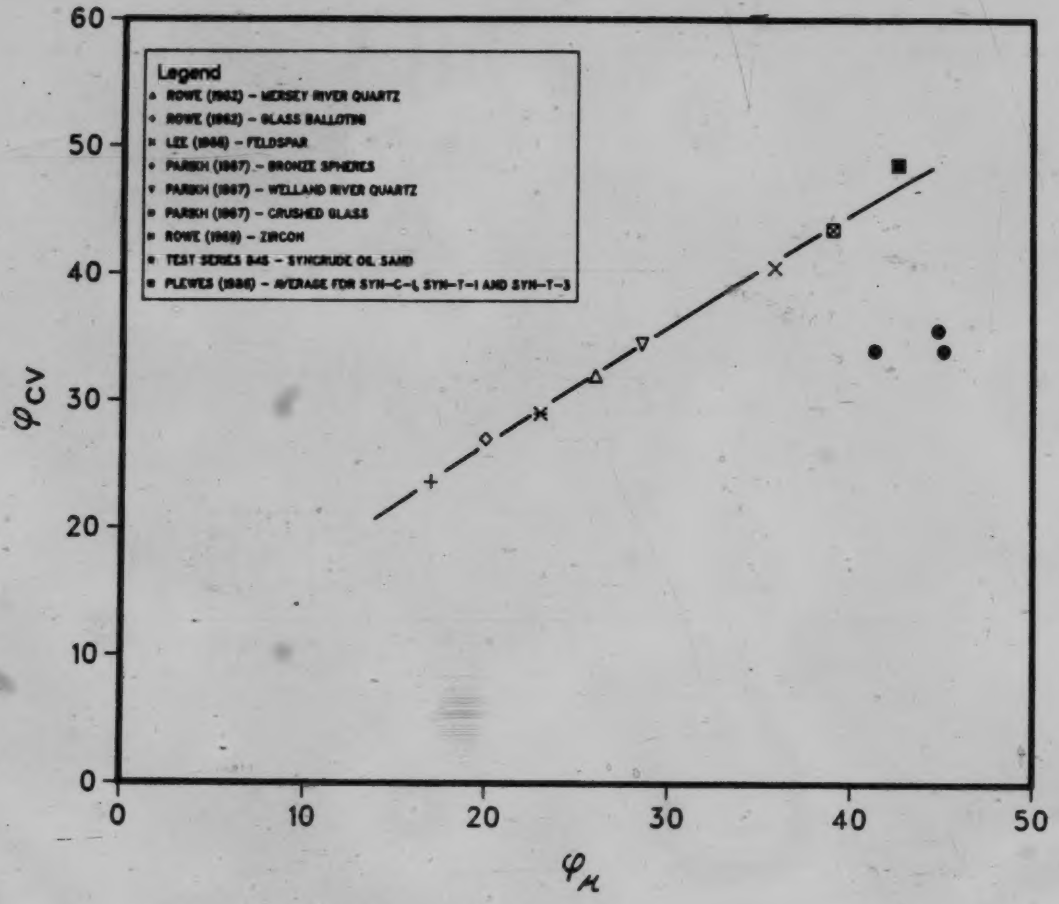

Figure 6.34 Comparison of $\phi_\mu$ and $\phi_{cv}$ for Syncrude oil sand with other Dense Sands at Low Stresses (After Rowe, 1969)

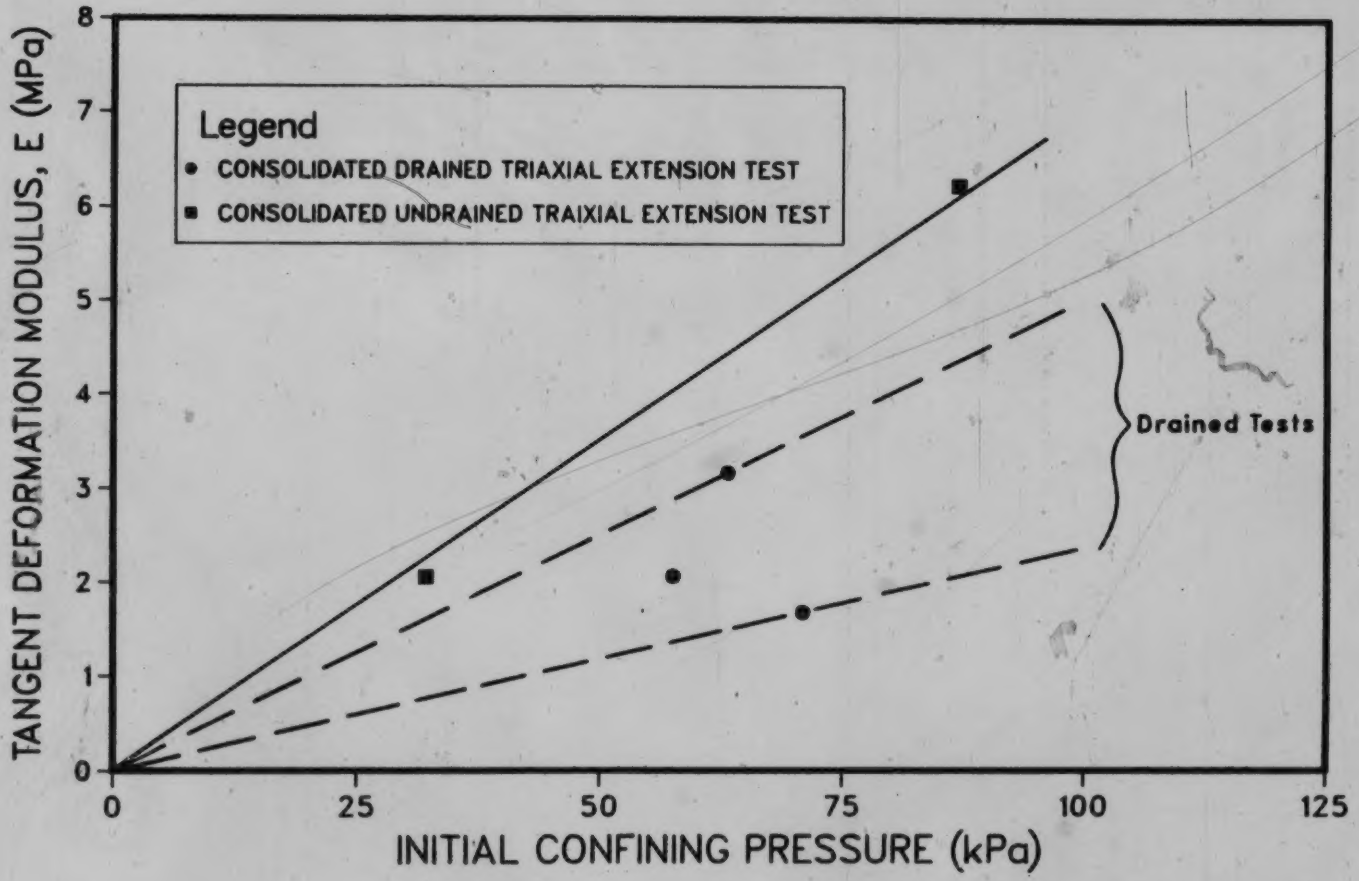

Figure 6.35 Tangent Modulus of Deformation Versus Initial Effective Confining Pressure for Extension Tests

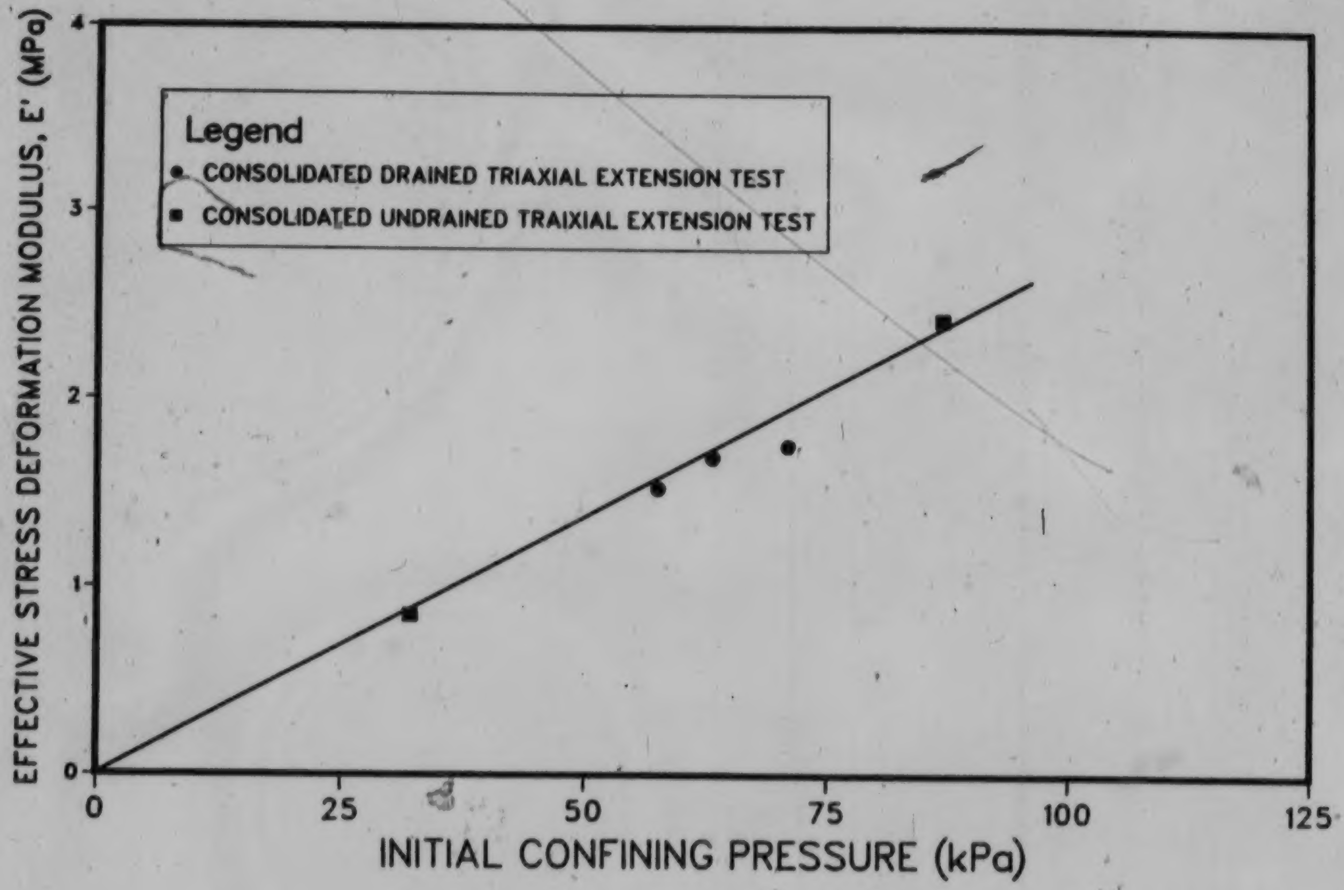

Figure 6.36 Effective Stress Modulus of Deformation, E' at 1.0 Percent Strain for Extension Tests

# 7. CONCLUSIONS AND RECOMMENDATIONS

## 7.1 General

The research documented in this thesis investigates the undrained behaviour of Athabasca oil sand. Undrained triaxial compression tests were conducted at room temperature (20°C) on intact and disturbed samples of Saline Creek oil sand. The behaviour over the range of confining pressures up to 8 MPa and strain rates up to 3.5 $s^{-1}$ was examined. Supplementary test procedures were performed to measure drained and undrained compressibility and evaluate grain alteration during testing.

Drained and undrained axial extension tests were conducted on intact samples of bitumen-poor Syncrude oil sand under confined and unconfined stress conditions. The method of shaped test specimens proposed by Bishop and Garga(1969) was used to show the absence of any tensile resistance in the interpenetrative grain structure of the oil sand tested.

The experimental results are discussed in Chapter 6. The conclusions and practical implications drawn from the research are outlined in the next sections.

## 7.2 Conclusions

### 1. Critical State Line

The complete critical state line for oil sand has been defined covering the range of porosity from the loosest state to the undisturbed state. The critical confining pressure for undisturbed laboratory specimens of Saline Creek oil sand ranges between 4.0 and 7.3 MPa. Accepting that some degree of sample disturbance and decrease in porosity has occurred among all laboratory test specimens, the critical confining pressure under in situ conditions is taken as the upper bound of 7.3 MPa.

### 2. Undrained Shear Strength

The angle of shearing resistance of oil sand at the maximum stress ratio in the undrained compression tests decreases non-linearly with effective normal stress. The shear strength correlates well with drained compression tests on oil sand with corrections for volume change during testing applied by Rowe's(1962) stress-dilatancy theory.

The angle of shearing resistance mobilized at the ultimate strength is 30° corresponding to conditions of constant volume at the critical confining pressure. The theoretical ultimate undrained shear strength mobilized under completely undrained conditions is identically equal to the critical confining pressure. The upper bound of undrained shear strength under in situ conditions is then predicted to be 7.3 MPa.

A generalized procedure for the prediction of undrained shear strength of oil sand under partially drained conditions or conditions of pore fluid cavitation is presented. The predicted undrained shear strength is solely a function of the pore pressure change at failure, $\Delta u_f$ and the initial effective confining pressure, $\sigma'_{3i}$:

$$\tau_u = f(\Delta u_f, \sigma'_{3i}) \qquad 7.1$$

The predictive procedure provides an accuracy of ± 25 percent in comparison with available published data for undisturbed and disturbed oil sand. This is considered within acceptable limits for predictive geomechanical analyses.

## 3. Undrained Stress-Strain Response

The undrained stress-strain response of oil sand in axial compression exhibits a distinct strain-hardening due to the progressive decrease in pore pressure and increase in effective confining pressure with strain. Failure is reached at the critical confining pressure as the dilatancy of the oil sand is suppressed by higher confining stresses.

The initial tangent modulus of deformation for the undrained compression tests is less than measured in drained compression tests at the same initial effective confining pressure. The difference in stress-strain response is shown to be a function of the effective stress path for the two types of tests rather than a difference in material behaviour.

The axial strain at the maximum principal stress ratio in both drained and undrained compression tests generally ranges between 1 and 2 percent for intact samples of oil sand. The predicted average strain in percent at the ultimate strength is given as:

$$\epsilon_f = 2.0 + 1.6\,(\sigma'_{3f} - \sigma'_{3i}) \quad \text{(MPa)} \qquad 7.2$$

For completely undrained tests, the final effective confining pressure is equivalent to the critical confining pressure. Hence:

$$\epsilon_f = 2.0 + 1.6\,(\sigma_{crit} - \sigma'_{3i}) \quad \text{(MPa)} \qquad 7.3$$

The strain at failure in completely undrained compression tests of undisturbed oil sand is predicted to range between 2 percent for $\sigma'_{3i} = \sigma_{crit} = 7.3$ MPa and 14 percent for $\sigma'_{3i} = 0$.

## 4. Influence of Strain Rate on Undrained Behavior

A transient response in pore pressure during undrained compression tests on Saline Creek oil sand was observed at strain rates greater than $10^{-2}$ $s^{-1}$, about two orders of magnitude of strain rate slower than for water saturated dense sands. The onset of transient response at slower strain rates is shown to be a direct function of the higher viscosity of the interstitial bitumen.

A 35 percent increase in ultimate shear strength and 600 percent increase in the modulus of deformation was measured between the strain rates of $10^{-2}$ and 3.5 $s^{-1}$. Strains at the ultimate strength increased very slightly over the same range of strain rate.

## 5. Behavior in Axial Extension

The average angle of shearing resistance of the Syncrude oil sand in axial extension is 68° over the range of mean effective stresses at failure up to 100 kPa. This corresponds to a relative increase in the angle of shearing resistance of 13 percent in comparison to axial compression, which agrees with the upper bound of increase for other dense sands reported in the literature.

The modulus of deformation for undrained extension ranges up to 75 percent greater than measured in drained extension. The difference in stress-strain reponse is shown to be a function of the difference in stress path between the two types of tests.

In terms of total stress, a significant apparent tensile strength may be mobilized during undrained unloading of oil sand. The magnitude of the mobilized undrained tensile strength increases with the initial confining pressure. Negligible tensile resistance was mobilized by the interstitial bitumen at room temperature (20°C).

## 6. Drained and Undrained Compressibility

The average coefficient of compressibility, $m_v$ of Saline Creek oil sand decreases almost one full order magnitude from $6 \times 10^{-6}$ to $0.8 \times 10^{-6}$ $kPa^{-1}$ over the range of effective confining stress between 0.1 and 7.0 MPa. It is recommended that the drained compressibility of oil sand should be referenced to a stress level rather than a broad range of stresses in geomechanical analyses.

The undrained pore pressure response to an increase in isotropic stress is governed by the theoretical relationship proposed by Bishop(1966, 1973) modified in Equation 6.1. The average compressiblity of the bitumen under saturated conditions is $2.0 \times 10^{-6}$ $kPa^{-1}$ over the range of pore fluid pressures between 1.0 and 6.0 MPa.

## 7. Assessment of Sample Disturbance

The classification of sample quality according to the index of disturbance proposed by Dusseault and Van Domselaar(1982) provided a reliable basis for differentation of sample condition. Based on a comparitive analysis of shearing resistance in the undrained compression tests, the index of disturbance for high quality geomechanical tests may be extended from 10 to 14 percent under controlled sampling and testing procedures.

## 7.3 Practical Implications of the Research

The following practical implications relevant to oil sand technology are drawn from the research:

1. Based on the critical confining pressure of 7.3 MPa, contractant behaviour should be anticipated under the in situ stress conditions at depths greater than 700 metres. At these depths, stress changes induced in the reservoir by injection of fluids or thermal heating could actually reduce the net permeability of the formation due to contraction of the oil sand and generation of fines.

2. The shear strength of oil sand under completely undrained conditions is extremely large compared to the stresses encountered in surface mining and most in situ recovery processes. Under such conditions, the mass behaviour of the oil sand will be

controlled by the weaker geological components in the formation. For example, the propagation of hydraulic fractures under very high rates of fluid injection will be favoured along the direction of weaker bedding planes or shale interbeds in the oil sand formation.

3. The undrained modulus of deformation is less than one-third that mobilized under drained conditions. Strains induced by fluid injection or thermal heating of reservoirs will therefore increase if sufficient pore fluid drainage and pore pressure drainage is not permitted. Ultimately, adverse strain gradients may develop between the oil sand and stronger indurated siltstone layers or weaker shale interbeds. Subsequent relaxation of the stresses and strains with pore fluid drainage could lead to damage or shearing of injection wells or neighbouring wells and shafts.

4. The apparent tensile strength mobilized during undrained unloading of oil sand explains the short term stability of very steep highwalls mined in the Athabasca oil sand by dragline and bucketwheel. Instabilities in the highwalls are almost always caused by weaker clay bedding planes dipping into the excavation.

The tensile strength developed by oil sand under undrained or partially drained conditions is an important consideration in the analysis and prediction of hydraulic fracturing. Further experiments to measure the undrained tensile strength mobilized at in situ stress levels are recommended.

5. The tensile resistance of the intersitial bitumen is nominally less than 2 kPa at 20°C. Greater tensile resistance could be drived from the viscosity of the bitumen at lower temperatures. This would enhance the stability and standup time of shafts and tunnels during excavation. For example, blind drilling of shafts with chilled brine solutions may reduce deformations of the unsupported shaft prior to installation of the shaft liner. Investigation of the tensile resistance of bitumen at lower temperatures is recommended for further research.

# REFERENCES

Agar, J.G. 1984. **Geotechnical Behavior of Oil Sands at Elevated Temperatures and Pressures.** Ph.D. Thesis, University of Alberta, 906 p.

Arthur, J.R.F., Dunston, T., Al-Ani, Q.A.J.L. and Assadi, A. 1977. Plastic Deformation and Failure in Granular Media. Geotechnique, Vol. 27, No. 1, pp. 53-74.

Au, K.S. 1984. **The Strength-Deformation Properties of Alberta Oil Sand.** M.Eng. Report, University of Alberta, 135 p.

Barden, L. and Khayatt, A.J. 1966. Incremental Strain Rate Ratios and Strength in the Triaxial Test. Geotechnique, Vol. 16, No. 4, pp. 338-357.

Barden, L. and Proctor, D.C. 1971. The Drained Strength of Granular Materials. Canadian Geotechnical Journal, Vol. 8, pp. 372-383.

Barnes, D.J. 1980. **Micro-Fabric and Strength Studies of Oil Sands.** M.Sc. Thesis, University of Alberta, 244 p.

Bishop, A.W. 1964. Correspondence on Shear Characteristics of a Saturated Silt Measured in Triaxial Compression. Geotechnique, Vol. 4, No. 1, pp. 43-45.

Bishop, A.W. 1966. Soils and Soft Rocks as Engineering Materials. Inaugaral Lecture, Imperial College of Science and Technology, 6, pp. 289-313.

Bishop, A.W. 1973. The Influence of an Undrained Change in Stress on the Pore Pressure in Porous Media of Low Compressibility. Geotechnique, Vol. 23, No. 3, pp. 435-442.

Bishop, A.W. and Eldin, A.K.G. 1950. Undrained Triaxial Tests on Saturated Sands and Their Significance in the General Theory of Shear Strength. Geotechnique, Vol. 1, No. 2, pp. 13-32.

Bishop, A.W. and Eldin, A.K.G. 1953. The Effects of Stress History on the Relation Between $\phi$ and Porosity of Sand. Proc. 3rd Int. Conf. Soil Mech. and Found. Eng., Vol. 1, pp. 100-105.

Bishop, A.W. and Henkel, D.J. 1962. **The Measurement of Soil Properties in the Triaxial Test.** Second Edition, Edward Arnold (Publishers) Ltd., London, U.K., 227 p.

Bishop, A.W. and Gibson, R.E. 1963. The Influence of the Provisions for Boundary Drainage on Strength and Consolidation Characteristics of Soils Measured in Triaxial Apparatus. Proc. Symp. on Laboratory Shear Testing of Soils, Ottawa, Ontario, ASTM SPT No. 361, pp. 435-451.

Bishop, A.W. and Green, G.E. 1965. The Influence of End Restraint on the Compression Strength of a Cohesionless Soil. Geotechnique, Vol. 15, No. 3, pp. 243-266.

Bishop, A.W., Webb, D.L. and Skinner, A.E. 1965. Triaxial Tests on Soil at Elevated Cell Pressures. Proc. 6th Int. Conf. Soil Mech. and Found. Eng., Vol. 1, pp. 170-174.

Bishop, A.W. and Garga, V.K. 1969. Drained Tension Tests on London Clay. Geotechnique, Vol. 19, No. 3, pp. 309-313.

Bishop, A.W. and Wesley, L.D. 1975. A Hydraulic Triaxial Apparatus for Controlled Stress Path Testing. Geotechnique, Vol. 25, No. 4, pp. 657-670.

Bjerrum, L., Kringstad, S. and Kummenje, O. 1961. The Shear Strength of a Fine Sand. Proc. 5th Int. Conf. Soil Mech. and Found. Eng., Vol. 1, pp. 29-37.

Black, D.K. and Lee, K.C. 1973. Saturating Laboratory Samples By Back Pressure. ASCE JSMFD, SM 1, Vol. 99, pp. 75-93.

Brooker, E.W. 1975. Tarsands Mechanics and Slope Evaluation. 10th Canadian Rock Mechanics Symposium, Kingston, Ontario, Sept. 1975, Vol. 1, pp. 409-446.

Casagrande, A. 1936. Characteristics of Cohesionless Soils Affecting the Stability of Slopes and Earth Fills. Contributions to Soil Mechanics 1925-1940, Boston Society of Civil Engineers, pp. 257-276.

Casagrande, A. and Shannon, W.L. 1948. Stress-Deformation and Strength Characteristics of Soils Under Dynamic Loads. Proc. 2nd Int. Conf. Soil Mech. and Found. Eng., Vol. 5, pp. 29-34.

Casagrande, A. and Shannon, W.L. 1949. Strength of Soils Under Dynamic Loads. Trans. ASCE, Vol. 114, pp. 755-773.

Coates, D.F. 1981. **Rock Mechanics Principles.** Publ. by Canadian Centre for Mineral and Energy Technology, Energy, Mines and Resources Canada, Monograph 874.

Cornforth, D.H. 1964. Some Experiments on the Influence of Strain Conditions on the Strength of Sand. Geotechnique, Vol. 14, No. 2, pp. 143-167.

Dusseault, M.B. 1977. **The Geotechnical Characteristics of Athabasca Oil Sands.** Ph.D. Thesis, University of Alberta, 1977.

Dusseault, M.B. 1983. Personal Communication of Unpublished Triaxial Test Results on Lean Oil Sand.

Dusseault, M.B. and Morgenstern, N.R. 1978a. Characteristics of Natural Slopes in the Athabasca Oil Sands. Canadian Geotechnical Journal, Vol. 15, pp. 202-215.

Dusseault, M.B. and Morgenstern, N.R. 1978b. Shear Strength of Athabasca Oil Sands. Canadian Geotechnical Journal, Vol. 15, pp. 216-238.

Dusseault, M.B. and Morgenstern, N.R. 1979. Locked Sands. Quarterly Jour. Eng. Geol., Vol. 12, pp. 117-131.

Dusseault, M.B. and Van Domselaar, H.R. 1982. Unconsolidated Sand Sampling in Canadian and Venezualian Oil Sand. Second Unitar Conference on the Future of Heavy Crudes and Tar Sands, Caracas, Venezuela.

Frossard, A. 1979. Effect of Sand Grain Shape on Interparticle Friction; Indirect Measurements by Rowe's Stress Dilatancy Theory. Geotechnique, Vol. 29, No. 3, pp. 341-350.

Gibson, R.E and Henkel, D.J. 1954. Influence of Duration of Tests at Constant Rate of Strain on Measured 'Drained' Strength. Geotechnique, Vol. 4, No. 1,pp. 6-15.

Hardy, R.M. and Hemstock, R.A. 1963. Shearing Strength Characteristics of Athabasca Oil Sands. In the K.A. Clark Volume on the Athabasca Oil Sands, Edited by M.A. Carrigy, Research Council of Alberta, Information Series No. 45, pp. 109-122.

Healy, K.A. 1963. The Dependence of Dilation in Sand on Rate of Shear Strain. MIT Report No. 13 to Office of the Chief Engineers, U.S. Dept. of the Army, Washington, D.C.

Henkel, D.J. and Gilbert, G.D. 1962. The Effect of the Rubber Membranes on the Measured Triaxial Compression Strength of Clay Samples. Geotechnique, Vol. 12, No. 3, pp. 20-29.

Horne, M.R. 1965. The Behavior of an Assembly of Rotund, Rigid Cohesionless Particles, Parts I and II. Proc.

Roy. Soc. Series A, Vol. 286, pp. 62-97.

Kirkpatrick, W.M. 1965. Effects of Grain Size and Grading on the Shearing Behavior of Granular Materials. Proc. 6th Int. Conf. Soil Mech. and Found. Eng., Vol. 1, pp. 273-277.

Kosar, K.M. 1983. **The Effect of Heated Foundations on Oil Sand.** M.Sc. Thesis, University of Alberta, 248 p.

Ladanyi, B. and Archambault, G. 1969. Simulation of Shear Behavior of a Jointed Rock Mass, 11th Symp. on Rock Mech., ASCE, Berkeley, Calif., pp. 105-125.

Lade, P.V. and Duncan, J.M. 1973. Cubical Triaxial Tests on Cohesionless Soil. ASCE JSMFD, SM 10, Vol. 99, pp. 793-811.

Lee, K.L. 1970. Comparison of Plane Strain and Triaxial Tests on Sand. ASCE JSMFD, SM 3, Vol. 96, pp. 901-923.

Lee, K.L. and Seed, H.B. 1967a. Drained Strength Characteristics of Cohesionless Soils. ASCE JSMFD, SM 6, Vol. 93, pp. 117-141.

Lee, K.L. and Seed, H.B. 1967b. Undrained Strength Characteristics of Cohesionless Soils. ASCE JSMFD, SM 6, Vol. 93, pp. 333-360.

Lee, K.L., Seed, H.B. and Dunlop, p. 1969. Effect of Transient Loading on the Strength of Sand. Proc. 7th Int. Conf. Soil Mech. and Found. Eng., Vol. 1, pp. 239-247.

McRoberts, E.C. 1986. Personal Communication of Unpublished Direct and Brazilian Tension Tests on Oil Sand.

Milligan, M.F. 1976. **Model Studies for a Friable Sandstone.** M.Sc. Thesis, University of Alberta, 146 p.

Mossop, G.D. 1978. Geological Controls on Reservoir Heterogeneity in Athabasca Oil Sands. In AOSTRA Seminar on Underground Excavation in Oil Sands, University of Alberta, Edmonton, Alberta, Paper No. 1, 27 p.

Mossop, G.D. 1980. Geology of the Athabasca Oil Sands. Science, Vol. 207, No. 11, January 1980, pp. 145-152.

Nash, K.L. and Dixon, R.K. 1961. The Measurement of Pore Pressure in Sand Under Rapid Triaxial Tests. Proc. Conf. on the Pressure and Suction in Soils, Butterworth, pp. 21-25.

Outrim, C.P. and Evans, R.G. 1978. Alberta's Oil Sands

Reserves and Their Evaluation. In Oil Sands of Canada-Venezuela, The Canadian Institute of Mining and Metallurgy Special Volume 17, pp. 36-66.

Peacock, D. 1986. Personal Communication of M.Sc. Thesis in Progress.

Rowe, P.W. 1962. The Stress Dilatancy Relation for Static Equilibrium of an Assembly of Particles in Contact. Roy. Soc. Series A, Vol. 269, pp. 500-527.

Rowe, P.W. 1969. The Relation Between the Shear Strength of Sands in Triaxial Compression, Plane Strain and Direct Shear. Geotechnique, Vol. 19, No. 1, pp. 75-86.

Rowe, P.W., Barden, L. and Lee, I.K. 1964. Energy Components During the Triaxial Cell and Direct Shear Tests. Geotechnique, Vol. 14, No. 3, pp. 247-261.

Reades, D.W. and Green, G.E. 1976. Independant Stress Control and Triaxial Extension Tests on Sand. Geotechnique, Vol. 26, No. 4, pp. 551-576.

Seed, H.B. and Lungren, R. 1954. Investigation of the Effect of Transient Loading on the Strength and Deformation Characteristics of Saturated Sands. Proc. ASTM, Vol. 54, pp. 1288-1306.

Seto, A.C.K 1985. **Thermal Testing of Oil Sand.** M.Sc. Thesis, University of Alberta, 320 p.

Skempton, A.W. 1954. The Pore Pressure Parameters A and B. Geotechnique, Vol. 4, No. 4, pp. 143-147.

Smith, L.B., Chatterji, P.K. Insley, A.E. and Sharma, L. 1978. Construction of Saline Creek Tunnel in Athabasca Oil Sand. In AOSTRA Seminar on Underground Excavation in Oil Sand, University of Alberta, Edmonton, Alberta, Paper No. 7, 58 p.

Sowers, G.B. and Sowers, B.F. 1951. **Introductory Soil Mechanics and Foundations.** MacMillan, New York.

Sutherland, H.B. and Mesdary, M.S. 1969. The Influence of the Intermediate Principal Stress on the Strength of Sand. Proc. 7th Int. Conf. Soil Mech. and Found. Eng., Vol. 1, pp. 391-399.

Taylor, D.W. 1948. **Fundamentals of Soil Mechanics.** J. Wiley, New York.

Triaxial Test Series 75S. Personal Communication of Unpublished Triaxial Test Results From Dr. J.D. Scott, Department of Civil Engineering, University of Alberta, Edmonton, Alberta.

Triaxial Test Series 78S. Personal Communication of Unpublished Triaxial Test Results From Dr. J.D. Scott, Department of Civil Engineering, University of Alberta, Edmonton, Alberta.

Triaxial Test Series 84S. Personal Communication of Unpublished Triaxial Test Results From Dr. J.D. Scott, Department of Civil Engineering, University of Alberta, Edmonton, Alberta.

Whitman, R.V. 1957. The Behavior of Soils Under Transient Loading. Proc. 4th Int. Conf. Soil Mech. and Found. Eng., Vol. 1, pp. 207-210.

Whitman, R.V. and Healy, K.A. 1962. Shear Strength of Sands During Rapid Loadings. ASCE JSMFD, SM 2, Vol. 88, pp. 99-132.

Vesic, A.S. and Barksdale, R.D. 1963. On Shear Strength of Sand at Very High Pressures. Proc. Symp. on Laboratory Shear Testing of Soils, Ottawa, Ontario, ASTM SPT No. 361, pp. 301-305.

Vesic, A.S. and Clough, G.W. 1968. Behavior of Granular Materials Under High Stresses. ASCE JSMFD, SM 3, Vol. 94, pp. 661-688.

# APPENDIX A - Compliance and Calibrations of Triaxial Test Apparatus

Table A.1 Calibration of Electronic Measuring Devices in High Pressure Triaxial Testing Facility

| ELECTRONIC MEASURING DEVICE | CALIBRATION | PRECISION |
|---|---|---|
| 1. 90 KN Strain Gauge Load Cell | 3.638 KN/mv | ± 0.07 KN(1) |
| - Amplified Signal | 8.40 KN/V | ± 0.10 KN(2) |
| 2. 14 MPa Strain Gauge Cell Pressure Transducer | 461 kPa/mv | ± 46 kPa(1) |
| 3. 14 MPa Strain Gauge Pore Pressure Transducer | 138 kPa/mv | ± 14 kPa(1) |
| - Amplified Signal | 1496 kPa/v | ± 40 kPa(2) |
| 4. Linear Voltage Displacement Transducer | 0.790 mm/V | ± 0.02 mm(1) |
| - Amplified Signal | 1.185 mm/V | ± 0.03 mm(2) |
| 5. Pore Fluid Volume Change Indicator | N/A | ± 0.0025 cc. |

1. Recorded by Servigor 460 Chart Recorder
2. Recorded by SE Labs SE6150 Oscillograph Chart Recorder

Table A.2 Measurement Of Piston Friction in High Pressure Triaxial Cell

| CELL PRESSURE (MPa) | RAM SPEED (mm/s) | PISTON FRICTION (N) |
|---|---|---|
| 12.5 | 0.10 | 231 |
| 12.5 | 0.51 | 295 |
| 12.5 | 5.08 | 300 |

Table A.3 Response of Pore Pressure Transducer Under Maximum Rate of Deformation

| CELL PRESSURE (MPa) | RAM SPEED (mm/s) | TIME INTERVAL (s) | CHANGE IN CELL PRESSURE, Δu (MPa) | | CALCULATED INERTIA FORCE OF PISTON RAM (N) |
|---|---|---|---|---|---|
| | | | LOAD CELL (MPa) | PORE PRESSURE TRANSDUCER (MPa) | |
| 4.9 | 50 | 0.135 | 1.78 | 1.65 | 68 |
| 6.7 | 50 | 0.130 | 1.62 | 1.50 | 60 |
| 10.1 | 50 | 0.140 | 1.99 | 1.86 | 69 |
| 12.1 | 50 | 0.120 | 1.62 | 1.53 | 49 |

Table A.4 Calibration of Electronic Measuring Devices in Low Pressure Triaxial Testing Facility

| ELECTRONIC MEASURING DEVICE | CALIBRATION | PRECISION[1] |
|---|---|---|
| 1. Internal Strain Gauge Load Cell | | |
| - Compression | 3.88 Kg/mv | ± 0.01 Kg |
| - Tension | 4.10 Kg/mv | ± 0.01 Kg |
| 2. 1.7 MPa Strain Gauge Cell Pressure Transducer | 21.24 kPa/mv | ± 0.02 kPa |
| 3. 2.1 MPa Strain Gauge Pore Pressure Transducer | 70.00 kPa/mv | ± 0.07 kPa |
| 4. Linear Voltage Displacement Transducers | 1.28 mm/V | ± 0.01 mm |
| | 1.43 mm/V | ± 0.01 mm |

1. Recorded by Fluke 2240B Datalogger

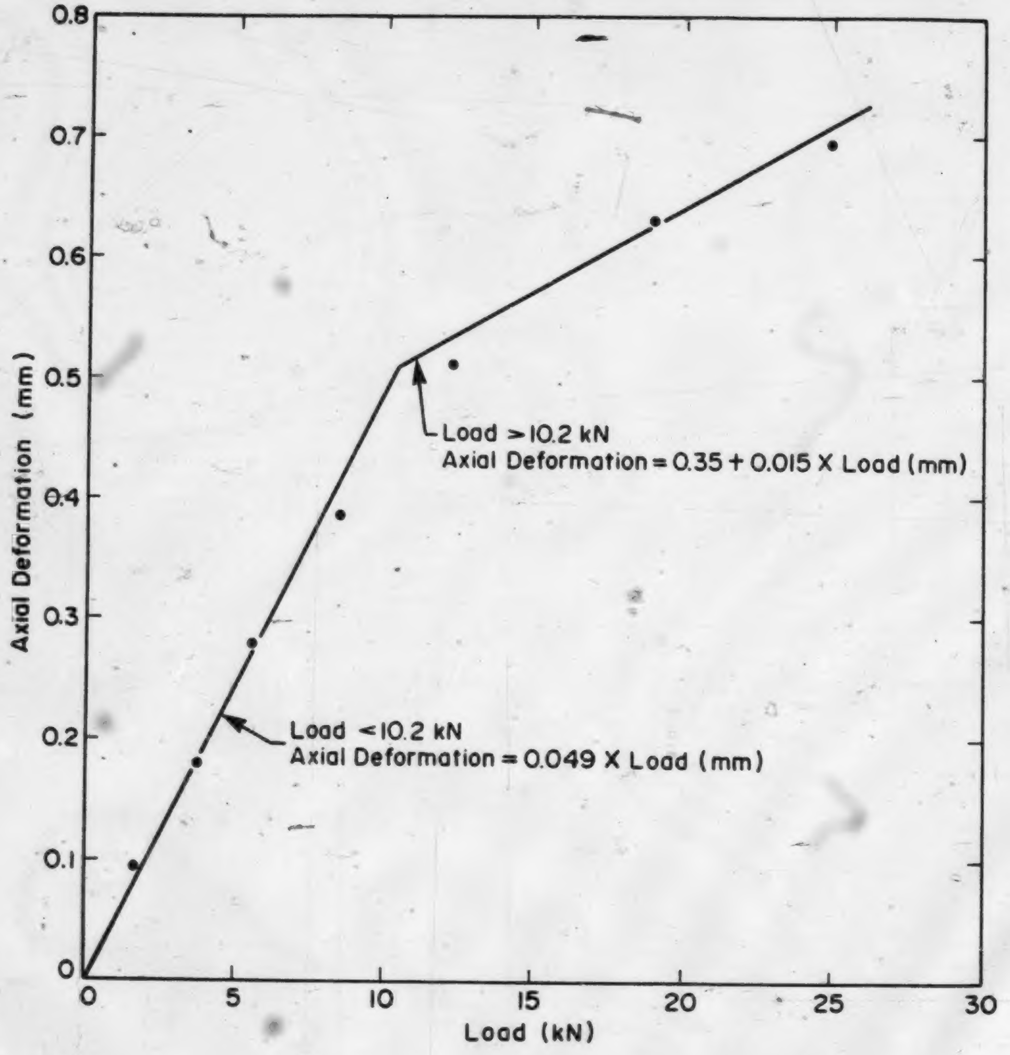

Figure A.1 Axial Compliance of Frictionless Platens (Steel Insert Sample Not Cyclically Compressed)

# APPENDIX B - Ottawa Sand Triaxial Test Results

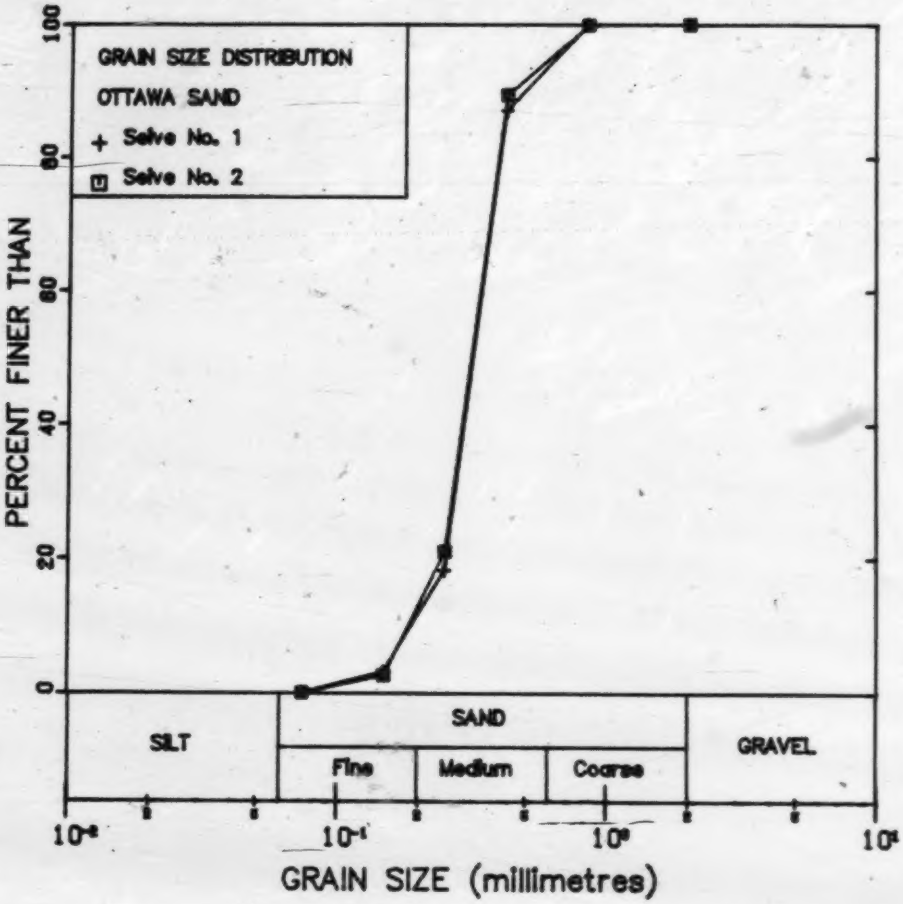

Figure B.1 Grain Size Distribution of Ottawa Sand

## TEST OS-S1: OTTAWA SAND

### PROCEDURAL DETAILS

1. Conventional 38.10 mm diameter loading platens were used.
2. The sample was saturated under back and confining pressures of 4.6 MPa and 6.6 MPa for 1.0 hours.
3. An undrained triaxial compression test was conducted at a strain rate of $6.42 \times 10^{-3}\ s^{-1}$.

### TEST DATA

DIAMETER = 37.96 mm BULK DENSITY = 2.061 Mg/$m^3$
HEIGHT = 19.58 mm
WEIGHT = 45.70 g.

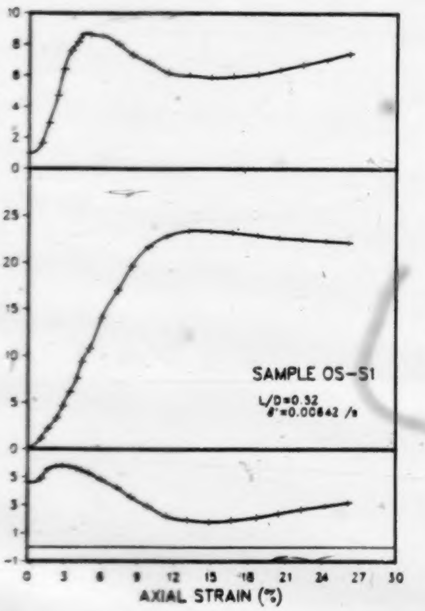

FIGURE B.2 OS-S1: Triaxial Test Results

# TEST OS-S2: OTTAWA SAND

## PROCEDURAL DETAILS

1. Conventional 38.10 mm diameter loading platens were used.
2. The sample was saturated under back and confining pressures of 4.6 MPa and 6.6 MPa for 1.0 hours.
3. An undrained triaxial compression test was conducted at a strain rate of $7.69 \times 10^{-3}$ $s^{-1}$.

## TEST DATA

DIAMETER = 38.13 mm   BULK DENSITY = 2.065 Mg/$m^3$
HEIGHT = 56.93 mm
WEIGHT = 133.70 g.

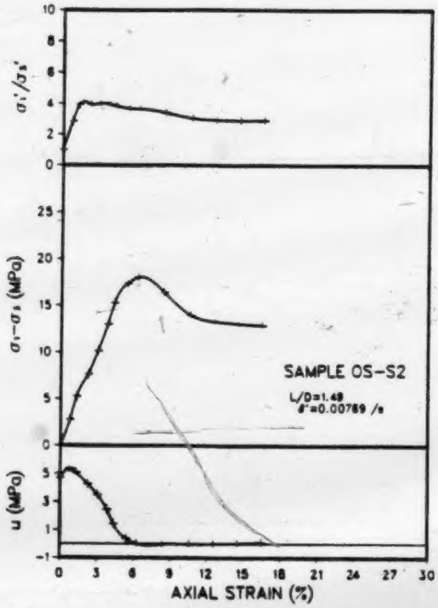

FIGURE B.3 OS-S2: Triaxial Test Results

# TEST OS-S3: OTTAWA SAND

## PROCEDURAL DETAILS

1. Conventional 38.10 mm diameter loading platens were used.
2. The sample was saturated under back and confining pressures of 4.6 MPa and 6.6 MPa for 1.0 hours.
3. An undrained triaxial compression test was conducted at a strain rate of $8.49 \times 10^{-3}$ $s^{-1}$.

## TEST DATA

DIAMETER = 38.07 mm     BULK DENSITY = 2.059 Mg/$m^3$
HEIGHT = 77.23 mm
WEIGHT = 181.00 g.

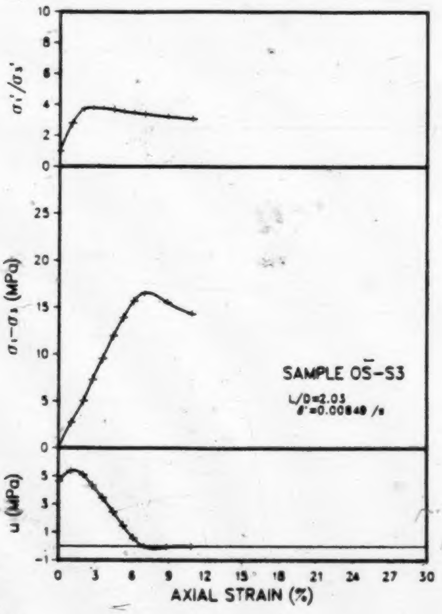

FIGURE B.4 OS-S3: Triaxial Test Results

## TEST OS-S4: OTTAWA SAND

### PROCEDURAL DETAILS

1. Conventional 38.10 mm diameter loading platens were used.
2. The sample was saturated under back and confining pressures of 4.6 MPa and 6.6 MPa for 1.0 hours.
3. An undrained triaxial compression test was conducted at a strain rate of $8.09 \times 10^{-3}$ $s^{-1}$.

### TEST DATA

DIAMETER = 38.10 mm
HEIGHT = 38.57 mm
WEIGHT = 90.00 g.

BULK DENSITY = 2.047 $Mg/m^3$

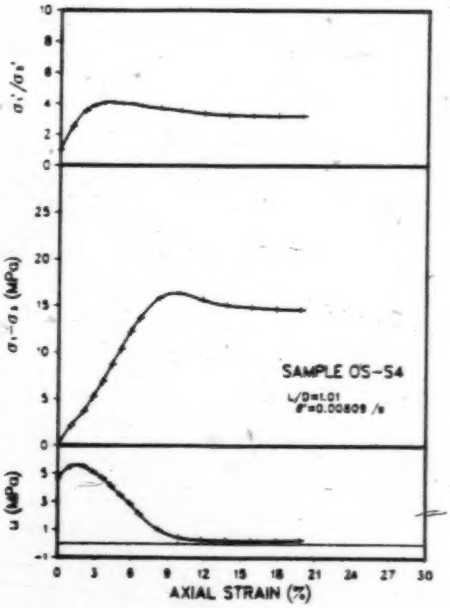

FIGURE B.5 OS-S4: Triaxial Test Results

## TEST OS-1A: OTTAWA SAND

### PROCEDURAL DETAILS

1. Conventional 38.10 mm diameter loading platens were used.
2. The sample was saturated under back and confining pressures of 4.6 MPa and 6.6 MPa for 1.5 hours.
3. An undrained triaxial compression test was conducted at a strain rate of $9.00 \times 10^{-3}\ s^{-1}$.

### TEST DATA

DIAMETER = 38.12 mm
HEIGHT = 20.75 mm
WEIGHT = 47.30 g.

BULK DENSITY = 2.000 $Mg/m^3$
WATER CONTENT = 21.10 %
VOID RATIO = 0.605
POROSITY = 0.377

Comments on sample failure:

Sample failed by bulging through the middle and radial expansion over the edges of the loading platens.

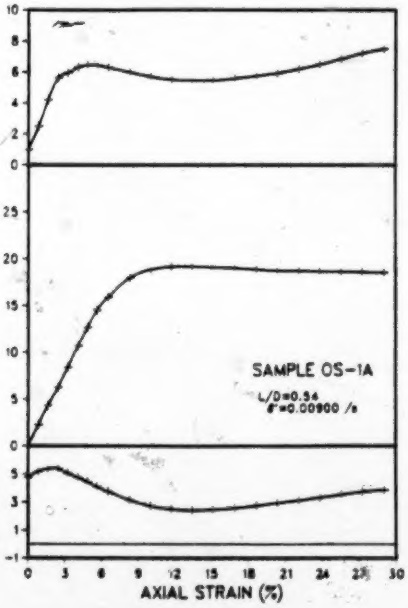

FIGURE B.6 OS-1A: Triaxial Test Results

## TEST OS-1B: OTTAWA SAND

### PROCEDURAL DETAILS

1. Conventional 38.10 mm diameter loading platens were used.
2. The sample was saturated under back and confining pressures of 4.6 MPa and 6.6 MPa for 1.5 hours.
3. An undrained triaxial compression test was conducted at a strain rate of $8.88 \times 10^{-3}\ s^{-1}$.

### TEST DATA

DIAMETER = 38.15 mm
HEIGHT = 38.60 mm
WEIGHT = 90.70 g.

BULK DENSITY = 2.056 $Mg/m^3$
WATER CONTENT = 16.93 %
VOID RATIO = 0.507
POROSITY = 0.336

### Comments on sample failure:

Sample failed by bulging through the middle and radial expansion over the edges of the loading platens.

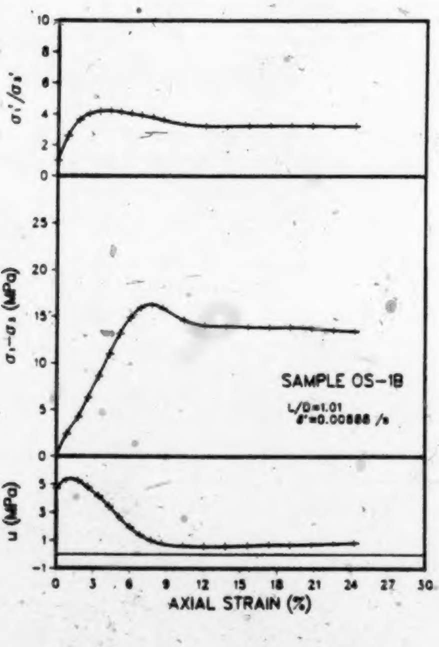

FIGURE B.7 OS-1B: Triaxial Test Results

## TEST OS-2A: OTTAWA SAND

### PROCEDURAL DETAILS

1. Conventional 38.10 mm diameter loading platens were used.
2. The sample was saturated under back and confining pressures of 4.6 MPa and 6.6 MPa for 1.0 hours.
3. An undrained triaxial compression test was conducted at a strain rate of $8.30 \times 10^{-3}$ $s^{-1}$.

### TEST DATA

DIAMETER = 38.10 mm
HEIGHT = 19.37 mm
WEIGHT = 44.10 g.

BULK DENSITY = 2.000 Mg/m$^3$
WATER CONTENT = 16.49 %
VOID RATIO = 0.543
POROSITY = 0.352

Comments on sample failure:

Sample failed by bulging through the middle and radial expansion over the edges of the loading platens.

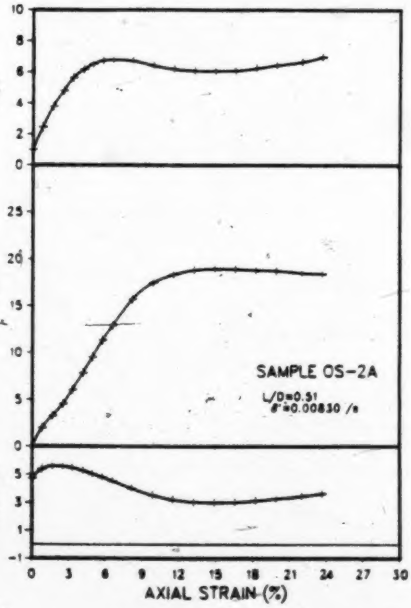

FIGURE B.8 OS-2A: Triaxial Test Results

## TEST OS-3B: OTTAWA SAND

### PROCEDURAL DETAILS

1. Enlarged 43.20 mm diameter loading platens were used. The faces of the platens were overlaid with two layers of greased rubber membranes.
2. The sample was saturated under back and confining pressures of 4.6 MPa and 6.6 MPa for 1.5 hours.
3. An undrained triaxial compression test was conducted at a strain rate of $8.83 \times 10^{-3}$ $s^{-1}$.

### TEST DATA

DIAMETER = 38.13 mm
HEIGHT = 19.08 mm
WEIGHT = 43.70 g.

BULK DENSITY = 2.006 $Mg/m^3$
WATER CONTENT = 18.75 %
VOID RATIO = 0.569
POROSITY = 0.363

Comments on sample failure:

Radial expansion occured uniformly throughout the height of the sample.

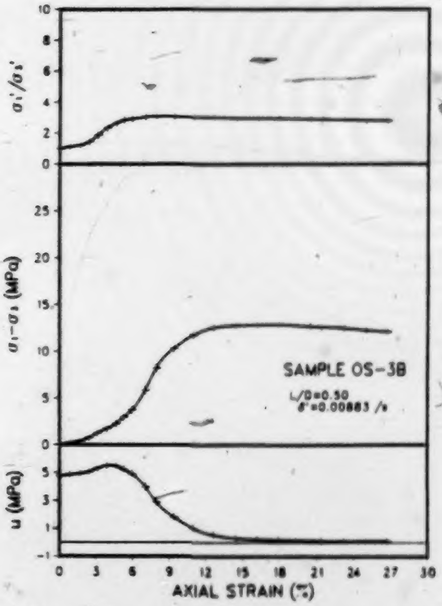

FIGURE B.9 OS-3B: Triaxial Test Results

# TEST OS-4: OTTAWA SAND

## PROCEDURAL DETAILS

1. Enlarged 43.20 mm diameter loading platens were used. The faces of the platens were overlaid with two layers of greased rubber membranes.
2. The sample was saturated under back and confining pressures of 4.6 MPa and 6.6 MPa for 1.0 hours. The pore pressure parameter B was then measured.
3. An undrained triaxial compression test was conducted at a strain rate of $8.90 \times 10^{-3}$ $s^{-1}$.

## TEST DATA

DIAMETER = 38.17 mm
HEIGHT = 38.37 mm
WEIGHT = 89.40 g.

BULK DENSITY = 2.036 Mg/m$^3$
WATER CONTENT = 17.86 %
VOID RATIO = 0.534
POROSITY = 0.348

PORE PRESSURE PARAMETER B = 0.91

Comments on sample failure:

Sample expanded radially at the base to the full width of the enlarged platen. Sample only partially expanded at the top platen.

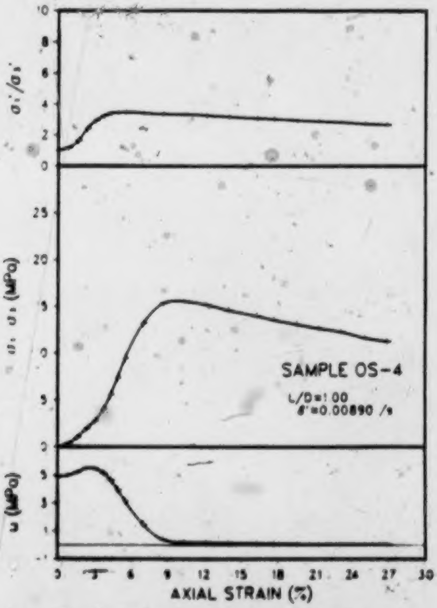

FIGURE B.10 OS-4: Triaxial Test Results

## TEST OS-5: OTTAWA SAND

### PROCEDURAL DETAILS

1. Enlarged 43.20 mm diameter loading platens were used. The faces of the platens were overlaid with two layers of greased rubber membranes.
2. The sample was saturated under back and confining pressures of 4.6 MPa and 6.6 MPa for 1.25 hours. The pore pressure parameter B was then measured.
3. An undrained triaxial compression test was conducted at a strain rate of $8.83 \times 10^{-3}$ $s^{-1}$.

### TEST DATA

DIAMETER = 38.20 mm
HEIGHT = 38.25 mm
WEIGHT = 89.40 g.

BULK DENSITY = 2.039 $Mg/m^3$
WATER CONTENT = 20.93 %
VOID RATIO = 0.572
POROSITY = 0.364

PORE PRESSURE PARAMETER B = 0.88

Comments on sample failure:

Sample expanded fully to the edges of the enlarged platens. Expansion was uniform throughout the height of the sample.

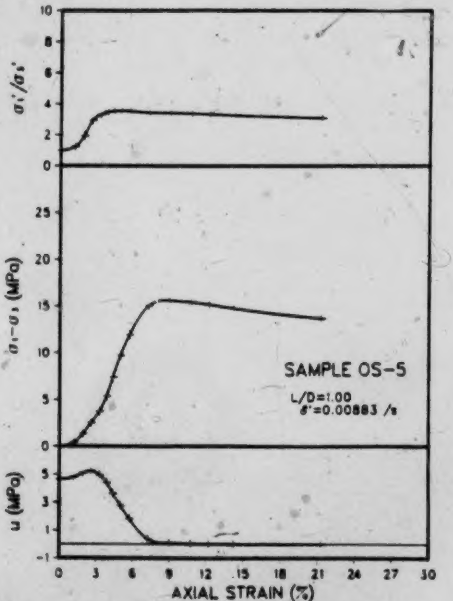

FIGURE B.11 OS-5: Triaxial Test Results

## TEST OS-6A: OTTAWA SAND

### PROCEDURAL DETAILS

1. Enlarged 43.20 mm diameter loading platens were used. The faces of the platens were overlaid with two layers of greased rubber membranes.
2. The sample was saturated under back and confining pressures of 4.6 MPa and 6.6 MPa for 1.5 hours. The pore pressure parameter B was then measured.
3. An undrained triaxial compression test was conducted at a strain rate of $8.68 \times 10^{-3}$ $s^{-1}$.

### TEST DATA

DIAMETER = 38.18 mm BULK DENSITY = 2.039 $Mg/m^3$
HEIGHT = 20.27 mm
WEIGHT = 47.33 g. PORE PRESSURE PARAMETER B = 0.84

Comments on sample failure:

Sample expanded fully to the edges of the enlarged platens. Expansion was uniform throughout the height of the sample.

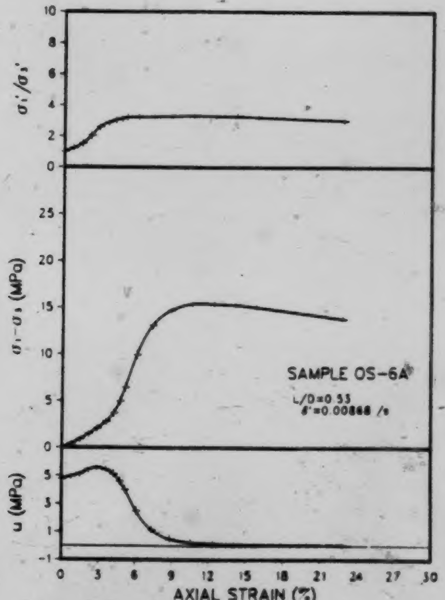

FIGURE B.12 OS-6A: Triaxial Test Results

## TEST OS-6B: OTTAWA SAND

### PROCEDURAL DETAILS

1. Enlarged 43.20 mm diameter loading platens were used. The faces of the platens were overlaid with two layers of greased rubber membranes.
2. The sample was saturated under back and confining pressures of 4.6 MPa and 6.6 MPa for 1.5 hours. The pore pressure parameter B was then measured.
3. An undrained compression test was conducted at a strain rate of $1.10 \times 10^{-4}$ $s^{-1}$.

### TEST DATA

DIAMETER = 38.10 mm
HEIGHT = 19.68 mm
WEIGHT = 44.73 g.

BULK DENSITY = 1.994 Mg/$m^3$
WATER CONTENT = 17.78 %
VOID RATIO = 0.565
POROSITY = 0.361

PORE PRESSURE PARAMETER B = 0.82

Comments on sample failure:

Sample expanded fully to the edges of the enlarged platens. Expansion was uniform throughout the height of the sample.

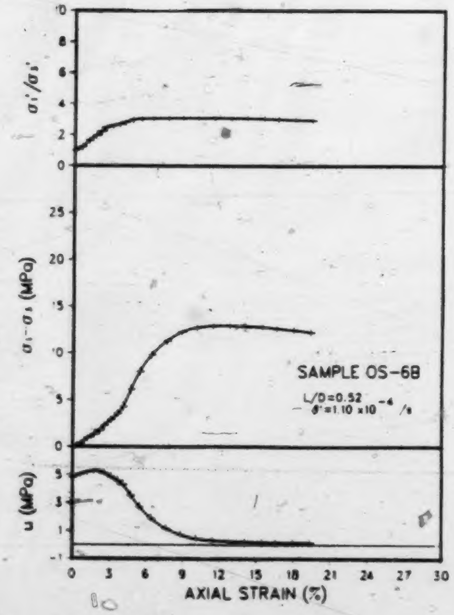

FIGURE B.13 OS-6B: Triaxial Test Results

## TEST OS-7A: OTTAWA SAND

### PROCEDURAL DETAILS

1. Enlarged 43.20 mm diameter loading platens were used. The faces of the platens were overlaid with two layers of greased rubber membranes.
2. The sample was saturated under back and confining pressures of 4.6 MPa and 6.6 MPa for 1.5 hours. The pore pressure parameter B was then measured.
3. An undrained triaxial compression test was conducted at a strain rate of 1.10 x $10^{-1}$ $s^{-1}$.

### TEST DATA

DIAMETER = 38.07 mm
HEIGHT = 19.32 mm
WEIGHT = 43.70 g.

BULK DENSITY = 1.998 $Mg/m^3$
WATER CONTENT = 19.88 %
VOID RATIO = 0.590
POROSITY = 0.371

PORE PRESSURE PARAMETER B = 0.79

Comments on sample failure:

Sample expanded fully to the edges of the enlarged platens. Expansion was uniform throughout the height of the sample.

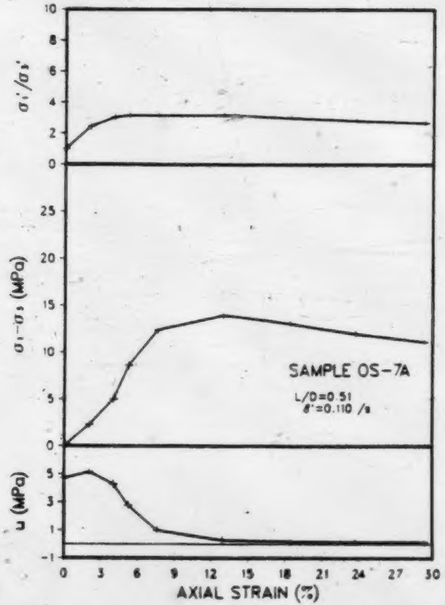

FIGURE B.14 OS-7A: Triaxial Test Results

## TEST OS-7B: OTTAWA SAND

### PROCEDURAL DETAILS

1. Enlarged 43.20 mm diameter loading platens were used. The faces of the platens were overlaid with two layers of greased rubber membranes.
2. The sample was saturated under back and confining pressures of 4.6 MPa and 6.6 MPa for 17 hours. The pore pressure parameter B was then measured.
3. An undrained triaxial compression test was conducted at a strain rate of $1.63 \times 10^{-5}$ $s^{-1}$.

### TEST DATA

DIAMETER = 38.05 mm BULK DENSITY = 2.014 $Mg/m^3$
HEIGHT = 17.28 mm WATER CONTENT = 19.88 %
WEIGHT = 39.58 g. VOID RATIO = 0.577
POROSITY = 0.366

PORE PRESSURE PARAMETER B = 0.84

Comments on sample failure:

Sample expanded fully to the edges of the enlarged platens. Expansion was uniform throughout the height of the sample.

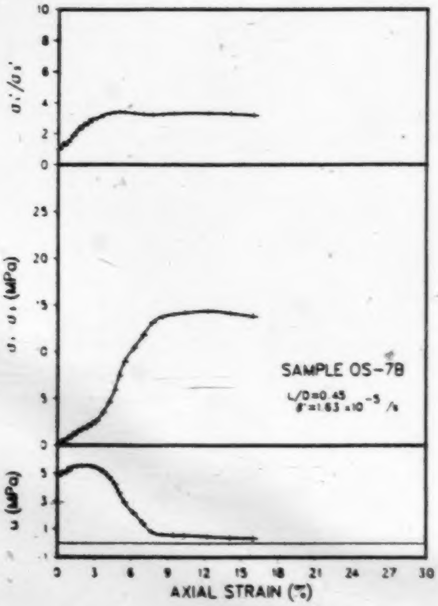

FIGURE B.15 OS-7B: Triaxial Test Results

## TEST OS-8A: OTTAWA SAND

### PROCEDURAL DETAILS

1. Enlarged 43.20 mm diameter loading platens were used. The faces of the platens were overlaid with two layers of greased rubber membranes.
2. The sample was saturated under back and confining pressures of 4.6 MPa and 6.6 MPa for 1.5 hours. The pore pressure parameter B was then measured.
3. An undrained triaxial compression test was conducted at a strain rate of $8.61 \times 10^{-3}$ $s^{-1}$.

### TEST DATA

DIAMETER = 38.03 mm BULK DENSITY = 2.004 $Mg/m^3$
HEIGHT = 19.28 mm WATER CONTENT = 18.07 %
WEIGHT = 43.91 g. VOID RATIO = 0.561
POROSITY = 0.360

PORE PRESSURE PARAMETER B = 0.86

Comments on sample failure:

Sample expanded fully to the edges of the enlarged platens. The sample slipped 1 mm to the side on the bottom platen.

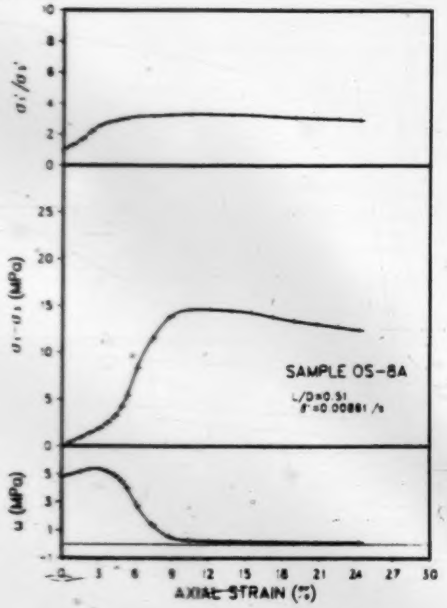

FIGURE B.16 OS-8A: Triaxial Test Results

## TEST OS-8B: OTTAWA SAND

### PROCEDURAL DETAILS

1. Enlarged 43.20 mm diameter loading platens were used.
2. The sample was saturated under back and confining pressures of 4.6 MPa and 6.6 MPa for 1.0 hours. The pore pressure parameter B was then measured.
3. An undrained triaxial compression test was conducted at a strain rate of $8.51 \times 10^{-3}$ $s^{-1}$.

### TEST DATA

DIAMETER = 38.10 mm BULK DENSITY = 2.014 Mg/m$^3$
HEIGHT = 19.30 mm WATER CONTENT = 18.07 %
WEIGHT = 44.31 g. VOID RATIO = 0.554
POROSITY = 0.356

PORE PRESSURE PARAMETER B = 0.74

Comments on sample failure:

Sample expanded fully to the edges of the enlarged platens. Slight bulging of the sample at mid-height.

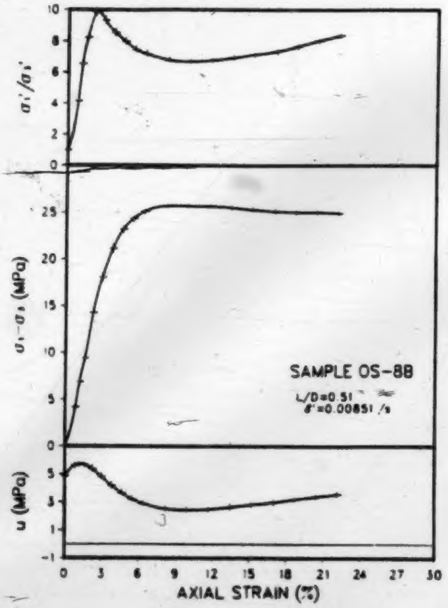

FIGURE B.17 OS-8B: Triaxial Test Results

## TEST OS-11: OTTAWA SAND

### PROCEDURAL DETAILS

1. Enlarged 43.20 mm diameter loading platens were used. The faces of the platens were overlaid with two layers of greased rubber membranes.
2. The sample was saturated under back and confining pressures of 9.9 MPa and 12.2 MPa for 1.0 hours. The pore pressure parameter B was then measured.
3. An undrained triaxial compression test was conducted at a strain rate of 2.40 $s^{-1}$.

### TEST DATA

DIAMETER = 37.76 mm    BULK DENSITY = 1.959 $Mg/m^3$
HEIGHT = 19.08 mm
WEIGHT = 41.84 g.    PORE PRESSURE PARAMETER B = 0.83

Comments on sample failure:

Sample expanded fully to the edges of the enlarged platens. Expansion was uniform throughout the height of the sample.

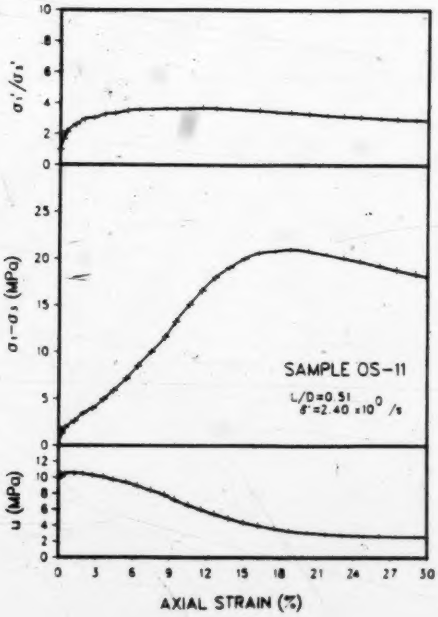

FIGURE B.18 OS-11: Triaxial Test Results

## TEST OS-12: OTTAWA SAND

### PROCEDURAL DETAILS

1. Enlarged 43.20 mm diameter loading platens were used.
2. The sample was saturated under back and confining pressures of 4.6 MPa and 6.6 MPa for 1.75 hours. The pore pressure parameter B was then measured.
3. An undrained triaxial compression test was conducted at a strain rate of $8.82 \times 10^{-3}\ s^{-1}$.

### TEST DATA

DIAMETER = 38.07 mm     BULK DENSITY = 2.058 $Mg/m^3$
HEIGHT = 72.13 mm
WEIGHT = 169.00 g.     PORE PRESSURE PARAMETER B = 0.90

Comments on sample failure:

Shear plane developed as shown in the sketch below. Sample bulged over the lower 2/3 of the sample height.

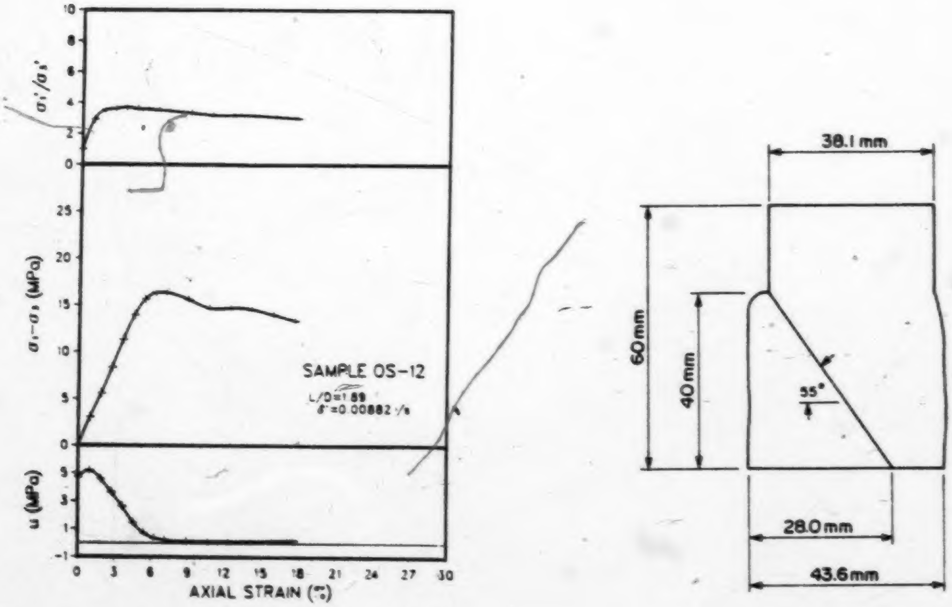

FIGURE B.19 OS-12: Triaxial Test Results

## TEST OS-13: OTTAWA SAND

### PROCEDURAL DETAILS

1. Enlarged 43.20 mm diameter loading platens were used. The faces of the platens were overlaid with two layers of greased rubber membranes.
2. The sample was saturated under back and confining pressures of 4.6 MPa and 6.6 MPa for 17 hours. The pore pressure parameter B was then measured.
3. An undrained triaxial compression test was conducted at a strain rate of $8.72 \times 10^{-3}$ $s^{-1}$.

### TEST DATA

DIAMETER = 38.18 mm BULK DENSITY = 2.045 Mg/$m^3$
HEIGHT = 73.98 mm
WEIGHT = 173.21 g. PORE PRESSURE PARAMETER B = 0.90

Comments on sample failure:

Bulging of sample confined to the middle of the sample. Radial expansion at the ends was minimal.

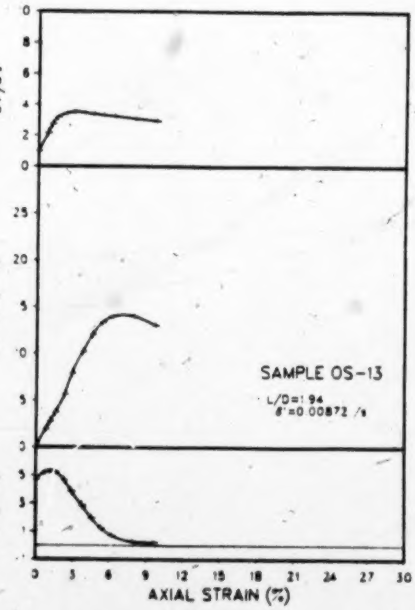

FIGURE B.20 OS-13: Triaxial Test Results

## TEST OS-14: OTTAWA SAND

### PROCEDURAL DETAILS

1. Enlarged 43.20 mm diameter loading platens were used.
2. The sample was saturated under back and confining pressures of 4.6 MPa and 6.6 MPa for 1.0 hours. The pore pressure parameter B was then measured.
3. An undrained triaxial compression test was conducted at a strain rate of $1.14 \times 10^{-4}$ $s^{-1}$.

### TEST DATA

DIAMETER = 38.07 mm    BULK DENSITY = 2.061 Mg/$m^3$
HEIGHT = 76.32 mm
WEIGHT = 179.06 g.    PORE PRESSURE PARAMETER B = 0.90

Comments on sample failure:

Shear plane developed as shown in the sketch below.

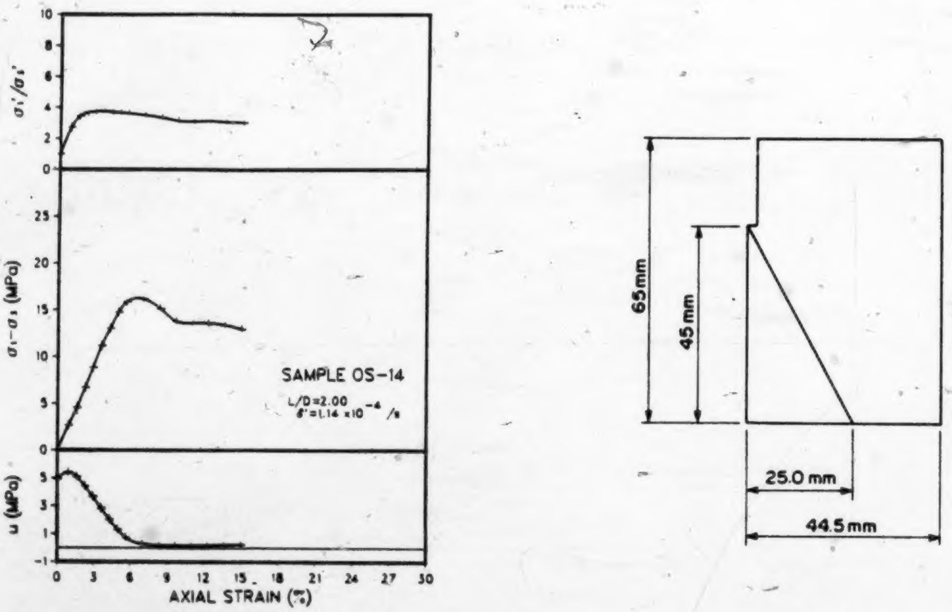

FIGURE B.21 OS-14: Triaxial Test Results

# TEST OS-15A: OTTAWA SAND

## PROCEDURAL DETAILS

1. Enlarged 43.20 mm diameter loading platens were used. The faces of the platens were overlaid with two layers of greased rubber membranes.
2. The sample was saturated under back and confining pressures of 4.6 MPa and 6.6 MPa for 1.25 hours. The pore pressure parameter B was then measured.
3. An undrained triaxial compression test was conducted at a strain rate of $1.10 \times 10^{-1}$ $s^{-1}$.

## TEST DATA

DIAMETER = 38.13 mm    BULK DENSITY = 2.022 $Mg/m^3$
HEIGHT = 19.72 mm
WEIGHT = 45.53 g.    PORE PRESSURE PARAMETER B = 0.84

Comments on sample failure:

Sample expanded fully to the edges of the enlarged platens. Expansion was uniform throughout the height of the sample.

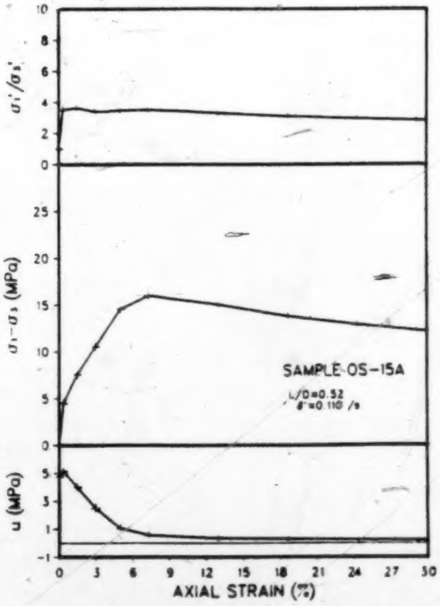

FIGURE B.22 OS-15A: Triaxial Test Results

## TEST OS-16A: OTTAWA SAND

### PROCEDURAL DETAILS

1. Enlarged 43.20 mm diameter loading platens were used. The faces of the platens were overlaid with two layers of greased rubber membranes.
2. The sample was saturated under back and confining pressures of 4.6 MPa and 6.6 MPa for 1.0 hours. The pore pressure parameter B was then measured.
3. An undrained triaxial compression test was conducted at a strain rate of $1.13 \times 10^{-4}$ $s^{-1}$.

### TEST DATA

DIAMETER = 38.18 mm  BULK DENSITY = 2.014 $Mg/m^3$
HEIGHT = 19.30 mm
WEIGHT = 44.54 g.  PORE PRESSURE PARAMETER B = 0.84

Comments on sample failure:

Sample expanded fully to the edges of the enlarged platens. Expansion was uniform throughout the height of the sample.

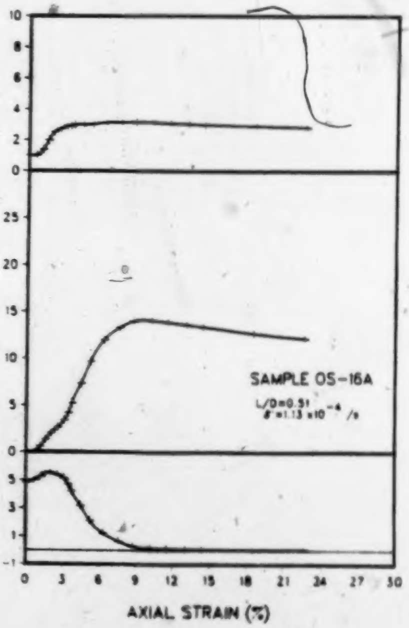

FIGURE B.23 OS-16A: Triaxial Test Results

## TEST OS-18A: OTTAWA SAND

### PROCEDURAL DETAILS

1. Enlarged 43.20 mm diameter loading platens were used. The faces of the platens were overlaid with two layers of greased rubber membranes.
2. The sample was saturated under back and confining pressures of 10.2 MPa and 12.3 MPa for 1.0 hours. The pore pressure parameter B was then measured.
3. An undrained triaxial compression test was conducted at a strain rate of $3.10\ s^{-1}$.

### TEST DATA

DIAMETER = 37.73 mm    BULK DENSITY = $1.936\ Mg/m^3$
HEIGHT = 19.93 mm
WEIGHT = 43.13 g.    PORE PRESSURE PARAMETER B = 0.82

Comments on sample failure:

Sample expanded fully to the edges of the enlarged platens. Expansion was uniform throughout the height of the sample.

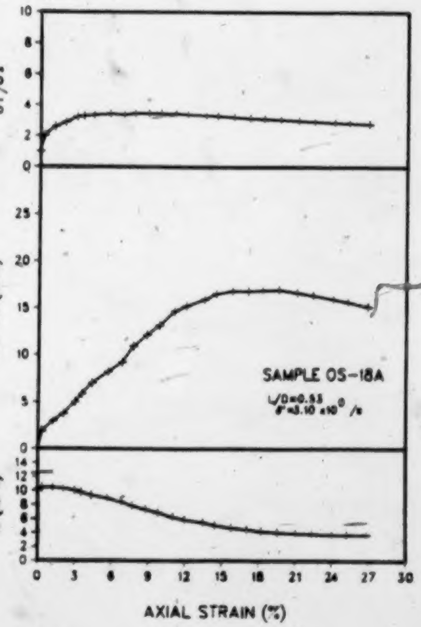

FIGURE B.24 OS-18A: Triaxial Test Results

## TEST OS-19A: OTTAWA SAND

### PROCEDURAL DETAILS

1. Enlarged 43.20 mm diameter loading platens were used.
2. The sample was saturated under back and confining pressures of 4.6 MPa and 6.6 MPa for 1.25 hours. The pore pressure parameter B was then measured.
3. An undrained triaxial compression test was conducted at a strain rate of 7.43 x $10^{-2}$ $s^{-1}$.

### TEST DATA

DIAMETER = 38.07 mm BULK DENSITY = 2.049 Mg/$m^3$
HEIGHT = 76.42 mm
WEIGHT = 178.25 g. PORE PRESSURE PARAMETER B = 0.89

Comments on sample failure:

Shear plane developed as shown in the sketch below.

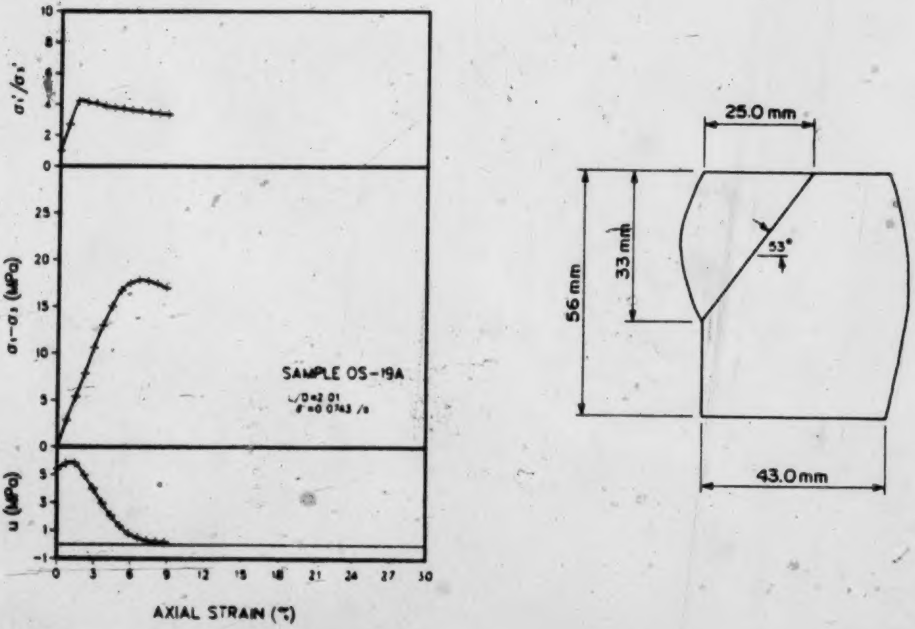

FIGURE B.25 OS-19A: Triaxial Test Results

## TEST OS-19B: OTTAWA SAND

### PROCEDURAL DETAILS

1. Enlarged 43.20 mm diameter loading platens were used. The faces of the platens were overlaid with two layers of greased rubber membranes.
2. The sample was saturated under back and confining pressures of 4.6 MPa and 6.6 MPa for 17 hours. The pore pressure parameter B was then measured.
3. An undrained triaxial compression test was conducted at a strain rate of 1.52 x $10^{-5}$ $s^{-1}$.

### TEST DATA

DIAMETER = 37.98 mm  BULK DENSITY = 2.021 Mg/$m^3$
HEIGHT = 19.30 mm
WEIGHT = 44.17 g.  PORE PRESSURE PARAMETER B = 0.79

Comments on sample failure:

Sample expanded fully to the edges of the enlarged platens. Expansion was uniform throughout the height of the sample.

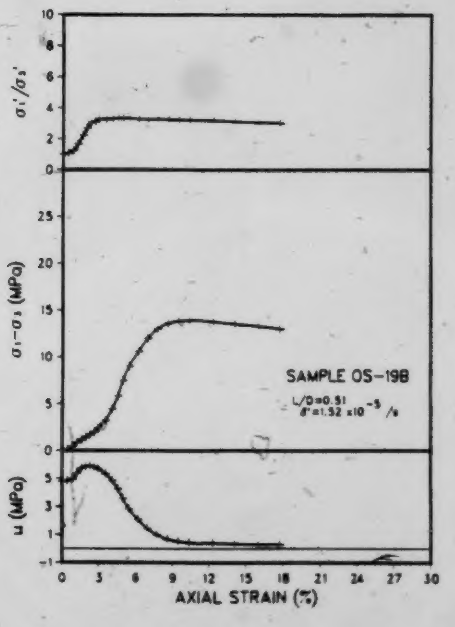

FIGURE B.26 OS-19B: Triaxial Test Results

## TEST OS-21: OTTAWA SAND

### PROCEDURAL DETAILS

1. Enlarged 43.20 mm diameter loading platens were used.
2. The sample was saturated under back and confining pressures of 4.6 MPa and 6.6 MPa for 1.0 hours. The pore pressure parameter B was then measured.
3. An undrained triaxial compression test was conducted at a strain rate of $1.59 \times 10^{-5}$ $s^{-1}$.

### TEST DATA

DIAMETER = 38.05 mm
HEIGHT = 71.57 mm
WEIGHT = 167.27 g.

BULK DENSITY = 2.055 $Mg/m^3$
PORE PRESSURE PARAMETER B = 0.90

Comments on sample failure:

Shear plane developed as shown in the sketch below.

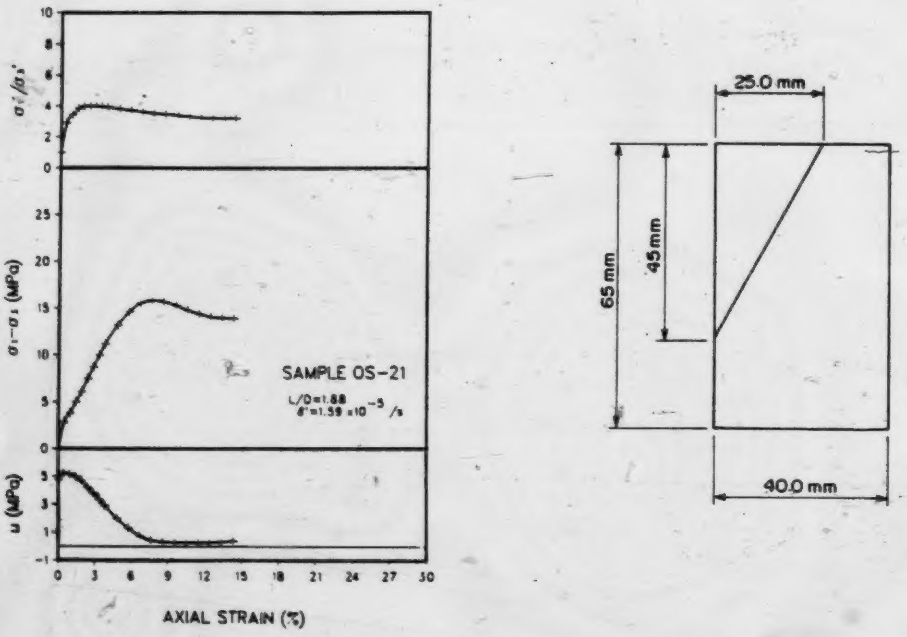

FIGURE B.27 OS-21: Triaxial Test Results

## TEST OS-22: OTTAWA SAND

### PROCEDURAL DETAILS

1. Enlarged 43.20 mm diameter loading platens were used.
2. The sample was saturated under back and confining pressures of 2.0 MPa and 4.0 MPa for 16.0 hours. The pressures were subsequently raised to 4.6 MPa and 6.6 MPa for a additional period of 3.0 hours. The pore pressure parameter B was then measured.
3. An undrained triaxial compression test was conducted at a strain rate of $1.10 \times 10^{-2}$ $s^{-1}$.

### TEST DATA

DIAMETER = 37.93 mm     BULK DENSITY = 2.018 $Mg/m^3$
HEIGHT = 19.30 mm
WEIGHT = 44.02 g.     PORE PRESSURE PARAMETER B = 0.81

Comments on sample failure:

Sample expanded fully to the edges of the enlarged platens. Expansion was uniform throughout the height of the sample.

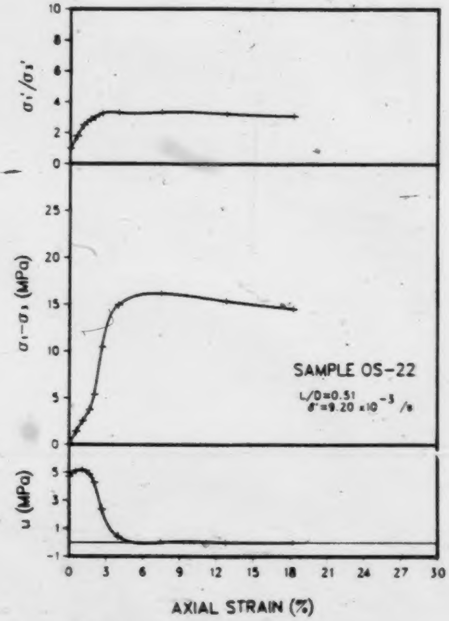

FIGURE B.28 OS-22: Triaxial Test Results

# APPENDIX C - Saline Creek Oil Sand Triaxial Test Results

## TEST SC-83-22D: SALINE CREEK OIL SAND

### PROCEDURAL DETAILS

1. Conventional 50.00 mm diameter loading platens were used.
2. The sample was thawed under cell and back pressures of 0.25 and 0.20 MPa for 12 hours.
3. B tests were conducted at an effective confining pressure of 0.14 MPa with incremental increases in pore pressure until saturation was reached.
4. An isotropic compressibility test was conducted with three cycles of effective confining stress up to 5 MPa. A constant pore pressure of 1.33 MPa was maintained throughout the test.
5. A second series of B tests were conducted at a confining pressure of 2.15 MPa following the cyclic compression of the sample.
6. Test data from the triaxial compression test has been lost.

### TEST DATA

DIAMETER = 50.86 mm
HEIGHT = 101.70 mm
WEIGHT = 411.0 g.
BULK DENSITY = 1.989 $Mg/m^3$
WATER CONTENT = 1.3 %
BITUMEN CONTENT = 13.4 %
SATURATION = 79.1 %
POROSITY = 0.360

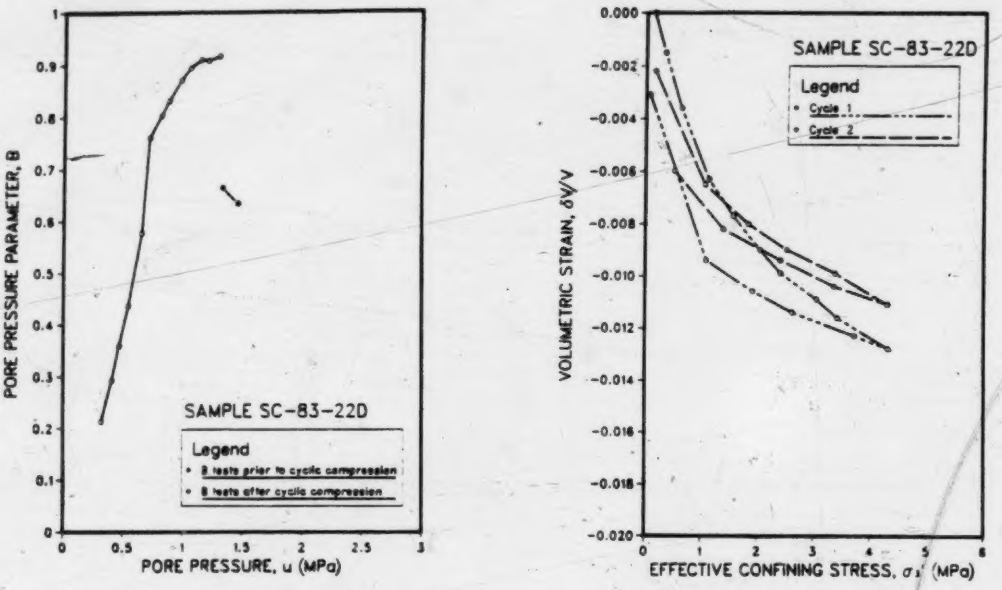

Figure C.1 SC-83-22D: Triaxial Test Results

# TEST SC-83-22U: SALINE CREEK OIL SAND

## PROCEDURAL DETAILS

1. Conventional 50.00 mm diameter loading platens were used.
2. The sample was thawed under cell and back pressures of 0.25 and 0.20 MPa for 12 hours.
3. B tests were conducted at an effective confining pressure of 0.05 MPa with incremental increases in pore pressure until saturation was reached.
4. An isotropic compressibility test was conducted with three cycles of effective confining stress up to 5 MPa. A constant pore pressure of 1.37 MPa was maintained throughout the test.
5. A second series of B tests were conducted at a confining pressure of 2.14 MPa following the cyclic compression of the sample.
6. The sample was consolidated under back and cell pressures of 1.52 MPa and 3.55 MPa. An undrained triaxial compression test was conducted at a strain rate of $1.4 \times 10^{-5}$ $s^{-1}$.

## TEST DATA

DIAMETER = 50.80 mm
HEIGHT = 102.24 mm
WEIGHT = 417.0 g.
BULK DENSITY = 2.012 $Mg/m^3$
WATER CONTENT = 1.6 %
BITUMEN CONTENT = 13.1 %
SATURATION = 81.8 %
POROSITY = 0.352

Comments on Sample Failure:

A shear plane developed as shown in the sketch.

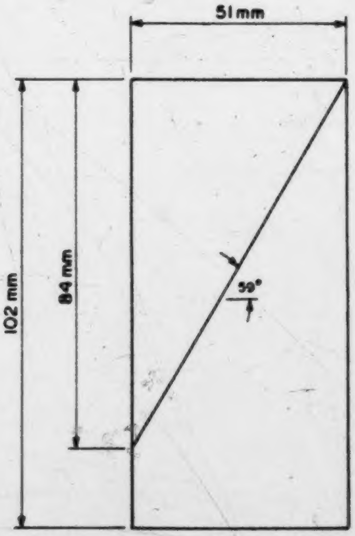

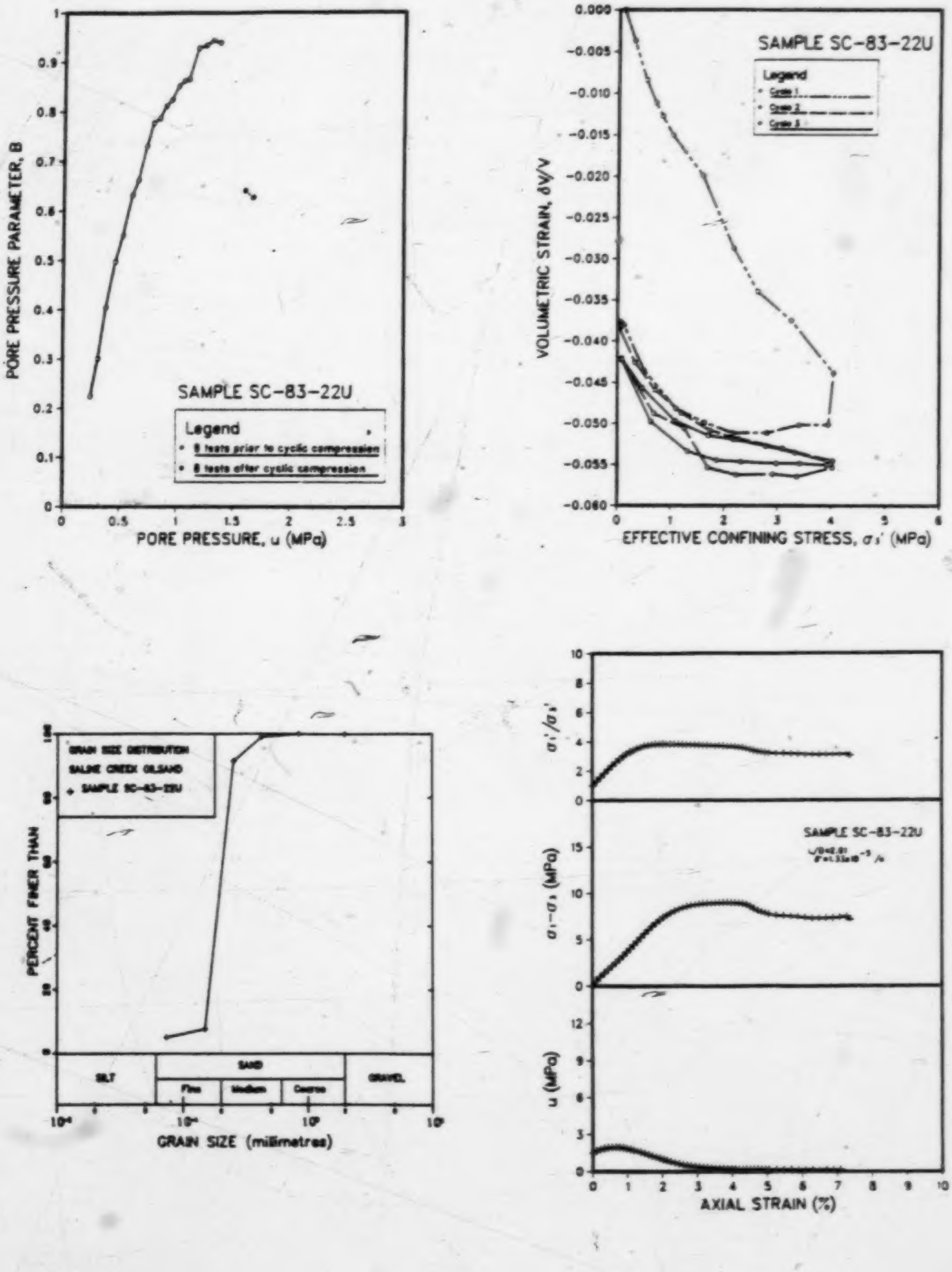

Figure C.2 SC-83-22U: Triaxial Test Results

## TEST SC-84-1: SALINE CREEK OIL SAND

### PROCEDURAL DETAILS

1. Enlarged 43.20 mm diameter loading platens were used. The faces of the platens were overlaid with two layers of greased rubber membranes.
2. The sample was thawed under cell and back pressures of 6.1 and 1.0 MPa for 16 hours.
3. B tests were conducted at an effective confining pressure of 5.0 MPa with incremental increases in pore pressure until saturation was reached.
4. The sample was consolidated under back and cell pressures of 3.55 MPa and 8.48 MPa. An undrained triaxial compression test was conducted at a strain rate of 1.4 x $10^{-3}$ $s^{-1}$.

### TEST DATA

DIAMETER = 38.69 mm
HEIGHT = 19.49 mm
WEIGHT = 46.24 g.
BULK DENSITY = 2.018 $Mg/m^3$
WATER CONTENT = 1.7 %
BITUMEN CONTENT = 14.8 %
SATURATION = 89.0 %
POROSITY = 0.364

Comments on Sample Failure:

Radial expansion occured uniformly throughout the full height of the sample.

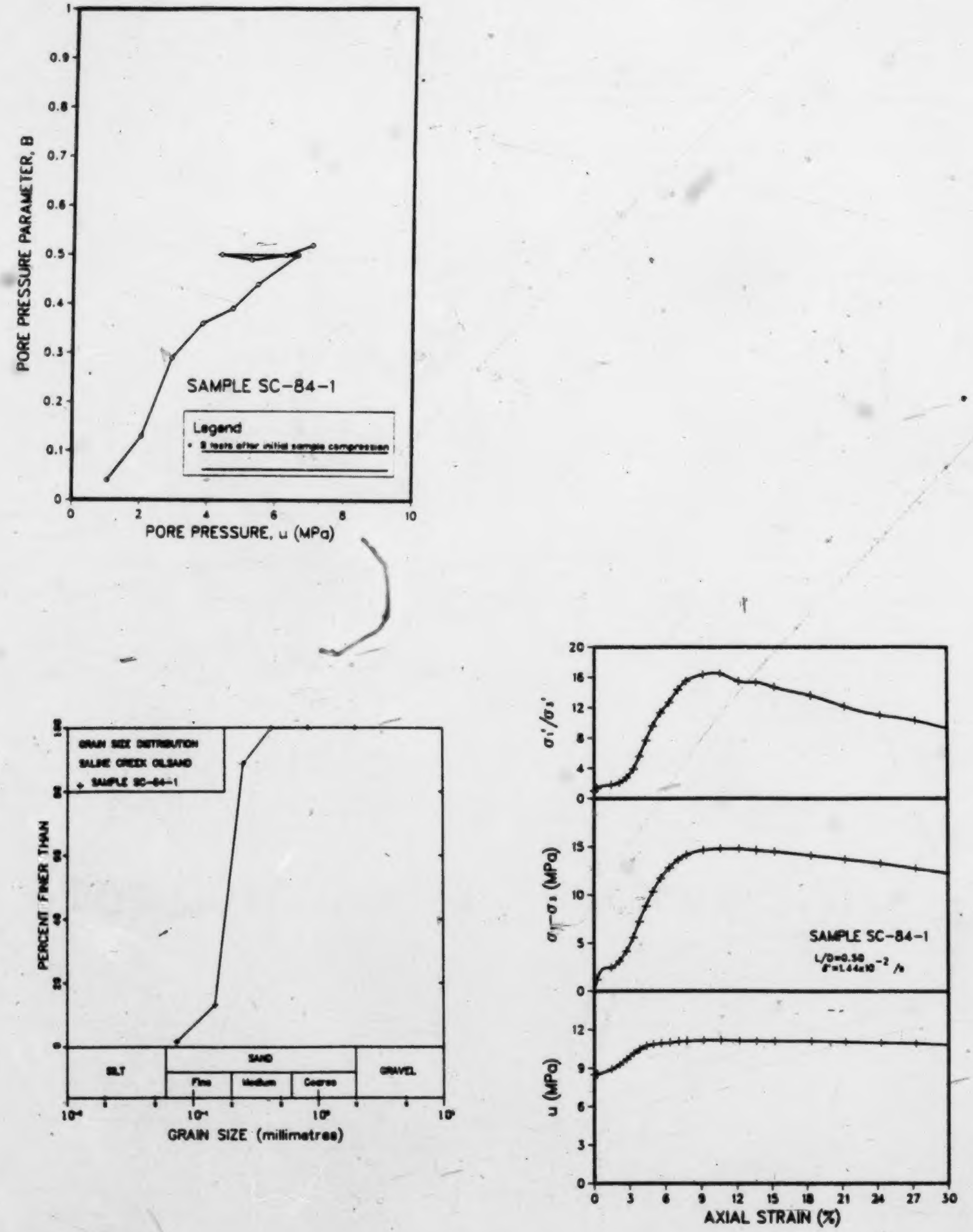

Figure C.3 SC-84-1: Triaxial Test Results

# TEST SC-84-3A: SALINE CREEK OIL SAND

## PROCEDURAL DETAILS

1. Enlarged 43.20 mm diameter loading platens were used. The faces of the platens were overlaid with two layers of greased rubber membranes.
2. The sample was thawed under cell and back pressures of 1.00 and 0.48 MPa for 2.0 hours.
3. B tests were conducted at an effective confining pressure of 0.50 MPa with incremental increases in pore pressure until saturation was reached.
4. An isotropic compressibility test was conducted with three cycles of effective confining stress up to 5 MPa. A constant pore pressure of 1.8 MPa was maintained throughout the test.
5. A second series of B tests were conducted at a confining pressure of 2.15 MPa following the cyclic compression of the sample.
6. The sample was consolidated under back and cell pressures of 10.63 MPa and 12.88 MPa. An undrained triaxial compression test was conducted at a strain rate of $8.4 \times 10^{-4}$ $s^{-1}$.

## TEST DATA

DIAMETER = 38.45 mm
HEIGHT = 19.33 mm
WEIGHT = 44.92 g.
BULK DENSITY = 2.002 $Mg/m^3$
WATER CONTENT = 2.6 %
BITUMEN CONTENT = 15.8 %
SATURATION = 93.5 %
POROSITY = 0.383

### Comments on Sample Failure:

Radial expansion occured uniformly throughout the full height of the sample.

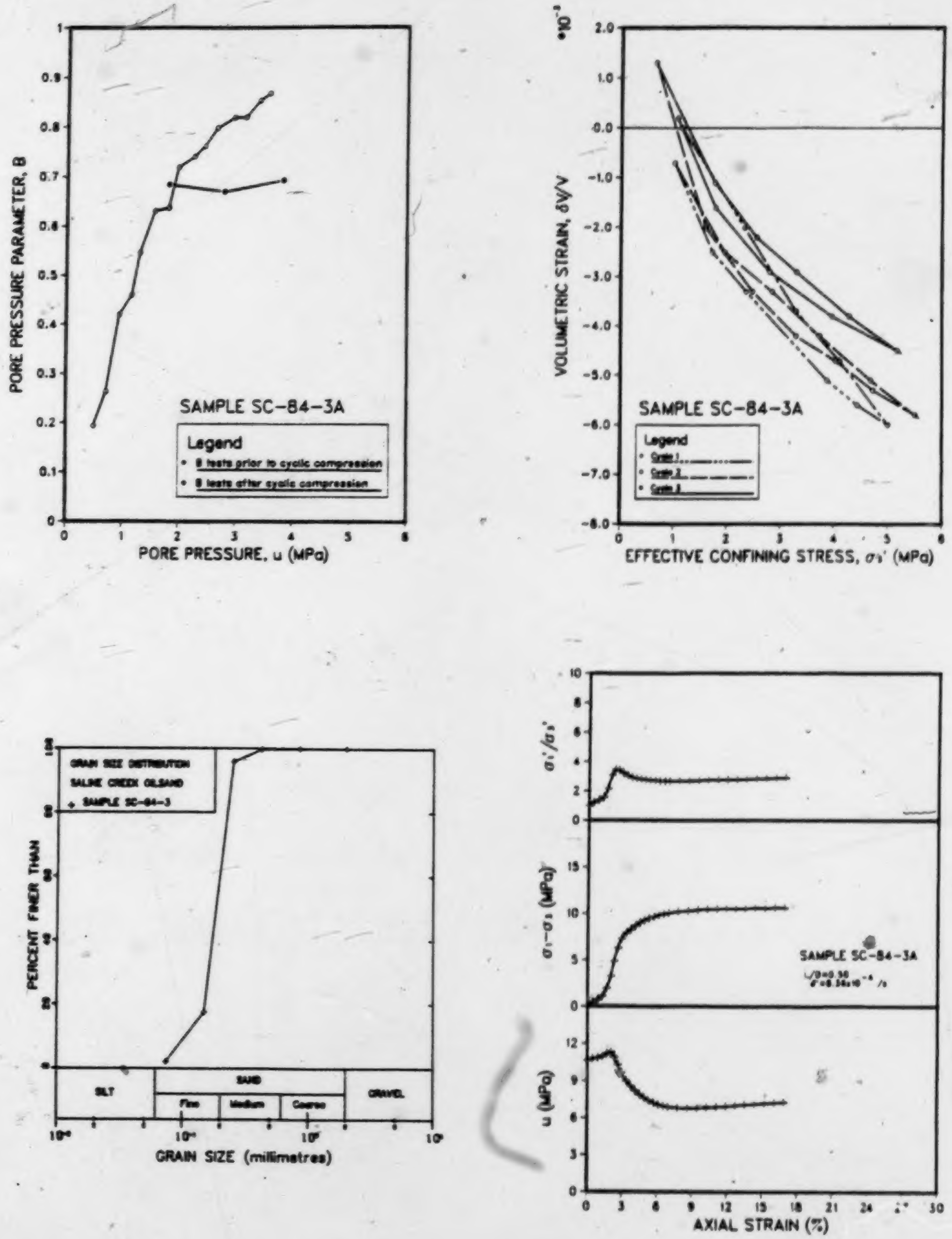

Figure C.4 SC-84-3A: Triaxial Test Results

## TEST SC-84-3B: SALINE CREEK OIL SAND

### PROCEDURAL DETAILS

1. Enlarged 43.20 mm diameter loading platens were used. The faces of the platens were overlaid with two layers of greased rubber membranes.
2. The sample was thawed under cell and back pressures of 1.02 and 0.50 MPa for 18 hours.
3. B tests were conducted at an effective confining pressure of 0.50 MPa with incremental increases in pore pressure until saturation was reached.
4. An isotropic compressibility test was conducted with three cycles of effective confining stress up to 5 MPa. A constant pore pressure of 1.8 MPa was maintained throughout the test.
5. A second series of B tests were conducted at a confining pressure of 2.30 MPa following the cyclic compression of the sample.
6. The sample was consolidated under back and cell pressures of 10.71 MPa and 12.88 MPa. An undrained triaxial compression test was conducted at a strain rate of 1.2 x $10^{-5}$ $s^{-1}$.

### TEST DATA

DIAMETER = 38.44 mm
HEIGHT = 19.35 mm
WEIGHT = 44.80 g.
BULK DENSITY = 1.994 $Mg/m^3$
WATER CONTENT = 2.6 %
BITUMEN CONTENT = 15.8 %
SATURATION = 92.5 %
POROSITY = 0.386

Comments on Sample Failure:

Radial expansion occured uniformly throughout the full height of the sample. A shear plane developed as shown in the sketch.

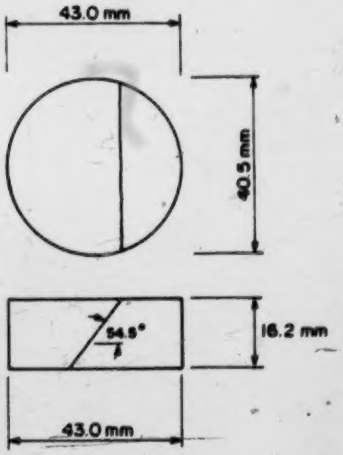

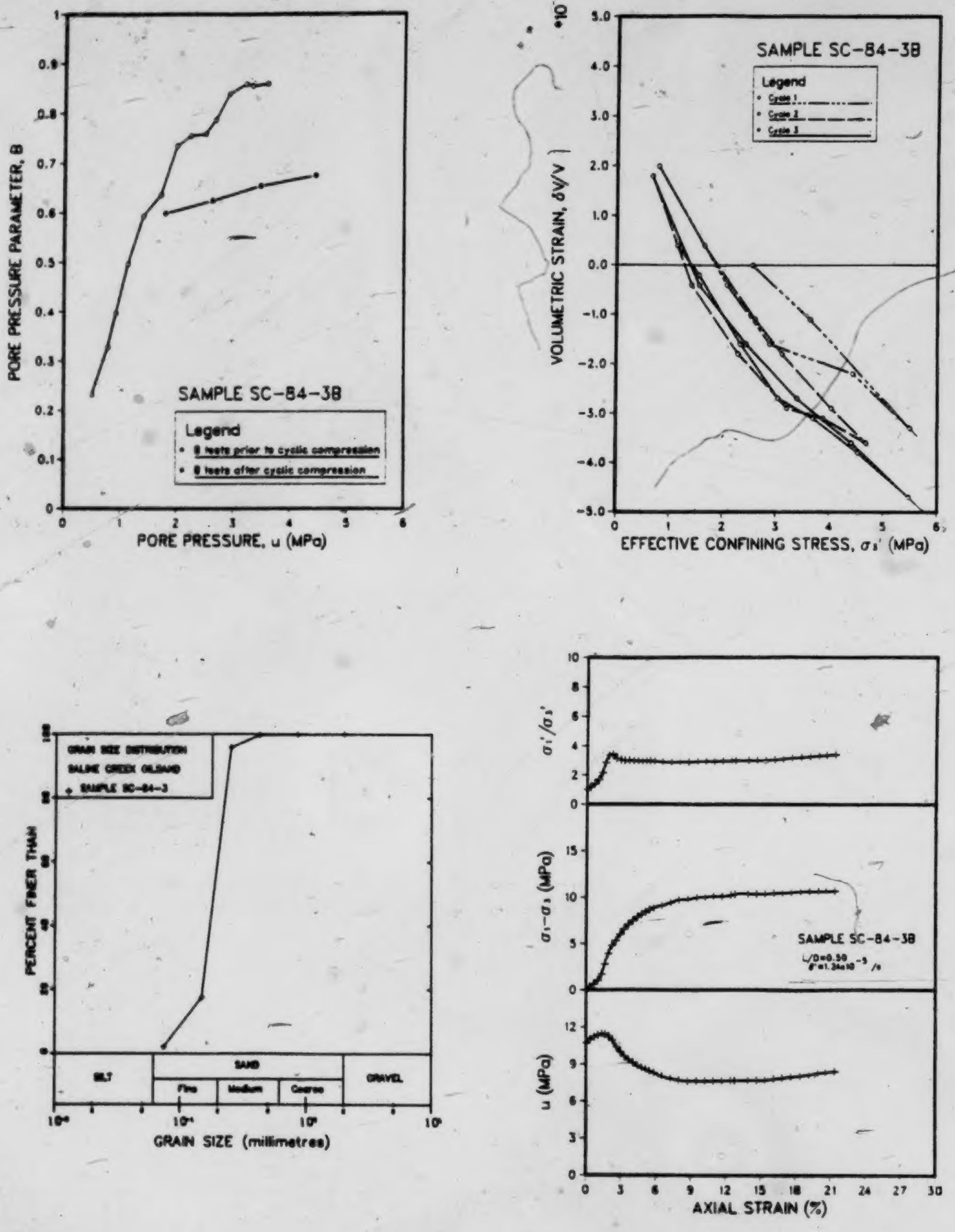

Figure C.5 SC-84-3B: Triaxial Test Results

# TEST SC-84-4A: SALINE CREEK OIL SAND

## PROCEDURAL DETAILS

1. Enlarged 43.20 mm diameter loading platens were used. The faces of the platens were overlaid with two layers of greased rubber membranes.
2. The sample was thawed under cell and back pressures of 0.73 and 0.30 MPa for 2.0 hours.
3. B tests were conducted at an effective confining pressure of 0.45 MPa with incremental increases in pore pressure until saturation was reached.
4. An isotropic compressibility test was conducted with three cycles of effective confining stress up to 5 MPa. A constant pore pressure of 1.8 MPa was maintained throughout the test.
5. A second series of B tests were conducted at a confining pressure of 2.20 MPa following the cyclic compression of the sample.
6. The sample was consolidated under back and cell pressures of 10.69 MPa and 12.70 MPa. An undrained triaxial compression test was conducted at a strain rate of $1.4 \times 10^{-5}$ $s^{-1}$.

## TEST DATA

DIAMETER = 38.27 mm
HEIGHT = 20.03 mm
WEIGHT = 45.36 g.
BULK DENSITY = 1.970 $Mg/m^3$
WATER CONTENT = 3.2 %
BITUMEN CONTENT = 15.9 %
SATURATION = 92.2 %
POROSITY = 0.399

### Comments on Sample Failure:

- Radial expansion occured uniformly throughout the full height of the sample.

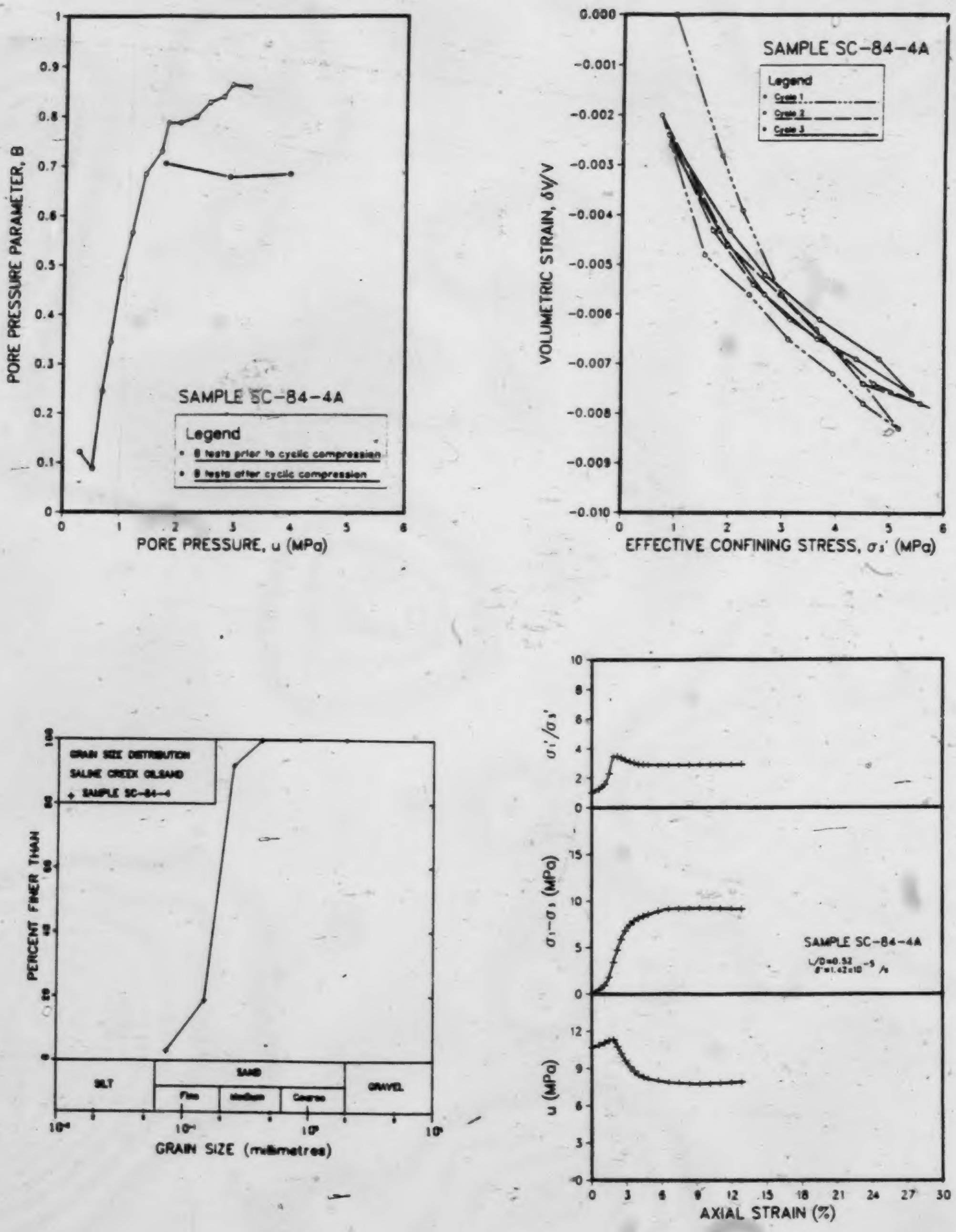

Figure C.6 SC-84-4A: Triaxial Test Results

## TEST SC-84-4B: SALINE CREEK OIL SAND

### PROCEDURAL DETAILS

1. Enlarged 43.20 mm diameter loading platens were used. The faces of the platens were overlaid with two layers of greased rubber membranes.
2. The sample was thawed under cell and back pressures of 0.88 and 0.51 MPa for 2.0 hours.
3. B tests were conducted at an effective confining pressure of 0.50 MPa with incremental increases in pore pressure until saturation was reached.
4. An isotropic compressibility test was conducted with three cycles of effective confining stress up to 5 MPa. A constant pore pressure of 1.75 MPa was maintained throughout the test.
5. A second series of B tests were conducted at a confining pressure of 2.15 MPa following the cyclic compression of the sample.
6. The sample was consolidated under back and cell pressures of 10.61 MPa and 12.76 MPa. An undrained triaxial compression test was conducted at a strain rate of $8.4 \times 10^{-4}$ $s^{-1}$.

### TEST DATA

DIAMETER = 38.27 mm
HEIGHT = 18.20 mm
WEIGHT = 41.21 g.
BULK DENSITY = 1.969 $Mg/m^3$
WATER CONTENT = 3.2 %
BITUMEN CONTENT = 15.9 %
SATURATION = 92.1 %
POROSITY = 0.399

### Comments on Sample Failure:

Radial expansion occured uniformly throughout the full height of the sample.

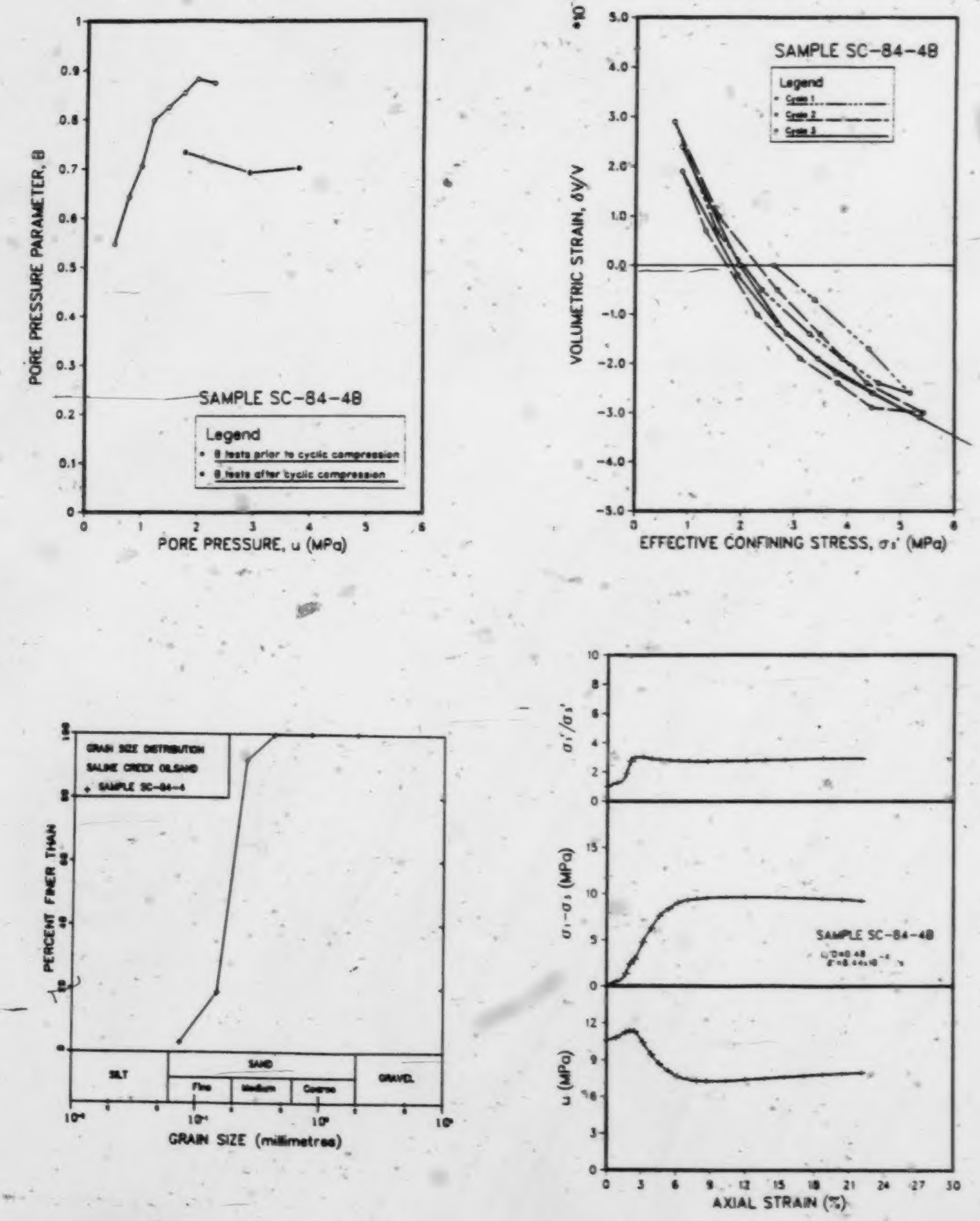

Figure C.7 SC-84-4B: Triaxial Test Results

## TEST SC-84-5A: SALINE CREEK OIL SAND

### PROCEDURAL DETAILS

1. Enlarged 43.20 mm diameter loading platens were used. The faces of the platens were overlaid with two layers of greased rubber membranes.
2. The sample was thawed under cell and back pressures of 1.08 and 0.48 MPa for 1.5 hours.
3. B tests were conducted at an effective confining pressure of 0.60 MPa with incremental increases in pore pressure until saturation was reached.
4. An isotropic compressibility test was conducted with three cycles of effective confining stress up to 5 MPa. A constant pore pressure of 1.80 MPa was maintained throughout the test.
5. A second series of B tests were conducted at a confining pressure of 2.15 MPa following the cyclic compression of the sample.
6. The sample was consolidated under back and cell pressures of 10.61 MPa and 12.77 MPa. An undrained triaxial compression test was conducted at a strain rate of $7.8 \times 10^{-2}$ $s^{-1}$. The sample slipped off the base pedestal during testing and the triaxial test results were considered erroneous.

### TEST DATA

DIAMETER = 38.31 mm
HEIGHT = 19.43 mm
WEIGHT = 44.85 g.
BULK DENSITY = 2.002 $Mg/m^3$
WATER CONTENT = 3.3 %
BITUMEN CONTENT = 14.0 %
SATURATION = 90.1 %
POROSITY = 0.375

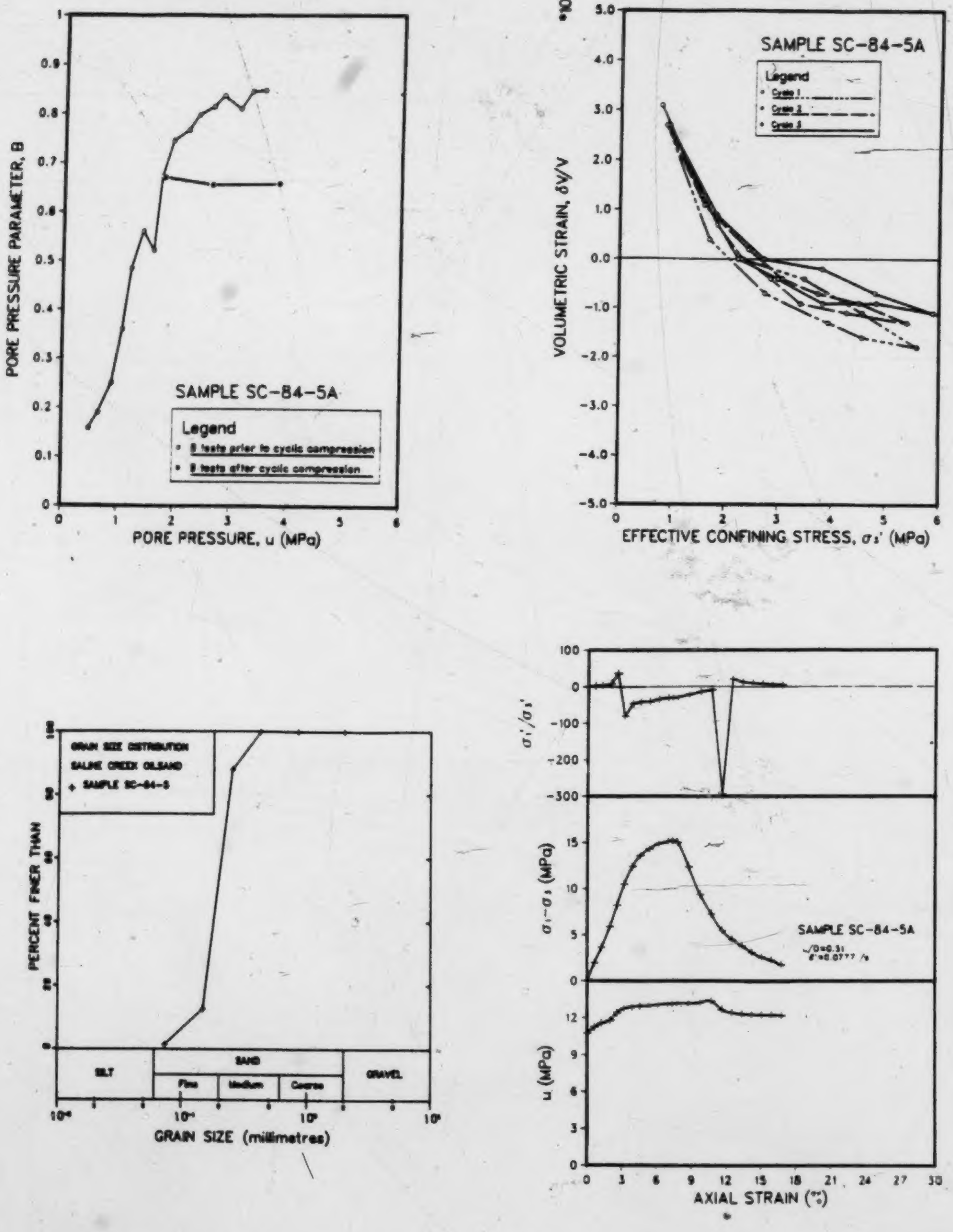

Figure C.8 SC-84-5A: Triaxial Test Results

# TEST SC-84-5B: SALINE CREEK OIL SAND

## PROCEDURAL DETAILS

1. Enlarged 43.20 mm diameter loading platens were used. The faces of the platens were overlaid with two layers of greased rubber membranes.
2. The sample was thawed under cell and back pressures of 1.03 and 0.47 MPa for 15 hours.
3. B tests were conducted at an effective confining pressure of 0.55 MPa with incremental increases in pore pressure until saturation was reached.
4. An isotropic compressibility test was conducted with three cycles of effective confining stress up to 5 MPa. A constant pore pressure of 1.80 MPa was maintained throughout the test.
5. A second series of B tests were conducted at a confining pressure of 2.20 MPa following the cyclic compression of the sample.
6. The sample was consolidated under back and cell pressures of 10.23 MPa and 12.21 MPa. An undrained triaxial compression test was conducted at a strain rate of 7.5 x $10^{-5}$ $s^{-1}$.

## TEST DATA

DIAMETER = 38.35 mm
HEIGHT = 19.63 mm
WEIGHT = 44.25 g.
BULK DENSITY = 1.952 $Mg/m^3$
WATER CONTENT = 3.3 %
BITUMEN CONTENT = 14.0 %
SATURATION = 84.4 %
POROSITY = 0.391

### Comments on Sample Failure:

Radial expansion occured uniformly throughout the full height of the sample.

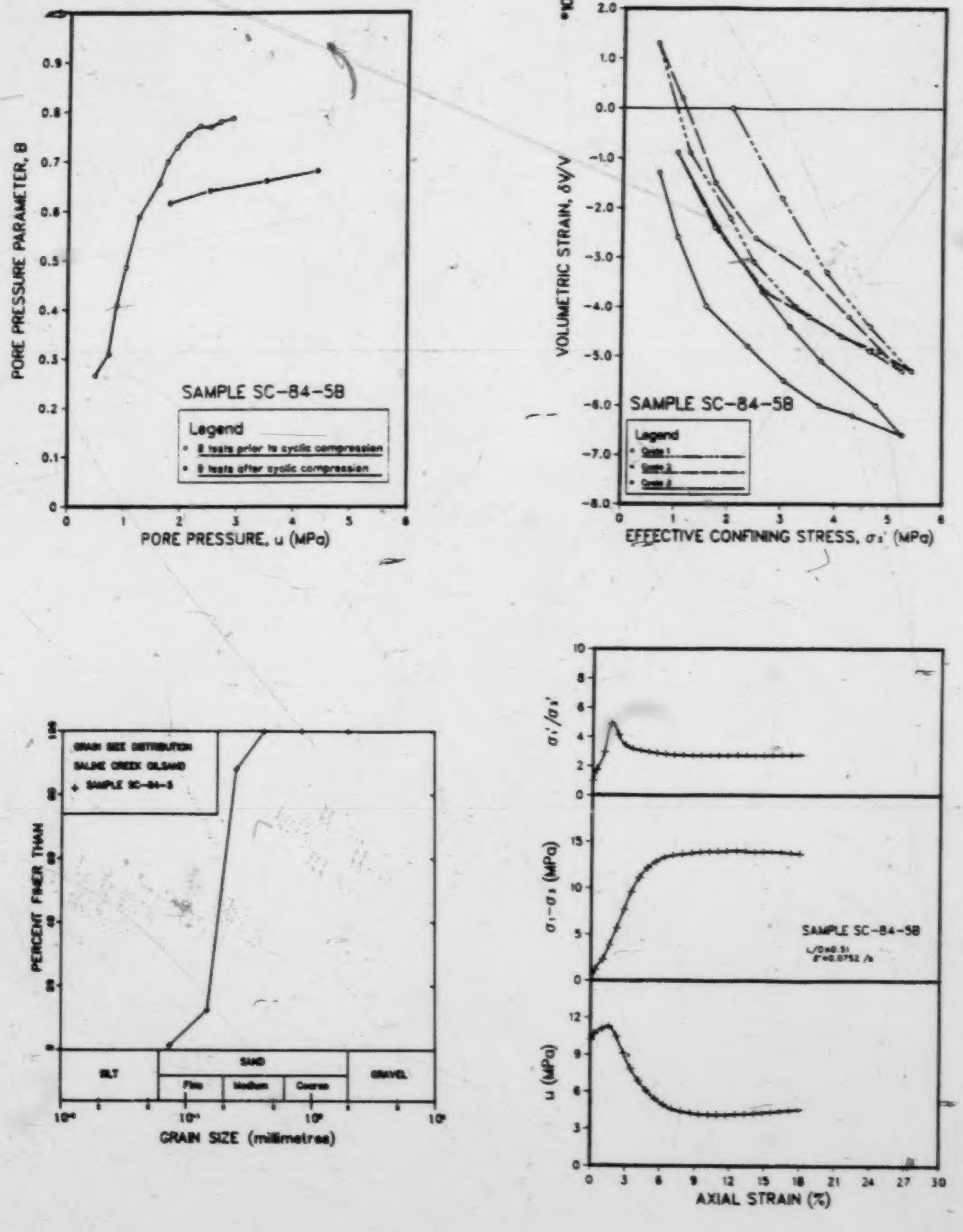

Figure C.9 SC-84-5B: Triaxial Test Results

# TEST SC-84-8A: SALINE CREEK OIL SAND

## PROCEDURAL DETAILS

1. Enlarged 43.20 mm diameter loading platens were used. The faces of the platens were overlaid with two layers of greased rubber membranes.
2. The sample was thawed under cell and back pressures of 1.02 and 0.51 MPa for 1.5 hours.
3. B tests were conducted at an effective confining pressure of 0.50 MPa with incremental increases in pore pressure until saturation was reached.
4. An isotropic compressibility test was conducted with three cycles of effective confining stress up to 5 MPa. A constant pore pressure of 1.80 MPa was maintained throughout the test.
5. A second series of B tests were conducted at a confining pressure of 2.00 MPa following the cyclic compression of the sample.
6. The sample was consolidated under back and cell pressures of 10.46 MPa and 12.53 MPa. An undrained triaxial compression test was conducted at a strain rate of 2.1 x $10^{-1}$ $s^{-1}$.

## TEST DATA

DIAMETER = 38.28 mm
HEIGHT = 19.35 mm
WEIGHT = 45.97 g.
BULK DENSITY = 1.985 $Mg/m^3$
WATER CONTENT = 2.0 %
BITUMEN CONTENT = 12.6 %
SATURATION = 76.9 %
POROSITY = 0.363

### Comments on Sample Failure:

Radial expansion occured uniformly throughout the full height of the sample.

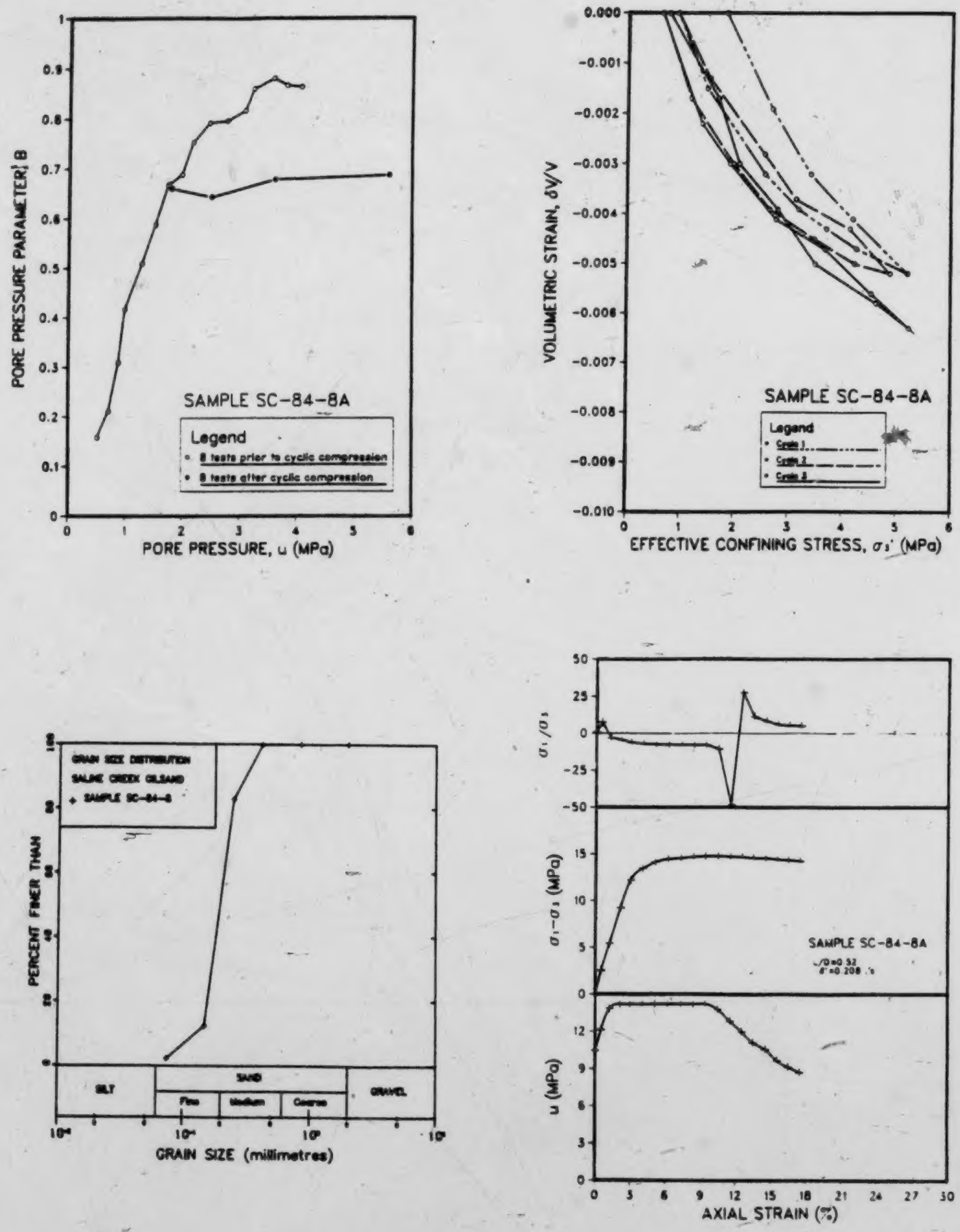

Figure C.10 SC-84-8A: Triaxial Test Results

## TEST SC-84-8B: SALINE CREEK OIL SAND

### PROCEDURAL DETAILS

1. Enlarged 43.20 mm diameter loading platens were used. The faces of the platens were overlaid with two layers of greased rubber membranes.
2. The sample was thawed under cell and back pressures of 1.10 and 0.64 MPa for 43 hours.
3. B tests were conducted at an effective confining pressure of 0.48 MPa with incremental increases in pore pressure until saturation was reached.
4. An isotropic compressibility test was conducted with three cycles of effective confining stress up to 5 MPa. A constant pore pressure of 1.80 MPa was maintained throughout the test.
5. A second series of B tests were conducted at a confining pressure of 2.30 MPa following the cyclic compression of the sample.
6. The sample was consolidated under back and cell pressures of 10.28 MPa and 12.35 MPa. An undrained triaxial compression test was conducted at a strain rate of 2.2 x $10^{-1}$ $s^{-1}$.

### TEST DATA

DIAMETER = 38.33 mm
HEIGHT = 20.07 mm
WEIGHT = 43.95 g.
BULK DENSITY = 1.974 $Mg/m^3$
WATER CONTENT = 2.0 %
BITUMEN CONTENT = 12.6 %
SATURATION = 78.1 %
POROSITY = 0.360

#### Comments on Sample Failure:

Radial expansion occured uniformly throughout the full height of the sample.

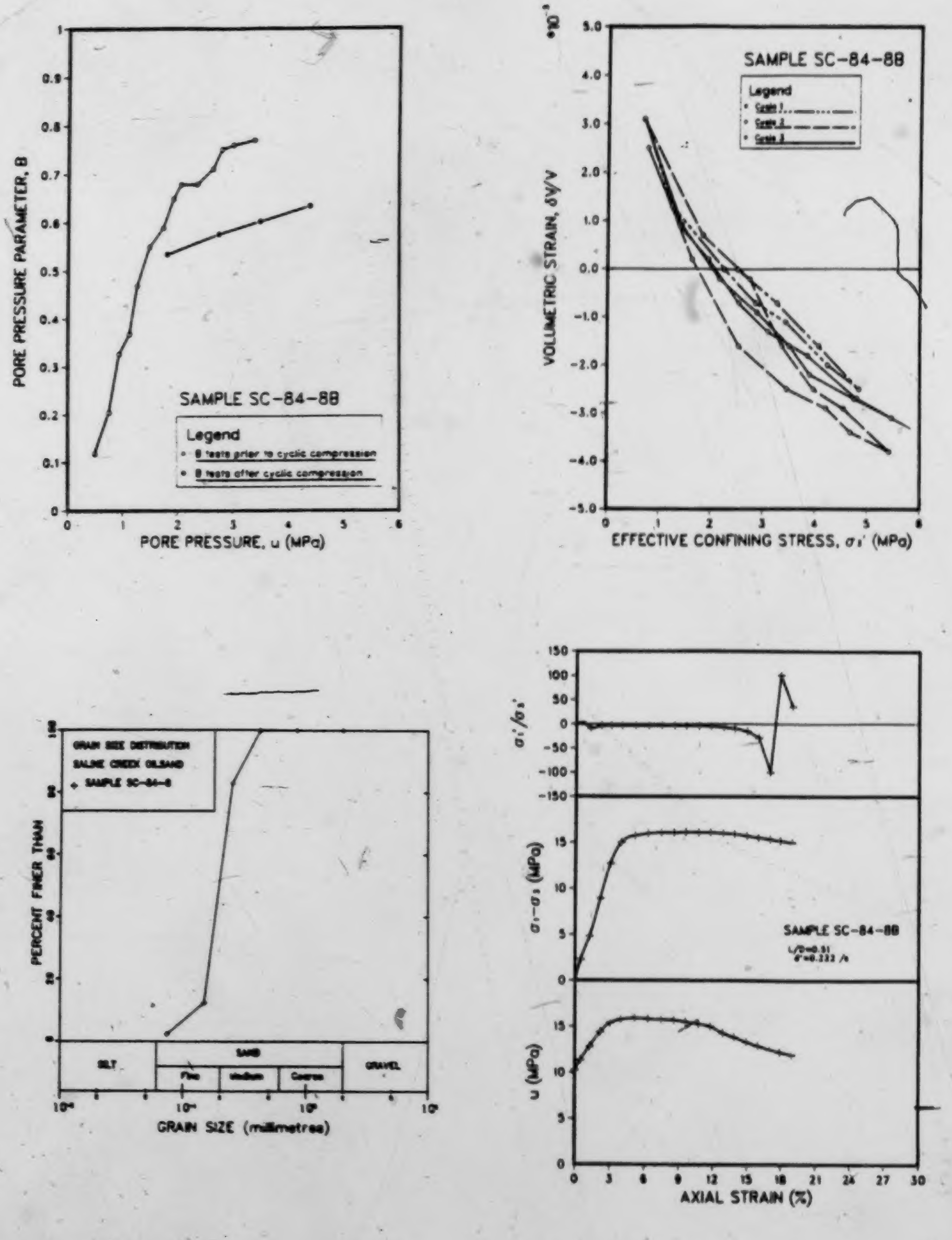

Figure C.11 SC-84-8B: Triaxial Test Results

## TEST SC-84-10: SALINE CREEK OIL SAND

### PROCEDURAL DETAILS

1. Enlarged 43.20 mm diameter loading platens were used.
2. The sample was thawed under cell and back pressures of 2.0 and 1.0 MPa for 17 hours.
3. B tests were conducted at an effective confining pressure of 1.03 MPa with incremental increases in pore pressure until saturation was reached.
4. The sample was consolidated under back and cell pressures of 10.98 MPa and 11.91 MPa. An undrained triaxial compression test was conducted at a strain rate of $2.6 \times 10^{-5}\ s^{-1}$.

### TEST DATA

DIAMETER = 38.75 mm
HEIGHT = 75.25 mm
WEIGHT = 178.03 g.
BULK DENSITY = 2.006 $Mg/m^3$
WATER CONTENT = 7.6 %
BITUMEN CONTENT = 12.2 %
SATURATION = 99.3 %
POROSITY = 0.394

### Comments on Sample Failure:

A shear plane developed as shown in the sketch.

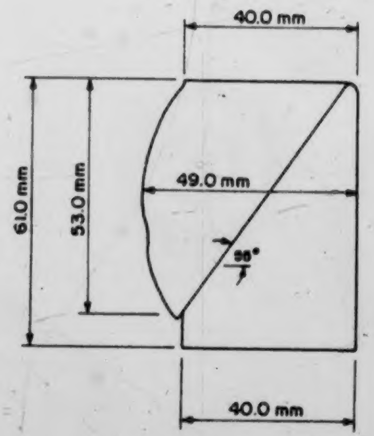

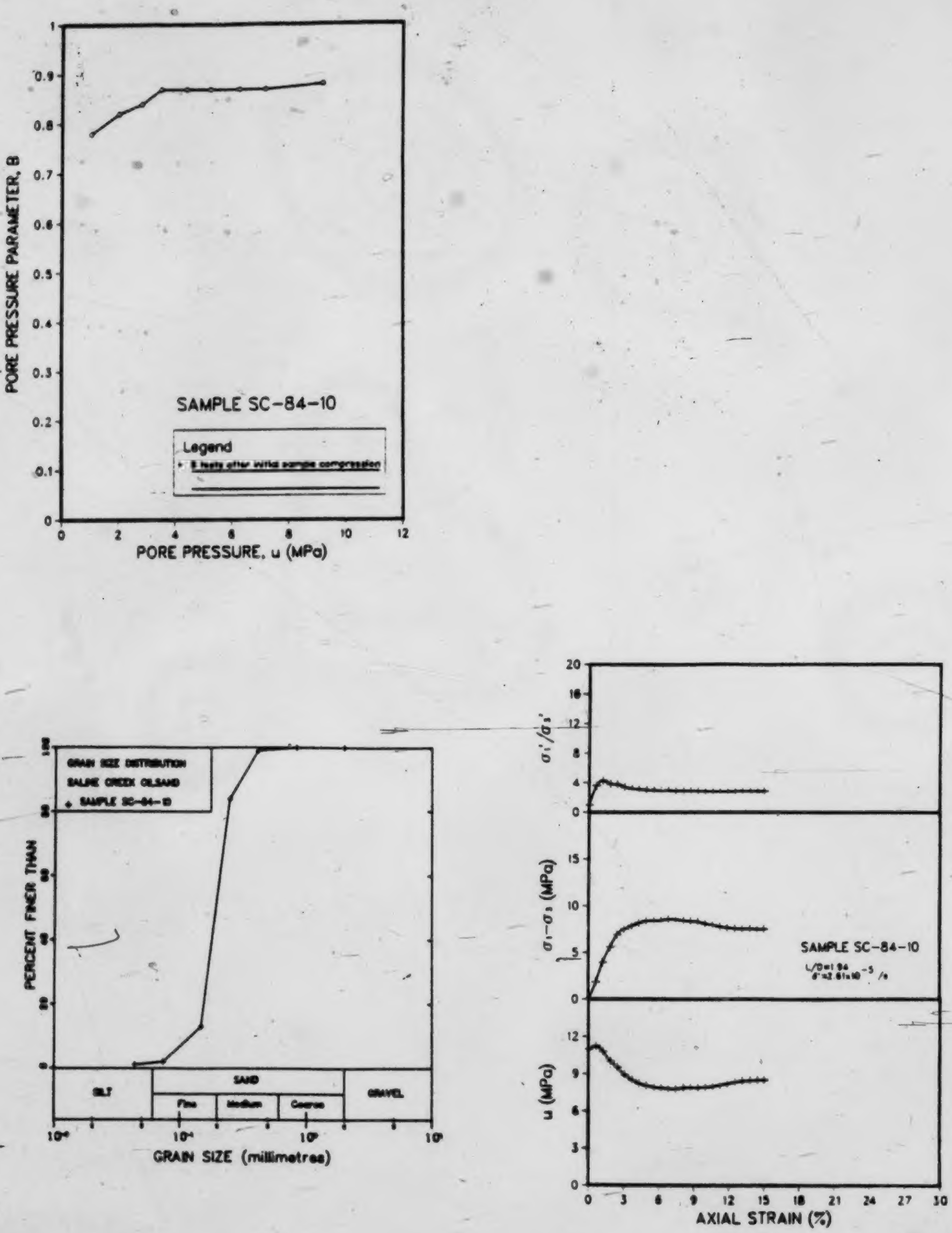

Figure C.12 SC-84-10: Triaxial Test Results

## TEST SC-84-13: SALINE CREEK OIL SAND

### PROCEDURAL DETAILS

1. Enlarged 43.20 mm diameter loading platens were used. The faces of the platens were overlaid with two layers of greased rubber membranes.
2. The sample was thawed under cell and back pressures of 2.2 and 1.2 MPa for 18 hours.
3. B tests were conducted at an effective confining pressure of 1.0 MPa with incremental increases in pore pressure until saturation was reached.
4. The sample was consolidated under back and cell pressures of 10.89 MPa and 11.94 MPa. An undrained triaxial compression test was conducted at a strain rate of $1.3 \times 10^{-5}$ $s^{-1}$.

### TEST DATA

DIAMETER = 38.50 mm
HEIGHT = 18.68 mm
WEIGHT = 43.81 g.
BULK DENSITY = 2.015 $Mg/m^3$
WATER CONTENT = 2.1 %
BITUMEN CONTENT = 15.2 %
SATURATION = 91.6 %
POROSITY = 0.383

### Comments on Sample Failure:

Radial expansion occured uniformly throughout the full height of the sample.

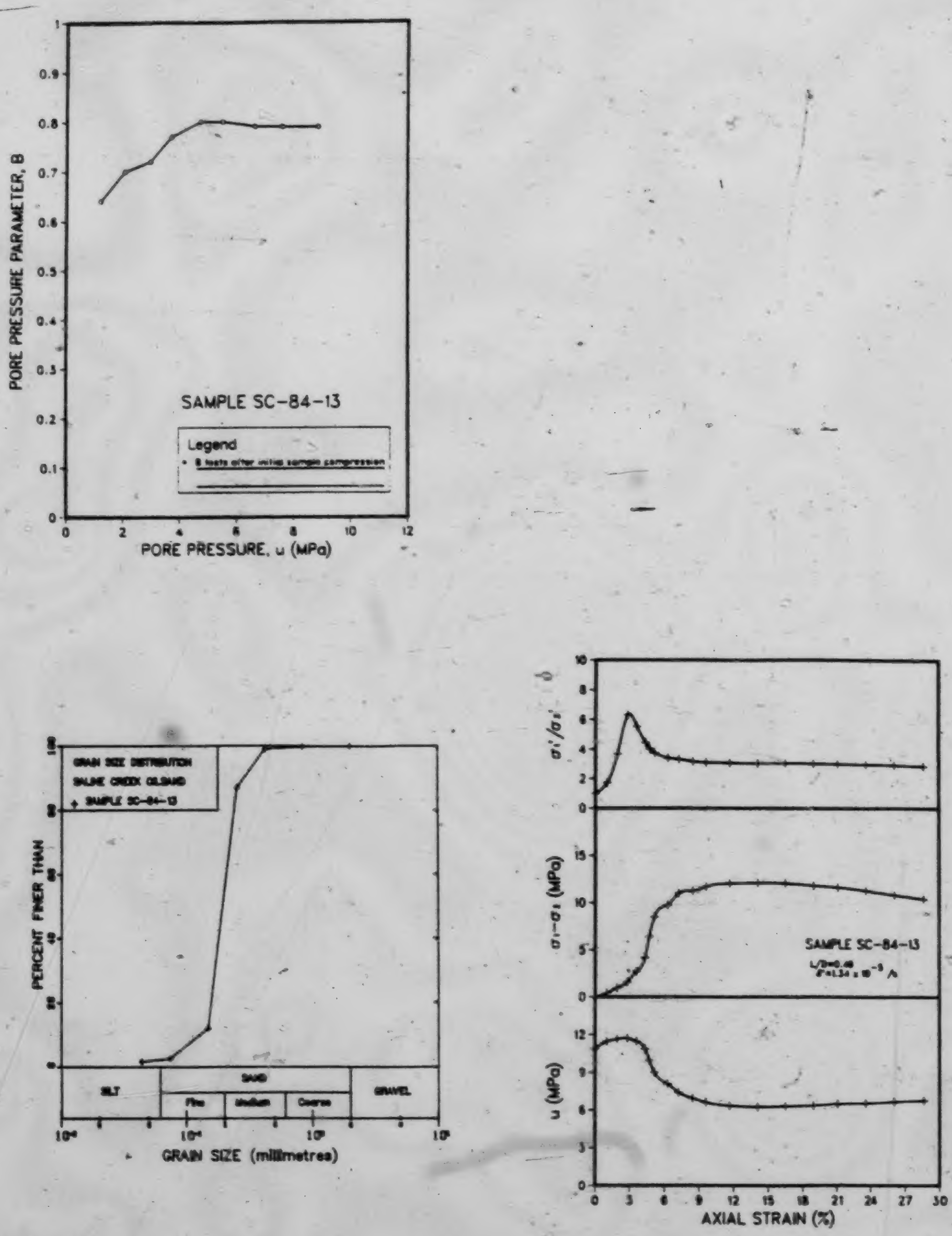

Figure C.13 SC-84-13: Triaxial Test Results

## TEST SC-84-14A: SALINE CREEK OIL SAND

### PROCEDURAL DETAILS

1. Enlarged 43.20 mm diameter loading platens were used. The faces of the platens were overlaid with two layers of greased rubber membranes.
2. The sample was thawed under cell and back pressures of 6.6 and 1.5 MPa for 16 hours.
3. B tests were conducted at an effective confining pressure of 5.0 MPa with incremental increases in pore pressure until saturation was reached.
4. The sample was consolidated under back and cell pressures of 7.80 MPa and 12.62 MPa. An undrained triaxial compression test was conducted at a strain rate of $1.5 \times 10^{-5}$ $s^{-1}$.

### TEST DATA

DIAMETER = 38.00 mm
HEIGHT = 18.81 mm
WEIGHT = 41.96 g.
BULK DENSITY = 1.966 $Mg/m^3$
WATER CONTENT = 5.1 %
BITUMEN CONTENT = 13.4 %
SATURATION = 91.9 %
POROSITY = 0.396

#### Comments on Sample Failure:

Radial expansion occured uniformly throughout the full height of the sample.

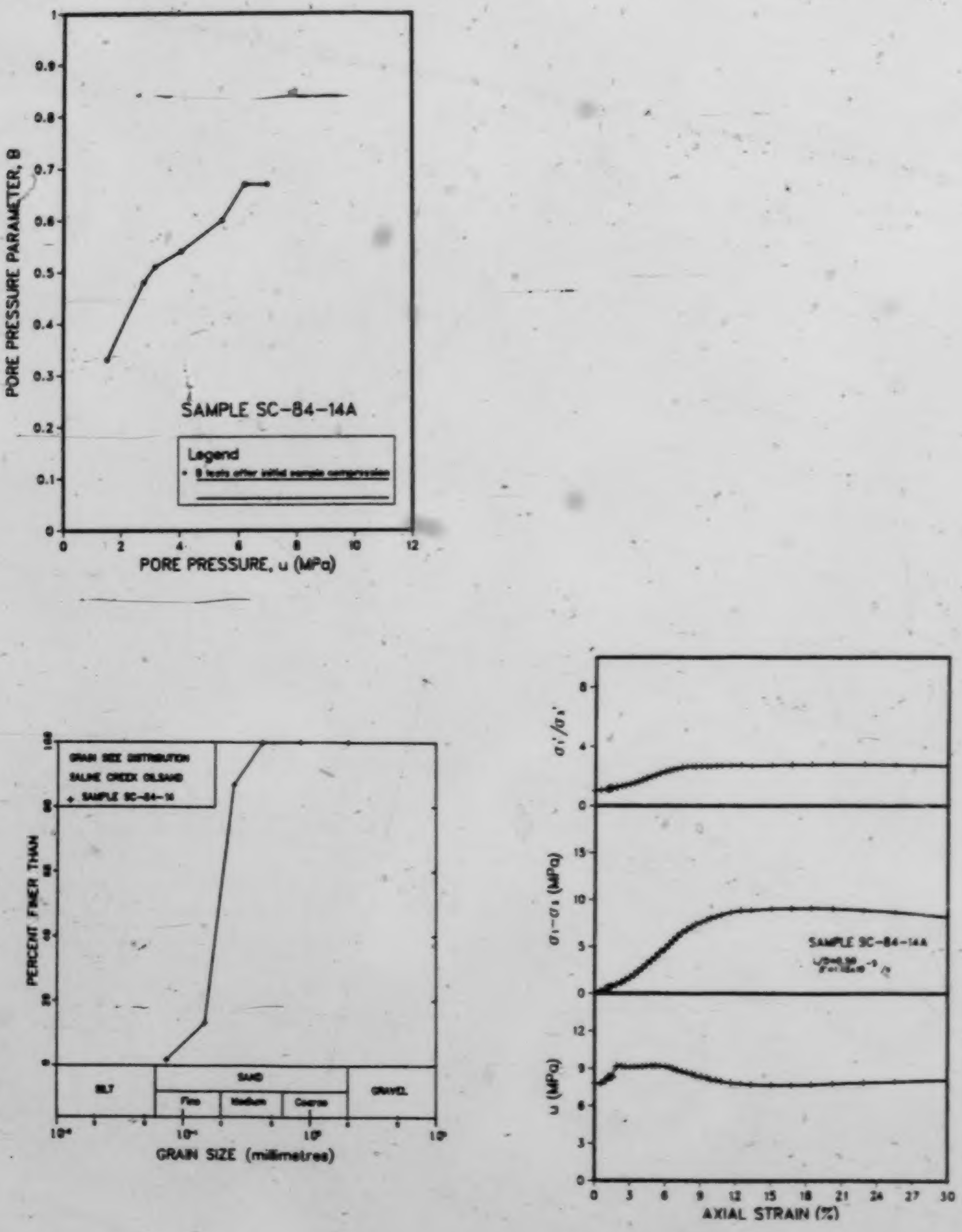

Figure C.14 SC-84-14A: Triaxial Test Results

# TEST SC-84-14B: SALINE CREEK OIL SAND

## PROCEDURAL DETAILS

1. Enlarged 43.20 mm diameter loading platens were used. The faces of the platens were overlaid with two layers of greased rubber membranes.
2. The sample was thawed under cell and back pressures of 6.6 and 5.7 MPa for 3.3 hours.
3. B tests were conducted at an effective confining pressure of 1.0 MPa with incremental increases in pore pressure until saturation was reached.
4. The sample was consolidated under back and cell pressures of 9.33 MPa and 10.30 MPa. An undrained triaxial compression test was conducted at a strain rate of $1.5 \times 10^{-2}$ $s^{-1}$.

## TEST DATA

DIAMETER = 38.10 mm
HEIGHT = 18.51 mm
WEIGHT = 40.96 g.
BULK DENSITY = 1.941 $Mg/m^3$
WATER CONTENT = 5.1 %
BITUMEN CONTENT = 13.4 %
SATURATION = 89.2 %
POROSITY = 0.403

### Comments on Sample Failure:

Radial expansion occured uniformly throughout the full height of the sample.

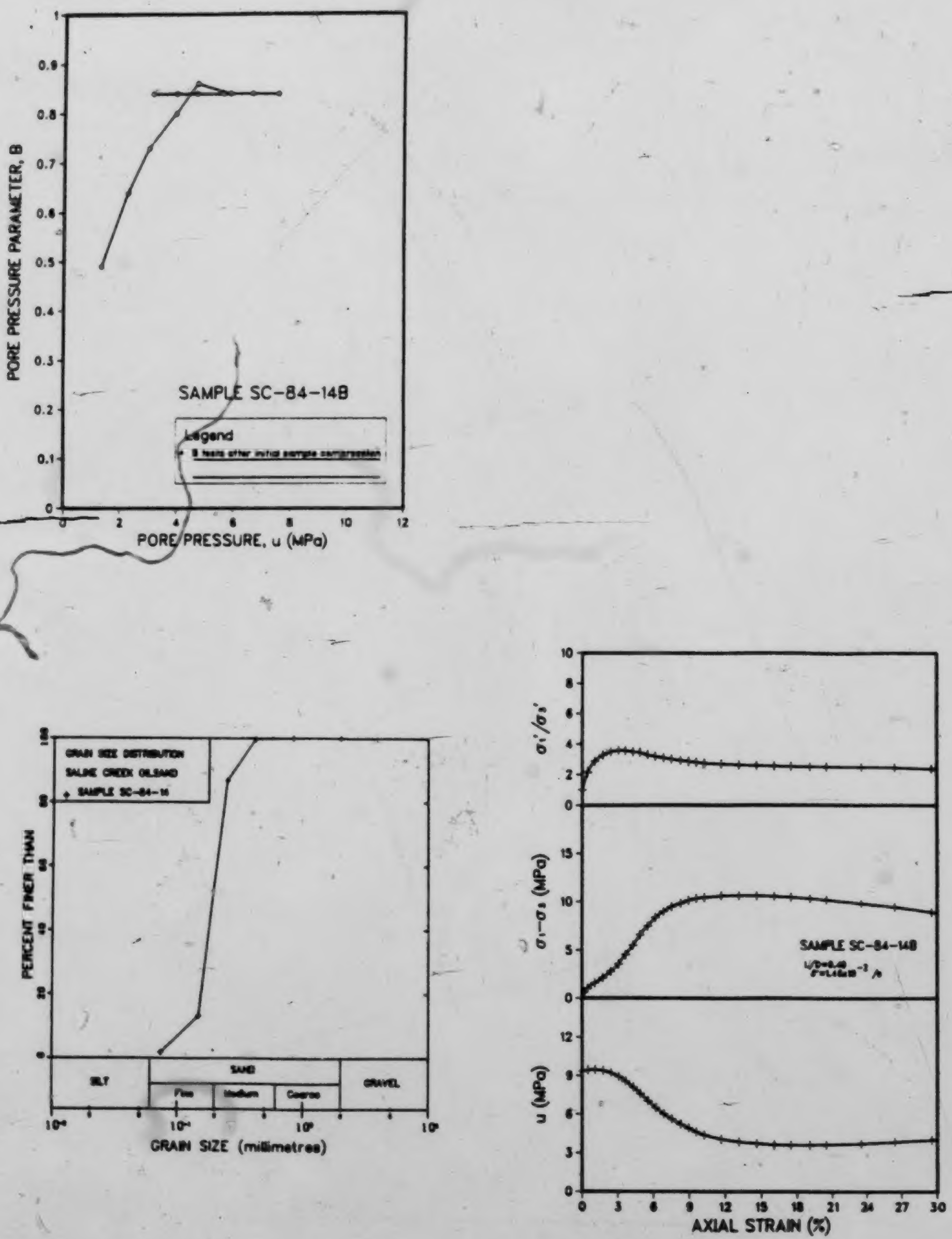

Figure C.15 SC-84-14B: Triaxial Test Results

# TEST SC-84-15A: SALINE CREEK OIL SAND

## PROCEDURAL DETAILS

1. Enlarged 43.20 mm diameter loading platens were used. The faces of the platens were overlaid with two layers of greased rubber membranes.
2. The sample was thawed under cell and back pressures of 2.68 and 2.11 MPa for 16 hours.
3. B tests were conducted at an effective confining pressure of 0.70 MPa with incremental increases in pore pressure until saturation was reached.
4. An isotropic compressibility test was conducted with three cycles of effective confining stress up to 5 MPa. A constant pore pressure of 1.91 MPa was maintained throughout the test.
5. A second series of B tests were conducted at a confining pressure of 2.20 MPa following the cyclic compression of the sample.
6. The sample was consolidated under back and cell pressures of 10.18 MPa and 12.24 MPa. An undrained triaxial compression test was conducted at a strain rate of $1.1 \times 10^{-2}$ $s^{-1}$.

## TEST DATA

DIAMETER = 37.95 mm
HEIGHT = 17.36 mm
WEIGHT = 39.69 g.
BULK DENSITY = 2.021 $Mg/m^3$
WATER CONTENT = 1.2 %
BITUMEN CONTENT = 16.5 %
SATURATION = 93.4 %
POROSITY = 0.373

Comments on Sample Failure:
Radial expansion occured uniformly throughout the full height of the sample. The sample slipped to one side of the base pedestal during the test. A line appeared across the top of the sample as shown in the sketch. The sample was broken in half and a fracture through the sample was not evident.

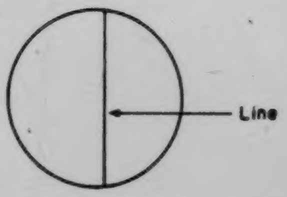

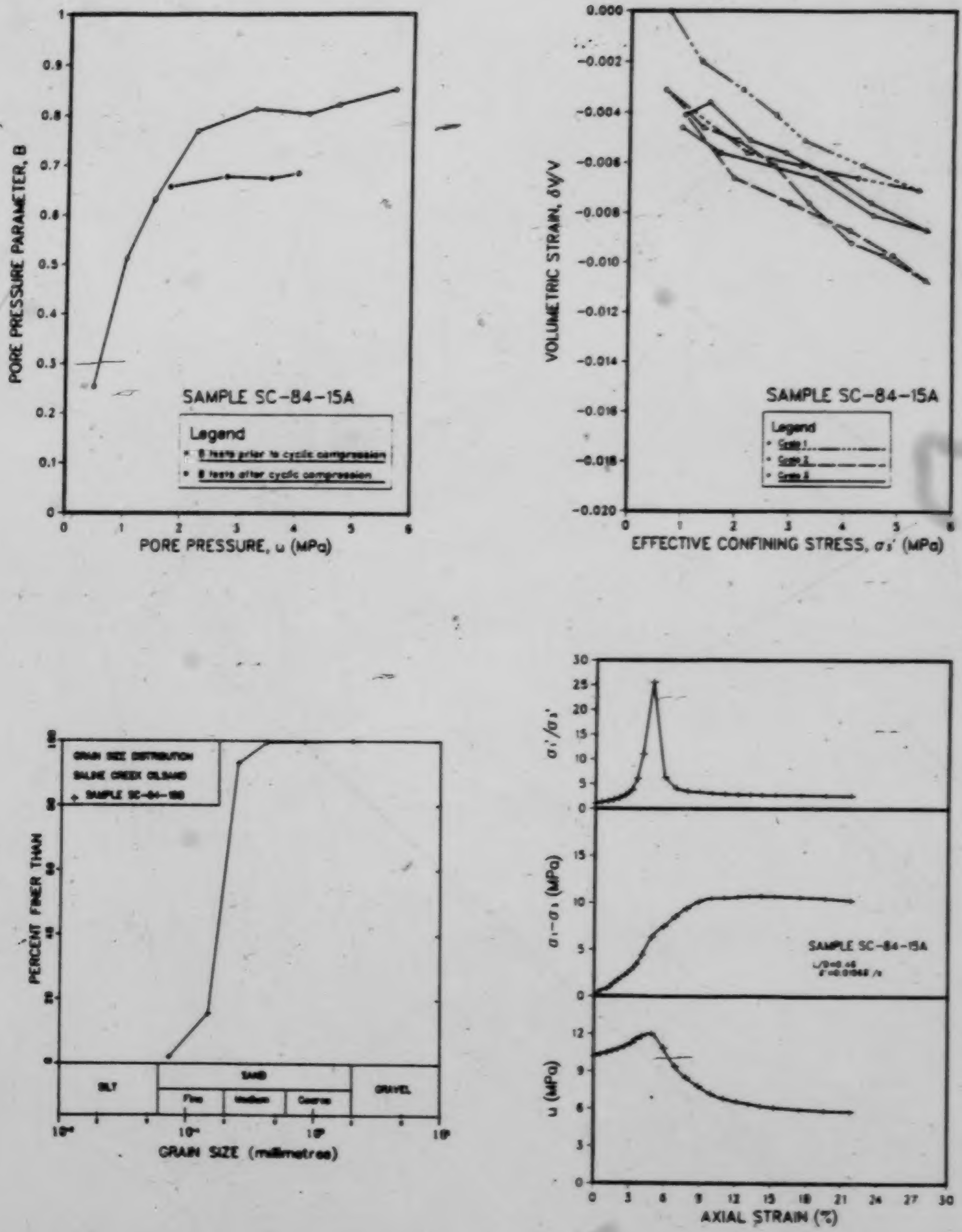

Figure C.16 SC-84-15A: Triaxial Test Results

# TEST SC-84-15B: SALINE CREEK OIL SAND

## PROCEDURAL DETAILS

1. Enlarged 43.20 mm diameter loading platens were used. The faces of the platens were overlaid with two layers of greased rubber membranes.
2. The sample was thawed under cell and back pressures of 0.96 and 0.06 MPa for 2.7 hours.
3. B tests were conducted at an effective confining pressure of 0.85 MPa with incremental increases in pore pressure until saturation was reached.
4. An isotropic compressibility test was conducted with three cycles of effective confining stress up to 5 MPa. A constant pore pressure of 4.30 MPa was maintained throughout the test.
5. A second series of B tests were conducted at a confining pressure of 1.80 MPa and -3.40 MPa following the cyclic compression of the sample.
6. The sample was consolidated under back and cell pressures of 10.24 MPa and 12.44 MPa. An undrained triaxial compression test was conducted at a strain rate of 8.4 x $10^{-3}$ $s^{-1}$.

## TEST DATA

DIAMETER = 37.95 mm
HEIGHT = 18.78 mm
WEIGHT = 42.16 g.
BULK DENSITY = 1.985 Mg/$m^3$
WATER CONTENT = 1.2 %
BITUMEN CONTENT = 16.5 %
SATURATION = 89.1 %
POROSITY = 0.384

### Comments on Sample Failure:

Radial expansion occured uniformly throughout the full height of the sample. Bitumen was found collected in the filter paper above the porous stone. The sides of the sample were light brown in colour indicating the flow of bitumen from the edge of the sample towards the porous stone.

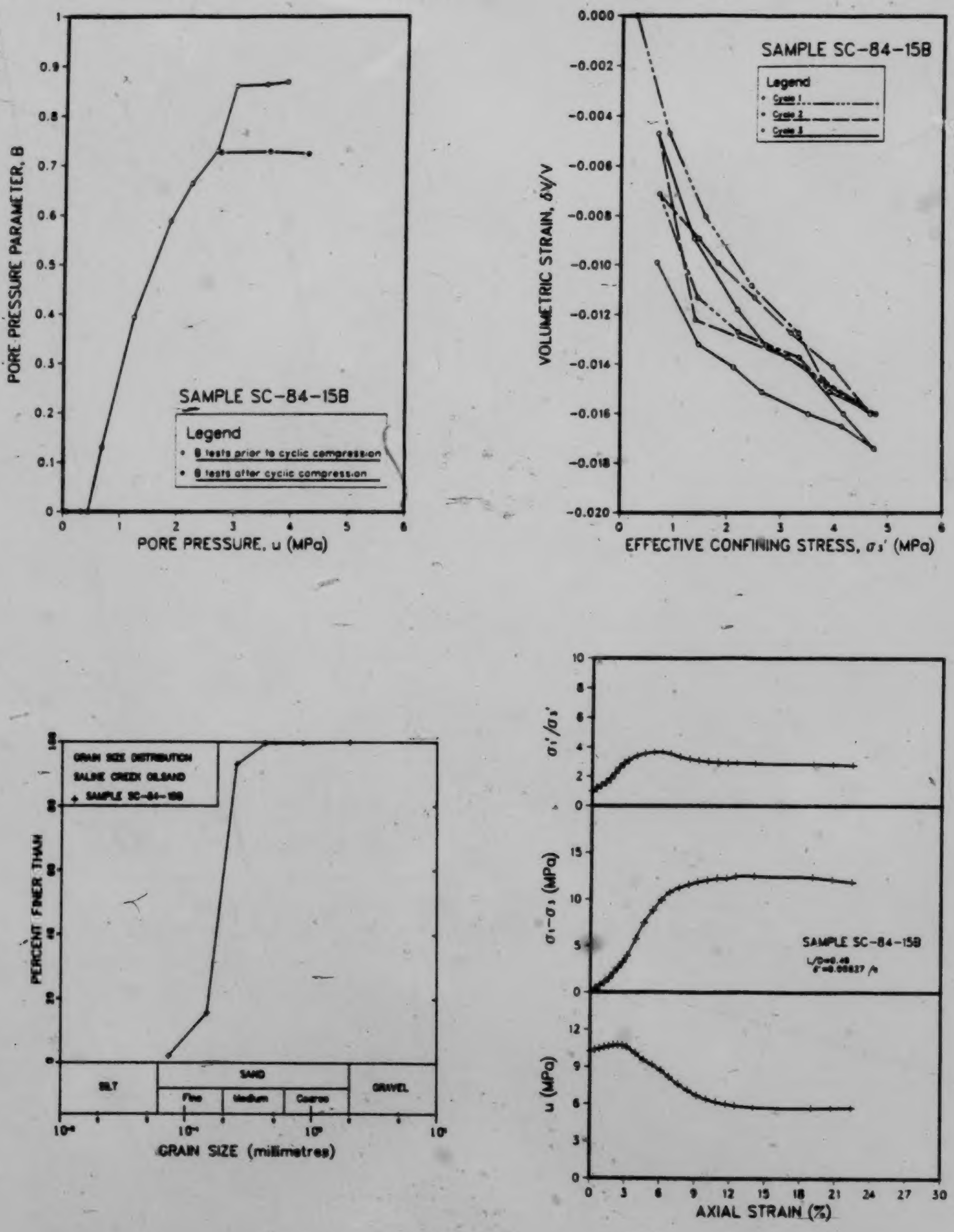

Figure C.17 SC-84-15B: Triaxial Test Results

## TEST SC-84-17: SALINE CREEK OIL SAND

### PROCEDURAL DETAILS

1. Enlarged 43.20 mm diameter loading platens were used. The faces of the platens were overlaid with two layers of greased rubber membranes.
2. The sample was thawed under cell and back pressures of 0.43 and 0.08 MPa for 2.0 hours.
3. B tests were conducted at an effective confining pressure of 0.35 MPa with incremental increases in pore pressure until saturation was reached.
4. An isotropic compressibility test was conducted with three cycles of effective confining stress up to 5 MPa. A constant pore pressure of 2.80 MPa was maintained throughout the test.
5. A second series of B tests were conducted at a confining pressure of 1.80 MPa and 4.00 MPa following the cyclic compression of the sample.
6. The sample was consolidated under back and cell pressures of 10.07 MPa and 12.37 MPa. An undrained triaxial compression test was conducted at a strain rate of $3.1 \times 10^{-2}$ $s^{-1}$.

### TEST DATA

DIAMETER = 38.22 mm
HEIGHT = 77.40 mm
WEIGHT = 174.51 g.
BULK DENSITY = 1.966 $Mg/m^3$
WATER CONTENT = 2.1 %
BITUMEN CONTENT = 16.1 %
SATURATION = 88.6 %
POROSITY = 0.393

### Comments on Sample Failure:

Shear plane developed along a bedding plane as shown in the sketch.

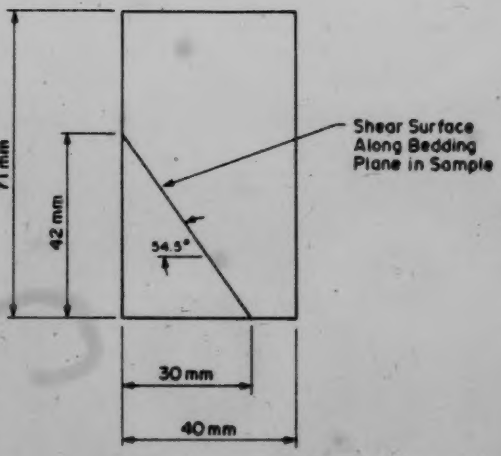

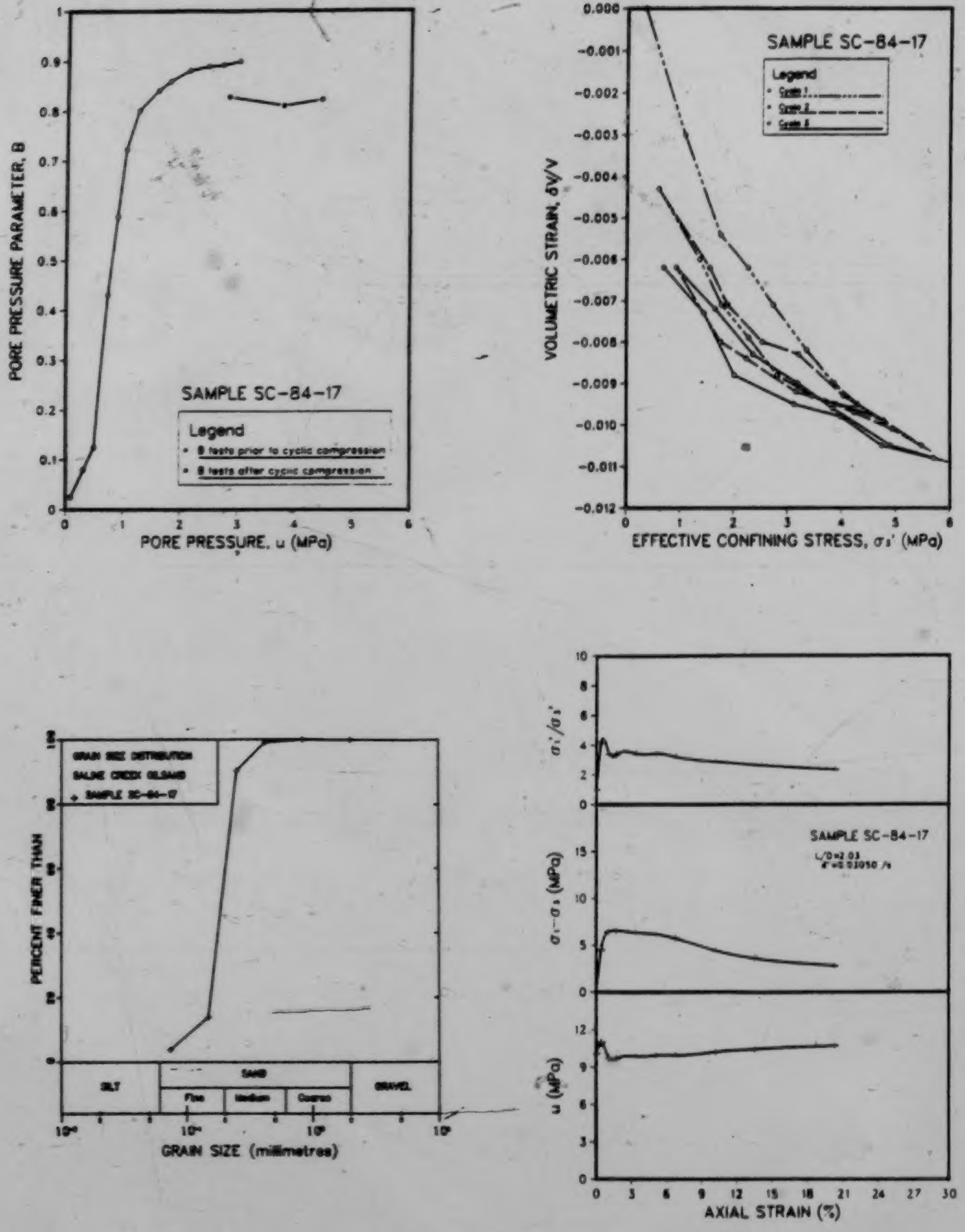

Figure C.18 SC-84-17: Triaxial Test Results

# TEST SC-84-22: SALINE CREEK OIL SAND

## PROCEDURAL DETAILS

1. Conventional 50.00 mm diameter loading platens were used.
2. The sample was thawed under cell and back pressures of 0.25 and 0.20 MPa for 12 hours.
3. B tests were conducted at an effective confining pressure of 0.07 MPa with incremental increases in pore pressure until saturation was reached.
4. An isotropic compressibility test was conducted with three cycles of effective confining stress up to 5 MPa. A constant pore pressure of 1.13 MPa was maintained throughout the test.
5. A second series of B tests were conducted at a confining pressure of 2.95 MPa following the cyclic compression of the sample.
6. The sample was consolidated under back and cell pressures of 11.46 MPa and 13.27 MPa. An undrained triaxial compression test was conducted at a strain rate of $1.9 \times 10^{-5}$ $s^{-1}$.

## TEST DATA

DIAMETER = 50.95 mm
HEIGHT = 102.50 mm
WEIGHT = 425.3 g.
BULK DENSITY = 2.035 $Mg/m^3$
WATER CONTENT = 2.8 %
BITUMEN CONTENT = 14.1 %
SATURATION = 92.7 %
POROSITY = 0.362

### Comments on Sample Failure:

A shear plane developed as shown in the sketch.

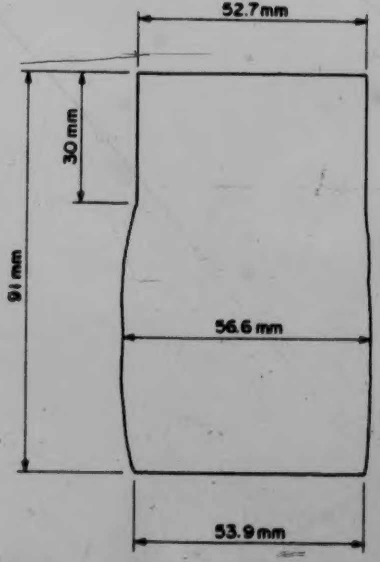

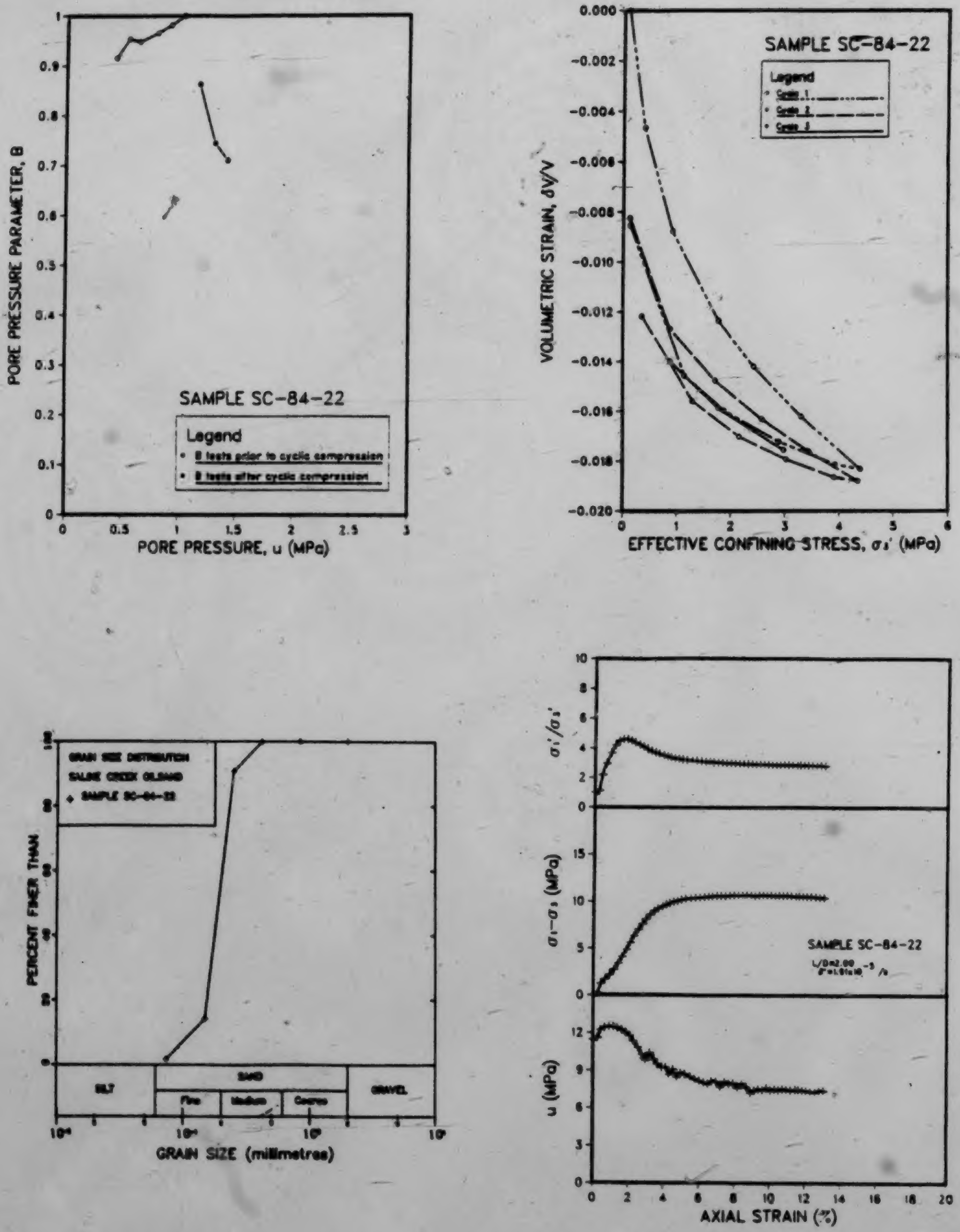

Figure C.19 SC-84-22: Triaxial Test Results

# TEST SC-84-23: SALINE CREEK OIL SAND

## PROCEDURAL DETAILS

1. Enlarged 43.20 mm diameter loading platens were used. The faces of the platens were overlaid with two layers of greased rubber membranes.
2. The sample was thawed under cell and back pressures of 0.82 and 0.34 MPa for 1.5 hours.
3. B tests were conducted at an effective confining pressure of 0.46 MPa with incremental increases in pore pressure until saturation was reached.
4. An isotropic compressibility test was conducted with three cycles of effective confining stress up to 5 MPa. A constant pore pressure of 0.75 MPa was maintained throughout the test.
5. A second series of B tests were conducted at a confining pressure of 2.40 MPa following the cyclic compression of the sample. The pore pressure response was very low and sluggish. Examination of the porous stone after testing showed the stone to be filled with bitumen. It is probable that the bitumen has also restricted volume change during the compressibility test, particularily in the last two cycles.
6. The sample was consolidated under back and cell pressures of 10.02 MPa and 11.98 MPa. An undrained triaxial compression test was conducted at a strain rate of 2.4 $s^{-1}$.

## TEST DATA

DIAMETER = 38.50 mm
HEIGHT = 21.70 mm
WEIGHT = 50.17 g.
BULK DENSITY = 1.986 Mg/$m^3$
WATER CONTENT = 3.3 %
BITUMEN CONTENT = 15.8 %
SATURATION = 93.7 %
POROSITY = 0.395

### Comments on Sample Failure:

Radial expansion occured uniformly throughout the full height of the sample.

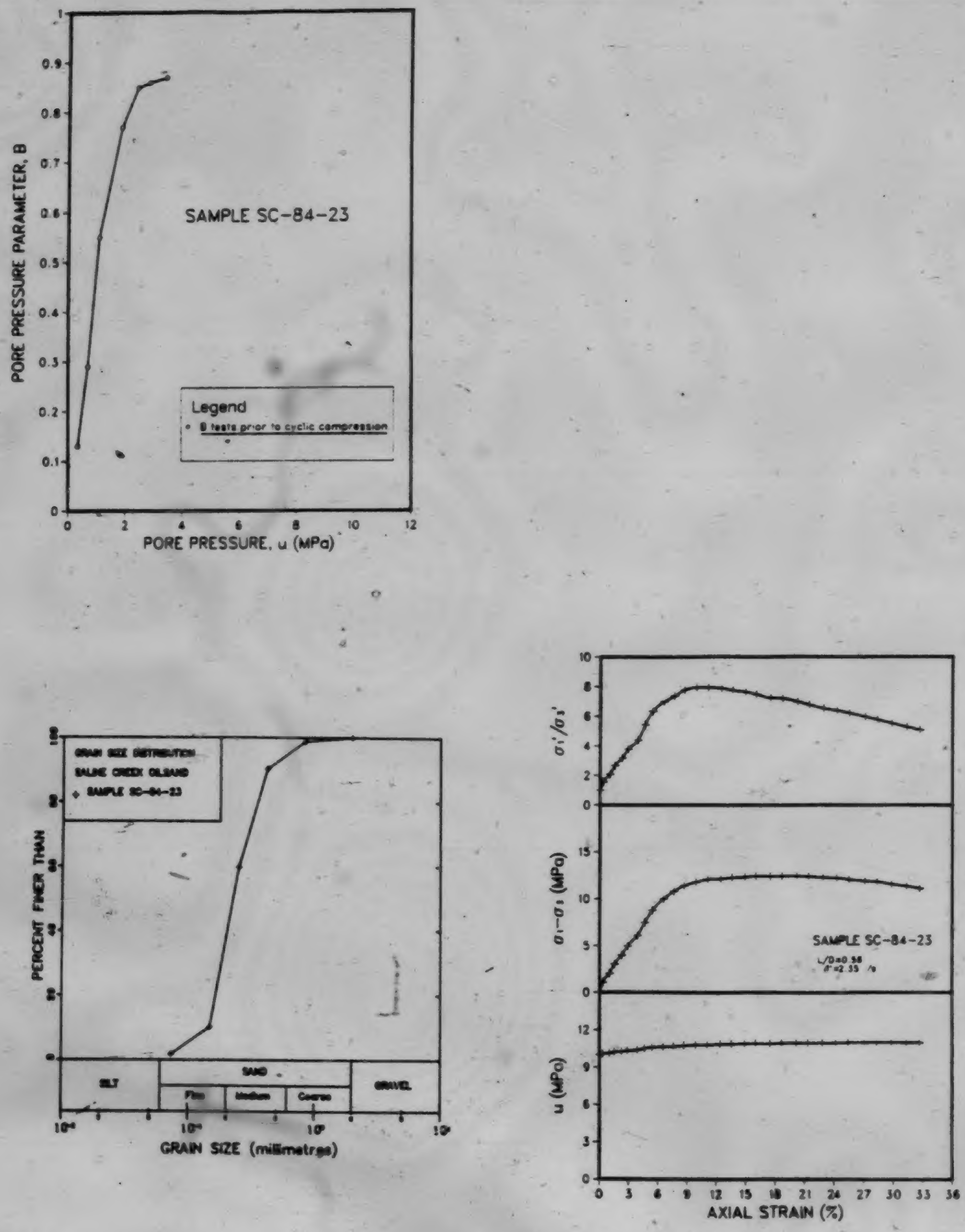

Figure C.20 SC-84-23: Triaxial Test Results

## TEST SC-84-24: SALINE CREEK OIL SAND

### PROCEDURAL DETAILS

1. Enlarged 43.20 mm diameter loading platens were used. The faces of the platens were overlaid with two layers of greased rubber membranes.
2. The sample was thawed under cell and back pressures of 0.66 and 0.37 MPa for 1.5 hours.
3. B tests were conducted at an effective confining pressure of 0.30 MPa with incremental increases in pore pressure until saturation was reached.
4. An isotropic compressibility test was conducted with three cycles of effective confining stress up to 5 MPa. A constant pore pressure of 1.70 MPa was maintained throughout the test.
5. A second series of B tests were conducted at a confining pressure of 2.20 MPa following the cyclic compression of the sample.
6. The sample was consolidated under back and cell pressures of 10.69 MPa and 12.81 MPa. An undrained triaxial compression test was conducted at a strain rate of $8.7 \times 10^{-5}$ $s^{-1}$.

### TEST DATA

DIAMETER = 38.20 mm
HEIGHT = 20.72 mm
WEIGHT = 46.45 g.
BULK DENSITY = 1.956 Mg/$m^3$
WATER CONTENT = 3.4 %
BITUMEN CONTENT = 16.2 %
SATURATION = 91.5 %
POROSITY = 0.408

#### Comments on Sample Failure:

Radial expansion occured uniformly throughout the full height of the sample.

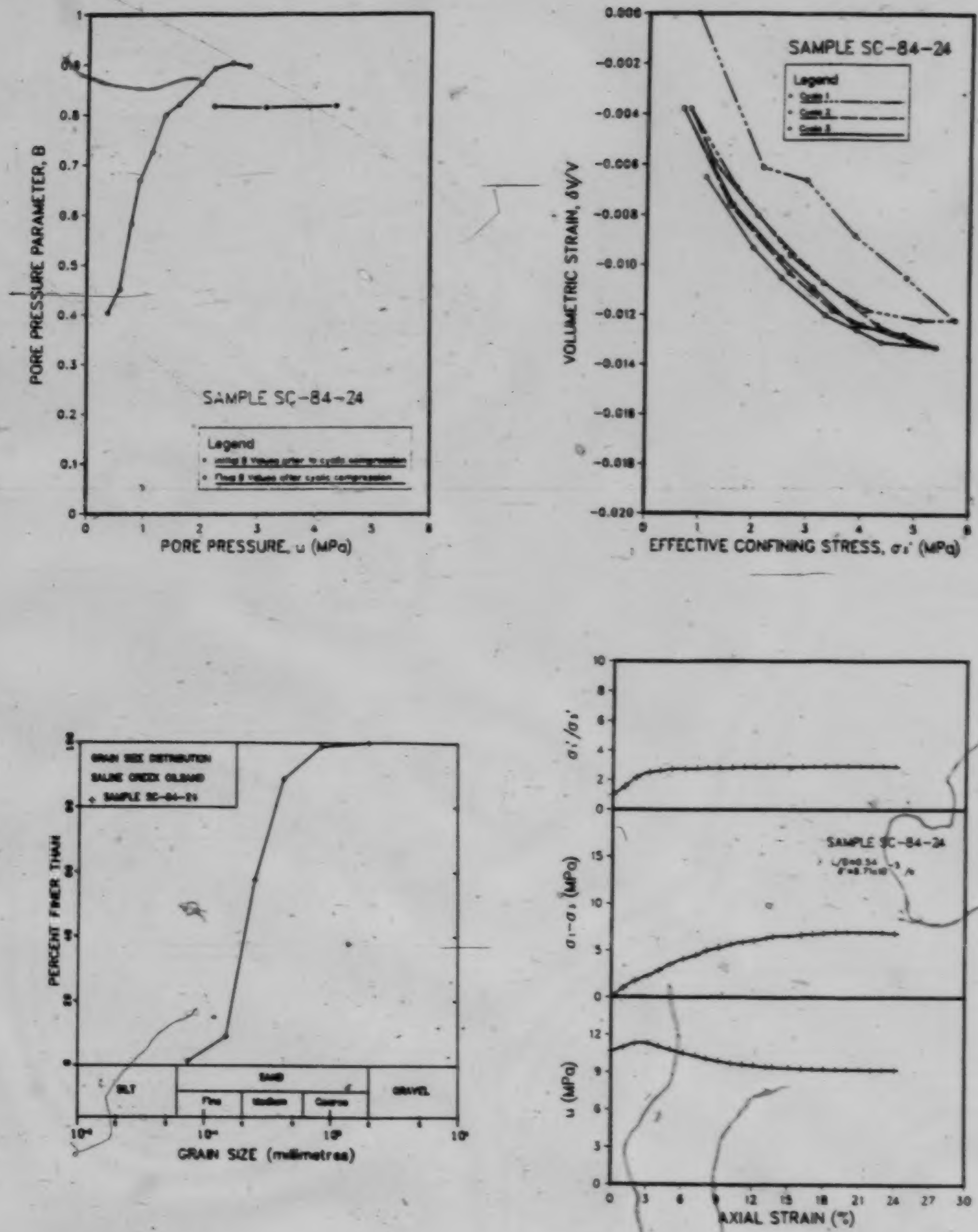

Figure C.21 SC-84-24: Triaxial Test Results

# TEST SC-84-25A: SALINE CREEK OIL SAND

## PROCEDURAL DETAILS

1. Enlarged 43.20 mm diameter loading platens were used. The faces of the platens were overlaid with two layers of greased rubber membranes.
2. The sample was thawed under cell and back pressures of 0.72 and 0.29 MPa for 2.0 hours.
3. B tests were conducted at an effective confining pressure of 0.43 MPa with incremental increases in pore pressure until saturation was reached.
4. An isotropic compressibility test was conducted with three cycles of effective confining stress up to 5 MPa. A constant pore pressure of 1.78 MPa was maintained throughout the test.
5. A second series of B tests were conducted at a confining pressure of 1.96 MPa following the cyclic compression of the sample.
6. The sample was consolidated under back and cell pressures of 10.32 MPa and 12.42 MPa. An undrained triaxial compression test was conducted at a strain rate of 8.4 x $10^{-5}$ $s^{-1}$. 5

## TEST DATA

DIAMETER = 38.00 mm
HEIGHT = 21.72 mm
WEIGHT = 49.36 g.
BULK DENSITY = 2.005 $Mg/m^3$
WATER CONTENT = 3.8 %
BITUMEN CONTENT = 12.9 %
SATURATION = 88.3 %
POROSITY = 0.370

### Comments on Sample Failure:

Radial expansion occured uniformly throughout the full height of the sample.

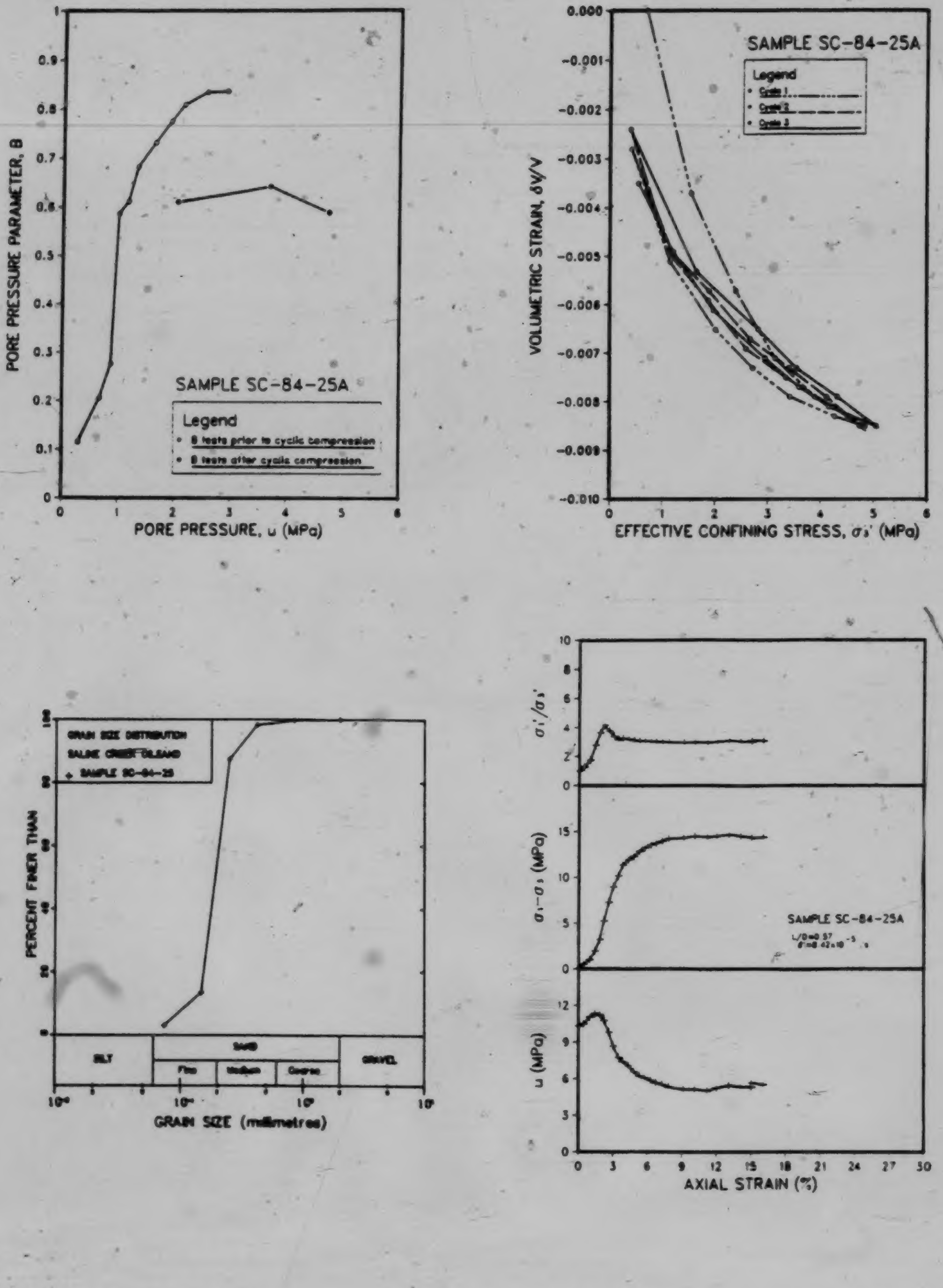

Figure C.22 SC-84-25A: Triaxial Test Results

## TEST SC-84-25B: SALINE CREEK OIL SAND

### PROCEDURAL DETAILS

1. Enlarged 43.20 mm diameter loading platens were used. The faces of the platens were overlaid with two layers of greased rubber membranes.
2. The sample was thawed under cell and back pressures of 0.77 and 0.35 MPa for 2.0 hours.
3. B tests were conducted at an effective confining pressure of 0.34 MPa with incremental increases in pore pressure until saturation was reached.
4. An isotropic compressibility test was conducted with three cycles of effective confining stress up to 5 MPa. A constant pore pressure of 1.72 MPa was maintained throughout the test.
5. A second series of B tests were conducted at a confining pressure of 2.45 MPa following the cyclic compression of the sample.
6. The sample was consolidated under back and cell pressures of 10.53 MPa and 12.63 MPa. An undrained triaxial compression test was conducted at a strain rate of $8.4 \times 10^{-5}$ $s^{-1}$.

### TEST DATA

DIAMETER = 38.00 mm
HEIGHT = 19.85 mm
WEIGHT = 45.00 g.
BULK DENSITY = 2.000 $Mg/m^3$
WATER CONTENT = 3.8 %
BITUMEN CONTENT = 12.9 %
SATURATION = 87.8 %
POROSITY = 0.371

#### Comments on Sample Failure:

Radial expansion occured uniformly throughout the full height of the sample.

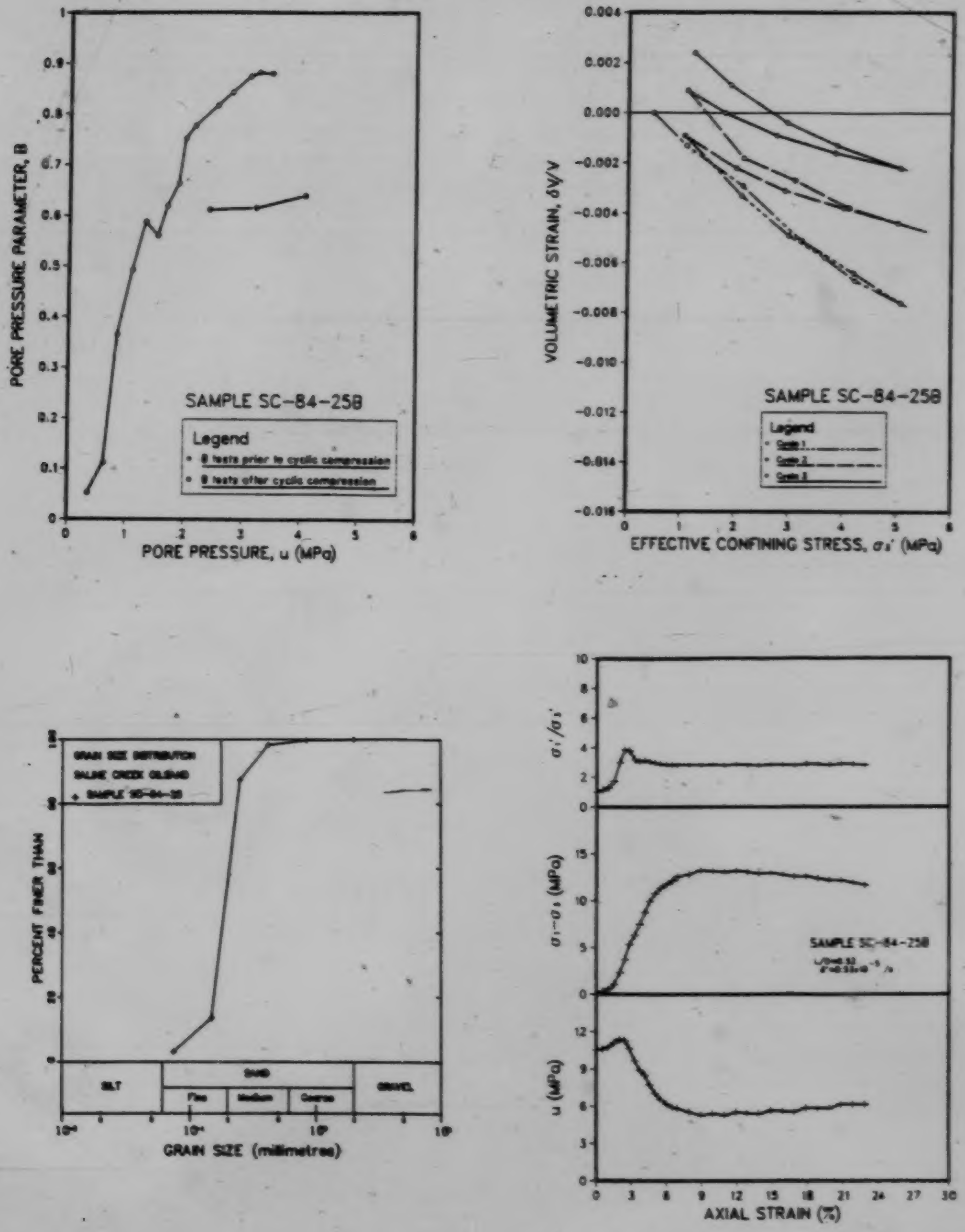

Figure C.23 SC-84-25B: Triaxial Test Results

## TEST SC-84-29: SALINE CREEK OIL SAND

### PROCEDURAL DETAILS

1. Enlarged 43.20 mm diameter loading platens were used. The faces of the platens were overlaid with two layers of greased rubber membranes.
2. The sample was thawed under cell and back pressures of 11.0 and 3.0 MPa for 20 hours.
3. B tests were conducted at an effective confining pressure of 8.0 MPa with incremental increases in pore pressure until saturation was reached.
4. The sample was consolidated under back and cell pressures of 3.23 MPa and 11.12 MPa. An undrained triaxial compression test was conducted at a strain rate of $1.1 \times 10^{-5}$ $s^{-1}$.

### TEST DATA

DIAMETER = 38.40 mm
HEIGHT = 20.73 mm
WEIGHT = 46.30 g.
BULK DENSITY = 1.929 $Mg/m^3$
WATER CONTENT = 2.0 %
BITUMEN CONTENT = 14.8 %
SATURATION = 80.1 %
POROSITY = 0.428

### Comments on Sample Failure:

Radial expansion occured uniformly throughout the full height of the sample.

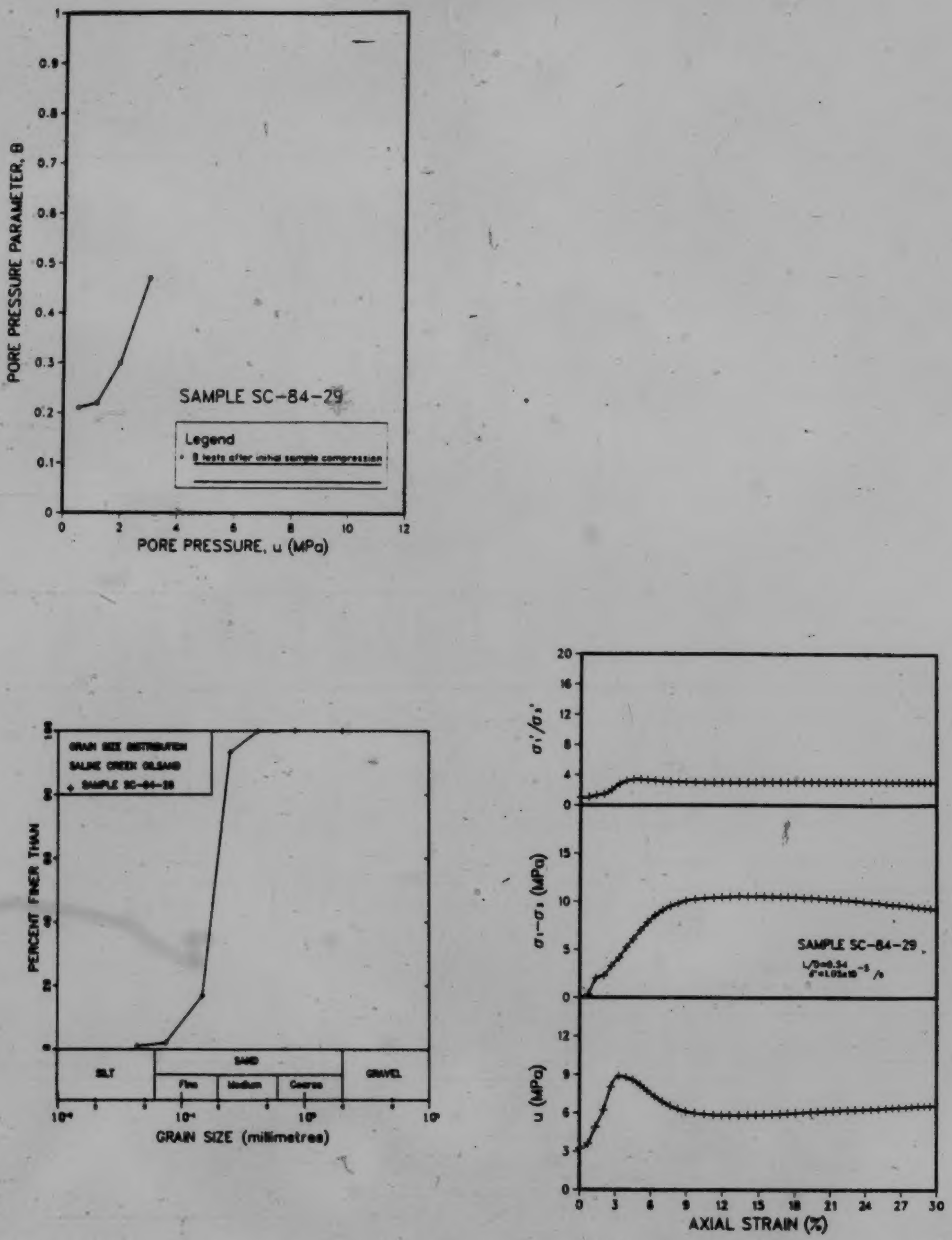

Figure C.24 SC-84-29: Triaxial Test Results

## TEST SC-84-30: SALINE CREEK OIL SAND

### PROCEDURAL DETAILS

1. Enlarged 43.20 mm diameter loading platens were used.
2. The sample was thawed under cell and back pressures of 11.2 and 3.0 MPa for 17 hours.
3. B tests were conducted at an effective confining pressure of 8.0 MPa with incremental increases in pore pressure until saturation was reached.
4. The sample was consolidated under back and cell pressures of 3.07 MPa and 11.13 MPa. An undrained triaxial compression test was conducted at a strain rate of $1.3 \times 10^{-5}$ $s^{-1}$.

### TEST DATA

DIAMETER = 38.23 mm
HEIGHT = 76.93 mm
WEIGHT = 170.80 g.
BULK DENSITY = 1.934 $Mg/m^3$
WATER CONTENT = 4.0 %
BITUMEN CONTENT = 13.9 %
SATURATION = 84.4 %
POROSITY = 0.428

#### Comments on Sample Failure:

A shear plane developed as shown in the sketch.

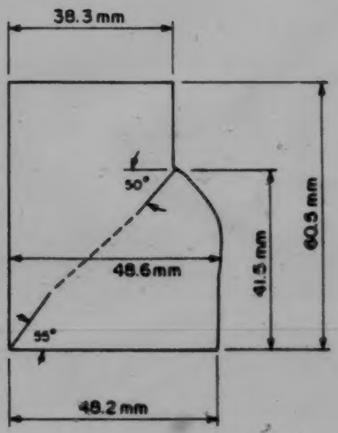

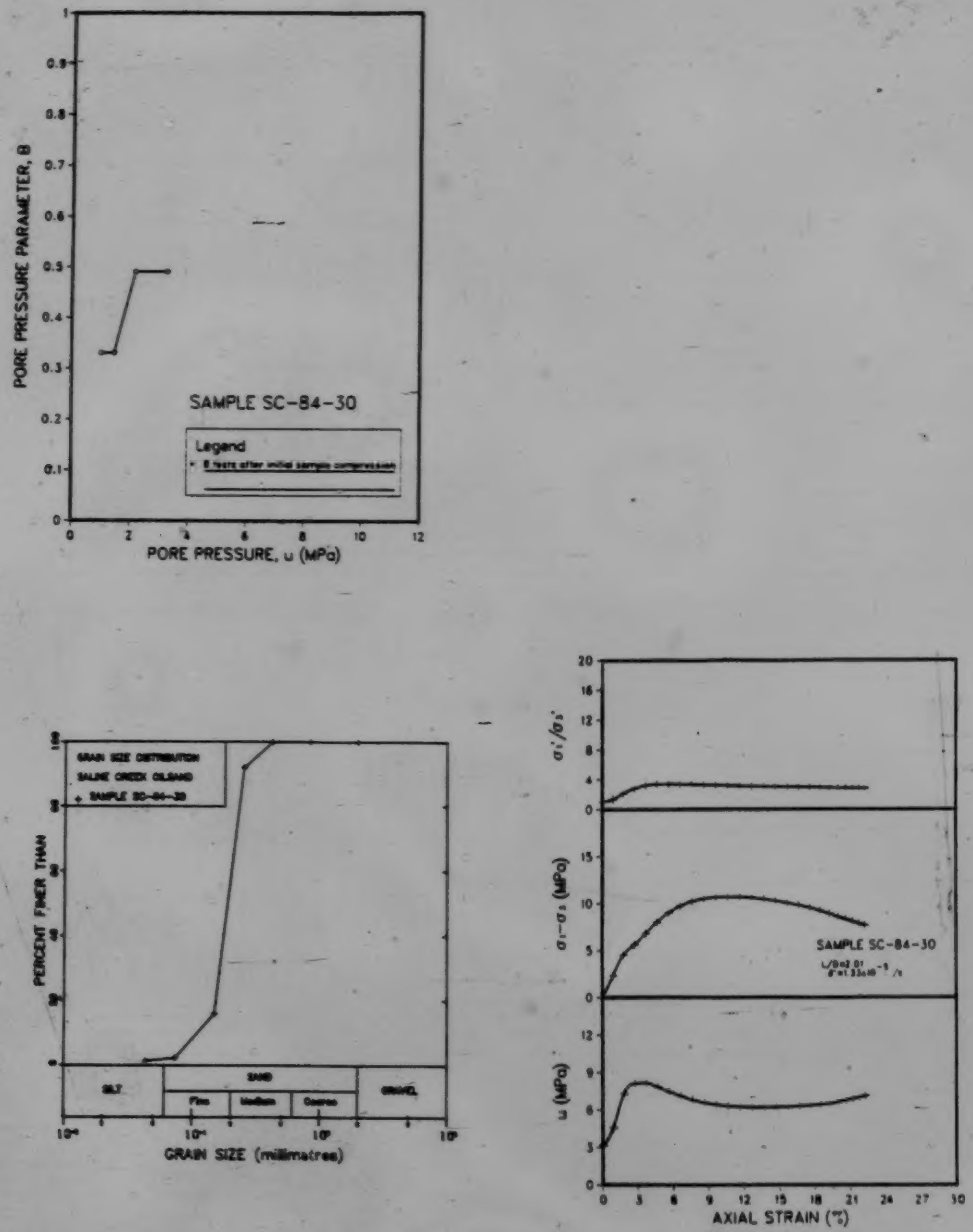

Figure C.25 SC-84-30: Triaxial Test Results

# TEST SC-84-31: SALINE CREEK OIL SAND

## PROCEDURAL DETAILS

1. Enlarged 43.20 mm diameter loading platens were used. The faces of the platens were overlaid with two layers of greased rubber membranes.
2. The sample was thawed under cell and back pressures of 5.65 and 0.65 MPa for 16 hours.
3. B tests were conducted at an effective confining pressure of 1.0 MPa with incremental increases in pore pressure until saturation was reached.
4. The sample was consolidated under back and cell pressures of 6.31 MPa and 11.31 MPa. An undrained triaxial compression test was conducted at a strain rate of 1.30 $s^{-1}$.

## TEST DATA

DIAMETER = 38.65 mm
HEIGHT = 17.40 mm
WEIGHT = 39.40 g.
BULK DENSITY = 1.930 $Mg/m^3$
WATER CONTENT = 2.3 %
BITUMEN CONTENT = 16.4 %
SATURATION = 86.3 %
POROSITY = 0.408

### Comments on Sample Failure:

Radial expansion occured uniformly throughout the full height of the sample.

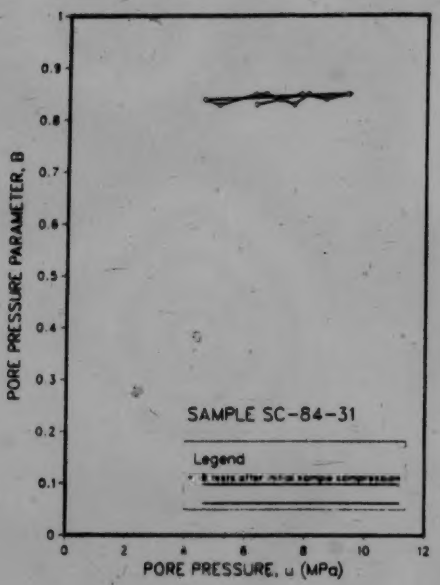

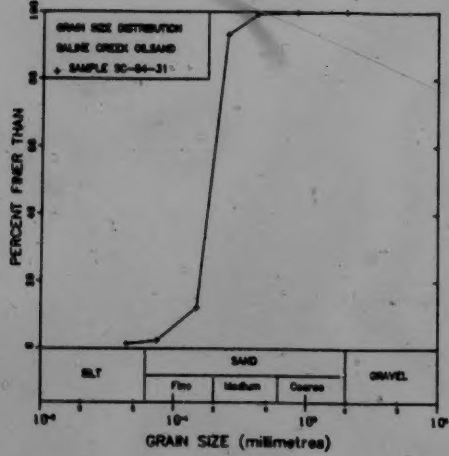

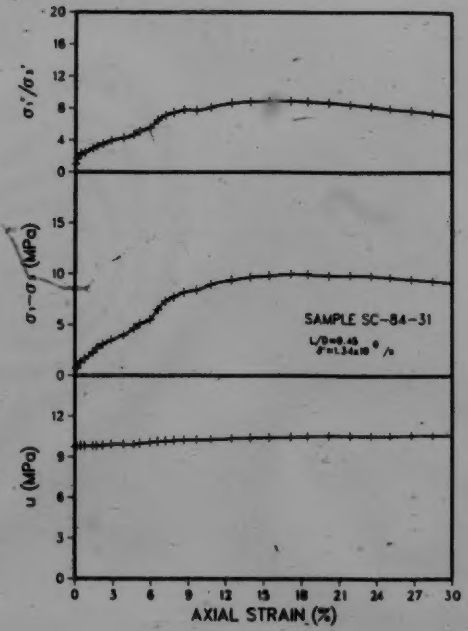

Figure C.26 SC-84-31: Triaxial Test Results

## TEST SC-84-33: SALINE CREEK OIL SAND

### PROCEDURAL DETAILS

1. Enlarged 43.20 mm diameter loading platens were used. The faces of the platens were overlaid with two layers of greased rubber membranes.
2. The sample was thawed under cell and back pressures of 5.65 and 0.65 MPa for 20 hours.
3. B tests were conducted at an effective confining pressure of 5.0 MPa with incremental increases in pore pressure until saturation was reached.
4. The sample was consolidated under back and cell pressures of 9.72 MPa and 10.76 MPa. An undrained triaxial compression test was conducted at a strain rate of 1.1 x $10^{-4}$ $s^{-1}$.

### TEST DATA

DIAMETER = 38.70 mm
HEIGHT = 19.94 mm
WEIGHT = 47.03 g.
BULK DENSITY = 2.005 $Mg/m^3$
WATER CONTENT = 3.9 %
BITUMEN CONTENT = 13.7 %
SATURATION = 91.6 %
POROSITY = 0.377

### Comments on Sample Failure:

Radial expansion occured uniformly throughout the full height of the sample.

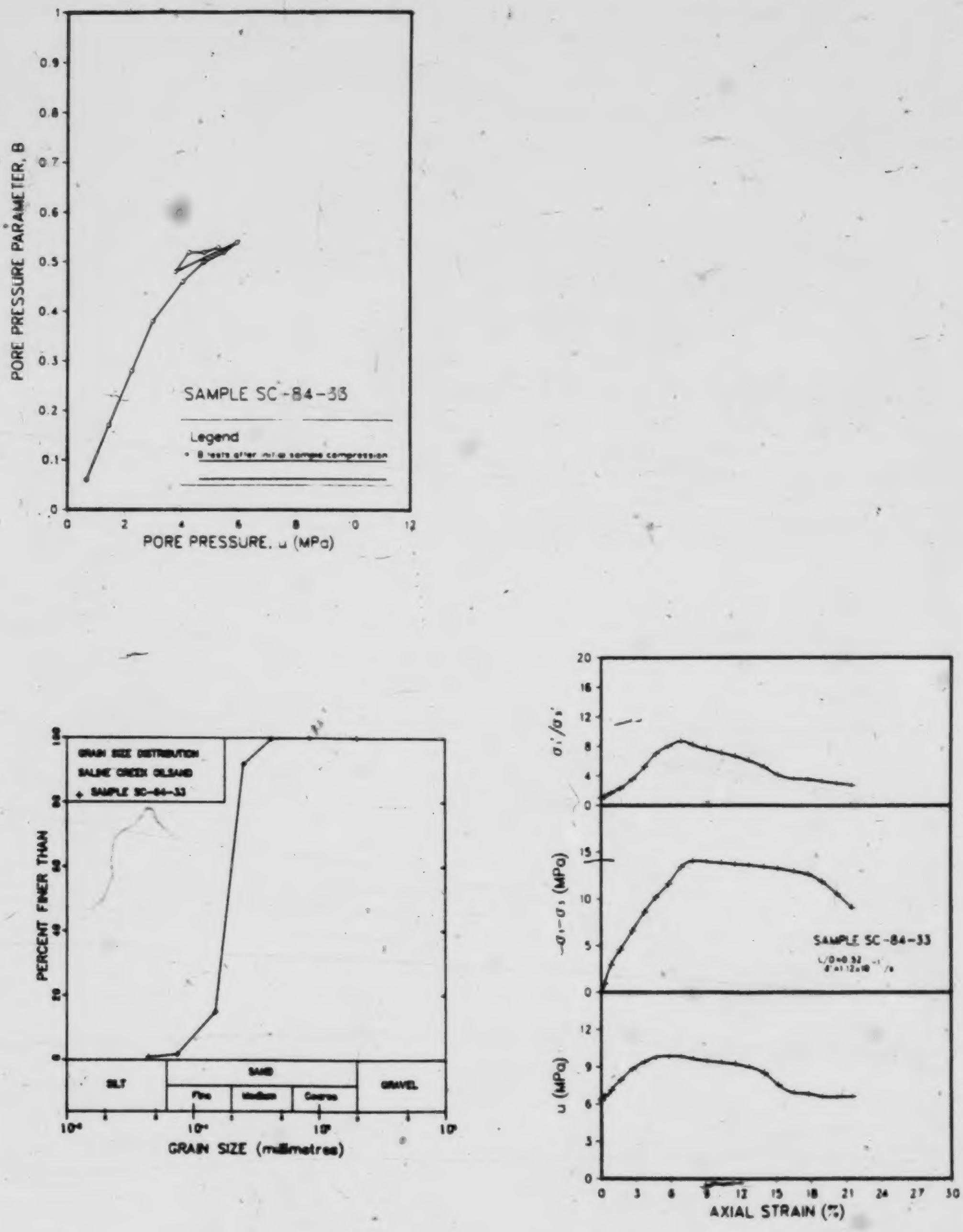

Figure C.27 SC-84-33: Triaxial Test Results

## TEST SC-84-34: SALINE CREEK OIL SAND

### PROCEDURAL DETAILS

1. Enlarged 43.20 mm diameter loading platens were used.
2. The sample was thawed under cell and back pressures of 5.82 and 0.82 MPa for 66 hours.
3. B tests were conducted at an effective confining pressure of 5.05 MPa with incremental increases in pore pressure until saturation was reached.
4. The sample was consolidated under back and cell pressures of 6.49 MPa and 11.50 MPa. An undrained triaxial compression test was conducted at a strain rate of $9.6 \times 10^{-4}$ $s^{-1}$.

### TEST DATA

DIAMETER = 38.50 mm
HEIGHT = 67.51 mm
WEIGHT = 162.08 g.
BULK DENSITY = 2.061 Mg/$m^3$
WATER CONTENT = 1.9 %
BITUMEN CONTENT = 14.8 %
SATURATION = 95.4 %
POROSITY = 0.358

### Comments on Sample Failure:

A shear plane developed as shown in the sketch.

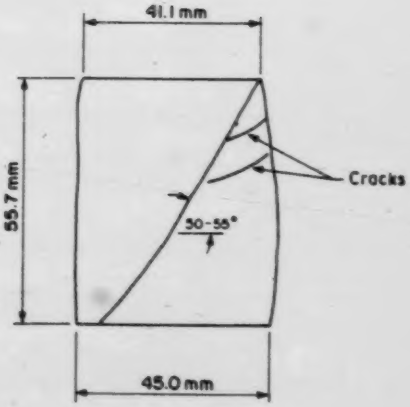

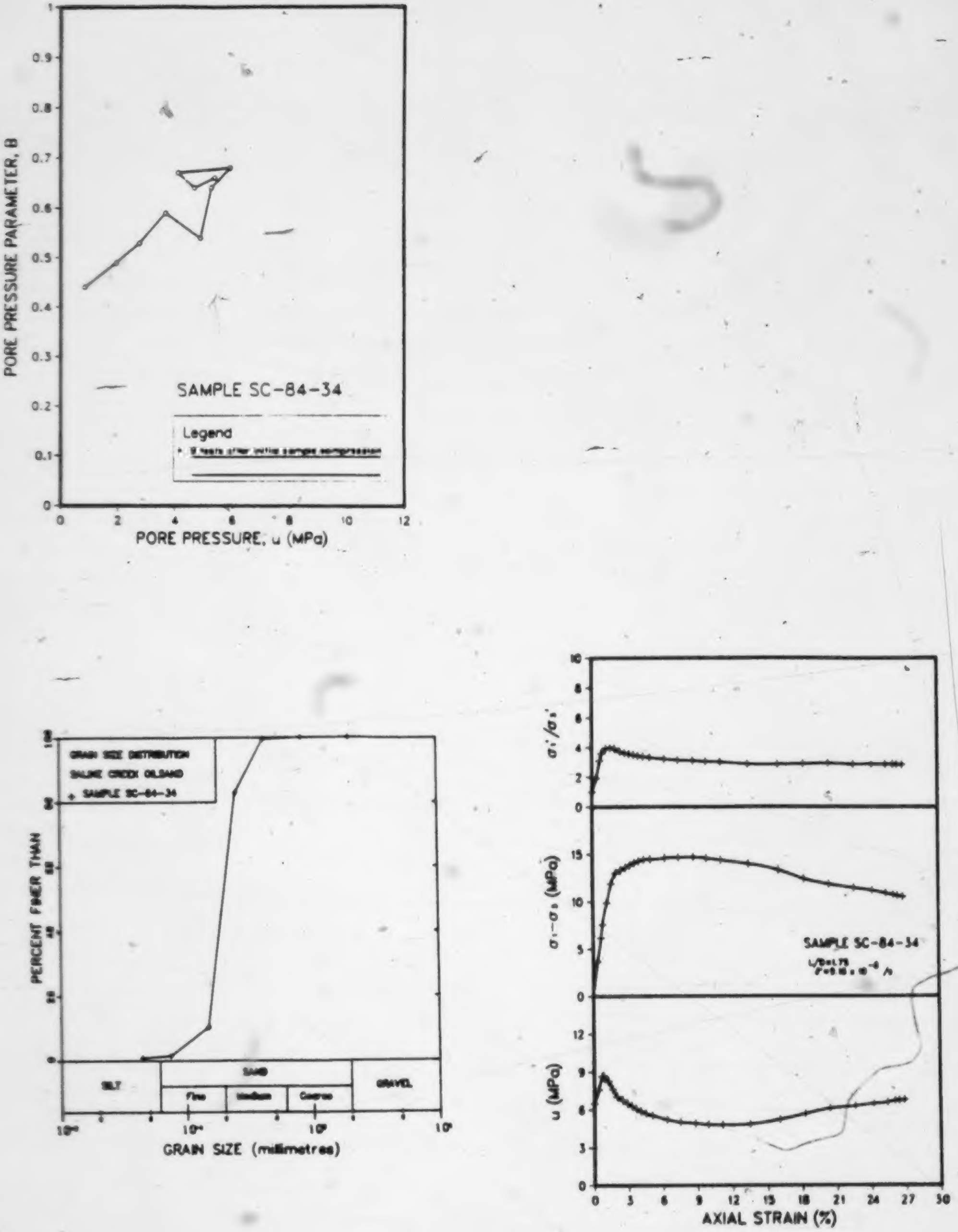

Figure C.28 SC-84-34: Triaxial Test Results

## TEST SC-84-39: SALINE CREEK OIL SAND

### PROCEDURAL DETAILS

1. Conventional 50.00 mm diameter loading platens were used.
2. The sample was thawed under cell and back pressures of 0.25 and 0.20 MPa for 12 hours.
3. B tests were conducted at an effective confining pressure of 0.15 MPa with incremental increases in pore pressure until saturation was reached.
4. An isotropic compressibility test was conducted with three cycles of effective confining stress up to 5 MPa. A constant pore pressure of 1.20 MPa was maintained throughout the test.
5. A second series of B tests were conducted at a confining pressure of 2.10 MPa following the cyclic compression of the sample.
6. The sample was consolidated under back and cell pressures of 4.46 MPa and 4.54 MPa. An undrained triaxial compression test was conducted at a strain rate of $1.8 \times 10^{-5}$ $s^{-1}$.

### TEST DATA

DIAMETER = 50.98 mm
HEIGHT = 102.10 mm
WEIGHT = 424.0 g.
BULK DENSITY = 2.034 $Mg/m^3$
WATER CONTENT = 1.4 %
BITUMEN CONTENT = 15.8 %
SATURATION = 94.0 %
POROSITY = 0.364

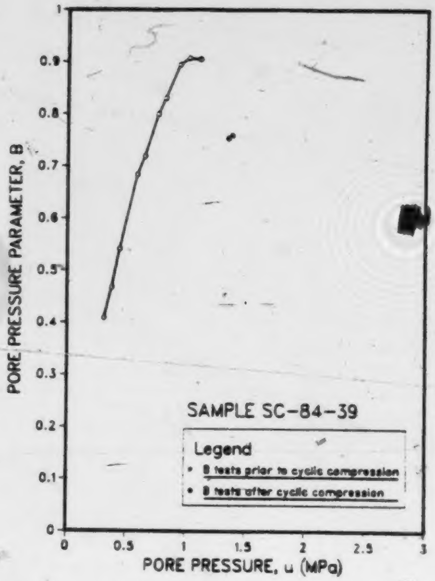

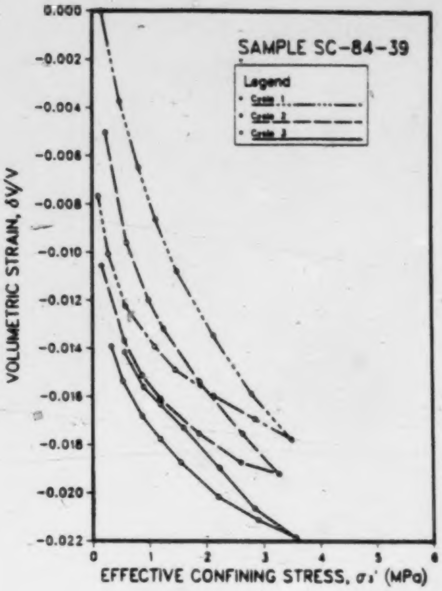

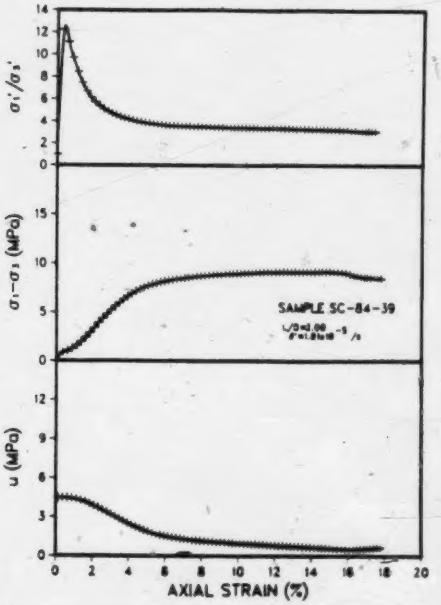

Figure C.29 SC-84-39: Triaxial Test Results

## TEST SC-84-40A: SALINE CREEK OIL SAND

### PROCEDURAL DETAILS

1. Enlarged 43.20 mm diameter loading platens were used. The faces of the platens were overlaid with two layers of greased rubber membranes.
2. The sample was thawed under cell and back pressures of 5.85 and 0.85 MPa for 2.5 hours.
3. B tests were conducted at an effective confining pressure of 5.0 MPa with incremental increases in pore pressure until saturation was reached.
4. The sample was consolidated under back and cell pressures of 7.20 MPa and 12.03 MPa. An undrained triaxial compression test was conducted at a strain rate of $1.5 \times 10^{-5}$ $s^{-1}$.

### TEST DATA

DIAMETER = 39.00 mm
HEIGHT = 18.83 mm
WEIGHT = 44.16 g.
BULK DENSITY = 1.963 $Mg/m^3$
WATER CONTENT = 2.6 %
BITUMEN CONTENT = 15.8 %
SATURATION = 89.1 %
POROSITY = 0.395

### Comments on Sample Failure:

Radial expansion occured uniformly throughout the full height of the sample.

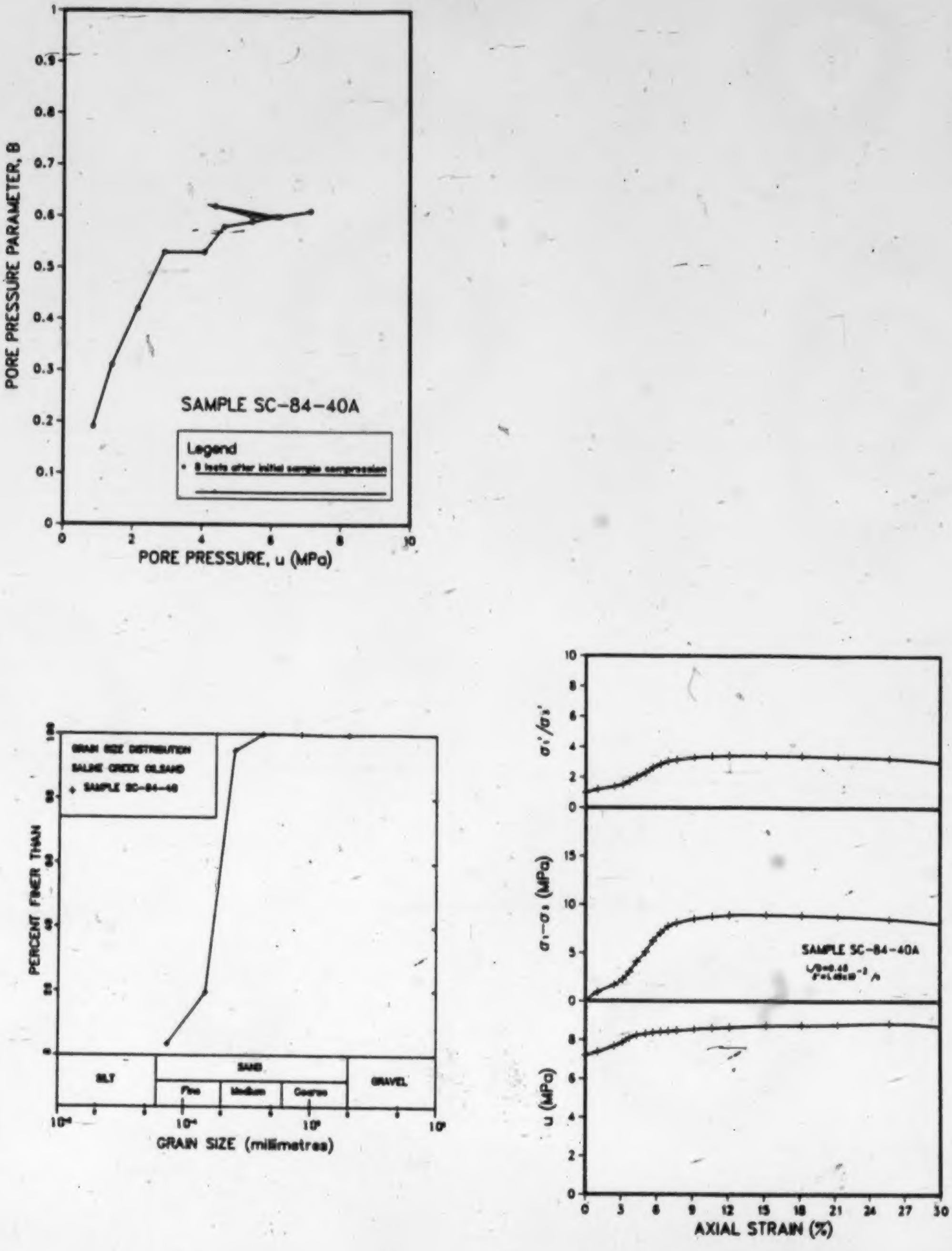

Figure C.30 SC-84-40A: Triaxial Test Results

## TEST SC-84-40B: SALINE CREEK OIL SAND

### PROCEDURAL DETAILS

1. Enlarged 43.20 mm diameter loading platens were used. The faces of the platens were overlaid with two layers of greased rubber membranes.
2. The sample was thawed under cell and back pressures of 5.70 and 0.78 MPa for 17 hours.
3. B tests were conducted at an effective confining pressure of 5.0 MPa with incremental increases in pore pressure until saturation was reached. The pore pressure response was very sluggish. Examination of the porous stone after testing showed the stone to contain bitumen.
4. The sample was consolidated under back and cell pressures of 4.83 MPa and 9.87 MPa. An undrained triaxial compression test was conducted at a strain rate of $1.3 \times 10^{-2}$ $s^{-1}$.

### TEST DATA

DIAMETER = 38.95 mm
HEIGHT = 20.53 mm
WEIGHT = 48.59 g.
BULK DENSITY = 1.987 $Mg/m^3$
WATER CONTENT = 2.6 %
BITUMEN CONTENT = 15.8 %
SATURATION = 91.7 %
POROSITY = 0.388

#### Comments on Sample Failure:

Radial expansion occured uniformly throughout the full height of the sample.

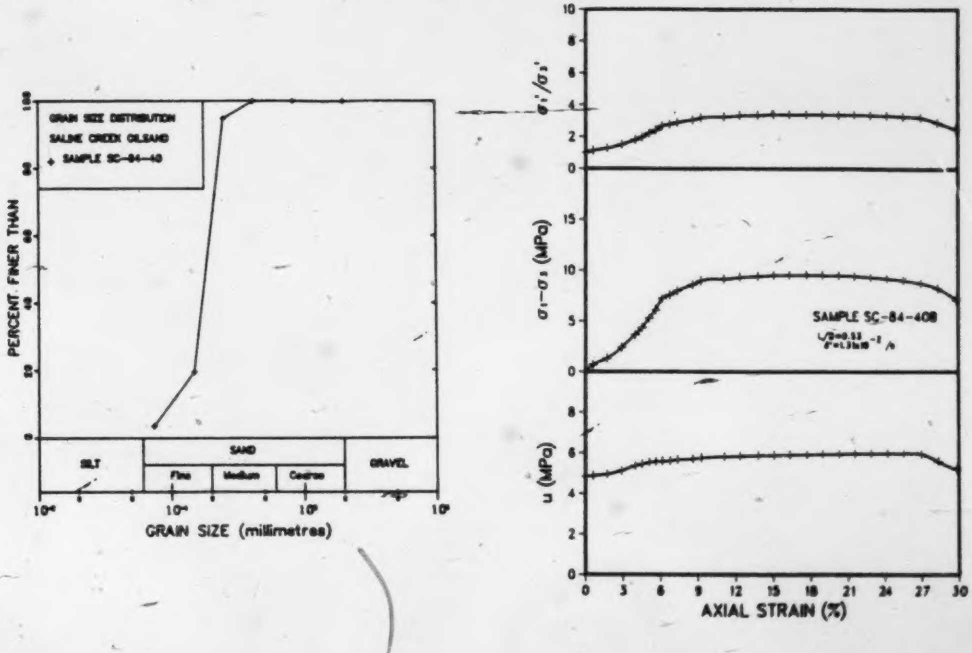

Figure C.31 SC-84-40B: Triaxial Test Results

## TEST SC-84-43: SALINE CREEK OIL SAND

### PROCEDURAL DETAILS

1. Enlarged 43.20 mm diameter loading platens were used. The faces of the platens were overlaid with two layers of greased rubber membranes.
2. The sample was thawed under cell and back pressures of 5.90 and 0.92 MPa for 18 hours.
3. B tests were conducted at an effective confining pressure of 1.0 MPa with incremental increases in pore pressure until saturation was reached. The pore pressure response was very sluggish. Examination of the porous stone after testing showed the stone to contain bitumen.
4. The sample was consolidated under back and cell pressures of 9.48 MPa and 10.40 MPa. An undrained triaxial compression test was conducted at a strain rate of $1.3 \times 10^{-8}$ $s^{-1}$.

### TEST DATA

DIAMETER = 38.45 mm
HEIGHT = 19.78 mm
WEIGHT = 44.85 g.
BULK DENSITY = 1.953 $Mg/m^3$
WATER CONTENT = 2.9 %
BITUMEN CONTENT = 17.4 %
SATURATION = 94.0 %
POROSITY = 0.411

### Comments on Sample Failure:

Radial expansion occured uniformly throughout the full height of the sample.

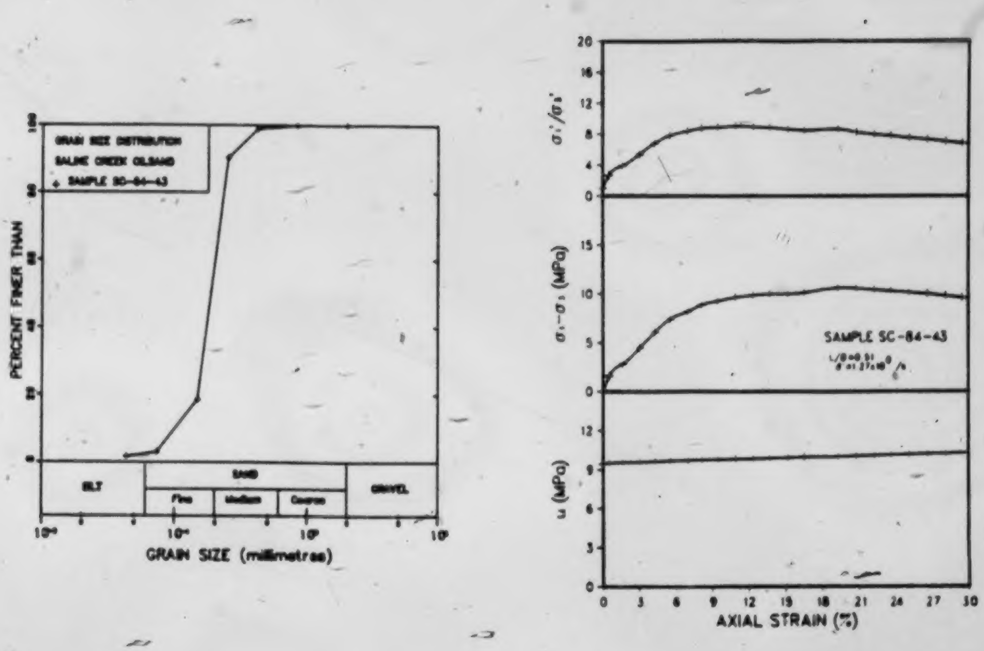

Figure C.32 SC-84-43: Triaxial Test Results

## TEST SC-84-49: SALINE CREEK OIL SAND

### PROCEDURAL DETAILS

1. Enlarged 43.20 mm diameter loading platens were used. The faces of the platens were overlaid with two layers of greased rubber membranes.
2. The sample was thawed under cell and back pressures of 5.52 and 0.52 MPa for 10 hours.
3. B tests were conducted at an effective confining pressure of 5.0 MPa with incremental increases in pore pressure until saturation was reached.
4. The sample was consolidated under back and cell pressures of 5.59 MPa and 10.44 MPa. An undrained triaxial compression test was conducted at a strain rate of 1.60 $s^{-1}$.

### TEST DATA

DIAMETER = 38.50 mm
HEIGHT = 19.30 mm
WEIGHT = 42.45 g.
BULK DENSITY = 1.890 $Mg/m^3$
WATER CONTENT = 3.1 %
BITUMEN CONTENT = 14.4 %
SATURATION = 78.6 %
POROSITY = 0.451

### Comments on Sample Failure:

Radial expansion occured uniformly throughout the full height of the sample.

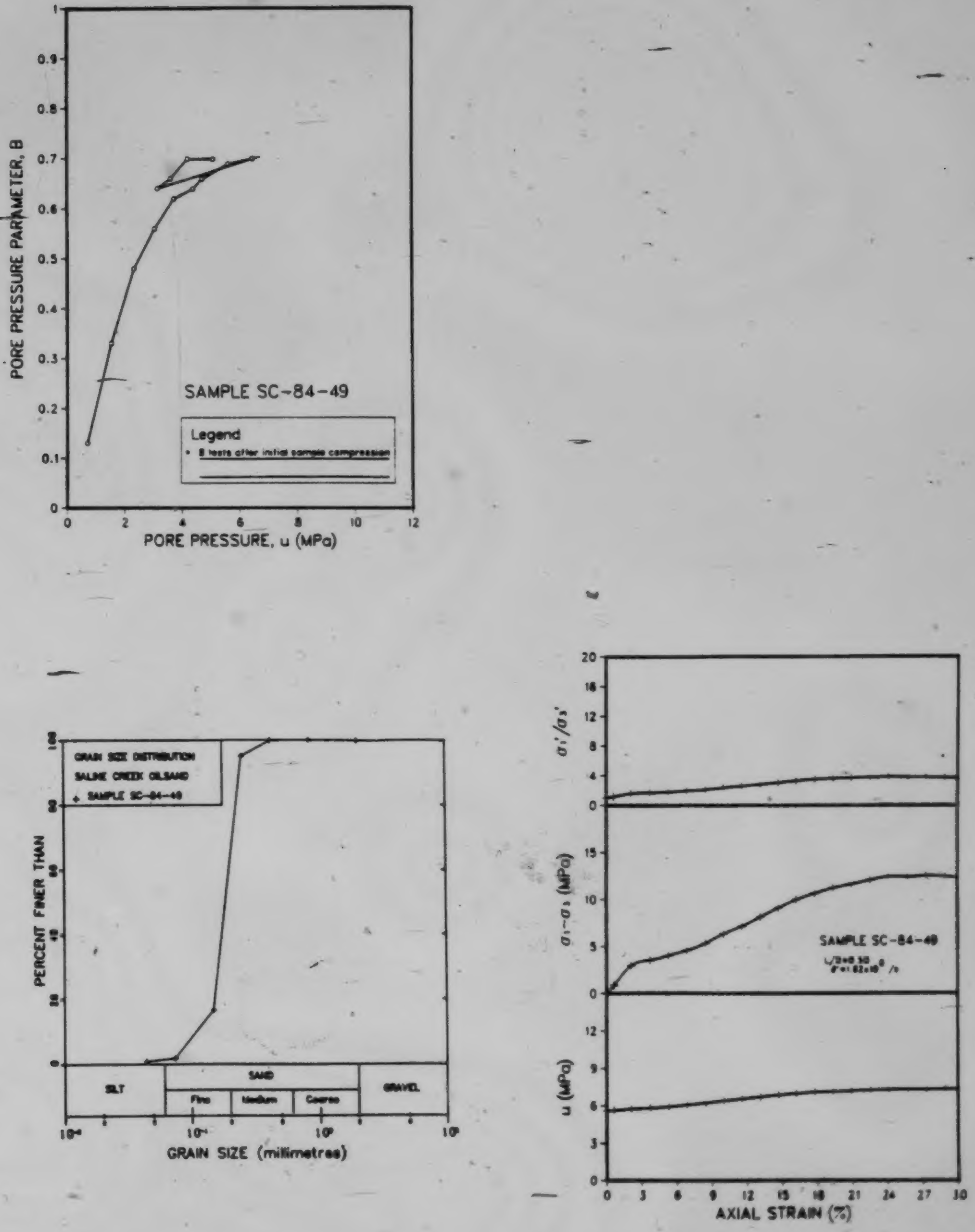

Figure C.33 SC-84-49: Triaxial Test Results

# TEST SC-84-51: SALINE CREEK OIL SAND

## PROCEDURAL DETAILS

1. Enlarged 43.20 mm diameter loading platens were used. The faces of the platens were overlaid with two layers of greased rubber membranes.
2. The sample was thawed under cell and back pressures of 5.52 and 0.52 MPa for 18 hours.
3. B tests were conducted at an effective confining pressure of 1.00 MPa with incremental increases in pore pressure until saturation was reached.
4. Test data for undrained triaxial compression test not recorded due to mis-triggering of data recorder.

## TEST DATA

DIAMETER = 38.47 mm
HEIGHT = 20.16 mm
WEIGHT = 45.61 g.
BULK DENSITY = 1.947 Mg/m$^3$
WATER CONTENT = 1.6 %
BITUMEN CONTENT = 16.9 %
SATURATION = 87.3 %
POROSITY = 0.423

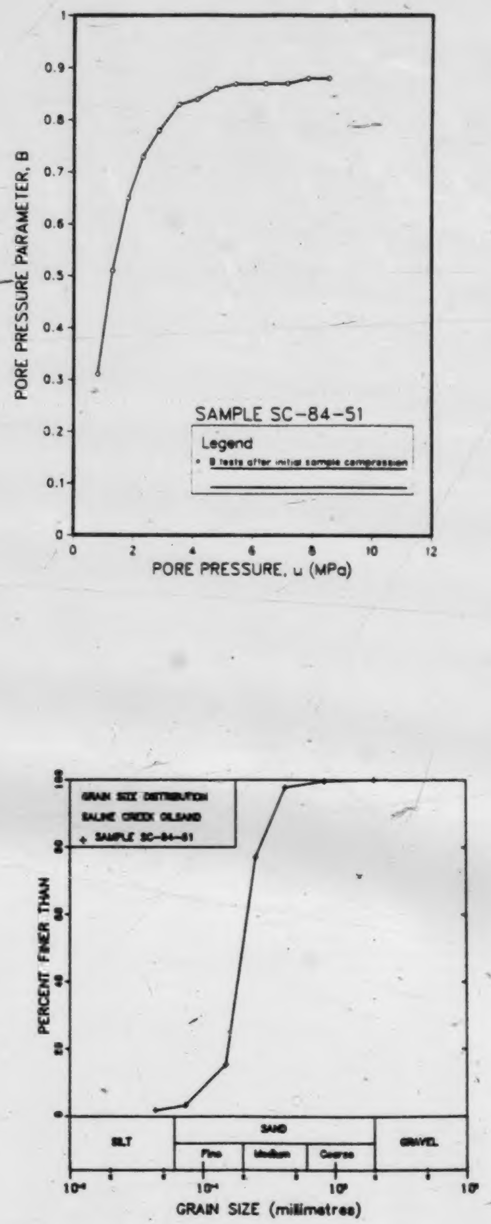

Figure C.34 SC-84-51: Triaxial Test Results

## TEST SC-84-52: SALINE CREEK OIL SAND

### PROCEDURAL DETAILS

1. Enlarged 43.20 mm diameter loading platens were used. The faces of the platens were overlaid with two layers of greased rubber membranes.
2. The sample was thawed under cell and back pressures of 5.67 and 0.67 MPa for 17 hours.
3. B tests were conducted at an effective confining pressure of 5.00 MPa with incremental increases in pore pressure until saturation was reached.
4. The sample was consolidated under back and cell pressures of 5.58 MPa and 10.63 MPa. An undrained triaxial compression test was conducted at a strain rate of 1.50 $s^{-1}$.

### TEST DATA

DIAMETER = 38.55 mm
HEIGHT = 19.68 mm
WEIGHT = 46.58 g.
BULK DENSITY = 2.027 $Mg/m^3$
WATER CONTENT = 4.2 %
BITUMEN CONTENT = 9.4 %
SATURATION = 79.7 %
POROSITY = 0.364

### Comments on Sample Failure:

Radial expansion occured uniformly throughout the full height of the sample.

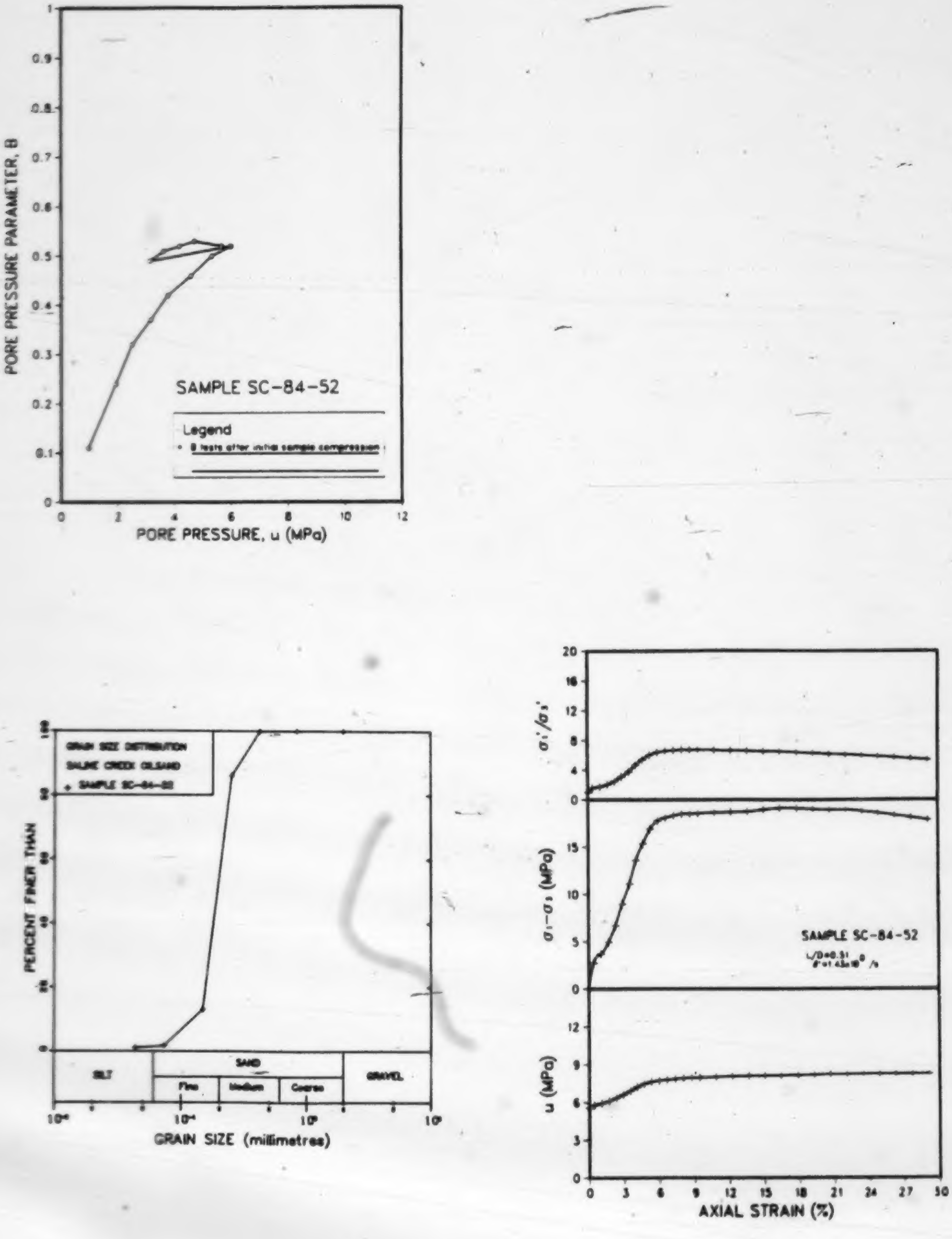

Figure C.35 SC-84-52: Triaxial Test Results

# TEST SC-84-53: SALINE CREEK OIL SAND

## PROCEDURAL DETAILS

1. Enlarged 43.20 mm diameter loading platens were used. The faces of the platens were overlaid with two layers of greased rubber membranes.
2. The sample was thawed under cell and back pressures of 8.35 and 0.35 MPa for 15 hours.
3. B tests were conducted at an effective confining pressure of 8.0 MPa with incremental increases in pore pressure. The pore pressure response was very low and sluggish. Examination of the porous stone after testing showed the stone to contain bitumen.
4. The sample was consolidated under back and cell pressures of 3.07 MPa and 11.08 MPa. An undrained triaxial compression test was conducted at a strain rate of $1.1 \times 10^{-5}$ $s^{-1}$.

## TEST DATA

DIAMETER = 38.52 mm
HEIGHT = 19.75 mm
WEIGHT = 44.80 g.
BULK DENSITY = 1.947 $Mg/m^3$
WATER CONTENT = 2.7 %
BITUMEN CONTENT = 17.8 %
SATURATION = 93.5 %
POROSITY = 0.427

### Comments on Sample Failure:

Radial expansion occured uniformly throughout the full height of the sample.

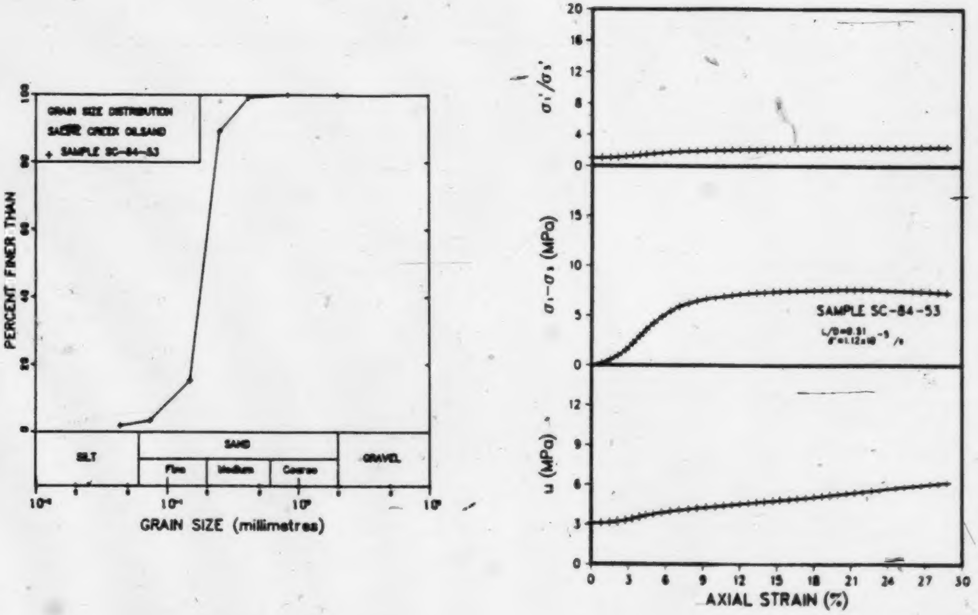

Figure C.36 SC-84-53: Triaxial Test Results

# TEST SC-84-55A: SALINE CREEK OIL SAND

## PROCEDURAL DETAILS

1. Enlarged 43.20 mm diameter loading platens were used. The faces of the platens were overlaid with two layers of greased rubber membranes.
2. The sample was thawed under cell and back pressures of 5.56 and 0.72 MPa for 1.2 hours.
3. B tests were conducted at an effective confining pressure of 2.00 MPa with incremental increases in pore pressure until saturation was reached.
4. The sample was consolidated under back and cell pressures of 10.38 MPa and 12.45 MPa. An undrained triaxial compression test was conducted at a strain rate of 2.90 $s^{-1}$.

## TEST DATA

DIAMETER = 38.65 mm
HEIGHT = 18.19 mm
WEIGHT = 41.91 g.
BULK DENSITY = 1.964 $Mg/m^3$
WATER CONTENT = 2.4 %
BITUMEN CONTENT = 16.3 %
SATURATION = 90.1 %
POROSITY = 0.398

### Comments on Sample Failure:

Radial expansion occured uniformly throughout the full height of the sample.

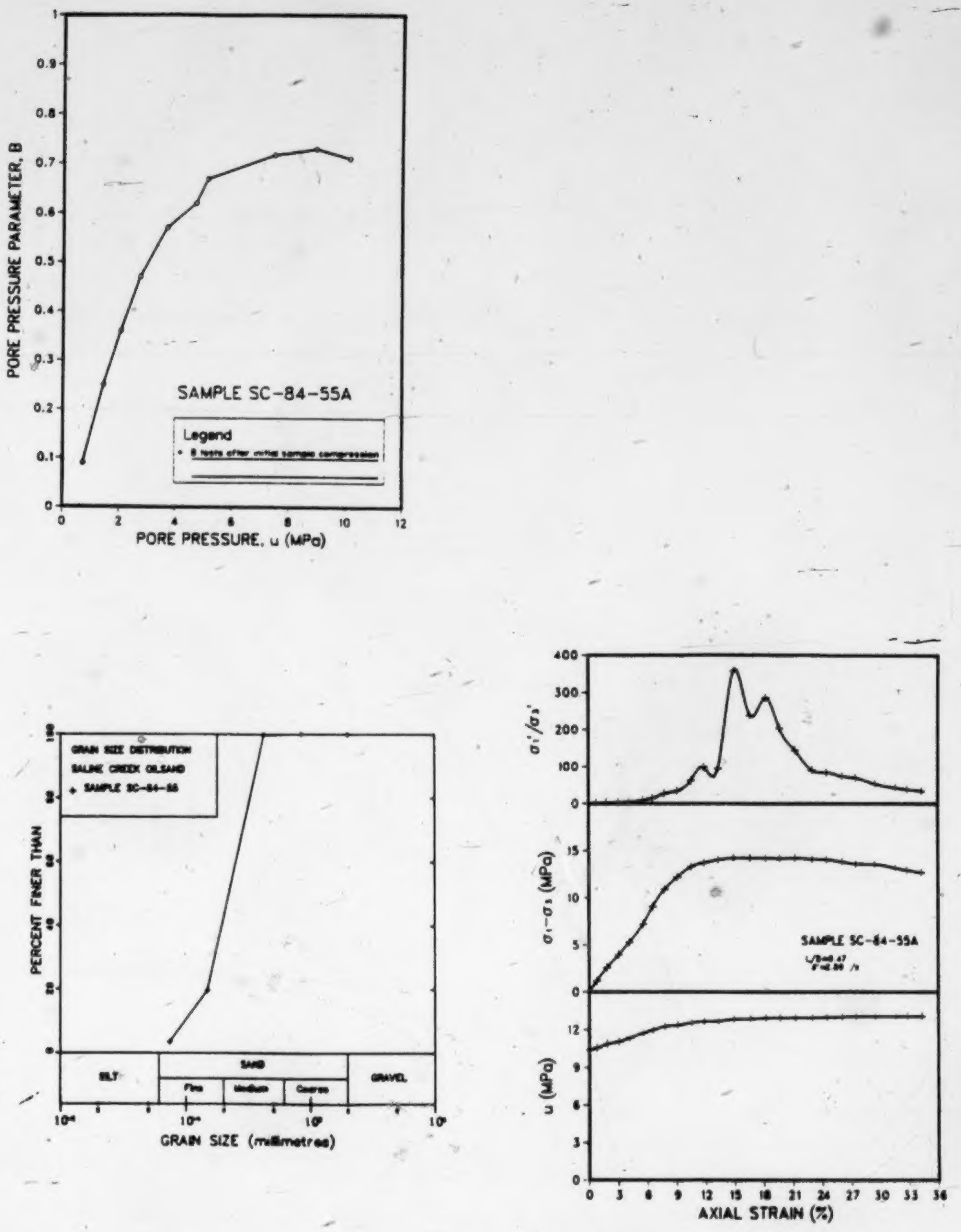

Figure C.37 SC-84-55A: Triaxial Test Results

# TEST SC-84-55B: SALINE CREEK OIL SAND

## PROCEDURAL DETAILS

1. Enlarged 43.20 mm diameter loading platens were used. The faces of the platens were overlaid with two layers of greased rubber membranes.
2. The sample was thawed under cell and back pressures of 6.27 and 0.58 MPa for 1.2 hours.
3. B tests were conducted at an effective confining pressure of 2.0 MPa with incremental increases in pore pressure until saturation was reached.
4. The sample was consolidated under back and cell pressures of 10.29 MPa and 12.31 MPa. An undrained triaxial compression test was conducted at a strain rate of 2.30 $s^{-1}$.

## TEST DATA

DIAMETER = 38.63 mm
HEIGHT = 20.98 mm
WEIGHT = 49.17 g.
BULK DENSITY = 1.999 $Mg/m^3$
WATER CONTENT = 2.4 %
BITUMEN CONTENT = 16.3 %
SATURATION = 94.3 %
POROSITY = 0.387

### Comments on Sample Failure:

Radial expansion occured uniformly throughout the full height of the sample.

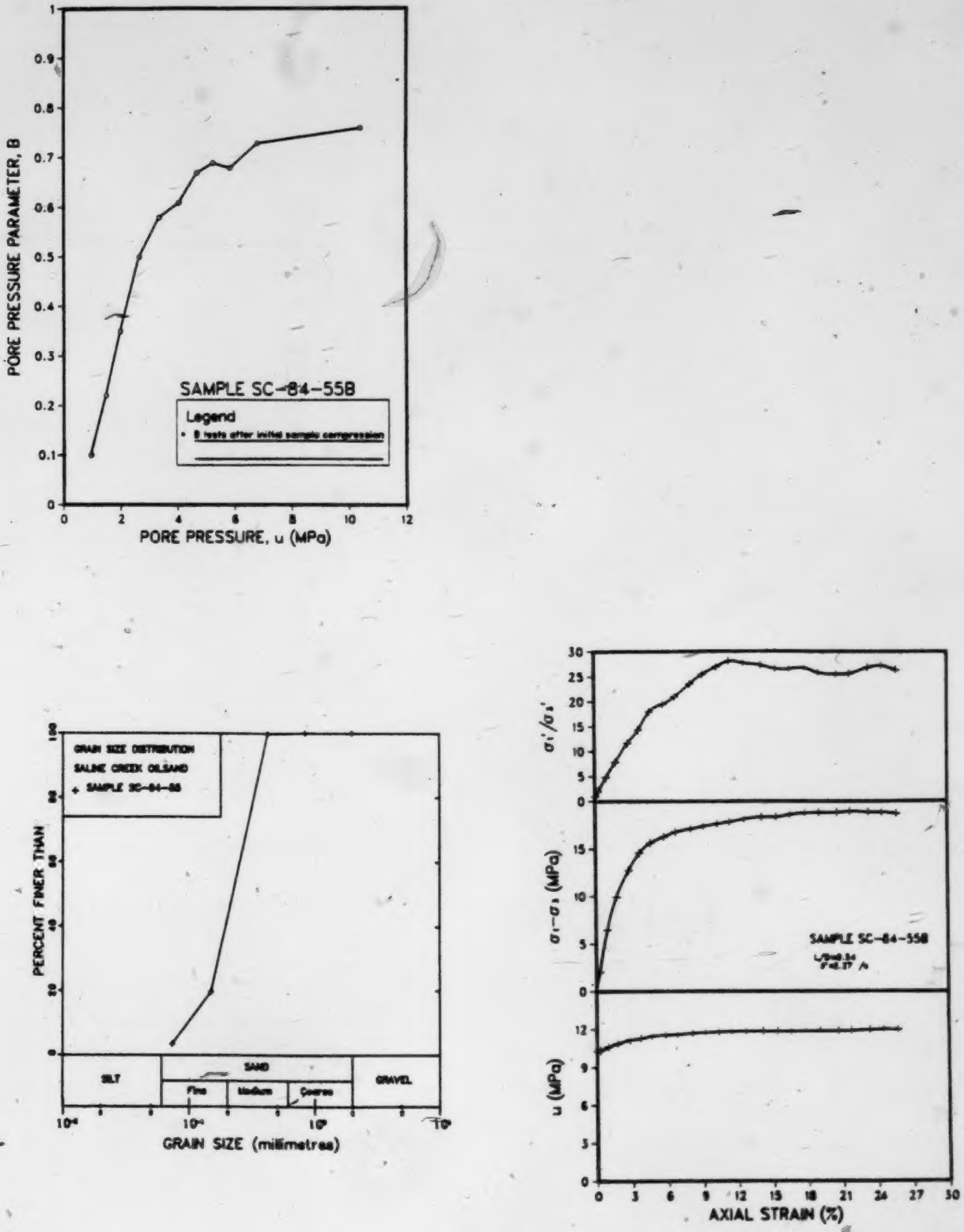

Figure C.38 SC-84-55B: Triaxial Test Results

# TEST SC-84-60: SALINE CREEK OIL SAND

## PROCEDURAL DETAILS

1. Enlarged 43.20 mm diameter loading platens were used. The faces of the platens were overlaid with two layers of greased rubber membranes.
2. The sample was thawed under cell and back pressures of 2.30 and 0.90 MPa for 17 hours.
3. B tests were conducted at an effective confining pressure of 1.00 MPa with incremental increases in pore pressure until saturation was reached.
4. The sample was consolidated under back and cell pressures of 10.94 MPa and 11.96 MPa. An undrained triaxial compression test was conducted at a strain rate of 1.4 x $10^{-1}$ $s^{-1}$.

## TEST DATA

DIAMETER = 38.80 mm
HEIGHT = 19.11 mm
WEIGHT = 44.61 g.
BULK DENSITY = 1.974 $Mg/m^3$
WATER CONTENT = 2.0 %
BITUMEN CONTENT = 15.3 %
SATURATION = 86.6 %
POROSITY = 0.405

### Comments on Sample Failure:

Radial expansion occured uniformly throughout the full height of the sample.

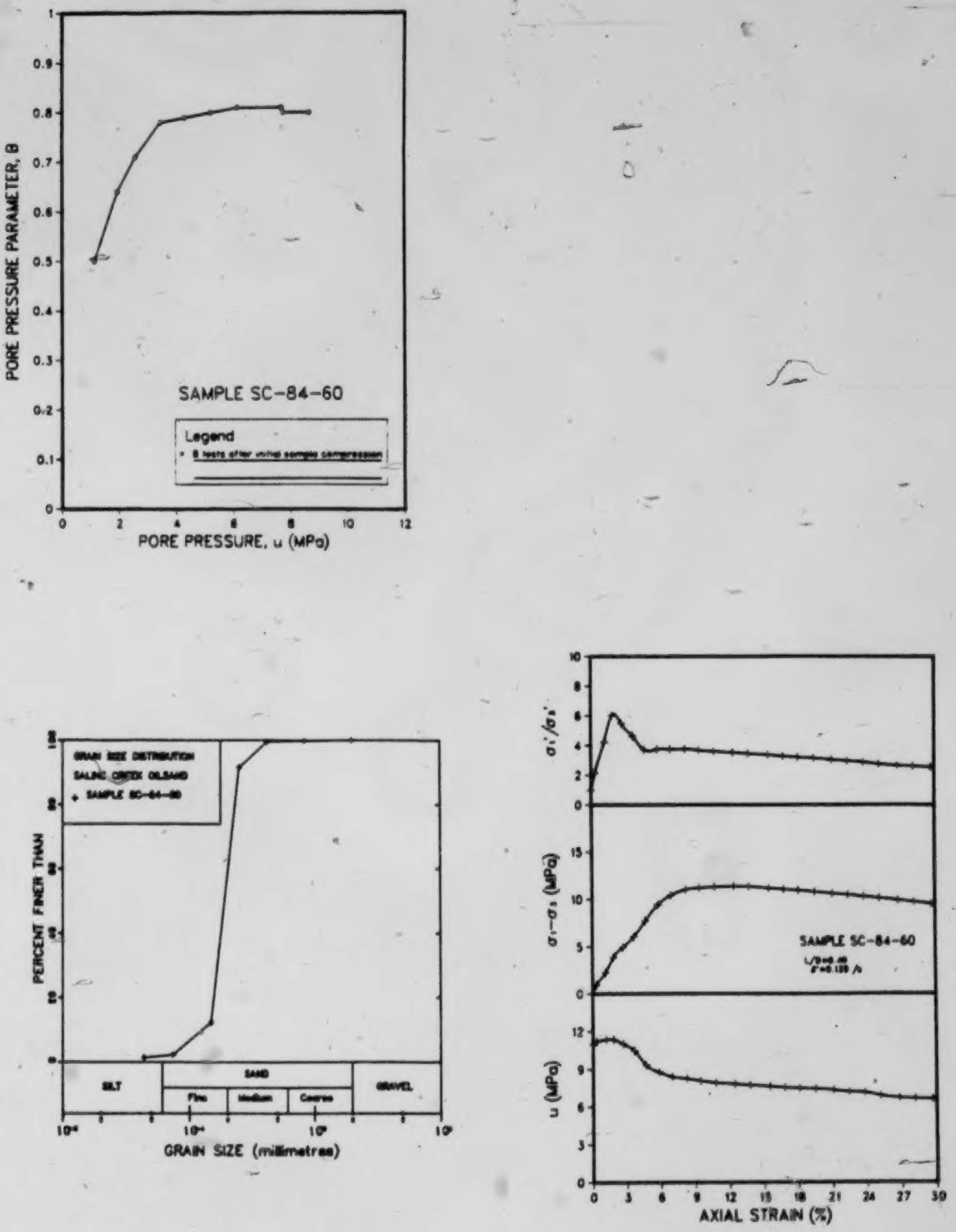

Figure C.39 SC-84-60: Triaxial Test Results

# TEST SC-84-115A: SALINE CREEK OIL SAND

## PROCEDURAL DETAILS

1. Enlarged 43.20 mm diameter loading platens were used. The faces of the platens were overlaid with two layers of greased rubber membranes.
2. The sample was thawed under cell and back pressures of 5.58 and 0.74 MPa for 1.0 hours.
3. B tests were conducted at an effective confining pressure of 2.00 MPa with incremental increases in pore pressure until saturation was reached.
4. The sample was consolidated under back and cell pressures of 9.71 MPa and 12.06 MPa. An undrained triaxial compression test was conducted at a strain rate of 2.30 $s^{-1}$.

## TEST DATA

DIAMETER = 38.58 mm
HEIGHT = 19.91 mm
WEIGHT = 45.59 g.
BULK DENSITY = 1.959 $Mg/m^3$
WATER CONTENT = 2.2 %
BITUMEN CONTENT = 15.5 %
SATURATION = 86.0 %
POROSITY = 0.392

### Comments on Sample Failure:

Radial expansion occured uniformly throughout the full height of the sample. A line appeared across the top of the sample as shown in the sketch. The sample was broken in half and a fracture through the sample was not evident.

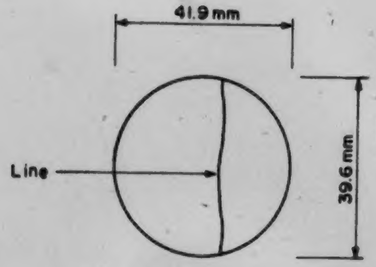

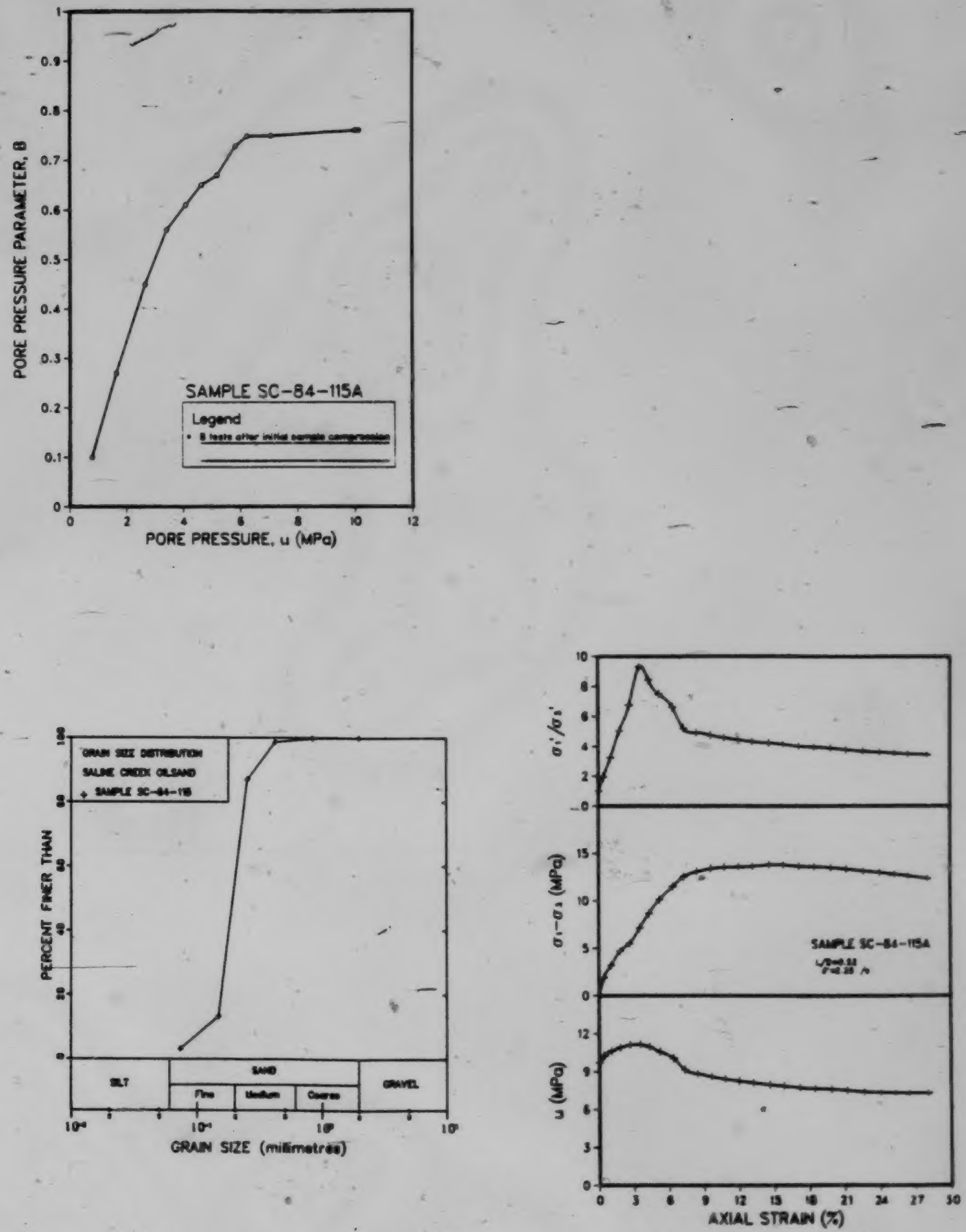

Figure C.40 SC-84-115A: Triaxial Test Results

# TEST SC-84-115B: SALINE CREEK OIL SAND

## PROCEDURAL DETAILS

1. Enlarged 43.20 mm diameter loading platens were used. The faces of the platens were overlaid with two layers of greased rubber membranes.
2. The sample was thawed under cell and back pressures of 5.85 and 0.95 MPa for 1.0 hours.
3. B tests were conducted at an effective confining pressure of 2.1 MPa with incremental increases in pore pressure until saturation was reached.
4. The sample was consolidated under back and cell pressures of 10.20 MPa and 12.33 MPa. An undrained triaxial compression test was conducted at a strain rate of 3.10 $s^{-1}$.

## TEST DATA

DIAMETER = 38.50 mm
HEIGHT = 14.28 mm
WEIGHT = 32.28 g.
BULK DENSITY = 1.948 Mg/$m^3$
WATER CONTENT = 2.2 %
BITUMEN CONTENT = 15.5 %
SATURATION = 85.1 %
POROSITY = 0.419

### Comments on Sample Failure:

Radial expansion occured uniformly throughout the full height of the sample.

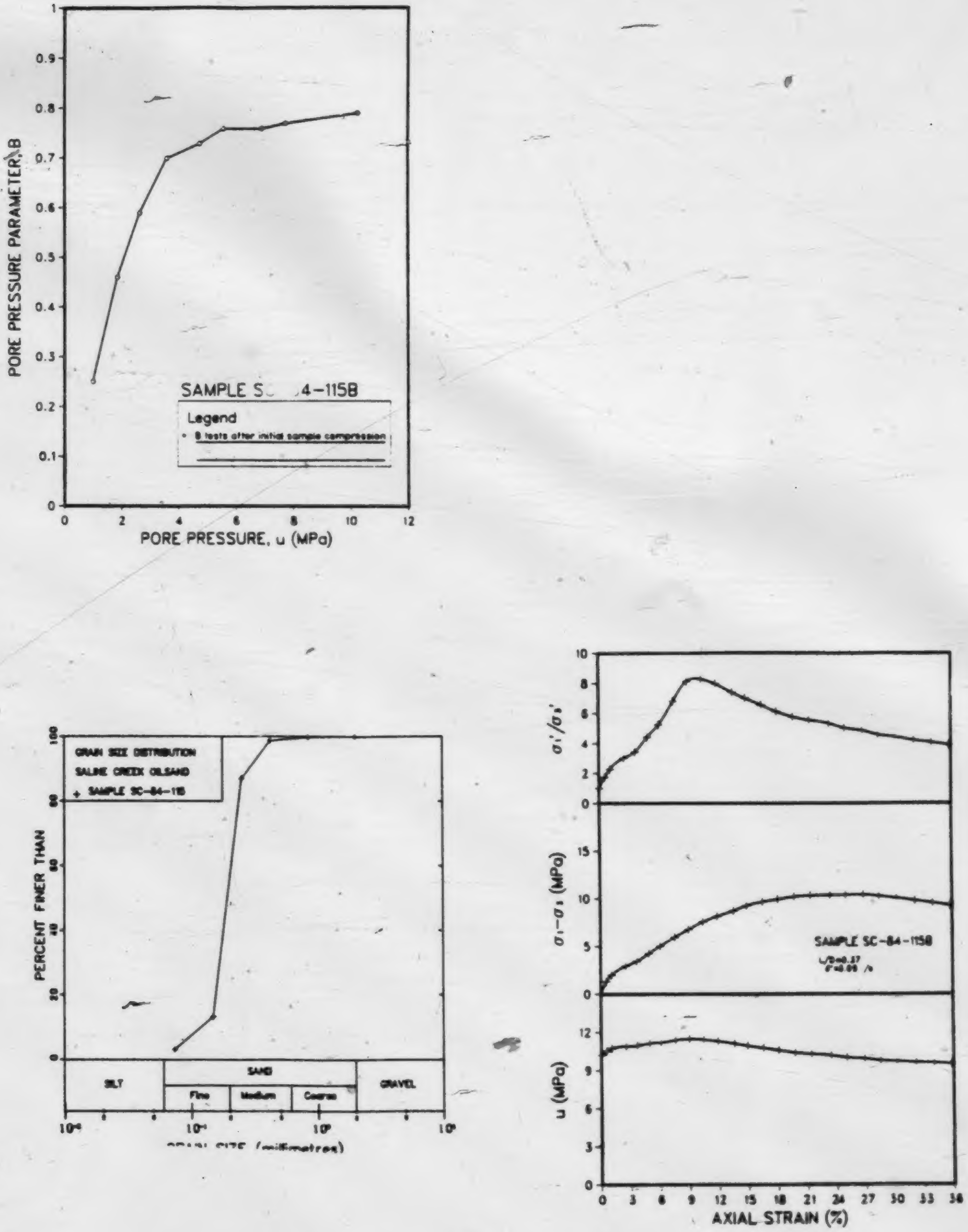

Figure C.41 SC-84-115B: Triaxial ~~Test~~ Results

## TEST SC-84-117: SALINE CREEK OIL SAND

### PROCEDURAL DETAILS

1. Enlarged 43.20 mm diameter loading platens were used. The faces of the platens were overlaid with two layers of greased rubber membranes.
2. The sample was thawed under cell and back pressures of 5.70 and 0.70 MPa for 20 hours.
3. B tests were conducted at an effective confining pressure of 5.02 MPa with incremental increases in pore pressure until saturation was reached.
4. The sample was consolidated under back and cell pressures of 6.43 MPa and 11.39 MPa. An undrained triaxial compression test was conducted at a strain rate of $1.1 \times 10^{-1}$ $s^{-1}$.

### TEST DATA

DIAMETER = 38.51 mm
HEIGHT = 19.45 mm
WEIGHT = 45.24 g.
BULK DENSITY = 1.997 $Mg/m^3$
WATER CONTENT = 2.9 %
BITUMEN CONTENT = 15.7 %
SATURATION = 93.7 %
POROSITY = 0.393

### Comments on Sample Failure:

Radial expansion occured uniformly throughout the full height of the sample.

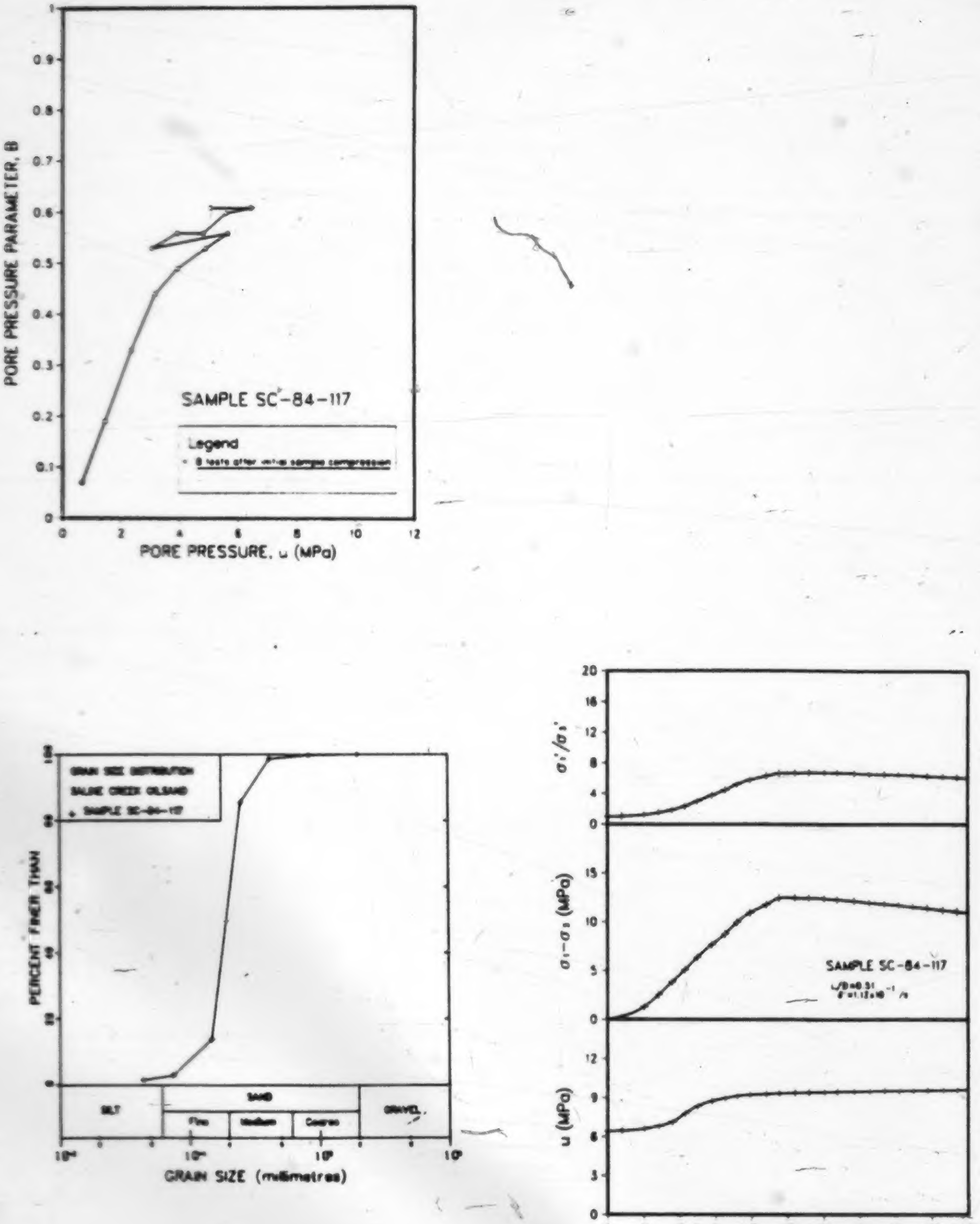

Figure C.42 SC-84-117: Triaxial Test Results

# APPENDIX D - Comparitive Grain Size Distribution of Saline Creek Oil Sand Before And After Testing

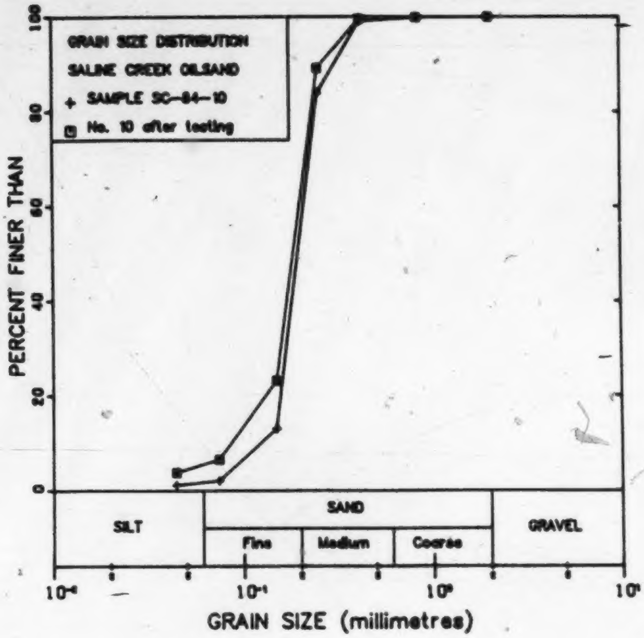

Figure D.1 SC-84-10: Grain Size Distribution Before And After Testing

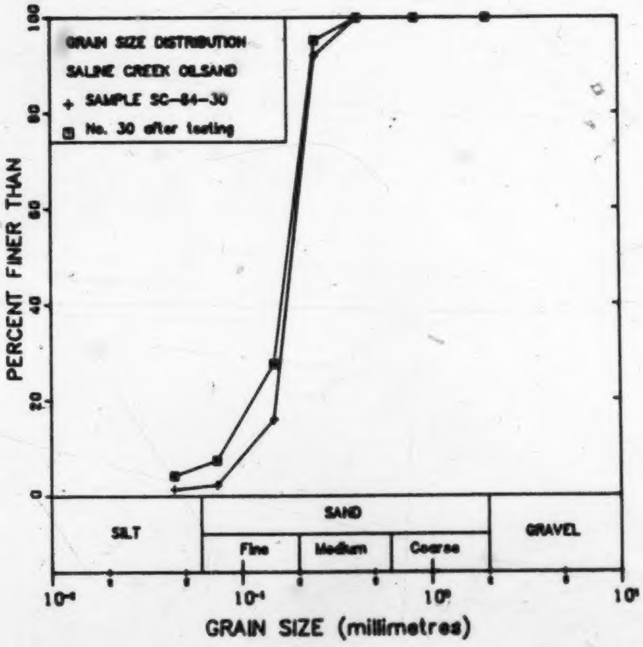

Figure D.2 SC-84-30: Grain Size Distribution Before And After Testing

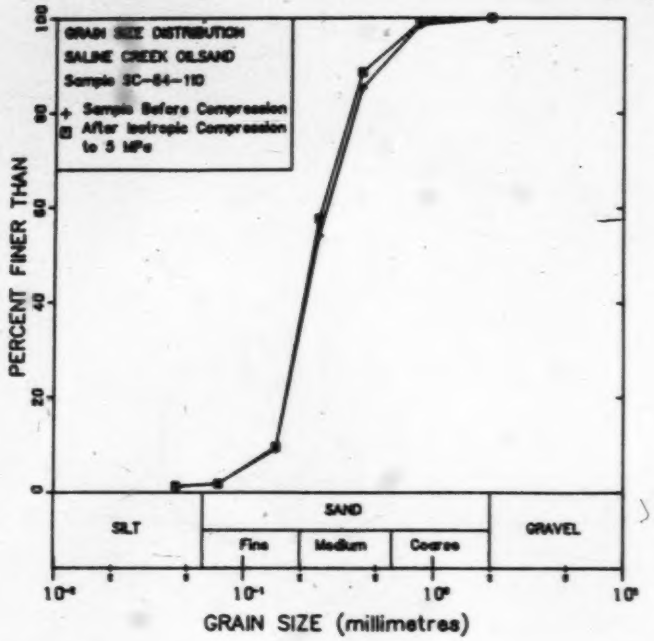

Figure D.3 SC-84-110: Grain Size Distribution Before And After Testing

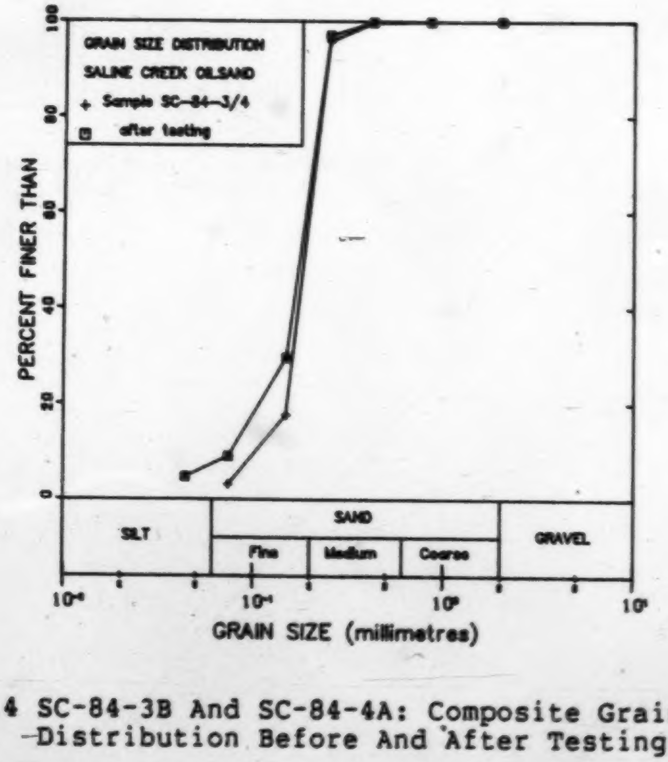

Figure D.4 SC-84-3B And SC-84-4A: Composite Grain Size Distribution Before And After Testing

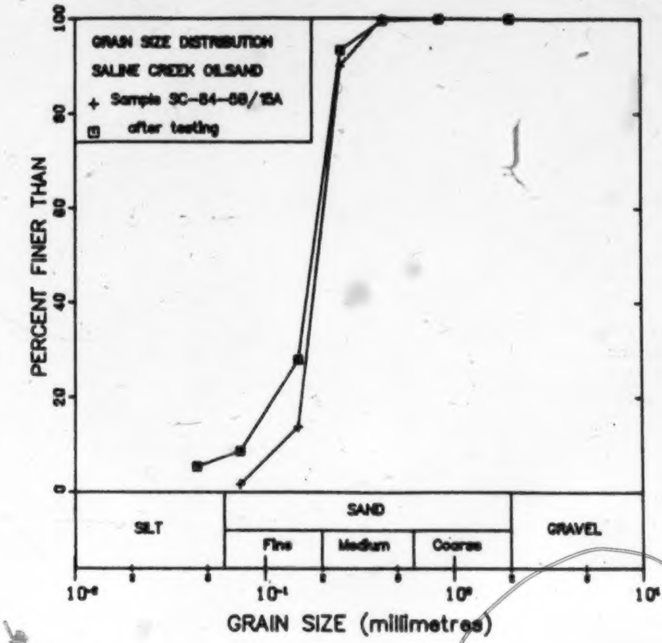

Figure D.5 SC-84-5B And SC-84-15A: Composite Grain Size Distribution Before And After Testing

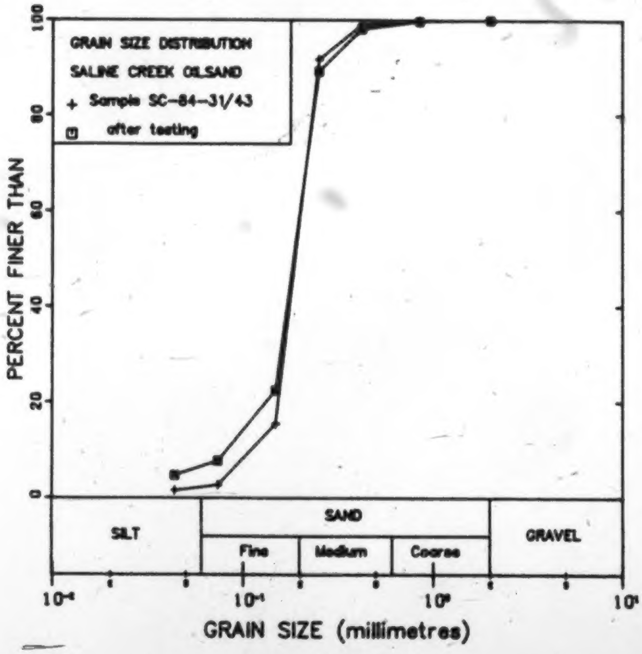

Figure D.6 SC-84-31 And SC-84-43: Composite Grain Size Distribution Before And After Testing

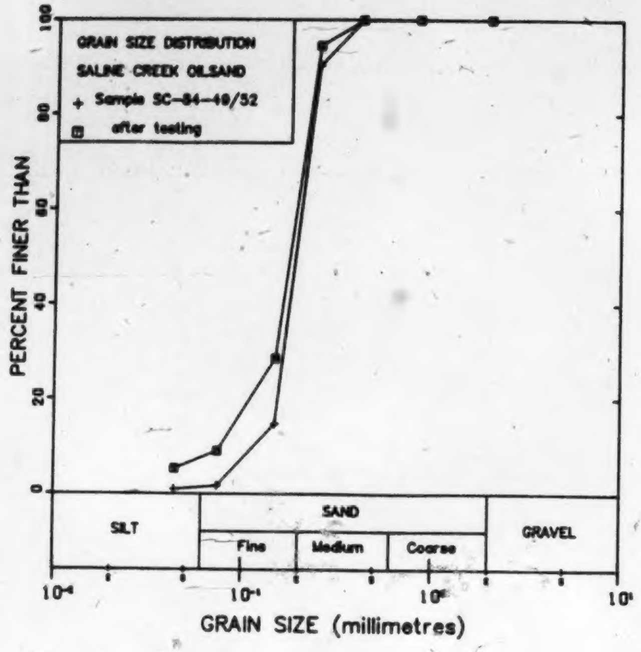

Figure D.7 SC-84-49 And SC-84-52: Composite Grain Size Distribution Before And After Testing

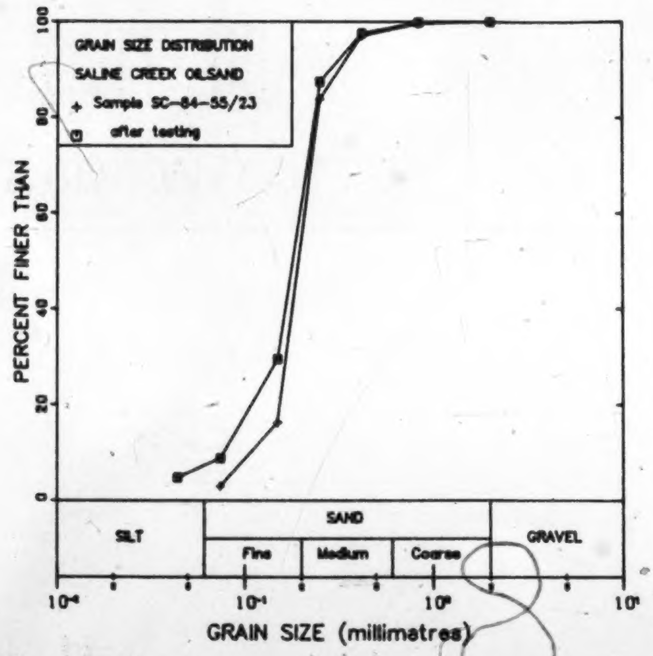

Figure D.8 SC-84-23, SC-84-55A And SC-84-55B: Composite Grain Size Distribution Before And After Testing

# APPENDIX E - Syncrude Oil Sand Triaxial Test Results

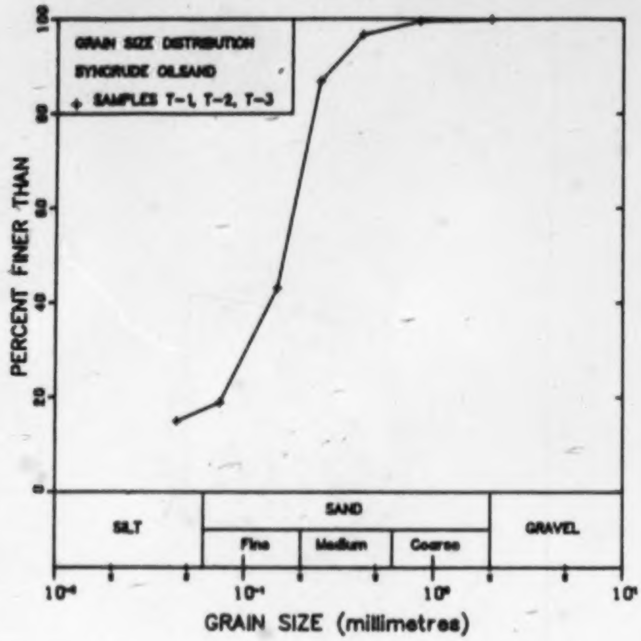

Figure E.1 SYN-T-1,T-2,T-3: Grain Size Distribution

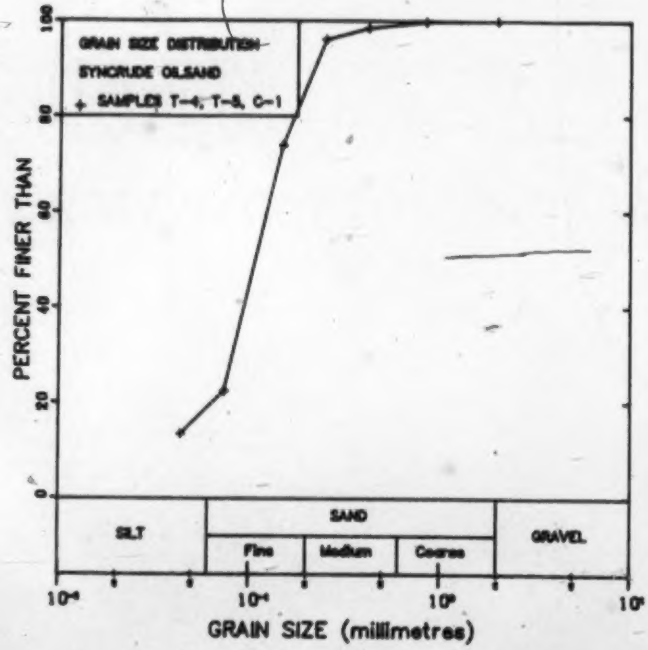

Figure E.2 SYN-T-4,T-5,C-1: Grain Size Distribution

## TEST SYN-C-1: SYNCRUDE OIL SAND

### PROCEDURAL DETAILS

1. The sample was installed in the triaxial cell and enclosed in a single membrane.
2. The sample was thawed under cell and back pressures of 539 and 398 kPa for 18 hours.
3. B tests were conducted at an effective confining pressure of 160 kPa with incremental increases in pore pressure until saturation was reached.
4. An isotropic compressibility test was conducted with one cycle of effective confining stress up to 791 kPa. A constant pore pressure of 408 kPa was maintained throughout the test.
5. A second series of B tests were conducted at a confining pressure of 84 kPa following the cyclic compression of the sample.
6. The sample was consolidated under an effective confining and back pressure of 14.8 kPa and 178 kPa. A drained axial compression test was conducted at a deformation rate of 0.223 mm per hour.

### TEST DATA

DIAMETER = 37.95
HEIGHT = 75.77 mm
INITIAL WEIGHT = 179.01 g.

BULK DENSITY = 2.089 $Mg/m^3$
WATER CONTENT = 9.8 %
BITUMEN CONTENT = 5.3 %
SATURATION = 94.3 %
POROSITY = 0.331

FINAL WEIGHT = 187.33 g.
FINAL WATER CONTENT = 12.5 %

### Comments on Sample Failure

The sample failed by shearing and splitting of the sample as shown in Figure E.6.

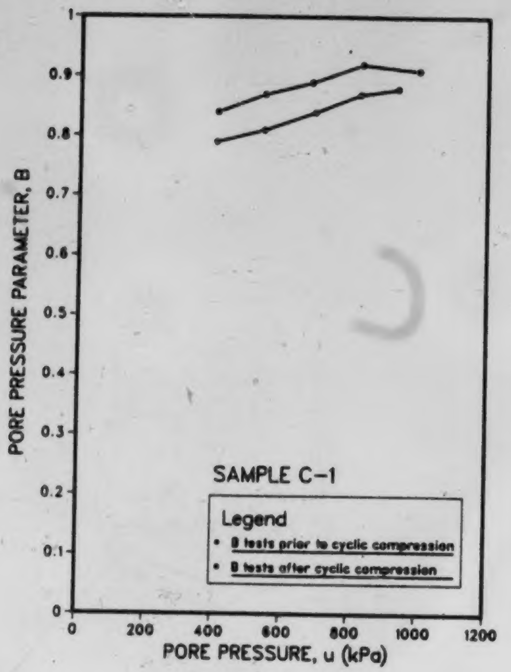

Figure E.3 SYN-C-1: Pore Pressure Parameter B

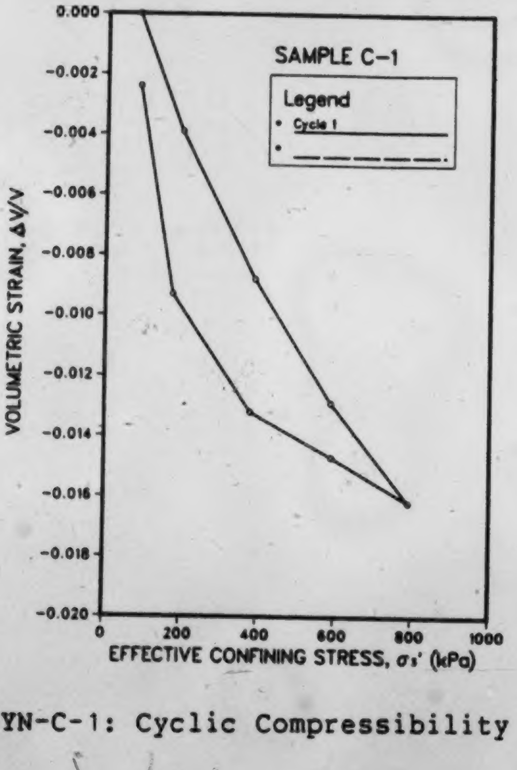

Figure E.4 SYN-C-1: Cyclic Compressibility Test

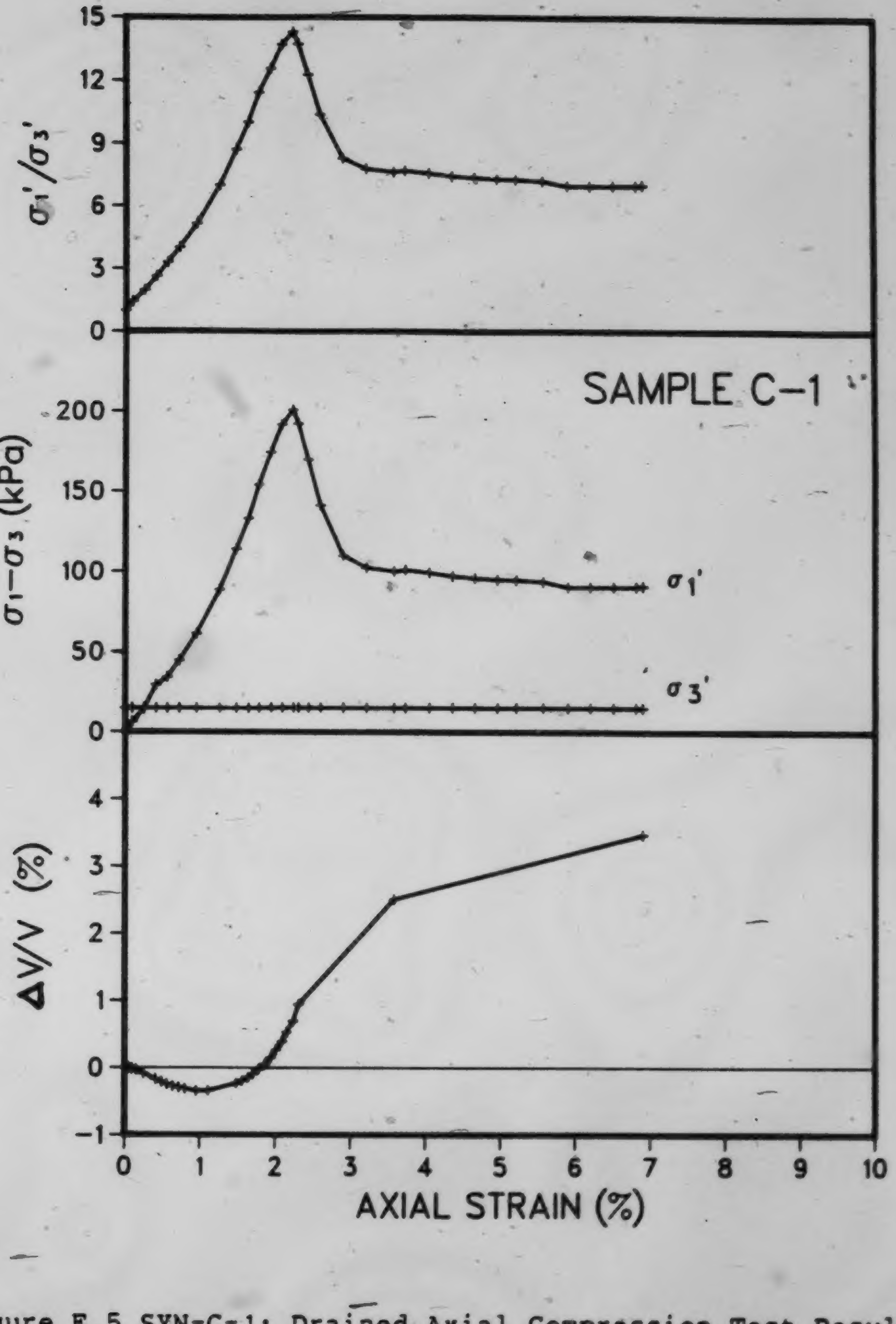

Figure E.5 SYN-C-1: Drained Axial Compression Test Results

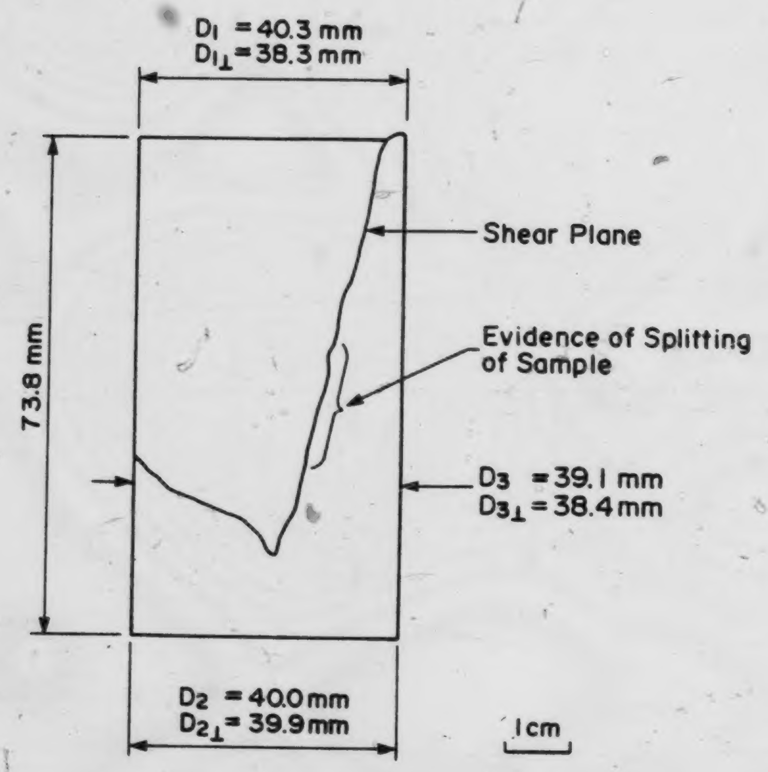
$D_1$ = 40.3 mm
$D_{1\perp}$ = 38.3 mm
73.8 mm
Shear Plane
Evidence of Splitting of Sample
$D_3$ = 39.1 mm
$D_{3\perp}$ = 38.4 mm
$D_2$ = 40.0 mm
$D_{2\perp}$ = 39.9 mm
1cm

Figure E.6 SYN-C-1: Condition of Sample After Testing

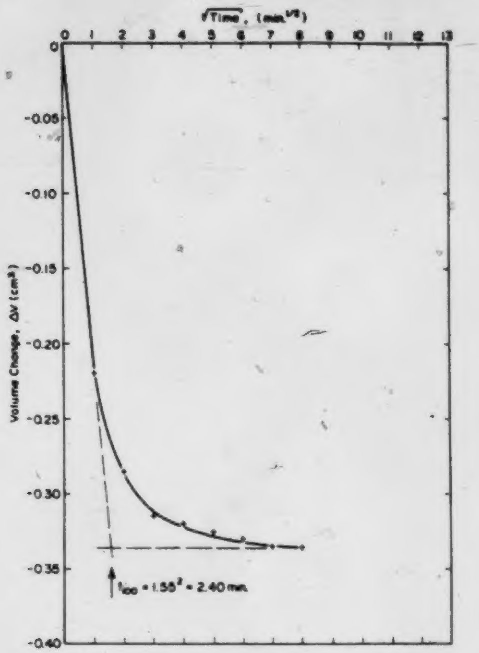

Figure E.7 SYN-C-1: Consolidation Under Loading Increment of Isotropic Stress From 81 To 198 kPa

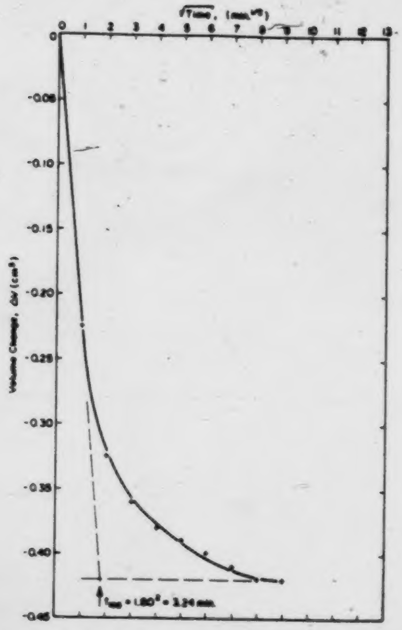

Figure E.8 SYN-C-1: Consolidation Under Loading Increment of Isotropic Stress From 198 To 389 kPa

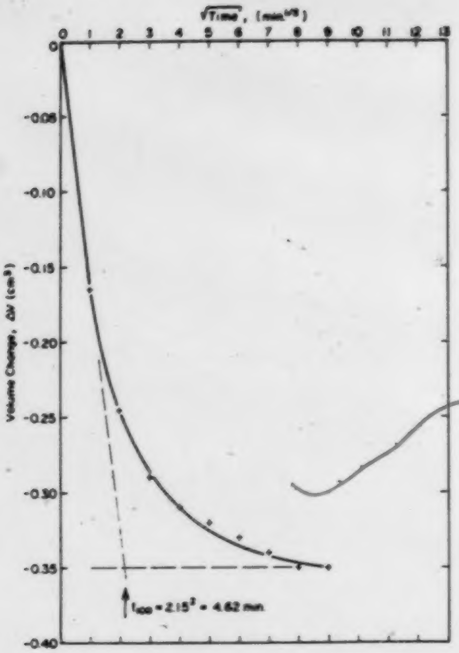

Figure E.9 SYN-C-1: Consolidation Under Loading Increment of Isotropic Stress From 389 To 589 kPa

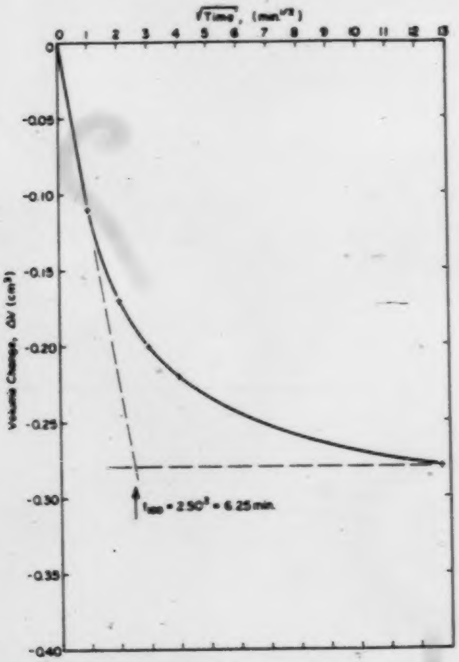

Figure E.10 SYN-C-1: Consolidation Under Loading Increment of Isotropic Stress From 589 To 791 kPa

## TEST SYN-T-1: SYNCRUDE OIL SAND

### PROCEDURAL DETAILS

1. The sample was installed in the triaxial cell and enclosed in a single membrane.
2. The sample was thawed under cell and back pressures of 730 and 550 kPa for 12 hours.
3. B tests were conducted at an effective confining pressure of 90 kPa with incremental increases in pore pressure until saturation was reached.
4. An isotropic compressibility test was conducted with two cycles of effective confining stress up to 750 kPa. A constant pore pressure of 400 kPa was maintained throughout the test.
5. A second series of B tests were conducted at a confining pressure of 75 kPa following the cyclic compression of the sample.
6. The sample was consolidated under an effective confining and back pressure of 57.5 kPa and 849 kPa. A drained axial extension test was conducted at a deformation rate of 1.12 mm per hour.

### TEST DATA

END DIAMETER = 37.90 mm
TOTAL HEIGHT = 70.22 mm
INITIAL WEIGHT = 140.68 g.

NOTCH DIAMETER = 28.95 mm
NOTCH LENGTH = 15.60 mm

BULK DENSITY = 2.066 $Mg/m^3$
WATER CONTENT = 11.4 %
BITUMEN CONTENT = 2.4 %
SATURATION = 86.5 %
POROSITY = 0.328

FINAL WEIGHT = 143.20 g.
FINAL WATER CONTENT - NOTCHED ZONE = 11.6 %
- SAMPLE ENDS = 11.1 %

### Comments on Sample Failure

The sample failed by parting at the bottom edge of the notched zone as shown in Figure E.14. No evidence of shearing at the ends of the sample were observed.

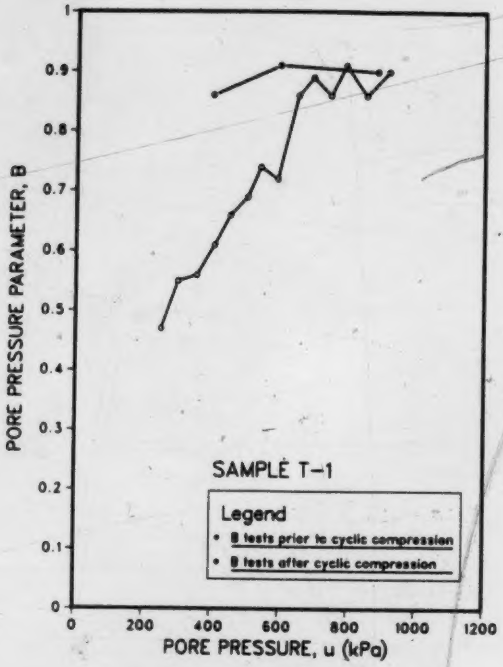

Figure E.11 SYN-T-1: Pore Pressure Parameter B

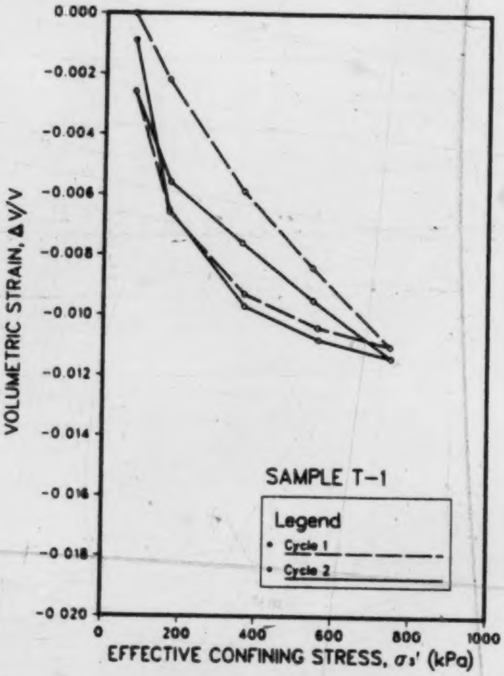

Figure E.12 SYN-T-1: Cyclic Compressibility Test

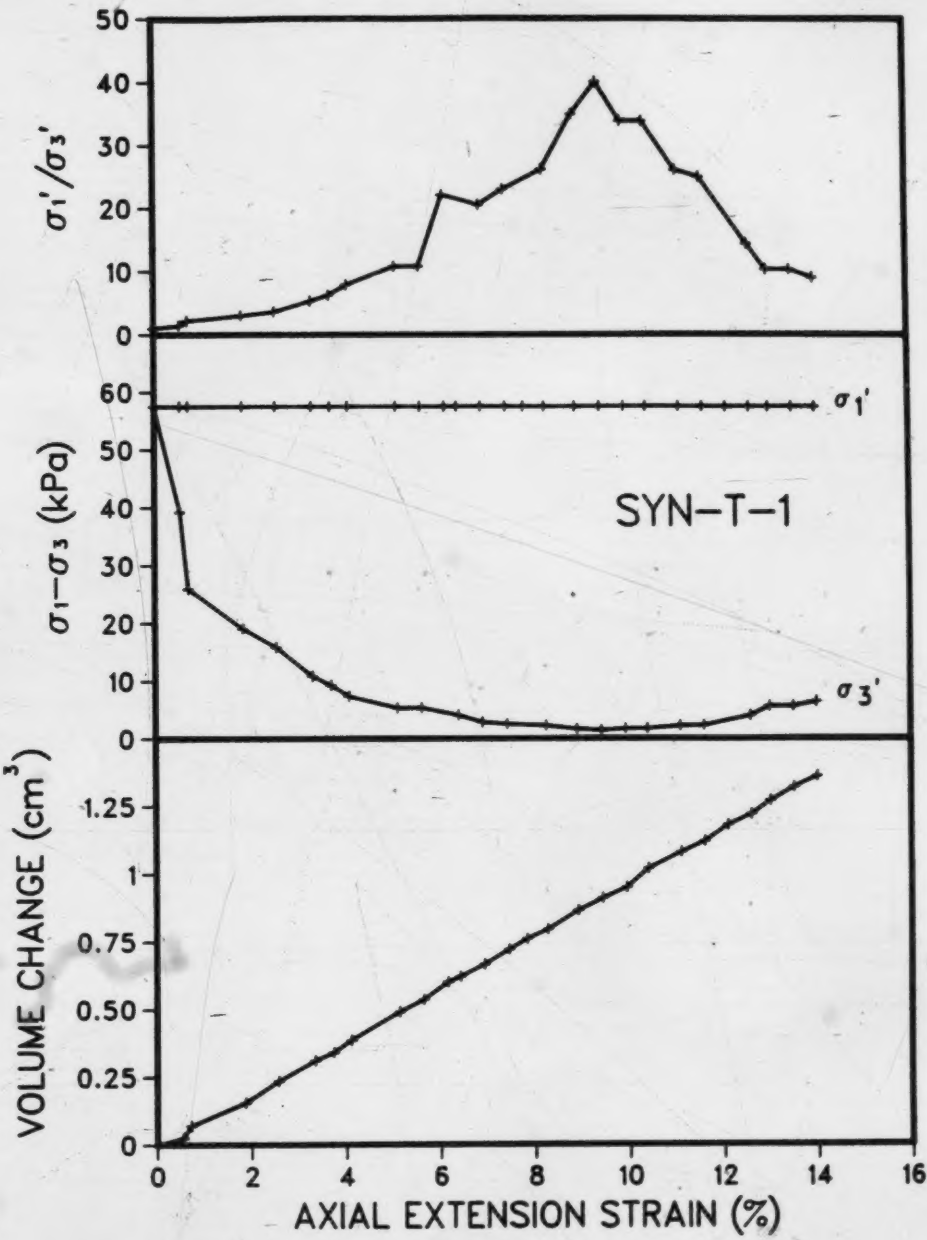

Figure E.13 SYN-T-1: Draine. ...ial Extension Test Results

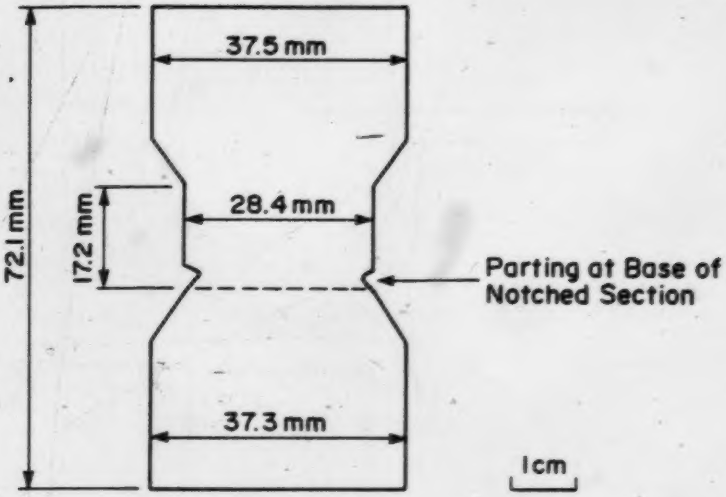
37.5 mm
28.4 mm
17.2 mm
72.1 mm
Parting at Base of Notched Section
37.3 mm
1cm

Final Total Length = 72.1 mm
Initial Total Length = 70.2 mm

Change in Total Length = 1.9 mm

Final Notch Length = 17.2 mm
Initial Notch Length = 15.6 mm

Change in Notch Length = 1.6 mm

Figure E.14 SYN-T-1: Condition of Sample After Testing

## TEST SYN-T-2: SYNCRUDE OIL SAND

### PROCEDURAL DETAILS

1. The sample was installed in the triaxial cell and enclosed in a single membrane with horizontal convolutions in the notched zone.
2. The sample was thawed under cell and back pressures of 441 and 310 kPa for 46 hours.
3. B tests were conducted at an effective confining pressure of 100 kPa with incremental increases in pore pressure until saturation was reached.
4. An isotropic compressibility test was conducted with two cycles of effective confining stress up to 780 kPa. A constant pore pressure of 408 kPa was maintained throughout the test.
5. A second series of B tests were conducted at a confining pressure of 88 kPa following the cyclic compression of the sample.
6. The sample was consolidated under an effective confining and back pressure of 70.9 kPa and 592 kPa. A drained axial extension test was conducted at a deformation rate of 0.223 mm per hour.

### TEST DATA

END DIAMETER = 37.90 mm NOTCH DIAMETER = 28.70 mm
TOTAL HEIGHT = 89.05 mm NOTCH LENGTH = 16.40 mm
INITIAL WEIGHT = 158.89 g.

BULK DENSITY = 2.059 Mg/m$^3$
WATER CONTENT = 11.4 %
BITUMEN CONTENT = 2.4 %
SATURATION = 85.6 %
POROSITY = 0.330

FINAL WEIGHT = -specimen disturbed during dismantling of triaxial cell
FINAL WATER CONTENT - NOTCHED ZONE = 11.5 %
- SAMPLE ENDS = 10.3 %

### Comments on Sample Failure

The sample failed by parting at mid-height of the notched zone as shown in Figure E.18. No evidence of shearing at the ends of the sample were observed.

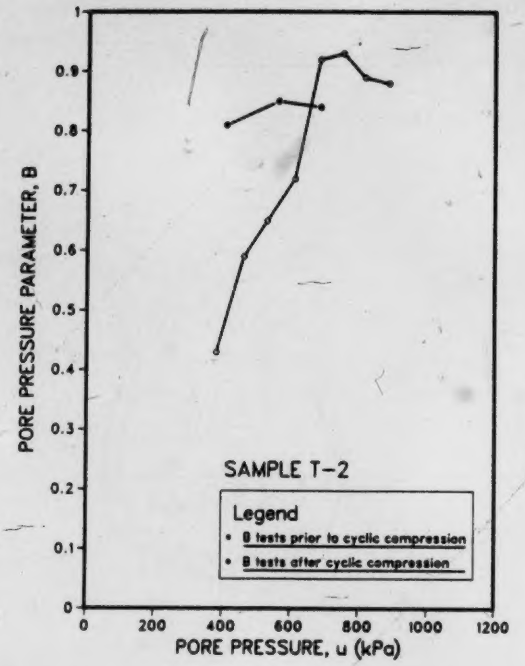

Figure E.15 SYN-T-2: Pore Pressure Parameter B

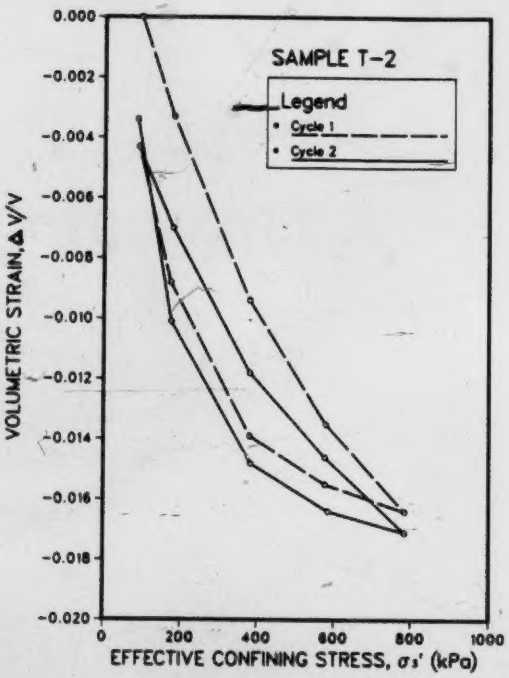

Figure E.16 SYN-T-2: Cyclic Compressibility Test

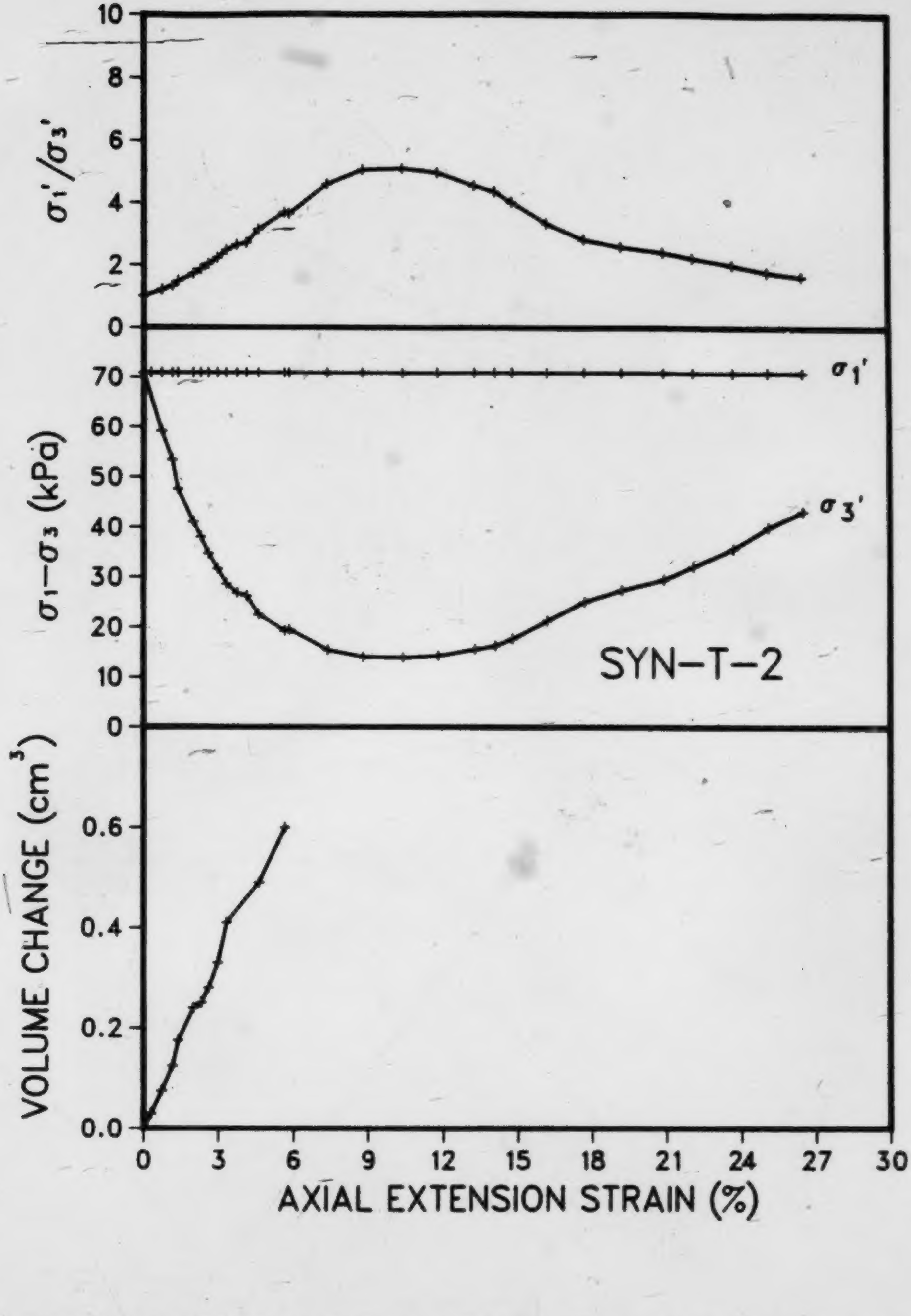

Figure E.17 SYN-T-2: Drained Axial Extension Test Results

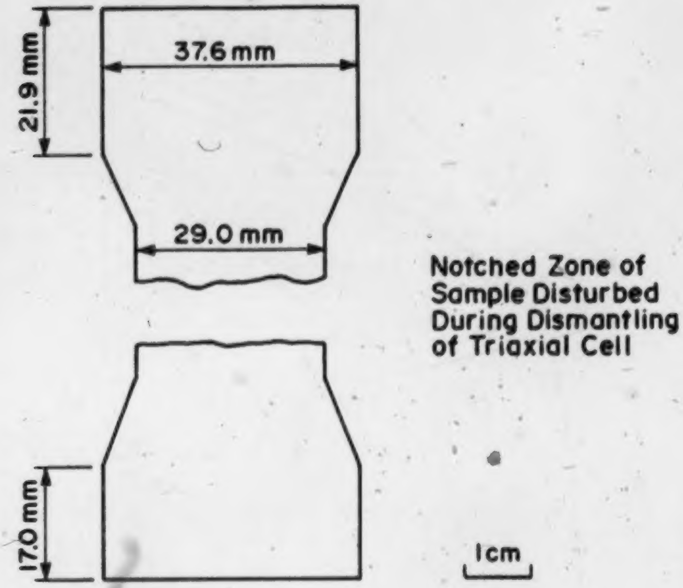
37.6 mm
21.9 mm
29.0 mm
Notched Zone of Sample Disturbed During Dismantling of Triaxial Cell
17.0 mm
1cm

Figure E.18 SYN-T-2: Condition of Sample After Testing

## TEST SYN-T-3: SYNCRUDE OIL SAND

### PROCEDURAL DETAILS

1. The sample was installed in the triaxial cell and enclosed in a single membrane with horizontal convolutions in the notched zone.
2. The sample was thawed under cell and back pressures of 463 and 319 kPa for 21 hours.
3. B tests were conducted at an effective confining pressure of 127 kPa with incremental increases in pore pressure until saturation was reached.
4. An isotropic compressibility test was conducted with two cycles of effective confining stress up to 758 kPa. A constant pore pressure of 420 kPa was maintained throughout the test.
5. A second series of B tests were conducted at a confining pressure of 72 kPa following the cyclic compression of the sample.
6. The sample was consolidated under an effective confining and back pressure of 63.1 kPa and 546 kPa. A drained axial extension test was conducted at a deformation rate of 0.223 mm per hour.

### TEST DATA

END DIAMETER = 37.68 mm
TOTAL HEIGHT = 81.73 mm
INITIAL WEIGHT = 138.80 g.

NOTCH DIAMETER = 25.50 mm
NOTCH LENGTH = 28.35 mm

BULK DENSITY = 2.060 Mg/m$^3$
WATER CONTENT = 11.4 %
BITUMEN CONTENT = 2.4 %
SATURATION = 85.7 %
POROSITY = 0.330

FINAL WEIGHT = 141.93 g.
FINAL WATER CONTENT - NOTCHED ZONE = 12.0 %
- SAMPLE ENDS = 11.5 %

Comments on Sample Failure

The sample failed by parting at mid-height of the notched zone as shown in Figure E.22. Initial parting surface inclined between 4° and 6° to horizontal. No evidence of shearing at the ends of the sample were observed.

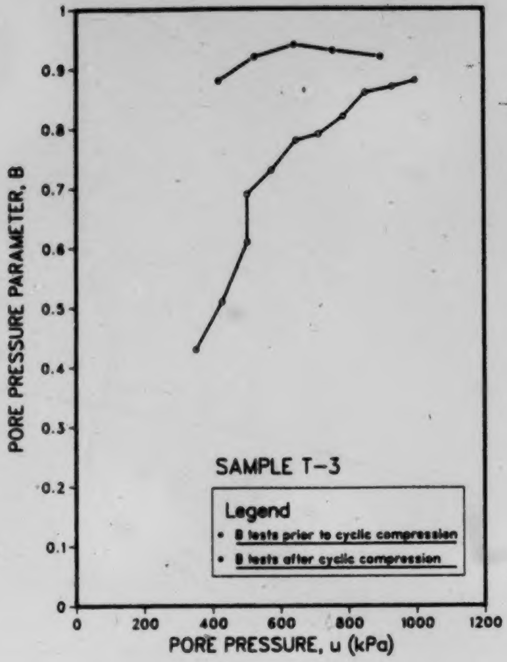

Figure E.19 SYN-T-3: Pore Pressure Parameter B

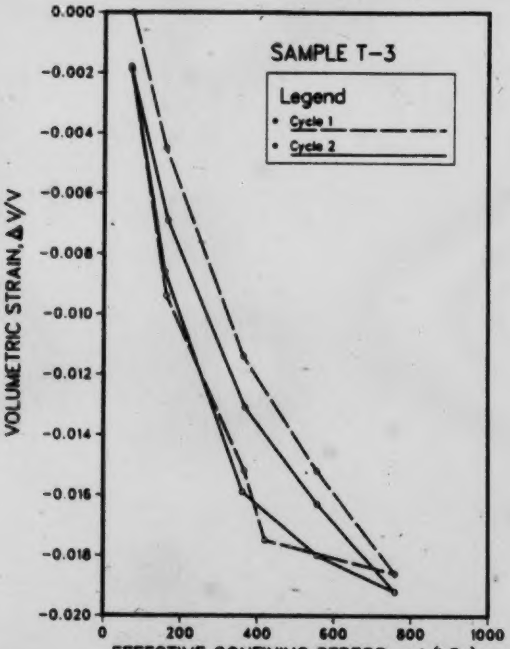

Figure E.20 SYN-T-3: Cyclic Compressibility Test

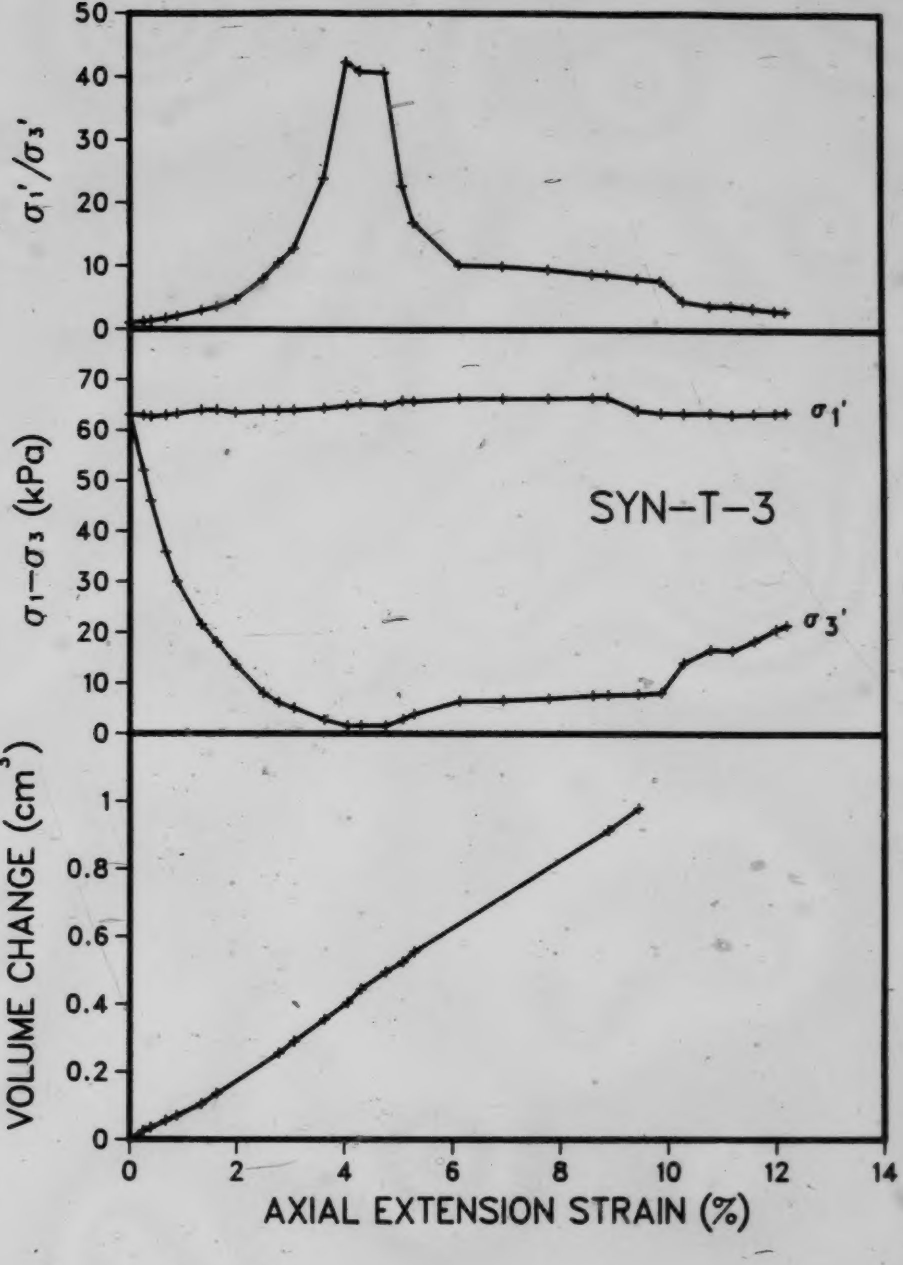

Figure E.21 SYN-T-3: Drained Axial Extension Test Results

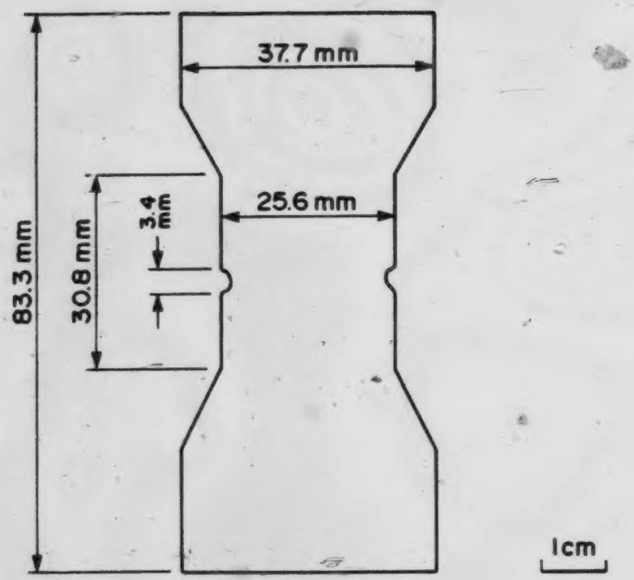
37.7 mm
25.6 mm
83.3 mm
30.8 mm
3.4 mm
1cm

Final Total Height = 83.3 mm
Initial Total Height = 81.7 mm

Change in Total Height = 1.6 mm

Final Notch Length = 30.8 mm
Initial Notch Length = 28.4 mm

Change in Notch Length = 2.4 mm

Figure E.22 SYN-T-3: Condition of Sample After Testing

## TEST SYN-T-4: SYNCRUDE OIL SAND

### PROCEDURAL DETAILS

1. The sample was installed in the triaxial cell and enclosed in a single membrane with horizontal convolutions in the notched zone.
2. The sample was thawed under cell and back pressures of 386 and 298 kPa for 17 hours.
3. B tests were conducted at an effective confining pressure of 107 kPa with incremental increases in pore pressure until saturation was reached.
4. An isotropic compressibility test was conducted with two cycles of effective confining stress up to 784 kPa. A constant pore pressure of 410 kPa was maintained throughout the test.
5. A second series of B tests were conducted at a confining pressure of 83 kPa following the cyclic compression of the sample.
6. The sample was consolidated under an effective confining and back pressure of 32.1 kPa and 620 kPa. An undrained axial extension test was conducted at a deformation rate of 0.223 mm per hour.

### TEST DATA

END DIAMETER = 38.35 mm

TOTAL HEIGHT = 89.60 mm

INITIAL WEIGHT = 157.20 g.

NOTCH DIAMETER = 25.60 mm

NOTCH LENGTH = 30.00 mm

BULK DENSITY = 2.092 $Mg/m^3$

WATER CONTENT = 9.7 %

BITUMEN CONTENT = 5.3 %

SATURATION = 94.8 %

POROSITY = 0.330

FINAL WEIGHT = 158.97 g.

FINAL WATER CONTENT - NOTCHED ZONE = 13.0 %

- SAMPLE ENDS = 10.6 %

Comments on Sample Failure

The sample failed by parting at mid-height of the notched zone as shown in Figure E.26. Occassional minute horizontal cracks visible above and below parting in notched section. No evidence of shearing at the ends of the sample were observed.

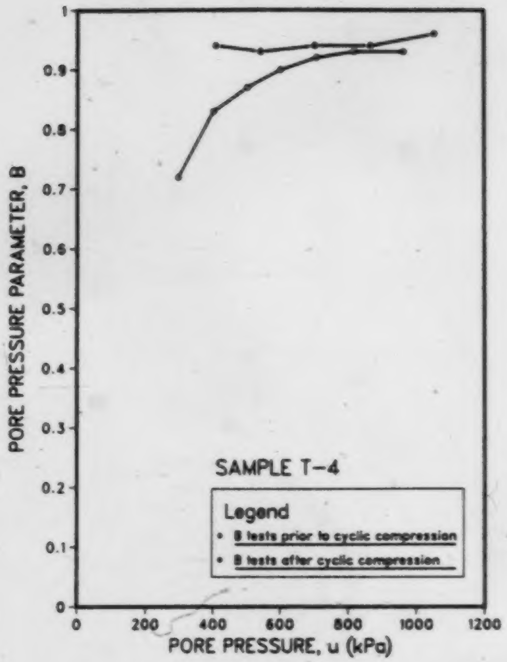

Figure E.23 SYN-T-4: Pore Pressure Parameter B

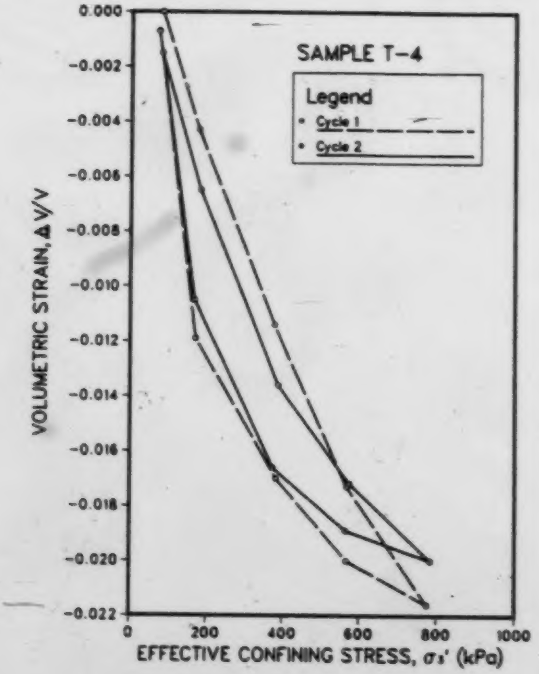

Figure E.24 SYN-T-4: Cyclic Compressibility Test

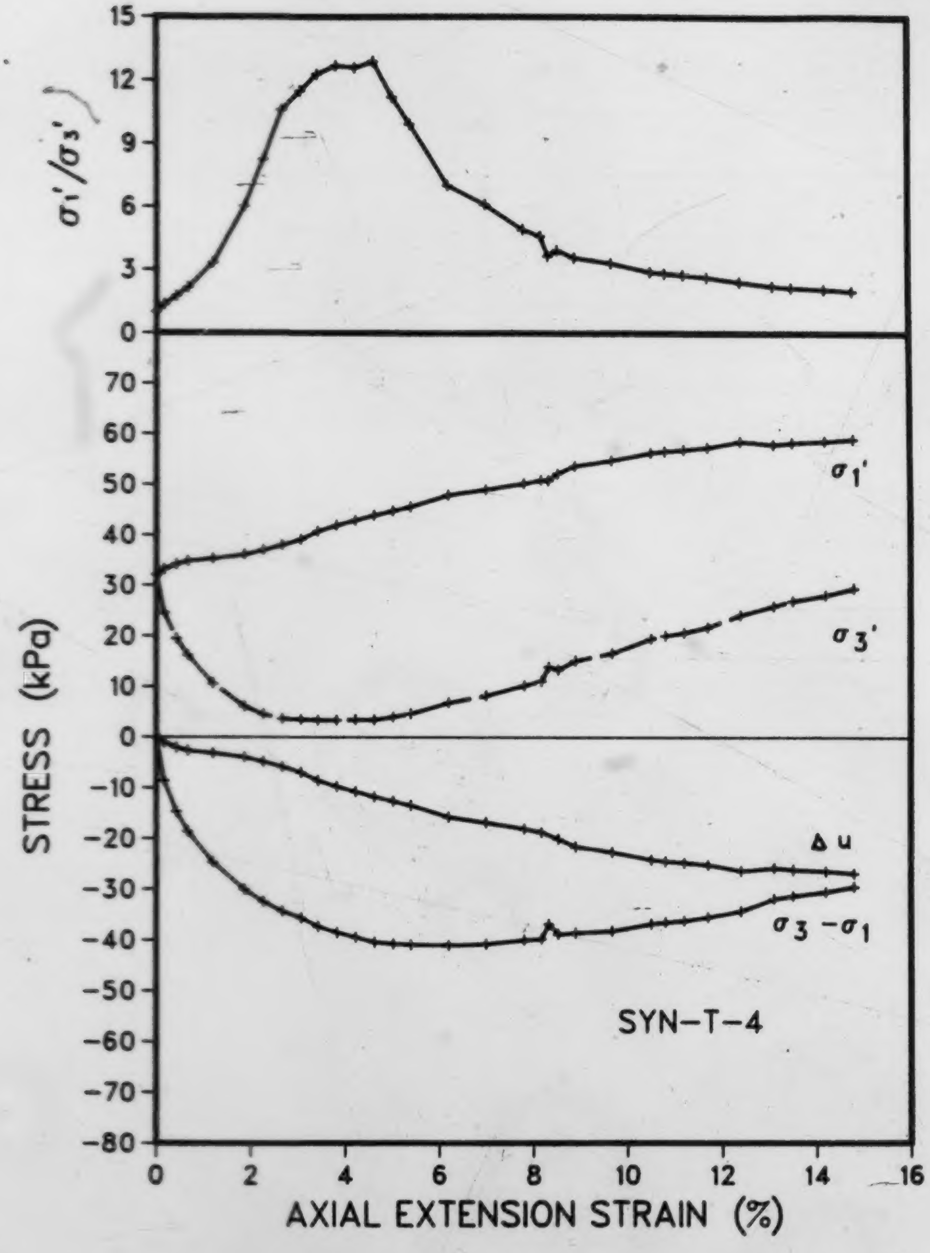

Figure E.25 SYN-T-4: Undrained Axial Extension Test Results

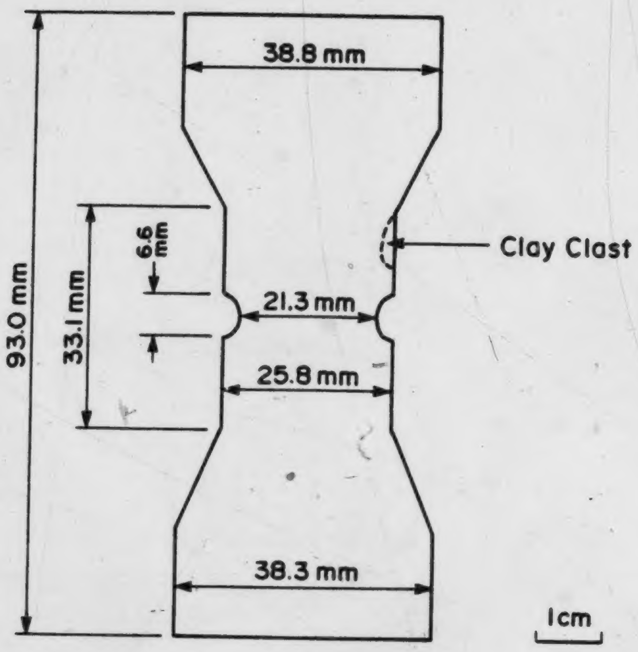
38.8 mm
Clay Clast
6.6 mm
93.0 mm
33.1 mm
21.3 mm
25.8 mm
38.3 mm
1cm

Final Total Length = 93.0 mm
Initial Total Length = 89.6 mm
Change in Height = 3.4 mm

Final Notch Length = 33.1 mm
Initial Notch Length = 30.0 mm
Change in Notch Length = 3.1 mm

Figure E.26 SYN-T-4: Condition of Sample After Testing

# TEST SYN-T-5: SYNCRUDE OIL SAND

## PROCEDURAL DETAILS

1. The sample was installed in the triaxial cell and enclosed in a single membrane with horizontal convolutions in the notched zone.
2. The sample was thawed under cell and back pressures of 494 and 146 kPa for 46 hours.
3. B tests were conducted at an effective confining pressure of 165 kPa with incremental increases in pore pressure until saturation was reached.
4. An isotropic compressibility test was conducted with two cycles of effective confining stress up to 781 kPa. A constant pore pressure of 408 kPa was maintained throughout the test.
5. A second series of B tests were conducted at a confining pressure of 73 kPa following the cyclic compression of the sample.
6. The sample was consolidated under an effective confining and back pressure of 86.9 kPa and 598 kPa. An undrained axial extension test was conducted at a deformation rate of 0.223 mm per hour.

## TEST DATA

END DIAMETER = 38.62 mm
TOTAL HEIGHT = 75.32 mm
INITIAL WEIGHT = 137.98 g.

NOTCH DIAMETER = 26.08 mm
NOTCH LENGTH = 22.30 mm

BULK DENSITY = 2.058 Mg/m$^3$
WATER CONTENT = 9.8 %
BITUMEN CONTENT = 5.3 %
SATURATION = 90.2 %
POROSITY = 0.341

FINAL WEIGHT = 140.75 g.
FINAL WATER CONTENT - NOTCHED ZONE = 12.0 %
- SAMPLE ENDS = 9.9 %

### Comments on Sample Failure

The sample failed by parting at mid-height of the notched zone as shown in Figure E.30. Initial parting surface inclined between 5° and 7° to horizontal. No evidence of shearing at the ends of the sample were observed.

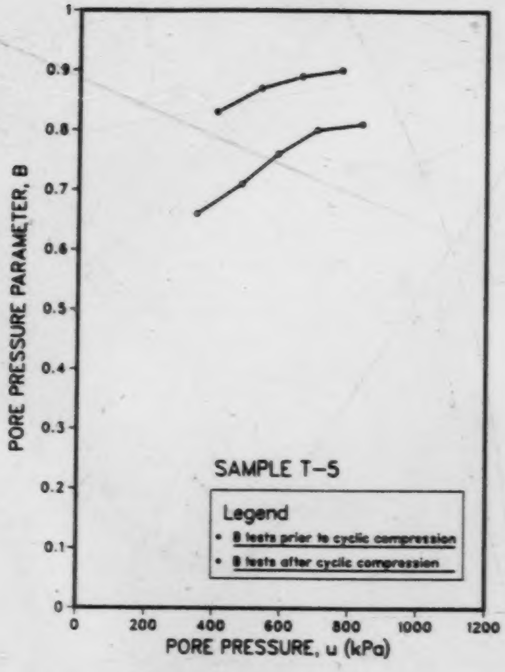

Figure E.27 SYN-T-5: Pore Pressure Parameter B

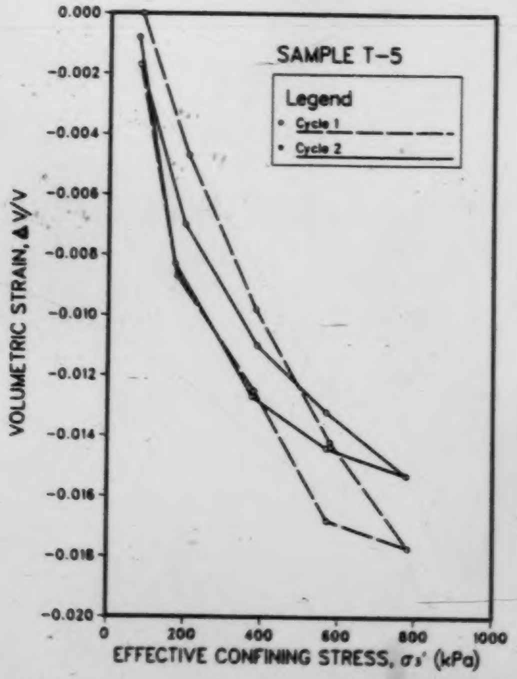

Figure E.28 SYN-T-5: Cyclic Compressibility Test

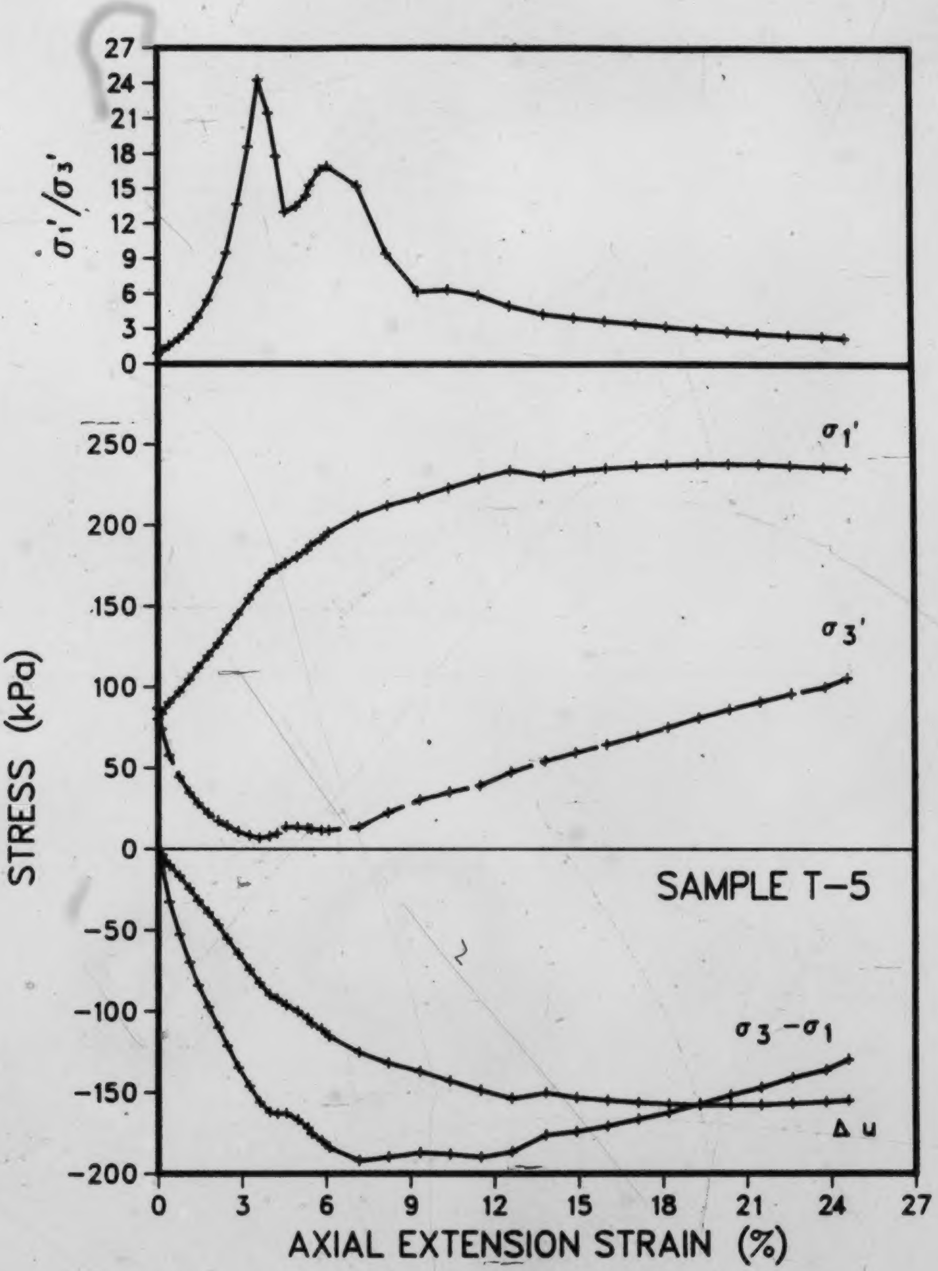

Figure E.29 SYN-T-5: Undrained Axial Extension Test Results

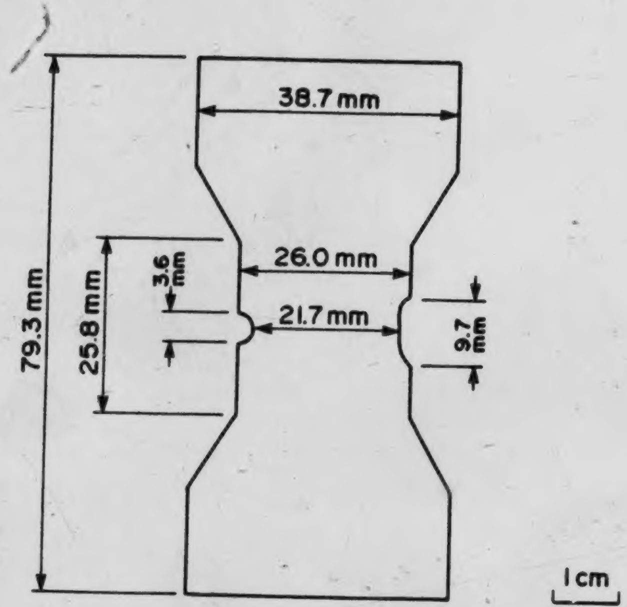
38.7 mm
26.0 mm
21.7 mm
79.3 mm
25.8 mm
3.6 mm
9.7 mm
1 cm

Final Total Length = 79.3 mm
Initial Total Length = 75.3 mm
Change in Length = 4.0 mm

Final Notch Length = 25.8 mm
Initial Notch Length = 22.3 mm
Change in Notch Length = 3.5 mm

Figure E.30 SYN-T-5: Condition of Sample After Testing

# TEST SYN-T-6: SYNCRUDE OIL SAND

## PROCEDURAL DETAILS AND OBSERVATIONS

1. The sample was installed in the holding hanger and suspended in the triaxial cell.
2. The sample was thawed under a cell pressure of 200 kPa.
3. The sample failed by horizontal parting at the midsection of the notch zone within 5 minutes of application of the cell pressure.
4. The cell pressure was increased to 400 kPa and the slaking of the sample observed for 4 days. The sample totally disintegrated after 4 days due to dispersion of the clay clasts within the oil sand.

## TEST DATA

Refer to Figure E.31 for initial specimen dimensions.

WATER CONTENT = 10.7 %
BITUMEN CONTENT = 2.5 %

INITIAL VOLUME = 669.9 $cm^3$
INITIAL WEIGHT = 1448 g.
BULK DENSITY = 2.162 $Mg/m^3$

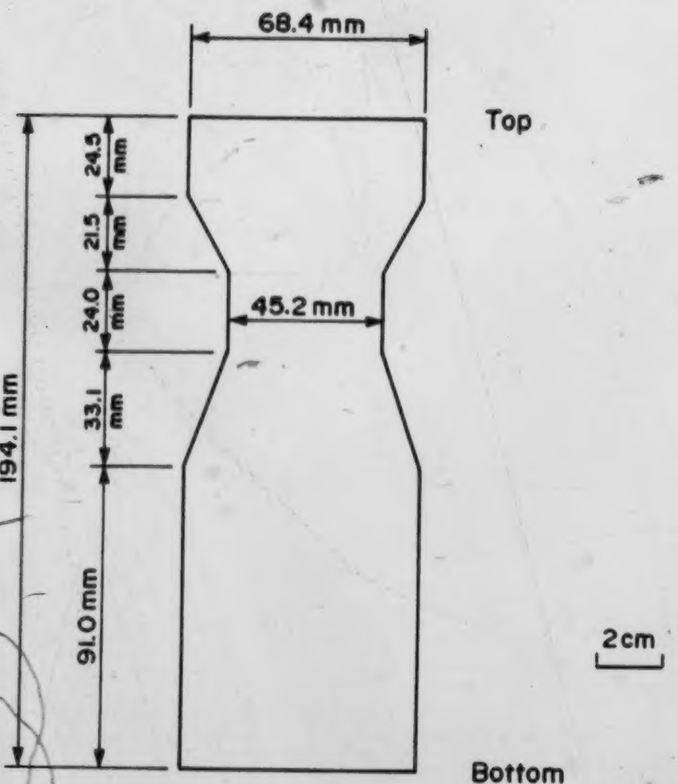
68.4 mm
Top
24.5 mm
21.5 mm
24.0 mm
45.2 mm
33.1 mm
194.1 mm
91.0 mm
2cm
Bottom

Figure E.31 SYN-T-6: Initial Sample Dimensions

# TEST SC-84-T-1: SALINE CREEK OIL SAND

## PROCEDURAL DETAILS AND OBSERVATIONS

1. The sample was installed in the holding hanger and suspended in the triaxial cell.
2. The sample was thawed under a cell pressure of 700 kPa.
3. The sample failed by horizontal parting at the midsection of the notch zone within 1 minute of application of the cell pressure.
4. The slaking of the sample was observed for 5 days under the cell pressure of 700 kPa. Virtually no disintegration of the sample was observed. Less than a 0.3 percent increase in the sample dimensions was measured indicating very minor expansion under pore pressures above the pore fluid saturation pressure.

## TEST DATA

Refer to Figure E.32 for initial specimen dimensions.

INITIAL VOLUME = 551.1 $cm^3$
INITIAL WEIGHT = 1048 g.
BULK DENSITY = 1.902 $Mg/m^3$

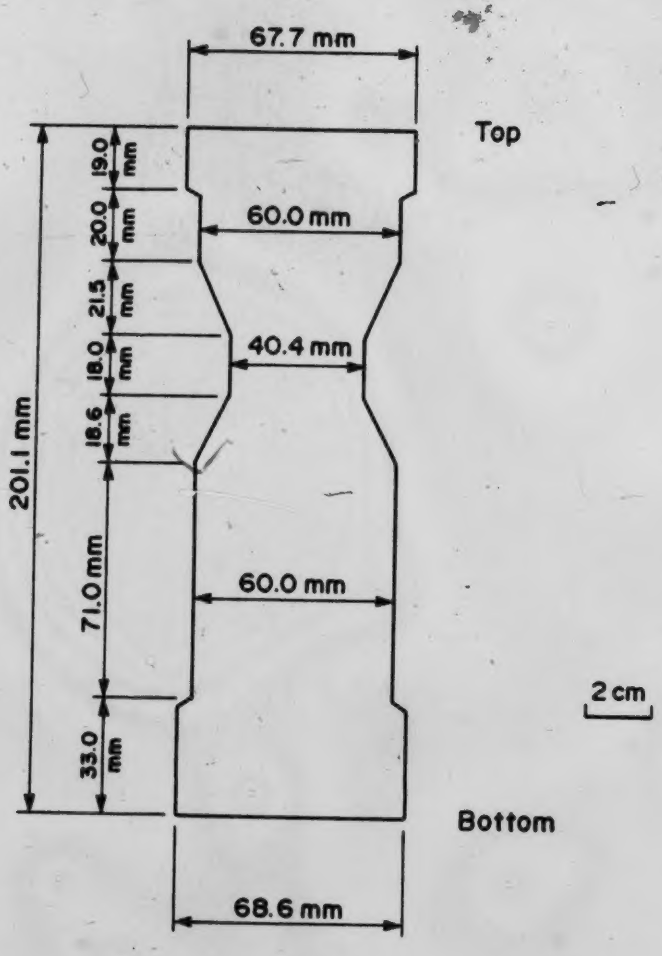
67.7 mm
Top
19.0 mm
20.0 mm
60.0 mm
21.5 mm
18.0 mm
40.4 mm
18.6 mm
201.1 mm
71.0 mm
60.0 mm
2 cm
33.0 mm
Bottom
68.6 mm

Figure E.32 SC-84-T-1: Initial Sample Dimensions

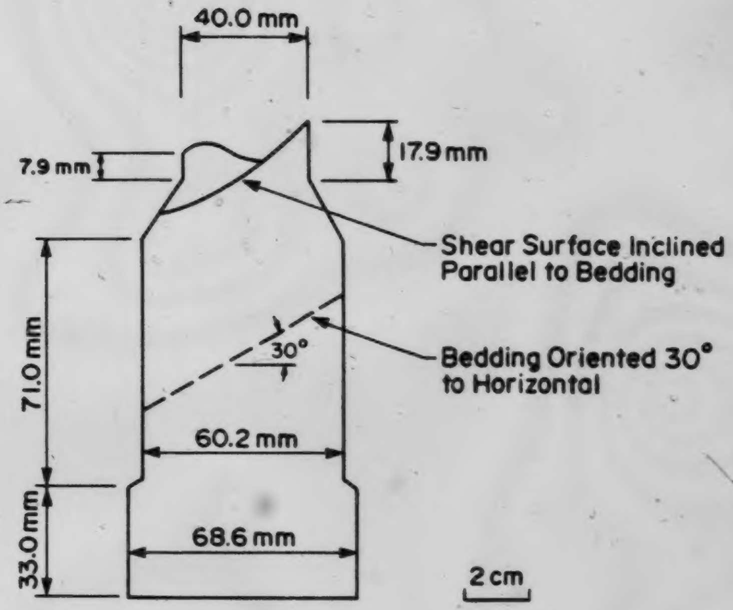
40.0 mm
7.9 mm
17.9 mm
Shear Surface Inclined Parallel to Bedding
Bedding Oriented 30° to Horizontal
30°
71.0 mm
60.2 mm
33.0 mm
68.6 mm
2 cm

Figure E.33 SC-84-T-1: Condition of Sample After 5 Days

## TEST SC-84-T-2: SALINE CREEK OIL SAND

### PROCEDURAL DETAILS AND OBSERVATIONS

1. The sample was installed in the holding hanger and suspended in the triaxial cell with the base of the sample resting on the bottom of the cell.
2. The sample was thawed under a cell pressure of 700 kPa for 3 hours.
3. The sample was raised slowly off the bottom of the triaxial cell at the rate of 0.5 mm per minute. A horizontal crack was initiated at the lower edge of the notched zone. The crack propagated through the sample with further extension as shown in Figure E.36. The parting of the sample in this manner was judged to be caused by eccentricity of loading while raising the sample off the bottom of the cell.
4. The sample was immediately removed from the cell and measured to estimate the degree of swell of the sample. The measurements are presented in Figure E.36. Virtually no swell of the sample was measurable. No evidence of slaking of the sample was observed during testing.

### TEST DATA

Refer to Figure E.34 for initial specimen dimensions.

INITIAL VOLUME = 603.8 $cm^3$
INITIAL WEIGHT = 1203 g.
BULK DENSITY = 1.992 $Mg/m^3$

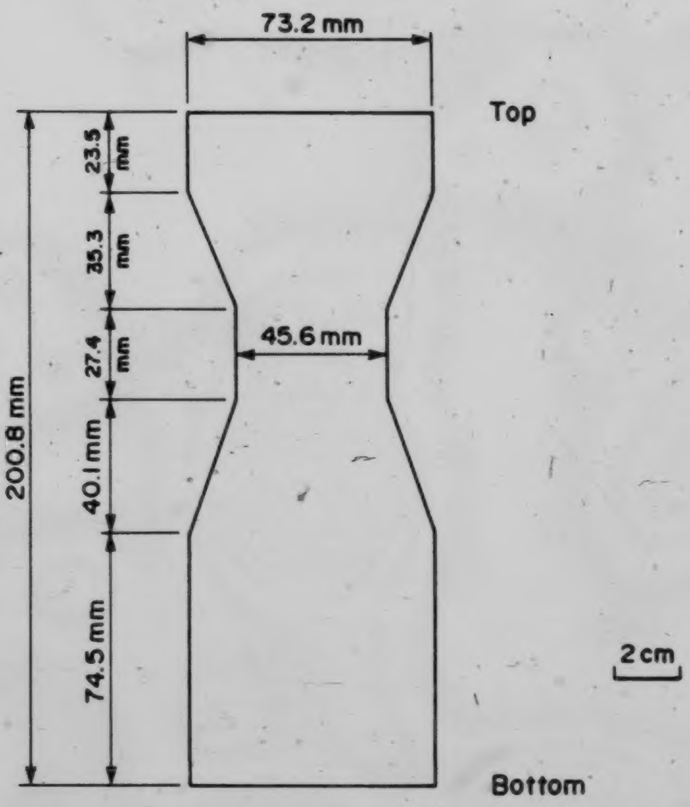
73.2 mm
Top
23.5 mm
35.3 mm
27.4 mm
45.6 mm
40.1 mm
74.5 mm
200.8 mm
2 cm
Bottom

Figure E.34 SC-84-T-2: Initial Sample Dimensions

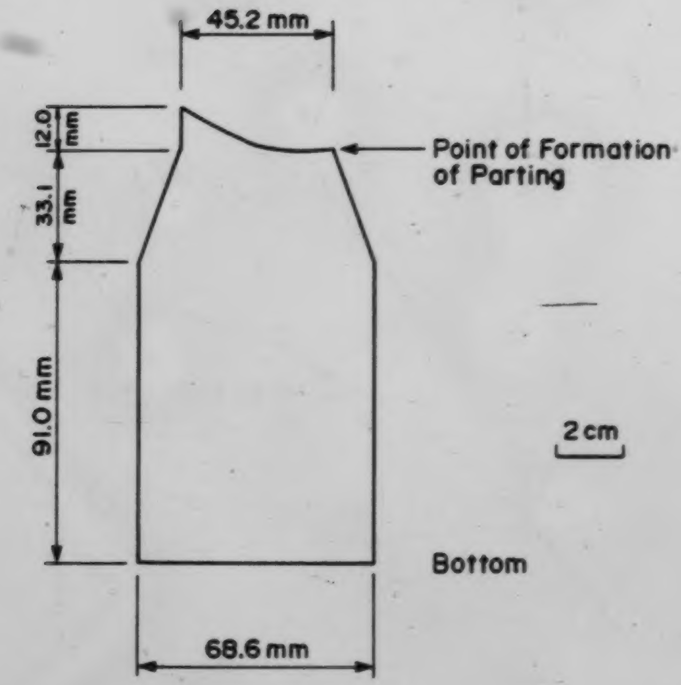
45.2 mm
12.0 mm
33.1 mm
91.0 mm
Point of Formation of Parting
2 cm
Bottom
68.6 mm

Figure E.35 SC-84-T-2: Condition of Sample After Failure